ORNL
MASTER COPY

ORNL-3849
UC-41 – Health and Safety
TID-4500 (44th ed.)

HEALTH PHYSICS DIVISION
ANNUAL PROGRESS REPORT
FOR PERIOD ENDING JULY 31, 1965

OAK RIDGE NATIONAL LABORATORY
operated by
UNION CARBIDE CORPORATION
for the
U.S. ATOMIC ENERGY COMMISSION

ChemRisk Document No. 727
#727

Printed in USA. Price $6.00. Available from the Clearinghouse for Federal Scientific and Technical Information, National Bureau of Standards, U.S. Department of Commerce, Springfield, Virginia

LEGAL NOTICE

This report was prepared as an account of Government sponsored work. Neither the United States, nor the Commission, nor any person acting on behalf of the Commission:

A. Makes any warranty or representation, expressed or implied, with respect to the accuracy, completeness, or usefulness of the information contained in this report, or that the use of any information, apparatus, method, or process disclosed in this report may not infringe privately owned rights; or

B. Assumes any liabilities with respect to the use of, or for damages resulting from the use of any information, apparatus, method, or process disclosed in this report.

As used in the above, "person acting on behalf of the Commission" includes any employee or contractor of the Commission, or employee of such contractor, to the extent that such employee or contractor of the Commission, or employee of such contractor prepares, disseminates, or provides access to, any information pursuant to his employment or contract with the Commission, or his employment with such contractor.

ORNL-3849
UC-41 – Health and Safety
TID-4500 (44th ed.)

Contract No. W-7405-eng-26

HEALTH PHYSICS DIVISION ANNUAL PROGRESS REPORT

For Period Ending July 31, 1965

K. Z. Morgan, Director
W. S. Snyder, Assistant Director
E. G. Struxness, Assistant Director

OCTOBER 1965

OAK RIDGE NATIONAL LABORATORY
Oak Ridge, Tennessee
operated by
UNION CARBIDE CORPORATION
for the
U. S. ATOMIC ENERGY COMMISSION

Summary

PART I. RADIOACTIVE WASTE DISPOSAL

1. Injection into Permeable Formations

Studies of sorption and desorption of iodine on mineral surfaces indicate that some species of iodine, probably I_2, can be actively adsorbed onto the mineral surface. In this event the adsorbed iodine is resistant to leaching, either by air or by water. Capillary condensation of HI and I_2 may also occur, but these forms are subject to further movement. No significant retention of methyl iodide (CH_3I) in Berea sandstone was observed.

2. Disposal by Hydraulic Fracturing

The sixth injection of a series was started on May 19, using a mix containing Kingston fly ash as a substitute for some of the portland cement. To control the proportioning of low-solids mixes with more consistency than was possible with the Densometer, a flowmeter was installed in the mixer hopper. During the injection, difficulty was experienced in maintaining the flow of solids. The cause of the plugging was found to be large clumps of solids which plugged the valves. Difficulties with the flowmeter were also experienced; in this case, a plastic cone, about 12 in. in diameter, came loose and plugged the hopper. Plugging of the hopper resulted in leakage of grout out into the mixer cell. The cell was decontaminated by flushing the grout into the concrete waste pit and pumping the contaminated wash water into the fracture.

After approximately 64,000 gal of waste had been injected, a leak developed in the high-pressure piping in the wellhead cell. After locating the leak at a connection between the plug container and the connecting piping, the well, filled with grout, was cleared by pumping water down the annulus, up the central tubing, and out through the leak in the wellhead. The wellhead cell was decontaminated with water, and the contaminated grout was flushed down to the emergency pit. The injection well has been kept open in order to determine the bleed-back characteristics of the grout.

3. Disposal in Natural Salt Formations

Preparations are nearly complete for the startup of Project Salt Vault, a demonstration of the disposal of high-level waste solids in a salt mine. Mining of the experimental area was completed at the end of March, and rehabilitation of the access to the experimental area has also been completed. All instrumentation for the measurement of salt movement has been installed, and most of the remaining experimental equipment has also been installed. Both the surface shipping carrier and the underground transporter have been completed.

Phosphate glass rods and ferrous sulfate chemical dosimeters both have been found to be usable at temperatures up to 250°C and doses up to 10^5 rads.

Operation of the prototype test has proved out the procedures for measurement of salt flow, temperature, etc., in the demonstration. It has also confirmed the expectation of trouble due to water in the shale below the original mine floor. However, no difficulties on this score are anticipated in the demonstration itself.

Creep tests have been run on scale-model salt pillars with axial loads from 1000 to 10,000 psi at temperatures up to 200°C. Results indicate that the effect of elevating the temperature is essentially the same as that of increasing the average pillar stress.

4. Clinch River Study

The field and laboratory work of the cooperative study of the Clinch River has been terminated. Tests of the effect of Melton Hill Dam water released at typical winter conditions have shown that minimum winter dilution factors at both CRM 14.4 and CRM 5.5 are only about one-third of the summer dilution factors.

The automatic water-sampling station for collections proportional to flow has been installed in the tailrace at Melton Hill Dam. The sampler for Gallaher Bridge has been fabricated.

Examination of the cores of bottom sediments from the Clinch River has shown that most of the sediment and the radionuclides are concentrated in the lower end of the reach, that the depth distribution of the gross gamma count is well correlated (coefficient of correlation, 0.80) with the annual release of ^{137}Cs and ^{60}Co, and that approximately 200 curies of radioactive material is stored in the bottom sediments. The bottom inventory shows 154.6 curies of ^{137}Cs, 17.5 curies of ^{60}Co, 15.5 curies of ^{106}Ru, 10.2 curies of rare earths, and 2.9 curies of ^{90}Sr. Of the radionuclides released through White Oak Dam (allowing for decay), 21% of the ^{137}Cs has been retained in the bottom sediments, 9% of the ^{60}Co, 0.4% of ^{106}Ru, and 0.2% of ^{90}Sr.

5. Movement of Nuclides in Terrestrial Environment

Sorption tests of three soils from the southeastern United States showed that ion exchange capacity was not the controlling factor in radiocesium sorption by these soils. Desorption with sodium acetate revealed a maximum in the time-desorption relationship, particularly in the subsurface horizons.

In the experimental field plots, the ^{137}Cs loss following six months of operation and after 27.92 in. of rain amounted to 17.9% from plot 1 (bare), 14.1% from plot 2 (clipped meadow), and 6.0% from plot 3 (tall meadow). The relationship between ^{137}Cs loss and soil loss was found to follow the equation

$$y = \exp\,(m \ln x - b), \quad 0 < y < 100, \; x > 16 \text{ g/m}^2,$$

where y = percent Cs loss and x = soil loss in g/m^2, and m is 0.6758, 0.6257, and 0.6382 and b is 1.3345, 0.4505, and 0.9029 for plots 1, 2, and 3 respectively. If we let $\ln y = z$, then, for plots 1, 2, and 3, z values fall in the ranges ±0.0468, ±0.0468, and ±0.0077 respectively.

After 19.7 in. of rain, the ^{137}Cs on the vegetation was measured. In both vegetation plots (2 and 3), approximately 25% of the radionuclide remained on the vegetation.

6. Mineral Exchange Studies

Solution-dispersion coefficients were measured in Berea sandstone as a function of flow rate. The experimental values of the dispersion coefficients varied as the 1.21 power of the solution velocity. This agrees more closely with the power of 1, expected on the basis of a statistical model, than with the power of 2, expected on the basis of a capillaric model. Molecular diffusion contributes negligibly to the total dispersion, except at very low flow rates.

If an ion exchange column is operated under continually changing chemical conditions, the distribution coefficient of the solute changes with time. Consequently, the relative velocity of the solute changes with respect to the transporting water. In such cases the relative dispersion of the solute will be different from that of the solvent.

7. Engineering, Economics, and Safety Evaluations

Analysis of the critical pathways of radiation exposure to man resulting from the discharge of radioactive materials to the Clinch River has shown that fish and water consumption are most important. Mathematical models have been constructed, and they show that the dose rate to the skeleton of the 14-year-old person drinking Clinch River water is twice the dose to standard man. The dose rate to the 14-year-old is still less than 1/10 of the present permissible limit. For those drinking Tennessee River water the dose rate to the skeleton of the 14-year-old is also about twice that of standard man and still less than 10% of the present permissible limit.

Based upon realistic but conservative assumptions, the estimated cumulative dose over a 20-year period received by the skeleton of the critical population group, the 18-year-old employed at ORGDP (assuming him to be a nonoccupational worker), was 3 rems, in comparison with a permissible dose of 60 rems.

8. Related Cooperative Projects

The U.S. Geological Survey cooperated in the preparation of a report on the soils and geology of White Oak Creek Basin.

The work of the multiagency steering committee for the Clinch River Study has continued.

One alien guest completed his assignment during the year.

Several members of the section have continued to participate in the following activities: the ASA Committee N5, the ASCE Committee on Sanitary Engineering Aspects of Nuclear Energy, and various ORNL special committees. One member has also served as an assistant editor of *Nuclear Safety* and assistant news editor for the United States for *Health Physics*. Two members have served part time with the Nuclear Safety Information Center.

In addition, courses and lectures have been given for ORSORT, ORINS, Vanderbilt University, University of Tennessee, and the U.S. Public Health Service.

PART II. RADIATION ECOLOGY

9. Radiation Effects and Radioactive Waste Area Studies

Studies of the effects of radiation on trees growing around the unshielded Health Physics Research Reactor showed radiation damage patterns extending into the forest up to 45 m from the reactor and covering an area of about 1200 m^2. Damage to deciduous species was confined to trees growing from 10 to 25 m from the reactor, where integrated fast-neutron doses (tissue dose in air) were 1273 to 197 rads delivered sporadically over a period of one year and two months. Beyond 25 m, only pine trees (*Pinus virginiana* Mill.) were visibly affected.

The effect of radiation and moisture stress on pines was tested in an experiment in which potted seedlings of two-year-old scrub pine (*P. virginiana*) received acute ^{60}Co doses of 388, 562, and 900 rads to their shoots. Three soil moisture treatments were given: no water, 150 ml/week, and 450 ml/week. Needle desiccation rates indicated that for a month following a near-lethal radiation stress, addition of a moisture stress may not augment the radiation effect. At lower doses the two stresses may be additive initially. After a two-month period the effect of the two stresses was additive in all cases.

Dormant stem cuttings from ten clones of *Populus deltoides* Marsh. (Eastern cottonwood) representing seven ecotypes from Alabama and one ecotype each from Mississippi, Kentucky, and Illinois were given an acute ^{60}Co gamma radiation dose of 7600 rads. A linear relationship was found between clonal growth performance and radiosensitivity. Clones which exhibited the best growth were the most radiosensitive. Interphase nuclear volumes of apical meristems provided no basis for differential radiosensitivity of clones.

Nine-day mimosa seedlings were given a total dose of 1350 rads (tissue dose in air) of fast neutrons delivered over a period of 47 min. Quantities of soluble and total ribonucleic acid (RNA) in the epicotyls were measured, and base compositions were calculated. The data suggest that levels of sRNA do not differ between irradiated and control seedlings, while levels in both decrease slowly as a result of aging (0.8 to 0.4% sRNA/dry weight from 9 to 19 days respectively). All base concentrations leveled off after six days post-irradiation. Correlations of base compositions with growth rates suggest an immediate flush of growth in the irradiated seedlings. No correlations between time following irradiation and amino acid acceptance of sRNA extracts have been found to date. Experiments were performed to investigate the interaction of ionizing radiation with short day length, which is critical for flowering in cocklebur (*Xanthium chinense* Mill.). Photoinduced plants receiving radiation produced more stem growth than controls, while noninduced irradiated plants did not differ from controls. Production of floral buds in plants irradiated before photoinduction did not differ significantly from controls, while those irradiated after photoinduction temporarily produced more.

Further surveys for distribution of radioactive mud-dauber wasp nests uncovered a relatively large number of old radioactive nests of the pipe-organ dauber, which heretofore had been considered rare. The source of radioactive mud was inferred to be from the radioactive seeps of the ORNL waste pits. Cesium-137 retention by suctorial insects was tested using two species, *Aphis fabae* and *Oncopeltus fasciatus*. Both of the species had elimination rates slower than predicted on the basis of size. *Oncopeltus* was predicted to have a T_b of 18 hr, but the measured T_b was 35 hr. For

Aphis, expected and measured values of T_b were 5 and 14 hr respectively. Both species showed a single-component elimination pattern.

Radiosensitivity studies and preparation of radiation profiles were undertaken for a number of insect species. These included the European brown cricket (*Acheta domestica*), common mealworm (*Tenebrio molitor*), evergreen bagworm (*Thyridopteryx ephemeraeformis*), giant milkweed bug (*Oncopeltus fasciatus*), and others. Data are presented on radiation effects on different life history stages and on life expectancy. Preliminary experiments were completed on beta radiation studies on several insect species using an ^{90}Sr plane source. Insects exposed to beta radiation lived about 50% longer than those exposed to equivalent gamma doses. This may be due to shielding of the intestine by the exoskeleton and body of the insect, which attenuate the dose to the gut.

Eight species of indigenous rodents, one species of shrew, and one strain (RF) of laboratory mouse were irradiated at eight doses ranging from 0 to 2000 rads. The two species of *Peromyscus* and the *singly caged* RF strain *Mus musculus* were the most radioresistant with respect to mortality. Rice rats and cotton rats were peculiar in that mortality changed from 0 to 100% within a narrow range (0 to 690 rads and 690 to 1060 rads respectively). Weight losses for all species were rapid at the higher doses, presumably resulting from a combination of anorexia and diarrhea that is caused by the intestinal-death syndrome that occurs in this dose range.

Studies were continued to test the usefulness of ^{131}IUDR (5-^{131}iodo-2′-deoxyuridine) as a physiological dosimeter. Cotton rats received acute doses of 100, 500, and 1000 rads prior to injection of ^{131}IUDR. The 100- and 500-rad doses reduced the amount of ^{131}IUDR incorporated by 28 and 65% of controls respectively. This reduction was due to decreased incorporation into the intestine. One thousand rads produced a combination of a reduction in intestinal incorporation and a change in iodine elimination.

10. Processes and Components of Terrestrial Ecosystems

Studies on loss of ^{137}Cs from the tagged *Liriodendron* forest confirmed the hypothesis that losses from the aboveground parts of tagged trees to the forest floor surface due to leaching by rain and fall of litter are exceeded by losses from underground parts of the tagged trees due to leaching by percolating ground water, exudation, and die-off of these root systems. Although the root contribution from tagged trees is greater than contributions of rainfall and leaf fall to the surrounding environment, the latter are more promptly transferred to other living components of the forest system.

Autecological studies on the behavior of radiocesium in herbivorous forest insects have utilized the evergreen bagworm, *Thyridopteryx ephemeraeformis*, as a model for uptake and transfer of this nuclide through metamorphosis. Pupating female larvae were removed to the laboratory for evaluation of the fate of the radiocesium body burden during transformation. Developmental times in the laboratory of about 40 days showed good agreement with values of about 38 days obtained with field populations. Essentially the entire body burden of radiocesium is transferred from the larval to the pupal stage. In the subsequent changes, 10% remains in the puparium, 40% is transferred to the egg clutch, and 50% remains in the female after oviposition.

The biological half-lives for radiocesium in arthropods of detritus-based food chains of the ^{137}Cs-tagged *Liriodendron* forest were determined to permit estimation of nuclide turnover rates within cryptozoan communities. Disregarding the rapid initial loss rates due to gut voidance, the retention curves were best characterized by either one or two exponential functions. All the Coleoptera were characterized by single-component systems, regardless of feeding mechanisms or trophic position. In the Orthoptera, crickets also exhibited single-component retention curves, while the retention curve for the wood roach consisted of two components. The diplopods also included species with both single- and double-component systems. All the isopods possessed two-component retention systems.

To complement previous experiments with tagged litter and with the ^{137}Cs *Liriodendron* forest, a 5- by 5-m plot in another *Liriodendron* forest was sprayed with a ^{137}Cs solution. After five months, the amounts of cesium in the litter and in successive 2.5-cm soil layers were 66, 27, 4, 1, 0.6, 0.6, and 0.4% of the total in 0 to 15 cm. The difference in distribution compared with the tagged forest, along with previously reported evidence that much of

the radiocesium in the tagged forest was associated with tree roots, reemphasized the importance of redistribution through living roots, in addition to downward percolation through water in natural soils.

In another radiocesium cycling study with herbaceous ecosystems, two 8- by 8-ft plots, one representing a tall meadow and a clipped one representing a short meadow, were each sprayed with 5 mc of ^{137}Cs diluted in water. Six days after inoculation, prior to any rainfall, more than 95% of the total ^{137}Cs tag was contained on the tall grass and about 85% was contained on vegetation materials on the short-meadow plot. After the plots had received 3.5 in. of rain, 47% ± 2.4 S.E. (S.E. = standard error) of the radiocesium was on the tall grass, while 50% ± 4.1 S.E. was associated with vegetation materials on the short-meadow plot.

A procedure was developed for random location of study units utilizing only one marker post, which provides for rapid relocation of permanent plots, permanent line transects, and permanently tagged individual plants for ecological studies. A circular plot area, with or without centers restricted from sampling, was subdivided by five intersecting diameters and an annulus of rings. Use of this system for locating plots, transects, or plants in ecological studies showed that considerable field time may be saved as compared with conventional methods of establishing sample locations.

11. Clinch River and Related Aquatic Studies

A previous study of the deposition of Sr and Ca in snail shells indicated a region of minimal Sr uptake, dependent on both Ca and Sr concentrations. In a similar experiment where Ca ranged from 0.10 to 180.0 ppm and Sr ranged from 0.02 to 8.0 ppm, calculations of the response surface again showed this area of minimal Sr uptake. These results indicate that both Ca and Sr amendments to an environment should be controlled carefully in order to effect a reduction in radiostrontium uptake.

A comparison of Sr concentrations in prehistoric (Indian midden) clam shells and present shells of the same species showed that the ancient shells had consistently greater concentrations of Sr. Also, inter- and intraspecific differences among the contemporary shells were small compared with the observed differences between contemporary and ancient shells. It was established that these differences were not due to construction of the Tennessee Valley Authority dams nor were they due to postmortem changes in the chemical composition of the midden shells resulting from solution and redeposition. It was hypothesized that the reduced Sr concentrations in modern shells result from a reduced Sr-Ca level in the rivers that has resulted from the removal of the forests and imposition of an agricultural economy over most of the watersheds of the Tennessee River system.

The distribution of ^{134}Cs in carp (*Cyprinus carpio*) was determined by feeding experiments and subsequent dissection. The uptake and subsequent loss of ^{134}Cs by the tissues indicated three types of cesium metabolism. Estimates of the biological half-life in days for each tissue were: heart, 16; kidney, 17.4; liver, 17.8; gills, 21.2; scales, 22.3; spleen, 24.1; skin, 26.6; blood, 39.5; bone, 97.0; and flesh, 280.0. The whole-body half-life was about 80 days. The long half-life of cesium in the flesh may be of significance when considering contaminated fish for human consumption.

Feeding rate and metabolism of carp in White Oak Lake were determined using the ^{137}Cs which is present as a contaminant. The average quantity of ^{137}Cs associated with algae and detritus samples taken from the lake is 18 and 9 $\mu\mu c$ per gram of wet weight respectively. The calculated amount of ^{137}Cs ingested by a yearling carp (146 g) was 81.2 $\mu\mu c$/day or 3.90 g of detritus per day and 2.56 g of algae per day. Based on the calorie content of the algae and detritus, the intake for maintenance by yearling carp was 6030 cal/day.

Comparison of methods for measuring primary production in aquatic systems indicated that radioisotopes other than ^{14}C may be useful for this purpose. Preliminary experiments with ^{85}Sr on Melton Hill Lake adjacent to the Oak Ridge Reservation suggest that it can be used for certain aspects of productivity measurement.

12. Theoretical and Systems Ecology

Theoretical studies were completed on the mathematical properties of food web structure based on the characteristics of mathematical graphs. Also a mathematical proof was developed to demonstrate equilibrium specific activity in two-compartment exchange systems.

A hypothetical food chain model was formulated for analog computer determinations of steady-state distributions and turnover rates of radioactivity in the system under a chronic input to the primary producers.

A FORTRAN program for ecosystem simulation was completed and tested using a generalized compartment model. The program was written with flexibility for digital simulation of compartment models, but was especially aimed at simulating ecological succession. This program also was used in simulating the redistribution of ^{137}Cs in a seven-compartment model of the tagged *Liriodendron* forest.

The kinetics of ^{134}Cs exchange in a microflora, soil, and millipede microcosm was explored using an analog computer compartment model system. Six computer experiments were performed to obtain transfer coefficients of ^{134}Cs for various partial systems and for the complete system.

A compartment model for the distribution of ^{134}Cs in carp was formulated and programmed for an analog computer study of exchange kinetics between the different organs. To obtain computer-generated curves which fit the empirical data for each organ, a synthetic blood curve was generated to which each organ could be coupled separately to determine transfer coefficients.

An indirect computer method for probabilistic estimates of forage intake by freely grazing animals was developed. This method has been applied to obtain estimates of precision for forage intake with data from experiments with grazing cattle and sheep.

Nonlinear programming and least-squares techniques were used to predict the attributes of individual species from knowledge of the attributes of the mixed sample and the species composition of the mixed sample. These techniques were applied successfully to data from experiments with cattle and sheep to predict the crude protein content of five dietary species groups from the botanical composition and the crude protein in the mixed sample.

PART III. RADIATION PHYSICS

13. General Radiation Physics

Continuing studies have shown that linear momentum transfer, which was used previously in the dosimetry of neutrons and gamma rays, can also be applied to charged particles in order to account for observed variations of RBE with physical characteristics of radiation. This extension implies that the concept of the LET dependence of RBE might be more specifically termed a velocity dependence, since charge dependence does not enter the new formulation. The absence of charge has been shown to be valid within the limits of applicability of the first Born approximation in quantum mechanics. An evaluation has been made of the maximum permissible flux of neutrons and protons in the energy range from 60 to 400 Mev. The investigation of instabilities produced by helical beams in a stationary plasma has been continued with particular reference to the excitation of hydromagnetic and whistler waves by gyrating electrons and to the excitation of hydromagnetic waves by gyrating protons. An investigation has been made of almost longitudinal waves excited by a linear beam in a stationary plasma immersed in a magnetic field.

14. Interaction of Radiation with Gases

Further studies of *alpha-particle ionization* in gas mixtures show that an empirical parameter can be associated with each component of the gaseous mixture which will allow the prediction of the amount of ionization in other mixtures to an accuracy of about 1%. These studies also show that in mixtures involving noble gases, an inverse Jesse effect exists which can be explained in terms of the Hornbeck-Mollnar process. In studies of *electron transport* in gases, it was found that for strongly polar molecules the cross section for momentum transfer can be predicted to within a factor of 2 from a macroscopic parameter, the dipole moment; whereas for *polarizable* (nonpolar) molecules the cross section predicted from polarizability alone is a factor of 20 to 80 larger than that observed. In the latter case, where forces are short range, many more details of molecular size, shape, etc., are important. *Methods* for the measurement of *electron transport* in gases have been advanced, and accurate assessment of errors in electron time-of-flight techniques has been given. Studies with these methods suggest that the electron diffusion coefficients differ significantly from those obtained from the competing Townsend-Huxley lateral diffusion method. An electron swarm technique has been developed which allows the determination of *electron capture cross sections at high temperatures* (up to 400°F) and is being applied to the study of molecules of

biological interest. We have shown that electron swarm and electron beam techniques can be combined to provide *electron capture cross sections as a function of electron energy*, even at energies less than 1 ev, for mass-identified reactions. The swarm-beam technique was applied to the study of *electron capture in a number of halogenated benzene derivatives*, and it was shown that these compounds capture electrons by dissociation even at thermal energies.

More emphasis has been given to theoretical treatments and discussions of electron transport and capture in molecules. A theory of *electron capture by rotational excitation* of a compound state was developed, and it explains the enhancement of elastic scattering cross sections observed in polar molecules, for example, H_2O, D_2O, and H_2S, for thermal electrons. A solution of the transport equation for the one-dimensional time-dependent case, where *electron capture and loss* are included, was found and will be applied to time-of-flight studies. *Electronic binding* energies in the field of permanent rigid dipoles have been calculated, and some evaluations have been made of appropriate wave functions. Calculations of the *interaction potential for diatomic molecules* have been initiated and will be extended to diatomic negative ions. A procedure has been found for the rapid *unfolding of experimental data* in which the sought function is convoluted with an observational fluctuation function. The unfolding procedure utilizes the Fourier integral transform and when applied to digital computations reduces the computational time by a factor of 20.

15. Interaction of Radiation with Solids

The transmission of photons through thin metal films, reflection of photons from opaque solids, and photon emission from electron-bombarded thin films have been investigated to determine the plasma frequencies of free electrons in various metals (e.g., Al, In, Cd, Tl, and Zn). The energy-loss functions Im ϵ^{-1} were calculated from optical constants n and k determined from reflectivity measurements and were compared with the results from electron energy-loss experiments. Unambiguous identification of the plasma losses is made possible by a knowledge of the optical constants since these losses arise at frequencies where the real part of the dielectric constant $\epsilon_1 = 0$ and the imaginary part ϵ_2 is small, whereas other losses due to one-electron (or interband) transitions are characterized by relative maxima in ϵ_2. The separation of plasma losses into surface and volume plasmons is made possible from studies of photon emission from electron-bombarded thin films since the probability of photon emission from surface plasmons is negligibly small and should not lead to observable emission. Reflection-type polarizers have been constructed and evaluated for use in the wavelength region 500 to 1300 A, for which polarizers have not previously been available. Absolute intensity measurements in this wavelength region are being made by the use of rare-gas tandem ion chamber techniques.

Improved data were obtained for slowing-down spectra in infinite, isotropic radioactive copper and gold media using an improved source design. Preliminary data were obtained for slowing-down spectra in chromium and yttrium media. A theoretical calculation for electron slowing down which illustrates the relative importance of successive generations of knock-on electrons was obtained in cooperation with workers at the National Bureau of Standards.

A criterion is proposed for locating the positions of small, chemically inert interstitial atoms in a crystal structure, and the interstitial diffusion coefficient is evaluated for the simple cubic, body-centered cubic, face-centered cubic, and diamond structures.

16. Physics of Tissue Damage

Transmission of electrons through films a few hundred atoms thick was measured over the energy range from 6 ev to 2 kev. Maxima in absorption for aluminum were identified as due to surface and volume plasmon excitation, electron-electron interactions, and L-shell ionization. Very long electron mean free paths (>300 A) were found at the lowest energy.

Calculations of an improved static dielectric constant $\epsilon(k)$ of a free-electron gas at metallic densities are being made, primarily for use in a theoretical treatment of the annihilation rate of positrons in metals, although $\epsilon(k)$ is of interest in many other connections. A Monte Carlo code for determining the penetration of electrons in metal foils has been written and is being applied to the analysis of experimental data. A theoretical expression has been given for the distribution of

transition radiation and bremsstrahlung from electrons obliquely incident on plane foils.

An investigation has been made of the effect of the mode of excitation on the excimer formation in solution and in the liquid state. The shape and position of the monomer-excimer emission and the excimer binding energy are the same for ultraviolet and x-ray excitation. Excimers are found to be formed by collision of an excited and an unexcited monomer molecule in a collision-controlled process. The ratio of the excimer and monomer quantum yields shows a strong dependence on the mode of excitation.

A crossed-beam technique was used to study vibrational excitation in N_2 by 2-ev electrons. Time-of-flight energy analysis showed electron energy losses of 0.6 and 1.0 ev attributed to $v = 0$ to $v = 2$ and $v = 0$ to $v = 3$ transitions.

17. Professional Health Physics Training

The Health Physics Training Program included 19 fellowship students from Vanderbilt University and the University of Tennessee who reported to ORNL for summer on-the-job instruction in applied and research health physics. Division personnel visited 32 colleges and universities for recruitment of students to this program and to give seminars on various research problems of current interest. A new curriculum was set up at the University of Tennessee in Advanced Health Physics which includes, in addition to the Ph.D. physics curriculum, courses entitled Radiation Chemical Physics, Radiation Biology, Physics of Polyatomic Molecules, Interaction of Electrons with Gases, Interaction of Electrons with Solids, and Interaction of Radiation with Matter. The Health Physics Division provided research facilities and advisors for eight master's and eight Ph.D. candidates to conduct their thesis research.

PART IV. RADIATION DOSIMETRY

18. Ichiban Studies

The major emphasis in the Radiation Dosimetry Section has been maintained in the area of dosimetry for human exposures. The Ichiban program for determining the radiation exposures of Japanese survivors of the nuclear bombings has yielded improved air-dose distributions and more precise shielding and epicenter information. An experiment was conducted in conjunction with Los Alamos Scientific Laboratory to determine the neutron and gamma-ray penetration of the Hiroshima bomb case.

19. Spectrometry and Dosimetry Research

Improved spectrometers have been developed for both neutrons and gamma radiation. The dose per neutron per square centimeter was measured for AmB and AmBe sources to an absolute accuracy of ±5%. Depth-dose studies in large animals were continued with measurements of the distribution of neutron and gamma dose in a burro exposed to the HPRR.

20. Dosimetry Applications

Measurements of the scattering coefficients for ^{60}Co and ^{137}Cs gamma radiation incident on concrete, lead, and water slabs were made. The albedos were determined to be 0.050, 0.0113, and 0.049 for ^{60}Co gamma rays incident on concrete, lead, and water, respectively, and 0.100, 0.013, and 0.083 for ^{137}Cs gamma rays incident on concrete, lead, and water, respectively.

Experimental and theoretical studies of sodium activation in anthropomorphous phantoms and animals have been extended, and calculations of the LET distribution in tissue for monochromatic neutrons of several energies and for fission spectra have been completed.

Dosimetry research centered on small solid-state dosimeters. The fading studies for metaphosphate glasses were completed for the third consecutive year; they emphasize the feasibility of this system for personnel monitoring.

Intercomparison and standardization measurements in conjunction with representatives from six laboratories were conducted at the HPRR. Further work of this nature is needed urgently due to the divergence of results from various laboratories.

21. Special Projects and HPRR Operations

The high-yield neutron source for the Operation HENRE experiments at the BREN tower in Nevada has been constructed and is being tested preparatory to use in the spring of 1966.

Operation of the HPRR has continued to serve a broad spectrum of dosimetric, radiobiological, and

radiation physics requirements, and studies of the reactor characteristics and performance were continued.

PART V. INTERNAL DOSIMETRY

22. Internal Dose Estimation

The program in internal dosimetry attempts to provide estimates of doses resulting from potential human exposure to radioactive materials that may enter the body. These dose estimates, in turn, constitute a basis for establishing criteria for control of radioactive contamination in air, water, or food. Such control criteria are needed for potential exposure of the entire population, as well as for occupational exposure, and are required for a wide variety of chemical forms of the material and for chronic as well as for acute exposure.

A Dose Estimate Based on Stable-Isotope Data

The metabolism of radioactive material by the body is essentially the same as for the corresponding material involving only stable isotopes. Thus, data on the daily intake of certain elements and on the concentrations of those elements in body tissues provide an estimate of the total dose that would be received from an intake of the radioactive material. Allowance must be made for decay when the radioactive half-life is rather short. This method of dose estimation is formulated more precisely, and its limitations are discussed in this article, and it is applied to several problems of estimation of dose for population exposure.

A Computer Code for Estimation of Body Burden of ^{90}Sr Based on O.R. and Bone Remodeling Which Are Age Dependent

The balance equation for metabolism of Sr has been given by Kulp and Rivera. The use of this method requires data on the observed ratio (O.R.) and on turnover rates of bone for the individual considered. Using preliminary estimates of the age dependence of these parameters, the equation has been used to obtain estimates of doses from ^{90}Sr for individuals of various ages.

Age Dependence of the Biological Half-Life of Iodine and Cesium in Man

The age dependence of the biological half-life of ^{137}Cs in the body and of ^{131}I in the thyroid has been studied by using data on the levels of these isotopes in the diet and in body tissues. In both cases it is found that there is considerable age variation, the infant and child having a shorter biological turnover time for these isotopes.

A Monte-Carlo Code for Estimation of Dose from Gamma-Ray Sources

A Monte-Carlo-type code has been written which enables one to compute the dose to a specified region of the body from a source of photons in another region of the body. The code is sufficiently flexible that body organs may be approximately represented by ellipsoids or by other simple geometrical shapes. Thus the dose from a gamma emitter can now be calculated more accurately since the code takes into account the multiple scattering of the radiation as well as the approximate sizes and shapes of the dose regions of interest.

An Age-Dependent Model for ^{90}Sr Metabolism

It is found that a single exponential which represents only the long-term retention of ^{90}Sr will provide a reasonably accurate model for ^{90}Sr metabolism if the fraction of intake absorbed into blood is considered to be age dependent. Such a simplified model is tested against the human data of Kulp on body burdens of ^{90}Sr from fallout as well as against data on dogs.

Derivation of a Power Function from a Linear Combination of Exponentials

The problem of determining conditions under which a sum of exponentials may be reasonably approximated by a power function is discussed. Several conditions are found to give this type of representation.

Stochastic Models for Representation of the Distribution of Radionuclides in Organs and Tissues

A mammillary compartment system in which the various peripheral compartments are randomly connected or disconnected to the central compartment is considered. The system is used to represent data on retention of ^{85}Sr in dogs.

23. Stable Element Metabolism

Data previously reported on concentrations of stable elements in tissues of grossly normal individuals have been studied to determine possible correlations of one element and/or tissue with another, and also for age dependence. In several cases, an element which shows little evidence of correlation with age in adults nevertheless shows considerable age dependence during preadult years. Improvements in laboratory techniques are also reported.

24. Information Center for Internal Exposure

Data on the absorption of plutonium compounds from gut to blood have been analyzed to determine the variations with the chemical form and with the pH of the material. Extreme variations are found extending over three orders of magnitude, and in some cases the ultimate distribution of the plutonium in body tissues varies as well as the amount reaching the blood.

PART VI. HEALTH PHYSICS TECHNOLOGY

25. Aerosol Physics

Surface contamination resuspension studies, described in the annual report for last year, have been extended to include several types of surface and surface treatment. A tracer dust (CuO) is dispersed and allowed to settle in a small room (8 × 12 × 8 ft high), and contamination samples are collected by a person wearing coveralls and a respirator. The amount of tracer dust collected in the various samples is determined by neutron activation analysis. These tests demonstrate the effectiveness of surface pretreatment in reducing particle resuspension, and show that the "smair" resuspension sampler is better correlated with the inhalation exposure probability per unit occupancy time than is the smear, or wipe, test.

An aerosol composed of electrically conductive particles was produced by exploding silver wires and observed in a grounded metallic chamber under a variety of conditions. The aerosol was treated to produce approximately an equilibrium distribution of electrical charge for some cases, and in other runs the particles were given a net excess of positive charge. Addition of ^{130}I vapor (1 mc/m^3) produced no change in the rate of decrease in particle concentration in the case of equilibrium change. The effect of this level of radioactivity on the positively charged aerosol was to reduce the rate of loss of particles, approximating that of the aerosol having an equilibrium charge distribution.

Adhesion of solid particles to solid surfaces is being studied theoretically and experimentally. Under normal environmental conditions, forces due to capillary phenomena apparently predominate; however, electrostatic and intermolecular forces may become significant depending upon the properties of the particles, of the surface, and of the environment. The most striking feature is the wide range of forces required to remove particles of the same size and composition from a surface in a given environment; for example, the force needed to remove 28.9-μ-diam glass particles from a glass surface in air at 40% relative humidity varied from about 1g (times the force of gravity) to >20,000g.

A practical extension of the adhesion study has provided preliminary information concerning the adhesion of particles to skin. Spherical particles (50 μ to 1 mm in diameter), made of a fluorescent wax, were dropped onto the forearms of six human volunteers, and the retention of the particles was observed by visual counting using an ultraviolet lamp. Retention is observed to vary greatly between persons and also between different skin areas of the same person, apparently depending upon the extent of oily, or otherwise moist, areas of the skin surface. In this study, particle retention as a function of time is described adequately by a linear combination of two exponentials; thus, one can define an average "lifetime" on the skin, which in the cases studied ranged from 5.3 ± 2 hr for 62-μ particles to 2 ± 1.4 hr for 1-mm particles. Such data may be useful in estimating radiation

dose to the skin of persons exposed to small radioactive particles.

In order to provide information for estimating radiation dose delivered by small, insoluble radioactive particles to the wall of the gastrointestinal (GI) tract, a study is being made of their pattern of movement in the alimentary canal. Fluorescent wax particles are fed to experimental animals until the GI tract is essentially in equilibrium with the rate of intake; after necropsy the viscera are frozen and cut into thin transverse sections. Ultraviolet lamp examination of the sections allows identification of the fluorescent particles on photomicrographs of the segments and permits determination of the number of particles in the various portions of the GI tract and their proximity to the wall. A pilot study with one rat showed that 51% of the particles were within 500 μ of the wall and that the highest concentration of particles per unit length of the GI tract was in the cecum.

An anthracene dosimeter has been developed to utilize the principle of extrapolation to zero volume in order to estimate radiation dose as a function of depth in tissue. This device will provide information on the volume energy transfer and, in some cases, linear energy transfer, as well as yielding estimates of radiation dose. Preliminary measurements with a crystal 1 mm in diameter by 20 μ thick indicate an adequate sensitivity to work with small sources containing on the order of 1 μc of ^{32}P.

26. Applied Internal Dosimetry

Scheduling of whole-body counts for the ORNL In Vivo Gamma-Ray Spectrometry (IVGS) Facility is based on a five-part priority system which places major emphasis on counting known, probable, and potential exposure cases. During the past year, 1462 persons were counted for a total of 1623 human counts. Approximately 88% of the counts showed an essentially normal human spectrum. Two employees, estimated to have approximately one maximum permissible lung burden of ^{90}Sr-^{90}Y ($SrTiO_3$), have been recounted at one-month intervals for 541 days after a single inhalation; the lung clearance half-time appears to exceed 500 days. Six unexposed employees were counted in the supine position to determine the relative contribution to the human gamma-ray spectrum of ^{40}K and ^{137}Cs for various positions of the crystal relative to the body; recalibrations using a bottle mannikin filled so as to give the same relative ^{40}K and ^{137}Cs counts for the given crystal positions have shown that old estimates, based on uniform filling, were approximately 4% too high.

Contents

SUMMARY iii

PART I. RADIOACTIVE WASTE DISPOSAL

1. INJECTION INTO PERMEABLE FORMATIONS 3
   Disposal of Gases 3
   Desorption of Iodine 3

2. DISPOSAL BY HYDRAULIC FRACTURING 8
   Plant Modification and Preparation 8
   Slotting and Injection 9
   Cleanup and Modifications 9
   Reslotting and Injection 9
   Hazards Analysis 10

3. DISPOSAL IN NATURAL SALT FORMATIONS 10
   Project Salt Vault 10

4. CLINCH RIVER STUDY 18
   Dispersion Studies 18
   Automatic Water-Sampling Stations 20
   Bottom Sediment Studies 20

5. MOVEMENT OF NUCLIDES IN TERRESTRIAL ENVIRONMENT 23
   Behavior of Radionuclides in Soils 23
   Adsorption of ^{137}Cs by Soils 23
   Desorption of ^{137}Cs by Soils 25
   Soil and Areal Description of Experimental Field Plots 26
   Soil Loss 28
   ^{137}Cs Loss from Soil 28
   ^{137}Cs Loss from the Plant Material 29
   Solid Waste Disposal 30

6. MINERAL EXCHANGE STUDIES 31
Dispersion in Laminar Flow 31
Experimental Studies 32
Effect of Changes in the Chemical Environment on the Dispersion of Strontium 33
7. ENGINEERING, ECONOMICS, AND SAFETY EVALUATIONS 35
Clinch River Safety Analyses 35
8. RELATED COOPERATIVE PROJECTS 41
Geologic and Hydrologic Studies by U.S. Geological Survey 41
Cooperation of Other Agencies in ORNL Studies 41
Visiting Investigators from Abroad 41
Nuclear Safety Review 41
Health Physics Journal 41
Committee Work 42
Participation in Educational Programs 42
Nuclear Safety Information Center 42

PART II. RADIATION ECOLOGY

9. RADIATION EFFECTS AND RADIOACTIVE WASTE AREA STUDIES 45
Vegetation Studies Around the HPRR 45
Radiation Studies on Forest Tree Populations 46
Biochemical Mechanisms Influencing Effects of Ionizing Radiation and Other Environmental Factors 47
Seasonal Changes in Radiosensitivity in Plants 49
Mineral Uptake Mechanisms Affected by Gamma Radiation 51
Transport of Radioactive Materials by Mud-Dauber Wasps 51
Radiocesium Retention by Suctorial Insects 53
Radiation Sensitivity of Insects 53
Radiation Profiles of Insects 55
Radiation Profile of the Evergreen Bagworm 56
Radiation Sensitivity of Immature Stages of the Giant Milkweed Bug 58
Effect of Beta Irradiation on Insects 59
Radiation Sensitivity in Indigenous Small Mammals 60
Incorporation of 5-^{131}Iodo-2′-deoxyuridine into Indigenous Rodents 62
10. PROCESSES AND COMPONENTS OF TERRESTRIAL ECOSYSTEMS 64
Analysis of Isotope Release from Decaying Leaves 64
Losses of ^{137}Cs from the Tagged *Liriodendron* Stand 65
Transfer of ^{137}Cs from Trees to Forest Undercover Vegetation 66
Nuclide Transfer and Microbial Respiration 68
Radiocesium Movement in a Foliage-Feeding Canopy Insect 68

Biological Half-Lives of ^{134}Cs in Forest-Floor Arthropods 70
Cesium Turnover in Forest Cryptozoa 71
Forest-Floor Tagging with ^{137}Cs 72
Pilot Studies of Herbaceous Interception of ^{137}Cs 73
Soil and Forest Site Studies of the Oak Ridge Reservation 74
Forest Management 76
Succession of Oak Ridge Vegetation 76
Succession at Copperhill, Tennessee 77
Prediction of Weight Composition from Point Samples 78
Random Locations for Sample Units in Circular Plots 78

11. CLINCH RIVER AND RELATED AQUATIC STUDIES 79
Deposition of Strontium and Calcium in Snail Shells 79
Microchemical Constituents of Contemporary and Indian Midden Clam Shells 80
Population Genetics and Radiation Effects Studies 84
^{134}Cs Distribution and Transport in the Carp 85
Feeding Rate and Metabolism of Carp in White Oak Lake 86
Radiation Effects on Carp Reproduction 87
^{85}Sr and Primary Productivity 87

12. THEORETICAL AND SYSTEMS ECOLOGY 89
Odd-Even Relationships in Food Webs 89
Equilibrium Specific Activity in Two-Compartment Exchange Systems 89
Stationary Distribution and Turnover of Radioactivity in a Hypothetical Food Chain 90
Digital Computer Program for Compartment Model Simulations of Cycling and Succession 92
First-Summer Redistribution of ^{137}Cs in *Liriodendron* Forest 92
^{134}Cs Leaching from Terrestrial Microcosms 94
Model of ^{134}Cs Distribution in Carp 96
Animal-Climate Interactions 97
Probabilistic Estimates of Forage Intake 98
Application of Some Operations Research Techniques to Ecological Analysis Problems 99
Information and Parameters Required for Modeling Macroecosystems 99
Related Activities 100

PART III. RADIATION PHYSICS

13. GENERAL RADIATION PHYSICS 103
General Concepts in Radiation Dosimetry 103
High-Energy Dosimetry 104
Excitation of Whistler and Hydromagnetic Waves in a Stream of Gyrating Electrons 105
Excitation of Hydromagnetic Waves by a Helical Proton Beam 105
Almost Longitudinal Instabilities in a Plasma-Beam System 105

14. INTERACTION OF RADIATION WITH GASES 106
Alpha-Particle Ionization of Binary Gas Mixtures 106
Interaction of Thermal Electrons with Polar and Polarizable Molecules 107
Electron Time-of-Flight Studies (Geiger-Mueller Detector) 110
Electron Time-of-Flight Studies Using Electron Multiplier Techniques 112
An Apparatus for Measurement of Electron Capture at Various Temperatures 113
An Electron Swarm-Beam Method for Measurement of Capture Cross Sections 114
Electron Capture by Benzene Derivatives 117
Lifetimes of Negative Ions 120
Theory of Electron Capture by Rotational Excitation of Polar Molecules 122
Calculations of One-Dimensional Electron Diffusion Through Gases with Capture and Loss 122
Fourier Transform Methods in the Unfolding of Experimental Data 123
Studies of Electronic Bound States in the Field of an Electric Dipole 124
Potential Energy Curves for Diatomic Molecules 124

15. INTERACTION OF RADIATION WITH SOLIDS 125
Angular Distribution and Thickness Dependence of Transition Radiation from Thin Aluminum Foils 125
Optical Emission Studies of the Characteristic Energy Losses in Cd, In, and Zn 126
Transition Radiation and Bremsstrahlung from Solids Irradiation by Obliquely Incident Electrons 128
Optical Constants and Energy-Loss Functions of Vacuum-Evaporated Films of Cd and Tl in the Vacuum Ultraviolet 129
The Dielectric Constant of an Electron Gas 130
Effect of Photon Refraction on Angular Dependence of Photoelectric Yields in the Wavelength Region 300 to 1200 A 131
Positron Annihilation in Metals 132
Polarization Studies in the Vacuum Ultraviolet 133
Polarization Calculations 135
Absolute Photon Intensity Measurements with Rare-Gas Ion Chambers 135
Electron-Slowing-Down Spectra in Chromium, Yttrium, and Gold 136
Interstitial Diffusion in Elements 139

16. PHYSICS OF TISSUE DAMAGE 140
Low-Energy Electron Transmission in Solids 140
The Penetration of Low-Energy Electrons in Metals 141
Optical Properties of Polystyrene 142
Excimer X-Ray Investigation 143
Time-of-Flight Electron Beam Spectrometer 146
Diffusion Pump Oil Deposition Measurements Utilizing Radioactive Tracers 147

17. PROFESSIONAL HEALTH PHYSICS TRAINING 149

PART IV. RADIATION DOSIMETRY

18. ICHIBAN STUDIES 153
Ichiban Leakage Experiment 153
Weapons Radiation Yield 155
Burst Point 155
Air Dose Curves 155
Ichiban Liaison 158

19. SPECTROMETRY AND DOSIMETRY RESEARCH 159
Radiation Spectrometry 159
Neutron-Dose-Conversion Factors for AmBe and AmB Sources 162
Burro Depth Dose Study 162

20. DOSIMETRY APPLICATIONS 163
Gamma-Albedo Experiment 163
Body Sodium Activation as a Dosimetric Tool in Nuclear Accidents 163
Distribution of Dose and Dose Equivalent in a Cylindrical Tissue Phantom from Fission Sources of Neutrons 166
Glass Dosimetry 171
Standardization of Nuclear Accident Dosimeter Systems for Applied Health Physics and the Puerto Rico Nuclear Center 172
Nuclear Accident Dosimeter Intercomparison Study 172

21. SPECIAL PROJECTS AND HPRR OPERATIONS 176
Operation HENRE 176
Health Physics Research Reactor 180

PART V. INTERNAL DOSIMETRY

22. INTERNAL DOSE ESTIMATION 185
A Dose Estimate Based on Stable-Isotope Data 185
A Computer Code for Estimation of Body Burden of ^{90}Sr Based on Observed Ratio and Bone Remodeling Which Are Age Dependent 188
Age Dependence of the Biological Half-Life of Iodine and Cesium in Man 190
A Monte-Carlo Code for Estimation of Dose from Gamma-Ray Sources 193
An Age-Dependent Model for ^{90}Sr Metabolism 195
Derivation of a Power Function from a Linear Combination of Exponentials 201
Stochastic Models for Representation of the Distribution of Radionuclides in Organs and Tissues 202

23. STABLE ELEMENT METABOLISM 204
Tissue Analysis Laboratory Progress Report 205
Improvements in the Methods for Analysis of Trace Elements in Biological Materials 206
Further Statistical Studies on Trace Elements in Subjects from the United States 207

24. INFORMATION CENTER FOR INTERNAL EXPOSURE 212
Estimates of f_1 for Plutonium Compounds 212

PART VI. HEALTH PHYSICS TECHNOLOGY

25. AEROSOL PHYSICS 217
Studies of Surface Contamination 217
Study of the Effects of Radioactive Iodine on Aerosols 219
Adhesion of Solid Particles to Solid Surfaces 220
Adhesion of Particles to Skin 221
Retention of Small Particles in the Gastrointestinal Tract and Their Proximity to the Wall During Transit 223
An Anthracene Extrapolation Dosimeter 224

26. APPLIED INTERNAL DOSIMETRY 227
ORNL in Vivo Gamma-Ray Spectrometry Facility 227
In Vivo Detection and Measurement of ^{90}Sr-^{90}Y Internal Contamination 227
Distribution of ^{40}K and ^{137}Cs in Calibration Mannikin 227

PAPERS, PUBLICATIONS, AND LECTURES

PAPERS 233
PUBLICATIONS 238
LECTURES 248

Part I. Radioactive Waste Disposal

F. L. Parker

1. Injection into Permeable Formations

D. G. Jacobs O. M. Sealand

DISPOSAL OF GASES

Sorption of Iodine Vapor by Berea Sandstone

Iodine vapor was generated by the oxidation of tagged KI with $FeNH_4(SO_4)_2$, and an attempt was made to pass it through a Berea sandstone core, which was 12 in. long and $1\frac{3}{4}$ by 2 in. Only about 50% of the iodine vapor reached the core (Table 1.1); the remainder plated out on lines leading to the specimen. Of the iodine reaching the core, 50% was removed in the first 0.7 in. of the core, 90% in the first 2.5 in., and 95% in the first 5 in. A small amount of iodine was detected all the way through the core (less than 1% of the concentration of the initial section of the core).

Water leaches indicated that 6% of the activity on the first 82-g section of the core (0.1 μc/g) and 10% of the activity on the second 182-g section of the core (0.05 μc/g) could not be removed by water at room temperature.

In a second series of experiments a solution of methyl iodide was tagged with ^{131}I. Air was passed over the CH_3I at room temperature and into a Berea sandstone core. The graph of the breakthrough of ^{131}I was a normal dispersion curve, with the inflection point corresponding to the pore volume of the core, indicating that the retention capacity of the sandstone for CH_3I is equal only to the available pore volume.

The cores were purged with air, then leached with water. The iodine removed by the water represented approximately 5% of the amount that had been present in the pore space before purging with air. When the cores were not purged with air, the amount of iodine leached by the water was about 17% of the total iodine retained in the pore space.

These preliminary tests are not conclusive, but they indicate that little holdup of CH_3I in the ground can be expected.

DESORPTION OF IODINE

Desorption with Air

Clinch River Floodplain Sediment. — Sediment from the Clinch River floodplain was contaminated with iodine vapor from the oxidation of tagged KI with $FeNH_4(SO_4)_2$ to a level of approximately 0.004 millimole of I_2 per gram of sediment. The surface area of the sediment sample, determined by the Analytical Chemistry Division, was about 4 m^2/g. Thus the original iodine loading of the sediment was about 10^{-7} millimole of I_2 per square centimeter.

One-gram samples of the sediment were weighed into glass sample tubes equipped with ground, tapered joints to accommodate inlet and outlet fittings. The assemblies were placed in small

Table 1.1. Distribution of Iodine in a 12-in. Berea Sandstone Core

Section	Length (in.)	Weight (g)	Loading (μc/g)	Incremental Iodine Adsorbed (μc)	Incremental Iodine Adsorbed (%)	Total Iodine[a] Adsorbed (μc)	Total Iodine Adsorbed (%)
End plate				272	53	272	53
1	0.8	82.1	1.66	137	27	409	80
2	2.7	181.9	0.43	78	15	487	96
3	4.1	137.3	0.045	6.2	1.2	493	97
4	5.5	132.4	0.034	4.5	0.88	498	98
5	7.2	163.7	0.029	4.7	0.92	502	98.5
6	8.5	129.7	0.021	2.7	0.53	505	99.1
7	9.6	103.8	0.014	1.5	0.29	507	99.5
8	11.3	173.4	0.012	2.1	0.41	509	100
9	12.0	63.5	0.011	0.7	0.14	509	100

[a]Five hundred microcuries of ^{131}I was introduced into the system.

ovens for temperature control, and air was passed through the samples at a rate of 120 ml/min. The outlet lines led into scrubbers containing 1 *M* NaOH. At various times the desorption process was halted, and the samples were counted in an NaI(Tl) well-type crystal with a single-channel analyzer.

The results (Fig. 1.1) show that desorption occurs in two phases. The initial desorption is quite rapid, with the rate dependent on temperature, apparently because the iodine is loosely bound. After the mobile iodine has been removed, the "bound" iodine is desorbed very slowly. After 300 hr, more than 30% of the iodine remained on the samples desorbed at room temperature. Experimentally, no relationship was found between temperature and the rate of desorption of the bound iodine.

An attempt was made to determine the activation energy for the desorption process from the desorption velocities at various temperatures.[1] The data were fitted to the equation

$$\ln u = a - E/RT , \qquad (1.1)$$

where

a = a constant,

u = the desorption velocity (moles cm^{-2} sec^{-1}),

E = the activation energy (cal/mole),

R = the gas constant,

T = the absolute temperature.

The values of E and a were obtained from the fit of the data and are shown in Table 1.2. The value of a remains constant with loading, but the activation energy increases with a decrease in loading. This indicates, as mentioned above, that two desorption processes are involved. By extrapolation to zero loading, it was estimated that the maximum activation energy was 16.7 kcal/mole. The apparent activation energy was assumed to be the weighted average of the activation energy of the iodine held with an activation energy of 16.7 kcal/mole and that held with a lesser activation energy. This treatment suggests that about 9.3 $\times 10^{-11}$ mole of I_2 per square centimeter is loosely bound, with an apparent activation energy of 6.5

[1]D. O. Hayward and B. M. W. Trapnell, *Chemisorption*, p. 141, Butterworths, Washington, D.C., 1964.

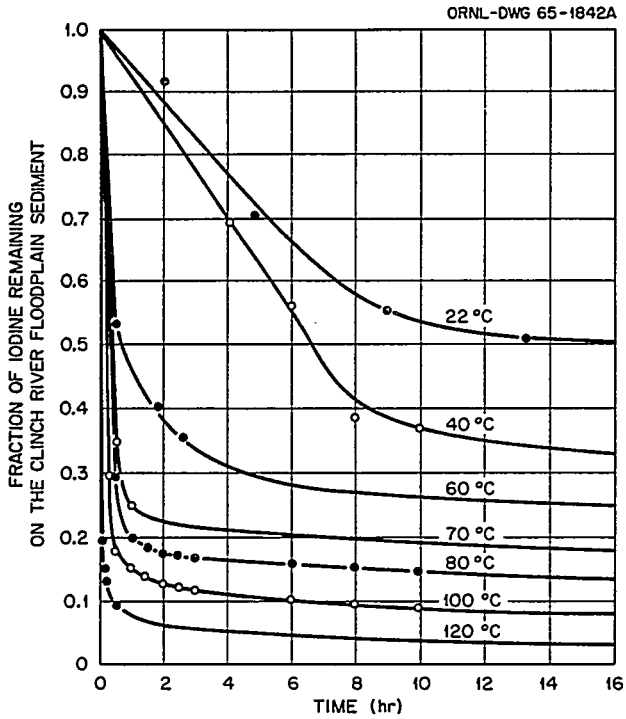

Fig. 1.1. Effect of Temperature on the Desorption of Iodine from Clinch River Floodplain Sediment Using Air.

Table 1.2. Desorption of Iodine from Clinch River Floodplain Sediment

Q^a (moles/cm^2)	a	E (kcal/mole)	β^b (moles/cm^2)
$\times 10^{-11}$			$\times 10^{-12}$
9	−21.0	7.31	6.85
8	−21.0	7.45	7.16
7	−21.1	7.54	6.90
6	−21.1	7.67	6.72
5	−21.9	7.98	7.12
4	−18.7	8.39	7.30
3	−20.1	8.95	7.13
2	−21.4	10.5	7.80
1	−20.8	13.5	6.85
0		(16.7) estd	

[a] Q is the loading of iodine on the sediment.
[b] β is the quantity of bound iodine.

kcal/mole, and that 0.7×10^{-11} mole/cm^2 is more tightly bound, with an apparent activation energy of 16.7 kcal/mole.

Recalculation of the desorption curves, using the extracted activation energies, indicates that the desorption equations used are too simple. The experimental curves have a greater initial desorption velocity and change more abruptly than the recalculated curves. This suggests that the quantity of "bound" iodine, as well as the rate of desorption of iodine, is a function of temperature.

Other Clay Materials

Several other clays were contaminated with iodine vapor from the oxidation of KI with $FeNH_4(SO_4)_2$, and desorption studies were carried out. The following conclusions can be made from the experimental observations:

1. The higher the temperature, the higher the desorption velocity, which qualitatively agrees with Eq. (1.1).
2. The higher the moisture content of the air, the higher the desorption velocity. This may be due to one of two phenomena, or both, that is, adsorption competition between the two polar adsorbates or chemical reaction of the iodine with the passing water vapor.
3. As the surface concentration of iodine is depleted, the remaining iodine becomes more difficult to displace. Finally, the desorption velocity becomes so slow that further changes in ^{131}I are masked by counting errors and the physical decay of the isotope.
4. The energies of desorption of the iodine suggest that three forms of iodine are present: HI, which has an energy of vaporization of 4.9 kcal/mole and which is most easily removed; I_2, which has an energy of sublimation of 14.7 kcal/mole; and actively adsorbed iodine, which is even more strongly retained.

5. The quantity of slowly desorbable iodine is dependent on the temperature and moisture content of the desorbing air (Table 1.3) but does not appear to be related to the nature of the adsorbing mineral.
6. The energy and the rate of desorption are functions of surface concentration but do not appear to be related to the nature of the adsorbing mineral.

Desorption with Water

Two 10-g samples of the contaminated Clinch River floodplain sediment were weighed into centrifuge tubes and leached with 25-ml increments of tap water for time intervals of 30 min. The supematant was decanted, and an aliquot removed for counting.

Most of the iodine was readily removed by the tap water (Fig. 1.2), but it was noted that about 10% of the iodine is removed at a much slower rate than the initial 90%.

In order to determine whether there is a finite retention of iodine against the leaching action of water, montmorillonite was contaminated with iodine (I_2) vapor. Air was passed over the samples at a rate of 120 ml/min at a number of constant temperatures for 16 hr. At the end of this time the samples

Table 1.3. Slowly Desorbable Iodine on Different Clays Under Different Experimental Conditions (millimoles/cm^2)

Conditions	Floodplain Sediment	Vermiculite	Montmorillonite	Kaolinite	Illite
	$\times 10^{-8}$	$\times 10^{-8}$	$\times 10^{-8}$	$\times 10^{-8}$	$\times 10^{-8}$
Original loading	10.0	1.69	1.69	0.906	0.783
Slowly desorbable at:					
25°C	4.67	1.69		0.879	
40°C	2.83				
60°C	2.32	1.32		0.867	0.783
70°C	1.77				
80°C	1.78				
100°C	1.25				
120°C	0.329	0.463		0.797	0.504
160°C		0.393	0.904	0.459	0.154
200°C		0.312	0.288	0.322	0.155
Slowly desorbable at 120°C oven temperature with air saturated at:					
25°C (vapor pressure of H_2O = 24 mm Hg or 1.5% R. H.[a])				0.797	
60°C (vapor pressure of H_2O = 149 mm Hg or 10% R. H.[a])				0.780	
100°C (vapor pressure of H_2O = 760 mm Hg or 50% R. H.[a])				0.336	

[a]R. H. = relative humidity.

were assayed for ^{131}I activity, and it was found, as previously, that the amount of ^{131}I remaining on the clay was a function of temperature (Table 1.4). These samples were then leached with five portions of tap water at room temperature (25°C) as above. After the five water leaches there was no significant difference in the amount of ^{131}I retained.

These results present further evidence that a finite concentration of iodine is actively adsorbed by mineral surface and that this portion of the iodine can be considered immobile.

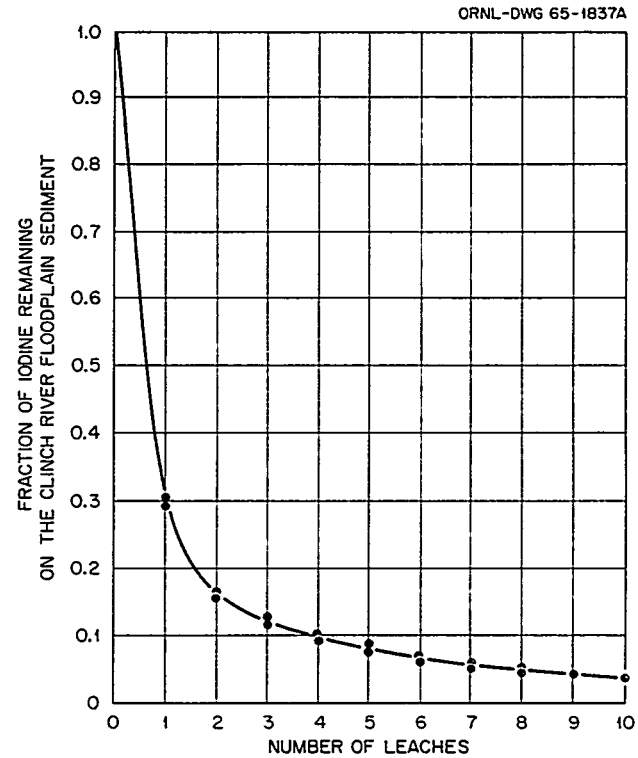

Fig. 1.2. Desorption of Iodine from Clinch River Floodplain Sediment with Tap Water.

Table 1.4. Effect of Loading of Iodine on Montmorillonite on the Amount of Iodine Not Leached by Water

Time of Assay	Temperature of Air Desorption (°C)						
	None[a]	25	60	80	120	160	200
Initial loading, 10^{-8} millimole/cm^2	4.12	4.11	4.11	4.13	4.15	4.12	4.12
After 16-hr air leach, 10^{-8} millimole/cm^2	4.03	3.79	3.64	3.53	1.38	0.798	0.570
After five water leaches, 10^{-8} millimole/cm^2	0.129	0.127	0.120	0.133	0.154	0.141	0.140

[a]This sample was capped for 16 hr with no air passing over it.

2. Disposal by Hydraulic Fracturing

Wallace de Laguna
Tsuneo Tamura
R. C. Sexton[1]
H. O. Weeren[2]
E. G. Struxness
F. S. Brinkley
B. L. Houser

The sixth injection in the series of tests with radioactive waste included the following objectives: (1) to evaluate a mix containing a cheaper substitute for cement, (2) to determine the ability of a mass flowmeter to measure the proportioning of low-solids mixes with more accuracy than was possible with the Densometer, and (3) to evaluate laboratory results of phase separation of the injected grout by measuring bleed-back of water from the grout. The waste solution had approximately three times the concentration of dissolved salts in normal ORNL waste. The activity of the waste solution in the underground tanks averaged 0.1 curie/gal.

PLANT MODIFICATION AND PREPARATION

The solids were mixed, blended over a five-day period, and stored in four bulk storage tanks and two blending tanks. During the loading of the cement into the transporters, an inexperienced operator was confused by the procedure and added too much cement to the trucks. This error was detected only after one of the bins was fully charged and a second bin partially charged. To correct the proportion of cement in the partially filled bin, the remainder of the mix was made with reduced cement content, and the bin was aerated to mix the entire content. The remaining bins were blended according to specifications. The total was 520,600 lb of solids, plus an unknown amount of excess cement in one of the bins.

The major modification to the injection facility consisted of the installation of a Halliburton mass flowmeter and associated equipment. The mass flowmeter is a device that will continuously weigh the solids passing through it, integrate this reading with a liquid flow rate measurement, and give a direct reading of the relative weights of solids and liquid that are being mixed to form the slurry. In preliminary tests this device has proven to give a much more sensitive indication of the solids-to-liquid ratio than the Densometer system previously used. The arrangement of the mass flowmeter in the mixing cell is shown in Fig. 2.1.

Other modifications included the addition of supplemental shielding on the wall of the mixing cell facing the operating platform, a modification in the sampler to reduce the likelihood of plugging, and a minor change in the vent piping. Since constant observation of the hopper was not necessary with the use of the mass flowmeter, and since it was desirable to reduce the radiation exposure of the operators, the window (Fig. 2.1) between the operating platform and the mixing cell was closed with lead bricks. The Plexiglas window in the mix hopper was replaced with the sheet metal.

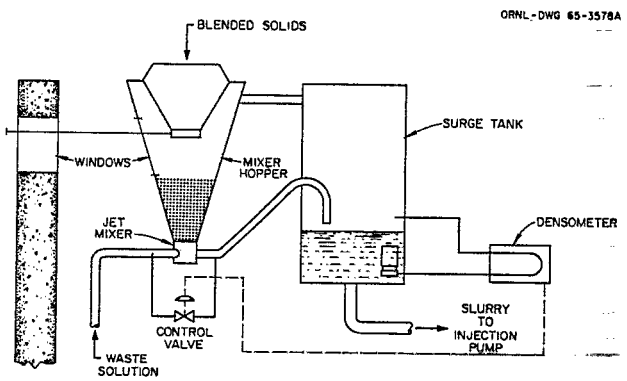

Fig. 2.1. Schematic of Hydrofracture Mixing System.

[1]Plant and Equipment Division.
[2]Chemical Technology Division.

SLOTTING AND INJECTION

The injection well was slotted at a depth of 880 ft on May 18, 1965. Breakdown pressure was approximately 5000 psi (wellhead measurement). A total of 760 gal of water was injected at this time to establish that the formation had fractured sufficiently.

The injection was started at 9:30 AM, May 19. Almost immediately after startup, it became evident that the cement was not flowing as expected – the mass flowmeter indicated a mix ratio of about 5 lb/gal, and the Densometer indicated a maximum slurry density of 10.8 lb/gal. The correct readings should have been 6.0 lb/gal and 11.7 lb/gal respectively. The injection was stopped after 2570 gal of slurry had been pumped to determine the cause of the trouble. The valve beneath bin 1 was found to be clogged with cement scale. The valve was cleared and the injection restarted. Again it became evident that the mixing was not normal; the flowmeter gave erratic readings, and the Densometer indicated a fluctuating density. The injection was stopped after a total of 4420 gal of waste had been pumped. The well pump and tub were washed clear of slurry, and a wiper plug was pumped down the well and overflushed.

Investigation revealed that either the mixer or the hopper had become plugged and that cement had filled the hopper and overflowed through a vent line to the mixer tub and through the valve handle opening into the mixer cell. Investigations also revealed that the cement in the mixer cell was contaminated.

CLEANUP AND MODIFICATIONS

The cement in the mixer cell was washed to the cell drain by water hoses operated from the cell roof. The cement-water slurry was drained to the waste pit, and from there it was pumped to the sump tub and down the injection well for disposal. A total of 18,800 gal of wash water was pumped into the well in this manner.

The mixer bowl was disconnected and found to be clear; the plugging was suspected to be in the hopper. After the packed cement was removed from the hopper, the accumulator tank was disconnected, and the tank and mass flowmeter were lifted out of the hopper. Inspection of the mass flowmeter revealed that a plastic cone about 12 in. in diameter had come loose. The cone had fallen into the hopper and caused the plugging.

Since repairs to the mass flowmeter would require several days, it was decided to continue the injection without repairing the flowmeter; control of the proportioning would be by the Densometer as in previous runs. It was further concluded that the large volume of waste water that had been pumped into the formation would make bleed-back measurements meaningless; hence it was decided to plug the slot and to cut a new fracture.

The accumulator tank was replaced in the mixer hopper. Screens made of $\frac{3}{4}$-in.-mesh woven wire were cut and inserted in the air slides as a precautionary measure to keep clumps from entering the system.

RESLOTTING AND INJECTION

The original slot at 880 ft was plugged, and a new slot was made at 872 ft. The well was pressurized, and breakdown occurred at approximately 3500 psi. A total of 820 gal of water was pumped to develop the fracture.

The injection was resumed on May 22. Within 10 min after startup, flow of solids had stopped. Switching to a second and third bin did not eliminate the problem; hence the injection was stopped and the screens that had been placed in the air slides were removed. The screens were found to be plugged with agglomerated solid particles. The injection was resumed without the screens.

For approximately an hour, the operation was smooth; then the pressure indicator on the injection pump showed that a pressure fluctuation was occurring in the high-pressure system. This fluctuation increased progressively, and it was decided to halt the injection after $3\frac{1}{2}$ hr operation to check the pump suction and valves, as well as to clear the air slide to bin 4, which had been found to be plugged.

The air slide to bin 4 was cleared of agglomerated solids. The pump was found to have a badly eroded valve. Evidently the valve had not been seating properly and the flow of slurry at high pressure past the valve seat had caused the erosion. The valves were replaced and the injection resumed.

The injection was continued for 45 min, when a leak was observed in the wellhead cell. The

injection was halted, and the standby unit was connected to the high-pressure piping manifold and used to pump water down the annulus and out the slot. Having located the leak at the connection between the plug container and the connecting piping, the master valve was then opened and the grout remaining in the central tubing was cleared. Having cleared the well, the pump surge tank and the piping manifold were washed. The wellhead cell was cleared first with hoses from the roof hatch and then by hosing from the inside by a man in an air suit. In this manner the contamination was reduced sufficiently so that the plug container could be removed from the wellhead and a direct connection made between the wellhead and the high-pressure manifold. About 2000 gal of water was then pumped down to clear the tubing and terminate the injection. The total waste volume pumped during the injection was 64,000 gal. The slot was kept open in order to make bleed-back tests. The grout was allowed to set for one week, after which the valve was opened and the liquid allowed to drain into a calibrated tank. The studies of the volume and nature of the bleed-back solutions are now in progress.

HAZARDS ANALYSIS

During the injection, two separate incidents caused contamination of the cells. Both in the mixer cell and the wellhead cell, decontamination was accomplished and repairs were made without exceeding the weekly permissible radiation dose to personnel. The highest radiation exposure to cleanup personnel involved in cell decontamination was 30 mr.

It was also necessary to make repairs to the pump in this injection. The general background with the heads off the pump was 20 mr/hr; the radiation inside the pump was 1 r/hr. One mechanic received an exposure of 20 mr; the other mechanic got 10 mr. These levels show that direct maintenance on the injection pump is feasible with wastes whose activity level is 0.1 curie/gal.

During injection the plant ran extremely smoothly; the Densometer, for example, operated smoother than had been the case previously. This injection demonstrated the ease with which an injection can be halted, repairs can be made, and the injection resumed. This was done twice during this injection; in both instances the injection was resumed without difficulty.

---

3. Disposal in Natural Salt Formations

PROJECT SALT VAULT[1]

W. J. Boegly, Jr.
R. L. Bradshaw
F. M. Empson
Hisashi Kubota[2]
T. F. Lomenick
W. C. McClain
F. L. Parker
W. F. Schaffer, Jr.[3]

Mine Preparations

W. J. Boegly, Jr.
F. M. Empson
W. C. McClain

Excavation and Mine Cleanup. — A ramp rising approximately 14 ft in 140 ft and having a level area at the top about 60 ft long was constructed by mining up from the floor in Entry 5. From this level space the experimental area has been mined. The main experimental entry is 310 ft long by 30 ft wide. From the entry, two rooms 32 ft wide by 60 ft long and two rooms 44 ft wide by 60 ft long were mined from the west rib. A room 30 ft wide by 50 ft long was mined from the east rib of the experimental area to the bottom of the waste shaft. Ceiling height in the entire area is 14 ft. Mining of the experimental area was completed at the end of March 1965.

---

[1]Demonstration of high-level waste solids disposal.
[2]Analytical Chemical Division.
[3]Chemical Technology Division.

Approximately 1840 linear feet of old tunnels in the Lyons Mine have been rehabilitated for access to the experimental area. This has consisted of taking down unsafe portions of the roof, cleaning up accumulations of trash, and taking up heaved and broken floor. In addition, a large amount of "spot" cleanup has been done in the old workings to provide safe access to plastic-flow gage locations.

Approximately 16,000 sq ft of floor space in Entry 5, rooms 7, 8, and 9, was prepared for use as work areas by removing 2 to 4 ft of roof and 1 ft of floor to give 17 ft of head room. This space is currently being used as storage space for experimental equipment, as a parking area for the waste transporter, and as the site for the Hole Liner Prototype Experiment. The radioactive array to be operated in the original mine floor will also be located in this area.

Drilling. – All instrumentation for the measurement of salt movement (plastic flow) in the experimental area was installed. This involved the drilling of 2631 linear feet of holes of various diameters and the installation of 359 different flow measurement gages. With the similar instrumentation installed last year, all salt-flow instrumentation is complete except for a minor amount to be installed around the floor array.

Drilling of holes for both the radioactive array and the electrical array is complete. Fourteen holes, 7 in each array, are approximately 12½ ft deep. The upper 5 ft is 16 in. in diameter, and the lower 7½ ft is 12 in. in diameter. The 22 pillar heater holes, each 12 ft deep, have also been completed. A total of approximately 110 thermocouple holes have been drilled in the four experimental rooms. All drilling is complete except for that associated with the array in the original mine floor.

Mine Ventilation. – A squirrel-cage-type fan, rated at 30,000 cfm, has been installed in the headframe to deliver ventilation air to the mine level. The air is delivered from the fan through two ducts, each 20 in. in diameter, to a point below the water collection rings, approximately 300 ft below the surface. Below that point the air moves through the timber-lined ventilation compartment in the shaft. At the mine level, it is channeled through airways controlled by recently constructed curtains to the demonstration site, and then back through the old workings to the shaft for exhausting it to the atmosphere.

Surface Charging Pad and Waste Shaft. – Drilling of the waste-charging shaft and casing with 20-in.-OD pipe was completed at the beginning of the year. A 26-in. casing is cemented around the top 300 ft of the 20-in. shaft for added protection against entry of water into the mine. A concrete pad with shield walls (2 ft to 3 ft 4 in. thick) and a headframe for use in lowering the demonstration canisters into the mine have been constructed at the top of the waste shaft (Fig. 3.1). A small building protects the working area of the pad over the waste shaft. The area around the waste shaft is paved and enclosed with a chain-link fence.

PHOTO 80192

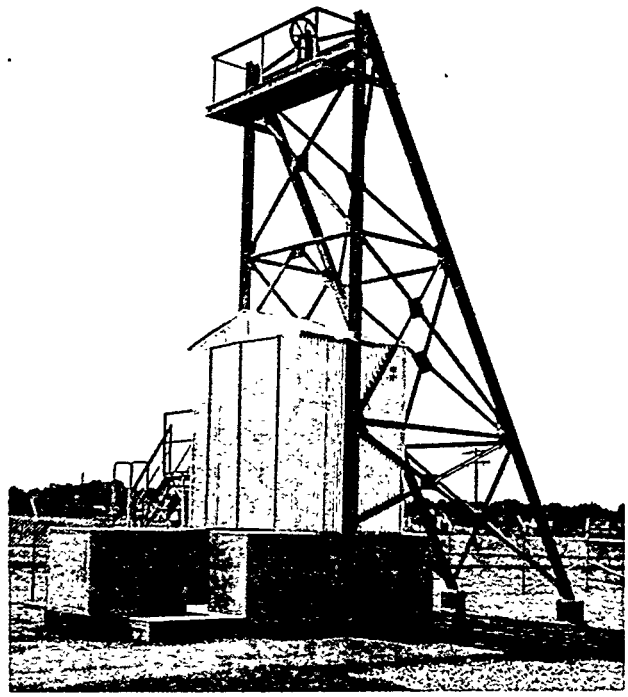

Fig. 3.1. Concrete Pad with Shield Walls and a Headframe for Use in Lowering the Demonstration Canisters into the Mine.

Installation of Experimental Equipment. – A major portion of the experimental equipment has been received at the mine, transferred underground, and installed. A 12- by 20-ft control room has been constructed at the top of the ramp, and the

temperature loggers and other instrumentation have been installed. The power-control panels and recorders have been installed at the end of pillar between rooms 1 and 2. The hole liners have been installed in both the main radioactive array and the electrical array, trenches have been cut, and the installation of off-gas and purge systems is under way.

Equipment Design and Fabrication

W. F. Schaffer, Jr. W. J. Boegly, Jr.

Underground Transporter. – The underground waste transporter was delivered to the site by Stowers Machinery Corporation, disassembled by Stowers personnel, transferred underground by mine personnel, and reassembled by Stowers personnel. No difficulties have been encountered in maneuvering and operating the machine on the ramp, in the waste shaft room, or in experimental room No. 1, where the radioactive array is located.

Surface Shipping Carrier. – Renovation of an existing fuel-element carrier for transporting the seven canisters from Idaho to Lyons was completed. The carrier and associated cooling equipment was heat tested with simulated fuel assemblies. In general, the fuel-element temperatures ran below those calculated theoretically. With coolant circulating, the carrier safely dissipated 14 kw, twice the power anticipated from the ETR assemblies. A test with 7 kw and no coolant flow was operated for about 16 hr, and indications were that it could have been extended for several hours more without approaching the melting point of either the fuel assemblies or the lead shielding.

Fuel Assembly Canisters. – Fabrication of the fuel canisters is in progress at ORNL. All the uranium shield plugs have been canned and heat tested. Eight canisters have been assembled and tested.

Dosimeter Development

R. L. Bradshaw Hisashi Kubota
T. W. Hodge, Jr.

Project Salt Vault presents a unique problem in dosimetry. The dosimeter will be placed in the center plane of the canisters in order to study both the shielding properties of the salt and the radiation damage incurred by the salt. The requirements that must be met by the dosimeter are:

1. it must react accurately to dose rates as high as 10^5 rads/hr and integrated doses as high as 10^5 rads,
2. its temperature dependence must be known from ambient to 250°C,
3. it must be able to withstand a saturated salt atmosphere during the period of irradiation,
4. the dosimeter must be essentially energy independent over a wide spectrum of energies,
5. the package, probe, or dosimeter must be limited in size to about 2 cm in diameter, and 6 cm in length.

The limiting requirement seems to be that of the elevated temperature, since most dosimeters are not stable at such temperatures. Most dosimetry is carried out at room temperature. In the past, dosimetry at high-temperature sites has frequently been achieved by cooling the dosimeter as it was being irradiated. Artificial cooling for exposure times up to several hours appeared to be an undesirable complexity for the demonstration, so it was decided to investigate the high-temperature response of the two most promising types of dosimeters, the phosphate glass rod and the chemical dosimeter.

The Toshiba II glass rods were found not to be usable, since the radiation-induced photoluminescence anneals rapidly at 250°C. Both the high-Z and the low-Z rods, manufactured by the Bausch and Lomb Company, have been found to give an excellent response when irradiated to doses of more than 10^5 rads at temperatures to 250°C for times up to 1 hr. It is thus only necessary to select the appropriate shield to flatten the low-energy response and to determine the calibration curve as a function of temperature.

Both the Fricke (ferrous sulfate) and the ceric sulfate dosimeter have very flat response to radiation in the energy range of 0.1 Mev to over 2 Mev.[4] There are reports on the use of the Fricke dosimeter up to 65°C (ref. 5) and the ceric sulfate up to 90°C (ref. 6).

---

[4]T. F. Kircher and R. G. Bowman, *Effects of Radiation in Materials and Component*, p. 57, Reinhold, New York, 1964.

[5]C. J. Hochanadel and J. A. Ghormley, *Radiation Res.* 16, 653 (1962).

[6]H. Hotta and K. Shimada, *Bull. Chem. Soc. Japan* 33, 114 (1960).

Sealed tubes of Fricke, ceric sulfate, and oxalic acid dosimetric solutions have been heated to temperatures as high as 250°C to study thermal stabilities. It was found that oxalic acid readily decomposes above 100°C and is not usable, while ceric sulfate hydrolyzes, forming a white insoluble precipitate, when heated above 150°C. This hydrolysis can be repressed by increasing acidity; however, there is reduction of ceric to cerous. The Fricke ferrous sulfate solution has shown the greatest thermal stability and has been chosen for use to complement the glass rods.

Studies thus far show that the deaerated Fricke dosimeter contained in a sealed glass tube can be used to make gamma dose rate measurements at temperatures up to 250°C with a precision of 10% or better. The *G* value remains nearly constant at 7.6 ± 0.2 at 25°C to 7.6 ± 0.4 at 200°C and drops to 7.3 ± 0.4 at 250°C. A slight decrease in *G* sets in after the exposure dose exceeds 10^5 rads. The lower limit for reliable dose rate measurements is about 10^3 rads.

Prototype Test

W. C. McClain R. L. Bradshaw
F. M. Empson

Startup of phase I of the prototype test was previously reported.[7] Operation throughout the duration of phase I of the test proceeded without significant incident. The test was terminated on July 20, 1964, after running 48 days.

When the liner was opened, the prototype canister was placed in the liner; it went in with no difficulty. From this test and other observations, it was concluded that there had been essentially no temperature distortion of the lower part of the liner.

When the lower part of the liner was removed, it was found to have a bright red oxide film on all welds, and a little corrosion at those places where water had dripped back from the off-gas and caliper ports. The main body of the lower liner, however, was completely unaffected and practically indistinguishable from its original state.

A total of 30 pins were shot into the floor around the prototype hole liner for periodic measurement of floor uplift. Figure 3.2 illustrates the areal extent and shape of the maximum measured uplift by contours (on July 20, 1964, just before turning off the heat).

The conclusions which can be drawn from the floor-leveling part of the prototype test are:

1. that standard leveling techniques will provide a sufficient accuracy (about 0.002 ft) and a satisfactory method of measurement in the demonstration;
2. that the magnitude of total uplift is of the order which was anticipated (about ½ in.);
3. that the floor leveling results, in conjunction with the temperature measurements, will provide a valuable adjunct to the investigation of the thermal-plastic properties of salt.

[7] F. L. Parker *et al.*, *Health Phys. Div. Ann. Progr. Rept. July 31, 1964*, ORNL-3697, p. 26.

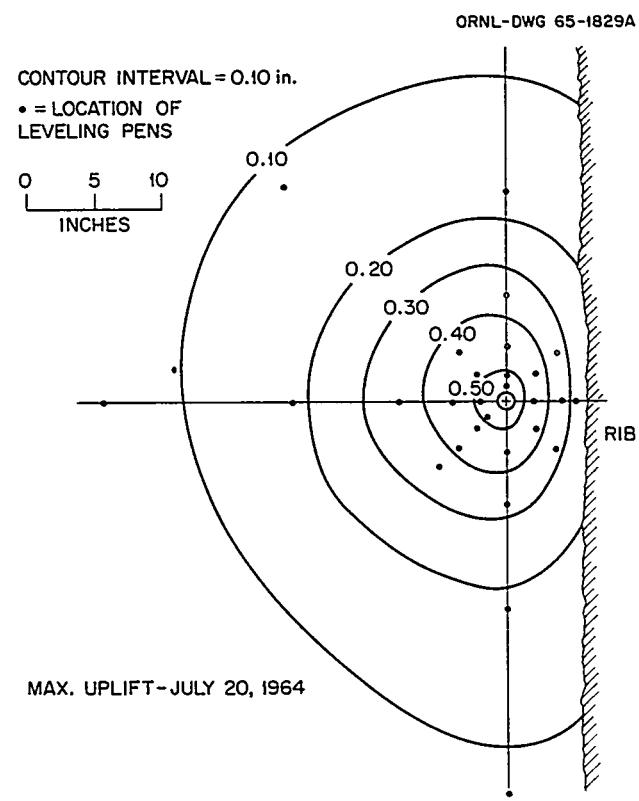

Fig. 3.2. Prototype Test Phase I – Floor Uplift Contours.

The room containing the prototype hole liner was instrumented with rock mechanics gages in order to gain some insight into the type of behavior to be expected from the experimental arrays. This instrumentation consisted of borehole extensometer stations (Potts' internal strain gages) in the roof, floor, and both pillars.

The results, on a time-deformation plot, of the two horizontal stations are shown in Fig. 3.3. A comparison of the two stations, P-2-W and P-5-E, indicates that the extensometer stations will be very sensitive to changes induced by heating. The strain rate at P-2-W was approximately twice that at P-5-E, and there was a significant decrease in strain rate when the heaters were turned off.

Most of the movement taking place at the floor station was probably induced by heat, and a sizable portion of it was recovered when the heaters were turned off. By contrast, very little movement took place at the roof station, indicating that the roof was not sagging appreciably. Figure 3.4 illustrates the movements of the floor and roof anchors relative to each other. This was constructed by assuming that the anchor 22 ft above the roof (U-1) did not move, and comparing the movements of all other anchors with it (by using convergence results). It is interesting to note that the anchor located 20 ft below the floor (D-1) shows essentially no movement.

The annulus between the 12-in.-diam hole and the outside of the lower liner was measured during the test by using a specially designed tube caliper. This instrument reads to $\frac{1}{16}$ in. and has an estimated accuracy of about $\frac{1}{16}$ in. Its primary purpose is to monitor the closure of the salt hole in order to avoid damage to the liner. The radial hole closure measured with the caliper during phase I was between $\frac{1}{4}$ in. and $\frac{1}{2}$ in., which agrees with a measured diameter of 11.5 in. after the liner was removed (approximately $\frac{3}{4}$-in. decrease in diameter).

The temperature at the periphery of the 12-in.-diam hole was about 200°C, and temperatures in excess of 100°C extended out to about 2 ft from the center of the hole. As in previous tests, the floor uplift does *not* appear to be linearly related to the depth-integrated temperature rise.

ORNL-DWG 65-8317

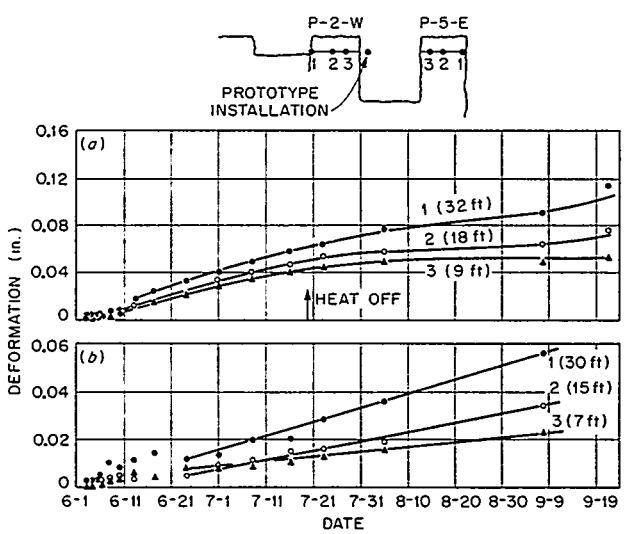

Fig. 3.3. Prototype Test Phase I – Rock Mechanics Gage Results, Stations P-2-W and P-5-E.

ORNL-DWG 65-1832A

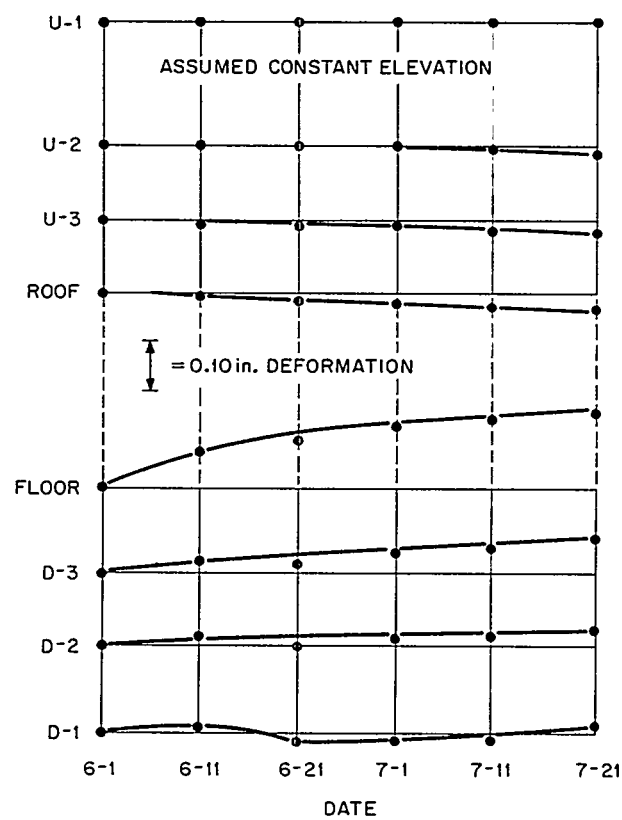

Fig. 3.4. Prototype Test Phase I – Relative Vertical Movements at Center of Room.

During the operation of phase I, about $2\frac{1}{2}$ liters of condensate was collected. Most of this condensate was heavily laden with stainless steel corrosion products, which came primarily from the condenser tube. For phase II a nickel condenser was installed, and the remainder of the equipment was put back together as before.

Phase II operation began on November 9, 1964, and lasted for about 100 days, during which time about two-thirds of a liter of condensate was collected. Examination of the hole liner indicated little change from the conditions at the end of phase I.

Phase III operation began on January 26, 1965, and lasted for about 50 days. The off-gas system was not operated during this phase, except for about 1 hr near the middle of the test, during which time about 40 ml of condensate was collected. The purpose of this test was to simulate an actual disposal in the floor of an existing mine in a bedded deposit. During the operation there were indications of some refluxing of water in the caliper guide tube, off-gas line, dosimeter hole, etc., as had been anticipated. When the lower liner was pulled for inspection at the end of phase III, the bottom 1 to 2 in. of the liner remained frozen in the bottom of the hole. The break was sharp and appeared to have taken place before the end of the test, since almost the entire area of the break had an oxide coating. There was salt on the liner and other evidence of splashing up to a distance of about 4 to 6 in. from the bottom.

Such an occurrence would not be anticipated in the demonstration itself due to several reasons: (1) no water should be present in the main radioactive array; (2) the off-gas system will be operated continuously on both the arrays; (3) the end of the liner will not be in contact with the salt and, thus, there should be no axial stress on the liner, such as was produced in the prototype due to the flow of salt into the bottom of the hole; and (4) the liners will be made of 304L steel instead of 304 as was the case with the prototype.

The bottom foot of the lower liner has been cut off, and a new section made of 304L steel has been welded on. The bottom of the hole has been deepened to avoid contact with the liner, and phase IV was started on June 2, 1965. During phase IV there will be no air flushing of the hole.

Lithology of Ceiling in Experimental Area

T. F. Lomenick

A series of ten representative cores, ranging from 3.5 to 11 ft in length, has been taken in the roof of the experimental area of the Lyons Mine to define more specifically the lithology of the salt section. From the cores, a generalized cross section of the first 11 ft of roof in the experimental area has been prepared (Fig. 3.5). In general, the salt is medium to coarsely crystalline and contains inclusions of shale, clay, polyhalite, and, occasionally, anhydrite. The shale, clay, and polyhalite inclusions tend to be concentrated along lines or zones that are parallel to bedding, thus giving the salt a characteristic banded appearance. With an increase in the amounts of shale or clay inclusions, banded salt grades into salt with thin shale partings. Shale or clay partings that are intermediate between banded salt and distinct shale beds may be referred to as "marginal" shale partings. Distinct shale beds, varying from $\frac{1}{16}$ in. to 6 in. in thickness, occur at distances of about 2, 5, $8\frac{1}{2}$, and 9 ft above the present ceiling, while several marginal shale partings occur principally within the 2- to 5-ft section of salt above the ceiling.

From the ceiling to the first shale bed at about 2 ft the salt grades from almost clear halite, which is in a few places somewhat friable and also contains a few blebs of polyhalite, to smoky or banded salt that contains numerous clay blebs. The first shale bed, which begins a little less than 2 ft above the ceiling, varies from 2 to 5 in. in thickness over the experimental area and contains interbedded anhydrite stringers and lenses, as well as some halite crystals. Generally the shale makes a sharp, straight-line contact with the overlying salt, but the contact with the underlying salt is more irregular and undulating. Above this shale bed and up to about 5 ft the salt contains varying amounts of polyhalite, which gives the salt a characteristic orange-to-reddish color. In several places the concentration of clay or shale along bedding is great enough so that banded salt grades into salt having marginal shale partings. The shale parting at 5 ft is generally $\frac{1}{16}$ in. or less in thickness. From 5 to 11 ft the salt column, which contains some shale, polyhalite, and anhydrite impurities, is interrupted by shale beds at about $8\frac{1}{2}$ and 9 ft. The shale bed at $8\frac{1}{2}$ ft is as

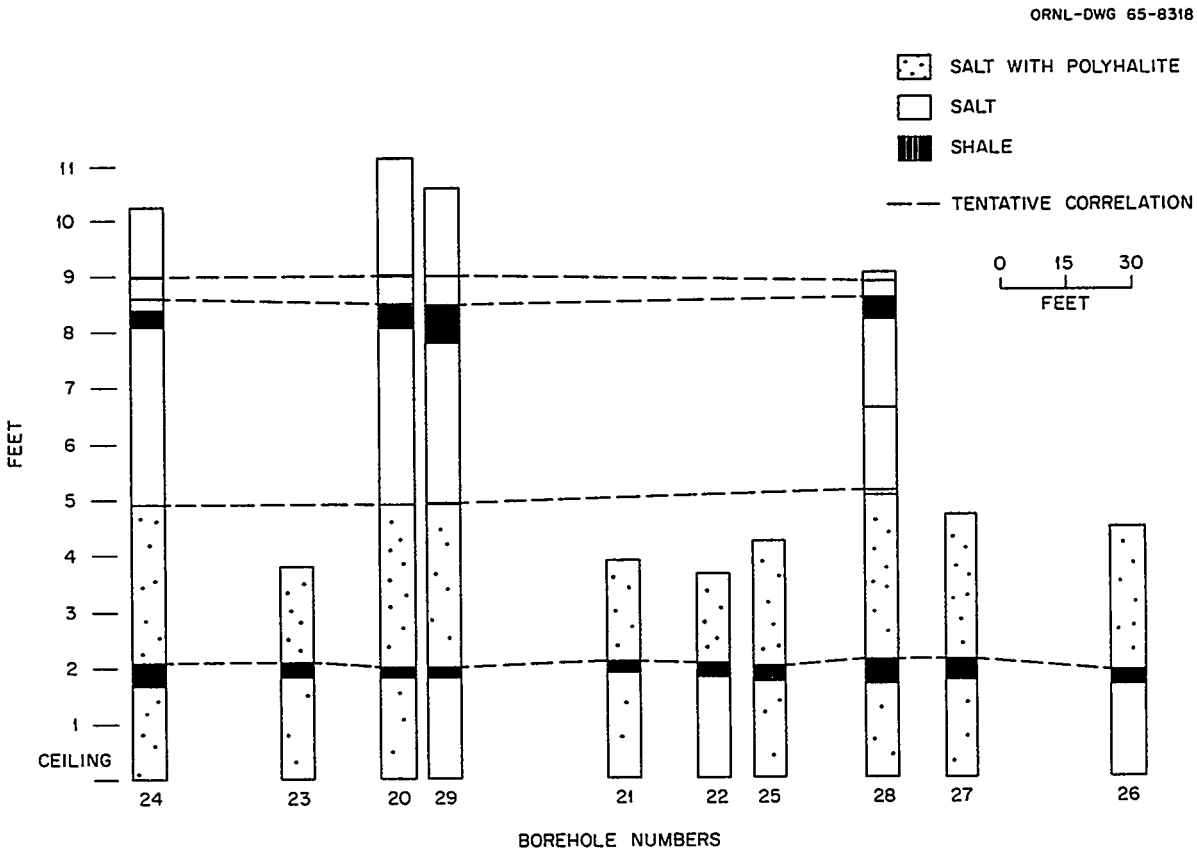

Fig. 3.5. Generalized Cross Section Through a Portion of the Roof in the Experimental Area of the Lyons Mine.

much as 6 in. thick and contains anhydrite stringers, as well as a few large halite crystals, while the shale at 9 ft is only about ½ in. thick and is essentially all shale.

Pillar Model Tests

T. F. Lomenick R. L. Bradshaw
H. J. Wyrick

Recent work has shown that flow in salt pillars may be approximated by uniaxially testing scale models.[8] To simulate pillar, roof, and floor conditions, samples of salt are used as models of salt pillars and their surrounding rooms. The test specimens are cylindrical, with a portion of the center section ground out to form the pillar, surrounding rooms, roof, and floor. Steel rings are epoxied around the ends of the samples to simulate the confining pressure that exists in the roof and floor of the mine. (See Fig. 3.6.) Cavity closure (floor to ceiling) is measured by two dial gages, mounted 180° apart on the rings. Constant uniaxial loads are applied to the models by hydraulic compression testers. All model tests are conducted in a controlled-temperature room that is equipped with automatic dehumidifiers to prevent moisture condensation on the samples during extremely damp periods. The elevated-temperature tests are performed with the specimens inside a cylindrical heating jacket and with barrier heaters on top and bottom between the specimen and the platens.

Tests are being conducted on samples of the type of salt that will comprise the pillars for Project Salt Vault. Axial loads from 1000 to 10,000 psi are being applied at temperatures of

[8]F. L. Parker *et al.*, *Health Phys. Div. Ann. Progr. Rept. July 31, 1964*, ORNL-3697, pp. 28–31.

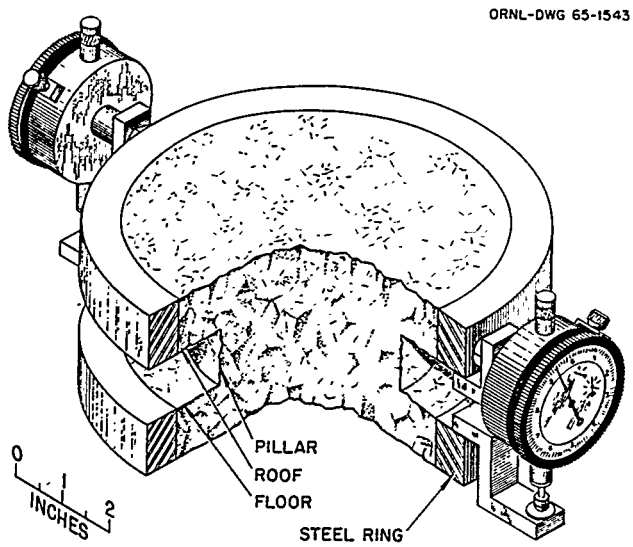

Fig. 3.6. Model of Salt Pillar.

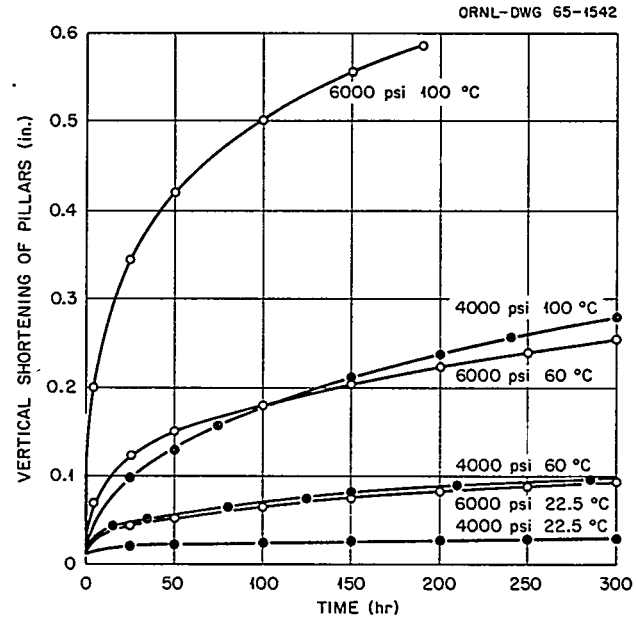

Fig. 3.7. Deformation of Model Rock-Salt Pillars.

ambient, 60, 100, and 200°C to models with a pillar width-to-height ratio of 4. More than 40 samples have now been tested, but the data have not yet been completely analyzed. Duration of the tests varies from a few hours to several thousand hours. For certain temperature and load combinations, duplicate or triplicate tests were run in order to obtain an approximate measure of variation from sample to sample.

From these tests it was observed that the deformation of the pillars increased markedly with increasing loads. However, even more significant was the greatly accelerated creep rates of the salt at elevated temperatures. The cavity closure with time for models axially loaded to 4000 and 6000 psi at temperatures of 22.5, 60, and 100°C are shown in Fig. 3.7. These curves, along with those at higher and lower stresses and at 200°C, all show general similarities. For each curve, there is initially a high creep rate that decreases with time. Tests of longer duration show that creep rates continue to decline even after 5000 hr. This is in agreement with measurements made in the Kansas salt mines, which show that closure rates are still decreasing with time in openings several years old.[9] At room temperature (22.5°C) the percentage cavity closure (inches shortening of the pillar) for the 4000-psi sample was about 3% after 300 hr and that for the 6000-psi model was approximately 10%, while for the 4000- and 6000-psi samples heated to 60°C, the closure for the same period of time was about 10 and 25% respectively. When the temperature is increased to 100°C, the increase in the rates of cavity closure is even more pronounced. The deformational behavior of the salt pillar loaded to 4000 psi at a temperature of 60°C is approximately the same as the behavior of the sample loaded to 6000 psi at room temperature. Too, the creep curve for the 4000-psi model at 100°C shows a close correlation with the behavior of the 6000-psi sample at 60°C. This strongly suggests that salt pillars subjected to elevated temperatures will behave like salt pillars under higher stresses.

The following empirical equations have been fitted to the results of the first 13 ORNL pillar-model tests for times greater than 10 hr. The equations require modification to fit the data from zero time.

$$\dot{\epsilon} = 3.2 \times 10^{-36}\, T^{10.9}\, \sigma^{3.2}\, t^{-0.65} ,$$

$$\epsilon = 9.2 \times 10^{-36}\, T^{10.9}\, \sigma^{3.2}\, t^{0.35} + A ,$$

[9] R. L. Bradshaw, *Waste Treatment and Disposal Progr. Rept. May–October 1963*, ORNL-TM-757 (R. E. Blanco and F. L. Parker, eds.), p. 132 (1964).

where

$\dot{\epsilon}$ = strain rate (vertical convergence, μin. in.$^{-1}$ hr^{-1}),

ϵ = cumulative deformation (μin./in.),

T = absolute temperature (°K),

σ = average pillar stress (psi),

t = time (hr),

A = constant adjusted to fit the experimental curve at 10 hr.

At ambient temperature these equations give approximately the same results as the ones derived from the tests at the Applied Physics Laboratory, U.S. Bureau of Mines. Although the data are still too sparse to attempt a statistical analysis, the results appear to corroborate a previously developed hypothesis[7] that the effect of elevating the temperature is essentially the same as that of increasing the average pillar stress, and that the relationship between creep rate and axial stress follows the same power law regardless of the temperature.

---

4. Clinch River Study

P. H. Carrigan, Jr.[1] F. L. Parker
K. E. Cowser B. J. Frederick[1]
R. J. Pickering[1]

The Clinch River Study has been continued in cooperation with the U.S. Atomic Energy Commission, U.S. Geological Survey, U.S. Public Health Service, Tennessee Valley Authority, Tennessee Game and Fish Commission, Tennessee State Department of Public Health, and the Tennessee Stream Pollution Control Board.

DISPERSION STUDIES

P. H. Carrigan, Jr.[1] F. L. Parker
B. J. Frederick[1] E. R. Eastwood
J. E. Jackson

Intermittent water releases (Fig. 4.1) from Melton Hill Lake, due to its function as a peaking hydroelectric plant, cause intermittent releases of radioactive waters from White Oak Creek into the Clinch River. An increase in water releases from no flow or from some intermediate flow rate causes a very rapid rise in the water level of the Clinch River in the vicinity of the mouth of White Oak Creek. This rise in water level acts as a control at the mouth of White Oak Creek, stopping the creek flow into the river and resulting in upstream flow in the creek to White Oak Dam. A decrease in water releases rapidly lowers the river level, resulting in immediate and large releases of radioactive waters from the creek into the river. If the release is completely terminated (no flow), waters released from White Oak Creek stagnate in the vicinity of the creek mouth.

Effects of typical summer patterns of water releases on diffusion of radioactive solutes released into the river were investigated during the summer of 1963.[2] Results of this study clearly indicated that the most critical concentration of radioactivity throughout the lower Clinch River resulted from the prolonged shutdown of power during the weekend. From consideration of this and earlier work concerned with diffusion of solutes, it was expected that dilution of the large mass of tracer released during a winter weekend would be less than the dilution observed during summer flow conditions.

[1]On loan from Water Resources Division, U.S. Geological Survey.

[2]F. L. Parker *et al.*, *Health Phys. Div. Ann. Progr. Rept. July 31, 1964*, ORNL-3697, pp. 35–37.

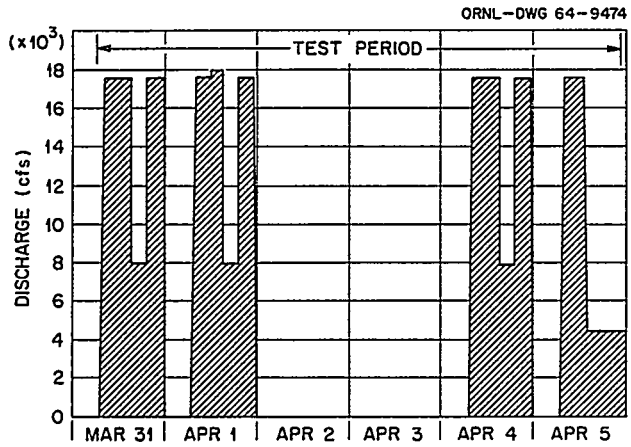

Fig. 4.1. Estimated Winter Discharge Pattern from Melton Hill Reservoir.

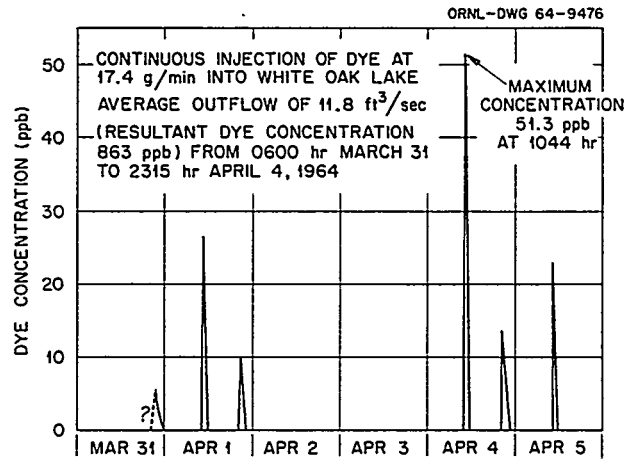

Fig. 4.2. Variation in Rhodamine B Concentration with Time During Period March 31 to April 5, 1964, at Clinch River Mile 14.4.

A tracer test was conducted in the Clinch River from March 31 to April 4, 1964, with injection of fluorescent dye at White Oak Dam. Rhodamine B was continuously released into the overflow at White Oak Dam for 113 hr. Variations in dye concentrations with time were continuously monitored at two sections, 6.4 and 15.3 miles downstream from the creek mouth, at the ORGDP water intake (CRM 14.4) and above the Emory River (CRM 5.5). Generating equipment was not fully installed at Melton Hill Dam; variations in flow for tests were simulated by TVA through controlled releases under the spillway gates.

Variations in dye concentration with time, observed at CRM 14.4 (ORGDP water intake), are shown in Fig. 4.2.

The minimum dilution factor at CRM 14.4 is much less for winter power patterns than is the minimum dilution factor for summer patterns (Table 4.1).

The threefold reduction in minimum dilution from summer to winter conditions is due to the combined influence of greater velocities in the Clinch River, slightly increased water releases, greater changes in storage in White Oak Creek embayment, substantially faster velocities in the embayment at times of decreased water releases, and less diffusion of the moving mass of dye.

Table 4.1. Seasonal Minimum Dilution Factors at CRM 14.4 and CRM 5.5

Flow Condition	CRM 14.4		CRM 5.5	
	Factor	Ratio	Factor	Ratio
Summer	54.1	3.3	122	3.3
Winter	16.8		36.9	

An extremely reliable method of predicting peak concentrations has been developed. This method requires information on channel geometry of White Oak Creek embayment, on rate of release of solutes and of flow through White Oak Dam, on the relationship between flow and water level at the creek mouth for various elevations of water surface at Watts Bar Dam, and on the empirically defined diffusion characteristics of a solute mass transported downstream in the study reach.

Results of the winter test again confirmed that time of arrival of peak concentration may be reasonably predicted as shown in Table 4.2.

Table 4.2. Comparison of Predicted and Observed Peak Concentrations at CRM 14.4 (ppm)

Peak Number[a]	Concentration	
	Predicted	Observed
1		
2	26.9	25.9
3	8.5	9.8
4	53.0	51.3
5	11.4	13.8
6	15.9	22.9

[a]See Fig. 4.1.

AUTOMATIC WATER-SAMPLING STATIONS

P. H. Carrigan, Jr.[1] W. F. Johnson[3]

Results of the dye tracer tests conducted in 1963 and in 1964 have shown that the water releases from Melton Hill Reservoir will have a significant effect on the concentration of radioactive wastes in the lower Clinch River. For short periods of time, the dilution of radioactive waters may be 10 to 30 times less than median values observed before construction of Melton Hill Dam.

Before power generation at Melton Hill Dam began, there were only fourfold to fivefold variations in the concentration of radionuclides at the mouth of White Oak Creek. Farther downstream in the river, these variations in concentration were almost completely attenuated. Because of the small fluctuations in concentration with time, a simple grab sample of the river water was collected.

With the change in flow conditions in the Clinch River, due to hydroelectric operations at Melton Hill Dam, a more sophisticated system of collecting water samples has been recommended by the Subcommittee on Water Sampling and Analysis of the Clinch River Study. It was suggested that the sampling equipment be fully automated so that water samples would be continuously collected in proportion to the flow. Two automatic water-sampling stations have been designed and fabricated for the tailrace at Melton Hill Dam and near the former site of Gallaher Bridge. The sampling equipment shown in Fig. 4.3 has been installed at the site near Melton Hill Dam.

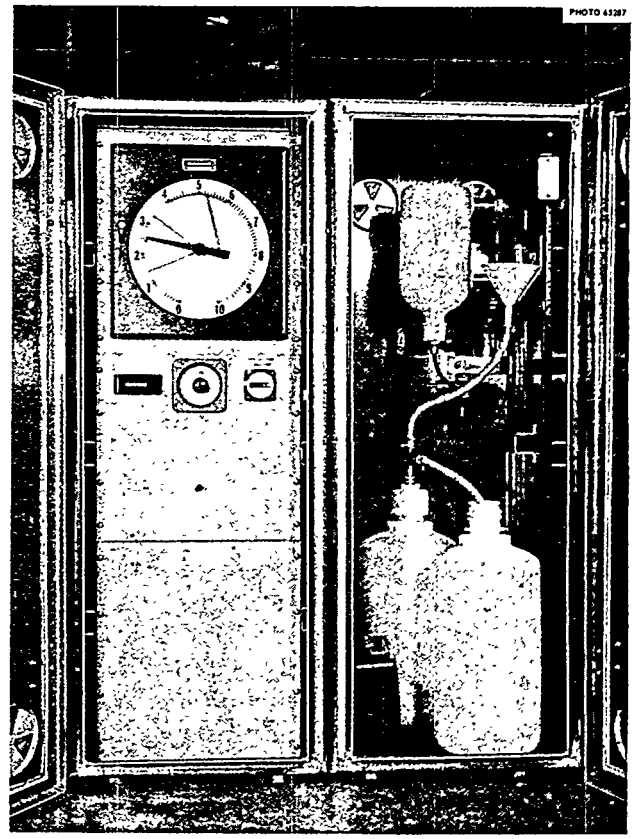

Fig. 4.3. Automatic Water-Sampling Station at Tailrace of Melton Hill Dam.

[3]Instrumentation and Controls Division.

BOTTOM SEDIMENT STUDIES

P. H. Carrigan, Jr.[1] R. J. Pickering[1]
E. R. Eastwood J. E. Jackson

Distribution of Radioactive Materials in Clinch River Bottom Sediment

A total of 163 undisturbed cores of bottom sediment were taken at 18 cross sections on the Clinch River and two major tributary streams, with

the Swedish Foil Sampler, for use in this and other investigations of radionuclides in Clinch River bottom sediments.[4]

Vertical distribution of gross gamma radioactivity in each intact core was determined by means of the core scanner.[4] Vertical distribution of the three most important gamma-emitting radionuclides – ^{137}Cs, ^{106}Ru, and ^{60}Co – in nine cores was determined through use of a multichannel pulse-height analyzer with the core scanner.

The greatest thicknesses of both radioactive and total sediment occur in the lower 13 miles of the Clinch River. The core showing the greatest thickness of radioactive sediment, 8.7 ft, was obtained at CRM 7.5. In accord with the general pattern of sediment accumulation in the Clinch River, radioactive sediment occurs along the sides of the channel. In the lower 13 miles of channel, sediment extends toward midchannel, and near CRM 12, sediment extends across the entire channel.

Several cores from the lower portion of the Clinch River showed a persistent pattern of gross gamma distribution with depth. This pattern is similar to the pattern of annual releases of ^{137}Cs from White Oak Lake. Statistical comparisons of the patterns for 27 cores with the pattern for annual releases of ^{137}Cs resulted in a mean correlation coefficient of 0.76. If the release pattern for ^{60}Co is included in such a comparison, a mean coefficient of correlation of 0.80 is obtained.

Measurements of the vertical distribution of ^{137}Cs, ^{60}Co, and ^{106}Ru in nine bottom sediment cores showed that about 81% of the gross gamma radioactivity was due to ^{137}Cs, 12% due to ^{60}Co, and 7% due to ^{106}Ru. Vertical distribution of ^{60}Co was similar to that of ^{137}Cs in all nine cores (coefficient of correlation, 0.88).

The persistent pattern of vertical distribution of ^{137}Cs and of ^{60}Co in the sediment at several coring sites downstream from CRM 18 indicates more or less regular, persistent deposition of sediment at these particular sites, and thus long-term net accumulation of sediment at these sampling sections.

Incorporation of ^{137}Cs in Clinch River bottom sediment of cesium-bearing aluminosilicate minerals entering the Clinch River from ORNL is indicated by (1) similarity in vertical distribution of ^{137}Cs in cores, (2) knowledge that nearly 70% of ^{137}Cs released to the river is associated with suspended solids, and (3) known preferential sorption of ^{137}Cs by such minerals.

Radionuclide concentration of ^{137}Cs is related to sediment thickness and location in study reach. This relationship is shown in Fig. 4.4.

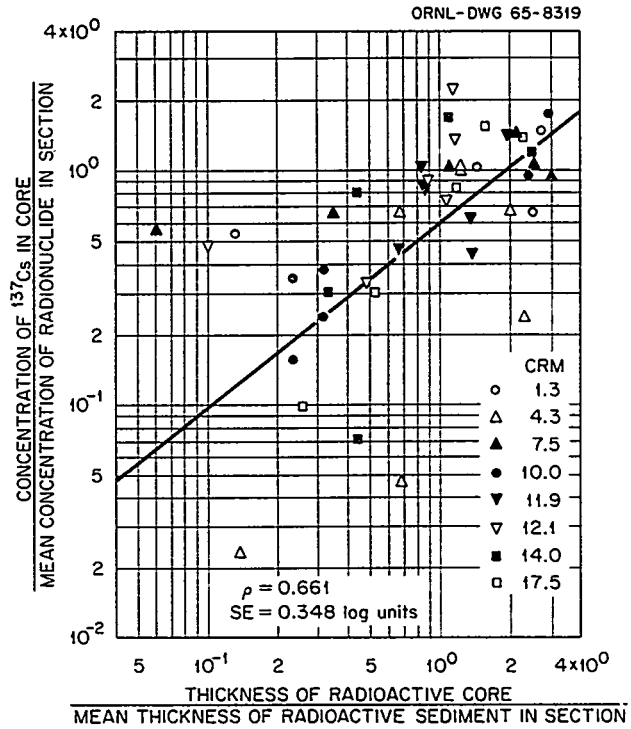

Fig. 4.4. Relationship of ^{137}Cs Content of Clinch River Bottom Sediment to Sediment Thickness.

Physicochemical Characteristics of Clinch River Bottom Sediment

Particle-size analyses showed that most of the sediment in cores was clayey silt. Total cation exchange capacities of 2-in. samples from two selected cores were moderately low and showed little variation. Exchange capacities were highest in the clay-size fractions. The only exchangeable cations in the sediment were calcium and magnesium.

[4]F. L. Parker *et al.*, *Health Phys. Div. Ann. Progr. Rept. June 30, 1964*, ORNL-3697, pp. 34–35.

Sand-size fractions of the samples contained 70 to 80% quartz, with lesser amounts of feldspar, dolomite, and mica. Silt-size fractions contained 60 to 70% quartz, with lesser amounts of mica, vermiculite, kaolinite, feldspar, and dolomite. Quartz content in the clay-size fraction was 10 to 20%. Dolomite and calcite were present in minor amounts; mica, kaolinite, and vermiculite made up the remainder. The content of free aluminum oxide, free iron oxide, and organic carbon was less than 3%, in general.

No strong correlations were observed between radionuclide contents and physicochemical properties of sediment samples.

Inventory of Radionuclides

An inventory of radionuclides associated with the bottom sediments has been made in the lower Clinch River. The reach included in this inventory extends from the mouth of White Oak Creek to the mouth of the river, a distance of 21.0 miles.

The quantities of radionuclides associated with the bottom sediments are: 154.6 curies of ^{137}Cs, 17.5 curies of ^{60}Co, 15.5 curies of ^{106}Ru, 10.2 curies of rare earths, and 2.9 curies of ^{90}Sr. The total activity is 200.7 curies. Cesium-137 constitutes 77% of the total radioactivity. The following percentages of the total activity were found for the other radionuclides: ^{60}Co, 8.7; ^{106}Ru, 7.7; rare earths, 5.1; and ^{90}Sr, 1.5.

Most of the radioactive material was found to be downstream from mile 15; approximately 95% of the identified radionuclides were in this downstream reach. At least 50% of the identified radionuclides were downstream from mile 8.7.

Comparison of the quantities of radionuclides associated with the bottom sediment to the quantities of these radionuclides released through White Oak Dam (allowing for decay) indicates that about 21% of the ^{137}Cs released has been retained in the sediments, about 9% of the ^{60}Co, about 0.4% of the ^{106}Ru, and about 0.2% of the ^{90}Sr. It is difficult to estimate the percent of retention for the rare earths because of the variety of half-lives involved in trying to compensate for the decay of releases. From meager information on content of ^{144}Ce in cores (three samples), the retention of rare earths may approach, possibly exceed, 25%.

The longitudinal variations of mean concentrations of the radionuclides, of radioactive sediment area, and of radioactive sediment thickness are shown in Figs. 4.5–4.7.

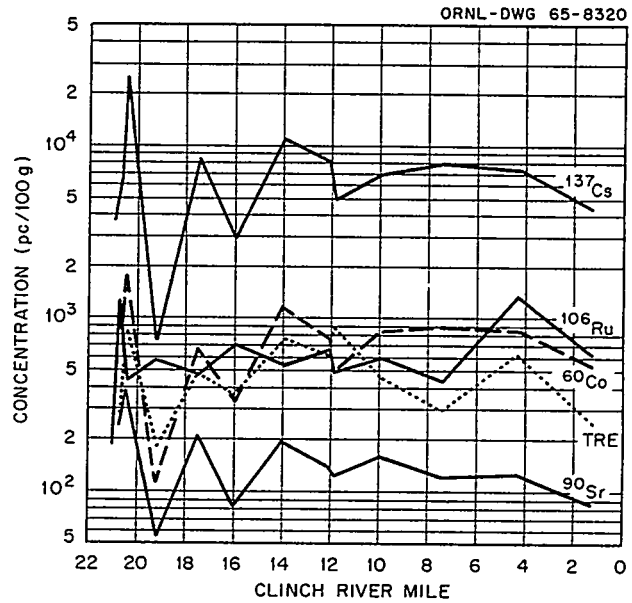

Fig. 4.5. Longitudinal Variation in Mean Concentration of Principal Radionuclides in Bottom Sediments of Clinch River.

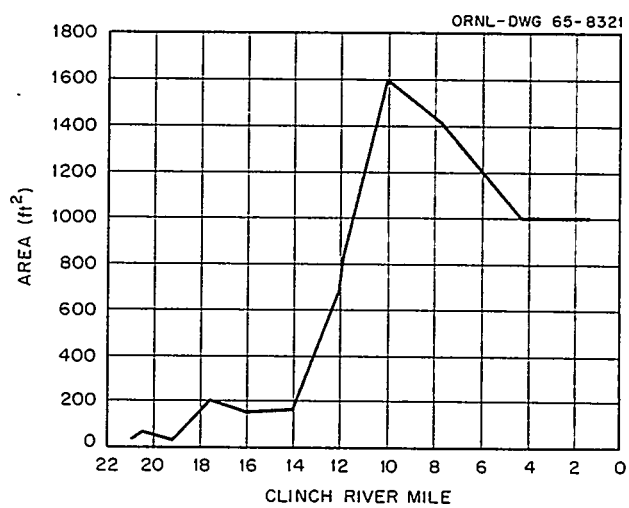

Fig. 4.6. Longitudinal Variation in Cross-Sectional Area of Radioactive Bottom Sediments of Clinch River.

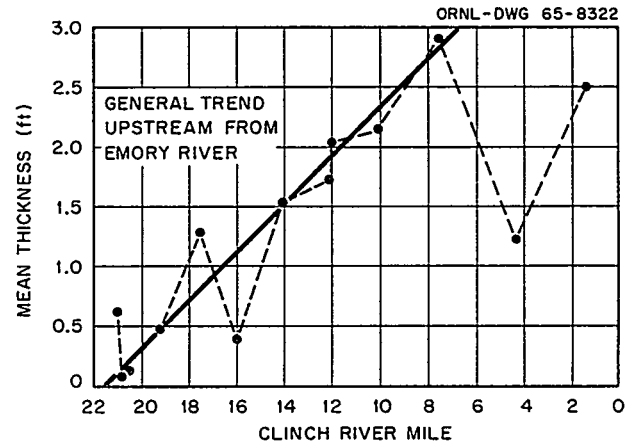

Fig. 4.7. Longitudinal Variation in Mean Thickness of Radioactive Bottom Sediments in Clinch River.

5. Movement of Nuclides in Terrestrial Environment

BEHAVIOR OF RADIONUCLIDES IN SOILS

Tsuneo Tamura A. S. Rogowski
E. R. Eastwood O. H. Myers

The major long-term objective of the soil studies is to obtain information from field and laboratory investigations on the behavior of radionuclides in soils and to synthesize this information so that predictions may be made of the fate of radionuclides released to the soil environment. One aspect of this study is the characterization of the reactions of radionuclides in the different horizons of the developed soil. Another aspect is the movement of radionuclides from the soil surface by runoff and erosion.

Studies of fission product movement by runoff and erosion have been concerned with fallout contamination, particularly with radiostrontium.[1,2] Very little information is available on the movement of ^{137}Cs by runoff and erosion; indeed, the high sorption of this element by most soils suggests immediate fixation and stabilization in the surface soil.[3] It was felt that the concentration of ^{137}Cs at or very near the surface of the soil would make its movement by runoff and erosion most important, because the surface particles are more susceptible to movement by these mechanisms. Furthermore, the use of long-lived radiocesium would permit following the behavior of that radionuclide over a long time span.

ADSORPTION OF ^{137}Cs BY SOILS

Tsuneo Tamura A. S. Rogowski
E. R. Eastwood O. H. Myers

In Table 5.1 the distribution coefficient (K_d)[4] for cesium is tabulated for three soil types found in the southeastern United States. The lowest adsorption of cesium is noted for the Fullerton soil, whose clay mineral content was found to be

[1] R. G. Menzel, *Science* 131, 499 (1960).

[2] M. H. Frere and M. Roberts, Jr., *Proc. Soil Sci. Soc. Am.* 27, 82 (1963).

[3] J. R. Miller and R. F. Reitemeier, *Proc. Soil Sci. Soc. Am.* 27, 141 (1963).

[4] K_d is defined as the ratio of ^{137}Cs adsorbed per gram of material to the ^{137}Cs remaining per milliliter of solution.

Table 5.1. The Adsorption of ^{137}Cs and the Ion Exchange Capacity of Three Soils in the Southeastern United States

Horizon	Depth (in.)	Ion Exchange Capacity (meq/100 g)	Distribution Coefficient (K_d)[a]		
			24 hr	48 hr	192 hr
		Fullerton Silt Loam			
A_1	0–1	18.1	872	1,130	2,030
A_2	1–7	6.8	1,850	2,320	3,840
A_3	7–9	7.8	3,190	4,830	9,420
B_1	9–11	10.2	6,130	9,380	16,540
B_2	11–26	10.0	5,430	9,320	14,690
B_3	26–48	10.4	6,300	11,180	18,450
C	48–60	11.1	4,110	6,030	10,020
		Sequoia Silt Loam			
A_1	0–2	10.1	11,860	22,070	31,900
A_2	2–8	4.2	7,540	11,130	14,100
B_1	8–12	5.4	25,970	37,450	40,460
B_2	12–18	7.9	22,540	52,640	71,530
C	18–27	7.0	51,910	85,340	112,900
		Captina Silt Loam			
A_p	0–6	8.5	7,880	14,350	30,840
A_3	6–8	10.4	13,080	29,300	45,620
B_1	8–13	8.6	11,420	27,500	48,240
B_2	13–23	6.4	12,040	28,300	56,140
B_3M_1	23–35	5.2	8,490	16,710	33,840
B_3M_2	35–68	6.5	16,780	28,820	44,620

[a] K_d is the ratio of adsorbed radionuclide per gram of soil to the remaining radionuclide per milliliter of solution.

primarily kaolinite. The surface horizon, with the highest exchange capacity (18.1 meq/100 g), showed the lowest K_d; the B_3 horizon, with 10.4 meq/100 g of exchange, showed the highest K_d. The high exchange capacity of surface soils is generally attributable to organic matter. The data show that the high capacity is not favorable for ^{137}Cs sorption. Both the Sequoia and Captina soils showed high affinity for radiocesium; both soils were found to contain appreciable illite and mica in them. Although the latter two soils show a lower exchange capacity than the Fullerton soil, they sorb a higher percentage of the radiocesium in a demineralized water system. The lowest exchange capacity of the two illitic soils was observed in the A_2 horizon (4.2 meq/100 g) of the Sequoia profile; the K_d of 14,100 of this horizon may be compared to the K_d of 18,450 in the B_3 horizon of the Fullerton with its exchange capacity of 10.4 meq/100 g. The high K_d for trace levels

of radiocesium has been explained on the basis of the favorable mineral structure of illite, and the reader is referred to the earlier papers on the mechanism of sorption.[5–7]

It should be pointed out that the Captina sample represents a cultivated profile, as evidenced by the A_p horizon; in contrast, the Fullerton and the Sequoia samples are from a forested environment with minimal disturbance by man. The latter situation results in a soil with observable and measurable differences in soil characteristics near the upper surface of the profile. Note, for example, that the A_2 horizon (zone of eluviation) samples show lower exchange capacities than the overlying A_1 horizon samples; the higher capacity of the A_1 is largely due to organic material in this upper zone. The Captina soil sample was taken from the field plot site where runoff and erosion studies are being made. The high K_d of the A_p horizon makes it particularly interesting to follow the runoff and erosion characteristics, since the high K_d tells us that the ^{137}Cs is at or very near the ground surface.

DESORPTION OF ^{137}Cs BY SOILS

Tsuneo Tamura A. S. Rogowski
E. R. Eastwood O. H. Myers

The samples which had been used to sorb radiocesium were washed once with water prior to the addition of 25 ml of 1 *M* sodium acetate to desorb the nuclide. The water wash resulted in less than 3% of the activity being leached from the solid. Desorption was followed as a function of time, and the data are given in Table 5.2. The highest leaching of ^{137}Cs is observed in the kaolinitic Fullerton samples. After only 5 min of solid-solution contact time, the deeper soil horizons show higher desorption than the samples near the surface. However, this relationship is not maintained with longer contact time. After a maximum is reached in the deeper horizons, the amount of cesium in solution is decreased in these horizons. In the A_1 horizon, the cesium continues to be leached even after 264 hr of contact, and in the A_2 the maximum appears to be reached after 120 hr; whereas in the A_3, the maximum is noted after 24 hr. With depth, the time to reach maximum desorption is reduced; in the *B* and *C* horizons, 4 hr contact showed maximum desorption.

In both the Sequoia and Captina soils, similar behavior is noted for the profiles; the difference appears to be mainly in the contact time needed for maximum desorption. The *C* horizon of the Sequoia soil may be likened to Conasauga shale, since it is the source of this soil. In this horizon the maximum desorption is observed after the shortest contact period of 5 min. During this period, approximately 40% of the ^{137}Cs was desorbed; with longer contact time the amount gradually decreased until, after 264 hr of contact, the desorbed cesium was 14.4%. It is interesting to note that the A_1 horizon of the Sequoia soil did not follow the same desorption behavior as the A_1 horizon of the Fullerton, though both samples appear to show organic exchange characteristics. However, the two samples differed in that the high exchange in the Fullerton did not increase ^{137}Cs sorption, whereas in the Sequoia sample the K_d for cesium was as high as the A_p horizon of the Captina, which suggests the dominating influence of illite.

Desorption of radiocesium in these soils is being further evaluated, using calcium chloride solutions. Similar behavior would not only confirm the sodium acetate observations but would cast doubt on interpretations of desorption of radiocesium that have been made based on values obtained after a single contact time. Further tests are in progress to compare the behavior of potassium in similar systems in order to establish the response of the alkali ions.

---

[5] T. Tamura and D. G. Jacobs, *Health Phys.* 2, 391–98 (1960).

[6] T. Tamura, *Nucl. Safety* 5, 262 (1964).

[7] T. F. Lomenick and T. Tamura, "Naturally Occurring Fixation of ^{137}Cs on Sediments of Lacustrine Origin," accepted for publication in the *Proceedings of the Soil Science Society of America* (1965).

Table 5.2. Percentage Desorption of ^{137}Cs of Three Soils from the Southeastern United States by Sodium Acetate

Values for maximum desorption are underlined

Horizon	Contact Time						
	5 min	45 min	4 hr	24 hr	96 hr	120 hr	264 hr
				Fullerton Silt Loam			
A_1	32.2	46.2	59.3	75.3	80.6	83.7	86.7
A_2	45.4	58.2	68.3	77.9	78.9	79.1	77.4
A_3	54.8	65.1	71.7	73.3	69.7	70.8	67.6
B_1	57.2	65.0	68.8	66.5	60.8	61.6	57.1
B_2	67.0	74.4	75.1	70.5	68.2	68.0	65.4
B_3	61.8	72.4	72.7	67.9	64.8	65.5	62.8
C	76.0	86.4	88.6	85.7	82.5	83.6	80.9
				Sequoia Silt Loam			
A_1	47.8	50.8	49.0	37.1			17.7
A_2	62.3	72.2	72.4	63.9			41.5
B_1	59.6	53.4	44.9	31.1			24.1
B_2	44.3	39.2	31.6	21.0			15.1
C	40.4	35.2	27.7	18.8			14.4
				Captina Silt Loam			
A_p	27.0	33.4	36.5	33.7	32.3		29.4
A_3	24.8	31.1	33.4	29.2	27.7		25.4
B_1	31.4	36.5	36.3	31.9	29.2		26.5
B_2	33.6	39.9	38.8	35.3	32.6		30.9
B_3M_1	41.3	45.7	46.3	42.9	38.8		36.7
B_3M_2	42.7	45.5	44.9	40.7	35.5		33.6

SOIL AND AREAL DESCRIPTION OF EXPERIMENTAL FIELD PLOTS

Tsuneo Tamura A. S. Rogowski
E. R. Eastwood O. H. Myers

The experimental area where the behavior of ^{137}Cs in the field is being studied is located on the alluvial plain of the north bank of the Clinch River at the Oak Ridge reservation. The soil belongs to the alluvial Captina series, which occupies low to intermediate areas along the Clinch River. The soil has a virtually impermeable fragipan layer at about 21 to 24 in. Laboratory samples described as the Captina soil in the earlier section came from this area. As a result of the fragipan layer, waterlogged conditions prevail in the upper 4 ft of the profile during most of the fall, winter, and spring; and during these periods, the soil is subject to erosion even by minor storms.

The experimental portion of the area is covered with a mixture of crabgrass and fescue, with crabgrass predominating. Using a point sampler, there was, on the average, 73% surface plant cover and 8.9% basal plant cover, with 300 to 500 g of plant material (on the dry basis) per square meter of surface. The slopes found in the field ranged from 2 to 15%. Three experimental plots were chosen for tagging with 5 mc of ^{137}Cs per plot. Each plot measured 2.5 by 2.5 m.

In the first plot, the vegetation was removed; in the second, the meadow was clipped and the litter was left on the ground; and in the third, the meadow was fertilized and allowed to grow. In Fig. 5.1 a general view of the experimental plot area is shown. Each of the plots was enclosed by a 15-cm-wide metal strip, sunk to a depth of 7 cm into the ground. The fourth plot (shown in the figure) was kept in reserve for future use. At the lowest corner of each plot a runoff catchment sink was cemented in place and connected by means of a rubber hose, encased in galvanized pipe, to the runoff catchment pans. Each catchment pan was equipped with calibrated drums and a water-level recorder to measure runoff. A recording rainfall gage was also installed in the experimental area.

PHOTO 67014

Fig. 5.1. General View of Experimental Plot Area.

SOIL LOSS

Tsuneo Tamura A. S. Rogowski
E. R. Eastwood O. H. Myers

Results reported here cover the period of five months following the application of ^{137}Cs to the plots. The results of the initial 81-day period were reported earlier.[8] Rainfall in four of the five months was below normal; it was above normal in the remaining month. The total precipitation during this period was 70.92 cm. The erosion index (EI) values for the study period were above normal in three of the five months, but the differences between the observed and expected values were found to be not significant at the 5% level. The EI value is a numerical evaluation of the capacity of a specific rainfall pattern to erode soil from the unprotected field; it is the product of rainfall energy and its maximum 30-min intensity.[9]

The total soil loss for the five-month period amounted to 573 g/m^2 on the bare soil, plot 1; 182 g/m^2 on the clipped meadow, plot 2; and 63 g/m^2 on the tall meadow, plot 3. Computed regression coefficients for the soil loss as a function of EI values were found not to be significantly different for the bare soil and the tall meadow plots when compared with regression coefficients derived from observed soil loss values. The regression coefficient from the observed values for the clipped meadow plot was, however, significantly lower than predicted. The discrepancy is most likely due to the difficulty in selecting a proper cover factor in the equation[10,11] and to the short study period involved.

^{137}Cs LOSS FROM SOIL

Tsuneo Tamura A. S. Rogowski
E. R. Eastwood O. H. Myers

The total loss of ^{137}Cs for the five-month period was 17.9% of the applied amount from the bare soils, 14.1% from the clipped meadow plot, and 6.0% from the tall meadow plot. In Fig. 5.2 the cumulative ^{137}Cs loss is plotted against the cumulative soil loss on a logarithmic scale. Cesium loss appears to be occurring at three different rates for the vegetation plots 2 and 3 and at two different rates for plot 1 (bare soil). Though the data are not plotted, the line for the first stage was drawn to the first cumulative points for each plot from measured values of specific activity. It was found that the specific activity of cesium in the runoff was higher during the first 46 days of the test period than in the next 35 days. This higher initial loss was likely due to lack of intimate contact of the cesium with the soil and vegetation when applied. Poor contact may have been due to the rapid evaporation of the fine spray during application, leaving the radionuclide at the surface without a strong bond to the adsorbing material.

During the second stage the cesium loss was highest in the bare plot; however, the specific activity was lowest in this plot. It is believed that the higher specific activity in the vegetation plots was due to "washoff" from the vegetation. This phenomenon is discussed more fully in a separate section. Finally, in the third stage, the slope is decreased further in the vegetated plots but remains the same as in the second stage in the bare soil plot. The latter behavior suggests that a "steady state" has been reached for the bare plot. More time is needed to establish "steady state" for plots 2 and 3.

For the second stage for plot 1 and third stage for plots 2 and 3, the curves fit the equation

$$y = \exp(m \ln x - b), \quad 0 < y < 100,\ x > 16\ g/m^2,$$

with percent loss of ^{137}Cs given by y and soil loss in g/m^2 given by x, and where m is 0.6758, 0.6257, and 0.6382 and b is 1.3345, 0.4505, and 0.9029 for plots 1, 2, and 3 respectively. If we let $\ln y = z$, then, for plots 1, 2, and 3, z values fall in the ranges ±0.0539, ±0.0468, and ±0.0077 respectively.

The use of the inverse of equation 1, namely, $x = \exp(\ln y + b)/m$, is anticipated for predicting soil losses from changes in observed fallout levels of radionuclides sorbed by different surface soils.

---

[8] A. S. Rogowski and T. Tamura, *Health Phys.* 11 (1965) (in press).

[9] W. H. Wischmeier and D. D. Smith, *Trans. Am. Geophys. Union* 39, 285 (1958).

[10] W. H. Wischmeier *et al.*, *Agr. Eng.* 39, 458 (1958).

[11] "*Soil Loss Estimation in Tennessee,*" unpublished proceedings of Soil Loss Conference, University of Tennessee, Knoxville, 1959.

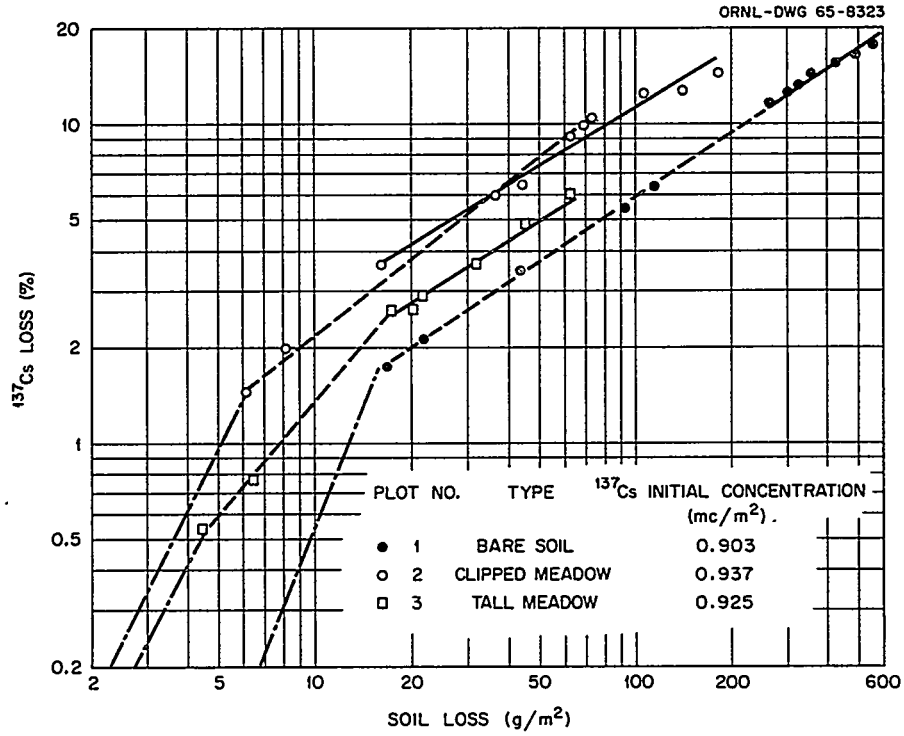

Fig. 5.2. Cumulative ^{137}Cs Loss as a Function of Soil Loss for the Bare Soil (Plot 1), Clipped Meadow (Plot 2, plus Border), Tall Meadow (Plot 3), and Clipped Meadow Corrected to Exclude Border (Plot 2, Minus Border).

^{137}Cs LOSS FROM THE PLANT MATERIAL

Tsuneo Tamura A. S. Rogowski
E. R. Eastwood O. H. Myers

Following the application of 5 mc of ^{137}Cs on the plots with vegetation (plots 2 and 3), it was found[12] that practically all the radionuclide was on the plant and litter material. Five months later, 25.7% of the radionuclide was still found on the vegetation in plot 3 (tall meadow); in plot 2, 24.0% was still on the plant material and 28.7% on the litter material.

A large standard error was obtained in determining the ^{137}Cs content of the vegetation samples, particularly on the litter and plant samples from plot 2. Only a limited number and size of samples could be taken without disturbing the runoff and erosion characteristics of the individual plots, and these contributed to the large error.

On the basis that all the ^{137}Cs was on the vegetation initially, Fig. 5.3 shows the percentage of cesium leached from the vegetation as a function of rain. Using the data points for plot 3, the following equation is derived with y representing the percent of ^{137}Cs leached from the vegetation and x representing the total rainfall in centimeters,

$$y = 10 \ln (x - 6.5) + 34 , \qquad x > 6.5 , \; 0 \leqq y \leqq 100 .$$

Obviously, more points are necessary to establish the accuracy of the equation; nevertheless, the data show that most rapid loss of ^{137}Cs from vegetation occurred during the initial 20 cm of rain. In Fig. 5.2 the starting points of the solid

[12]Data supplied by H. D. W. Waller, Radiation Ecology Section.

lines for plots 2 and 3 (16.4 g/m^2 and 17.4 g/m^2 of soil loss respectively) correspond to the 15.4 cm of rain on plot 2 and 29.7 cm of rain on plot 3. The low rate of leaching following these rainfall levels suggests that loss of ^{137}Cs was due to soil loss by erosion. On the other hand, the high specific activity of the ^{137}Cs initially coming off plots 2 and 3 (stage 2) is likely due to leaching loss from vegetation. When approximately 70% of ^{137}Cs was leached off the vegetation, the "rate" of radionuclide loss from the vegetated plots approached the "rate" from the bare soil.

These radionuclide loss data were obtained from field plots. The information, though incomplete, suggests interesting changes in the behavior of radiocesium. Studies in the field are continuing, and further characterization of the movement of radionuclide from vegetation to the soil is now in progress, using a rainfall simulator.

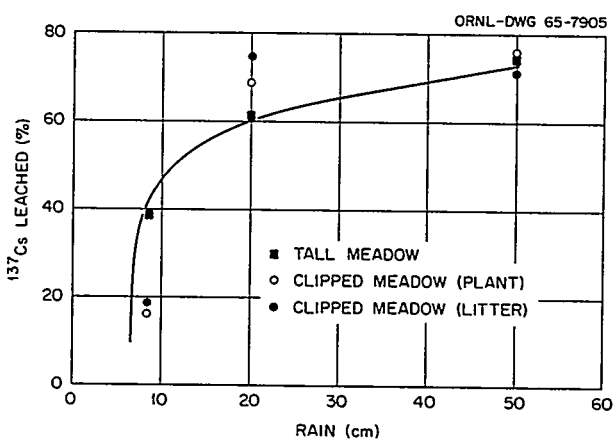

Fig. 5.3. Leaching Loss of ^{137}Cs as a Function of Total Rain for Plot 2 (Litter), Plot 2 (Plant), and Plot 3 (Plant).

SOLID WASTE DISPOSAL

T. F. Lomenick

The proposed burial ground 6 is located in Melton Valley, immediately southwest of the Oak Ridge National Laboratory liquid-waste seepage-pit area and northwest of White Oak Lake (see Fig. 5.4). The area includes about 70 acres of gently to moderately sloping land, divided into several smaller sections by natural surface cuts. The site is underlain by the Conasauga shale formation of Cambrian age, consisting mainly of multicolored calcareous and noncalcareous shales interbedded with limestone lenses and resistant siltstones. In general, there is an increase in the amount of limestone and a decrease in silty layers toward the southeast. Weathering persists generally to a depth of 5 ft or less in areas of low topography, and in excess of 20 ft in areas of high topography. In the extreme southern portion of the area, well-rounded pebbles and cobbles of quartzite and other resistant materials, along with sands, silts, and clay, are found immediately overlying the shale. The pebbles and cobbles, which are not representative of the surrounding bedrock, are believed to be remnants of an ancient floodplain of the nearby Clinch River.

Water-level measurements are being made periodically in a series of 40 shallow observation wells that were only recently completed within the proposed burial area, along with several existing deep churn wells, to determine seasonal variations in the depth to groundwater and to define water-table configurations.

From the available information, it appears that in areas of high elevations within the burial site the weathered shale should be easily excavated, and the depth to groundwater is sufficient to allow the waste to be suspended a considerable distance above the water table. However, about half the 70-acre area is believed to be unsuitable, because it is either too steep for convenient operations, has a "high" water table, or lies beneath power wires.

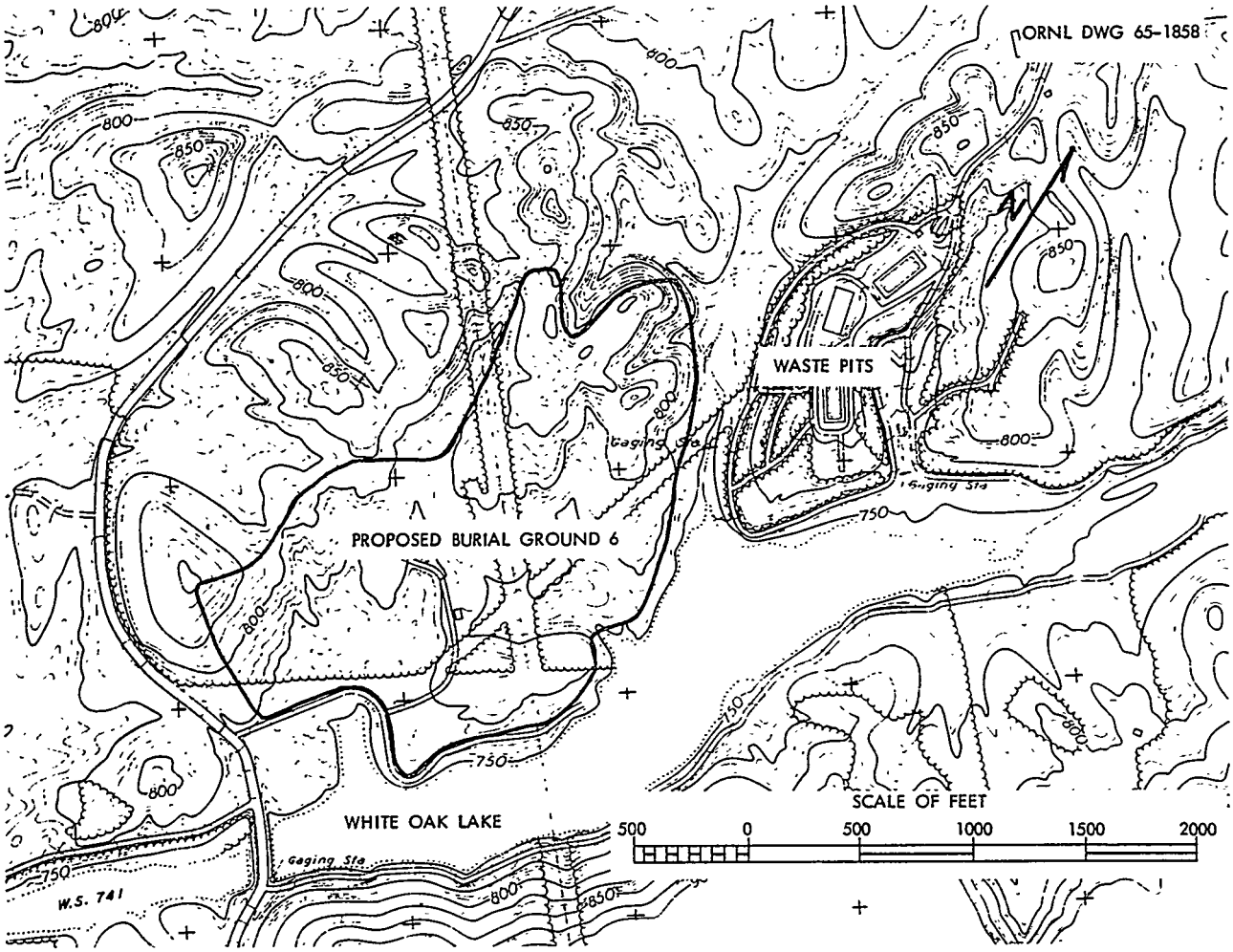

Fig. 5.4. Map of a Portion of Melton Valley, Showing Location of Proposed Burial Ground 6.

6. Mineral Exchange Studies

D. G. Jacobs
M. U. Shaikh[1]
O. M. Sealand
Susan M. Burke[2]

DISPERSION IN LAMINAR FLOW

The net dispersion of a tracer solution in a porous medium can be attributed to the following factors: (1) Poiseuille's velocity distribution, (2) distribution of pore size, (3) noncylindrical geometry of the pores, (4) random paths of fluid flow, (5) molecular diffusion, (6) bed packing or heterogeneity, and (7) viscosity, density, and thermal gradients in the liquid. Due to the wide variety of these parameters, dispersion in porous

[1]Noncitizen guest from Pakistan Atomic Energy Commission.

[2]Summer employee.

media cannot be predicted completely by any theoretical approach based on simplifying assumptions. By adopting different approaches based on different assumptions, numerous investigators have studied the dispersion phenomena in the laminar flow through porous media.

There are essentially two models that have been proposed to describe dispersion of solution in porous media – the capillaric model theory and the statistical or random walk theory.[3] The underlying assumption for the capillaric model theory is that the flow through a porous medium is equivalent to flow through a bundle of capillary tubes, so that the velocity distribution for a tracer is obtained by summing Poiseuille's parabolic velocity distribution for individual capillary tubes. In the statistical theory it is assumed that the porous medium is isotropic and homogeneous and that an event occurring in any one elemental time step is entirely independent of events occurring in any other time step. This implies a random distribution of "residence times." Both theories give an error-function expression for the distribution of tracer concentration in the laminar flow through porous media. According to the capillaric model theory, the coefficient of dispersion should vary as the square of the velocity, while in the random walk model it should be linearly proportional to the velocity of the tracer particle. The results of the studies of various observers indicate that the effect of molecular diffusion in the longitudinal direction is negligible, except at very low velocities.

EXPERIMENTAL STUDIES

Measurements of dispersion coefficients at different flow rates were made on a cylindrical core (10 by $1\frac{3}{4}$ in.) of Berea sandstone enclosed in an aluminum pipe, the space between the pipe and core being filled with epoxy resin. Twelve runs at different flow rates were made with 0.01 N $CaCl_2$ tagged with ^3H, and the breakthrough data were analyzed according to the method of Hashimoto *et al.*[4] The solution for the problem of miscible displacement in a column of finite length is

$$\frac{C}{C_0} = \frac{1}{2}\left(1 - \operatorname{erf}\sqrt{P}\frac{1-\tau}{\sqrt{\tau}}\right), \qquad (6.1)$$

where

$P = UL/4D$ (P is the Peclet number; U, the velocity of the fluid; L, the length of the column; and D, the dispersion coefficient), and

$\tau = V_i/\bar{V}$ (V_i is the throughput volume and $\bar{V}$ is the equivalent pore volume of the column).

From the breakthrough data for each run, a set of values of C/C_0 and the corresponding throughput volume, V_i, are known. Values of P and $\bar{V}$ are carefully guessed and are varied in small increments so as to minimize the difference between the observed C/C_0 and that calculated from Eq. (6.1). The values of P and $\bar{V}$ that give the best fit of the theoretical curve to the experimental data were determined by successive approximations with the CDC 1604-A computer.

The ratio of the experimental dispersion coefficient, D, divided by the molecular diffusion coefficient, D', is plotted in Fig. 6.1 as a function of the dimensionless parameter $\bar{v}r/D'$. Here, $\bar{v}$ is the mean pore velocity defined as $\bar{v} = F/fA$ (cm/sec), where F is the volumetric injection rate (cm^3/sec), f is the fractional porosity, and A is the cross-sectional area of the core (cm^2), and r is the average particle radius. For the displacement experiments in unconsolidated sands, the experimental data of Beran and von Rosenberg (after Collins[5]) can be fitted by a line having a slope of 1.17. As discussed by Collins, the value of the slope obtained by Rifai *et al.*[6] for a sand of a different texture is nearly the same, although the curve is displaced. Collins suggests that the position of the curve may reflect the difference in texture. For the present study it was found that the slope of the straight-line portion of the best-fitting continuous curve is 1.21. The displacement of our curve to the left indicates that dispersion is relatively greater in a consolidated sandstone, having a

---

[3] A. E. Scheidegger, *The Physics of Flow Through Porous Media*, p. 259, Macmillan, New York, 1950.

[4] I. Hashimoto *et al.*, *Ind. Eng. Chem., Fundamentals* 3(3), 213–18 (1964).

[5] R. E. Collins, *Flow of Fluids Through Porous Materials*, p. 209, Reinhold, New York, 1961.

[6] M. N. E. Rifai *et al.*, *Dispersion Phenomena in Laminar Flow Through Porous Media*, Progress Report No. 2, Sanitary Engineering Research Laboratory, University of California, Berkeley (July 1956).

wider range of pore sizes and a definite pattern of structure, than in unconsolidated sand. These studies suggest that the experimental value of the slope is closer to the theoretical value of unity, expected if the dispersion in porous media is to be explained on the basis of a statistical model or a random walk model, than to the value of 2, expected on the basis of the capillaric model.

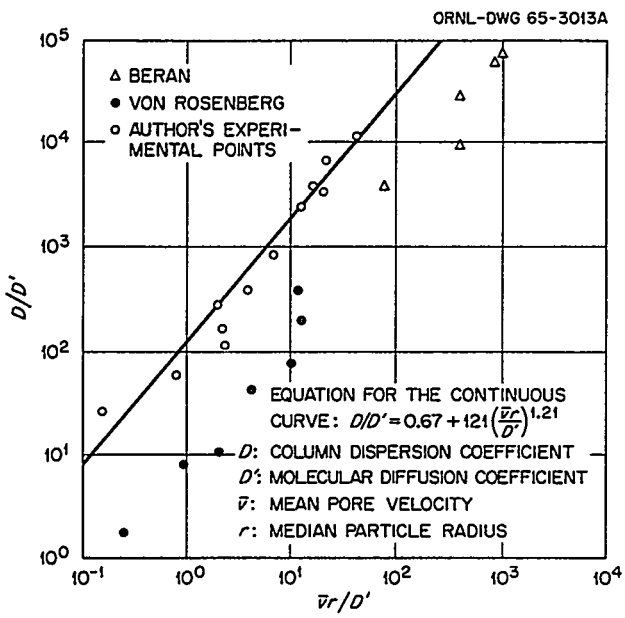

Fig. 6.1. Dispersion Coefficients for Sandstone Core, Showing the Effect of Displacement Velocity.

EFFECT OF CHANGES IN THE CHEMICAL ENVIRONMENT ON THE DISPERSION OF STRONTIUM

In the application of Eq. (6.1) it is assumed that the value of $\bar{V}$, the equivalent pore volume or the 50% breakthrough volume, remains constant during the course of an experiment. If the chemical environment is maintained at a constant concentration and composition and the exchange isotherm of the tracer is linear, this condition is met within practical limits. However, in many cases of interest, the discharge of radioactive contaminants into the ground is accompanied by a solution whose composition and concentration are much different from those of the natural ground waters. This changes the chemical environment during the period of discharge, but the system reverts gradually to the initial conditions after the discharge is completed. In such cases the distribution coefficient changes with time; consequently the relative velocity of the tracer changes with respect to the transporting water and the value of $\bar{V}$ in Eq. (6.1).

If an ion exchange column having a fixed Peclet number of the transporting solution is operated under two different but constant sets of conditions, giving different distribution coefficients, the relative breakthrough curves will be similar but will be displaced from one another according to the value of $\bar{V}$. If, on the other hand, one set of chemical conditions is gradually displaced by another, the breakthrough of the tracer will at first tend to follow the breakthrough expected for the original conditions. As the conditions are changed during the course of the experiment, the breakthrough tracer will tend toward the curve expected for the second set of chemical conditions. If the distribution coefficient in the original solution is lower than that in the succeeding influent solution, the breakthrough curve will become flatter; under the inverse conditions the breakthrough curve will become sharper.

In order to observe the influence of changing chemical environments on the movement of radionuclides through vermiculite, four columns were set up. Each column contained 10 g of vermiculite which had been pretreated for iron removal and saturated with NaCl. The first column was washed and filled with distilled water, the second with 0.01 *N* $CaCl_2$, the third with 1 *N* $CaCl_2$, and the fourth with 0.3 *M* Na_3PO_4 (pH = 12). Each of the columns was saturated with 0.01 *N* $CaCl_2$ tagged with ^{85}Sr. The effluent from each column was collected in 25-ml increments, using metering pumps (Beckman model 746) in the effluent line to control the flow rates.

In Fig. 6.2 in a log-probability plot are shown the concentration histories of strontium for four columns. The apparent number of theoretical plates, *N*, in the column is calculated from Glueckauf's[7] breakthrough equation. If we take

[7]E. Glueckauf, *Trans. Faraday Soc.* 51, 34 (1955).

V_{90} as the throughput volume corresponding to 90% breakthrough and V_{10} that for 10% breakthrough, then

$$N = \frac{(2.56)^2 V_{90} V_{10}}{(V_{90} - V_{10})^2},$$

where the quantity 2.56 corresponds to the number of standard deviations between V_{90} and V_{10}. Table 6.1 shows the apparent number of theoretical plates, N, the dispersion coefficients, D, and the throughput volumes corresponding to the 50% breakthrough of strontium for each of the columns.

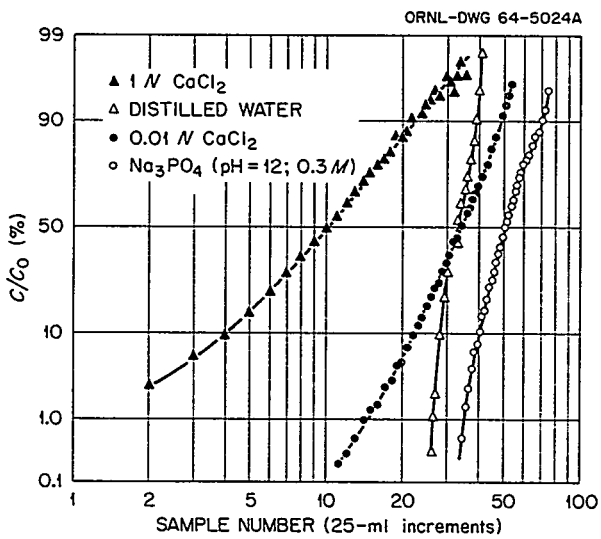

Fig. 6.2. Breakthrough Curves for ^{85}Sr in a Presaturated Vermiculite Column.

It is seen from the table that in the case of the Na_3PO_4-saturated column, 50% strontium breakthrough is delayed by a factor of about 5.5 times compared to the strontium breakthrough in the column saturated with 1 N $CaCl_2$, and about 1.5 times compared to the breakthroughs in the columns saturated with 0.01 N $CaCl_2$ and distilled water. The breakthrough curve for the Na_3PO_4-saturated column is quite sharp compared to those in the columns presaturated with 1 N and 0.01 N $CaCl_2$. As is seen from the third column of Table 6.1, strontium dispersion in the Na_3PO_4-saturated column is considerably smaller than in the 1 N and 0.01 N $CaCl_2$–saturated columns. The results agree qualitatively with the behavior expected in columns with changing chemical composition.

The slowing down of radionuclide migration by the introduction of chemicals to act as barriers in the columns is a transient situation which no longer exists after the chemical has been displaced by the continuous passage of the influent solution. Actually, in a short interval of time most of the chemical barrier is washed away from the columns in a piston-like displacement by the incoming solution. The effectiveness of chemical barriers in retarding the radionuclides' migration can be maintained only by the continuous addition of these chemicals.

Table 6.1. Variations of the Coefficient of Dispersion with Different Chemical Barriers in Vermiculite Columns

Chemical Barrier	Apparent Number of Theoretical Plates, N	D (cm^2/sec)	V (ml)
		$\times 10^{-3}$	
1 N $CaCl_2$	1.9	29	250
0.01 N $CaCl_2$	9	5.9	875
Distilled water	95	0.6	875
0.3 M Na_3PO_4	43	1.3	1375

7. Engineering, Economics, and Safety Evaluations

K. E. Cowser

CLINCH RIVER SAFETY ANALYSES

In most situations in which radioactive material is released to the environment, there are a number of pathways by which radionuclides may cause radiation exposure of man. Calculations have been made of the likely dose received by population groups as a result of discharge of radioactive fluids to the Clinch River. Previous reports include information on calculational procedure, the estimated dose from consumption of contaminated water and fish, and the external exposure from contaminated water, bottom sediments, and sludge accumulations in water systems utilizing river water.[1–3] This report includes additional calculations of the internal exposure due to consumption of contaminated water and fish and an estimate of the cumulative exposure to critical population groups.

Criteria of permissible radiation exposures adopted by the International Commission of Radiological Protection (ICRP), the Federal Radiation Council (FRC), and the National Committee on Radiation Protection and Measurements (NCRP) are accepted as guides.[4–8] The $(MPC)_w$ values that are employed to assess radiation dose to man follow the recommendations of ICRP found in Publications 2 and 6. In Publication 6 the ICRP recommended an increase in the $(MPC)_w$ values of ^{90}Sr when the skeleton and total body are the organs of reference. They consider that metabolic data provide a sounder basis for estimating the MPC values for ^{90}Sr than the exponential model used previously in their calculations. For continuous occupational exposure, the $(MPC)_w$ (skeleton) is increased from 1×10^{-6} to 4×10^{-6} μc/ml and the $(MPC)_w$ (total body) is increased from 4×10^{-6} to 7×10^{-6} μc/ml. As a result of these changes the estimates of internal dose to the skeleton and total body due to ingestion of ^{90}Sr in previous reports are conservative and are now overestimated by factors of 4 and $^7/_4$, respectively.

Contaminated Water and Fish

Mathematical models that permitted machine computations of critical organ burdens and dose due to ingestion of known concentrations of radionuclides were devised and coded for the CDC 1604. Correction factors were included to take into account differences in rate of intake and organ size as a function of the age of the individuals. Calculations were performed by assuming that individuals of ages 0 (newborn infant) through 45 and standard man begin in 1944 to drink untreated water from the Clinch River (mile 14.5) and from the Tennessee River (mile 471). They continued to drink water from these sources through 1963, following which water is obtained from an uncontaminated supply. It was also assumed that all water taken into the body in food or other form is equally contaminated and that intake and organ mass vary with age.

[1] K. E. Cowser *et al.*, *Proceedings of Conference on Transport of Radionuclides in Fresh Water, January 30, 31, and February 1, 1963, Austin, Texas*, TID-7664, pp. 17–39 (July 1963).

[2] K. E. Cowser, *Waste Treatment and Disposal Quart. Progr. Rept. February–April 1963*, ORNL-TM-603, pp. 98–103 (Dec. 16, 1963).

[3] K. E. Cowser, *Waste Treatment and Disposal Progr. Rept. May–October 1963*, ORNL-TM-757, pp. 157–68 (April 1964).

[4] *Report of Committee II on Permissible Dose for Internal Radiation*, ICRP Publication 2, Pergamon, New York, 1959.

[5] "Background Material for the Development of Radiation Protection Standards," *U.S. Federal Radiation Council Staff Report No. 1*, U.S. Govt. Printing Office, Washington, D.C., May 13, 1960.

[6] "Background Material for the Development of Radiation Protection Standards," *U.S. Federal Radiation Council Staff Report No. 2*, U.S. Govt. Printing Office, Washington, D.C., Sept. 26, 1961.

[7] "Maximum Permissible Body Burdens and Maximum Permissible Concentrations of Radionuclides in Air and in Water for Occupational Exposure," *Natl. Bur. Std. (U.S.) Handbook 69*, pp. 1–95, U.S. Govt. Printing Office, Washington, D.C.

[8] *Recommendations of the International Commission on Radiological Protection* (as amended 1959 and revised 1962), ICRP Publication 6, Pergamon, New York, 1964.

An example of the computed annual dose received by the skeleton of males drinking Clinch River water is shown in Fig. 7.1. At the end of 1963 the dose rate to the skeleton of the potentially critical population group, the 14-year-old, is about twice that to the skeleton of standard man. Thereafter any dose received is due to radionuclides that have accumulated in the skeleton during the period Clinch River water is consumed. The dose rate received by the skeleton of males in other age groups is less than that to the skeleton of the 14-year-old (see Table 7.1). The differences in dose rate are attributed to differences in intake and size of the skeleton. Strontium-90 is responsible for more than 99% of the skeleton dose; thus, smaller releases of this radionuclide in 1950 to 1952 and 1960 to 1963 are reflected by a reduction in annual dose received by the skeleton. Notice that the dose rate to the skeleton of the potentially critical group is smaller than 3.0 rems per year; that is, smaller than $^1/_{10}$ of the continuous occupational level that ICRP recommends not be exceeded. Dose rate to the total body and thyroid of the potentially critical group in 1963 is about 50% larger than that to the total body and thyroid of standard man. Similar differences are found for the Tennessee River (Table 7.1), but in all cases the dose rates to the critical organ of the potentially critical groups is at least one order of magnitude smaller than permissible levels. The dose rate received by males is larger than that received by females for all age groups and critical organs considered.

Another interesting comparison is the total dose received by individuals during the period in which Clinch River and Tennessee River water is consumed. As shown in Table 7.2, the skeleton of a 14-year-old male may receive a total dose of 2.9 rems by use of Clinch River water and 0.37 rem by use of Tennessee River water – about twice that to the skeleton of standard man. The total body of the 14-year-old attains a 50% larger dose than the total body of standard man. About 99% of the total body dose is due to ^{90}Sr, and fluctuations in dose rate reflect changes in ^{90}Sr release, as well as differences in intake and organ mass. The thyroid of the newborn infant receives the largest dose, which is about twice that to the thyroid of standard man. Strontium-90 and iodine-131 are responsible for 70% and 30% of the total thyroid dose, respectively. Of the organs analyzed, the skeleton of man receives the largest dose.

A second interpretation can be made of the internal dose calculations. As a consequence of radionuclides with long effective half-lives, and in particular ^{90}Sr, the dose to the critical organ will continue for many years after the exposure period. Therefore, there is a dose commitment for the future, at least in part, rather than just a

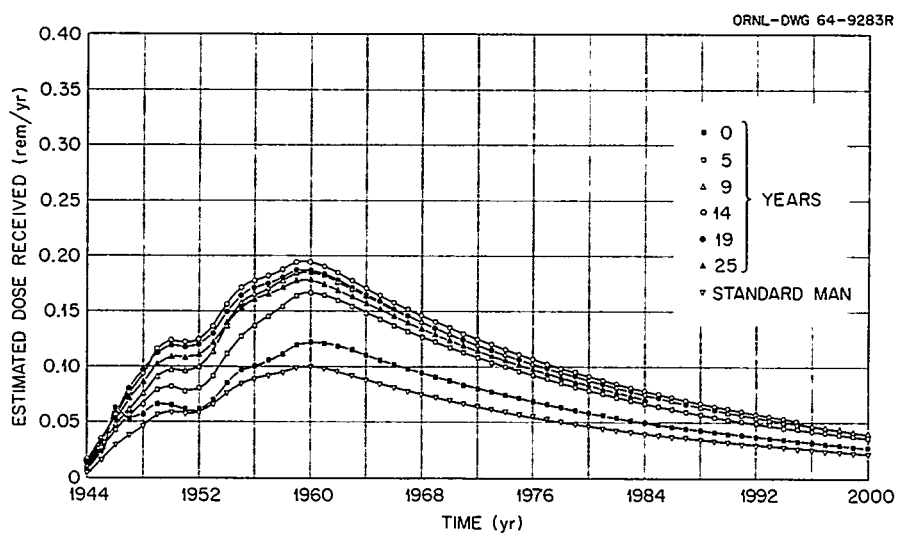

Fig. 7.1. Estimated Dose Received by Skeleton of Males from Drinking Clinch River Water.

Table 7.1. Dose Rate to Critical Organs of Males from Drinking Water[a]

(rems/year)

Age at Start of Exposure	Clinch River Water			Tennessee River Water		
	Skeleton	Total Body	Thyroid	Skeleton	Total Body	Thyroid
0	0.16	0.0097	0.023	0.017	0.0014	0.0032
5	0.17	0.013	0.027	0.023	0.0018	0.0038
9	0.18	0.014	0.029	0.025	0.0019	0.0039
14	0.19	0.014	0.028	0.026	0.0019	0.0039
19	0.18	0.014	0.027	0.025	0.0018	0.0037
25	0.17	0.013	0.025	0.023	0.0017	0.0034
Standard man	0.099	0.0097	0.017	0.013	0.0013	0.0024
Maximum permissible dose[b]	3.0	0.5	3.0	1.00	0.05	1.0

[a]The cumulative dose rate at the end of 1963.

[b]According to recommendations of ICRP Publication 2, values of annual dose rate for continuous occupational exposure are reduced to $\frac{1}{10}$ and applied to the Clinch River and are reduced to $\frac{1}{30}$ for skeleton and thyroid as critical organ and to $\frac{1}{100}$ for total body as critical organ and applied to the Tennessee River.

Table 7.2. Dose Received by Critical Organs of Males from Drinking Water[a]

(rems)

Age at Start of Exposure	Clinch River Water			Tennessee River Water		
	Skeleton	Total Body	Thyroid	Skeleton	Total Body	Thyroid
0	1.7	0.20	0.65	0.23	0.026	0.087
5	2.3	0.22	0.61	0.30	0.029	0.082
9	2.6	0.23	0.60	0.34	0.029	0.079
14	2.9	0.23	0.59	0.37	0.030	0.078
19	2.8	0.22	0.53	0.36	0.028	0.070
25	2.6	0.20	0.48	0.34	0.026	0.063
Standard man	1.5	0.15	0.32	0.19	0.019	0.042
Maximum permissible dose[b]	60	10	60	20	1	20

[a]The cumulative dose for the period 1944 to 1963.

[b]According to recommendations of ICRP Publication 2, values of annual dose rate for continuous occupational exposure are reduced to $\frac{1}{10}$ and applied to the Clinch River and are reduced to $\frac{1}{30}$ for skeleton and thyroid as critical organ and to $\frac{1}{100}$ for total body as critical organ and applied to the Tennessee River.

dose actually received during the period the individual was present in the area. The dose will be delivered during various periods following the intake, depending upon the effective half-life of the radionuclides involved. The dose commitments for future years associated with the consumption of Clinch River and Tennessee River water are given in Table 7.3. These are the cumulative doses that persons of various ages may receive and that begin in 1964 and extend to age 65 for each individual; they result from the retention of radionuclides in critical organs due to the ingestion of contaminated water during the period 1944 through 1963. For reasons previously enumerated, the critical organs of standard man have a smaller dose commitment (in general) than the organs of other individuals. In all cases the dose commitments are well below prescribed limits. The computational methods referred to above are used to calculate the dose commitment and thus have value in estimating future radiation exposures.

The dose received by the skeleton, total body, and thyroid of man due to consumption of contaminated water and fish is also calculated by use of the models. In addition to the assumptions previously listed for contaminated drinking water, it is also assumed that 37 lb per year of the flesh of bottom feeders is consumed by standard man during the period 1960 to 1963. The contribution to skeleton and total body exposure from consuming the flesh of bottom feeders (fish prepared to approximate normal human consumption) is about equal to the average exposure received from drinking untreated water. A recent survey of 80 fishermen by the Tennessee Fish and Game Commission lends support to the thesis that consumption of "fishburgers" is at most uncommon. Although the number of fishermen interviewed is small, not one indicated even occasional use of a mixture of flesh and bone. Without information on the actual rate of fish consumption as a function of age, it is further assumed that the intake of fish is distributed as the intake of water. Another way to state this assumption is that the ratio of fish eaten by an individual to that of standard man is equal to the ratio of water consumed by the individual to that of standard man.

Figure 7.2 shows the computed annual dose to the skeleton due to the consumption of contaminated water and fish. By comparison with Fig. 7.1, it is seen that the net increase in dose rate to the skeleton of individuals is small. This is due to inclusion of only 4 years of data (1960–1963) in the calculations to the long effective half-life of the critical radionuclide, ^{90}Sr, and to the reduction in ^{90}Sr released to the river. It is likely that findings of current research studies by the Radiation Ecology Section will eventually permit an estimate to be made of ^{90}Sr in processed fish flesh (and the consequent dose to man) for periods in which fish data are lacking.

Table 7.3. Dose Commitment to Critical Organs of Males from Drinking Water[a]

(rems)

Age at Start of Exposure	Clinch River Water			Tennessee River Water		
	Skeleton	Total Body	Thyroid	Skeleton	Total Body	Thyroid
0	2.6	0.18	0.36	0.35	0.024	0.051
5	3.3	0.23	0.46	0.45	0.030	0.063
9	3.5	0.24	0.47	0.43	0.032	0.066
14	3.4	0.23	0.46	0.45	0.031	0.062
19	3.0	0.21	0.41	0.41	0.027	0.055
25	2.5	0.17	0.34	0.34	0.023	0.046
Standard man	2.0	0.18	0.32	0.28	0.024	0.044

[a]The cumulative dose commitment beginning in 1964 and extending to age 65.

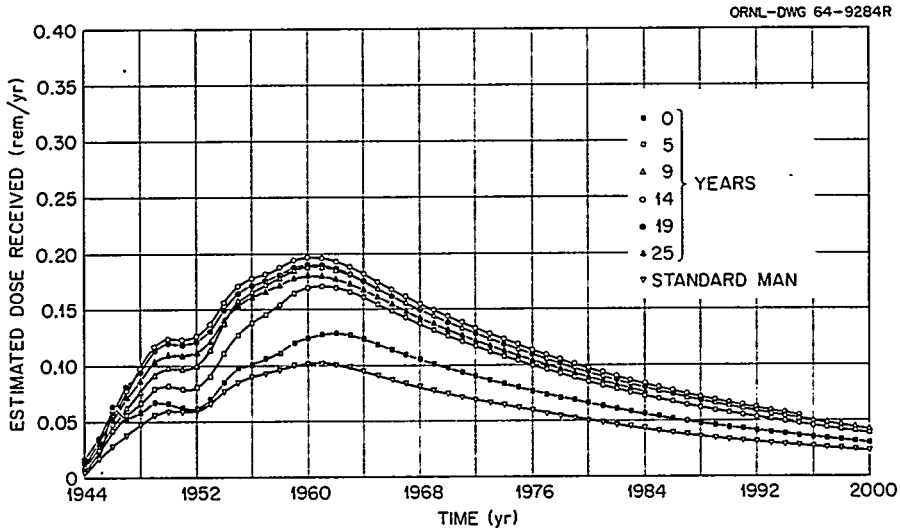

Fig. 7.2. Estimated Dose Received by Skeleton of Males from Drinking Clinch River Water and Consuming Contaminated Fish.

The cumulative dose over the 4-year exposure period is not excessive, with the skeleton of the 14-year-old receiving the largest increase of about 30 millirems. Consumption of "fishburgers" could result in an increase of the cumulative dose by a factor of 5 to 10. However, available information does not justify such a pessimistic assumption, but does emphasize the need to define the habits of individuals residing near the river system.

Cumulative Dose to Exposed Populations

The aggregate exposures of individuals or critical population groups that result from disposal of radioactive waste to the Clinch River cannot be stated precisely. One of the principal reasons for this difficulty is the lack of information on the habits and characteristics of the potentially exposed groups. Data on the location and age distribution of potentially exposed populations, the amounts of important food-stuffs consumed, the methods of food preparation, and the principal recreational habits are needed to define the cumulative dose. Differences in metabolic rates or processes of children or adults as they relate to the important radionuclides, in radionuclide removal from river water by suspended solids and by water treatment processes, and in the transfer of radionuclides from contaminated water to fish must also be considered. Although a single critical population group may be defined for a particular exposure pathway, there is no categorical reason to suppose the same critical population group for all exposure pathways. Unless founded on factual information, the dose estimates to critical population groups for the various exposure pathways cannot be added and assumed to be the maximum exposure realized.

By selecting reasonable values for periods of occupancy and dietary habits, an estimate is made of the aggregate exposure to the skeleton and total body of males working and residing in the Clinch River—Tennessee River environment (Table 7.4). The fractions of allowable dose received by the thyroid and GI tract are smaller than those received by the skeleton and total body and are not included. Since the Clinch River does not serve as a source of municipal water, children are not involved in its consumption. Therefore, we assume the youngest age at the beginning of exposure to be the 18-year-old who is employed at the Oak Ridge Gaseous Diffusion Plant. Only half of the daily fluid intake takes place on the job and results in an estimated total exposure over 20 years of 1.4 rems and 0.11 rem to the

Table 7.4. Estimated Cumulative Dose Received by Critical Organs of Males from Use of Clinch River and Tennessee River[a]

(rems)

Critical Pathway	Clinch River		Tennessee River	
	Skeleton	Total Body	Skeleton	Total Body
Drinking water	1.4	0.11	0.38	0.030
Recreation	0.018	0.019	0.003	0.003
Fish	1.8	0.14	0.070	0.0057
Total	3.2	0.27	0.45	0.039
Maximum permissible dose[b]	60	10	20	1.0

[a]Aggregate exposure for the period 1944 to 1963.

[b]As recommended by ICRP (see refs. 4 and 8), the annual dose rates for occupational exposure are reduced to $^1/_{10}$ and applied to the Clinch River and are reduced to $^1/_{30}$ for bone as critical organ and to $^1/_{100}$ for total body as critical organ and applied to the Tennessee River.

skeleton and total body, respectively. The Tennessee River is used as a municipal water supply, and, consequently, the 14-year-old is the likely critical population group. The cumulative dose from drinking water is as previously described. The radiation dose from recreational use of the environment (listed in Table 7.4) is based on the following assumptions: (1) an exposure time of 100 hr per year; (2) an attenuation of bottom sediment radiation by 3 ft of water; (3) the use of the average concentrations of radionuclides found in water and sediments to estimate dose for periods where data are lacking; and (4) the adsorption of beta particles by the flesh of man, thus limiting the exposure of the skeleton to gamma radiation. Only the feet of the swimmer would frequently be subjected to the total radiation from contaminated bottom sediments, but even this would not be expected to exceed about 30 times the dose given in Table 7.4 for recreational use of the river. Occupational exposure from work within a water treatment plant is not significantly different from background radiation and is not considered in these calculations.

The likely dose due to consumption of contaminated fish is even more difficult to define. As previously mentioned, the fraction of maximum permissible intake attained by standard man from consuming 37 lb per year of the flesh of contaminated bottom feeders is about equal to that from drinking untreated water. However, the average fish consumption in the South is only 24 lb per year. As a first approximation (and a likely upper limit) we assume the total dose from eating Clinch River fish is $^{24}/_{37}$ of the dose due to drinking Clinch River water continuously and amounts to 1.8 rems and 0.14 rem to the skeleton and total body, respectively. We further assume that bottom feeders taken from the Tennessee River are diluted with other East Tennessee fish and result in a total dose of 0.07 rem to the skeleton and 0.0057 rem to the total body. As a consequence of discharging radioactive wastes to the Clinch River, the estimated cumulative dose to the skeleton of the 18-year-old utilizing the Clinch River is largest at 3.2 rems. The estimated dose to the skeleton of the 14-year-old residing along the Tennessee River is 0.45 rem. In all cases the dose estimate to the critical organs is less than one-tenth of the maximum permissible dose. The cumulative doses are believed to be high as a result of the conservative assumptions made in their estimation. When better information is factored into the calculations, a reduction is expected in the likely dose received.

8. Related Cooperative Projects

GEOLOGIC AND HYDROLOGIC STUDIES BY THE U.S. GEOLOGICAL SURVEY

A generalized soils map of the White Oak Creek Basin and an explanatory text that describes the soil characteristics and associated geologic units was issued.

COOPERATION OF OTHER AGENCIES IN ORNL STUDIES

The research and development program of the Radioactive Waste Disposal Section of this Division is of special interest to various public and private agencies. Several study projects provide an opportunity for others to participate, both to supplement the Laboratory's research effort and to gain information and experience of value to the other agency. The ways in which another agency may cooperate include assignment of on-loan personnel as temporary additions to the ORNL staff, performance of specific work under cooperative agreements to augment ORNL programs, work authorized under ORNL subcontracts and performed by the contracting agency, or coordination of related work projects with ORNL projects for mutual benefit.

Clinch River Study

This is a cooperative study under the guidance of the Clinch River Study Steering Committee, which coordinates arrangements for participation of the agencies represented by membership on the committee. These include, in addition to ORNL, the U.S. Geological Survey, the U.S. Public Health Service, the Tennessee Valley Authority, the Tennessee Department of Public Health and Stream Pollution Control Board, the Tennessee Game and Fish Commission, the Divisions of Reactor Development and Biology and Medicine of the U.S. Atomic Energy Commission, Washington, D.C., and the Biology Division of the U.S. Atomic Energy Commission, Oak Ridge Operations. The activities of the Steering Committee, participation by the several agencies, and the results during the past year are presented in Chap. 4.

Disposal in Salt Formations

Agencies participating in this program during the past year have included the U.S. Bureau of Mines and the Carey Salt Company of Hutchinson, Kansas, an ORNL subcontractor. The results of this cooperative program are given in Chap. 3.

Disposal in Deep Wells

The subcommittee of the Committee on Research of the American Association of Petroleum Geologists published its study of the deep sedimentary basins of the United States to identify those best suited to radioactive waste disposal. Cooperation between this group, the U.S. Geological Survey, and ORNL had been active but informal. The introduction to the report had been written by a staff member.

VISITING INVESTIGATORS FROM ABROAD

During the year, one noncitizen guest completed his assignment as a temporary member of the research staff of the Radioactive Waste Disposal Section. Mohammad Unis Shaikh of Pakistan completed his thesis on an experimental and theoretical study of the flow of fluids through porous media in a five-spot array.

NUCLEAR SAFETY REVIEW

One member of the Section served on the staff of *Nuclear Safety* as assistant editor. During the year, several individuals in the Section contributed review articles which were published under the category "Consequences of Activity Release."

HEALTH PHYSICS JOURNAL

One member of the section served as assistant news editor for the United States.

COMMITTEE WORK

American Standards Association

Several members of the staff of the Radioactive Waste Disposal Section have continued to serve on working groups of ASA Sectional Committee N5, Nuclear Fuel Cycle Engineering, its subcommittee N5.2, Radioactive Waste Disposal, and working group N5.2.2, Site Selection Criteria.

ASCE – Committee on Sanitary Engineering Aspects of Nuclear Energy

The section leader served as a member of the Committee on Sanitary Engineering Aspects of Nuclear Energy of the American Society of Civil Engineers.

PARTICIPATION IN EDUCATIONAL PROGRAMS

During the ten weeks of field training of the AEC Fellowship course in applied radiation physics at ORNL, three students were assigned to work five weeks in the Radioactive Waste Disposal Section under the supervision of four staff members.

The course in physical geology conducted by ORSORT, given again by one member of the Radioactive Waste Disposal staff, comprised approximately 30 lectures to a class of about 40 students, some American and some from other countries.

Four lectures and a field tour of the Laboratory's waste disposal facilities and ecological research activities were provided at ORNL by the staff of the section as part of the course conducted by the U.S. Public Health Service on "Reactor Safety and Environmental Health Problems."

NUCLEAR SAFETY INFORMATION CENTER

Two members of the section served as part-time staff members of the Nuclear Safety Information Center.

Part II. Radiation Ecology

S. I. Auerbach

9. Radiation Effects and Radioactive Waste Area Studies

S. I. Auerbach[1]
G. N. Brown[1]
D. A. Crossley, Jr.
J. W. Curlin[1]
P. B. Dunaway
J. M. Inglis[2]
E. F. Menhinick
J. A. Payne
D. E. Reichle[3]
A. F. Shinn
J. P. Witherspoon[1]
Gladys J. Dodson
Lovell L. Lewis
T. P. O'Farrell[4]
M. H. Shanks
J. D. Story
F. G. Taylor, Jr.[1]

VEGETATION STUDIES AROUND THE HPRR

J. P. Witherspoon F. G. Taylor, Jr.

Initial studies on the effects of radiation on trees around the Health Physics Research Reactor (HPRR) were reported last year. Mortality and growth anomalies were observed out to 20 m from the reactor. Additional studies through the 1964 growing season showed radiation damage patterns extending into the forest up to 45 m from the reactor and covering an area of about 1200 m^2. Damage to deciduous species was confined to trees growing from 10 to 25 m from the reactor, where integrated fast-neutron doses (tissue dose in air) were 1273 to 197 rads delivered sporadically over a period of one year and two months. Beyond 25 m only pine trees (*Pinus virginiana* Mill.) were visibly affected. At the end of the 1964 growing season, 153 terminal shoot samples were collected from 26 pine trees growing from 25 to 80 m from the reactor. Shoot and needle lengths were measured to ascertain 1964 growth. Figure 9.1 shows the relationship between 1964 average needle length and distance of sampled trees from the reactor.

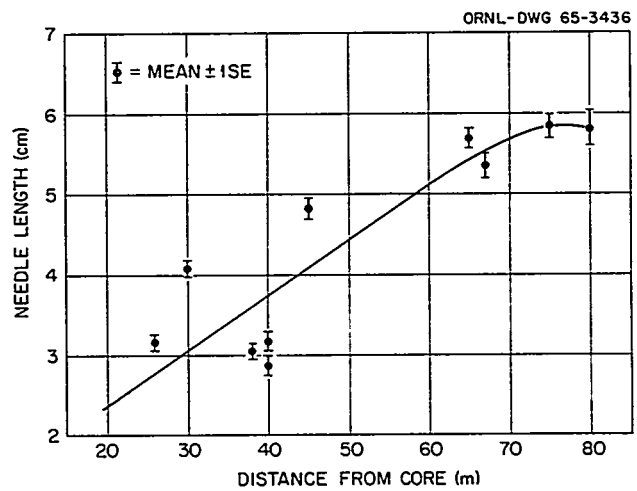

Fig. 9.1. Length of 1964 Virginia Pine Needles vs Distance of Trees from Reactor.

Trees within 40 m had needles which fell below the length (4 to 8 cm) characteristic of this species. This growth retardation occurred in an integrated dose range of 102 to 248 rads delivered over a one year and four month period. Needles sampled from 45 to 80 m (79 to 20 cumulated rads) fell within the normal range of lengths for this species. Shoot lengths averaged 3.7 cm ± 0.7 SE for trees growing between 25 and 40 m and 6.1 ± 0.3 cm for trees from 45 to 80 m from the reactor.

[1]Dual capacity.
[2]ORINS Summer Research Participant, 1964.
[3]AEC Postdoctoral Fellow.
[4]AEC Graduate Fellow.

Trees growing on exposed, eroded edges of the forest had more foliage growth retardation than trees within the forest, thus suggesting an interaction between radiation effect and poor site conditions. By the end of September 1964 mortality of needles was evident in almost all pines growing within 40 m.

As reactor operations continue, patterns of radiation damage are expected to extend deeper into the forest in the case of conifers, and the more resistant deciduous species can be expected to exhibit anomalous growth or phenological patterns.

RADIATION STUDIES ON FOREST TREE POPULATIONS

J. P. Witherspoon J. W. Curlin

Studies of the effects of gamma or fast-neutron radiation on experimental plant populations continue to provide information useful in interpreting or predicting radiation damage to forests, such as that surrounding the DOSAR. Moreover, these studies serve to ascertain the importance of environmental, population, or seasonal factors which may modify plant responses to ionizing radiation.

Potted seedlings of two-year-old scrub pine (*Pinus virginiana*) received acute ^{60}Co gamma doses of 388, 562, and 900 rads to their shoots. These plants and controls were maintained at 68°F nights and 86°F days (16 hr at 3700 ft-c) in a plant growth chamber. Soil moisture levels were varied with pots receiving no water, 150 ml/week (50 ml thrice weekly), and 450 ml/week (150 ml thrice weekly). During the study apical needle moisture content was determined [(wet wt – dry wt)/dry wt] until it dropped below 65%, a point below which no seedlings survived. Plants in all dose groups and controls reached this needle moisture level in 19 to 21 days in the "no water" group, and no significant difference was found between radiation treatments. In groups receiving 150 ml/week (moisture stress), plants in the 562- and 900-rad treatments required 55 to 64 days to reach the 65% end point, while those in the 388-rad and control groups required only 49 to 52 days. Plants in the higher-dose groups may have required less water due to physiological impairments, therefore surviving the moisture stress for a longer period. In the groups receiving 450 ml/week (adequate water), controls and plants receiving the 388-rad treatment maintained relatively constant needle moisture, while those in the 562- and 900-rad groups showed a linear decrease in moisture content with time at the rate of 0.6 to 1.0%/day, respectively, for 60 days. Needle desiccation rates indicated that for a month following a near-lethal radiation stress, addition of a moisture stress may not augment the radiation effect. At lower doses, however, the two stresses may be additive initially. After a two-month period the effect of the two stresses was additive in all cases.

Dormant stem cuttings from ten clones of *Populus deltoides* Marsh. (Eastern cottonwood), representing seven ecotypes from Alabama and one ecotype each from Mississippi, Kentucky, and Illinois, were given an acute ^{60}Co gamma radiation dose of 7600 rads. These irradiated cuttings, along with controls from each clone, were placed in aerated nutrient solutions and maintained under constant environmental conditions in a plant growth chamber. Clones were scored for time of leaf emergence, callus formation, and root emergence. Shoot height was measured during the initial rapid growth phase (20 days), and shoot and root biomass was measured on harvested plants. Statistically significant (1% level) differences in growth rate, biomass, and size were found between control clones. This was presumably related to genetically controlled growth factors in the clones. Statistically significant growth differences also were found between irradiated clones. Average retardation of shoot height ranged from 60 to 85% of control clones; shoot biomass reduction, 64 to 95%; inhibition of callus formation, 0 to 45%; and root biomass reduction, 56 to 100%. Formation of callus tissue was least affected, while root production was most affected. A linear relationship was found between clonal growth performance and radiosensitivity. Clones which exhibited the best growth were more radiosensitive when irradiated in the dormant condition. Histological examination of apical meristematic tissue showed interphase nuclear volumes of 78 to 90 μ^3, suggesting no nuclear basis for differential radiosensitivity of clones. Figure 9.2 illustrates the growth responses of two populations, both from Alabama. Although each population had its growth in height reduced about 60% by an acute

dose of 7600 rads, the irradiated A-8 population does not differ significantly in height from the control A-13 population under identical growth conditions. If, by chance, control individuals of the A-8 population were compared experimentally with irradiated individuals of A-13, the apparent shoot height reduction would be 81%. If, on the other hand, A-13 controls were, by chance, compared with irradiated A-8, the growth reduction would be only 17%. These ecotypic variations in growth phenomena serve to illustrate the amount of variations possible in response to radiation by various populations of the same species. Many of the widely used criteria of radiosensitivity such as degree of ploidy, nuclear volume, age, size, etc., would not lead one to predict such variations.

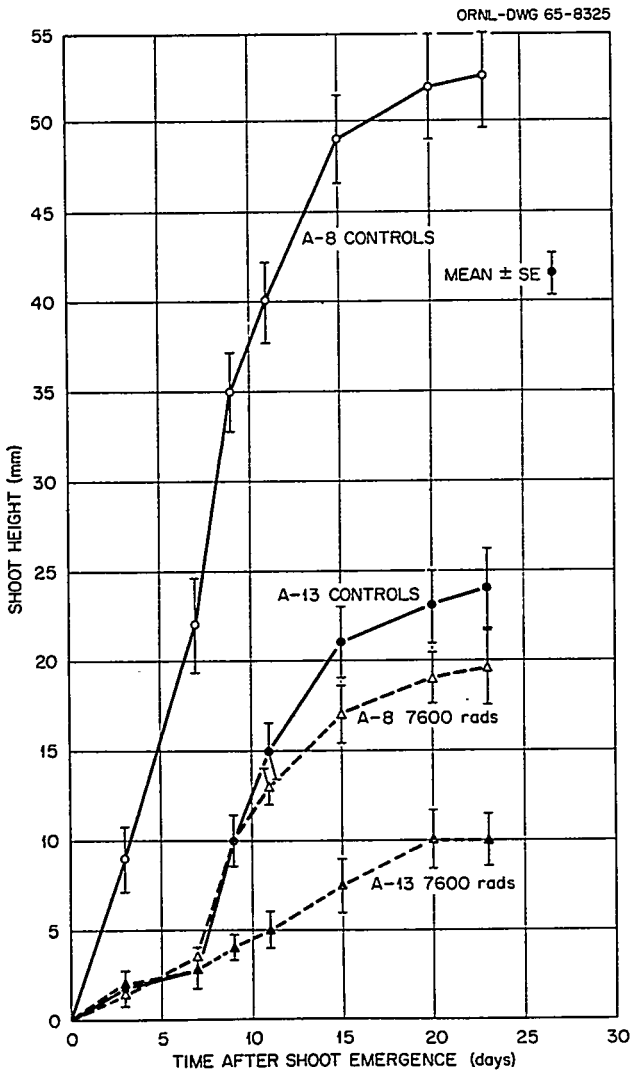

Fig. 9.2. Mean Shoot Growth of Two Populations of Eastern Cottonwood After an Acute Gamma Irradiation of 7600 rads.

The extent to which irradiated roots may affect shoot response to irradiation is usually unknown in plant experiments. In studies with potted plants this information may help explain variation in apparent shoot damage such as desiccation of foliage. Bundles of two-year-old seedlings of *Pinus strobus* were irradiated with 900 rads of ^{60}Co. One group received only shoot exposures; another, only root exposures; and a third group received both root and shoot exposures. Needle moisture, length, and mortality were measured for six months. Needle moisture reached critical levels first (after two weeks) in groups in which roots were irradiated. Plants with both root and shoot exposures showed needle mortality after one month. Data on plant damage following root irradiation and additional dosimetry experiments in soil and root systems of potted plants indicate that pot size may affect dose delivered to root systems and introduce variability in shoot biological end points.

BIOCHEMICAL MECHANISMS INFLUENCING EFFECTS OF IONIZING RADIATION AND OTHER ENVIRONMENTAL FACTORS

G. N. Brown F. G. Taylor, Jr.

Radiosensitive mechanisms in plants apparent at levels of visible growth and differentiation should be reflected at molecular and subcellular levels. These molecular and subcellular effects should appear at an earlier time than ultimate developmental responses. In order to better understand these responses to radiation, both the visible effects and the preceding subcellular effects are being analyzed together. Biochemical mechanisms presently being investigated include protein synthesis and photosynthetic mechanisms.

Previous studies[5] using mimosa (*Albizzia julibrissin*) indicated a correlation between soluble ribonucleic acid (sRNA) base compositions and temperature-controlled growth rates (Fig. 9.3).

[5]G. N. Brown, *Plant Physiol.* 40, 557 (1965).

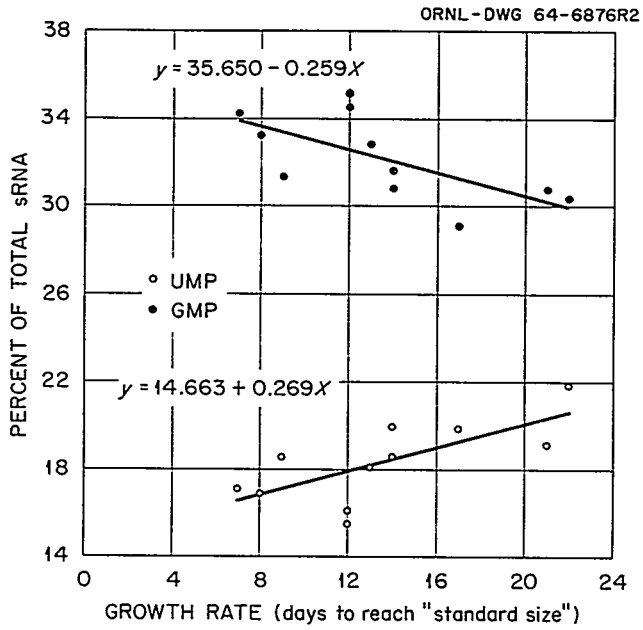

Fig. 9.3. Relationship Between Growth Rate and Soluble Ribonucleic Acid Guanylic Acid (GMP) and Uridylic Acid (UMP) in Mimosa Seedlings.

Since stem elongation is visibly affected following fast-neutron irradiation, normal sRNA characteristics might be altered relatively earlier during this postirradiation period. Any changes in sRNA base compositions suggest differential synthesis of sRNA molecules which would be reflected in both the quantitative and qualitative characteristics of the proteins and enzymes synthesized. Such shifts in enzyme properties would result in visible growth effects and might eventually clarify interactions of radiation and other factors.

Nine-day mimosa seedlings were given a total dose of 1350 rads (tissue dose in air) of fast neutrons delivered over a period of 47 min. Epicotyls of irradiated and controlled mimosa seedlings were excised at three-day intervals following irradiation. Soluble and total RNA were extracted, and total quantities determined. Base compositions were calculated. Finally, amino acid acceptance tests were done for samples of sRNA. Purity of sRNA extracts from ribosomal breakdown products was checked by determination of sedimentation coefficients (3.18), amino acid acceptances, and individual base ratio differences.

The data suggest that levels of sRNA do not differ between irradiated and control seedlings, while levels in both decrease slowly as a result of aging (0.8 to 0.4% sRNA/dry weight from 9 to 19 days respectively). Base compositions varied, with relative guanine and cytosine concentrations in irradiated seedlings showing immediate increases, and uracil and adenine corresponding decreases, as compared to controls. Changes in concentrations of sRNA bases from time of irradiation to six days postirradiation were as follows:

	Percentage of Concentration at Time of Irradiation			
	Adenine	Cytosine	Guanine	Uracil
Irradiated	−10.5	+17.0	+2.8	−14.3
Control	−3.0	−6.8	0.0	−9.3

All base concentrations leveled off after six days postirradiation. Correlations of base compositions with growth rates[5] suggest an immediate flush of growth in the irradiated seedlings. No correlations between time following irradiation and amino acid acceptance of sRNA extracts have been found to date.

These variations in sRNA base compositions suggest shifts in mechanisms or sRNA synthesis and later protein synthesis following irradiation. Such changes in patterns of protein synthesis could result in phenological alterations in mimosa.

Photosynthetic responses to ionizing radiation have been of interest to many radiation biologists. However, effects on specific metabolic reactions have been ignored for the more gross measurements involving CO_2 and O_2 exchange in closed chambers following plant irradiations. In order to pinpoint locations of radiosensitivity in photosynthetic mechanisms, enzymatic conversions of sugars and fixation of CO_2 must be examined.

Two-year-old yellow poplar (*Liriodendron tulipifera*) seedlings received 3000 rads over a two-day period from a ^{60}Co source. At three-day intervals following irradiation, seedlings were placed in closed chambers and subjected to an atmosphere of $^{14}CO_2$ under controlled light intensities. Plants were removed from the chambers at time intervals of 1 to 10 min following the introduction

of $^{14}CO_2$ and immediately frozen for later sugar and amino acid extraction. The sugars and amino acids were separated and quantitatively determined to detect points of accumulation or depletion. Thus far, a large chamber enabling effective, rapid $^{14}CO_2$ generation and uptake has been designed, and present techniques for sugar and amino acid extraction and separation have been modified for use with yellow poplar leaf material. Processing of data and analysis are still under way.

Should significant accumulations of metabolites be found following plant irradiation, an enzymatic pathway inhibition will be indicated at the next step beyond the accumulation point. On the other hand, should depletion of a metabolite be found, an inhibition of the step preceding this metabolite will be indicated, or possibly a modified shuttle pathway which would drain off the depleted metabolite. Such observations should aid in pinpointing radiosensitive steps in photosynthetic molecular pathways.

SEASONAL CHANGES IN RADIOSENSITIVITY IN PLANTS

G. N. Brown F. G. Taylor, Jr.

Photoperiod (day length) is a seasonal variable in the natural environment, and many plant mechanisms respond to changes in photoperiod. Among these photoperiodic mechanisms are flower differentiation and seed production. Any interaction between photoperiodic mechanisms and even brief sublethal exposures to ionizing radiation could modify normal flower differentiation and alter the seed populations available for growth the following year.

Experiments were designed to investigate the interaction of ionizing radiation with short-day-length treatment, which is critical for flowering in cocklebur (*Xanthium chinense* Mill.). Seedlings were grown for 70 days at 68°F night and 80°F day temperatures, at 90% relative humidity, and were given 17 hr of light per day. The photoinduction period consisted of 12 hr of light per day for five days. Ten-week plants were separated into four groups: those irradiated before, during, and after photoinduction, and those not receiving short-day treatment. Nonirradiated controls also included photoinduced and noninduced plants. Each irradiated group received 5000 rads of gamma radiation from a ^{60}Co source over a five-day period.

Photoinduced plants receiving radiation produced more stem growth than nonirradiated controls, while noninduced irradiated plants did not differ from corresponding controls. Irradiated plants of all four groups produced more leaves than controls. Production of floral buds in plants irradiated before photoinduction did not differ significantly from controls, while those irradiated during photoinduction permanently produced significantly fewer bands, and those irradiated after photoinduction temporarily produced more (Fig. 9.4).

A second experiment was designed to investigate differential radiosensitivity during either the dark or light period of photoinduction in cocklebur irradiated simultaneously with photoinduction. Both the dark- and light-irradiated plants showed a flush of vegetative growth over the nonirradiated, but photoinduced, controls. Results at 27 days postirradiation (stem elongation: night – 2.9 times controls; day – 1.8 times controls) indicate that plants irradiated only during the light period show an inhibition in flowering as compared to controls (0.2 to 0.7 flower per plant respectively), while plants irradiated only during the dark period show an initial stimulation (1.6 to 0.7 flower per plant respectively). Future results should elucidate differential radiosensitivity of flowering in *Xanthium*, depending on whether plants are irradiated during the dark or light period of photoinduction.

The average interphase nuclear volumes and estimated chromosome volumes (nuclear volume/somatic chromosome number) of 14 local tree species have been determined from January to December 1964 to aid predictions of changes in radiosensitivity of trees and plant communities under field conditions. Seasonal changes in nuclear volumes suggest that both coniferous and deciduous trees are most radiosensitive between April and September (Fig. 9.5) during active division of shoot meristem cells and formation of new DNA. The ratios of the changes in average nuclear volume and chromosome volume, actively growing to dormant plants, varied from 1.2 to 2.0 in species, indicating a wide range in interseasonal radiosensitivity. Information of this nature is needed in interpreting plant radiation experiments and in predictions of sensitivity which previously made little or no allowance for intraseasonal growth.

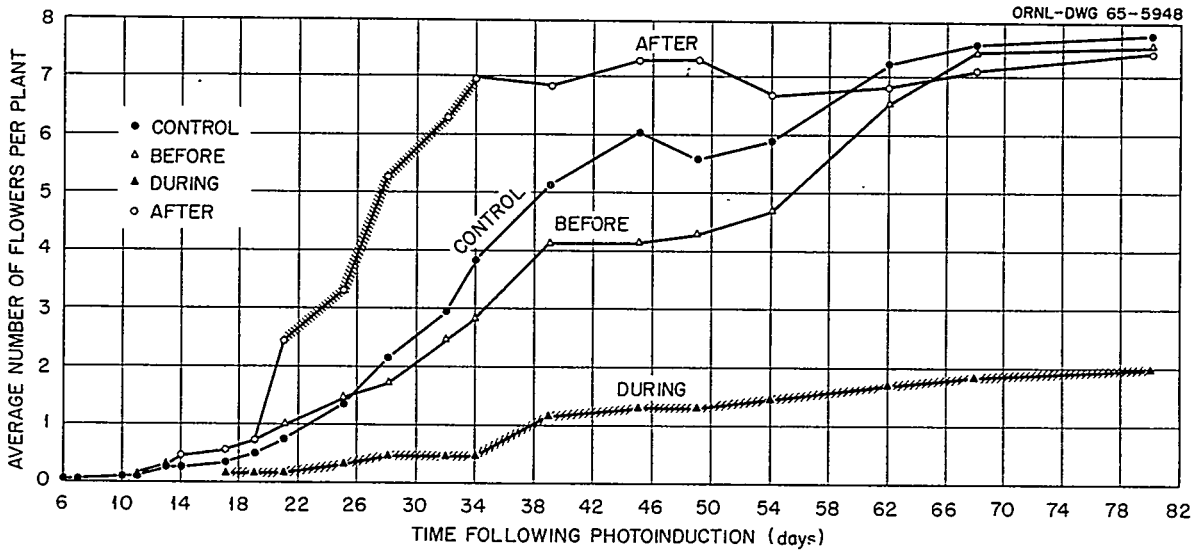

Fig. 9.4. Photoinduced Cockleburs Which Were Gamma Irradiated Either Before, During, or After Photoinduction. ++++++++++ = significantly different from controls at 5% level.

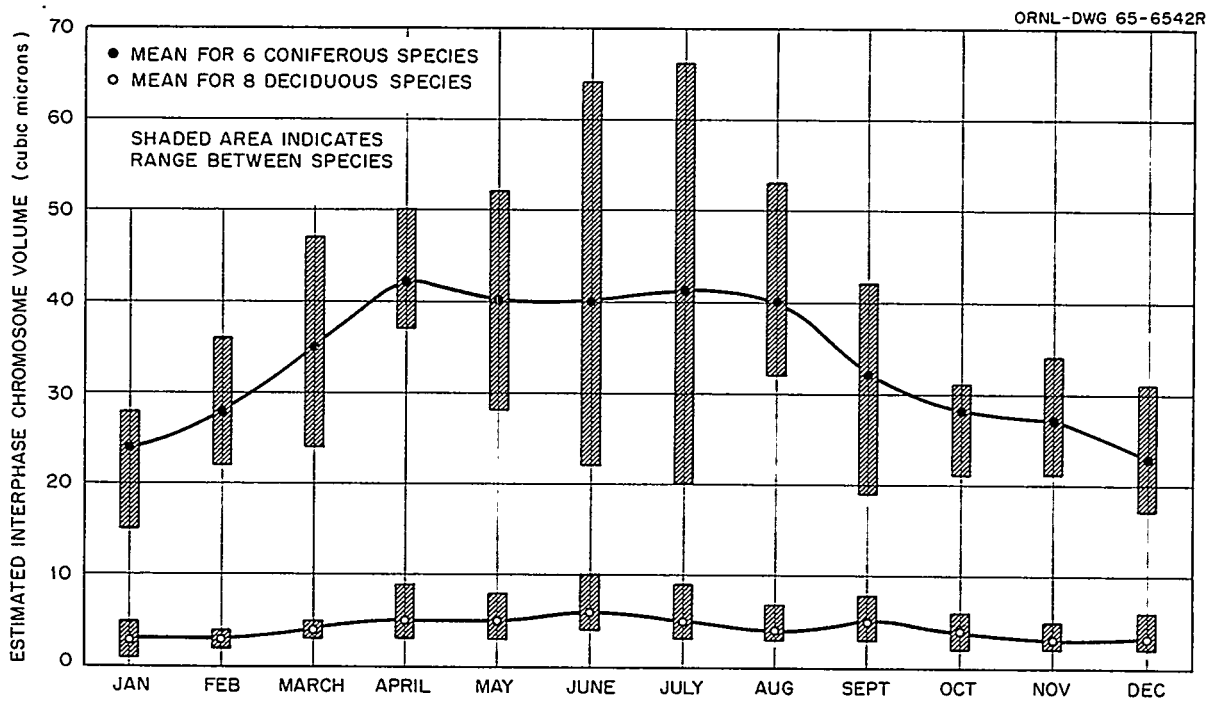

Fig. 9.5. Seasonal Changes of the Estimated Volume, in Cubic Microns, of the Interphase Chromosome of 14 Representative Coniferous and Deciduous Tree Species at Oak Ridge, Tennessee (1964).

MINERAL UPTAKE MECHANISMS AFFECTED BY GAMMA RADIATION

G. N. Brown F. G. Taylor, Jr.

Mineral uptake by plant roots and translocation to leaves involve several physiological mechanisms. Growth retardation by ionizing radiation may affect mineral uptake, or growth may be inhibited by impairment of mineral uptake mechanisms. An experiment has been initiated to determine effects of fast-neutron irradiation on uptake of ^{65}Zn from the soil. Zinc-65 was chosen since zinc participates metabolically in the synthesis and activity of plant growth hormones. Also zinc has a soil exchange capacity favorable for plant uptake studies. Two groups of potted red oak (*Quercus rubra*) seedlings (three years old) received shoot irradiations of 505 and 1011 rads, respectively (tissue dose in air), of fast neutrons delivered over a period of 8 min. Potted soil of irradiated plants and controls was inoculated with 50 μc of ^{65}Zn per pot. Leaf disks for radioanalysis and growth measurements were taken twice weekly. Preliminary data at nine days postirradiation suggest that plants receiving the lower level of radiation have initially greater ^{65}Zn uptake than controls (5.92 counts per leaf disk as compared to 1.59), while the higher-level plants and controls do not differ (0.92 and 1.59 counts per leaf disk respectively). Both levels of irradiation inhibited stem elongation and leafing out but produced no anomalous leaves.

Since temporary growth stimulation is frequently seen in plants subjected to low-level irradiation, the higher ^{65}Zn uptake in this group might have been expected as a result of increased growth and not as a direct response to radiation. However, since an immediate growth flush has not been observed at the lower level of irradiation in this experiment, it suggests that uptake or translocation mechanisms may be directly affected by fast-neutron irradiation at lower doses.

TRANSPORT OF RADIOACTIVE MATERIALS BY MUD-DAUBER WASPS

A. F. Shinn M. H. Shanks

A survey of the ORNL area and the general vicinity of the waste disposal area of the adjoining AEC Reservation was conducted to determine the distribution of radioactive mud-dauber nests. The rarity of radioactive nests of the pipe-organ dauber and the relative abundance of radioactive nests of the black-and-yellow dauber in the waste disposal area have already been reported.[6] During the past year a relatively large number of old radioactive nests of the pipe-organ dauber were uncovered at a single locality along with a few others at scattered localities.

Radioactive pipe-organ nests were found at the following places: (1) east and west seepage from waste pit 4; (2) White Oak Creek gaging station; (3) ^{137}Cs-tagged poplar forest; (4) White Oak Lake boathouse; and (5) White Oak Dam. The gamma activity of pipe-organ nests was a maximum of 1000 pc/g at (3), (4), and (5), and was one-fourth to one-hundredth that of black-and-yellow dauber nests at the same sites. The nests at (2) gave gamma activity up to 11,600 pc/g, but no clump nests were available for comparison. At (1), about 58 nests were discovered hidden under the false bottoms of two monitor cabinets. One nest had been made in the summer of 1964, but the rest could be dated no closer than summer 1962 or earlier because of the lack of gamma assays for muds from previous years. The gamma activity was almost exclusively from ^{106}Ru-^{106}Rh. Figure 9.6 shows the distribution of the radioactivity among nests. Mud from temporary puddles, formed

[6] A. F. Shinn, *Health Phys.* 10, 618 (1964).

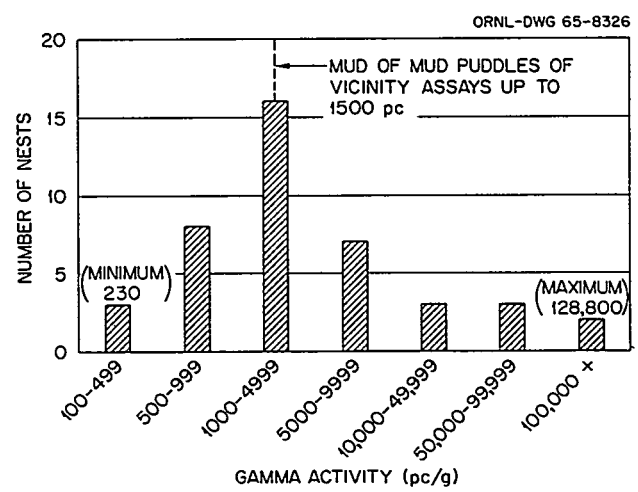

Fig. 9.6. Gamma Activity in Pipe-Organ Dauber Nests from East and West Seeps.

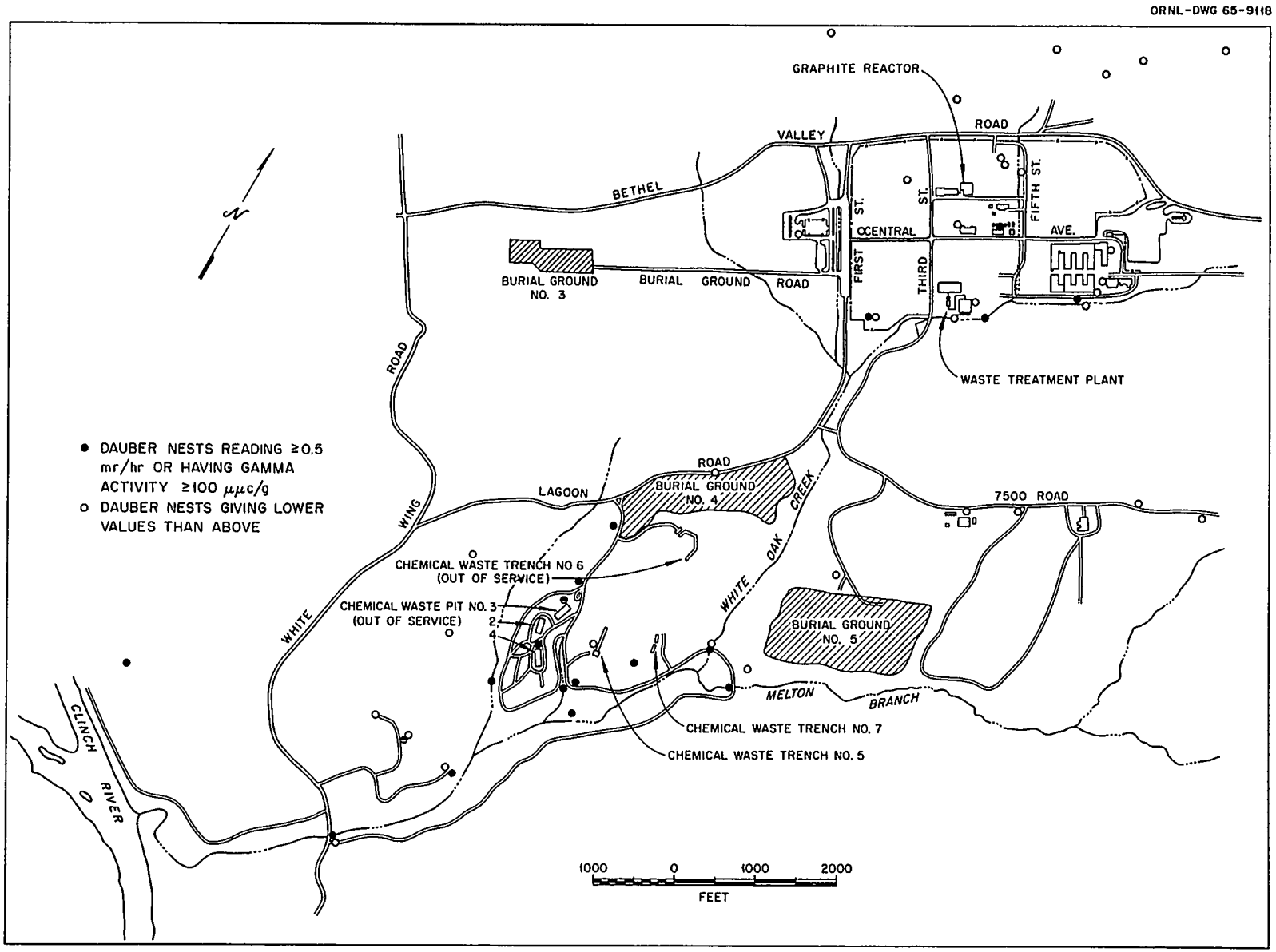

Fig. 9.7. Locations of Mud-Dauber Nests Surveyed for Radioactivity on the ORNL Area and the AEC Reservation.

in the vicinity of the seep after a rain, assayed 1500 pc/g gross gamma activity. Forty percent (17 of 42) of the nests exceeded this level of radioactivity, which suggests that their source of mud was the radioactive seeps from the waste pits. An explanation for this use of radioactive mud may be that in a period of drought the pipe-organ dauber may use contaminated mud because it is the only mud available.

The results of the survey of ORNL and the AEC Reservation are shown in Fig. 9.7. In contrast to nests found in the waste disposal area, which gave survey meter readings as high as 1 r/hr, those from the ORNL area were mostly less than 0.5 mr/hr, with a maximum of 2 mr/hr. Nests in the ORNL area are often secreted among objects or between walls which then act as effective shields for the low level of radiation from the nests.

RADIOCESIUM RETENTION BY SUCTORIAL INSECTS

D. A. Crossley, Jr. Gladys J. Dodson

Previous studies have applied radiocesium turnover in insect communities as a means of measuring feeding rates and metabolic rates, as well as estimating food chain transfer of ^{137}Cs. An observed relationship between size of insect and biological half-life (T_b) for cesium was used to derive an average T_b for the entire insect community on herbaceous vegetation on White Oak Lake bed. However, the community T_b was based on experiments with insects having chewing mouthparts. Since preliminary results showed that suctorial insects may have longer retention times than chewing species, experimentation has been performed on radiocesium retention by insect species with suctorial mouthparts.

For retention studies with the bean aphid, *Aphis fabae*, tagged nasturtium plants were utilized. Seedlings were placed for 18 hr in nutrient solution containing 1.1 μc of ^{134}Cs per milliliter. Activity density for the seedlings thus tagged was about 1.5 μc per plant, with satisfactory distribution of tracer among the plant parts (0.95, 0.71, 0.90 μc per gram of fresh weight in roots, stems, and leaves respectively). After tagging, seedlings were transferred to untagged nutrient solution or were repotted in soil. Aphids then were transferred to the seedlings, and their radioactivity was measured through time. Results showed that there was a marked daily fluctuation in radiocesium content of the aphids, which may have been the result of diurnal changes in transpiration rate in the nasturtium seedlings. Biological half-lives were estimated by transferring the aphids to untagged, potted nasturtium seedlings and following their radiocesium loss rates.

Milkweed bugs (*Oncopeltus fasciatus*) were supplied with drinking water containing 1.63 μc of ^{134}Cs per milliliter. After three days the tagged water was replaced with untagged, and the retention of radiocesium was measured through time.

Both of the species had elimination rates slower than predicted on the basis of size. Based on the size-T_b relationship for chewing insects, *Oncopeltus* (fresh weight, 75 mg) was predicted to have a T_b of 18 hr, but the measured T_b was 35 hr. For *Aphis*, expected and measured values for T_b were 5 and 14 hr respectively. Both species showed a single-component elimination pattern. The copious fluid intake by suctorial insects evidently has led to ion conservation mechanisms which enhance radiocesium retention. Future studies of large insect communities may require that suctorial and chewing insects be handled separately.

RADIATION SENSITIVITY OF INSECTS

E. F. Menhinick Gladys J. Dodson

Information on the comparative radiosensitivity of different species of insects would be useful to estimate ranges in sensitivity of species not examined. No general principle for predicting radiosensitivity of insects has thus far been elaborated (similar to the nuclear volume method for higher plants).

Thirteen species of insects and other terrestrial arthropods were irradiated in a ^{60}Co source at 3 or 30 kr/min and given total doses of 1 to 512 kr in 100% increments. Insects were maintained at 28°C, and records were kept on mortality until all organisms were dead. In contrast to the study of radiation profiles, effects were expressed as median life expectancy corrected for control mortality. This was necessary because of the wide variation in life expectancies of the different examined species.

A dose of 512 kr was immediately lethal to all species except dermestids. A dose of 256 kr killed all species immediately except dermestids, *Crematogaster, Oncopeltus, Tenebrio,* and *Blatta.* None of the species were immediately killed by 128 kr. Lower doses resulted in longer life expectancies. Life expectancy was significantly lower than control for all species exposed to 8 kr or more. Most species were affected by 4 kr; *Acheta* and *Crematogaster* were affected by doses as low as 2 kr. However, several species exposed to 1 kr outlived controls.

To compare radiation sensitivity of different species, the median life expectancy corrected for control mortality was examined for doses of 8, 16, and 32 kr (Table 9.1). With three exceptions, life expectancy decreased with increasing dose. Species in Table 9.1 are arranged according to increasing sensitivity, with the most sensitive forms toward the bottom of the list. Life expectancy varied from 1.9 days (*Periplaneta* exposed to 32 kr) to 83 days (*Armadillidium* exposed to 8 kr). Most species given doses of 8 kr or more lived less than 20 days.

Attempts were made to correlate radiosensitivity with other characteristics of the species; such correlations would be useful in predicting sensitivity of species not examined. This information would enable evaluation of postattack insect problems and would be useful in control of insects by radiation. Related forms (those in the same order) varied in sensitivity as much as did those in different orders (Table 9.1). Therefore, there seemed to be little relation of sensitivity to taxonomic grouping. Comparison of sensitivity and wet weight of adult insects showed a very general trend in which larger forms were most sensitive, but unrelated forms having similar weight varied greatly in sensitivity (i.e., *Armadillidium, Sceliphron*).

Within each order, however, species weighing more were more sensitive. A striking example of this is seen with cockroaches. *Periplaneta* (937 mg) was more sensitive than *Blatta* (683 mg); and those two species were more sensitive than *Blattella* (102 mg) (Table 9.1). Likewise, larger Coleoptera were more sensitive than smaller ones. Further experiments are needed to establish whether these relationships are generally applicable to insects and to determine mechanisms of radiation damage.

Table 9.1. Arthropod Median Life Expectancy Corrected for Control Mortality

Taxon	Order	Wet wt (mg)	Median Life Expectancy (days)		
			8 kr[a]	16 kr[a]	32 kr[a]
Dermestid	Coleoptera	4	70.6	73.2	52.5
Armadillidium	Isopoda	76	83.0	44.5	23.3
Thermobia	Thysanura	23	72.5	28.0	11.0
Crematogaster	Hymenoptera	½	20.1	19.0	12.4
Blattella	Orthoptera	102	22.3	16.3	6.6
Oncopeltus	Hemiptera	56		9.5	10.5
Tenebrio	Coleoptera	53	21.0	13.4	8.8
Blatta	Orthoptera	683	22.2	13.0	3.4
Malacosoma	Lepidoptera	102		8.0	6.4
Sceliphron	Hymenoptera	107	15.2		
Acheta	Orthoptera	398	9.3	5.9	3.4
Harpalus	Coleoptera	152	4.3	6.0	3.0
Periplaneta	Orthoptera	937	4.7	3.0	1.9

[a]Exposure dose.

RADIATION PROFILES OF INSECTS

E. F. Menhinick Gladys J. Dodson

Laboratory studies describing the relative radiosensitivity of the various life history stages of insect species (radiation profiles) are a necessary first step in the interpretation of radiation effects on insect populations in contaminated areas. Different developmental stages of European brown crickets (*Acheta domestica*) and mealworms (*Tenebrio molitor*) were irradiated in a ^{60}Co source at 3 or 30 kr/min and given total exposure doses of 1 to 512 kr in 100% increments. Insects were maintained at 28°C. Effects were expressed as mean life expectancy.

Mean life expectancy was plotted as a function of exposure dose for different developmental stages of *Acheta* (Fig. 9.8). Life expectancy increased after small doses of radiation: with but one exception the different stages of *Acheta* exposed to 1 kr lived (on the average) longer than controls (Fig. 9.8). Examination of survival data shows that these irradiated insects began to outlive controls after 75 days for small nymphs, after 42 days for large nymphs, and after 19 days for adults. Threshold doses (doses causing statistically significant decreases in life expectancy) occurred between 1 and 2 kr for cricket nymphs and between 2 and 4 kr for adults. After a sudden initial drop in life expectancy, the dose-effect curves tended to become more linear (Fig. 9.8). Exposures to 256 kr immediately killed all nymphs and most adults; 512 kr killed all stages. Differences in mean life expectancy between the developmental stages of *Acheta* were most pronounced at total doses of 1 or 2 kr and disappeared at about 16 kr.

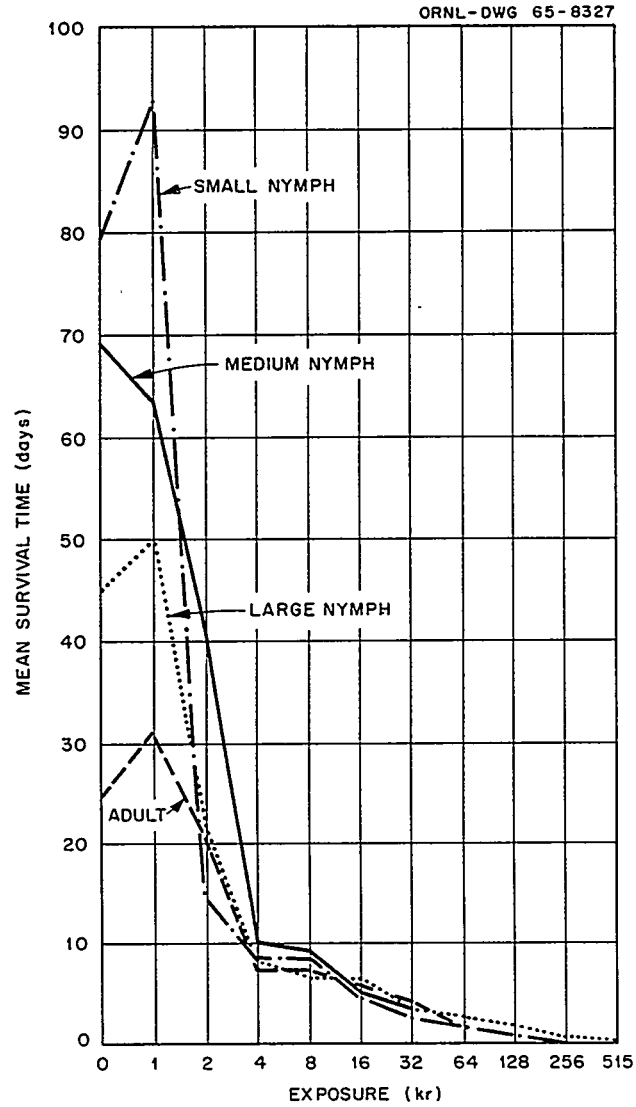

Fig. 9.8. Mean Life Expectancy of *Acheta* Exposed to Gamma Radiation.

Although *Tenebrio* larvae exposed to 1 kr had shorter life expectancy than controls, an increased life expectancy was observed in those exposed to 2 kr (Fig. 9.9). None of these differences were statistically significant, however. Threshold doses occurred between 2 and 4 kr for small and medium larvae and pupae, and between 4 and 8 kr for large larvae and adults. Mortality curves tended to level out from 4 to 16 kr, depending upon stage. Radiation profiles of *Tenebrio* exposed to 4, 8, and 16 kr showed that younger larvae were more sensitive than older ones (Fig. 9.9). Pupae and adults were more sensitive than larvae; after 32 kr, survival was similar for all stages. Immediate 100% mortality occurred around 512 kr, although some larvae survived for a short time at this large dose.

Between 4 to 64 kr, survival of *Tenebrio* pupae was about the same, approximately nine days. There was little change over this range, perhaps because death resulted from the same radiation injury. Irradiation of larvae did not appear to prevent pupation except when doses exceeded 64 kr. However, no pupae from irradiated larvae emerged as adults at doses higher than 4 kr.

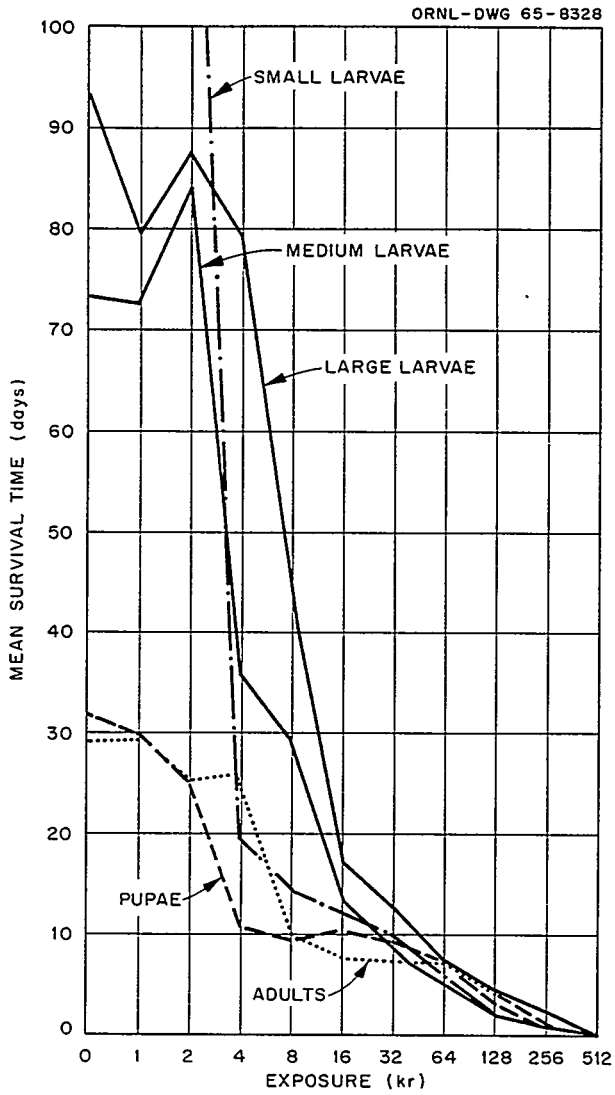

Fig. 9.9. Mean Life Expectancy of *Tenebrio* Exposed to Gamma Radiation.

Aberrations in the development of irradiated pupae presented striking examples of effect of dose. Pupae exposed to 2 kr developed into phenotypically normal adults. Pupae exposed to 4 kr, however, developed into adults having wings which were cracked and otherwise distorted, particularly on the ends. At 8 kr, wings were stunted to less than one-half of their normal length. At 16 kr, wings did not develop, and the emerged "adult" closely resembled the pupa except for leg development, which appeared to be basically normal. At 32 kr, development was usually prevented. No adults emerged from pupae irradiated at doses greater than 64 kr.

Dose-effect curves give some insight into mechanisms of radiation damage. Generally, mortality curves were composed of three components: (1) a slight increase in life expectancy at low doses, (2) a sharp decline at slightly higher doses, and (3) a gradual decline at increasingly higher doses. Increase in life expectancy, an apparently "beneficial" effect of low doses of radiation, has been observed since 1919.[7] This may be due to a slowing down of metabolic activity which would increase life expectancy of insects in much the same manner as lowering environmental temperature. Decrease in life expectancy following doses of 2 to 4 kr was probably due to the effect on most actively dividing cells. At higher doses (64 and 128 kr) paralysis of the insects indicated damage to the nervous system. Immediate mortality at 256 and 512 kr suggests that destruction of basic chemicals may have occurred.

RADIATION PROFILE OF THE EVERGREEN BAGWORM

D. E. Reichle

The responses of insect populations in irradiated ecosystems are important factors involved in the functional and structural stabilization of the system. Irradiations of natural landscapes could result in increased densities of herbivorous insects, owing to their relative radioresistance (both innate and that afforded by protected habitats), high potential rates of increase, and the possible alteration of predator populations. Laboratory studies describing the relative radiosensitivity of life history stages (radiation profiles) are necessary to evaluate critical periods in the life cycles of these species. The crucial considerations are the effects upon subsequent population sizes and, therefore, an emphasis on fecundity and egg survival as well as adult responses.

[7]W. P. Davey, *J. Exptl. Zool.* **28**, 447 (1919).

Bagworms are feeders upon a variety of plant species and have been selected as analogs for other lepidopterans. They offer the experimental advantage of large numbers and restricted clones. Cases containing eggs of the evergreen bagworm (*Thyridopteryx ephemeraeformis*) were collected in late winter and maintained in their overwintering state in the laboratory at 7°C. Dormancy was broken by raising the temperature to 30°C. Eggs, in replicated sets of 25, were irradiated in a ^{60}Co gamma source (exposure dose rate of 14.4 r/sec) at dose levels of $100(2^n)$, where $n = 1, 2, \ldots, 9$, and at increasing time intervals after breaking dormancy, thus permitting analyses of dose-age interactions.

The results of these experiments involving 4000 individuals are graphically illustrated in Fig. 9.10. Numbers of individuals hatching at each dose level were expressed as a percentage of controls for that egg stage. The mean hatching time for all controls was 14.1 ± 0.07 days. Mean percentage hatching of controls was 82.0 ± 3.9.

ORNL-DWG 65-8329

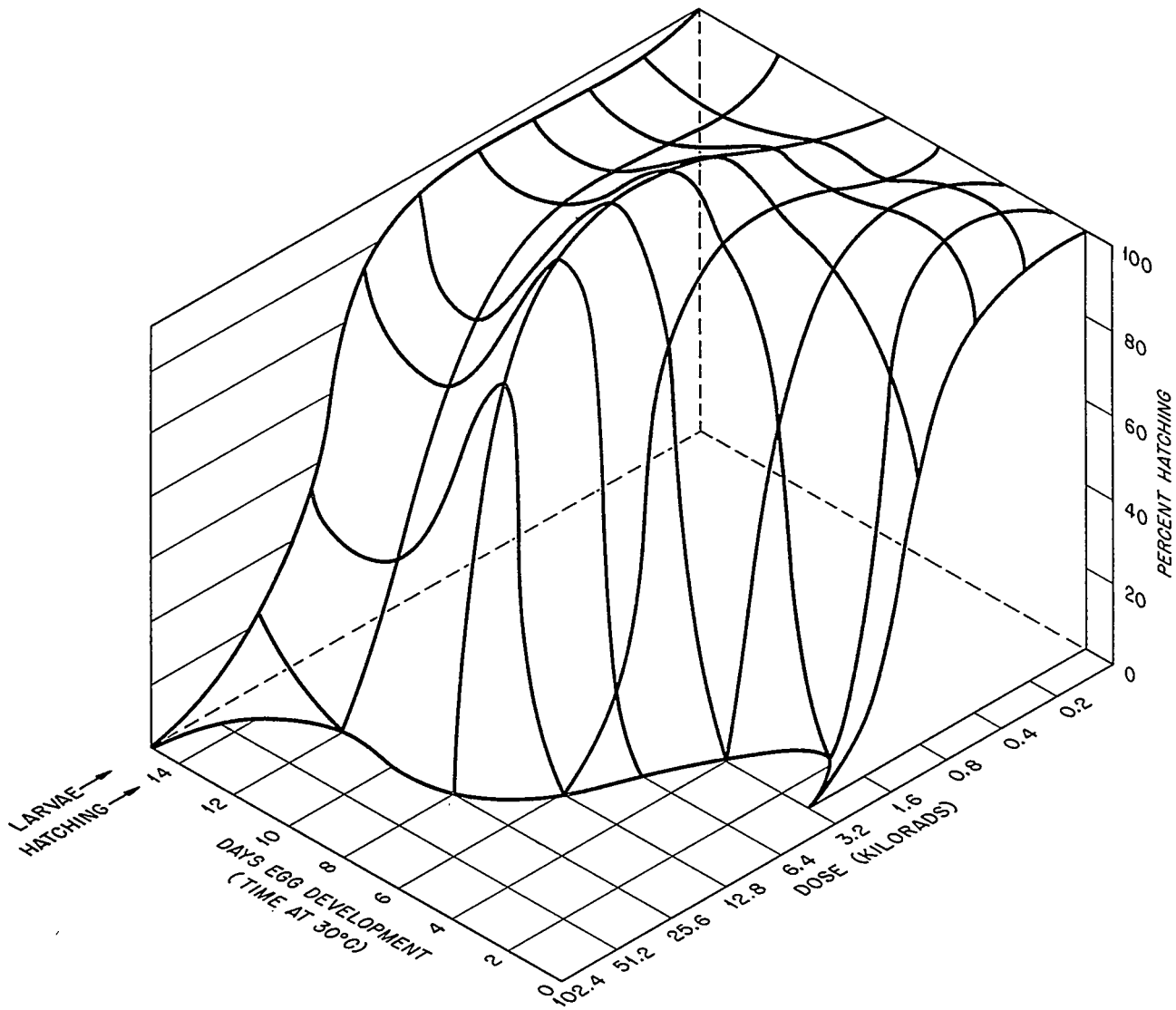

Fig. 9.10. Radiation Sensitivity of Bagworm Eggs.

Radiosensitivity decreased with increasing age of embryonic development. Two-day eggs showed no hatching at doses at or above 1600 rads, while a minimum of 25,600 rads was required to prevent hatching of 8- to 12-day eggs. Eggs during early embryonic development thus appear to be about 16 times more radiosensitive than eggs in stages immediately preceding hatching. One-day-old larvae were fourfold more radioresistant than prehatch eggs, as indicated by lethal dose effects after 20 days (a time interval equivalent to longest development time for eggs). One-day eggs were somewhat more resistant than two-day eggs, implying that eggs in the dormant state may not be as radiosensitive as those in initial stages of development. The plateau region in the figure reflects the relative radioresistance of different ages to low doses. One-day eggs showed a significant decrease in hatching at 400 rads, while eight-day eggs to day-old larvae were unaffected by doses below 3200 rads.

Besides the obvious effects of acute irradiations on egg hatching and subsequent larval survival, alterations in normal behavioral patterns were detectable in the larval stage. In those individuals irradiated in late embryonic development, immediate posthatch mortality could be anticipated by cessation of feeding, while protracted lethal effects were often indicated by reduced locomotor activity. The most prominent behavior pattern in these insects is the construction of a protective larval case or "bag" – typically within one to two days after hatching. In all instances, the characteristic case-building behavior of newly hatched irradiated individuals was impaired at dose levels 0.5 below those at which mortality was first apparent. The ecological significance of this impairment would be realized in resultant deleterious effects limiting population size.

In certain instances it appears that low doses may have an enhancing effect upon hatching; however, verification of this phenomenon will require additional data. More-refined analyses of dose, time, and dose × time interactions will be made when the profile is completed and information is available for larval development and overwintering eggs. The preliminary results of these experiments indicate that bagworm eggs are the most radiosensitive stage in the life cycle and, therefore, a most critical period for radiation disruption of normal population structure. The significance of this stage is further enhanced by the probability of radiation insult occurring during this period, since the greater portion of the life cycle (October through April or about 60% of total time) is passed in the egg stage.

RADIATION SENSITIVITY OF IMMATURE STAGES OF THE GIANT MILKWEED BUG

D. A. Crossley, Jr. M. H. Shanks

In laboratory studies preliminary to investigations of radiation effects on natural populations of insects, sensitivity to gamma radiation was examined for immature stages of the giant milkweed bug, *Oncopeltus fasciatus* (Dallas). This species is typical of those insects which spend their entire life cycle upon the host plant and thus would receive little or no environmental protection from gamma radiation. *Oncopeltus* is unusually well suited to combined laboratory-field experimentation since colonies can be maintained in laboratory conditions on a diet of milkweed seeds and water, and field populations can be maintained on milkweed plants themselves (several species of *Asclepias*). The preliminary studies were designed to discover the range of radiation exposure eliciting a significant response by the immature stages, since in general immature insects are more radiosensitive than are adult insects. The ability of nymphs to molt or of eggs to hatch following irradiation was used as a biological end point in description of radiation effects.

Irradiations were performed with a ^{60}Co gamma source at a dose rate of 14.4 rads/sec. Clutches of 20 eggs each were given doses of 0, 0.5, 1, 2, 4, 8, or 16 kilorads. Nymphs were given these doses and 32 and 64 kilorads in addition. Following irradiation, insects were kept in controlled environment chambers at 75°F and a 16-hr day.

Comparatively low doses of gamma radiation affected hatchability. One-day-old eggs showed reduction of hatchability by more than 50% at the lowest dose level used (500 rads). No eggs hatched after receiving 2000 rads, but 8000 rads was required to halt all embryonic development. Three-day-old eggs were somewhat less sensitive, 1000 rads being the dose which reduced hatchability to less than 50%. Normal duration of the egg stage is five days; irradiation of five-day-old

eggs has not been completed. These ranges of radiation sensitivity are similar to those reported[8] for eggs of other insect species.

Radiosensitivity of nymphs was measured for instars I through IV (*Oncopeltus* has five instars). Results showed no evidence of a decrease in radiosensitivity with age, when ability to molt is used as a criterion of radiation survival. In each instar, survival at molt after 4000 rads was about 70% (and not significantly different from controls); 8000 rads reduced survival to about 50%; 16,000 rads to about 30%; and 32,000 rads to about 10%. Further refinement of these experiments is desirable in order to compare molting as a biological end point with the more commonly used criterion of mortality.

Survival of nymphs after irradiation was compared with survival of *Oncopeltus* adults exposed to similar radiation doses.[9] Adults showed a radiation response similar to the nymphal stages; mean survival time was 26 days for controls, 23 days for adults receiving 8000 rads, and 8 days for adults receiving 16,000 rads. Thus the major reduction in survival occurred after radiation doses in the vicinity of 8000 to 16,000 rads, as was the case with nymphs receiving these doses. These comparisons would indicate that a radiation profile for *Oncopeltus* would show little change in radiation sensitivity except for the egg stages. In that event this insect species would be well suited for field experiments in radiation sensitivity.

EFFECT OF BETA IRRADIATION ON INSECTS

E. F. Menhinick Gladys J. Dodson

Beta irradiations of insects are necessary to determine effects of the beta component of environmental contamination. The most feasible approach to this problem appeared to be with the use of the plane sources.[10] Exposure dose to x-ray or gamma radiation is expressed in roentgens. An equivalent measurement for dose of beta radiation must be made in rads (absorbed dose), in air, at the point of exposure.

In these studies, insects were placed on the source, where the air dose was 3600 rads/hr. Insects were given doses varying from 877 to 224,000 rads in 100% increments. Five replicates of ten individuals each were made for each dose. Developmental stages included small (3.0-mg), medium (26.3-mg), and large (300.0-mg) cricket nymphs (*Acheta domestica*); small (1.1-mg), medium (16.0-mg), and large (52.0-mg) mealworms (*Tenebrio molitor*); small (4.4-mg) and large (801.1-mg) American roach nymphs (*Periplaneta americana*); and small (1.9-mg) and large (101.6-mg) German roach nymphs (*Blattella germanica* L.). Insects were irradiated at room temperature and kept at 28°C before and after radiation. Effects were expressed as median life expectancy corrected for control mortality.

Median life expectancy of large *Acheta* nymphs exposed to beta and gamma radiation (3600 rads/hr beta; 25,000 rads/min gamma) is shown in Fig. 9.11. Insects exposed to beta radiation lived about half again as long as those exposed to equivalent amounts of gamma radiation. Approximately twice as much total dose of beta radiation as gamma radiation was required to produce a given effect. To explain this difference in dose effect, several factors must be considered.

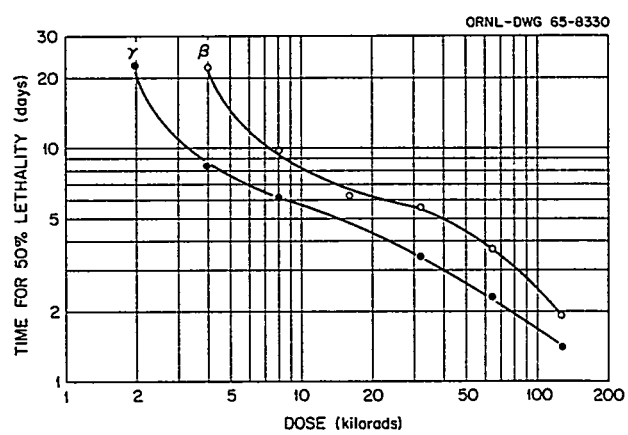

Fig. 9.11. Median Survival of Large Cricket Nymphs Exposed to Gamma and Beta Radiation.

[8] D. J. Jefferies, p. 213 in *Radiation and Radioisotopes in Entomology*, IAEA, Vienna, 1962.

[9] E. F. Menhinick, ORNL, unpublished data.

[10] S. I. Auerbach *et al.*, *Health Phys. Div. Ann. Progr. Rept. July 31, 1964*, ORNL-3697, p. 78.

Table 9.2. Median Life Expectancy (Days) of Insects Exposed to Beta Radiation

Dose (kilorads)	Cricket			Mealworm			American Roach		German Roach	
	Small	Medium	Large	Small	Medium	Large	Small	Large	Small	Large
3.5	8.3	11.6	20.2	24.0			11.4		24.8	
7.0	8.2	8.0	9.7	14.6	34.2		5.1	64.5	20.9	25.6
14.0	7.9	6.7	6.2	12.4	16.5	23.5	3.2	55.6	16.0	26.7
28.0	9.4	4.1	5.6	8.4	12.0	12.5	2.9	8.8	10.2	18.7
56.0	4.4	4.0	3.7	3.8	6.2	6.7	1.9	5.6	2.1	5.8
112.0	1.8	1.7	1.9	2.9	2.7	3.4	1.5	3.1	1.1	2.7

Film calibration of the plaques gave a half-value layer of 164 mg/cm^2 (E. D. Gupton, Dosimetry, Health Physics Division). Assuming a tissue density of about 1.0, there would be a 50% reduction in absorbed dose for every 1.6 mm of tissue. Large cricket nymphs averaged about 5 mm in diameter, resulting in a dose to the center of the gut of about 34% of that received by the ventral surface. This difference in gut dose to surface dose would more than compensate for the difference in effect of beta and gamma radiation if mortality resulted primarily from gut damage.

If mortality resulted from gut damage, one would expect that larger forms (with correspondingly more tissue shielding the gut) would be less affected by external beta radiation than would smaller forms (with less tissue shielding the gut). Experimental evidence shows that larger forms were more resistant than smaller forms of the same species (Table 9.2). However, larger forms of the same species have been found to be more sensitive to gamma radiation than smaller forms (see "Radiation Profiles of Insects," this chapter). Gamma radiation from ^{60}Co has a half-value layer in water of about 5 in. (ref. 11). All tissues of insects would receive nearly equal exposure from ^{60}Co gamma radiation. Comparisons were then made of the relative effect of beta to gamma radiation to eliminate variation in sensitivity of different life history stages. The term "RBE" (relative biological effectiveness) is restricted to studies having similar dose rates and similar absorbed doses. Relative effect of 3600 rads/hr beta radiation and 25,000 rads/min gamma radiation varied with dose and was not related to size of the organisms. This indicated (if the RBE of beta radiation to the gut is 1.0) that the gut is not a primary critical organ, but rather that the most sensitive organ lies closer to the skin. Also, variation in relative sensitivity to beta and gamma radiation may have been due to differences in dose rate or to a different RBE of the two radiations. Further experiments are necessary to determine the relative importance of these two factors.

RADIATION SENSITIVITY IN INDIGENOUS SMALL MAMMALS

P. B. Dunaway J. A. Payne
Lovell L. Lewis J. D. Story
J. M. Inglis

A wide range of radiation sensitivity has been reported for laboratory mammals. For example, LD_{50-30} estimates for these mammals range from ~300 to 800 r. More recently, radiation responses of several species of wild rodents have been investigated, and comparatively high radiation resistance has been reported for some of these species. Gambino and Lindberg[12] calculated LD_{50} estimates of 1520 r for the little pocket

[11] J. Moteff, *Nucleonics* 13, 24 (1955).

[12] J. J. Gambino and R. G. Lindberg, *Radiation Res.* 22, 586 (1964).

mouse (*Perognathus longimembris*) and 1300 r for the longtail pocket mouse (*P. formosus*). Chang *et al.*[13] reported survival of nine out of ten Mongolian gerbils (*Meriones unguiculatus*) at 1000 r, and one out of ten survived 1500 r. Golley *et al.*[14] calculated LD_{50} doses of 1125 r for old-field mice (*Peromyscus polionotus*) and 1130 r for cotton mice (*P. gossypinus*).

Laboratory measurements of lethality, survival time, and weight change in wild mammals began at ORNL during the summer of 1964. The need for such research is threefold: (1) Radiation responses of various species under standard conditions must be known before interactions between radiation and other environmental variables can be measured. (2) Comparisons of radiation effects in native species and laboratory mammals are necessary for evaluations of the applicability of radiobiological data from laboratory animals to wild species. (3) Interspecies and interfamily comparisons of radiation effects may help demonstrate to what extent radiation response is related to taxonomic status; should such interrelationships be demonstrated, predictions of radiation effects in closely related taxa may be possible.

Eight species of indigenous rodents, one species of shrew, and one strain (RF) of laboratory mouse were irradiated at eight levels ranging from 0 to 2000 rads in a ^{60}Co unit[15] (15.1 rads/sec; May 4, 1964).

The two species of *Peromyscus* and the singly caged RF strain *Mus musculus* were the most radioresistant, with respect to mortality, of the mammals tested (Table 9.3). The rice rat was the most radiosensitive rodent by far, but the wild house mouse, Norway rat, and harvest mouse also were relatively radiosensitive. Too few least shrews were irradiated to make even a preliminary estimate of the LD_{50} range, but it appears that this species is relatively radiosensitive. Cotton rats were peculiar in that mortality changed from 0 to 100% within a narrow range (690 to 1060 rads). A seasonal response may have been present for the golden mice. About half were caught during late winter and early spring, and some of these animals died at lower doses than did animals caught during the fall.

Survival times at the lower doses (500 to 1060 rads) were much the same for the various wild species, except that the least shrews died at relatively short times (3 to 6 days) in comparison to the 7 to 12 days for the other species. In general, survival times at the highest doses were shorter for each species, as expected, but survival times for the least shrew and the murid wild house mouse and Norway rat (4 to 5 days) were shorter than the times for the cricetids (6 to 8 days). Michaelson and Odland[16] suggested that radiation recovery time is inversely related to metabolic rate (i.e., size of mammal). However, this relationship did not hold true invariably for survival times at the generic levels in our experiments, because smaller species often survived longer than larger species.

Weight losses for all species were rapid at the higher doses, presumably resulting from a combination of anorexia and diarrhea during the intestinal-death syndrome that occurs in this dose range. At lower radiation doses at which death occurred, the rates of weight loss were less, of course, and considerable variation was seen in onset, magnitude, and recovery of weight loss among the various species. However, although the average percent weight loss at death ranged from ~15 to 30%, there were no significant differences in weight losses at the various doses at which lethality occurred. Some of the weight losses in most species doubtless were caused by handling stresses, because control animals of these species also lost weight, especially during the first week.

Much of the laboratory radiobiological data accumulated in the past may not be very useful for direct evaluation of radiation effects in individuals since it appears that radiation effects may be confounded seriously with population density stresses. It has been common practice in many radiation experiments to house several animals in a cage and thus increase sample size. Hahn and Howland[17] found greater mortality and reduced survival times in multiply caged irradiated laboratory rats. The results of our initial experiments with RF mice caged singly or in groups of five also show much greater mortality and shorter survival times in the mice grouped five to a cage (Table 9.3). The results for the wild house mouse and the multiply caged RF mice were similar.

[13] M. C. Chang, D. M. Hunt, and C. Turbyfill, *Nature* 203, 536 (1964).

[14] F. B. Golley *et al.*, *Radiation Res.* 24, 350 (1965).

[15] Atomic Energy of Canada, Ltd., Ottawa, Canada.

[16] S. M. Michaelson and L. T. Odland, *Radiation Res.* 16, 281 (1962).

[17] E. W. Hahn and J. W. Howland, *Radiation Res.* 19, 678 (1963).

Table 9.3. Survival (%) of Wild Small Mammals and RF Strain Laboratory Mice

	Radiation Dose (rads)							
	0	500	690	875	1060	1250	1625	2000
Soricidae								
Cryptotis parva	100(3)[a]	100(1)	50(2)	33(3)	0(2)	0(1)	0(1)	0(1)
Cricetidae								
Reithrodontomys humulis	100(13)	100(11)	90(10)	40(10)	10(10)	0(12)	0(12)	0(10)
Peromyscus leucopus	*100(11)*	100(11)	100(10)	82(11)	50(10)	8(12)	0(11)	0(10)
Peromyscus nuttalli	90(10)	100(10)	100(10)	70(10)	40(10)	10(10)	0(10)	0(11)
Microtus pinetorum	100(10)	100(10)	100(10)	45(11)	20(10)	10(10)	0(10)	0(10)
Oryzomys palustris	100(7)	71(7)	16(6)	0(7)	0(6)	0(6)	0(6)	0(5)
Sigmodon hispidus	100(13)	100(10)	100(10)	70(10)	0(10)	0(10)	0(10)	0(10)
Muridae								
Mus musculus								
Wild	100(8)	91(11)	94(16)	42(12)	15(13)	0(10)	0(10)	0(10)
RF strain								
Caged singly	100(7)	100(7)	100(7)	86(7)	86(7)	29(7)	0(7)	0(7)
Five in cage	100(5)	100(5)	60(5)	40(5)	20(5)	0(5)	0(5)	0(5)
Rattus norvegicus	100(10)	100(10)	67(9)	40(10)	0(10)	11(9)	0(9)	0(9)

[a]Numbers in parentheses indicate number of individuals.

Unfortunately, radiation-effects data on multiply caged animals probably cannot be used to much extent for designing studies of radiation effects in natural populations. For instance, extrapolating the "population" density of the multiply caged mice used in our experiment gives a density of about 450,000 mice per acre, an obviously unrealistic population density for natural environments.

INCORPORATION OF 5-^{131}IODO-2′-DEOXYURIDINE INTO INDIGENOUS RODENTS

T. P. O'Farrell

The thymidine analog 5-^{131}iodo-2′-deoxyuridine (^{131}IUDR) enters into DNA synthesis and has proven to be a useful tool for in vivo measurement of cell proliferation and DNA synthesis.[18] Since radiation alters the amount of incorporation of this antimetabolite,[19] studies were continued to test the usefulness of ^{131}IUDR as a physiological dosimeter. The objectives of these recent experiments were to determine the tissue distribution of radioactivity following injections of ^{131}IUDR into cotton rats, *Sigmodon hispidus*, as an aid in interpretation of whole-body retention curves, and to measured changes in incorporation following acute radiation of the same species.

[18]W. L. Hughes *et al.*, *Federation Proc.* 23, 640 (1964).

[19]D. Gitlin *et al.*, *Science* 133, 1074 (1961).

Most of the methods were reported previously.[20] During tissue distribution studies, groups of three cotton rats were killed at 24-hr intervals postinjection, and their tissues were removed, weighed, and assayed for ^{131}I. Animals used in the radiation-effects studies received 100, 500, and 1000 rads in a 323-curie ^{60}Co source prior to injection of $^{131}IUDR$. Groups of five animals were killed at 48 hr and 20 days postinjection to determine the contributions of the various tissue concentrations to the in vivo measurements.

Radioiodine was diffused throughout most of the body from 12 to 48 hr after injection of $^{131}IUDR$, but the unincorporated portion was being eliminated at a high rate. After this initial elimination phase, 65 to 75% of the activity was found in the washed intestines; the biological half-life in the intestines was about 60 hr. Activity in the gut was much higher than that in other tissues from two to ten days postinjection, and the rate of loss of gut activity determined the slope of the whole-body retention curve during this period. Other proliferating tissues such as the bone marrow, stomach, and spleen also incorporated $^{131}IUDR$ (Fig. 9.12). Extrathyroidal iodine pools such as the skin, hair, and male reproductive tract retained significant amounts of activity, probably as iodide dehalogenated from unincorporated $^{131}IUDR$, and from 10 to 20 days postinjection the ^{131}I in these pools was the major contributor to the whole-body measurements.

Tissue analyses following injection of $Na^{131}I$, the major catabolic product of $^{131}IUDR$, indicated a rapid loss of about 95 to 99% of the initial activity and retention of the remaining iodide in long-half-lived traps or pools such as the hair, skin, and male reproductive tract (Fig. 9.12).

[20] S. I. Auerbach *et al.*, *Health Phys. Div. Ann. Progr. Rept. July 31, 1964*, ORNL-3697, p. 83.

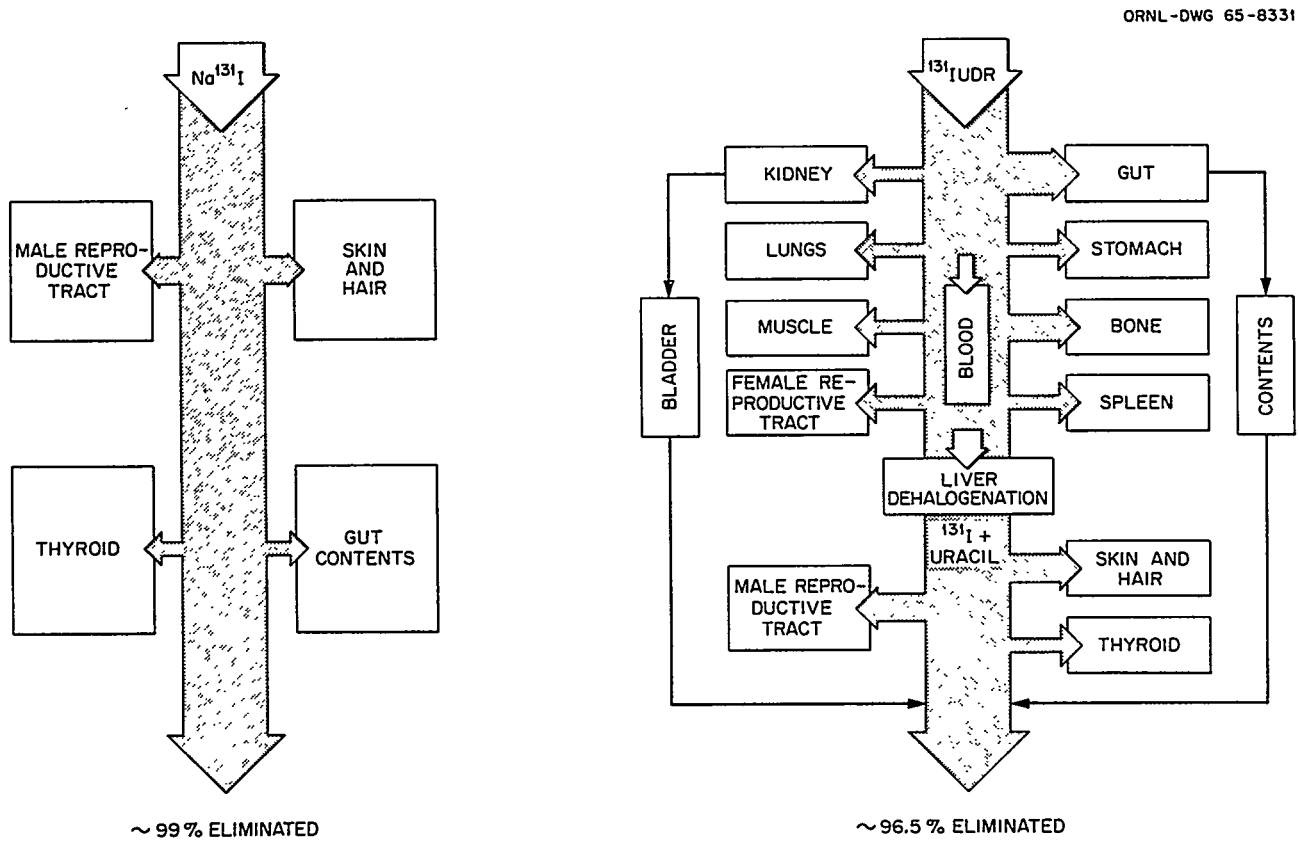

Fig. 9.12. Preliminary Model of Tissue Distribution of Radioactivity 48 hr Postinjection of $^{131}IUDR$ or $Na^{131}I$ in Cotton Rats. The sizes of the arrows indicate relative amounts of activity. Most compartments are closed because data describing outgoing movements are lacking.

Retention of iodine in the male reproductive tract was of interest since a relatively high proportion (0.4%) of the initial dose was retained regardless of whether ^{131}IUDR or Na^{131}I was injected. The radioiodine in the tract had a long biological half-life; in fact, the data were insufficient to demonstrate that the elimination rate differed from zero. This compartment may be important in internal-dose calculations, since high initial doses would subject the male reproductive system to chronic radiation and possible damage.

Acute radiation of 100 and 500 rads reduced the amount of ^{131}IUDR incorporated by 28 and 65% of controls, respectively, but the rate of loss remained the same as the rate for controls. Tissue distribution data indicated that the major portion of the changes in incorporation as measured with whole-body techniques was due to a reduction of activity incorporated into the intestine. Midlethal doses of 1000 rads altered incorporation to such an extent that no difference could be detected between the slopes and intercepts of the ^{131}IUDR and Na^{131}I curves. This indicated that activity measured in vivo was probably iodide contamination rather than incorporated ^{131}IUDR. The merging of whole-body retention curves with increasing doses of radiation was probably due to a coaction of reduced incorporation of ^{131}IUDR and a change in the elimination rate of iodine, the metabolic by-product. The clearance time for radioiodine within various organs was prolonged, and there was a striking retention of activity in the contents of the gastrointestinal tract. Gross pathological examinations indicated that the latter accumulation may have been related to a delayed emptying syndrome, which has been noted in other radiation studies.[21]

The cotton rat intestinal tract, because of its bulk and rapid rate of cell proliferation, incorporates most of the activity retained following an injection of ^{131}IUDR, and for the first ten days postinjection this activity level determines the shape of in vivo retention curves. Acute radiation alters the cells in this relatively radiosensitive organ in such a way that ^{131}IUDR incorporation is inversely proportional to absorbed doses in the sublethal range. It appears that in vivo measurements can be used as an index to the degree of radiation insult.

[21] R. A. Conrad, *Am. J. Physiol.* 165, 375 (1951).

10. Processes and Components of Terrestrial Ecosystems

G. N. Brown[1]
J. W. Curlin[1]
J. S. Olson
G. M. Van Dyne[1]
J. P. Witherspoon
Martin Witkamp
Regina M. Anderson
W. C. Cate
Marilyn L. Frank
F. G. Taylor, Jr.[1]
H. D. Waller
G. Cristofolini[2]
Simonetta Cristofolini[3]

ANALYSIS OF ISOTOPE RELEASE FROM DECAYING LEAVES

J. S. Olson H. D. Waller
Regina M. Anderson

Comparative experiments in the cycling of radionuclides have shown considerable effects of climate, leaf species, and vegetation cover on the rate parameters of litter decay. Such decay is normally responsible for the release of nutrients, and also radioactive contaminants, for transfer through animal food chains and for recycling through vegetation. Experiments with tagged leaves have been analyzed

[1] Dual capacity.

[2] NATO Fellow.

[3] Consultant.

and have shown how much more rapidly radiocesium is released than several other nuclides. Certain of these experiments also included intact slabs of the forest floor, to estimate retention of the ions after release from the tagged leaves.

The slowest leaf decomposition among several deciduous species found in the Great Smoky Mountains and Oak Ridge was that of beech, *Fagus grandifolia.* A further experiment with artificially tagged beech leaves at Oak Ridge confirmed slow decomposition (67, 64, and 57% of the weight remaining after one year) in pine, oak, and maple forests. Yet, the percentages of the original radiocesium remaining in litter were only 21 to 34, 10 to 16, and 5 to 9 after seven weeks, one year, and two years respectively. A 2.5-cm slab of soil in plastic and screen boxes placed under the litter bags retained 66, 66, and 42% of the original cesium applied in the pine, oak, and maple forests after two years. Thus, soils retain much, but far from all, of the cesium that is promptly released during the decay and leaching of the litter. These results have led to further concentration of larger-scale tagging experiments on radiocesium.

LOSSES OF ^{137}Cs FROM THE TAGGED *LIRIODENDRON* STAND

J. S. Olson W. C. Cate
H. D. Waller Regina M. Anderson

Previously reported data[4] on net transfers of ^{137}Cs from tree boles to other compartments of a tagged-tulip-poplar forest ecosystem have required interpretation in terms of simultaneous income and loss rates for several major compartments in an idealized model of the forest. A computer program for simulating these transfers and estimates of the fractional turnover rates for the data from summer of 1962 are discussed in Chap. 12.

Extrapolation of this model into later years, even with due allowance for decreased transfer rates during the winter, implies that there should be large decreases in the activity of the foliage concentrations. Continuing inventories of the tree stand and major losses from it confirmed this expected decrease in 1963 and 1964. Results also confirm the hypothesis that losses from the above-ground parts of tagged trees to the forest floor surface due to leaching by rain and fall of litter are exceeded by losses from underground parts of the tagged trees due to leaching by percolating ground water, exudation, and die-off of these root systems.

Figure 10.1 shows that the foliage concentration of ^{137}Cs (microcuries per gram of lead) decreased nearly one order of magnitude between the growing seasons of 1962 and 1964. In each of these years, radiocesium reached a maximum concentration in June and then decreased by about 50% from June to September due to transfer of ^{137}Cs from the leaves to woody tissue and to the surrounding environment.

Records have been kept since the beginning of this experiment in 1962 on the main transfers of ^{137}Cs from the tagged trees to the forest floor surface. Table 10.1 gives a summation of these data by years.

The weight data on fallen leaves collected beneath the tagged forest canopy (column 1, Table 10.1) also give one tentative basis for estimating the radiocesium activity of living leaves per unit ground area ($\mu c/m^2$). Preliminary data on the woody parts of these trees indicate that there is no increase in the ^{137}Cs concentration in wood to account for this large decrease in the forest canopy between years and that these trees are not growing

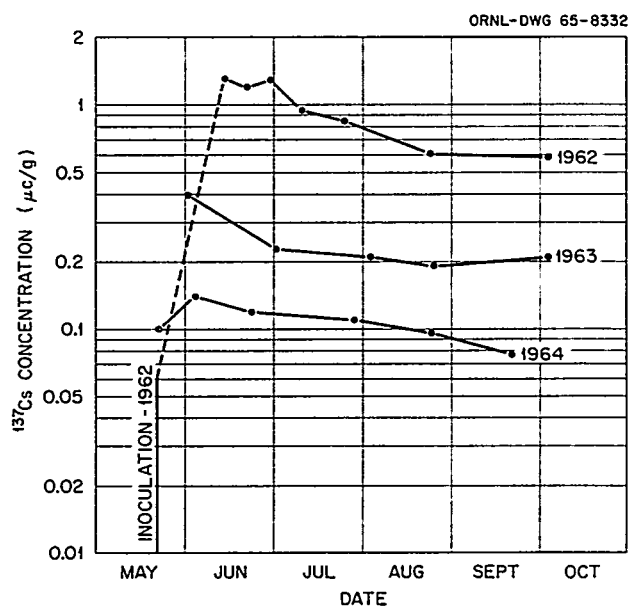

Fig. 10.1. Tagged Forest Canopy Concentration.

[4]S. I. Auerbach *et al., Health Phys. Div. Ann. Progr. Rept. July 31, 1964,* ORNL-3697, pp. 85–90.

Table 10.1. Surface Losses of ^{137}Cs from a Tagged Forest Canopy

Year	Litter Fall – *Liriodendron* Leaves		Rainfall Activity ($\mu c/m^2$)	Loss to Plot Area Activity ($\mu c/m^2$)
	Weight (g/m^2)	Activity ($\mu c/m^2$)		
1962	196	47.8	13.3	61.1
1963	204	21.4	5.5	26.9
1964	146	8.1	3.0	11.1

fast enough for dilution of ^{137}Cs by new tissues to account for a decrease of this magnitude. It is obvious that a substantial loss to or through the roots must account for the observed decrease. There has been some dispersal of tagged leaves out of the plot, but these losses are comparable to the influx of untagged leaves (total – 196 g/m^2). Therefore, a provisional estimate of foliage cesium per unit of ground area may be derived by subtraction:

1. ^{137}Cs in forest canopy (tentative):

June 1962

$$196 \text{ (g of leaves per m}^2) \times 1.3\ (\mu c/g) = 254.8\ \mu c/m^2$$

June 1963

$$204 \text{ (g of leaves per m}^2) \times 0.4\ (\mu c/g) = 91.6\ \mu c/m^2$$

$$163.2\ \mu c/m^2$$

2. Subtracting the total surface loss measured in 1962 (Table 10.1) from this total decrease in canopy concentration suggests a magnitude for expected below-ground transfer:

June 1962–June 1963 decrease in canopy concentration	163.2 $\mu c/m^2$
Measured surface losses from 1962–1963	61.1 $\mu c/m^2$
Deficit not accounted for by surface losses	102.1 $\mu c/m^2$

An inventory made at the end of the first growing season indicated that almost 50% of the total amount of ^{137}Cs introduced into the tree boles (467 mc) had moved into the medium, fine, or very fine roots.[4] Detailed analysis of soil and root fractions at the end of October suggests that as much as 100 μc of ^{137}Cs per square meter may have been released from roots to soil by the end of a full year.[5] This estimate of underground release (based on soil and root analysis) is thus of the same magnitude as the independent estimate of canopy losses which are not accounted for by leaching by rain and litter fall (surface losses).

TRANSFER OF ^{137}Cs FROM TREES TO FOREST UNDERCOVER VEGETATION

H. D. Waller J. S. Olson
G. Cristofolini

Although the root contribution from tagged trees is greater than contributions of rainfall and leaf fall to the surrounding environment, the latter are more promptly transferred to other living components of the forest system. Table 10.2(*A*, *B*) shows that an inverse relationship exists between the ratio of concentrations of ^{137}Cs in plants and in soil for the first growing season and the ratio for the second. Concentrations in plants decreased by factors of 5 to 10 while those in the soil increased by a factor of 8, suggesting that ^{137}Cs associated with soil had little effect on plant radioactivity during this season. The decrease is attributed largely to the decrease in ^{137}Cs content of the tagged overstory (Fig. 10.1) from the first to the second season. Other data on plant parts and autoradiograms prepared from the overstory plants suggest that the radiocesium was distributed throughout the plant organs.

Potted plants of Christmas fern (*Polystichum acrostichoides*) were placed inside the area to obtain a direct measurement of foliar uptake. Half these plants had only the vegetative material exposed (soil covered with paraffin wax); the remainder had vegetative material plus soil exposed to ^{137}Cs in rainfall. The sample units were placed in pairs inside the tagged forest area. Results from this experiment indicate that: (1) plants with covered soil had 91% as much ^{137}Cs as was found within plants in which the soil as well as foliage

[5] H. D. Waller and J. S. Olson, "Prompt Transfer of ^{137}Cs to the Soils of a Tagged *Liriodendron* Forest" (manuscript).

Table 10.2. Contrasts in Undercover Radioactivity due to Foliar Absorption vs Root Uptake (August)

Ground Cover	Sample Weight (g/m^2)	Distribution of ^{137}Cs by Species (%)	Plant Concentration of ^{137}Cs ($\mu c/g$)	Plant/Soil Ratio
			$\times 10^{-2}$	
A. 1962 – 1st Season in Tagged Forest				
Christmas fern (*Polystichum acrostichoides*)	28.44	35	5.62	76[a]
Hydrangea (*Hydrangea aborescens*)	39.46	53	5.55	75[a]
Virginia creeper (*Parthenocissus quinquefolia*)	3.84	3	9.13	124[a]
Other species	14.16	9	11.64	158[a]
B. 1963 – 2d Season in Tagged Forest				
Christmas fern (*Polystichum acrostichoides*)	23.21	14	0.88	1.4[b]
Hydrangea (*Hydrangea aborescens*)	16.14	49	0.64	1.0[b]
Virginia creeper (*Parthenocissus quinquefolia*)	4.17	35	0.34	0.5[b]
Other species	2.26	2	2.59	4.1[b]
C. Root Uptake from Surface – Sprayed Plots – 1st Season				
Christmas fern (*Polystichum acrostichoides*)	4.75	67.50	7.86[c]	0.48[d]
Hydrangea (*Hydrangea aborescens*)	6.14	7.79	0.37	0.02[d]
Virginia creeper (*Parthenocissus quinquefolia*)	0.77	1.05	0.33	0.02[d]
Other species[e]		12.96	0.76	0.05[d]
Other species[c]		10.70	7.75[c]	0.48[d]

[a]Based on mean soil activity of 0.08×10^{-2} $\mu c/g$ due mainly to rainout from tagged overstory.

[b]Based on mean soil activity of 0.64×10^{-2} $\mu c/g$ due mainly to release from litter and roots.

[c]Indicates plants that received direct contamination from spray application of this radionuclide. This includes early spring flowering plants (orchids, violets, etc.) or perennial plants that contain their foliage throughout most of the winter months.

[d]Based on mean soil activity of 16.2×10^{-2} $\mu c/g$ sprayed directly on forest floor, Apr. 1, 1964.

[e]Indicates those species that had a minimal amount of direct foliar contamination when the radionuclide was applied.

was exposed; (2) comparison of the August collection (prior to leaf fall) with the December collection (after leaf fall) indicated that post-August absorption, either foliar or through fern crown sections, was apparently of a greater magnitude than uptake during the normal growing season; and (3) large differences that existed between the exposed and covered units for the December collection suggest that there was considerable absorption into exposed fern crown and shallow roots occupying the organic layer, as well as increased foliar uptake between the August and December collections. Cesium-137 leached from fallen leaves which had lodged on the plants would be especially important for those evergreen plants (such as Christmas fern) that remain metabolically active until most leaves have fallen from the overstory.

NUCLIDE TRANSFER AND MICROBIAL RESPIRATION

Martin Witkamp Marilyn L. Frank

Microbial storage and turnover of radionuclides depend directly on the abundance and metabolic activity of the microflora and the concentration and availability of the nuclides. Most of the year was used to analyze data and prepare eight manuscripts describing microbes, nuclides, and their interaction in the field and in the laboratory.

Abundance of microbes and microbial mass in various broadleaf and confierous forests in all four seasons,[6–8] as well as their metabolic activity, were described.[6,7,9] The effects of temperature, moisture, litter age and species,[6–9] soil fauna,[10] and depth of the soil profile[8] were analyzed to predict microbial activity in other environments. A successful model for this was developed.[7]

Concentration, distribution availability, and turnover of ^{137}Cs in the tulip poplar stand, and of ^{137}Cs and ^{90}Sr in arctic vegetation, were discussed.[11,12] Local differences in distribution of ^{137}Cs in the forest floor varied up to 3 orders of magnitude due to irregularities in root distribution.[11] Laboratory studies of the influence of time, moisture, temperature, pH, litter age, species, fragmentation, leaching, mode of contact, and species and age of microbes on accumulation of radiocesium by fungi have aided in understanding the variation in ^{137}Cs burdens in mushrooms of the tagged forest.[13]

RADIOCESIUM MOVEMENT IN A FOLIAGE-FEEDING CANOPY INSECT

D. E. Reichle Gladys J. Dodson

Biological distribution and cycling of radionuclides by insect populations in forest ecosystems are presently being analyzed in the ^{137}Cs-tagged forest. Although emphasis to date has been upon detritus-based food chains of the forest floor, investigations on selected canopy species are in progress. Autecological studies on the behavior of radiocesium in herbivorous insects have utilized the evergreen bagworm, *Thyridopteryx ephemeraeformis*, as a model for uptake and transfer of this nuclide through metamorphosis. The locally abundant cedar, *Juniperus virginiana*, is a preferred host for this ubiquitous insect and, congruent with these objectives, one *Juniperus* was tagged by stem inoculation of 5.69 mc of ^{134}Cs in mid-August 1964.

Translocation of the nuclide was comparable to the behavior of alkali metals in other tree species for this season. Detectable movement into apical leaves was observed within half an hour after inoculation, with near maximal values occurring within one week. Activity densities for leaves

[6]Martin Witkamp, "Environmental Influences on Microbial Populations and Activity of the Forest Floor," *Proc. Intern. Congr. Soil Sci., 8th, Bucharest, 1964* (in press).

[7]Martin Witkamp, "Decomposition of Leaf Litter in Relation to Environmental Conditions, Microflora, and Microbial Respiration," *Ecology* (in press).

[8]Martin Witkamp, "Macroflora, Mycoflora, and Soil Relationships in a Pine Continuum," submitted for publication in *Ecology*.

[9]Martin Witkamp, "Rates of Carbon Dioxide Evolution from the Forest Floor: Measurement, Environmental Effects, and Relation to CO_2 from Litter," submitted for publication in *Ecology*.

[10]D. A. Crossley, Jr., and Martin Witkamp, "Effects of a Pesticide on Biota and Breakdown of Forest Litter," *Proc. Intern. Congr. Soil Sci., 8th, Bucharest, 1964* (in press).

[11]Martin Witkamp and Marilyn L. Frank, *Radiation Botany* 4, 485–95 (1965).

[12]Martin Witkamp, "Biological Concentrations of ^{137}Cs and ^{90}Sr in Arctic Food Chains," submitted for publication in *Nuclear Safety*.

[13]Martin Witkamp, "Environmental Effects of Microbial Turnover of Some Mineral Elements," submitted for publication in *Ecology*.

(picocuries/mg dry wt) at successive heights after eight weeks were: 2 ft, 33 pc/mg; 5 ft, 167 pc/mg; 10 ft, 333 pc/mg; 18-ft apex, 724 pc/mg. Last-instar bagworm larvae placed on the cedar in containment cages exhibited rapid uptake of radiocesium through consumption of vegetation. Maximum mean values of 32.7 pc/mg were recorded within three days, but cessation of active feeding during this period immediately preceding pupation may bias any interpretation of this as an equilibrium value. Elimination rates during this prepupal period are prolonged and may be indicative of a changing metabolic rate prior to pupation.

Pupating female larvae were removed to the laboratory for evaluation of the fate of the radiocesium body burden during transformation. Individuals were placed in artificial cases simulating actual bagworm cases in which normal development would have occurred, and reared to adults at a mean field temperature of 72°F. Developmental times in the laboratory of about 40 days from case closure to oviposition showed good agreement with values of about 38 days obtained from field populations, and it was assumed that the behavior of radiocesium in laboratory cultures could be applied to natural populations. Figure 10.2 illustrates the pathways of radiocesium movement in female bagworms. Regardless of body-burden concentrations in mature larvae and equilibrium states with vegetation, the percentage transferred during metamorphosis should be applicable for varying inputs of radiocesium. Essentially the entire body burden of radiocesium is transferred from the larval to the pupal stage, with only 0.3% being lost with the cast skin at ecdysis; however, the activity density in the pupa increases by about 16% over that in the larval stage. Of the total radiocesium concentration in the pupal stage, 10% remains associated with the puparium and miscellaneous residues. Slightly less than half the female body burden of radiocesium (44.5%) is transferred in egg production, which in itself accounts for 82.4% of the total female biomass. Expressed as a percent of pupal activity the distribution is: 10% to puparium, 40% to egg clutch, and 50% to female after oviposition. Since the mean number of eggs per clutch is 665, this yields a value of 2 pc/egg or 22.3 pc/mg egg.

The bagworm life cycle includes a seven-month inactive period (October through April) during which the eggs overwinter in a dormant state. Silver metaphosphate glass rod dosimetry showed an accumulated dose to eggs of 19 rads during this period from the background of contaminated vegetation. Combined with a calculated internal dose of about 8 rads from the puparium and egg clutch itself, this yielded a total of 27 rads delivered to eggs during the dormant period — a value far below any for which radiation effects have been observed for this insect (see "Radiation Profile of the Evergreen Bagworm," Chap. 9).

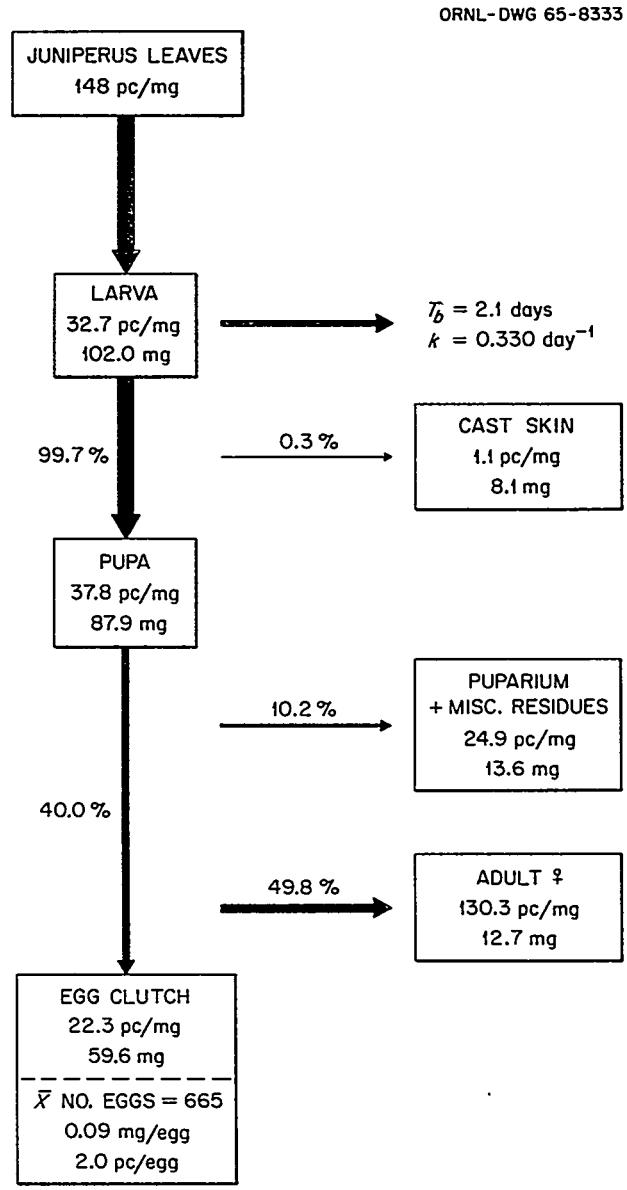

Fig. 10.2. Fate of Radiocesium Body Burden in Transforming Bagworm Larvae.

BIOLOGICAL HALF-LIVES OF ^{134}Cs IN FOREST-FLOOR ARTHROPODS

D. E. Reichle Gladys J. Dodson

The biological half-lives for radiocesium in arthropods of detritus-based food chains were determined to permit estimation of nuclide turnover rates within cryptozoan communities.[14] Those species studied belonged to the natural fauna of the ^{137}Cs-tagged *Liriodendron* forest and were selected to serve as analogs for the remaining faunal elements. Individuals were fed on ^{134}Cs-contaminated food, and eliminations were measured in the laboratory at 20°C. Disregarding the rapid initial loss rates due to gut voidance, the retention curves were best characterized by either one or two exponential functions.

Figure 10.3 illustrates the typical radiocesium retention curves for single-component (beetle, *Sphaeroderus stenostomus*) and double-component (wood roach, *Parcoblatta*) retention systems, which can be described, respectively, by the equations

$$k = \frac{0.693}{T_b}$$

and

$$k = \frac{0.693}{a_1 T_{b_1} + a_2 T_{b_2}} .$$

Table 10.3 gives the biological half-lives, T_b, for radiocesium in the 12 cryptozoan species examined. The first column contains the T_b (days) for those species typified by single-exponential retention curves. For the remaining species with double-component retention systems, the T_b for each component is given in the second column, together with its associated *a* value (proportion of whole-body radioactivity eliminated through each component).

Coleoptera (Carabidae, Passalidae) were all characterized by single-component systems, regardless of feeding mechanisms or trophic position. In the Orthoptera, crickets (Gryllidae) also exhibited single-component retention curves, although the retention curve for the wood roach (Blattidae) consisted of two components. The diplopods (millipedes) were also heterogeneous and included species with both single- and double-component systems. In most cases the T_{b_1} averaged about one day, with *a* values above 35%, and the longer second-component half-lives were associated with <65% of the body burden. Elimination constants (*k*) calculated for these systems were comparable to those for single-component systems. All the isopods possessed two-component retention systems with relatively long T_{b_2}'s (>20 days) associated with over 80% of body activity and, consequently, were characterized by elimination rates for radiocesium that were much longer than those for other arthropods. Values for *k* ranged from a low of 0.031 day^{-1} for the isopod *Armadillidium vulgare* to a maximum of 0.578 day^{-1} for the xystodesmid millipede *Apheloria montana*.

Temperature appears to be the most important abiotic variable affecting elimination rates. Laboratory experiments indicated a Q_{10} relationship of approximately 2 between 10°C and 30°C for the isopods *Cylisticus convexus* and *Armadillidium vulgare*, geometrid larvae, and the millipede *Dixidesmus erasus*. Biological half-lives for radiocesium also appeared to be related to the size of

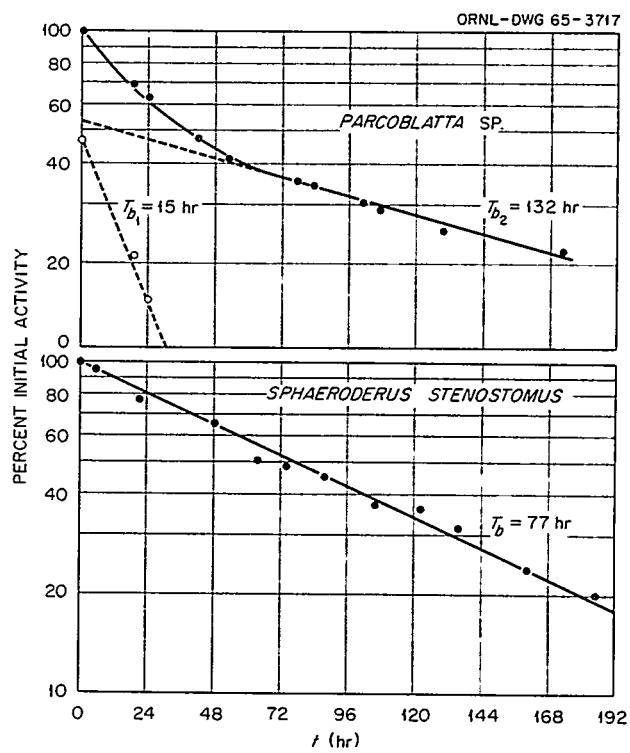

Fig. 10.3. Retention of ^{134}Cs by Two Cryptozoan Species.

[14] D. E. Reichle and D. A. Crossley, Jr., *Health Phys.* 11 (in press).

Table 10.3. Biological Half-Life (T_b) of ^{134}Cs in Selected Forest Cryptozoans Maintained in Laboratory Culture at 20°C

Species	Half-Life (days)				
	Single-Component System	Two-Component System			
	T_b	T_{b_1}	a_1	T_{b_2}	a_2
Coleoptera					
Evarthrus sodalis	4.0				
Sphaeroderus stenostomus	3.2				
Popilius disjunctus	3.8				
Orthoptera					
Parcoblatta sp.		0.6	0.47	5.5	0.53
Ceuthophilus gracilipes	3.8				
Acheta domesticus	3.9				
Diplopoda					
Dixidesmus erasus	2.4				
Cambala annulata		1.5	0.38	12.4	0.62
Ptyoiulus impressus		0.8	0.35	20.0	0.65
Apheloria montana	1.2				
Isopoda					
Armadillidium vulgare		2.7	0.18	27.0	0.82
Cylisticus convexus		2.3	0.16	20.0	0.84

the animal, showing good agreement with the curve given by Crossley[15] relating insect mass to elimination rate.

CESIUM TURNOVER IN FOREST CRYPTOZOA

D. E. Reichle D. A. Crossley, Jr.
Gladys J. Dodson

Radiocesium movement in cryptozoan food chains of the ^{137}Cs-tagged *Liriodendron* forest was examined during the autumn and winter months, when cesium inputs to the forest floor were minimized and detritus comprised the major food base.[14] Movement of ^{137}Cs from a generalized food base through selected saprovores in a detritus-based food web is shown in Fig. 10.4. An average value of 25 pc/mg was used for ^{137}Cs concentrations in leaf litter; the mean activity densities for arthropods were based upon weekly field collections for the same period. Input was estimated from the relationship

$$I = kQM$$

where I is the input (pc/day), k is the elimination constant (day^{-1}), Q is the ^{137}Cs activity density (pc/mg) for each species, and M is the mass (mg dry wt) per individual. The first three compartments are orthopterans – the crickets *Nemobius* and *Ceuthophilus*, and the wood roach *Parcoblatta*. The five species comprising the remaining three components are all millipedes. Outgo from saprovore compartments by elimination is expressed both as the T_b and k (both corrected to mean environmental temperatures). Equilibrium is expressed as activity density (pc/mg). At equilibrium, outgo (kQM) is equal to input (I), and consumption of leaf litter is calculated by dividing intake (pc/day) by ^{137}Cs concentration in leaf litter. Since consumption is normally a function of body size, relative input rates are given as a percent of body weight consumed per day.

[15] D. A. Crossley, Jr., p. 46 in *Radiation and Radioisotopes Applied to Insects of Agricultural Importance*, IAEA, Vienna, 1963.

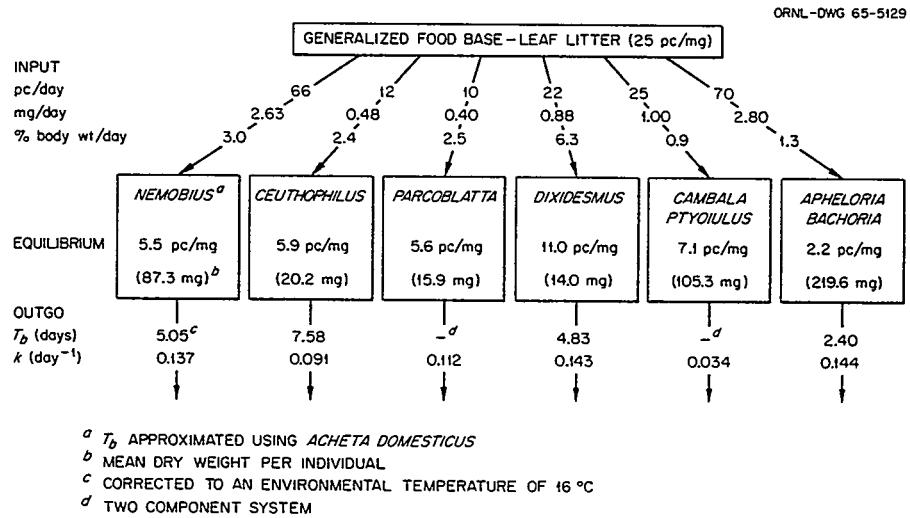

Fig. 10.4. Litter Consumption by Arthropods Estimated from Radiocesium Turnover Rates.

The arthropod species examined had similar rates of food consumption per body weight, although they differed in size, elimination constants, equilibrium concentrations of ^{137}Cs, and inputs of radiocesium. Estimates ranged from 0.9 to 6.3% of body weight per day, with a mean of 2.7% per day for the eight species. These food consumption rates were lower than those which have been found with radiocesium tracer techniques for herbivorous insects and suggest a small turnover of radiocesium by cryptozoa. These turnover rate estimates need yet to be evaluated for cesium assimilation from detritus and for dilution of tagged biomass (and thus ^{137}Cs activity densities) by migrations of the fauna. Investigation continues with the objectives of contrasting the dynamics of radiocesium movement in different types of food chains and of using rates of radiocesium movement to specify energy transfer along them.

FOREST-FLOOR TAGGING WITH ^{137}Cs

H. D. Waller J. S. Olson

To complement previous experiments with tagged litter and with tagging of a forest through tree boles, a 5- by 5-m plot in a yellow poplar (*Liriodendron*) forest was sprayed with a ^{137}Cs solution April 1, 1964 (Fig. 10.5). After five months, the amounts of cesium in the litter and in successive 2.5-cm soil layers were 66, 27, 4, 1, 0.6, 0.6, and 0.4% of the total in 0 to 15 cm. The high percentage retained in litter and organic fragments through the summer in spite of leaching fits the interpretation of important microbial immobilization suggested by laboratory microbiology work. The comparatively high retention in the surface 2.5 cm of soil confirms the indications obtained by litter bag and box experiments, in a situation involving less disturbance of the soil. Within only five months after tagging of the *Liriodendron* forest through tree boles, ^{137}Cs was more evenly distributed at corresponding depths (5.1, 26, 22, 15, 13, ~9, and ~9% of the total to 15 cm) and had penetrated to greater depths (to at least 30 cm). The difference in distribution, along with previously reported evidence[16] that much of the cesium in the tagged forest was associated with tree roots, reemphasized the importance of redistribution through living roots, in addition to downward percolation through water in natural soils.

In order to test the hypothesis that undercover activity in the stand of tagged trees was due mainly to rainout from these trees, the present plot served to indicate the amount of uptake that could be expected by local species from soil and litter. Data in Table 10.2 (C) indicate that the

[16] S. I. Auerbach *et al.*, *Health Phys. Div. Ann. Progr. Rept. July 31, 1964*, ORNL-3697, pp. 85–90.

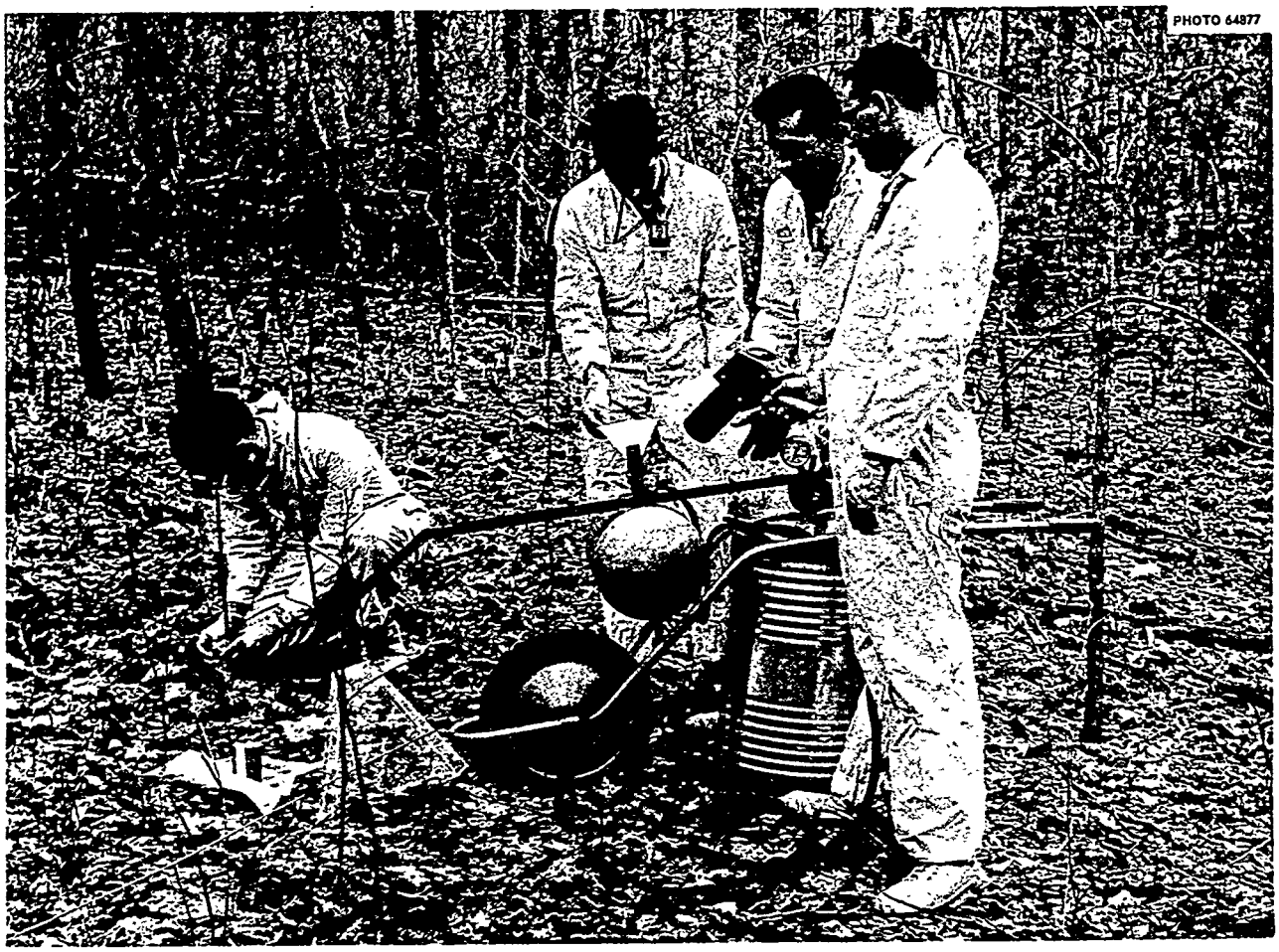

Fig. 10.5. Ecology Personnel Recharging a Modified Orchard Sprayer with a ^{137}Cs Tracer Solution Prior to Surface Tagging of an Experimental Plot. A plastic shield enclosing the head of the spray nozzle directs the spray to the ground surface, preventing excessive wind drift. Constant pressure supplied by a compressed air tank helps maintain a uniform spray discharge. Aluminum foil was wrapped around woody plants so that direct spray contamination would not be confused with root uptake from the soil.

plant activity/soil activity ratio is in the range of 0.02 to 0.05, except for the evergreen Christmas fern and a few other species which may have been exposed to spray directly during the tagging operation. These plant/soil ratios are so much smaller than those in either the 1962 or 1963 samples from the forest that these results strongly confirm the hypothesis that undercover vegetation becomes radioactive mainly as a result of rainout and recycling of ^{137}Cs released during prompt decay of litter.

PILOT STUDIES OF HERBACEOUS INTERCEPTION OF ^{137}Cs

H. D. Waller

A pilot project initiated by U.S. Geological Survey personnel and continued in cooperation with the Waste Disposal Section is using 8- by 8-ft enclosed plots for aid in planning operational procedures and preparing a hazard analysis for a proposed 20-acre ^{137}Cs-tagged old-field facility.

A successful test of pressure spray application used 5 mc of ^{137}Cs diluted in 4 liters of water, which gave a quantity sufficient for five complete spray coverages with alternate spray applications at right angles to one another. A modified orchard sprayer (shown in Fig. 10.5) was used with a constant pressure of 50 psi and required 5 min for the complete plot.

Two types of vegetative plots (one representing a tall meadow and a clipped one representing a short meadow) were sprayed with a ^{137}Cs solution to ascertain the effect of grass vegetation (*Festuca* and *Digitaria*) on the interception and subsequent rain leaching of the tagging solution. Six days after inoculation, prior to any rainfall, more than 95% of the total ^{137}Cs tag was contained on the tall grass and about 85% was contained on vegetation materials (short grass stubble and grass litter) on the short-meadow plot. After the inoculated plots had received six individual rains totaling 3.5 in. (five weeks after tagging), 47% ± 2.4 S.E. (S.E. = standard error) of the total ^{137}Cs applied was found on the tall grass; 50% ± 4.1 S.E. was associated with vegetation materials (short grass stubble, ~30%; litter, ~20%) on the short-meadow plot.

A series of tap-water leaches showed a similar order in the percent of water-leachable cesium: tall grass (11.6%) > short grass (2.3%) > litter (1.8%), after a 32-cm simulated rain extending over a two-day period (Fig. 10.6). Cumulative leachate percent cesium, y, for different amounts of leaching (between 2.5 and 33 cm) may be approximated by $y = 7.76 \log x$ for tall grass.

For the short-meadow plot, released cesium is more directly proportional to the amount of rainfall, $y = 0.063x$ and $y = 0.026x$ for grass and litter respectively.

Thus, much of the ^{137}Cs associated with vegetation is potentially leachable, but it appears to be in small increments during successive rains over a period of many weeks. An implication of this work, which is being tested by actual runoff studies reported in the Waste Disposal Section, is that optimum vegetative treatment prior to spraying of larger plots or the 20-acre old field may well include clipping of dense sod to reduce total interception by vegetation, followed by moderate regrowth plus natural matting of litter, to protect the ground surface from rain splash and sheet erosion of both litter and soil.

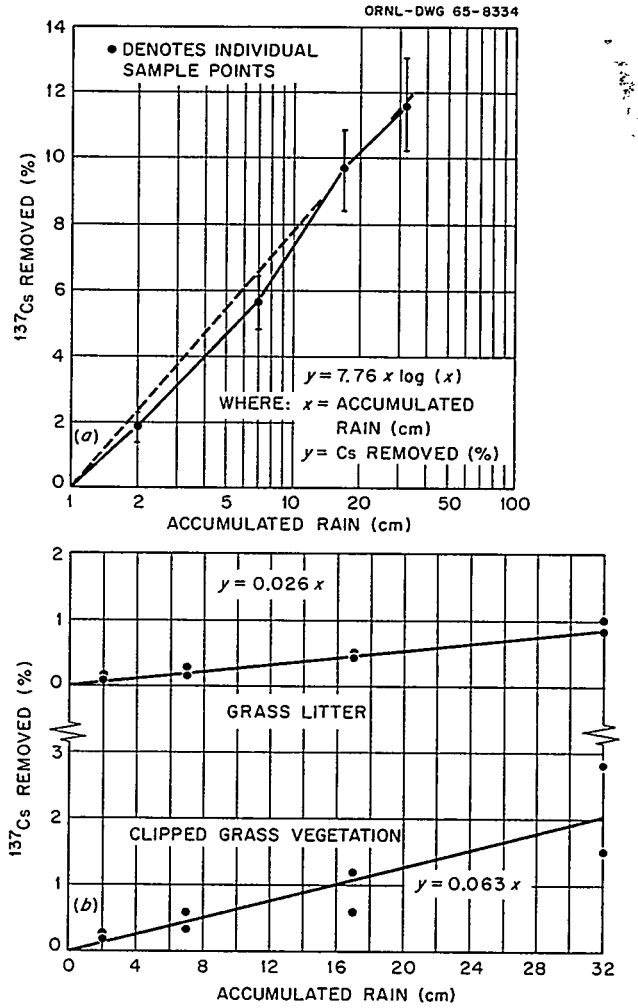

Fig. 10.6. Water-Leachable ^{137}Cs Associated with Vegetation Collected from Sprayed Plots. (*a*) Tall grass; (*b*) clipped grass plot, including litter and grass.

SOIL AND FOREST SITE STUDIES OF THE OAK RIDGE RESERVATION

H. D. Waller F. P. Neumann

Textural analysis was completed for soils collected from study stations, representing the contrasting soil types whose distribution was mapped in earlier annual reports and in a separate memorandum.[17]

[17] W. M. McMaster and H. D. Waller, *Geology and Soils of White Oak Creek Basin, Tennessee*, ORNL-TM-1108 (May 1965).

ORNL-DWG 65-8335

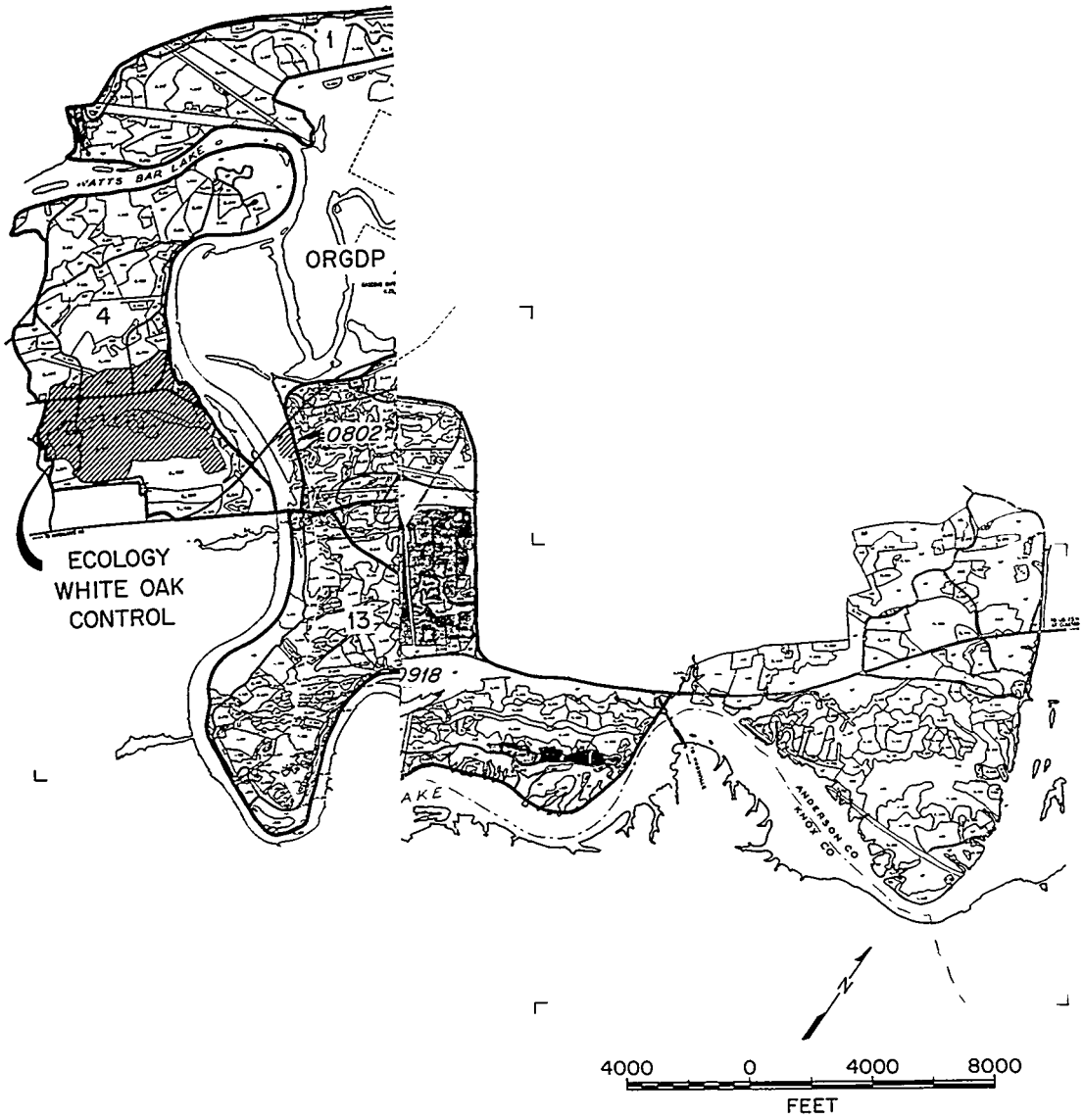

Table 10.4. Percentage of Area Transformed from a Given Vegetation Type in 1935 to Another Type by 1959

Numbers on the main diagonal represent percentages remaining in same vegetation type. This matrix times 0.01 gives $(pjk) = P$, expressing model of successional changes in vegetation type.

Dominant Vegetation in 1935			Dominant Vegetation in 1959							
			Conifer		Deciduous		Deciduous Plus			Nonforest
			Pine	Cedar	Lowland	Uplant	White Pine	Yellow Pine	Red Cedar	10
			1+2	3	4	5+6	7	8	9	
Conifer	Pine	1+2	93	1	0	3	0	3	0	0
	Cedar	3	10	68	0	6	0	14	2	0
Deciduous	Lowland	4	2	0	98	0	0	0	0	0
	Upland	5+6	0	0	0	96	0	2	0	0
Mixed	White pine—deciduous	7	0	0	0	0	100	0	0	0
	Yellow pine—deciduous	8	5	0	0	16	0	79	0	0
	Cedar—deciduous	9	0	0	0	2	0	0	98	0
Nonforest		10	55	18	2	11	0	10	3	0
Percent of present area			34	8	1	36	0	18	3	0

Previously open land (mostly pasture or other fields) showed highest probability (0.55) of becoming pine: Virginia (*Pinus virginiana*), shortleaf (*P. echinata*), planted shortleaf, loblolly (*P. taeda*), or white pine (*P. strobus*). Red cedar (*Juniperus virginiana*) had a higher probability (0.18) than either deciduous or mixed deciduous-pine cover (0.11 and 0.10) for invading nonforested land. Red cedar in turn tends to be transformed to yellow pine—deciduous mixtures (0.14) or pure pine (0.10) rather than hardwood (0.06) or cedar-hardwood mixtures (0.02). Cedar-hardwood remains a comparatively stable type (0.98 of the initial area of this type remaining in same type) — perhaps because of its persistence on favorable limestone outcrop sites. Only eight stands (only 51 acres) were typed as "white pine—hardwood," and these remained in the same category. The probability of persistence in the same state was almost as high for lowland deciduous (0.98) and upland deciduous forests (0.96). The impact of varying the probabilities of transfer due to natural trends, epidemics (e.g., southern pine beetle), or management policy can now be considered in simulations of long-term succession by comparison with a substantial body of empirical experience centering around our own research areas.

SUCCESSION AT COPPERHILL, TENNESSEE

Martin Witkamp Marilyn L. Frank

The five-year study (1960—1965) of buildup rates of living plant material, litter, humus, biota, carbon, and nitrogen in successional stages of a kudzu pioneer vegetation on denuded areas at Copperhill, Tennessee, showed a rapid accumulation of dead organic material (170 g m^{-2} $year^{-1}$) and especially nitrogen (8 g m^{-2} $year^{-1}$) on and in the soil (Table 10.5). However, in the nine-year-old stage, 30% of the nitrogen, 40% of the available potassium, and 70 to 80% of the available phosphorus above a soil depth of 2.5 cm are localized and partially immobilized in litter, thereby limiting the productivity of this pioneer ecosystem

Table 10.5. Carbon, Nitrogen, Phosphorus, and Potassium in Vegetation, Litter, and Humus plus Soil (to a Depth of 2.5 cm) of 2-, 5-, 7-, and 9-year-old Stages of Succession in a Kudzu Vine Vegetation on Eroded Soil at Copperhill, Tennessee

Means of triplicates in g/m^2

	Age (years)			
	2	5	7	9
Carbon				
Vegetation	11	105	184	250
Litter	19	323	582	803
Humus + soil	65	224	609	736
Total	95	652	1375	1789
Nitrogen				
Vegetation	0.4	4.5	6.7	7.9
Litter	0.5	13.7	23.6	23.3
Humus + soil	5.9	18.1	43.1	54.2
Total	6.8	36.3	73.4	85.4
Phosphorus				
Vegetation	0.02	0.16	0.21	0.31
Litter	0.02	0.47	1.14	1.11
Humus + soil	0.03	0.05	0.08	0.03
Total	0.07	0.68	1.43	1.45
Potassium				
Vegetation	0.4	3.2	4.1	5.4
Litter	0.1	1.9	2.9	4.4
Humus + soil	0.8	1.2	1.1	1.6
Total	1.3	6.3	8.1	11.4

severely and making its nutrient reserve very susceptible to removal by erosion in case of further disturbance. These accumulations and potential losses are important in the regeneration process of soil and for the prevention of irreversible loss of fertility following catastrophic removal of vegetation, such as might occur as a result of nuclear war or mismanagement of resources.

PREDICTION OF WEIGHT COMPOSITION FROM POINT SAMPLES

G. M. Van Dyne

Field point sampling of foliage and basal cover is frequently used to determine percentage species composition in ecological studies. Recently, laboratory point sampling has been employed to determine composition of forage samples taken from fistula samples, but reports of attempts to estimate percent weight composition with point sampling are scarce. Field time is more limited than laboratory time in many ecological studies, especially those conducted in radioactive areas such as White Oak Lake bed and an old field proposed to be tagged with ^{137}Cs.

Studies were conducted to develop and to test equations to predict percent weight composition (Y) of herbage samples from percent point composition (X), and consideration was given to transformation of variates, to adjusting equations through or not through the origin, to variations in equations for individual species vs groups, to effects of plant maturity stages, and to evaluating vegetational composition effects.[20]

Regression analyses showed that percentage botanical composition by weight can be estimated from composition determined with the laboratory point method based on point sampling of clipped herbage with a binocular microscope and hand separation of the same material. Satisfactory results were obtained by analysis of the percentage data on a linear basis through the origin if differences among species, seasons of growth, and botanical composition were taken into account.

RANDOM LOCATIONS FOR SAMPLE UNITS IN CIRCULAR PLOTS

G. M. Van Dyne

A procedure was developed from random location of study units utilizing only one marker post, which provides for rapid relocation of permanent plots, permanent line transects, and permanently tagged individual plants for ecological studies.[21] A circular plot area, with or without centers restricted from sampling, was subdivided by five intersecting diameters and an annulus of rings wherein the radii of the rings were determined by the following equation:

$$r_i = \sqrt{\frac{r_m^2 - r_0^2}{10} + r_{i-1}^2},$$

[20] H. F. Heady and G. M. Van Dyne, *J. Range Management* 18, 144–48 (1965).

[21] G. M. Van Dyne, *J. Range Management* 18, 150–51 (1965).

where r_m is the maximum plot radius and r_0 is the minimum radius. Distances from plot centers to sampling points were calculated with a computer program for plots with maximum radii varying from 25 to 200 ft in steps of 25 and containing center areas restricted from sampling at 0, 10, and 20% of the maximum radii. Use of this system for locating plots, transects, or plants in ecological studies showed that considerable field time may be saved as compared with conventional methods of establishing sampling locations.

---

11. Clinch River and Related Aquatic Studies

S. I. Auerbach[1] D. J. Nelson N. A. Griffith
B. G. Blaylock B. C. Patten[1] Margaret C. Merlini[2]
N. R. Kevern R. C. Early R. L. Iverson[3]

DEPOSITION OF STRONTIUM AND CALCIUM IN SNAIL SHELLS

D. J. Nelson Margaret C. Merlini

A previous study of the deposition of Sr and Ca in snail shells showed that Sr uptake was dependent primarily on the environmental Sr concentration with a slight negative interaction from Ca.[4] The response surface calculated from the previous experiment indicated an interesting area of minimal Sr uptake, dependent on both Ca and Sr concentrations. A similar experiment was performed with the range of 0.10 to 180.0 ppm Ca and 0.02 to 8.0 ppm Sr. Additional experimental points were used in the experiment design to define further the region of minimal Sr uptake. As in the previous experiment, the Ca and Sr inputs were rigidly controlled by analysis of all chemicals used in the media for adventitious Ca and Sr. Calcium and Sr uptake response surfaces (Figs. 11.1 and 11.2) were calculated from a least-squares fit of the uptake data. Experimental points within the range of Sr and Ca concentrations are indicated by circles on the figures.

Calcium uptake (Fig. 11.1) may be expressed by the equation: Ca uptake (atoms $\times 10^{16}$) = $-3.061 \times 10^{21} + 1.848 \times 10^{20}$ Sr $+ 8.205 \times 10^{19}$ Ca $- 8.421 \times 10^{16}$ Ca^2 $- 1.014 \times 10^{18}$ SrCa. This quadratic expression (without the Sr^2 term) is different from the planar response obtained in the prior experiment. The difference may be due to the increased number of experimental points which gave a more precise fit of the uptake data, or to an alteration of the basic chemical composition of the experimental environments. In this experiment the Mg and K concentrations were reduced. From other brief experiments with snails, it appeared that the Mg concentration was an important factor.

Strontium uptake was expressed by the equation: Sr uptake (atoms $\times 10^{15}$) = $4.558 \times 10^{19} + 2.660 \times 10^{18}$ Sr $- 5.775 \times 10^{17}$ Ca $+ 1.611 \times 10^{15}$ Ca^2 $- 6.571 \times 10^{15}$ SrCa. The response surface (Fig. 11.2) is similar to that obtained in the previous experiment. The occurrence of a minimal Sr uptake within the range of experimental concentrations was particularly gratifying. While Sr uptake at the low Ca concentrations is largely dependent on the environmental Sr concentration, a region at higher Ca concentrations exists where a minimal Sr uptake occurs. At still higher Ca concentrations, the Sr uptake again increases. This shows that both Ca and Sr amendments to an environment should be controlled carefully in order to effect a reduction in radiostrontium uptake. Other biological systems should be tested to see if they respond similarly to different Ca and Sr concentrations.

---

[1]Dual Capacity.

[2]Consultant.

[3]Temporary summer employee.

[4]S. I. Auerbach *et al.*, *Health Phys. Div. Ann. Progr. Rept. July 31, 1964*, ORNL-3697, p. 96.

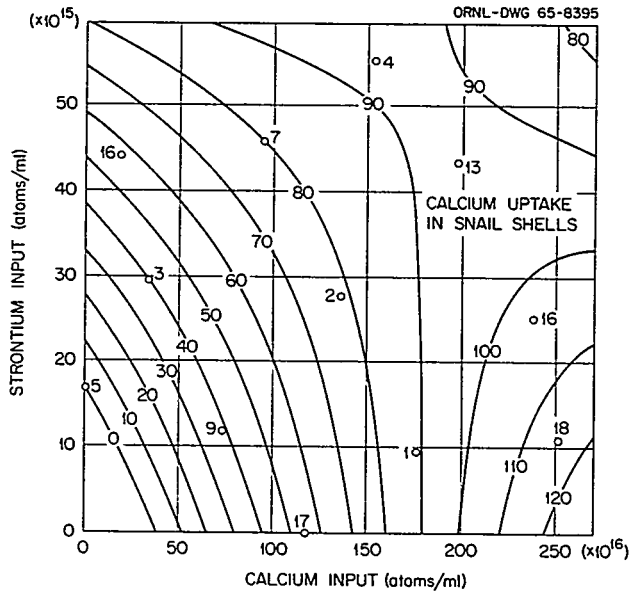

Fig. 11.1. Calcium Uptake (Atoms $\times 10^{-4}$) in Snail Shell as a Function of Environmental Calcium and Strontium Concentrations. 50×10^{16} atoms Ca/ml = 33.22 ppm Ca; 10×10^{15} atoms Sr/ml = 1.46 ppm Sr.

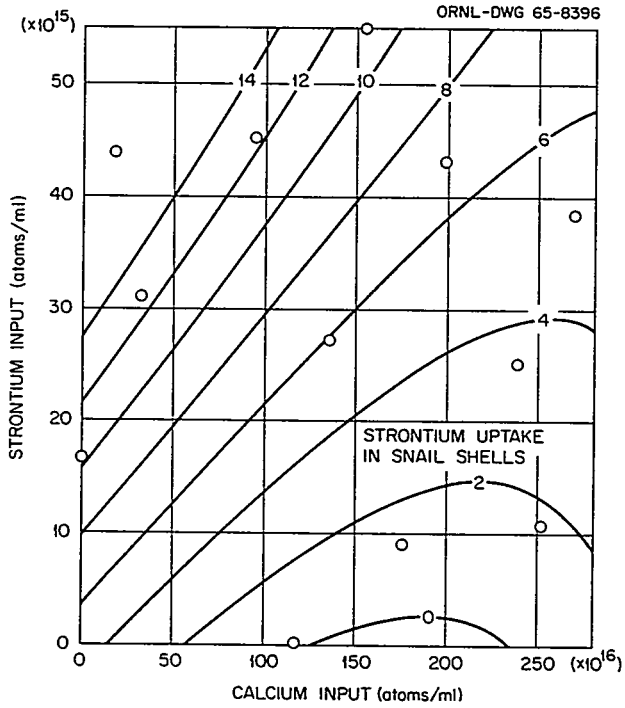

Fig. 11.2. Strontium Uptake (Atoms $\times 10^{-4}$) in Snail Shell as a Function of Environmental Calcium and Strontium Concentrations. 50×10^{16} atoms Ca/ml = 33.22 ppm Ca; 10×10^{15} atoms Sr/ml = 1.46 ppm Sr.

MICROCHEMICAL CONSTITUENTS OF CONTEMPORARY AND INDIAN MIDDEN CLAM SHELLS

D. J. Nelson

Trace-element incorporation into biogenic calcareous materials is used frequently by geochemists to interpret paleochemical environments. These studies have been applied mostly to geologic ages and marine environments. In connection with our previous studies of Sr and ^{90}Sr deposition in contemporary Clinch and Tennessee River mollusk shells, a number of 1000- to 2000-year-old Indian midden clam shells were analyzed for their microchemical constituents, particularly Sr, to see if relatively recent shells could be used in a manner analogous to geologic materials.

In one locality contemporary shells were collected from the river and midden shells on the bank. Thus, shells from the same species were similar except for the difference in time. The shells were analyzed either by flame spectrophotometry or by emission spectrography, and results from either technique were comparable.

The Sr concentrations in midden shells of several species of clams were consistently greater than those of the contemporary shells (Table 11.1). Differences in the Sr concentrations among contemporary shells existed and were probably due to localized habitat variables as well as age of the shells analyzed. Generally, inter- and intraspecific differences in Sr concentrations among the contemporary shells were small compared with the observed differences between the contemporary and ancient shells.

Several possible explanations were explored to determine the reasons for the higher Sr concentrations in Indian midden shells. The possible causal factors considered were the following: (1) environmental changes induced by the construction of Tennessee Valley Authority dams, (2) postmortem changes in the chemical composition of the shells resulting from solution and redeposition, (3) biological changes in the clams resulting in a different metabolism of mineral elements, (4) alteration of the chemical composition of river water resulting from erosion of different rock strata, and (5) alteration of the chemical composition of river water because of man's activities, particularly cutting of forests and imposition of an agricultural economy on the watershed.

Table 11.1. Strontium Concentrations in Contemporary and Indian Midden Clam Shells

Species	Collecting Site	Contemporary N	Contemporary Sr (μg/g ± S.E.)	Midden N	Midden Sr (μg/g ± S.E.)
Elliptio crassidens	TRM521	15	211.4 ± 3.66	5	330.6 ± 7.03
	CRM47	10	260.9 ± 5.00		
	TRM425	7	196.4 ± 6.40		
	TRM100	5	228.2 ± 15.5		
	UMMZ	6	178.8 ± 10.3		
E. dilatatus	CRM66	2	222 ± 6.52		
	CRM47	10	206 ± 5.16		
	TRM425	1	218		
	TRM521			12	336.6 ± 10.2
	UMMZ	7	195 ± 6.47		
Pleurobema cordatum	CRM47	10	201 ± 5.63		
	TRM427	11	237.3 ± 6.60		
	TRM521			10	335.9 ± 12.4
Actinonaias carinata gibba	CRM47	7	185.7 ± 5.55		
	TRM521			10	304.1 ± 7.28
Plagiola lineolata	TRM425	3	199.7 ± 4.06		
	TRM521			5	343.8 ± 17.1

N = number of shells analyzed.
S.E. = standard error of the mean.
TRM = Tennessee River Mile.
CRM = Clinch River Mile.
UMMZ = University of Michigan Museum of Zoology.

The Tennessee Valley Authority dams changed the discharge and temperature regimes in the rivers. The effect of these structures could be verified by analyzing shells collected in this area prior to the construction of dams. Shells from the University of Michigan Museum of Zoology collected prior to the construction of dams (UMMZ, Table 11.1) were analyzed. The Sr concentrations in the museum specimens of *Elliptio crassidens* and *E. dilatatus* were similar to those in other contemporary specimens, showing that environmental changes produced by the dams were not the factor.

Biological evolution, resulting in an alteration of mineral metabolism, is impossible to test. However, it is considered highly improbable that a natural population would alter its metabolism significantly within 1000 to 2000 years. Similarly, it is unlikely that changes in drainage patterns from the geologic strata occurred which would affect the chemical composition of river water.

Geochemists generally recognize that solution and redeposition of mineral elements occur in deposited materials. Fortunately, it is possible to test this factor by analyzing annual layers in the clam shell. Previous studies showed that there was a heterogeneous distribution of Sr within the shell of fresh-water clams.[5] In cross sections of the clam shells, two distinct nacreous layers may be observed (Fig. 11.3). An outer *P* layer and an inner *L* layer exists for each year of a clam's growth. Strontium concentrations in the *P* layers are low and do not differ greatly with age of the clam at the time of deposition. Conversely, Sr concentrations in the inner *L* layers are similar to those in the *P* layers during the first five to eight years, and higher Sr concentrations are present in the annual layers in subsequent years. Because of the two distinct nacreous layers and the differential deposition of Sr, a unique heterogeneous distribution of Sr occurs within each shell. This unique distribution of Sr would be obliterated if solution and redeposition of Sr occurred.

[5]D. J. Nelson, *Intern. Ver. Theoret. Angew. Limnol. Verhandl.* 15, 893–902 (1964).

Analyses of the annual layers in several *E. crassidens* shells showed that the heterogeneous distribution of Sr exists in the midden shells (Table 11.2). Furthermore, Sr concentrations in annual layers of midden shells were approximately 50 to 100% higher than in corresponding annual layers of contemporary shells. These differences in Sr concentrations in the annual growth layers were similar to those observed from the analyses of individual shells. From the results it is apparent that measurable solution and redeposition had not occurred after the shells were discarded in the midden.

Strontium inclusion in living mollusk shells is almost directly proportional to the concentration of Sr in the aquatic environment. Thus, we can conclude that when the midden shells were living in the river, the water contained 50 to 100% more Sr than now.

Circumstantial evidence accounting for higher Sr concentrations may be inferred from changes in the landscape resulting from colonization. Prior to the arrival of white settlers, this region was heavily forested. The virgin forests had a rich litter-humus layer on the forest floor and an abundance of roots in the soil. Respiratory activity in

ORNL-LR-DWG 71784

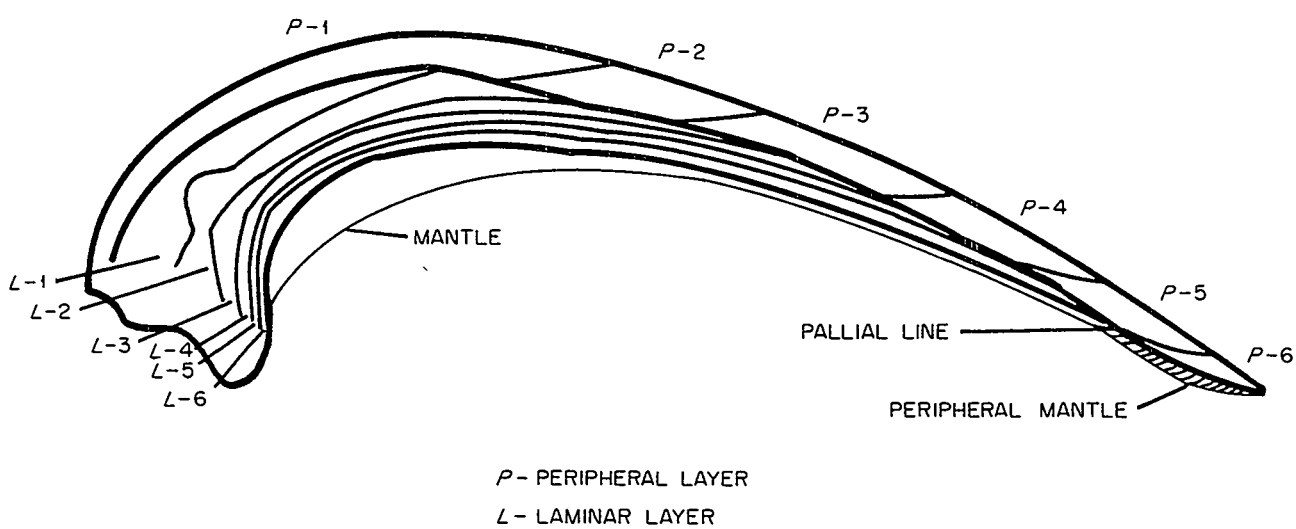

Fig. 11.3. Cross Section of a Six-Year Old *Elliptio crassidens* Shell, Showing the Relationship of the Peripheral and Laminar Layers.

the humus layer and of the tree roots resulted in a soil atmosphere rich in carbon dioxide. The carbon dioxide, together with the large amount of percolating ground water, was ideal for the formation of carbonic acid and the dissolution of alkaline-earth carbonates as the bicarbonates. Cutting of these forests for lumber and farming portions of the watershed reduced the quantity of carbon dioxide in the soil and also resulted in a decrease in the proportion of rainwater percolating through the soil to enter the ground water. It is suggested that in the period 1000 to 2000 years ago the ground water and river water contained higher concentrations of dissolved minerals.

Clam shells are essentially pure calcium carbonate with trace concentrations of other elements such as Sr, Ba, Mg, Mn, Na, and K. It is not possible to assess the levels of Ca in river water on the basis of clam shells because increased Ca deposition would result in increased growth. However, examination of prehistoric and contemporary shells indicates no disparity in growth rates. In addition to the higher levels of Sr, comparative data show that the Ba and Mn concentrations are also higher in the midden shells and no difference exists in the Na concentrations. Additional results which are not directly comparable suggest that Mg occurs at greater concentrations in the midden shells and no difference exists in the K concentrations.

From these results we may infer that the imposition of an agricultural economy on a forested landscape resulted in significant changes in the geochemical relationships between a watershed and the river. Perhaps of even greater importance is the fact that we have shown that mollusk shells have a heterogeneous distribution of trace elements which may be used to determine whether postmortem replacement has occurred. This capability is important for interpreting the long-term behavior of Sr and other elements present in the shells.

Table 11.2. Strontium Concentrations ($\mu g/g$) in Peripheral and Laminar Layers of Indian Midden and Contemporary *Elliptio crassidens* Shells

Year of Layer	Midden								Contemporary							
	928		929		930		931		461	463	1		462		464	
	P^a	L^b	P	L	P	L	P	L	L	L	P	L	P	L	P	L
1	318	331						383	245	235	210	240				
2			292	307					230	220	210	230	215	235		225
3					359	300			215	220	210	220	235	255	235	240
4	327	405					343	422	220	255	210	250	225	230	245	250
5									235	235	190	240	215	265	240	225
6									245	245	180	300	215	295	245	240
7			356	370					250	270	190	300	245	370	215	275
8	296	403			331	396			345	280	200	350			215	235
9										320					255	330
11				524			296	393								
12						482										
13			328	534												
15					314	496		470								
19							380	510								

[a] P = peripheral layer.
[b] L = laminar layer.

POPULATION GENETICS AND RADIATION EFFECTS STUDIES

B. G. Blaylock R. C. Early

The population of *Chironomus tentans* inhabiting White Oak Creek has merited continuing investigation because it is a natural population that has been exposed to approximately 230 rads/year of chronic environmental radiation for over 120 generations. Previously we have shown that in this population there is an increase of new chromosomal aberrations which are eliminated rapidly. Also, we have studied the chromosomal polymorphism produced by three endemic inversions in this population. These inversions are well established in the population at certain frequencies which do not fluctuate seasonally and have not changed significantly for the past five years.

A pertinent question is whether the exposure to chronic low-level radiation has affected the fitness of the population to survive in its environment. Others have shown in studies of laboratory populations that chromosomal polymorphic populations are superior to monomorphic populations in their ability to produce a greater biomass and more individuals on the same amount of food. Also, it has been shown that polymorphic populations have a greater capacity for increase. Since in some cases large acute doses of radiation may decrease chromosomal polymorphism in a population, a comparison of the chromosomal polymorphism in the chronically irradiated natural population of *C. tentans* was made with a nonirradiated population. A decrease in chromosomal polymorphism therefore could indicate a decrease in fitness of the irradiated population. Table 11.3 shows no significant difference in the frequencies of the three endemic inversions in collections made from 1962 to 1964 in White Oak Creek and Ten Mile Creek. It appears that the exposure of these organisms to chronic irradiation which is capable of producing a detectable increase of new chromosomal aberrations has not affected the frequencies of the endemic inversions. Or, if there was an initial effect produced on the frequencies of the inversions by ionizing radiation, the population has compensated for it.

In conjunction with the studies on the natural populations of *C. tentans,* laboratory populations of *Drosophila melanogaster* were established to study the effects of acute and chronic irradiation on balanced chromosomal polymorphism. An inversion was needed that would reach equilibrium at a high frequency. The inversion 3-R-Payne, which is found in natural populations, was tried in population cages that would support approximately 5000 *D. melanogaster.* Analyses of the salivary gland chromosomes were made to determine the frequency of the inversion in the population. After approximately ten generations in a population cage that had been started with 100 males and 100 females that were heterozygous for the inversion, 58.8% of the individuals were heterozygous for the chromosomal arrangement. About four generations later, 64.3% of the individuals were heterozygous for the inversion. Thus, inversion 3-R-Payne appears to be an excellent inversion to use in studying the

Table 11.3. Frequency of Inversions Heterozygotes in Irradiated and Nonirradiated Natural Populations of *Chironomus tentans*

	Irradiated Population of White Oak Creek in 1962–64	Nonirradiated Population of Ten Mile Creek in 1962–64	χ^2	P (1 degree of freedom)
No. of larvae analyzed	439	407		
Inversion 1Ra	67	74	1.29	0.50–0.25
Inversion 2Lab	99	90	0.02	0.90
Inversion 3Ra	36	37	0.22	0.75–0.50

effects of ionizing radiation on chromosomal polymorphism. Consequently, a population of *D. melanogaster* that had been established for approximately two generations was given an acute dose of 2000 rads. The frequency of the inversion heterozygote, which had been approximately 60% before irradiation, was 30% two generations after the population was irradiated. It appears that in the case of inversion 3-R-Payne the administering of 2000 rads to the population drastically reduces the frequency of the inversion heterozygote. This work is in the preliminary stage, and larger samples are needed before conclusions can be reached. However, these preliminary results suggest that experiments with inversion 3-R-Payne can be used to determine whether chronic low-level radiation will reduce chromosomal polymorphism in laboratory populations. In this case it may be possible to detect the effect of ionizing radiation by a decrease in the frequency of inversion heterozygotes.

^{134}Cs DISTRIBUTION AND TRANSPORT IN THE CARP

N. R. Kevern N. A. Griffith

The distribution of ^{134}Cs in carp (*Cyprinus carpio*) was determined by feeding a single tagged meal to the fish, sacrificing and dissecting the fish, and counting the various parts. The redistribution of ^{134}Cs was studied by sacrificing a series of fish from 16 hr to 79 days. The tissues and organs counted were blood, gut, liver, heart, gills, kidney, spleen, skin, scales, flesh, and bone. The carp used were similar but not uniform in size, and the amount of ^{134}Cs ingested was not constant for each fish, necessitating that the data be normalized. Data were plotted as the ratio of activity per gram of tissue to initial activity per gram of whole body. Analog computer traces which fit the data are shown in Fig. 11.4. (See Theoretical and Systems Ecology Section for discussion.)

The ^{134}Cs was absorbed and transferred rapidly by the gut. Although blood is the common vehicle for transferring cesium throughout the fish, analog computer analysis suggested that lymph may be important in conveying cesium from the gut to the blood. Activity in the gut peaked before the first sample was taken and thus showed a sharp decline (Fig. 11.4*a*). The uptake and subsequent loss of ^{134}Cs by the tissues indicated three types of cesium metabolism. Skin, scales, and spleen paralleled the blood, having peak activities between 3 and 5 days and then declining rapidly (Fig. 11.4*a*). Liver, heart, gills, and kidney, active organs which process blood in some manner in addition to having a blood supply, demonstrated the highest and earliest (about 1 day) initial activity and then declined exponentially (Fig. 11.4*b*). Bone and flesh accumulated cesium slowly, probably through an active transport system, peaked at 6 and 15 days, respectively, and then declined very slowly (Fig. 11.4*c*).

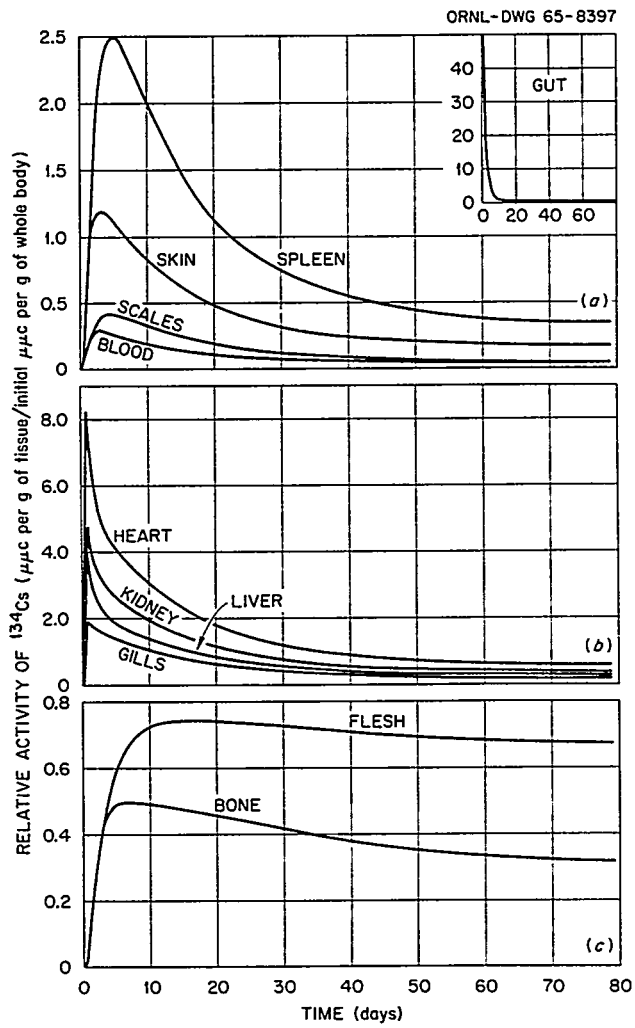

Fig. 11.4. Uptake and Loss of ^{134}Cs by Organs and Tissues of Carp. (*a*) Spleen, skin, scales, blood, and gut; (*b*) heart, liver, kidney, and gills; and (*c*) flesh and bone.

Estimates of the biological half-life for cesium in the various tissues were calculated from the computer curves. The biological half-life in days for each tissue was as follows: heart, 16; kidney, 17.4; liver, 17.8; gills, 21.2; scales, 22.3; spleen, 24.1; skin, 26.6; blood, 39.5; bone, 97.0; and flesh, 280.0. The half-life for cesium in the gut was 1.8 days for the initial rapid loss and 25 days for the slower component. The long half-life of cesium in the flesh may be of significance when considering contaminated fish for human consumption. The whole-body half-life for ^{134}Cs in carp at similar water temperatures would be about 80 days.[6] Fish that were contaminated with radioactive cesium and kept in uncontaminated water to allow biological turnover to reduce the body burden would have a higher flesh burden than would be indicated by whole-body data.

FEEDING RATE AND METABOLISM OF CARP IN WHITE OAK LAKE

N. R. Kevern N. A. Griffith

A continuing project on White Oak Lake includes studies of the cycling of radionuclides, especially ^{137}Cs, in an aquatic environment, the role of detritus in aquatic food chains, and various other ecological aspects of the plants and animals in the lake. The availability of a lake contaminated with ^{137}Cs offers a unique opportunity to estimate the feeding rate of fish in a natural population and their caloric requirements for maintenance and growth. The study of the feeding rate and metabolism of carp has also involved the influence of these fish on the fate of ^{137}Cs in the lake and the importance of detritus in their diet. The equation used to calculate the feeding rate is based on the amount of radionuclide that must be ingested to maintain an equilibrium body burden when the radionuclide has a known assimilation and turnover by the organism. As first presented in an ecological sense by Davis and Foster,[7] the equation is

$$q = \frac{(p + b)Q}{a},$$

where q is the rate of ingestion of the radionuclide, p is the rate of physical decay, b is the rate of biological elimination of the radionuclide, Q is the body burden, and a is the fraction of the ingested radionuclide that is assimilated by the organism. The equation assumes that the radionuclide used enters the organism only through the food chain and that the organism is in equilibrium with the environment. Experiments have shown that freshwater fish do not accumulate cesium directly from the water. Autoradiograms of scales from carp taken from White Oak Lake demonstrate a uniform distribution of radioactivity in the scales, thus indicating that the carp have been in the lake since they were spawned and are in equilibrium with the lake environment.

The biological half-life for cesium in carp and the influence of temperature on the half-life have been determined in the laboratory.[8] The effective rate of turnover ($p + b$) for cesium in carp at an average temperature of 16.5°C is 0.01/day. The average body burden (Q) of ^{137}Cs in the carp is 24.2 $\mu\mu c/g$. The diet was determined by analysis of gut contents and was simplified to 40% algae and 60% detritus. The amount of ingested ^{137}Cs assimilated (a) by the carp was determined in the laboratory by feeding tagged food to the fish. Carp removed approximately 7% of the ^{137}Cs from detritus and 80% from algae. Cesium is adsorbed on the detritus and apparently not readily available to the fish, while cesium in algae exists largely as a labile pool in the cell which is released by digestion and readily absorbed by the gut. The average amount of ^{137}Cs associated with algae and detritus samples taken from the lake is 18 and 9 $\mu\mu c$ per gram of wet weight respectively. The calculated amount of ^{137}Cs ingested by a yearling carp (146 g) was 81.2 $\mu\mu c$/day or 3.90 g of detritus per day and 2.56 g of algae per day. Since growth is not included in the body burden, this food intake is for maintenance alone. Based on the caloric content of the algae and detritus, the intake for maintenance by yearling carp was 6030 cal/day. A mammal of comparable size requires about 21,000 cal/day for maintenance, most of which is used for maintaining body temperature and muscle tonus for support and therefore is not required by fish.

A one-year-old carp increases in weight about 200 g between the age of one and two years. Using

[6] S. I. Auerbach *et al.*, *Health Phys. Div. Ann. Progr. Rept. July 31, 1964*, ORNL-3697, p. 101.

[7] J. J. Davis and R. F. Foster, *Ecology* 39, 530–35 (1958).

[8] S. I. Auerbach *et al.*, *Health Phys. Div. Ann. Progr. Rept. July 31, 1964*, ORNL-3697, p. 101.

the same formula, the increase in mass and associated ^{137}Cs required an additional daily intake of 28.4 $\mu\mu c$, or 0.88 g of algae and 1.4 g of detritus. The total annual intake for growth is about 830 g of food, giving a conversion of food to fish of 24%. Assuming a carp population of 300 lb/acre, the fish would contain 3.3 μc of ^{137}Cs, would turn over 30 μc of ^{137}Cs per acre per year, and would consume 4000 lb of detritus per acre per year.

RADIATION EFFECTS ON CARP REPRODUCTION

N. R. Kevern B. G. Blaylock
N. A. Griffith

The effects of chronic low-level irradiation, which might exist over large areas should fallout levels increase or should there be a nuclear disaster, have not been studied as intensively as effects of acute high-level irradiation. Conditions in White Oak Lake provide an opportunity to study the long-range effects of low-level irradiation in a natural environment. Preparations have been made to study the effects of chronic low-level irradiation on the reproductive capacity of the carp population in White Oak Lake. Background data have been collected and techniques for spawning and hatching carp eggs have been tested. The accumulated radiation dose to the gonads of five-year-old carp, estimated by glass-rod dosimetry, is approximately 800 rads and is a result of body burdens, in micromicrocuries per gram of live weight, of ^{106}Ru, 19.7; ^{65}Zn, 6.4; ^{60}Co, 8.9; ^{137}Cs, 24.2; and ^{90}Sr (no data). Carp spawned in the East Tennessee area from April 20 through the first week of May 1965 after water temperatures had reached 21°C. Carp from White Oak Lake were collected and spawned in the laboratory on glass slides in plastic boxes and in plastic boxes containing a nylon cloth previously attached to the bottom. Hatchability of eggs on glass slides averaged 75%, while hatchability in nylon-lined boxes averaged 1%. Although the nylon-lined boxes had been rinsed for two months in springwater to remove toxic residues, some detrimental factor was still present. Hatcheries often achieve a 90% hatch of carp eggs; thus if the techniques used for the boxes with glass slides were adequate, some radiation effects may be indicated. The study will be continued during the next spawning season with controls from uncontaminated waters in the area.

^{85}Sr AND PRIMARY PRODUCTIVITY

B. C. Patten R. L. Iverson

A standard method for estimation of aquatic primary production is based on assimilation of ^{14}C. This isotope is difficult to work with because it is a weak beta emitter. Furthermore, it has recently been demonstrated[9] that significant quantities of newly synthesized photoassimilate are released into the medium by phytoplankton as ^{14}C-labeled dissolved organic matter.

A number of radioisotopes other than carbon have been indicated in the literature to have differential uptake by plankton organisms in light and dark, suggesting that these may have some potential for estimating primary production. These radionuclides include ^{32}P, ^{65}Zn, ^{89}Sr, ^{90}Sr, ^{99}Mo, and ^{137}Cs.

Preliminary experiments with natural water samples from Melton Hill Lake into which ^{85}Sr was admitted indicated that uptake of this isotope by plankton differed significantly in light and dark (Fig. 11.5). Because ^{85}Sr is a strong gamma emitter and therefore easy to count, it was decided to compare estimates of production parameters obtained from ^{85}Sr data with measurements made by the standard dark- and light-bottle oxygen method. A number of field experiments was performed in situ, and data from one of these are graphed in Fig. 11.6. In this experiment (July 29, 1964), water obtained from a depth of 8 ft was bottled, tagged, and resuspended for 6 hr at depths of 0, 2, 6, 10, 14, 18, and 22 ft. The thermocline was located at about 6 ft; water above this depth was about 28°C, and water below ranged from 13 to 18°C. The ambient concentration of stable Sr was about 0.07 mg/liter.

In Fig. 11.6 results obtained by the oxygen method are graphed against results computed from ^{85}Sr uptake differences in dark and light bottles. The graph for gross production shows a good relationship between the two methods except near the surface, where light intensities were highest. Photoinhibition of photosynthesis is typically observed in surface waters when determinations are made by the oxygen of ^{14}C methods. Since ^{85}Sr uptake continues to increase at 0 and 2 ft in Fig. 11.6, this may indicate that photoinhibition is actually an artifact resulting, perhaps, from significant changes in the photosynthetic quotient (ratio of

[9] J. A. Hellebust, *Limnol. Oceanog.* 10, 185 (1965).

CO_2 assimilated to O_2 released) accompanying changes in the kinds of organic compounds synthesized under high light conditions. The graph for net production also shows good correspondence between the oxygen and ^{85}Sr methods, except toward the surface. Results of respiration were not as satisfactory. As Fig. 11.6 shows, respiration of the samples when suspended near the surface was considerably greater than in and below the thermocline. However, the degree of increase was less by the ^{85}Sr method than by the oxygen procedure.

The data in Fig. 11.6 are typical and encouraging, but a number of problems remain to be worked out before ^{85}Sr can be considered seriously for estimating aquatic production.

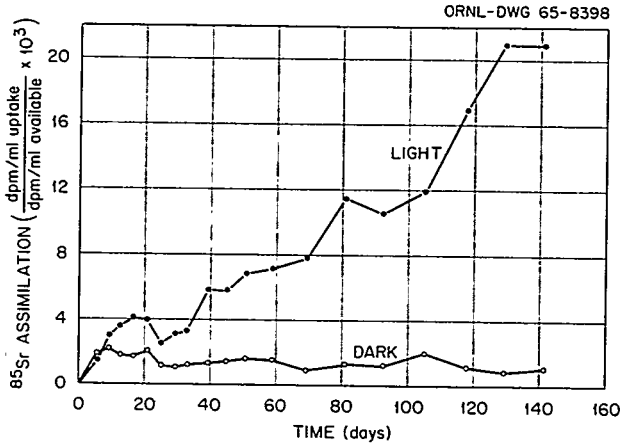

Fig. 11.5. Light and Dark Assimilation of ^{85}Sr by Plankton from Melton Hill Lake as a Function of Time.

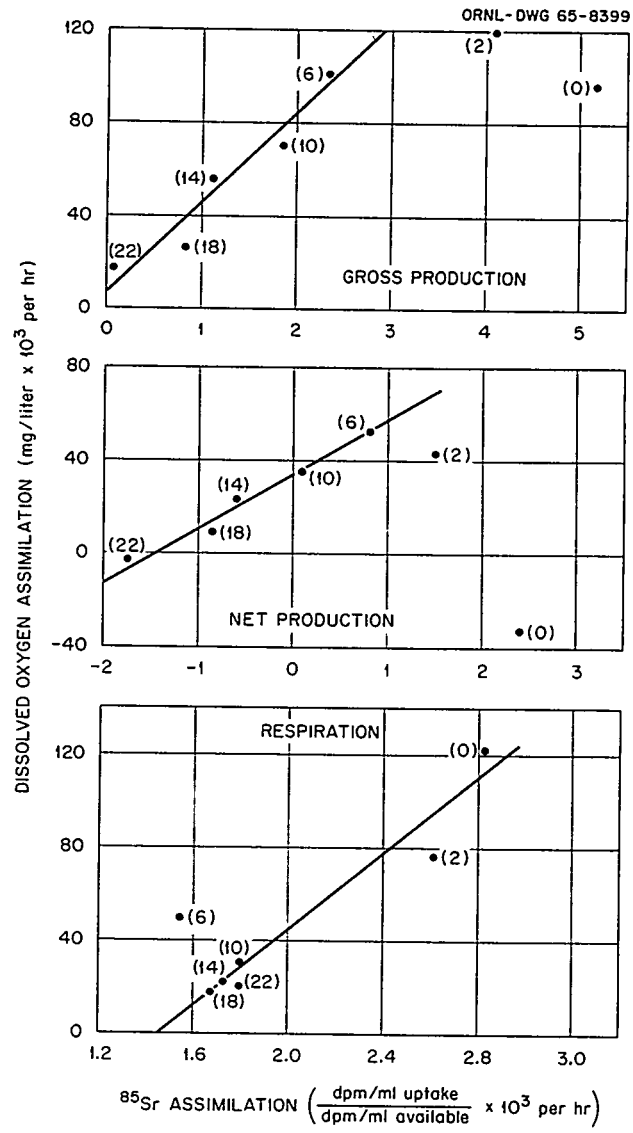

Fig. 11.6. Comparison of Gross Production, Net Production, and Respiration as Determined by the Dark- and Light-Bottle Oxygen Method and by ^{85}Sr Assimilation. Bottle suspension depths (ft) are indicated parenthetically.

12. Theoretical and Systems Ecology

B. C. Patten[1] G. M. Van Dyne[1]
J. S. Olson[1] L. J. Bledsoe, Jr.[2]

ODD-EVEN RELATIONSHIPS IN FOOD WEBS

B. C. Patten

Food webs in ecosystems are analogous to communication networks in other information-transferring systems. Movement of radionuclides requires a trophic network, and disruptions such as those produced by ionizing radiation imply breaks in various parts of an established food web. Consequently, mathematical properties of food web structure may be of interest. The following properties were derived from characteristics of mathematical graphs.[3]

1. Every food web contains an even number of species in trophic contact (eating or eaten by, or both) with an odd number. The number of species eating or eaten by an even number of species may be either even or odd.
2. The number of species eating an odd number of species has the same oddness and evenness as the number eaten by an odd number. The number of species which eats an even number of species is similarly odd or even as the number eaten by an even number is odd or even.
3. When the number of species in trophic contact with an even number of species is odd, then the number feeding upon an odd number is of opposite evenness and oddness from the number feeding on an even number, and the number eaten by an odd number is likewise of opposite evenness and oddness from the number eaten by an even number. When the number of species in trophic contact with an even number of species is even, the number eating an odd number, the number eating an even number, the number eaten by an odd number, and the number eaten by an even number are either all even or all odd.
4. When there is an odd number of species in trophic contact with an even number, both the total number of feeding species and the total number of species consumed are odd. When the number in trophic contact with an even number is even, then both the total number of species eating and eaten are even.

EQUILIBRIUM SPECIFIC ACTIVITY IN TWO-COMPARTMENT EXCHANGE SYSTEMS

B. C. Patten

It is commonly thought that when total-element equilibration occurs between two compartments, the specific activity (ratio of radioisotope concentration to total element) must be equal in both compartments. This is not necessarily true because three kinds of equilibria can actually occur in closed, two-compartment exchange systems: (1) equilibria of total element, stable element, and radioisotope occur simultaneously, at which time specific activities of the compartments become equal; (2) total element, stable element, and radioisotopic equilibria all develop as limit processes, and consequently specific activities never become strictly equal in an experiment of finite duration; and (3) total element equilibrium may be achieved in a finite experiment, but equilibria of radioisotope and stable element occur in the limit only, so that specific activities merely approach equality as time extends to infinity.

The latter case is a consequence of necessary and sufficient conditions for total element equilibrium, which can be developed as follows: Let

[1]Dual capacity.

[2]Consultant.

[3]O. Ore, *Theory of Graphs*, Am. Math. Soc. Colloq. Publ. 37, Cushing-Malloy, Ann Arbor, Mich., 1962.

$X_i \equiv$ concentration of radioisotope $[ML^{-3}]$ or number of atoms $[M]$ in compartment i $(i = 1, 2)$,

$Y_i \equiv$ concentration of stable element $[ML^{-3}]$ or number of atoms $[M]$ in compartment i,

$Z_i = X_i + Y_i \equiv$ total concentration $[ML^{-3}]$ or number of atoms $[M]$ of element in compartment i,

$R_i = Y_i/(X_i + Y_i) \equiv$ relative abundance of stable element [dimensionless] in compartment i,

$S_i = X_i/(X_i + Y_i) \equiv$ specific activity [dimensionless] in compartment i,

$\lambda_{ij} \equiv$ rate constant $[T^{-1}]$ for transfer of element from compartment i to j. Then, $\dot{X}_i = \dot{Y}_j$ *$(i,j = 1, 2;\ i \neq j)$ are necessary and sufficient for total element equilibrium.*

Proof: 1) The conditions are necessary.

a) $\dot{Z}_i = 0 \Rightarrow \dot{X}_i = -\dot{Y}_i$ because $\dot{Z}_i = \dot{X}_i + \dot{Y}_i$.

b) $\dot{X}_i = -\dot{X}_j$ and $\dot{Y}_i = -\dot{Y}_j$ from the system equations:

$$\dot{Z}_j = \lambda_{ij}Z_i - \lambda_{ji}Z_j ,$$

$$\dot{X}_j = \lambda_{ij}Z_iS_i - \lambda_{ji}Z_jS_j = \lambda_{ij}X_i - \lambda_{ji}X_j ,$$

$$\dot{Y}_j = \lambda_{ij}Z_iR_i - \lambda_{ji}Z_jR_j = \lambda_{ij}Y_i - \lambda_{ji}Y_j .$$

c) Therefore, $\dot{X}_i = \dot{Y}_j$.

2) The conditions are sufficient.

a) $\dot{X}_i = \dot{Y}_j \Rightarrow -\dot{X}_j = \dot{Y}_j$ from the system equations.

b) $-\dot{X}_j = \dot{Y}_j \Rightarrow \dot{X}_j + \dot{Y}_j = \dot{Z}_j = 0$.

There is nothing in these conditions for total element equilibrium which stipulates that $S_i = S_j$. If the specific activities should not be equal when total element equilibrium occurs, then both radioisotope and stable isotope concentrations will continue to change in the two compartments. The rate of change will be in the proportion $k = \lambda_{ij}Z_i(0)$ to the gradient $|S_i - S_j|$:

$$\dot{X}_i = k\,(S_j - S_i) ,$$

$$\dot{Y}_i = k\,(S_i - S_j) ,$$

and the direction of net movement will be controlled by the signs of $\dot{X}_i$ and $\dot{Y}_i$ ($S_j > S_i \Rightarrow X_i$ and Y_j increase, X_j and Y_i decrease; $S_j < S_i \Rightarrow X_i$ and Y_j decrease, X_j and Y_i increase).

Since the first derivatives of the specific activities with respect to time are $\dot{S}_i = \dot{X}_i/Z_i$, S_i and S_j have extrema when $\dot{X}_i = \dot{X}_j = 0$. These extrema are the same since $\dot{X}_i = \dot{X}_j = 0 \Rightarrow S_i = S_j$, but one is a maximum and the other a minimum because $\dot{X}_i = -\dot{X}_j$ from the system equations, so that if S_i increases then S_j must decrease. Thus, if $S_i \neq S_j$ when $\dot{X}_i = \dot{Y}_j$, the stable element and radioelement become redistributed between the compartments ($S_i \to S_j$ as $t \to \infty$) even though the total amount of element remains at equilibrium.

STATIONARY DISTRIBUTION AND TURNOVER OF RADIOACTIVITY IN A HYPOTHETICAL FOOD CHAIN

B. C. Patten

A hypothetical food chain model was formulated for analog computer determinations of steady-state distributions and turnover rates of radioactivity in the system under a constant chronic input to the primary producers. The model was intended for possible application to plankton systems, and is of the constant transfer coefficient variety. Computer experiments were performed to determine effects of altering various combinations of coefficients.

With $X_i \equiv$ radioactivity (expressed in computer volts) in compartment i ($i = 0, 1, \ldots, 4$; where $0 \equiv$ environment, $1 \equiv$ primary producers, $2 \equiv$ herbivores, $3 \equiv$ carnivores, and $4 \equiv$ pooled dead organic matter and decomposers), and $\lambda_{ij} \equiv$ transfer coefficients from compartment i to j ($j = 0, 1, \ldots, 4$), the model is

$$\dot{X}_1 = \lambda_{01}X_0 - (\lambda_{10} + \lambda_{12} + \lambda_{14})\,X_1 ,$$

$$\dot{X}_2 = \lambda_{12}X_1 + \lambda_{42}X_4 - (\lambda_{20} + \lambda_{23} + \lambda_{24})\,X_2 ,$$

$$\dot{X}_3 = \lambda_{23}X_2 - (\lambda_{30} + \lambda_{34})\,X_3 ,$$

$$\dot{X}_4 = \lambda_{14}X_1 + \lambda_{24}X_2 + \lambda_{34}X_3 - (\lambda_{40} + \lambda_{42})\,X_4 .$$

Six experiments were performed in which parameters were varied (Table 12.1) and steady-state distributions and turnovers of radioactivity were recorded (Table 12.2). The primary input to producers, $\lambda_{01}B_0$, was a constant 5 v in all experiments except experiment 3, where it was doubled.

Table 12.1. Parameter Values (Potentiometer Settings) in Six Analog Computer Experiments

For experiments 2 to 6, only differences with experiment 1 are indicated

Parameter ($i \neq j$)	Experiment No. 1	2	3	4	5	6
λ_{01}	0.05		0.10			
λ_{12}	0.05		0.075			
λ_{23}	0.05					
λ_{42}	0.00	0.05				
λ_{10}	0.10			0.40		
λ_{20}	0.20			0.30		
λ_{30}	0.30			0.20		
λ_{40}	0.40			0.10		
λ_{14}	0.05				0.01	0.10
λ_{24}	0.05					
λ_{34}	0.05				0.10	0.01

The only difference between experiments 1 and 2 was a nonzero input from organic matter-decomposers to herbivores (λ_{42} = 0.05 in Table 12.1). This gave a small increase in total system radioactivity (1.745 vs 1.741 v) and changed the stationary distribution so that herbivores and carnivores were more active and decomposers less active (Table 12.2). Turnover of the entire system was also slightly increased, but especially in compartment 4 (46.3 vs 40.8% dt^{-1}).

Doubling the input rate in experiment 3 accompanied by a 50% increase in transfer to herbivores (Table 12.1) did not double the total system activity at equilibrium (3.190 vs 1.741 v). The distribution of activity was different from experiment 1, particularly in the producers and herbivores. Total system turnover was only slightly changed (26.1 vs 23.2% dt^{-1}), considering the magnitude of the input change, and turnover of the individual compartments was substantially as in experiment 1.

In experiment 4 losses of radioactivity to the environment were reversed in order ascending the food chain, with greatest loss rates now at the lower trophic levels. This produced a significant reduction in total system radioactivity at equilibrium (0.861 vs 1.741 v) as well as marked redistribution among compartments (Table 12.2). Producer activity was reduced to 58.1% of the total system activity, while decomposer activity increased to 34.8%. Turnover of radioactivity was also markedly changed. System turnover increased to 35.5% dt^{-1}, producers to 50.0, herbivores to 41.7, and carnivores to 300.0, while decomposer turnover rate was reduced to 40.8% dt^{-1}.

Table 12.2. Stationary Distributions of Radioactivity and Turnover Rates

Turnover in each compartment was computed as follows: $1 \equiv \lambda_{01}X_0/X_1$, $2 \equiv (\lambda_{12}X_1 + \lambda_{42}X_4)/X_2$, $3 \equiv \lambda_{23}X_2/X_3$, and $4 \equiv (\lambda_{14}X_1 + \lambda_{24}X_2 + \lambda_{34}X_3)/X_4$. Turnover of the entire system was calculated as $[\lambda_{01}X_0 + (\lambda_{12} + \lambda_{14})X_1 + (\lambda_{23} + \lambda_{24})X_2 + \lambda_{34}X_3]/(X_1 + X_2 + X_3 + X_4)$.

Experiment No.	Total System	Standing Biomass (v) Compartment No. 1	2	3	4	Standing Biomass (% of total) Compartment No. 1	2	3	4	Total System	Turnover Rate (% dt^{-1}) Compartment No. 1	2	3	4
1	1.741	1.300	0.220	0.031	0.190	74.7	12.6	1.8	10.9	23.2	19.2	29.5	35.5	40.8
2	1.745	1.300	0.240	0.035	0.170	74.5	13.8	2.0	9.7	23.7	19.2	30.6	34.3	46.3
3	3.190	2.200	0.550	0.080	0.360	69.0	17.2	2.5	11.3	26.1	22.7	30.0	34.4	39.3
4	0.861	0.500	0.060	0.001	0.300	58.1	7.0	0.1	34.8	35.5	50.0	41.7	300.0	9.4
5	1.985	1.600	0.270	0.035	0.080	80.6	13.6	1.8	4.0	19.0	15.6	29.6	38.6	41.3
6	1.528	1.050	0.170	0.028	0.280	68.7	11.1	1.8	18.3	27.8	23.8	30.9	30.4	40.6

In experiment 5 transfer to compartment 4 (simulating mortality) was increased in successive trophic levels. This resulted in little change in distribution and turnover of radioactivity compared to experiment 1. In experiment 6 mortality was decreased up the trophic chain, and this produced a reduction in total system activity (1.528 vs 1.741 v), with less in producers and more in decomposers. System turnover was increased to 27.8% dt^{-1}, with turnover of the producers increasing and that of carnivores decreasing.

These results are instructive because they illustrate how a constant amount of radioactivity in an environment is subject to vastly different fates, and therefore potential effects on ecological systems, and this is determined by the character of the system; that is, how its components are coupled together in interaction.

DIGITAL COMPUTER PROGRAM FOR COMPARTMENT MODEL SIMULATIONS OF CYCLING AND SUCCESSION

J. S. Olson L. J. Bledsoe, Jr.

A FORTRAN program for ecosystem simulation was completed and tested using the generalized compartment model described previously.[4,5] The state of the system is here defined by a row vector **V**, which must be specified as an initial state $\mathbf{V}^{(0)}$ in the input. The continuous changes specified by the system of differential equations $\mathbf{V} = \mathbf{VF}$ are approximated by a sequence of matrix multiplications specifying the redistribution of the variable from part J to part K of the system. Here $\mathbf{F} = (f_{JK})$ specifies the fractions of the total variable associated with part J which are transferred to part K per unit time and can be allowed to vary as a function of time, environmental variables, or the current state of the system. Control cards allow many options on output, including numerical and graphical expression of the integrated change of as many ecosystem compartments as required.

This program was written with flexibility for digital simulation of compartment models, but was especially motivated by problems of simulating ecological succession. One aspect of succession concerns the redistribution of biomass (or energy or other constituents) among species, or between living and nonliving compartments, within some bounded unit area. The postulate which explains succession is that environmental changes diminish the flow of energy into species groups (including many pines) which can develop readily under initial conditions, and increase the flow into certain other species which are favored by environmental conditions which the pioneer species created. Mathematically, this corresponds with the changes in one or more terms in the matrix **F**, which now require further attention for empirical evaluation.

A second aspect of succession in a heterogeneous landscape follows from existence of changes in any given module of that landscape. This is reflected in a redistribution of ground (or water) *area* occupied by different community types. This requires expressing fractional rates of change of a given community type J to another community type K as a matrix **F**, which operates on the vector of community areas just as a matrix of fractional energy flow rates operates on a vector of compartment distributions within a given community. Evaluation of such a matrix was made for the broad vegetation types of the Oak Ridge Reservation and was reported in Chap. 10.

FIRST-SUMMER REDISTRIBUTION OF ^{137}Cs IN *LIRIODENDRON* FOREST

J. S. Olson

The compartment model program described above was used in simulating the redistribution of ^{137}Cs in a seven-compartment model of the tagged 20- by 25-m *Liriodendron* forest.[6] The initial dose of 467 mc was initially distributed in a "source" compartment (No. 1) consisting of the immediate vicinity of the trough through which the nuclide was introduced, 1 m above the ground, and the tree stem through which the cesium is quickly

[4] J. S. Olson, *Health Phys. Div. Ann. Progr. Rept. July 31, 1964*, ORNL-3697, p. 108.

[5] J. S. Olson, "Models for Simulating Ecological Systems with the Aid of Analog and Digital Computers," submitted to *Biometrics*.

[6] J. S. Olson, "Equations for Cesium Transfer in *Liriodendron* Forest," *Health Phys.* 11 (in press).

moved, as by transpiration. To account for the initial rise and later decline of radioactivity in foliage (compartment No. 2) shown in Fig. 12.1, certain losses from foliage (to undercover, No. 5, and the forest floor litter, No. 6) had been estimated directly, but these were found quite inadequate to account for observed changes. The fractional turnover rates specified in Table 12.3 were adjusted by successive simulation runs to account for the summer decrease in foliage by translocation to bark and coarse roots (compartment No. 3) and to medium-fine roots (compartment No. 4) which were sampled along with soil (compartment No. 7). Initially, almost all the soil activity consisted of material in roots rather than soil per se, but through late summer and autumn there was a continuing increase in amounts that were inseparable from mineral soil by mechanical means of flotation.[7]

The simulations in Fig. 12.1 were based on the matrix of Table 12.3, that is, on constant fractional coefficients f_{JK} of transfer from compartment J to compartment K. Hence, it was not expected to treat seasonal fluctuations, like those involving the autumn dropping of leaves, the corresponding seasonal peak in litter radioactivity, and the seasonal changes in translocation inside the trees.

[7]H. D. Waller *et al.*, *Health Phys. Div. Ann. Progr. Rept. July 31, 1964*, ORNL-3697, pp. 87–89.

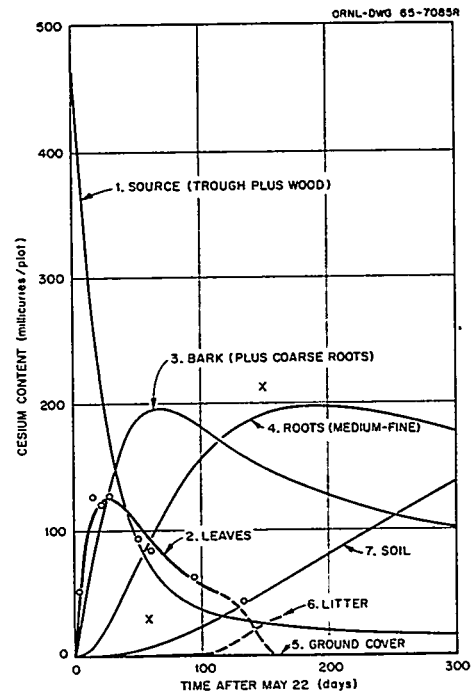

Fig. 12.1. Comparison of Observed Foliage Radioactivity (Circles) with Simulated Changes in Compartment Model for Radioactivity in Foliage (Compartment 2) and Other Parts of an Idealized *Liriodendron* Forest, Tagged in Tree Trunks May 22, 1962. Estimated soil and medium to fine root activity (x's) was based on 0 to 10 cm of soil in July and 0 to 30 cm in October and is expected to be slightly less than the total for these two compartments (7 and 4 respectively).

Table 12.3. Constant Coefficient Model for ^{137}Cs Transfer During First Year in *Liriodendron* Forest

J, Compartment of Origin	K, Receiving Compartment						
	1, "Source"	2, Leaves	3, Bark	4, Roots	5, Undercover	6, Litter Mat	7, Soil
1 "Source"	−0.036	0.028	0.008				
2 Leaves		−0.0444	0.044		0.00005	0.00035	
3 Bark	0.005	0.005	−0.03	0.015			
4 Roots			0.007	−0.01			0.003
5 Undercover					−0.02	0.02	
6 Litter mat						−0.02	0.02
7 Soil				0.0001	0.00001		−0.00011

^{134}Cs LEACHING FROM TERRESTRIAL MICROCOSMS

B. C. Patten Martin Witkamp

In experiments with ^{134}Cs-tagged white oak leaves with and without microflora, soil, and leaf-eating millipedes,[8] it was found that the microflora decreased ^{134}Cs leaching from the litter by 30 to 50%, while millipedes increased leaching by 15 to 20%. The presence of soil increased loss of ^{134}Cs from the overlying leaves by 17 to 20%, and all but 1 or 2% of this loss was adsorbed by the soil.

To determine the kinetics of ^{134}Cs exchange in this system and the effects of various combinations of compartments, a model was constructed for simulation by analog computer (Fig. 12.2). Six computer experiments were conducted to obtain values of the λ_{ij}'s (Fig. 12.2) for various partial systems and for the complete system. In all cases, constant λ_{ij}'s were adequate to fit computer-generated curves to the empirical data. Results are shown in Table 12.4.

[8] S. I. Auerbach *et al.*, *Health Phys. Div. Ann. Progr. Rept. July 31, 1962*, ORNL-3347, pp. 64, 65.

Table 12.4. Values of the λ_{ij}'s for Two-, Three-, Four-, and Five-Compartment Microcosms

Parameters	Expt. 1, (X_1,X_5)	Expt. 2, (X_1,X_2,X_5)	Expt. 3, (X_1,X_3,X_5)	Expt. 4, (X_1,X_2,X_3,X_5)	Expt. 5, (X_1,X_3,X_4,X_5)	Expt. 6, (X_1,X_2,X_3,X_4,X_5)
λ_{12}		0.071		0.083		0.097
λ_{13}			0.033	0.033	0.015	0.012
λ_{14}					0.012	0.006
λ_{15}	0.073	0.002	0.038	0.025	0.045	0.001
Σ	0.073	0.073	0.071	0.141	0.072	0.116
λ_{21}		0		0		0
λ_{23}				0		0
λ_{24}						0
λ_{25}		0		0		0
Σ		0		0		0
λ_{31}			0	0	0	0
λ_{32}				0		0
λ_{34}					0	0
λ_{35}			0	0	0	0
Σ			0	0	0	0
λ_{41}					0	0
λ_{42}						0
λ_{43}					0	0
λ_{45}					0	0
Σ					0	0

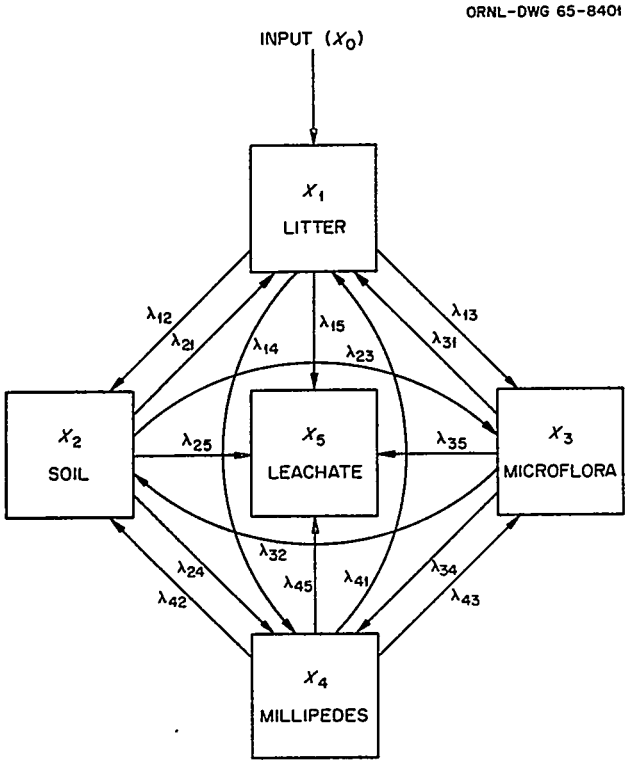

Fig. 12.2. Compartment Model of Litter-Soil-Microflora-Millipede-Leachate Microecosystem. Partial systems are produced by letting appropriate $\lambda_{ij} = 0$ in the system equations:

$$\dot{X}_1 = X_0 + \lambda_{21}X_2 + \lambda_{31}X_3 + \lambda_{41}X_4 - (\lambda_{12} + \lambda_{13} + \lambda_{14} + \lambda_{15})X_1 ,$$

$$\dot{X}_2 = \lambda_{12}X_1 + \lambda_{32}X_3 + \lambda_{42}X_4 - (\lambda_{21} + \lambda_{23} + \lambda_{24} + \lambda_{25})X_2 ,$$

$$\dot{X}_3 = \lambda_{13}X_1 + \lambda_{23}X_2 + \lambda_{43}X_4 - (\lambda_{31} + \lambda_{32} + \lambda_{34} + \lambda_{35})X_3 ,$$

$$\dot{X}_4 = \lambda_{14}X_1 + \lambda_{24}X_2 + \lambda_{34}X_3 - (\lambda_{41} + \lambda_{42} + \lambda_{43} + \lambda_{45})X_4 ,$$

$$\dot{X}_5 = \lambda_{15}X_1 + \lambda_{25}X_2 + \lambda_{35}X_3 + \lambda_{45}X_4 ,$$

where $\dot{X}_i$ are first derivatives with respect to time of ^{134}Cs activity, X_i, in compartments i, and $\lambda_{ij}(t)$ are functions expressing rates of ^{134}Cs exchange (day^{-1}) from compartments i to j ($i, j = 1, 2, \ldots, 5$).

In experiment 1, consisting of a litter-leachate system, 7.3%/day was transferred from litter to leachate. When soil was added (experiment 2), the loss rate from litter was unchanged, but 7.1%/day was transferred to soil and only 0.2%/day to the leachate. There was no exchange from soil back to litter (indicated by $\lambda_{21} = 0$), verifying that ^{134}Cs is adsorbed by the soil. When microflora were added without soil (experiment 3), loss rate from the litter was again essentially unchanged, but the partition was 3.3%/day transferred to microflora and only 3.8%/day to leachate. Microflora activity was not indicated to be exchangeable ($\lambda_{31} = \lambda_{35} = 0$). In experiment 4, with both soil and microflora present, interaction doubled the rate of activity loss from litter to 14.1%/day. Of this, 8.3%/day was transferred to soil (representing an increase over experiment 2), 3.3%/day to microflora (no change compared to experiment 3), and 2.5%/day to the leachate (different from all preceding experiments). Activities of soil and microflora were again both nonexchangeable ($\lambda_{21} = \lambda_{23} = \lambda_{25} = \lambda_{32} = \lambda_{35} = 0$).

Since millipedes could not be sterilized, it was impossible to obtain experimental data on a litter-millipede-leachate or a litter-soil-millipede-leachate system. A litter-microflora-millipede-leachate system was studied in experiment 5. Total activity loss rate from litter was unchanged over experiments 1, 2, and 3. The partition was 1.5%/day to microflora (a decrease compared to experiments 3 and 4), 1.2%/day to millipedes, and 4.5%/day to leachate (slightly higher than in experiment 3, where only microflora were present). Microflora and millipede activity were again nonexchangeable ($\lambda_{31} = \lambda_{34} = \lambda_{35} = \lambda_{41} = \lambda_{43} = \lambda_{45} = 0$). In experiment 6, with the complete system, activity loss from the litter (1.16%/day) was increased over experiment 5 (soil absent) but was not as great as in experiment 4 (millipedes absent). Hence, while millipedes cause increased leaching from the litter (experiment 4), this effect is reduced in the presence of soil (experiment 6). In experiment 6 transfer to soil was the highest recorded (9.7%/day) and that to leachate the lowest (0.1%/day); 1.2%/day went to microflora and 0.6%/day to millipedes. Soil, microflora, and millipede activities were again indicated to be nonexchangeable ($\lambda_{ij} = 0$, where $i = 2, 3, 4$, $j = 1, 2, \ldots, 5$, and $i \neq j$).

MODEL OF ^{134}Cs DISTRIBUTION IN CARP

A. L. Kretchmar[9] B. C. Patten
N. R. Kevern

A compartment model for the distribution of ^{134}Cs in carp (as described in Chap. 11) was formulated (Fig. 12.3) and programmed for an analog computer study of exchange kinetics between the different organs. To obtain computer-generated curves which fit the empirical data for each organ, a synthetic blood curve was generated to which each organ could be coupled separately to determine transfer coefficients.

With this procedure it was possible to fit the data for skin, scales, and spleen (Fig. 11.4*a*) with first-order kinetics, that is, with constant transfer coefficients. The data for flesh and bone (Fig. 11.4*c*) could not be duplicated in this way, and several alternative hypotheses were explored on the computer. The one accepted was that ^{134}Cs transfer from blood to flesh and blood to bone required active transport.

The liver, heart, gills, and kidney, which in addition to having a blood supply also serve some blood-processing function, could not be simulated with any of the hypotheses previously explored. To obtain suitable fits to the data (Fig. 11.4*b*) it was necessary to postulate some kind of connections (direct or indirect) between these organs and the gut. This required a revision of the model shown in Fig. 12.3. The new model is shown in Fig. 12.4 as a block diagram, with a schematic representing the postulated movement of ^{134}Cs between the four organs. Reference to anatomical and physiological literature led to the tentative conclusion that the pathways required to simulate the experimental data have real counterparts in the fish, namely, the lymphatic and hepatic portal systems.

To complete the model the separate compartments must be coupled together in accordance with the block diagram of Fig. 12.4. This is difficult because with so many compartments available, combinational problems are great. It is possible that further revision of the model may be required before the entire system can be simulated satisfactorily. The significant point at this stage of the investigation is that by use of the analog computer, hypotheses which might not otherwise have been considered were revealed, tested, and either accepted or rejected. The two accepted – active transport to muscle and bone and revision of the model from Fig. 12.3 to Fig. 12.4 – would not have been suggested readily by experimentation; but if they are accepted in the final version of the model they can be evaluated in the laboratory with a high probability of verification.

[9]Oak Ridge Institute of Nuclear Studies.

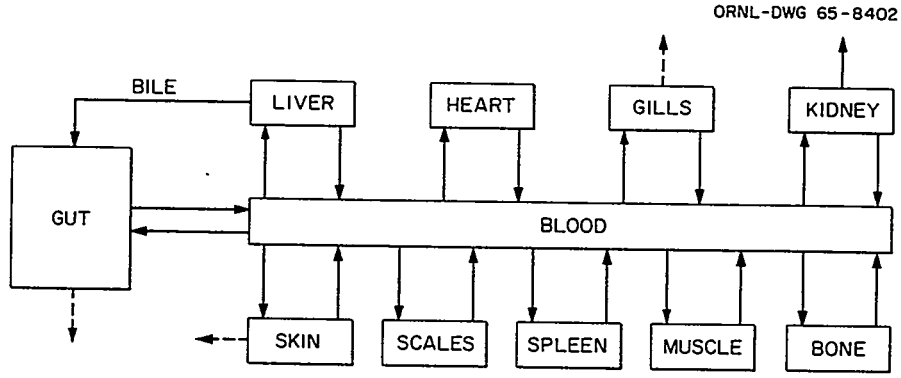

Fig. 12.3. Block Diagram of Original Compartment Model for Distribution of ^{134}Cs in Carp.

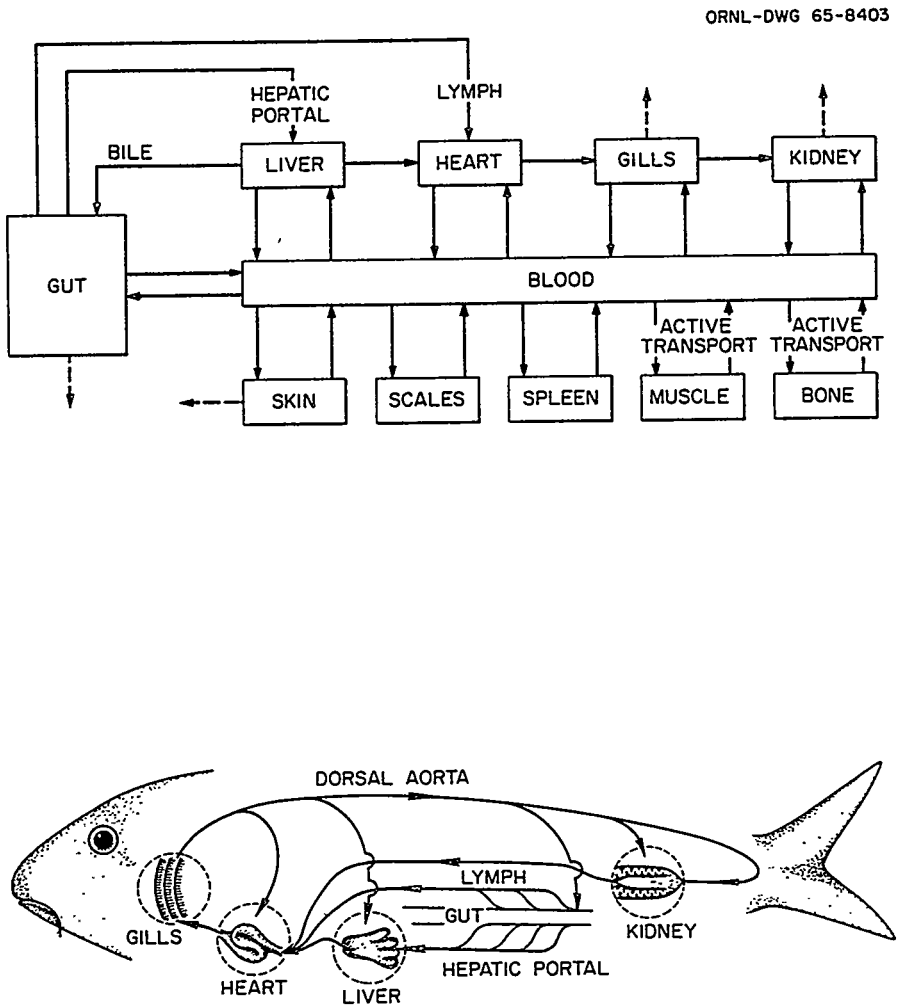

Fig. 12.4. Block Diagram of Revised Model for ^{134}Cs Distribution in Carp, and Schematic Showing Transfer Pathways Between Kidney, Liver, Heart, and Gills.

ANIMAL-CLIMATE INTERACTIONS

G. M. Van Dyne

One of the problems arising in simulation of macroecosystems is determination of the response of freely moving animals to climatic conditions. Data were obtained from grazing experiments conducted elsewhere with cattle and sheep on foothill winter ranges to investigate these responses. Study of dietary chemical composition, obtained from esophageal fistulated heifers and ewes grazed in adjacent pastures under herd and band conditions, revealed no significant differences between morning and afternoon grazing.[10] Furthermore, under these conditions, no significant differences were found among animals, but highly significant differences were found among dates which were related to climatic variations.

The influences of climate on energy expenditure in grazing, as determined from distances grazed and elevations climbed, were investigated also for sheep under the same conditions.[11] The average distance traveled by sheep in the band

[10] G. M. Van Dyne *et al.*, *Proc. West. Sect. Am. Soc. Animal Sci.* 15(LXI), 1–6 (1964).

[11] G. M. Van Dyne and J. L. Van Horn, *Proc. West. Sect. Am. Soc. Animal Sci.* 16(LXXIV), 1–6 (1965).

averaged winterlong was 7.6 km, and the elevation climbed each day varied from 85 to 280 m. Energy expenditure for grazing, calculated using Blaxter's constants of 0.030 and 0.322 kcal/m, respectively, for horizontal and vertical movement of a 50-kg sheep, varied from 137 to 406 kcal/day per sheep. The average energy expenditure for grazing, 235 ± 62 kcal/day, of which less than 3% was expended for climbing, represents about 20% of the basal metabolic requirement, and is thus significant for the total energy budget of range ecosystems. Wind movement was the most important climatic variable affecting energy expenditure by the grazing sheep. There was no apparent lag influence of climate on grazing and on energy expenditure for grazing.

PROBABILISTIC ESTIMATES OF FORAGE INTAKE

G. M. Van Dyne

In proposed research on White Oak Lake bed, it will be necessary to determine by indirect means the total forage, and subsequently radionuclide, intake by freely grazing animals. Daily forage intake (F) may be calculated by the equation

$$F = 100 \cdot E \cdot E_c / (100 \cdot F_c - F_c \cdot M_c) , \qquad (1)$$

where E is the quantity of feces produced per day, E_c is the percent cellulose content of the feces, F_c is the percent cellulose content of the diet, and M_c is the percent microdigestion of dietary cellulose. Generally, E, E_c, and M_c are measured with one group of animals, and F_c is measured with a second group of animals grazing with the first group. Estimates are obtained by sampling of the means and standard deviations of these variates and of correlations among E, E_c, and M_c, and it is assumed that these variates follow a normal distribution. No measure of precision of F is obtained by conventional procedures. An estimate of the precision of F may be obtained by generating a large number of such values and examining the distribution. For this purpose it is assumed that E, E_c, and M_c are to be sampled from a trivariate normal population. This is accomplished by first generating three mutually independent standard normal deviates designated as u, v, and w. Values for x, y, and z are selected by letting $x = u$ and then calculating y and z by Eqs. (2) and (3):

$$y = r_1 \cdot u + a \cdot v , \qquad (2)$$

where r_1 is the correlation between E and E_c, and a is calculated from the variance of y: $a = 1 - r_1^2$;

$$z = a \cdot u + b \cdot v + c \cdot w , \qquad (3)$$

where a is given as above, and b and c are calculated by (4) and (5);

$$b = \frac{r_3 - r_1 \cdot r_2}{a} , \qquad (4)$$

where r_2 is the correlation between E and M_c, and r_3 is the correlation between E_c and M_c;

$$c = \frac{1 - r_1^2 - r_2^2 - r_3^2 + 2r_1 \cdot r_2 \cdot r_3}{a} . \qquad (5)$$

The deviates x, y, and z (from a standard trivariate normal population) are "scaled" by Eqs. (6):

$$\begin{aligned} E &= x \cdot s_E + \bar{E} , \\ E_c &= y \cdot s_{E_c} + \bar{E}_c , \\ M_c &= z \cdot s_{M_c} + \bar{M}_c , \end{aligned} \qquad (6)$$

where s_E, s_{E_c}, and s_{M_c} are the measured standard deviates, and $\bar{E}$, $\bar{E}_c$, and $\bar{M}_c$ are the means.

This method has been applied to obtain estimates of precision for forage intake estimates with data from experiments with grazing cattle and sheep.[12] From 1000 to 10,000 values of F were generated and their distributions examined. For cattle the distribution of F was approximately normal, whereas for sheep it was skewed to the right. Coefficients of variation, in percent, for cattle in three experiments with decreasing herbage availability were 19, 24, and 20, whereas for sheep under identical conditions they were 31, 28, and 36. The principal conclusions are (1) more precise estimates of forage intake are obtained with cattle than with sheep, and (2) availability of herbage does not influence precision of the estimate.

[12] G. M. Van Dyne, *Proc. West. Sect. Am. Soc. Animal Sci.* 16(LXXVII), 1–6 (1965).

APPLICATION OF SOME OPERATIONS RESEARCH TECHNIQUES TO ECOLOGICAL ANALYSIS PROBLEMS

G. M. Van Dyne

In many ecological studies samples are obtained which contain a mixture of species. Some attributes of the mixed sample are measured, and percentage composition in the samples is determined. Often, however, because of practical or technical reasons the same attributes for each species in the sample cannot be measured. Nonlinear programming and least-squares techniques were used to predict the attributes of individual species from knowledge of the attributes of the mixed sample and the species composition of the mixed sample.[13] Samples with known attributes were constructed and were used in computer studies to show the effect on accuracy of estimates of the species attributes due to (1) variability in the attribute for a given species from sample to sample, (2) variability in percent composition of a given constituent in each species in the sample, (3) the grouping of species in the sample, and (4) bias in determination of percent composition of a given constituent for a species in the sample.

The relation between the composition of a given chemical in the ith mixed sample (C_i), the chemical composition of the jth species, plant part, or plant group in the sample (P_j), and the weight of the jth species, plant part, or plant group in the ith sample (W_{ij}) is

$$C_i = \sum_{j=1}^{m} (P_j W_{ij}) , \qquad (1)$$

where $j = 1, 2, \ldots , m$ species, parts, or groups in the sample. Given data for C_i and W_{ij}, we desire to estimate the P_j. This is accomplished by using least-squares and nonlinear programming routines to solve for the P_j by minimizing a function Q as follows:

$$Q = \sum_{i=1}^{n} \left[C_i - \sum_{j=1}^{m} (P_j W_{ij}) \right]^2 , \qquad (2)$$

subject to $0 \leqq P_j \leqq 100$, where $i = 1, 2, \ldots , n$ samples. Known P_j and W_{ij} were used to test these techniques. Known variability of P_j and W_{ij} was obtained using random number generators, and known bias was included in some W_{ij} values in 30 computer experiments. Values of $\hat{P}_j$, predicted by the above methods from the generated C_i and W_{ij}, were compared to P_j, the true values used in generating the data. Both least-squares and nonlinear programming gave acceptable $\hat{P}_j$ in most instances. Poor estimates of $\hat{P}_j$ were found only if P_j were small and if the corresponding W_{ij} were small and of low variability.

These techniques were applied successfully to data from experiments with cattle and sheep to predict the crude protein content of five dietary species groups from the botanical composition and the crude protein in the mixed sample.[12]

[13] G. M. Van Dyne, "Application of Some Operations Research Techniques to Food Chain Analysis Problems," *Health Phys.* 11(12), in press.

INFORMATION AND PARAMETERS REQUIRED FOR MODELING MACROECOSYSTEMS

G. M. Van Dyne

In order to model mathematically and to simulate macroecosystems, much information and many parameters will be required to relate soil-plant, plant-animal, and animal-soil interactions, and the effect of climatic influences on these interactions. Toward this end, analyses and papers were completed on research initiated elsewhere. The purpose of these analyses was to provide necessary data, parameters, and methods which will be used in proposed radiation ecology researches on modeling of macroecosystems and their response to catastrophic insults such as radiation contamination, fire, or physical disturbance.

Detailed analyses were made of dietary chemical and botanical composition relationships with special attention to individual variations in and factors influencing dietary composition.[14–16]

[14] G. M. Van Dyne and H. F. Heady, *J. Range Management* 18, 78 (1965).

[15] G. M. Van Dyne and H. F. Heady, "Dietary Botanical Composition of Cattle and Sheep Sharing a Mature California Annual Range," *Hilgardia* (in press).

[16] G. M. Van Dyne and H. F. Heady, *J. Animal Sci.* 24, 305 (1965).

Methods of measuring microdigestion of herbages and forages under both range and drylot conditions were summarized[17] and were utilized in a study of the chemical composition and digestibility of range plants from annual range and from pure-stand plots.[18] Additional data were obtained and tabulated on seasonal variations in chemical composition of grasses and shrubs which are important in some mixed prairie ranges.[19]

RELATED ACTIVITIES

During the past year graduate and undergraduate classes in ecology and mammalogy toured the laboratory and were briefed on the ORNL ecology program. These classes were from Ohio State University and the University of Tennessee respectively.

A graduate class in Production Limnology from the University of Indiana also visited the Ecology Section. A special one-day workshop in productivity was given by members of the Section to this class.

Two members of the Section were appointed Ford Foundation professors at the University of Tennessee. Together with a third member they organized and presented a new one-year course in "Systems Ecology."

The Section again participated in the summer institute in radiation ecology which was held at the Oak Ridge Institute of Nuclear Studies. This institute was attended by 20 college and university teachers.

---

[17] G. M. Van Dyne and W. C. Weir, "Comparison of Microdigestion Techniques Under Range and Drylot Conditions," *J. Agr. Sci.* (in press).

[18] G. M. Van Dyne, "Chemical Composition and Digestibility of Range Plants from Annual Range and from Pure-Stand Plots," *J. Range Management* (in press).

[19] G. M. Van Dyne, O. O. Thomas, and G. F. Payne, *Chemical Composition of Individual Range Plants from U.S. Range Station, Miles City, Montana from 1955–1960*, ORNL-TM report (in preparation).

Part III. Radiation Physics

G. S. Hurst

13. General Radiation Physics

Jacob Neufeld
R. H. Ritchie

V. E. Anderson[1]
J. C. Ashley[2]
Julian Crowell[3]
Kenneth Fox[4]
R. N. Hamm
H. J. Howe, Jr.[5]
H. C. Schweinler
W. S. Snyder
J. E. Turner
C. L. Wiginton[4]
H. A. Wright

GENERAL CONCEPTS IN RADIATION DOSIMETRY

Previous work[6] on the possible role of linear momentum transfer in radiation dosimetry was extended to include not only neutrons and gamma radiation but also charged particles.[7] The new work confirms the hypothesis that linear momentum transfer appears to offer a useful description of the observed relative biological effectiveness (RBE) of various kinds and mixtures of radiations, at least insofar as RBE depends on physical characteristics of radiation and its interaction with matter. Based on momentum transfer, an equation analogous to the empirical one published in the 1962 RBE Committee Report[8] was derived for charged particles.[9] The two equations are similar, as the following comparison shows:

$$(\mathrm{RBE})_{\mathrm{ICRP/U}} = 0.9 + 0.05\,\bar{L}\,,$$

$$(\mathrm{RBE})_{\mathrm{momentum}} = 0.94 + \frac{0.047}{\beta}\,.$$

The quantity $\bar{L}$ is the rate of linear energy transfer (LET) of the particles expressed in kilo-electron volts per micron, and β is the velocity of the particles in units of the velocity of light. As Fig. 13.1 shows, the two equations give practically the same numerical results for singly charged particles over the energy ranges for which the momentum theory has been worked out (e.g., ~0.075 to ~100 Mev for protons). If the momentum theory is justified, then it implies that the RBE of a charged particle should depend on the velocity of the particle but not on its charge. Specifically, one should distinguish between LET dependence and velocity dependence for RBE. It appears possible to delineate exactly the conditions under which this distinction is necessary by describing the action of radiation quantum mechanically in the formalism of successive Born approximations.[10]

---

[1]On loan from Central Data Processing Facility (ORGDP).

[2]Temporary leave.

[3]Oak Ridge Graduate Fellow.

[4]Consultant.

[5]AEC Health Physics Fellow.

[6]J. E. Turner and H. Hollister, *Health Phys.* 8, 523 (1962).

[7]J. E. Turner, *Health Physics* (in press).

[8]Report of the RBE Committee to the International Commissions on Radiological Protection and on Radiological Units and Measurements, *Health Phys.* 9, 357 (1963).

[9]H. Hollister and J. E. Turner, submitted for publication in *Health Physics*.

[10]J. E. Turner and H. Hollister, submitted for publication in *Nature*.

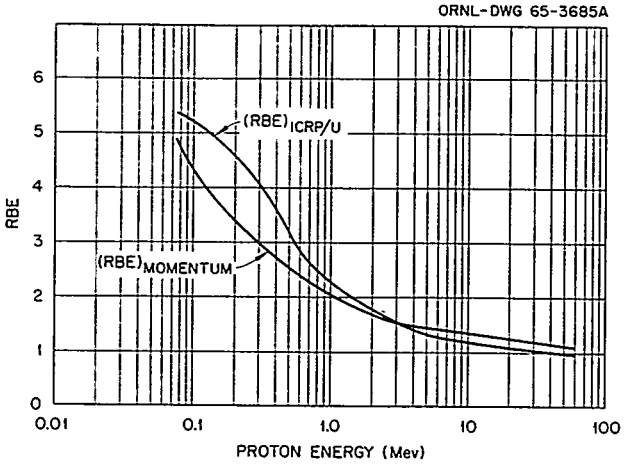

Fig. 13.1. Comparison of Empirical Equation from 1962 ICRP-ICRU Report with That Based on Linear Momentum Transfer.

HIGH-ENERGY DOSIMETRY

An evaluation has been made of the permissible flux of neutrons and protons in the energy range from 60 to 400 Mev. The data based on the calculations made by Turner *et al.*,[11] Zerby and Kinney,[12] and Bertini[13] are given in Figs. 13.2 and 13.3. Figures 13.2 and 13.3 contain graphs representing particle flux densities that deliver a dose equivalent at a rate of 2.5 millirems/hr as a function of the incident energy. Exposure to these fluxes for 40 hr/week results in a dose equivalent of 5 rems in 50 weeks. Curves 1*A* and 2*A* represent, respectively, doses due to neutrons and protons normally incident on the tissue slab, whereas curves 1*B* and 2*B* represent, respectively, doses due to neutrons and protons isotropically incident on the tissue slab 30 cm thick. The curves 1*C* and 2*C* represent the corresponding data published in the report of Committee IV of the International Commission on Radiation Protection.[14]

The codes used in the calculation of dose due to high-energy protons in the paper by Turner *et al.* have been modified in such a way that dose can now be calculated in a tissue phantom in the shape of either a rectangular parallelepiped of arbitrary dimensions or of a right circular cylinder of arbitrary dimensions.

[11] J. E. Turner *et al.*, *Health Phys.* 10, 783 (1964).

[12] C. D. Zerby and W. E. Kinney, *Calculated Current-to-Dose Conversion Factors for Nucleons Below 400 Mev*, ORNL-TM-1038 (May 1965).

[13] H. W. Bertini, *Phys. Rev.* 131, 1801 (1963).

[14] *Recommendations of the ICRP: Report of Committee IV (1953–1959) on Protection Against Electromagnetic Radiation Above 3 Mev and Electrons, Neutrons, and Protons*, pp. 3–4, MacMillan, New York, 1964.

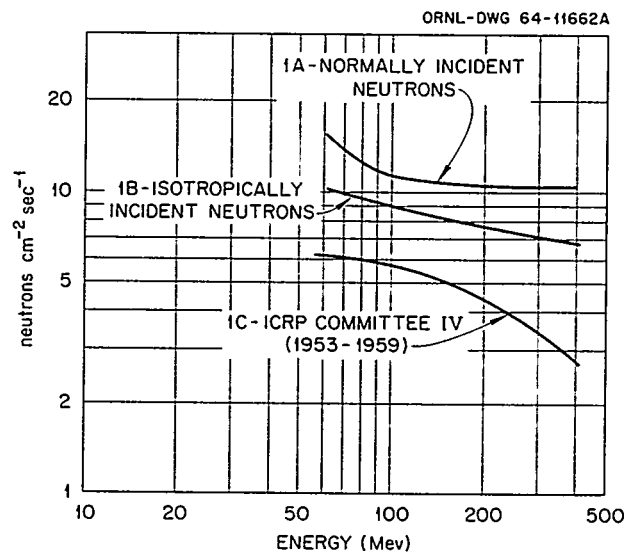

Fig. 13.2. Flux Density of Neutrons to Deliver a Dose Rate of 2.5 Millirems/hr as a Function of Neutron Energy.

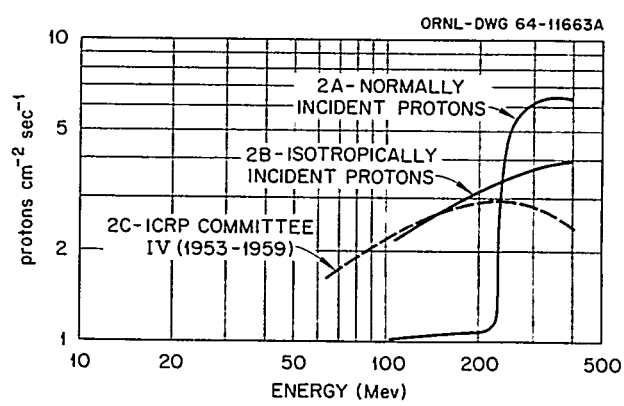

Fig. 13.3. Flux Density of Protons to Deliver a Dose Rate of 2.5 Millirems/hr as a Function of Proton Energy.

EXCITATION OF WHISTLER AND HYDROMAGNETIC WAVES IN A STREAM OF GYRATING ELECTRONS

This investigation deals with the excitation of whistler and hydromagnetic waves by a stream of electrons moving along spiral trajectories in a cold and uniform ionized medium immersed in a static magnetic field $\mathbf{B}_0$. The electrons have velocity components $v_{\parallel} = \beta_{\parallel} c$ and $v_{\perp} = \beta_{\perp} c$ which are, respectively, parallel and perpendicular to $\mathbf{B}_0$ (c is the velocity of light). It is assumed that $\beta_{\parallel} \ll \beta_{\perp}$ and, consequently, the assembly of electrons forms an "almost circular stream."

It has been found that the excitation of waves in the relatively low frequency range (below the electron gyrofrequency of the stationary plasma) is characterized by a continuous spectral distribution which includes both whistler and hydromagnetic waves. Both whistler and hydromagnetic waves occur for any $\beta_{\perp}$ whether in the relativistic or nonrelativistic range. It is significant that for values of $\beta_{\perp}$ less than approximately 0.97 all the excited waves, both whistler and hydromagnetic waves, have the same rate of growth $|\mathrm{Im}\ \delta|$ equal to $(\sqrt{2}/2)\sigma^{1/2}\omega_e(1 - \beta^2)^{1/2}\beta_{\perp}$, where ω_e is the plasma frequency of the ionized medium, β is equal to $(v_{\parallel}^2 + v_{\perp}^2)^{1/2}/c$, and σ is the ratio of the density of electrons in the beam to the density of the electrons in the plasma-beam medium. Thus the rate of growth $|\mathrm{Im}\ \delta|$ is independent of the frequency of the excited waves within the entire frequency range under consideration.

EXCITATION OF HYDROMAGNETIC WAVES BY A HELICAL PROTON BEAM

The hydromagnetic approximation has been applied to the dispersion equation of a plasma-beam system, and it has been found that the hydromagnetic waves excited by a helical proton beam represent superluminous and counterstreaming instabilities, whereas the hydromagnetic excitation produced by a linear proton beam can only be superluminous. Physical conditions under which hydromagnetic P and B instabilities may occur are investigated with particular reference to the intensities of the helical proton beam and the rate of growth of the excited waves. In some instances the qualitative behavior of instabilities is significantly different when the beam intensities increase from relatively small to relatively large values. When the beam is very tenuous, the hydromagnetic B instability is "weak," that is, it is characterized by a relatively small rate of growth, whereas the hydromagnetic P instability is "strong," that is, the corresponding rate of growth is relatively large. The contrast between the weak B instability and the strong P instability decreases for increasing beam intensity, and for less tenuous beams the situation is reversed, that is, the P instability is weak, whereas the B instability is strong. The excitation of hydromagnetic waves having very low frequencies has been discussed with particular reference to an aperiodic instability which occurs in the limiting case in which the frequency tends to zero.

ALMOST LONGITUDINAL INSTABILITIES IN A PLASMA-BEAM SYSTEM

A plasma-beam system immersed in a magnetic field $\mathbf{B}_0$ has been investigated under the assumption that the plasma is stationary, cold, uniform, and extended and that the beam of charged particles is uniform in density and moving in a direction parallel to that of $\mathbf{B}_0$. Instabilities which are almost longitudinal are investigated with respect to conditions of occurrence, strength and type of instabilities, and dependence on the angle between the direction of $\mathbf{B}_0$ and the direction of the excited waves. Two logically distinct types of waves which occur have been defined and investigated. An almost longitudinal Cherenkov wave has a phase velocity equal to the projection of the beam velocity in the direction of the wave. An almost longitudinal cyclotron wave has a frequency equal to the Doppler-shifted gyrofrequency of the particles in the beam. Certain simple analytical expressions which apply to the significant regions of instability have been derived and tabulated. Numerical analysis of typical cases has been carried out.

14. Interaction of Radiation with Gases

G. S. Hurst

T. E. Bortner[1]
Ada E. Carter
L. G. Christophorou[1]
R. N. Compton[2]
J. T. Cox
F. J. Davis
Kenneth Fox[1]
Anthony Hadjiantoniou[3]
J. A. Harter
A. G. Kenerly[4]
C. E. Klots
J. E. Parks[5]
Devon Pittman
P. W. Reinhardt
R. H. Ritchie
H. C. Schweinler
J. E. Turner
E. B. Wagner

ALPHA-PARTICLE IONIZATION OF BINARY GAS MIXTURES

Measurements of W (electron volts per ion pair) and G (ion pairs per 100 electron volts) in irradiated gases have long been pursued because of the role these quantities may play in particle-detection and radiation dosimetry schemes. The present work has yielded simple empirical formulas with which the above quantities may be estimated for any binary mixture of some 18 molecular gases. The formulas are of the form:

$$G_{(p_i,p_j)} = G_i \frac{ap_i}{ap_i + p_j} + G_j \frac{p_j}{ap_i + p_j} ,$$

where p_i, p_j are the partial pressures of the species i and j and a is an empirical parameter unique to each binary combination. This formulation has been known for some time.[6]

It has been found that, to an excellent approximation, any a is composed of two molecular parameters in the sense:

$$a = Z_i'/Z_j' .$$

Through repeated examination of various binary mixtures, a scale of Z_i for the 18 gases has thus been established and is reproduced in Table 14.1. These parameters are of intrinsic interest. They may be interpreted[7] as weighting factors dictating

[1]Consultant.

[2]Oak Ridge Graduate Fellow.

[3]AEC Health Physics Fellow.

[4]Instrumentation and Controls Division.

[5]Graduate student.

[6]T. E. Bortner and G. S. Hurst, *Phys. Rev.* 93, 1236 (1954).

[7]C. E. Klots, *J. Chem. Phys.* 39, 1571 (1963).

Table 14.1. W Values and Energy Partition Coefficients for Various Gases[a]

Gas	W_i	Z_i'	Gas	W_i	Z_i'
H_2	36.25	3.08 ±0.03	C_2H_6	26.62	16.3 ±0.2
O_2	32.41	6.25 ±0.06	c-C_3H_6	25.97	20.5 ±0.3
N_2	(36.60)	7.05 ±0.05	C_3H_6	27.16	22.8 ±0.1
NO	29.03	7.90 ±0.09	C_3H_8	26.30	22.9 ±0.2
CO	34.73	8.38 ±0.10	C_4H_{10}	25.87	28.8 ±0.4
CH_4	29.19	(10.00)	*i*-C_4H_{10}	26.32	29.6 ±0.2
CO_2	34.35	10.95 ±0.20	C_4H_8-1	26.63	29.5 ±0.1
C_2H_2	27.51	14.7 ±0.04	*i*-C_4H_8	26.65	29.8 ±0.1
C_2H_4	28.03	15.50 ±0.15	*cis*-C_4H_8	26.33	30.1 ±0.2

[a]Parentheses denote assigned values.

the partitioning of dose among various components of a mixture subject to high-energy irradiation. This initial partitioning must be known if subsequent energy- and charge-transfer processes are to be assessed.

One such application lies in the discovery in this laboratory of a negative Jesse effect in mixtures containing a rare gas. Thus, for example, excited states of krypton are apparently generated which ordinarily react by the well-known Hornbeck-Mollnar process,

$$Kr^* + Kr \rightarrow Kr_2^+ + e\,,$$

but which may be quenched by an additive:

$$Kr^* + M \rightarrow Kr + M^*\,.$$

A kinetic analysis of this competition may be performed similar to that applied to the normal Jesse effect.[8] These several effects are under further investigation as part of a program to determine the yields with which selected electronic states of the rare gases are generated by high-energy radiation.

INTERACTION OF THERMAL ELECTRONS WITH POLAR AND POLARIZABLE MOLECULES

The swarm method is applied in an attempt to study the role of short-range (polarizable) and long-range (polar) forces involved in electron-molecule interactions. Ethylene is used as a carrier gas to provide a swarm of thermal electrons (low E/P),[9] and the increase in the electron swarm drift time when nonpolar and/or polar molecules are used in mixtures with ethylene provides useful information on the electron-molecule interaction. The experimentally obtained electron drift velocity w is related to the cross section for momentum transfer σ by[10]

$$w = \frac{4\pi}{3}\,\frac{e}{m}\,\frac{E}{P}\,\frac{1}{n}\int_0^\infty f_0\,\frac{d}{dv}\,(v^2/\sigma)\,dv\,, \qquad (1)$$

where E is the electric field, P is the gas pressure, n is the gas density at 1 torr and 300°K, e and m are the electron charge and mass, v is the electron velocity, and f_0, in our case of thermal electrons, is

$$f_0 = \left(\frac{m}{2\pi kT}\right)^{3/2} e^{-(mv^2/2kT)}\,. \qquad (2)$$

From Eq. (1), using experimental data on w, σ can in principle be calculated. The cross sections can then be compared with the cross sections calculated from idealized force fields in an effort to see if the macroscopic quantities, polarizability and dipole moment, are adequate characterizations of the electron interactions with molecules. In these cases cross sections obtained from simple theory can be tested in Eq. (1).

For nonpolar molecules, Vogt and Wanier[11] have given a quantum mechanical calculation of the cross section for spiraling collisions, $\sigma_{\mathrm{V.W.}}$, equal to

$$\sigma_{\mathrm{V.W.}} = 4\pi\left(\frac{e^2\alpha}{mv^2}\right) = \frac{A_{\mathrm{V.W.}}}{v}\,, \qquad (3)$$

where $A_{\mathrm{V.W.}} = 4\pi e m^{-1/2}\alpha^{1/2}$ for electrons (or gaseous ions) of charge e, relative mass m, and relative velocity v which move through a gas of nonpolar molecules of polarizability α.

Altshuler[12] has calculated the cross section for polar molecules by making use of the Born approximation. He finds

$$\sigma = \frac{8\pi}{3}\left(\frac{\mu e}{\hbar v}\right)^2 = \frac{A_I'}{v^2}\,, \qquad (4)$$

where $A_I' = \frac{8\pi}{3}\left(\frac{\mu e}{\hbar}\right)^2 = 1.72\mu^2$ (μ in Debye units), μ is the permanent molecular dipole moment, e and m are the electron charge and mass, respectively, and $\hbar = h/2\pi$, where h = Planck's constant.

We have integrated Eq. (1) assuming a v^{-1} and a v^{-2} dependence of σ for nonpolar and polar molecules, respectively, and from our data on

[8] G. S. Hurst *et al.*, *J. Chem. Phys.* 42, 713 (1965).

[9] J. A. Stockdale and G. S. Hurst, *J. Chem. Phys.* 41, 255 (1964).

[10] W. P. Allis, p. 413 in *Handbuch der Physik* (ed. by S. Flügge), vol. XXI, Springer, Berlin, 1956.

[11] E. Vogt and G. H. Wanier, *Phys. Rev.* 95, 1190 (1954).

[12] S. Altshuler, *Phys. Rev.* 107, 114 (1957).

w [for very low E/P, where f_0 in Eq. (1) is Maxwellian], we have determined σ for nonpolar gases with ethylene.

Figure 14.1 and Table 14.2 compare A_{exp} ($= \sigma v$) as calculated from our data on pure nonpolar gases with $A_{V.W.}$ ($= \sigma_{V.W.}\ v$) as determined by the theory of ref. 11. Table 14.3 and Fig. 14.2 show similar results, but obtained from studies of nonpolar gases mixed with ethylene. Our results for mixtures involving polar molecules with ethylene are shown in Table 14.4 and Fig. 14.3. In Fig. 14.3, in addition to the theoretical line, a second line has been fitted to the experimental points which correspond to the benzene derivatives. The good fit of the experimental points to a straight line indicates that within a particular group of molecules A_I'/A_E' vs μ^2 is linear but with a different slope and intercept than that predicted by the theory. In Fig. 14.3 the points represented by asterisks were taken from ref. 13.

Our experimental cross sections for nonpolar molecules are much smaller than those obtained from theory, and, in fact, Figs. 14.1 and 14.2 clearly show that the correlation between theoretical and experimental values is quite poor. For polar molecules, the theory, however, is in relative agreement with experiment; the agreement becomes better for small molecules with large permanent dipole moments. For large asymmetric molecules and for $\mu \rightarrow 0$, where the assumption of a central force and the negligence of the short-range effects of the detailed molecular structure are no longer valid, the theory breaks down. Apparently, simple theory is much more successful in predicting the scattering cross section for the long-range force than it is for the short-

[13]G. S. Hurst *et al.*, *J. Chem. Phys.* **38**, 2572 (1963).

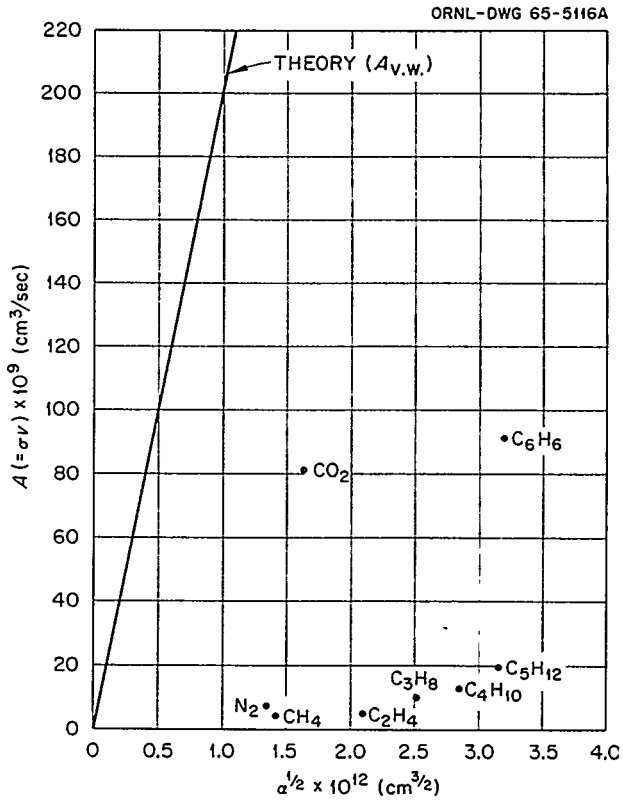

Fig. 14.1. A vs $\alpha^{1/2}$ for Various Nonpolar Gases.

Table 14.2. Data on Nonpolar Gases

Molecule	α (cm^3)	$\alpha^{1/2}$ (cm$^{3/2}$)	A_{exp} (cm^3/sec)	$A_{V.W.}$ (cm^3/sec)	$A_{V.W.}/A_{exp}$
	$\times 10^{-24}$	$\times 10^{-12}$	$\times 10^{-9}$	$\times 10^{-9}$	
N_2	1.8	1.34	7.2	269	37.3
CO_2	2.65	1.63	81.5	328	4
C_2H_4	4.3	2.08	5.3	418	78.8
C_3H_8	6.29	2.51	10	504.5	50.4
C_4H_{10}	8.12	2.85	12.7	573	45
C_5H_{12}	9.95	3.16	19.3	635	32.9
C_6H_6	10.32	3.21	91.4	645	7

range force. In the case of nonpolar molecules many factors in addition to the polarizability must be included in an accurate calculation. These factors would certainly include molecular size, shape, noncentral interaction forces, and repulsive force terms encountered near the nucleus.

Table 14.3. A_I/A_E for Nonpolar Aromatic and Other Molecules

Molecule	A_I (cm^3/sec)	α (cm^3)	$\alpha^{1/2}$ (cm$^{3/2}$)	A_I/A_E
	$\times 10^{-9}$	$\times 10^{-24}$	$\times 10^{-12}$	
N_2	7.2	1.8	1.34	1.358
CO_2	81.5	2.65	1.63	15.377
C_2H_4	5.3	4.3	2.08	1
C_3H_8	10	6.29	2.51	1.886
C_4H_{10}	12.7	8.12	2.85	2.396
C_5H_{12}	19.3	9.95	3.16	3.641
C_6H_6	91.4	10.32	3.21	17.245
C_6H_{12}		10.8	3.29	6.662
p-$C_6H_4(CH_3)_2$		14.2	3.88	12.407
p-$C_6H_4Cl_2$		14.5	3.97	63.877

Table 14.4. A_I'/A_E' for Aromatic Molecules

Molecule	α (cm^3)	μ (Debye units)	μ^2	A_I'/A_E
	$\times 10^{-25}$			
C_6H_6	103.2	0	0	16.423
C_6H_{12}	108.7	0	0	6.662
p-$C_6H_4(CH_3)_2$	142	0	0	12.407
p-$C_6H_4Cl_2$	145	0	0	67.4
m-$C_6H_4(CH_3)_2$	141.8	0.37	0.137	15.08
o-$C_6H_4(CH_3)_2$	141	0.55	0.303	29.998
o-$C_6H_4CH_3Br$		1.44	2.067	77.046
m-$C_6H_4Cl_2$	142.3	1.5	2.25	84.727
C_6H_5Br	136.2	1.55	2.40	107.725
C_6H_5Cl	122.5	1.61	2.59	101.037
o-$C_6H_4Cl_2$	141.7	2.20	4.84	170

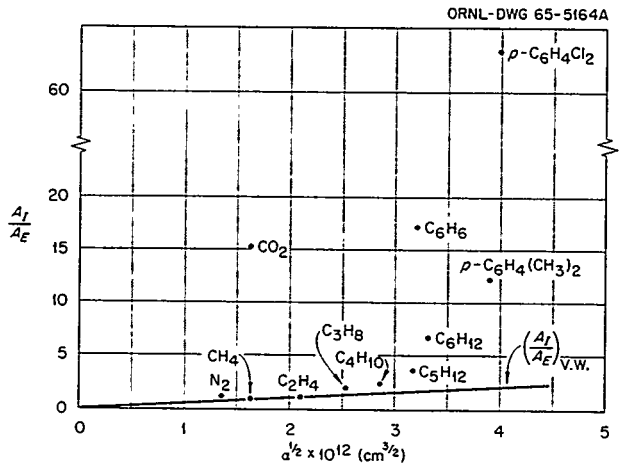

Fig. 14.2. A_I/A_E vs $\alpha^{1/2}$ for Nonpolar Gases.

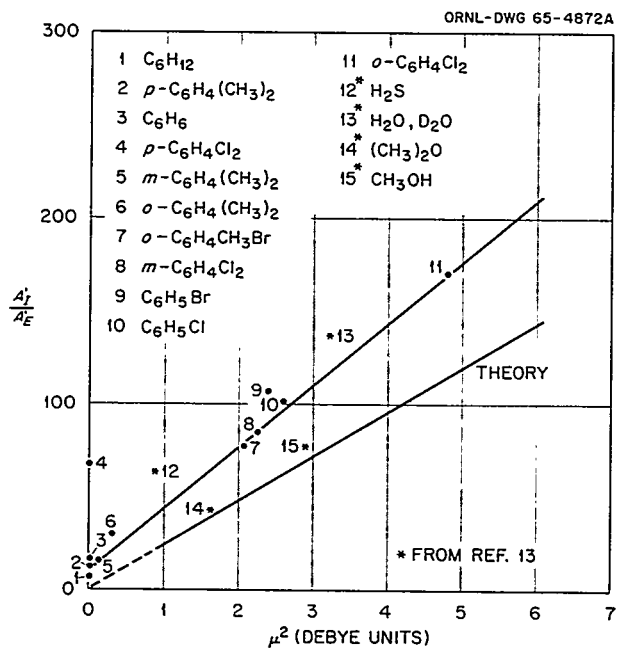

Fig. 14.3. A_I'/A_E' vs μ^2 for Polar Gases.

ELECTRON TIME-OF-FLIGHT STUDIES (GEIGER-MUELLER DETECTOR)

A more detailed analysis of the electron time-of-flight method[14] for the measurement of diffusion coefficient D and drift velocity w has been carried out. It was previously suggested that the macroscopic swarm parameters, D and w, could be obtained from a single time-of-flight function, $E(t)$. The function $E(t)$, giving the number of electrons arriving at a detector at a fixed distance from a uniform plane of electrons generated at time $t = 0$, was obtained from a solution of the transport equation.

An experiment was carried out to verify that the detecting of single electrons using a Geiger-Mueller counter in the time-of-flight technique follows Poisson statistics. Cases were studied where instrumentation error was negligibly small compared to the measured distribution. The measured electron time-of-flight distribution $E''(t)$ was verified to be given by

$$E''(t) = E(t) \exp\left[-\int_0^t E(T)\, dT\right],$$

where $E''(t)$ differs from $E(t)$ due to counts lost during counter deadtime. A distribution $E_1''(t)$ was measured first for a case where $\int_0^\infty E(t)\, dt \ll 1$ such that

$$E_1''(t) \cong E(t) .$$

Then a second distribution $E_2''(t)$ was measured for a case where

$$\int_0^\infty E(t)\, dt > 1 .$$

From the $E_1''(t)$ distribution a theoretical distribution, $E_3''(t)$, was calculated for the second case. Results for an $E_2''(t)$ distribution where

$$\int_0^\infty E(t)\, dt = 3.35$$

are shown in Fig. 14.4. The numerical factor was determined from the ratio of the total number of counts to the total number of light flashes used to generate the pulse of electrons.

Measurement of an electron time-of-flight distribution $E(t)$, smeared with an error function, $T_0(t)$, results in a distribution $E'(t)$, given by

$$E'(\tau) = \int_0^\tau E(t)\, T_0(\tau - t)\, dt .$$

[14] G. S. Hurst *et al.*, *J. Chem. Phys.* 39, 1341 (1963).

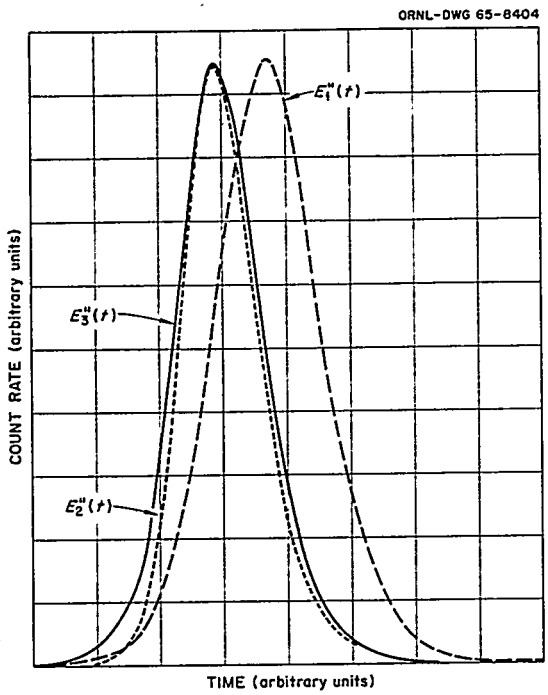

Fig. 14.4. Effect of Counting Losses, Due to Counter Deadtime, on the Time-of-Flight Distribution. The distribution $E_1''(t)$ applies to the no-loss case, $E_2''(t)$ is the measured distribution, and $E_3''(t)$ is the calculated distribution for a case of moderate loss.

In order to find $E(t)$, from which the drift velocity and the diffusion coefficient are computed, $T_0(t)$ and $E'(t)$ were measured; $E(t)$ was unfolded and the data were fitted to theory by a numerical method of Ritchie and Anderson (see "Fourier Transform Methods in the Unfolding of Experimental Data," this chapter). Plots of the measured points of $T_0(t)$ and $E'(t)$ are shown in Fig. 14.5. along with the unfolded $E(t)$ function and the convolution of $E(t)$ and $T_0(t)$. Figure 14.6 shows again the measured $E'(t)$ function with the best fit of $E(t)$ to those points. Comparing the $E(t)$'s of Figs. 14.5 and 14.6, where the error function is taken into account and where it is not, one can see the effect of error fluctuations. Although drift velocity data would agree rather well between the two methods, the diffusion coefficient is a factor of 4 too high. As one might expect, it should be noted that the fit in Fig. 14.6 is not too good.

The unfolding process has produced diffusion data for pure ethylene and ethylene and water mixtures, independent of pressure and in the expected range of values. Diffusion data, when plotted out on an expanded scale, reveals fluctuations in the data. The higher values of the

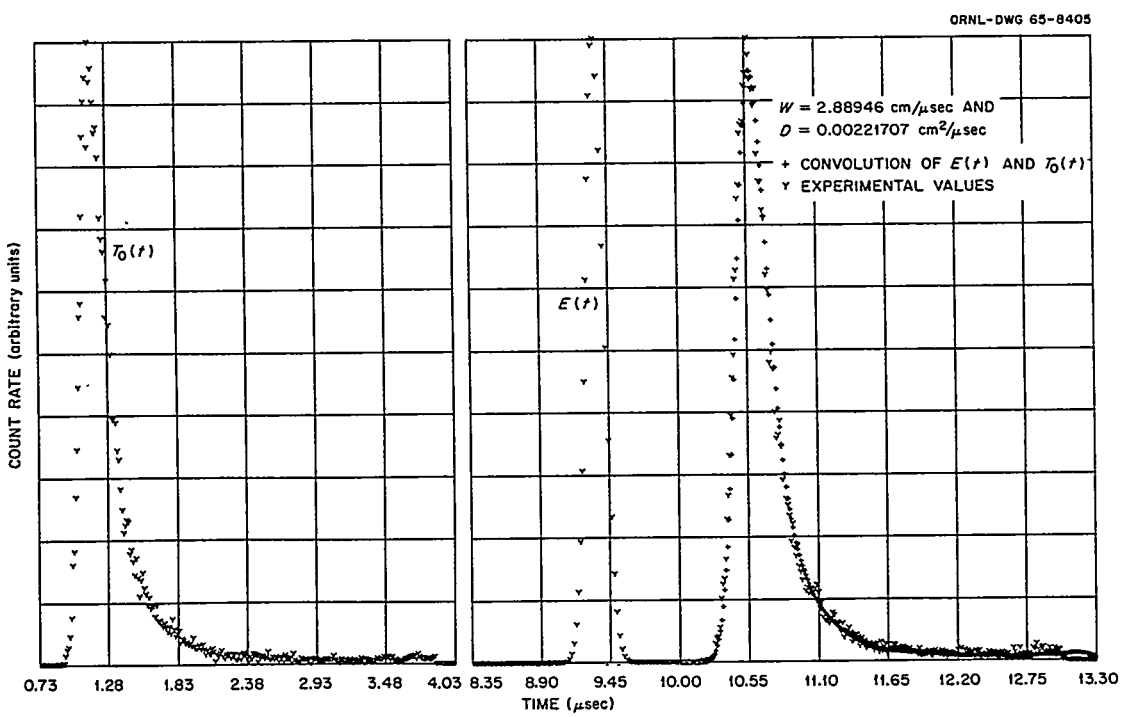

Fig. 14.5. $T_0(t)$, $E'(t)$, and $E(t)$ for Ethylene. $E/P = 1.0$, $P = 100$ torrs.

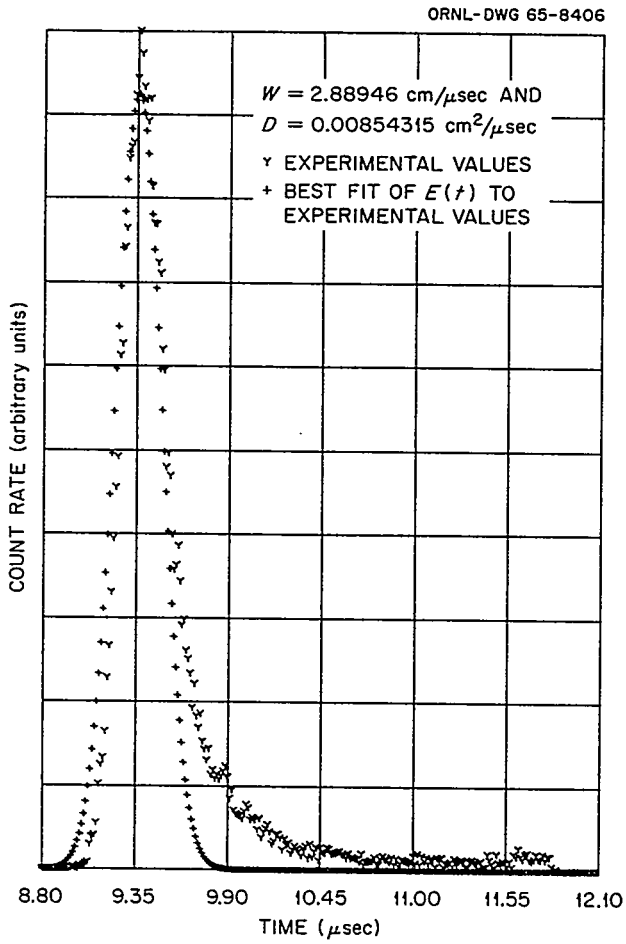

Fig. 14.6. Time-of-Flight Distribution in Ethylene, Where Error Fluctuations Are Neglected. E/P = 1.0, P = 100 torrs.

diffusion coefficient can be correlated to poor fittings of data to theory. Therefore, by looking at plots of the data fits, questionable data points may be repeated. High values of the diffusion coefficient have been tentatively attributed to impurities which cause long-duration collisions. More-precise data are to be taken with frequent changes of the gas so that impurities that might leak in will have no effect on the data.

Calculations of momentum transfer cross sections for C_2H_4 and H_2O, using diffusion data thus far obtained, agree well with those using drift velocity data. A comprehensive data analysis is yet to follow.

ELECTRON TIME-OF-FLIGHT STUDIES USING ELECTRON MULTIPLIER TECHNIQUES

Modifications on the electron time-of-flight apparatus described previously[15,16] include a shorter, simplified electron lens system which diminishes electron scattering with gas molecules in the intermediate-pressure region. This allows a much higher yield of electrons at higher gas pressures in the reaction chamber. The electron detector now chosen is the RCA model C7185J 14-stage copper-beryllium dynode, open-window electron multiplier. A longer reaction chamber of 1.5 m length has been constructed and can be interchanged with the present 24-cm chamber.

Experiments have been performed measuring the mobility, μ, and diffusion, D, of various gases. The ratio D/μ, which is a measure of the agitation energy, is shown for nitrogen, hydrogen, ethylene, and carbon dioxide in Figs. 14.7–14.10. For comparison are shown values obtained by other experimenters, all of whom used the Townsend method. In the first three gases the present values are considerably lower than values obtained by

[15] R. D. Birkhoff *et al.*, *Health Phys. Div. Ann. Progr. Rept. June 30, 1963*, ORNL-3492, p. 135.

[16] R. D. Birkhoff *et al.*, *Health Phys. Div. Ann. Progr. Rept. July 31, 1964*, ORNL-3697, p. 134.

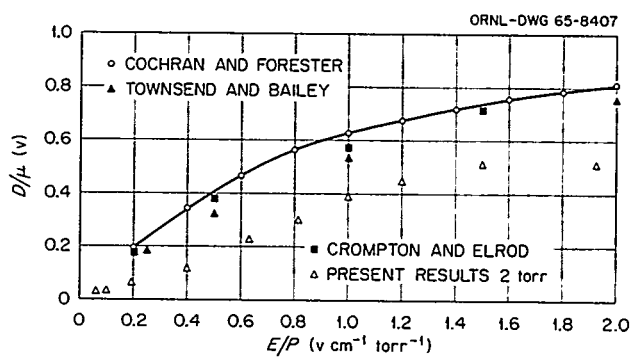

Fig. 14.7. Ratio D/μ as a Function of E/P in Nitrogen. Data from L. W. Cochran and D. W. Forester, *Phys. Rev.* 126, 1785 (1962); J. S. Townsend and V. A. Bailey, *Phil. Mag.* 42, 873 (1921); and R. W. Crompton and M. T. Elrod, "The Ratio of Drift Speed to Diffusion Coefficient for Quasi-Thermal Electrons in Nitrogen and Hydrogen," *Proc. Intern. Conf. Ionization Phenomena Gases, 6th, Paris, 1963.*

the Townsend method. In carbon dioxide our values lie between two sets of data taken with the Townsend method. In the present apparatus, D and μ are measured independently, instead of only their ratio as in the Townsend method. Comparison of the mobility of these same gases with values obtained by Bortner *et al.*[17] and Lowke[18] show that the present values are, in general, higher by 5 to 15%.

If our preliminary results are valid, they represent a significant development in electron diffusion studies. The substantial difference in the present results and those of others should be considered from the point of view that there exist only two methods for measuring electron diffusion, the Townsend method and the time-of-flight method. All other observers used the Townsend method; hence our disagreement with others may be due to the fundamentally different approach employed.

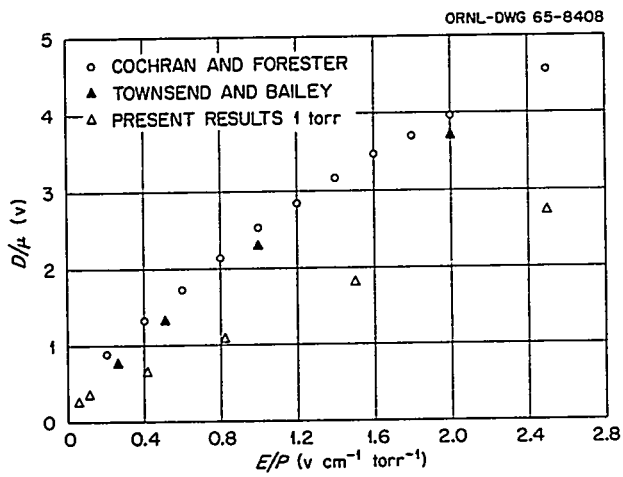

Fig. 14.8. Ratio D/μ as a Function of E/P in Hydrogen. Data from L. W. Cochran and D. W. Forester, *Phys. Rev.* 126, 1785 (1962) and J. S. Townsend and V. A. Bailey, *Phil. Mag.* 42, 873 (1921).

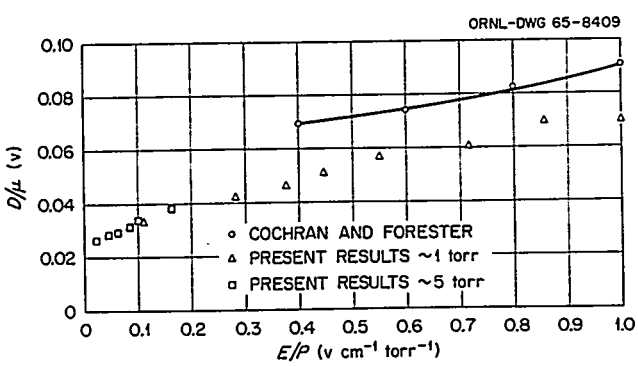

Fig. 14.9. Ratio D/μ as a Function of E/P in Ethylene. Data from L. W. Cochran and D. W. Forester, *Phys. Rev.* 126, 1785 (1962).

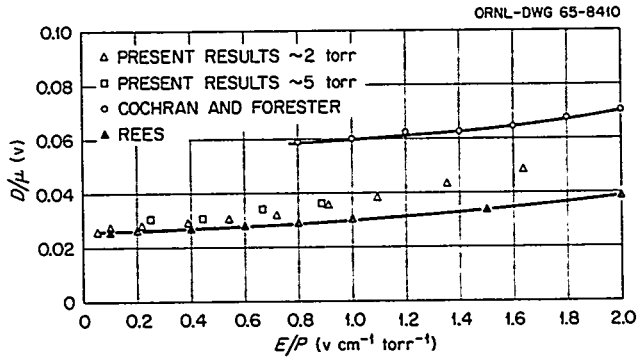

Fig. 14.10. Ratio D/μ as a Function of E/P in Carbon Dioxide. Data from L. W. Cochran and D. W. Forester, *Phys. Rev.* 126, 1785 (1962) and J. A. Rees, "Measurements of Townsend's Energy Factor k_1 for Electrons in Carbon Dioxide," September 1964 (unpublished) (*Ion Diffusion Unit*, The Australian National University, Canberra, Report 64-2).

AN APPARATUS FOR MEASUREMENT OF ELECTRON CAPTURE AT VARIOUS TEMPERATURES

An apparatus has been designed for electron-capture studies as a function of temperature (up to ~250°C). The development of such an apparatus was undertaken for two main reasons. First, organic molecules of biological interest, such as the four- and five-benzene-ring carcinogenic aromatic hydrocarbons, have very low vapor pressures at room temperature and thus could not be studied by our existing equipment, which was designed for room-temperature electron-capture studies. Second, temperature studies may be helpful in revealing mechanisms for electron

[17] T. E. Bortner *et al.*, *Rev. Sci. Instr.* 28, 103 (1957).
[18] J. J. Lowke, *Australian J. Phys.* 16, 115 (1963).

capture. For example, in studies with benzene derivatives (see "Electron Capture by Benzene Derivatives," this chapter), dissociative capture occurs in two separate ranges of electron energy. One possible explanation for these two processes involves vertical transitions from two vibrational levels ($v = 0$, $v = 1$) in the attractive electronic ground state to a common repulsive state leading to dissociation. Such ideas can be tested by studies of the capture cross section for the two processes as a function of temperature.

The main part of the apparatus, a parallel-plate ionization chamber designed for high-temperature experiments, is shown in Fig. 14.11. A block diagram of the apparatus is given in Fig. 14.12. The establishment of the apparatus is completed, and experiments are in progress.

AN ELECTRON SWARM-BEAM METHOD FOR MEASUREMENT OF CAPTURE CROSS SECTIONS

A method is described which combines electron-swarm and electron-beam techniques to obtain absolute electron-capture cross sections as a function of electron energy. As examples of the method, data on Cl^- from *o*-chlorotoluene (ca. 1 ev) and O^- from oxygen (ca. 7 ev) are presented and discussed.

The absolute values of the attachment coefficient $\alpha(E/P)$ and the electron drift velocity $w(E/P)$ are measured in the swarm method. Their product gives the absolute rate of electron capture, which is closely related to the capture cross section. Specifically, the attachment coefficient $\alpha(E/P)$, the capture cross section $\sigma_c(\epsilon)$ as a function of electron energy ϵ, and the electron drift velocity $w(E/P)$ are related by

$$\alpha(E/P) \times w(E/P)$$

$$= N_0(2/m)^{1/2} \int_0^\infty \epsilon^{1/2} \sigma_c(\epsilon) f(\epsilon, E/P)\, d\epsilon\,, \quad (1)$$

where N_0 is the number of sample gas molecules per cubic centimeter at 1 torr, m is the electron mass, and $f(\epsilon, E/P)$ is the electron energy distribution function. The left-hand side of Eq. (1),

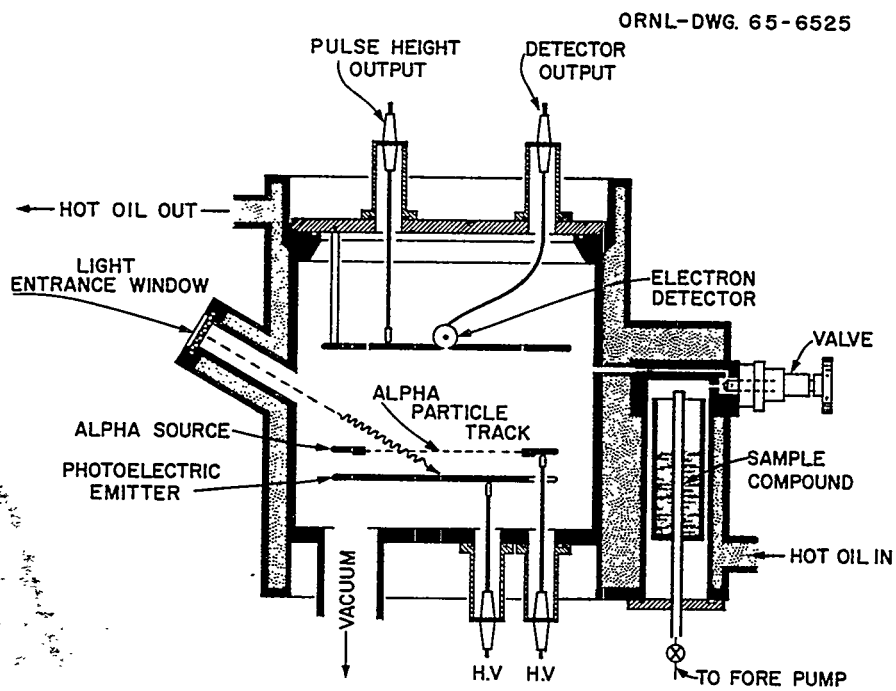

Fig. 14.11. Ionization Chamber for Measurement of Attachment Coefficients and Electron Drift Velocities at High Temperatures.

ORNL-DWG. 65-6588

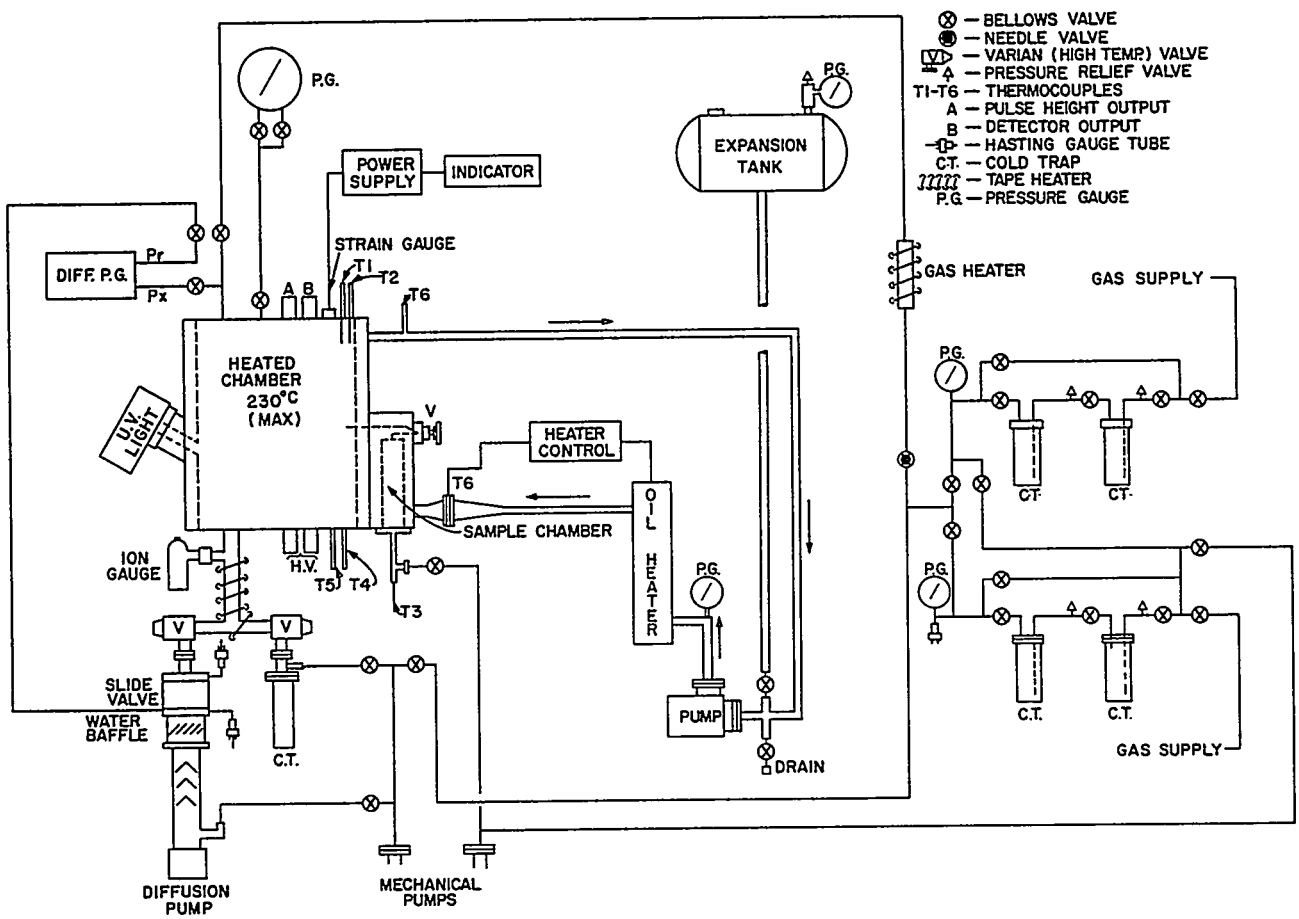

Fig. 14.12. Block Diagram of High-Temperature Electron-Capture Apparatus.

$\alpha(E/P) \times w(E/P)$, is the absolute rate of removal of electrons from the electron swarm due to capture.

Let us denote by $\alpha_i w_i$ the measured rate of attachment for the ith value of E/P and let us use various trial functions for cross section $\sigma_c(\epsilon)$ and denote by $(\alpha w)_{ij}$ the calculated αw for the ith value of E/P and the jth specification of the trial function. For each trial function j, a best fit to the experimental swarm data is obtained by

$$\sum_i [(\alpha w)_{ij} - \alpha_i w_i]^2 = \text{minimum} = M_j \,. \qquad (2)$$

Various trial functions j can be used in an effort to find a j for which $M_j \rightarrow$ minimum.

With the Bendix time-of-flight mass spectrometer we have obtained the ion current $I(\epsilon)$ as a function of the electron energy ϵ for o-$C_6H_4CH_3Cl$ and O_2. Let T_j be a simple translation of $I(\epsilon)$ along the energy axis and use $\sigma_{bj}(\epsilon)$ as a beam trial function, that is,

$$\sigma_{bj}(\epsilon) = K_j T_j \, I(\epsilon) \,. \qquad (3)$$

If we introduce this cross section into Eq. (2), we obtain

$$\sum_i \left[N_0 (2/m)^{1/2} K_j \int_0^\infty \epsilon^{1/2} T_j \, I(\epsilon) \, f_i(\epsilon) \, d\epsilon - \alpha_i w_i \right]^2 = M_j \,. \qquad (4)$$

Formally, then, each transformation T_j of $I(\epsilon)$ results in values of M_j and K_j which are found from Eq. (4) and the solution of

$$\frac{dM_j}{dT_j} = 0 \, . \tag{5}$$

In Fig. 14.13 the swarm experimental rates and the calculated capture rates (based on our beam data) for various energy translations T_j are plotted as a function of E/P for the case of o-$C_6H_4CH_3Cl$. For $T_j = 0 \rightarrow 0.42$ ev the swarm experimental rates are in complete agreement with those obtained from the beam data. In the case of O_2, Fig. 14.14, $T_j(\text{opt}) = 0 \rightarrow 0$ ev, and a positive or negative shift of the $I(\epsilon)$ curve along the energy axis by 0.5 ev results in a considerable disagreement between the beam calculated rates and the swarm experimental rates (the disagreement being more pronounced the larger the energy shift). This indicates the sensitivity of this method in determining the energy at which $\sigma_c(\epsilon)$ peaks. Using the method which has just been described, our $I(\epsilon)$ curves can be normalized, and absolute values of the capture cross section as a function of electron energy ϵ, $\sigma_c(\epsilon)$, can be calculated. Figures 14.15 and 14.16 show $\sigma_c(\epsilon)$ for o-C_7H_7Cl and O_2. The cross sections are plotted against electron energy in electron volts and are given in square centimeters. Since these cross sections are based on electron beam data which are just translated in energy and are then normalized in

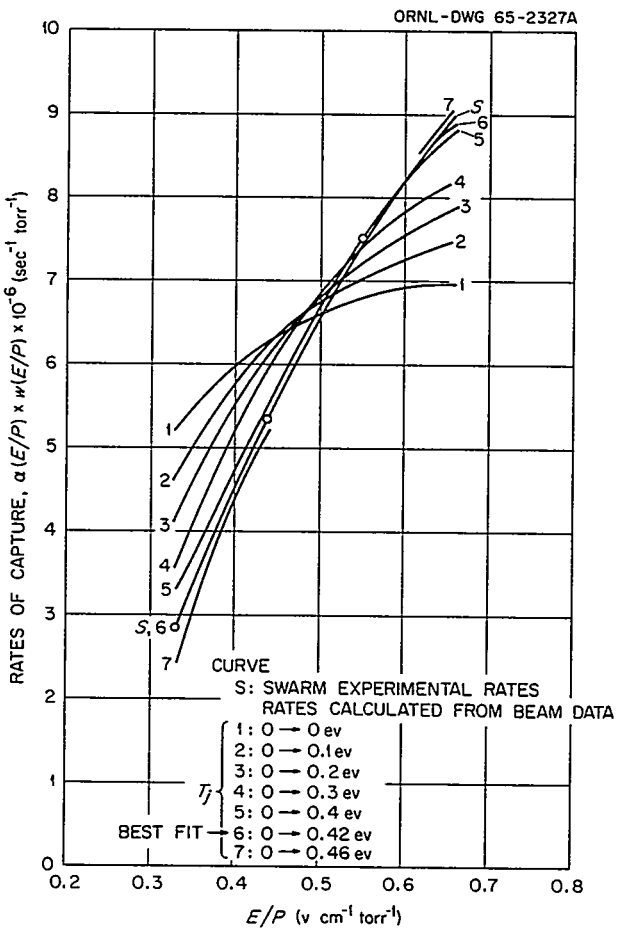

Fig. 14.13. Experimental and Calculated Rates of Capture vs E/P for o-Chlorotoluene for Trial Functions Based on Beam Experiments.

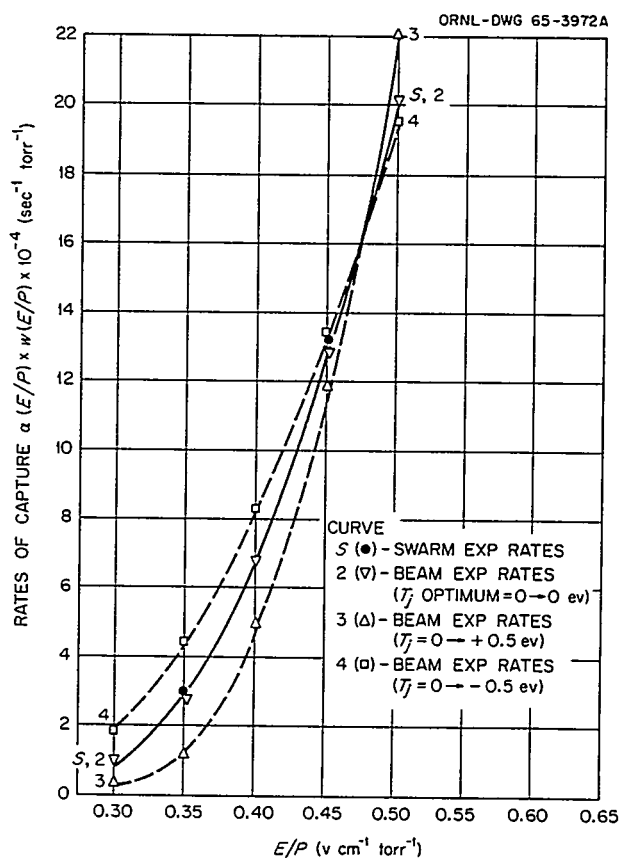

Fig. 14.14. Experimental and Calculated Rates of Capture vs E/P for Oxygen for Various Types of Trial Functions.

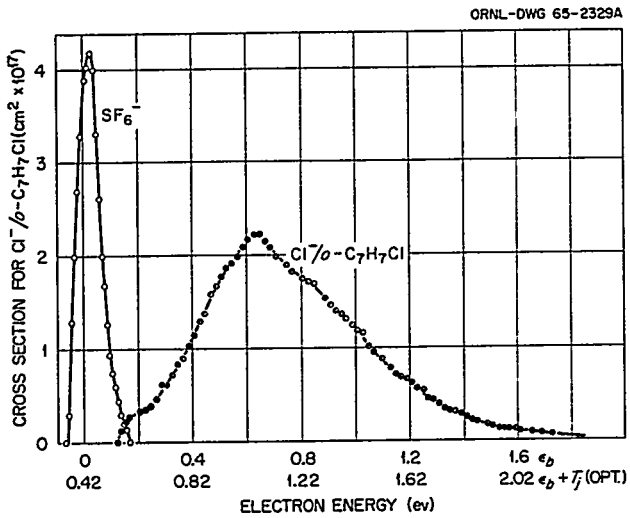

Fig. 14.15. Electron Capture Cross Section as a Function of Energy for Chlorine Negative Ions from *o*-Chlorotoluene.

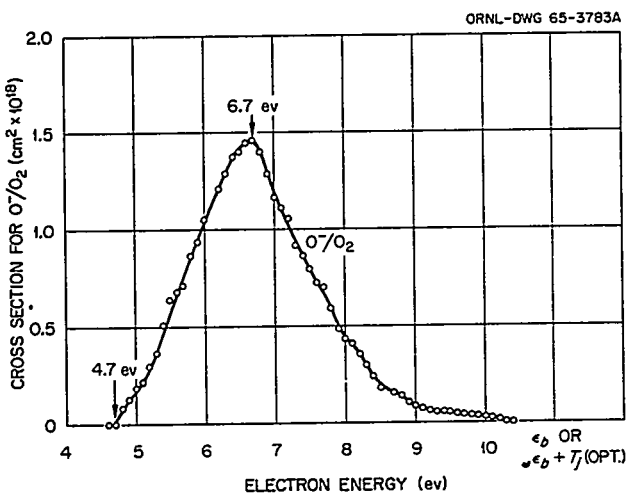

Fig. 14.16. Electron Capture Cross Section as a Function of Electron Energy for Oxygen Atomic Negative Ions from Oxygen.

magnitude, both operations being determined by fitting the swarm data, they may be appropriately described as "swarm-normalized beam cross sections."

The significance of the swarm-beam combination in determining absolute capture cross sections must be emphasized. As a rule, mass spectroscopy and beam experiments report relative cross sections, while in swarm experiments only the rate of capture, $\alpha(E/P) \times w(E/P)$, can be calculated. However, in a few cases absolute cross sections have been calculated from total ionization measurements which did not include mass analysis. Our value of the maximum cross section for O^-/O_2, 1.5×10^{-18} cm^2, is in relative agreement with that of refs. 19 to 21 and is in exact agreement with that of ref. 22, but disagrees with that given in ref. 23. The combined swarm-beam technique appears to be a powerful method for the determination of the absolute cross section (as a function of electron energy) for identified electron-capture processes.

ELECTRON CAPTURE BY BENZENE DERIVATIVES

We have used the combined swarm-beam method (described in the preceding section) to investigate the interaction of electrons with energies $\lesssim 2$ ev with organic vapors.

Using the swarm method we have calculated absolute capture rates, $\alpha(E/P) \times w(E/P)$, as a function of E/P (the pressure-reduced electric field), where $\alpha(E/P)$ is the attachment coefficient for the vapor under investigation in mixtures with a carrier gas for which the energy distribution in the electron swarm is known, and $w(E/P)$ is the electron drift velocity. Using the beam method, we measured the ion current $I(\epsilon)$ as a function of electron energy ϵ, and we identified the products of the electron-molecule interaction. A combination of the two sets of data allowed determination of the capture cross section, $\sigma_c(\epsilon)$, as a function of electron energy for mass-identified negative ions.

---

[19] I. S. Buchel'nikova, *Soviet Phys. JETP (English Transl.)* 35, 783 (1959).

[20] G. J. Schulz, *Phys. Rev.* 128, 178 (1962).

[21] R. K. Asundi *et al.*, *Proc. Phys. Soc. (London)* 82, 967 (1963).

[22] D. Rapp and D. D. Briglia, Lockheed Missiles and Space Company Technical Report 6-74-64-40 (unpublished).

[23] J. D. Craggs *et al.*, *Proc. Roy. Soc. (London)* A240, 473 (1957).

The halogenated benzene derivatives listed in Table 14.5 satisfy the condition

$$D(\mathrm{A}-\mathrm{X}) - EA(\mathrm{X}) \lesssim 0 ,$$

where $D(\mathrm{A}-\mathrm{X})$ is the dissociation energy of the halogenated benzene derivative AX, and $EA(\mathrm{X})$ is the electron affinity of the halogen X. In all cases, two separate dissociative processes have been observed, one peaking at *ca.* 1 ev and the other at energies $< 3/2\ kT$.

The *ca.* 1-ev Electron-Capture Process

Table 14.5 summarizes our swarm-beam data. The only ions observed in the time-of-flight mass spectrometer are the X^-. In columns 3 and 4 of Table 14.5, the energy $\epsilon_1(\delta)$ at which $\sigma_c(\epsilon)$ peaks and the energy-integrated cross section $\int_0^\infty \sigma_c(\epsilon)\, d\epsilon$ are given as determined by the swarm method on the assumption that $\sigma_c(\epsilon) \cong \delta$ function. The energy at which the ion current $I(\epsilon)$ peaks, as determined by our beam experiments, is given in column 5, and the corrected energy at which $\sigma_c(\epsilon)$ peaks is tabulated in column 6. Column 7 gives the maximum value $\sigma_c(\max)$ of $\sigma_c(\epsilon)$, determined by the swarm-beam method. The energy which is available for excitation of AX or A and/or X^- is given in column 8.

Figures 14.17 and 14.18 give representative results for $\alpha(E/P)$ and $\sigma_c(\epsilon)$, respectively, for the case of *o*-bromotoluene.

The Thermal Electron Capture Process

Figure 14.19 gives the "pulse height" vs E/P for the thermal process for *o*-bromotoluene, and Fig. 14.20 shows $\alpha \times w = f(E/P)$ for a number of halogenated benzene derivatives. The decrease in $\alpha \times w$ as E/P increases (for a certain E/P range) excludes the possibility that the thermal, pressure-independent dissociative capture is due to the low-energy tail of the *ca.* 1-ev process. In Table 14.6 the rates of capture for the thermal process are listed. These rates are much smaller than those of the *ca.* 1-ev process.

The actual mechanism for this process is not yet completely understood, and experiments are in progress to help understand all the data as well as the predicted connection of this process with that occurring at *ca.* 1 ev. It is, however,

Table 14.5. Swarm-Beam Data on the *ca.* 1-ev Dissociative Process

Compound	Ion	$\epsilon_1(\delta)$ (ev)	$\int_0^\infty \sigma_c(\epsilon)\, d\epsilon$ (cm^2ev)	$\epsilon_b(\max)$ (ev)	$\epsilon_b(\max) + T_j(\mathrm{opt})$ (ev)	$\sigma_c(\max)$ (cm^2)	Energy available for excitation = $[\epsilon_b(\max) + T_j(\mathrm{opt})] + [EA(\mathrm{X}) - D(\mathrm{A-X})]$ (ev)
			$\times 10^{-17}$			$\times 10^{-17}$	
Chlorobenzene	Cl^-	0.78	1.3	0.60	0.86	1.38	0.86
Bromobenzene	Br^-	67	4.7	0.51	0.84	9.6	1.33
Iodobenzene	I^-	~0.0	Very large	0.00			0.79
o-Dichlorobenzene	Cl^-	0.41	12.3	0.21	0.38	43	~0.38
o-Chlorotoluene	Cl^-	0.85	1.1	0.66	1.10	2.2	~1.10
o-Bromotoluene	Br^-	0.83	4.2	0.63	0.95	6.0	~1.44
Deuterated bromobenzene	Br^-	0.65	4.5	0.51	0.80	10.4	1.26

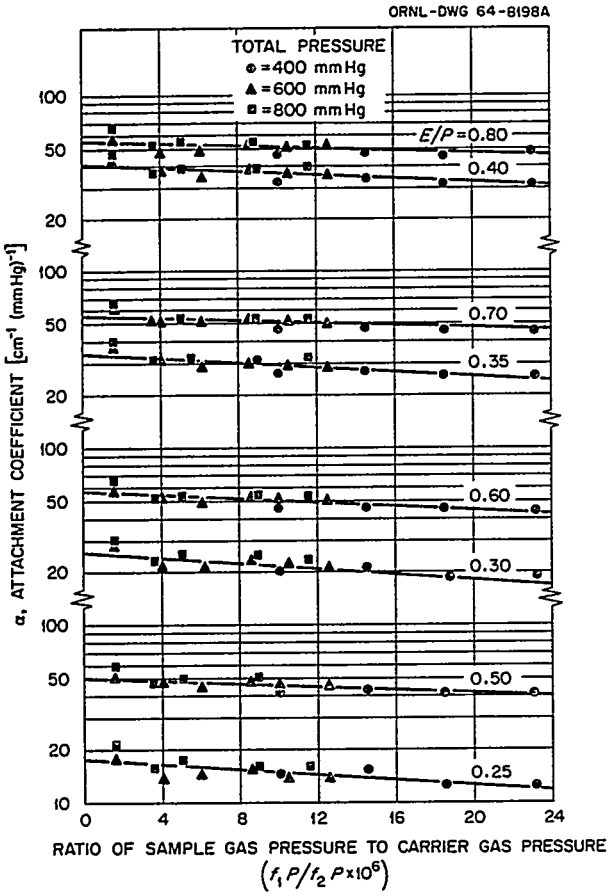

Fig. 14.17. Attachment Coefficient, $\alpha(E/P)$, as a Function of the Ratio of Sample Gas Pressure to Carrier Gas Pressure, f_1P/f_2P, for o-Bromotoluene.

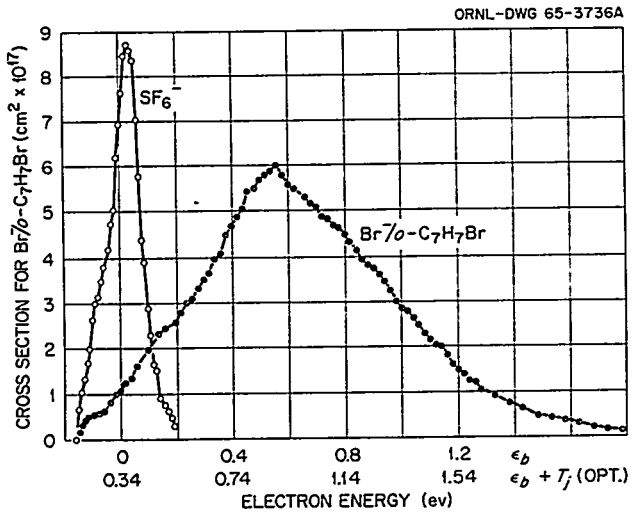

Fig. 14.18. Electron Capture Cross Section as a Function of Energy for Bromine Negative Ions from o-Bromotoluene.

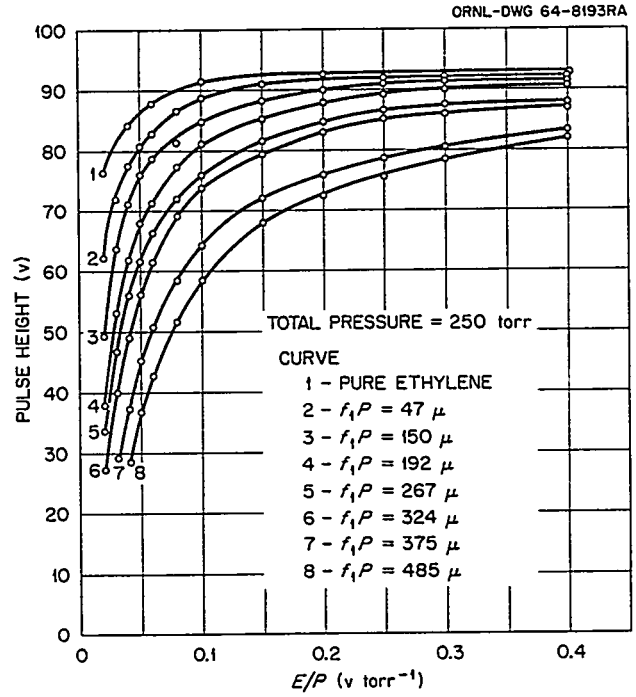

Fig. 14.19. Pulse Height as a Function of E/P for o-Bromotoluene in Ethylene.

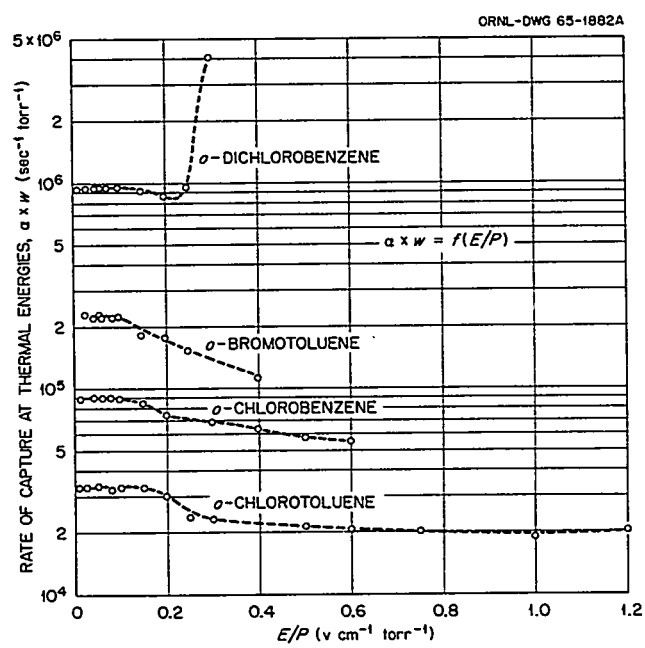

Fig. 14.20. Rate of Capture at Thermal Energies as a Function of E/P for Halogenated Benzene Derivatives in Mixtures with Ethylene.

Table 14.6. Swarm Data on the Thermal Dissociative Process

Compound	Rate of Capture at Thermal Energies (sec^{-1} $torr^{-1}$)
	$\times 10^4$
Chlorobenzene	9.7
Bromobenzene	30
Iodobenzene	Very large
o-Dichlorobenzene	95
o-Chlorotoluene	3.4
o-Bromotoluene	23
Deuterated bromobenzene	35

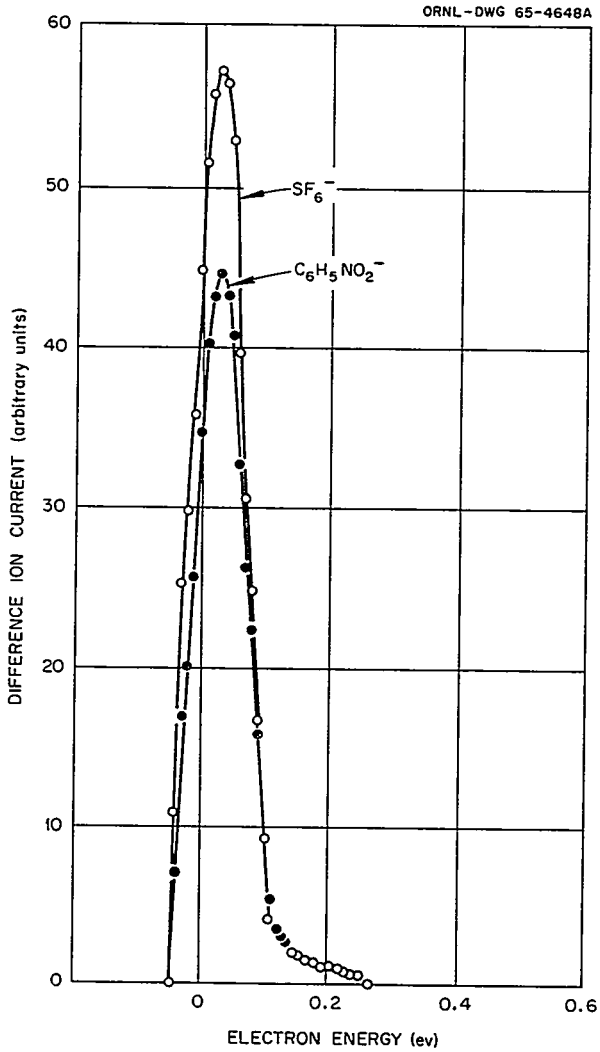

Fig. 14.21. Comparison of $C_6H_5NO_2^-$ Ion Current with SF_6^- Ion Current as a Function of Electron Energy.

clear that this group of molecules captures low-energy electrons (including thermal) dissociatively. This is in contradiction with previously published data that this group of organic molecules captures strongly low-energy electrons (thermal or near the thermal region) only by a resonance nondissociative process.

In addition to the halogenated benzene derivatives listed in Table 14.5, we have applied our techniques to study the electron capture processes in a number of other benzene derivatives including nitrobenzene and nitrotoluene. Both nitrobenzene and nitrotoluene are found to capture electrons through a very sharp nondissociative resonance process at approximately thermal electron energies. Figure 14.21 shows that the energy width of the nondissociative capture resonance is instrumental and is thus less than 0.1 ev. Two separate dissociative electron capture processes leading to NO_2^- were observed for nitrobenzene and nitrotoluene at higher electron energies, namely at 1.07 and 3.6 ev for both molecules.

LIFETIMES OF NEGATIVE IONS

Construction of a new negative-ion lifetime apparatus, shown in Fig. 14.22 and described previously,[24] is near completion and ready for testing of the major components. The apparatus will be used to measure lifetimes of negative ions in the range 10^{-9} to 10^{-6} sec.

[24]R. D. Birkhoff *et al.*, *Health Phys. Div. Ann. Progr. Rept. July 31, 1964*, ORNL-3697, p. 136.

ORNL-DWG 64-5967A

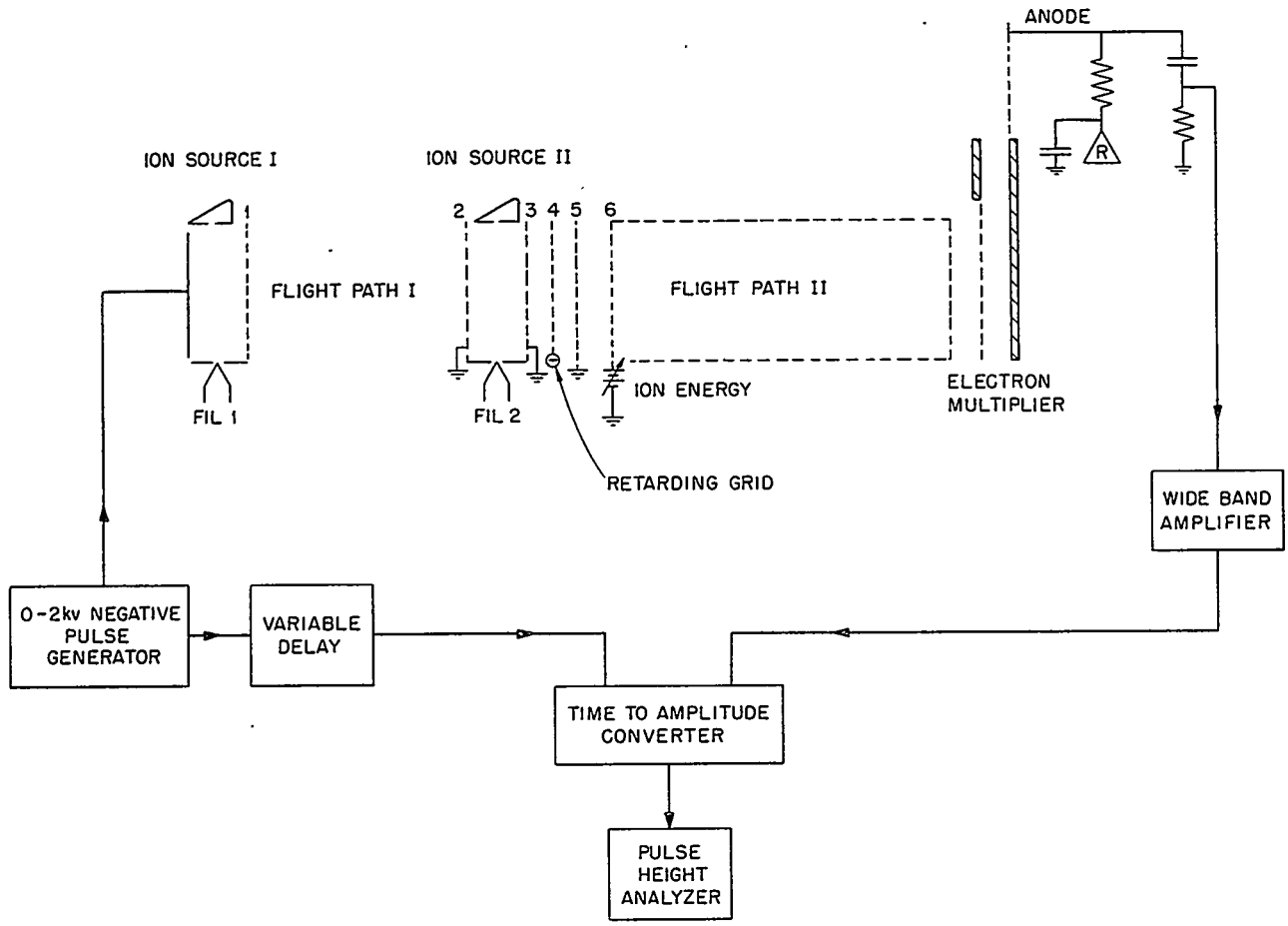

Fig. 14.22. Schematic Diagram of Negative-Ion Lifetime Apparatus.

Experiments are also in progress to determine lifetimes of long-lived temporary negative ions. Quite a number of molecules have been reported to attach electrons by unimolecular electron capture for times greater than 10^{-6} sec. These molecules are large and generally symmetric, so that the excess energy of the captured electron is shared with the many degrees of freedom of the molecule, allowing the negative ion to live long enough to be detected in a conventional mass spectrometer. Of particular interest is the study of temporary negative ions of organic molecules which have been observed in our electron attachment experiments.

A Bendix time-of-flight mass spectrometer is utilized to measure the long lifetimes. The experimental procedure can be illustrated by referring to Fig. 14.23. Temporary negative ions are created in the ion source by nondissociative electron capture and are immediately pulsed out of the source. The ions then travel down a field-free flight tube with a velocity v. Electrons become autodetached from the negative ions in their passage through the flight tube in accordance with an exponential decay law. A "flat top" potential at A decelerates the negative ions and leaves the neutral molecules unaffected. This potential barrier separates the negative ions from the neutral molecules after a time $t = l/v$ and therefore allows N^- and N^0 to be determined individually. A single-pulse counting technique is used to detect both the negative ions and the neutral

ORNL-DWG 65-8411

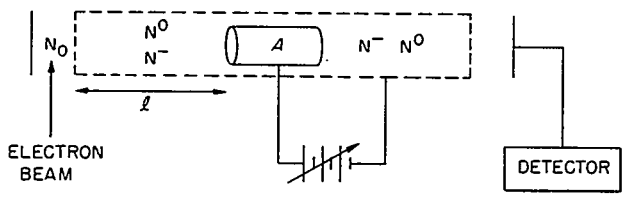

Fig. 14.23. Schematic Diagram of Experiment Employed to Determine Lifetimes of Long-Lived Negative Ions.

molecules. If an exponential decay law is assumed for the autodetachment of electrons from the molecules within the time t, then the mean lifetime can be determined from

$$\frac{1}{\lambda} = \frac{t}{\ln(N^- + N^0/N^-)} .$$

A preliminary measurement of the lifetime of the nitrobenzene negative ion has been carried out with the result $1/\lambda \approx 50$ μsec.

THEORY OF ELECTRON CAPTURE BY ROTATIONAL EXCITATION OF POLAR MOLECULES

A theoretical study of electron capture by rotational excitation of polar molecules was suggested as a result of previous experimental findings.[13,25] A calculation of capture cross sections and ion lifetimes for rotational transitions in a polar molecule along the lines of an earlier calculation by Bloch and Bradbury[26] for capture by vibrational excitation has been completed. In the present work the molecule is represented as a rigid dipole, free to rotate about its center. The results of the theoretical study indicate that there may be substantial contributions to momentum transfer cross sections (which are measured in swarm experiments) by capture and release of electrons from polar molecules that (1) have a large ratio of dipole moment to moment of inertia and (2) have a moment of inertia so small that successive rotational levels in the molecule have energies comparable with thermal energies kT. The theory predicts that the molecules HF, HCl, H_2O_2, and NH_3 should show an increase in the cross section calculated only from elastic scattering[12] similar to that of H_2O, D_2O, and H_2S in swarm experiments.[13] Numerical evaluation gives capture cross sections of approximately 5×10^{-19} cm^2 and negative-ion lifetimes of approximately 10^{-13} sec.

CALCULATIONS OF ONE-DIMENSIONAL ELECTRON DIFFUSION THROUGH GASES WITH CAPTURE AND LOSS

The diffusion of electrons in one dimension through a system of molecules that capture and lose electrons is governed by the equations:

$$\frac{\partial n}{\partial t} = D\frac{\partial^2 n}{\partial x^2} - w\frac{\partial n}{\partial x} - \beta n + \gamma N ,$$

$$\frac{\partial N}{\partial t} = \beta n - \gamma N .$$

Here $n = n(x, t)$ is the volume density of electrons at the position x and time t, $N(x, t)$ is the volume density of molecules (considered stationary) which have captured electrons, w is the drift velocity, D is the diffusion coefficient of electrons in the gas, β is the probability of electron capture per unit time, and γ is the reciprocal of the lifetime of the negative ions. The system physically is one in which electrons in a swarm diffusing through a gas can be captured by the gas molecules and subsequently released back into the swarm.

If a source of electrons is released at the position $x = 0$ at time $t = 0$ (1 electron/cm^2), then the Fourier components $\bar{n}(s, \omega)$ of the Laplace transform of $n(x, t)$ are given by

$$\bar{n}(\omega, s) = \frac{1}{D\omega^2 + iw\omega + \Gamma} ,$$

where $\Gamma = \beta + s - \beta\gamma/(s + \gamma)$, and

$$n(x, t) = \frac{1}{4\pi^2 i}\int d\omega \int ds\, e^{i\omega x + st}\, \bar{n}(\omega, s) .$$

[25] G. S. Hurst *et al.*, *Nature* 195, 66 (1962).

[26] F. Bloch and N. E. Bradbury, *Phys. Rev.* 48, 689 (1935).

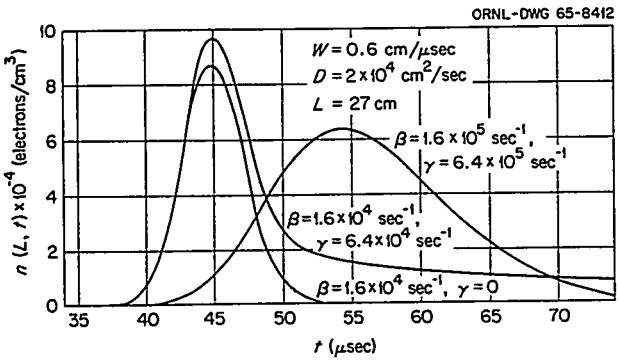

Fig. 14.24. Time Variation in the Density of Electrons at a Distance L from a Plane Source in a Gas Subject to a Uniform Electric Field. The electron diffusion coefficient is D and the drift velocity is w. The capture rate of electrons on molecules of the gas is β and the decay rate is γ.

For $\gamma = 0$, electrons are permanently captured by molecules, and the density is given exactly by

$$n(x, t) = \frac{w}{\sqrt{4\pi Dt}} \exp\left[-(x - wt)^2/4Dt - \beta t\right] .$$

As a function of time this distribution has the characteristic shape shown in Fig. 14.24 when the other parameters take the values given there. For $\gamma \neq 0$, no exact solution for $n(x, t)$ has been found in closed form, although the inverse Laplace transform and the inverse Fourier transform, separately, can both be found analytically. Numerical integration for two sets of values β, γ gives the distributions shown in Fig. 14.24. An account of this work and numerical results are being prepared for publication.

FOURIER TRANSFORM METHODS IN THE UNFOLDING OF EXPERIMENTAL DATA

In most physical experiments, data are subject to unavoidable "smearing" effects introduced by the apparatus. It is possible, for a certain important class of experiments, to represent $E(t)$, the variation of the experimental data with an independent variable t, in the form of a convolution integral:

$$E(t) = \int_0^t F(t - \tau)\, G(\tau)\, d\tau . \qquad (1)$$

Here we suppose that $F(t)$ represents the real data in the absence of smearing, while $G(\tau)$ is a "smearing" function, which is presumed to be known.

If one has definite information concerning the form that $F(t)$ should take, for example, from a knowledge of the physics involved in the experiment, one may consider it to depend upon a set of parameters $\boldsymbol{\beta} = \beta_1, \beta_2, \ldots, \beta_n$ and write $F_{\boldsymbol{\beta}}(t)$ to denote the analytically specified function.

The conventional generalized least-squares method for deriving a "best" set of parameters $\boldsymbol{\beta}$ from the data involves the minimization of the quantity

$$R = \int_0^\infty dt\, \left[E(t) - \int^t F_{\boldsymbol{\beta}}(t - \tau)\, G(\tau)\, d\tau\right]^2 \qquad (2)$$

with respect to $\boldsymbol{\beta}$. This procedure may be prohibitively time consuming, even with the use of electronic computers.

An alternative procedure is to utilize Fourier integral expansions of the quantities involved in Eq. (1). Thus, if the functions E, F, and G may be represented by expansions like

$$f(t) = \frac{1}{2\pi} \int_{-\infty}^{\infty} e^{-i\omega t}\, \bar{f}(\omega)\, d\omega ,$$

one may show by standard methods that Eq. (1) may be represented in Fourier space by

$$\bar{E}(\omega) = \bar{F}_{\boldsymbol{\beta}}(\omega)\, \bar{G}(\omega) . \qquad (3)$$

Also one may write Eq. (2) as

$$R = \frac{1}{\pi} \int_0^\infty d\omega\, \left|\bar{E}(\omega) - \bar{F}_{\boldsymbol{\beta}}(\omega)\, \bar{G}(\omega)\right|^2 , \qquad (4)$$

which may be minimized with respect to the $\boldsymbol{\beta}$ much more economically than Eq. (2).

A computer program has been written to analyze data obtained on time of flight in electron swarm experiments. In this case one fits experimental

data with a theoretical expression having the form

$$F(t) = \frac{A}{\sqrt{t}} e^{-(L - wt)^2/4Dt - \gamma t},$$

where the set of parameters $\beta = \{D, w, A, \gamma\}$ are to be found from the condition that R be a minimum. The quantities $\bar{E}(\omega)$ and $\bar{G}(\omega)$ are computed from experimental data on $E(t)$, the number of electrons drifting to a detector at time t, and $G(t)$, an experimentally determined smearing function. An automatic search for the best β is made in the course of the calculation.

This scheme has worked very well in the present application. It is faster by a factor of 10 to 100 than the direct method of minimizing Eq. (2) and is being used extensively in this research activity. A more complete account of this scheme will be published in the near future.

STUDIES OF ELECTRONIC BOUND STATES IN THE FIELD OF AN ELECTRIC DIPOLE

In relation to the problem of electron capture by polar molecules described previously in this chapter, some detailed studies and calculations of the bound states of an electron in the field of an electric dipole were made. The Schrödinger wave equation for an electron in the field of a finite electric dipole is separable, and numerical calculations have been made by Wallis *et al.*[27] for dipole moments down to 2.14×10^{-18} esu-cm. These calculations were not continued below this value because of the slow convergence of the expansions employed. They do not include, therefore, one of the important molecules studied experimentally,[13] namely, water, which has a dipole moment of only 1.85×10^{-18} esu-cm.

A variational trial function was sought which would show that an electron could be bound to a dipole with a moment smaller than that at which the numerical calculations had been discontinued. For a point dipole it was found that an electronic wave function of the form $\phi = C_0 Y_{00} r^{-p} e^{-\alpha r^t} + C_1 Y_{10} r^{-q} e^{-\beta r^s}$, in which C_0, C_1, α, β, s, t, p, and q are variational parameters and Y_{00} and Y_{10} are S- and P-state angular functions, gives binding for a moment as small as 1.65×10^{-18} esu-cm. In this case the trial function takes the simple form $\phi = e^{-\alpha r^t} (C_0 Y_{00} + C_1 Y_{10})$, with t taking a small positive value.

An argument based on the uncertainty principle indicates that bound states might exist for dipole moments as small as 0.2×10^{-18} esu-cm. A solution of purely classical electron–finite-electric-dipole problem has been achieved via the Hamilton-Jacobi theory. A detailed account of all these studies and calculations is being prepared as an ORNL report.

POTENTIAL ENERGY CURVES FOR DIATOMIC MOLECULES

Using as input the experimental term values T_{evJ} for the states of a diatomic molecule with electronic configuration e, vibrational quantum number v, and rotational quantum number J, Klein[28] has derived equations which provide the potential energy for nuclear motion $U_e(r)$ as a function of internuclear distance r. We have modified these equations in two ways: (1) by introducing the reduced mass in a way which will make the comparison of potential energy curves for isotopically different molecules easier, and (2) by modifying an important concomitant function of Klein's theory so that it is expressed in terms of the integral variables v and J. This latter modification is important because the concomitant function (of two variables) is obtained by a single numerical integration and must be numerically differentiated subsequently.

The resulting equations are ready for programming for an automatic computer. The first potential energy curves to be computed are those for HF and DF; the results can be checked against values in the literature.[29]

---

[27] R. F. Wallis *et al.*, *J. Mol. Spectry.* 4, 51 (1960).

[28] O. Klein, *Z. Physik* 76, 226 (1932); for earlier related work see O. Oldenberg, *Z. Physik* 56, 563 (1929) and R. Rydberg, *Z. Physik* 63, 376 (1931).

[29] R. J. Fallon *et al.*, *J. Chem. Phys.* 32, 698 (1960); *ibid.*, 33, 944 (1960).

15. Interaction of Radiation with Solids

R. D. Birkhoff

E. T. Arakawa
L. C. Emerson
W. F. Hanson[1]
R. N. Hamm
J. A. Harter
R. J. Herickhoff[1]
G. E. Jones, Jr.[2]
A. G. Kenerly[3]
R. A. MacRae[4]
W. J. McConnell
Devon Pittman
R. H. Ritchie
H. C. Schweinler
J. L. Stanford[1]

ANGULAR DISTRIBUTION AND THICKNESS DEPENDENCE OF TRANSITION RADIATION FROM THIN ALUMINUM FOILS

The spectral distribution of photons emitted by aluminum foils bombarded by 80-kev electrons was determined in the wavelength region from 600 to 1400 A for various angles of observation on the electron emergence or front side of the foil ($\theta = 0$ to 90°) and on the electron incidence or back side of the foil ($\theta = 90$ to 180°). A trace of the spectrum recorded at $\theta = 160°$ is shown in Fig. 15.1 to illustrate the signal-to-noise ratio and the breadth of the peak at 830 A. The spectrometer resolution is about 40 A. No other peaks were observable from 600 to 1400 A. Similar spectra were obtained at other angles of observation.

Figure 15.2, which shows the peak intensity as a function of angle of observation, summarizes the results obtained. The experimental peak intensities for the front side are slightly higher than the experimental intensities for the back side. This relationship also holds for the peak intensities of the theoretical curves. The angles for which the experimental curves have maximum intensity are $\theta = 22°$ on the front side and $\theta = 157°$ on the back side, while the angles for which the theoretical curves exhibit maximum intensity are $\theta = 15°$ and $\theta = 168°$. This discrepancy may be due to differences between the optical constants of the foils used in this experiment and those of the foils used in the optical constant determination.

Figure 15.3 shows that the energies of the experimental peak intensities on the front side decrease with increasing angle of observation, in agreement with theory. However, the shift of the experimental energy of the peak intensity with angle of observation on the back side is opposite to that of the theoretical shift. This discrepancy may be due to the previously mentioned differences

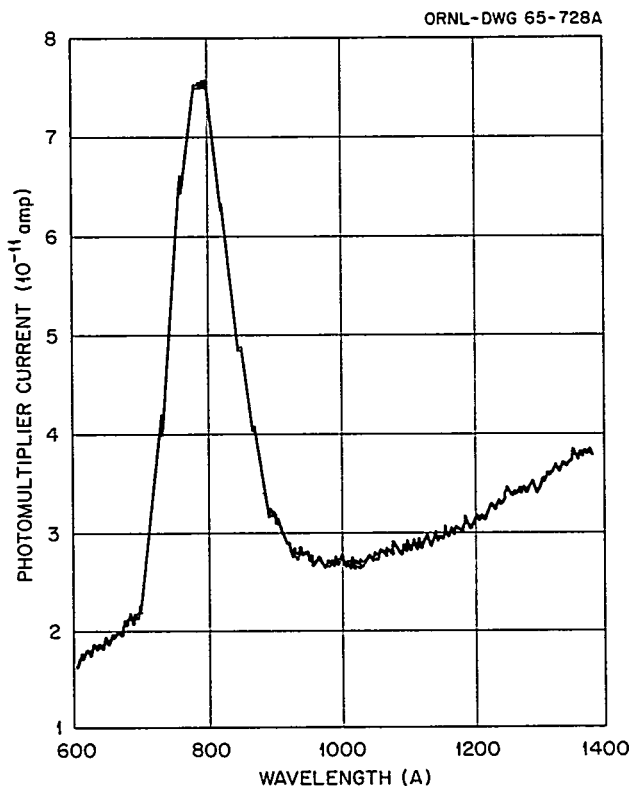

Fig. 15.1. Recorder Trace of Photon Emission from Electron-Bombarded Al Foil, 320 A Thick ($\theta = 160°$, $E = 80$ kev).

[1]Graduate student.

[2]Research participant.

[3]On loan from Instrumentation and Controls Division.

[4]Summer faculty.

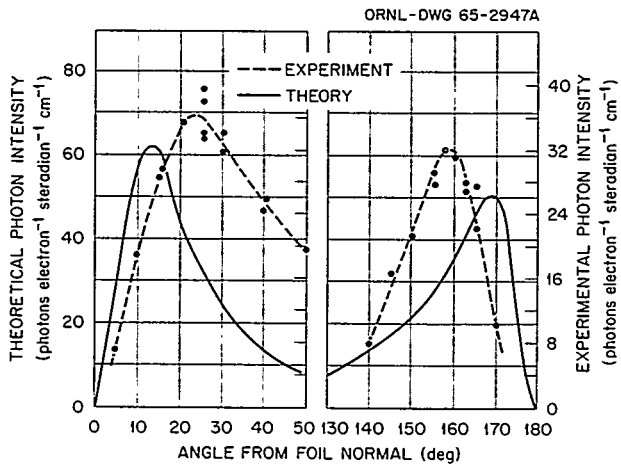

Fig. 15.2. Theoretical and Experimental Peak Intensities as a Function of Angle of Observation.

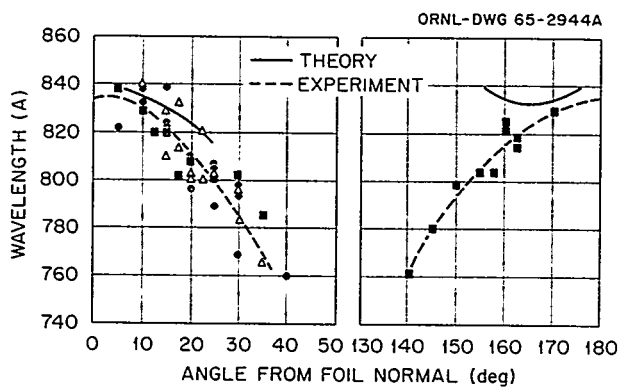

Fig. 15.3. Variation of Peak Wavelength as a Function of Angle of Observation.

in optical constants. The shift of peak energy with angle is predicted by the generalized transition-radiation theory[5] and is qualitatively explained in terms of refraction of light at the surface of the dielectric. In the frequency range where the foil is transparent to photons, $\omega < \omega_p$, photons which originate in the foil interior and strike the surface at an angle θ' with respect to the foil normal will undergo refraction and are bent toward the normal. The exit angle θ is related to θ' by Snell's law, $\epsilon^{1/2} \sin \theta' = \sin \theta$.

[5]R. H. Ritchie and H. B. Eldridge, *Phys. Rev.* 126, 1935 (1962).

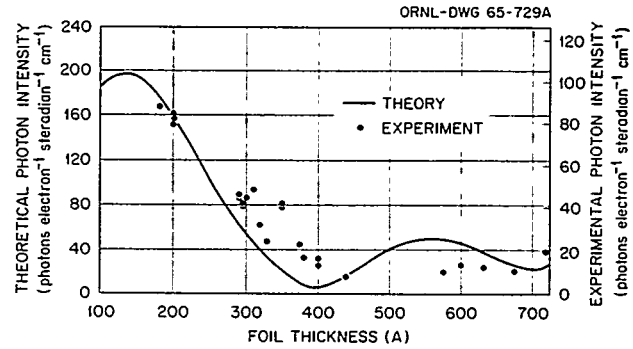

Fig. 15.4. Photon Intensity at Peak Wavelength as a Function of Foil Thickness.

Setting $\theta' = \pi/2$ (the maximum angle of photons in the foil interior) and $\epsilon = 1 - \omega_p^2/\omega^2$, Snell's law reduces to $\omega = \omega_p/\cos \theta$. Thus, for a given frequency $\omega < \omega_p$ there is a value of θ beyond which photons originating inside the foil will not be observed. In the transition-radiation theory the maximum in the photon intensity distribution should occur at $\omega = \omega_p/\cos \theta$. Thus, the curve through the points in Fig. 15.3 extrapolated to 0° should give the plasma wavelength, λ_p = 835 A or E_p = 14.9 ev. This value is in agreement with previous electron energy-loss experiments.[6]

A sine-squared variation of intensity with thickness is predicted by the generalized transition-radiation theory. The first maximum is predicted to occur for a thickness around $\beta\lambda_p/2$, where β is the electron velocity relative to that of light and λ_p is the wavelength of the peak. Secondary maxima are weaker than the first maximum because of increased photon absorption in the foil for increasing foil thickness. Comparison of the experimental results with theory in Fig. 15.4 confirms the essential correctness of the transition-radiation description.

OPTICAL EMISSION STUDIES OF THE CHARACTERISTIC ENERGY LOSSES IN Cd, In, AND Zn

Recent investigations of light emission from electron-bombarded Al and Mg foils yielded results

[6]A. W. Blackstock *et al.*, *Phys. Rev.* 100, 1078 (1955).

in good agreement with the theory of plasma oscillations in metals and the electron energy-loss experiments. Since the optical method is a more accurate means of measuring the plasma frequency and studying the characteristic energy losses than the electron energy-loss method, optical emission studies were continued by bombarding Cd, In, and Zn foils 600 to 1000 A in thickness with 60- to 100-kev electrons, and analyzing the light emitted at 30° from the foil normal with a Seya-Namioka vacuum ultraviolet spectrometer.

The spectra of light emitted by the foils are shown in Figs. 15.5 to 15.7. These spectra have been corrected for the spectrometer response, which includes a measured grating efficiency and an assumed uniform fluorescent quantum efficiency of sodium salicylate. The corresponding electron energy-loss data of Robins[7] are plotted on the same energy scale. The breadth of the energy losses in Robins' data results from his instrumental resolution of about 2.0 ev, whereas for the present experiment an energy separation of 0.22 ev can be detected at 1500 A. Hence the optical method not only provides detail that cannot be obtained from electron energy-loss spectra but also makes possible a study of the inherent widths of the characteristic loss lines. The levels marked N_4, N_5, and $M_{4,5}$ are the levels of the metals determined by soft-x-ray spectroscopy.[8] Also shown for Cd and In is k, the imaginary part of the complex index of refraction determined by optical methods. The theoretical spectrum for In was calculated using the transition-radiation equation of Ritchie and Eldridge,[5] and the optical constants required for the calculations were determined by Hunter[9] from λ = 800 to 1050 A and by us from λ = 1000 to 3000 A.[10]

A sharp, intense peak with a half-width of 0.9 ev was observed in Cd at 9.1 ev, and a less-intense peak was observed in In at 11.8 ev, whereas no peak was seen in Zn. The spectra of all three

[7] J. L. Robins, "The Energy Losses of Electrons Scattered from Solid Elements," Ph.D. dissertation, July 1961, University of Western Australia, Nedlands, Western Australia (unpublished).

[8] A. E. Sandstrom, p. 226 in *Handbuch der Physik* (ed. by S. Flügge), vol. XXX, Springer, Berlin, 1957.

[9] W. R. Hunter, *J. Phys. Radium* 25, 154 (1964).

[10] R. H. Huebner, "The Optical Constants of Vacuum Evaporated Films of Ag and In," M.S. thesis, 1965, Vanderbilt University, Nashville, Tenn. (unpublished).

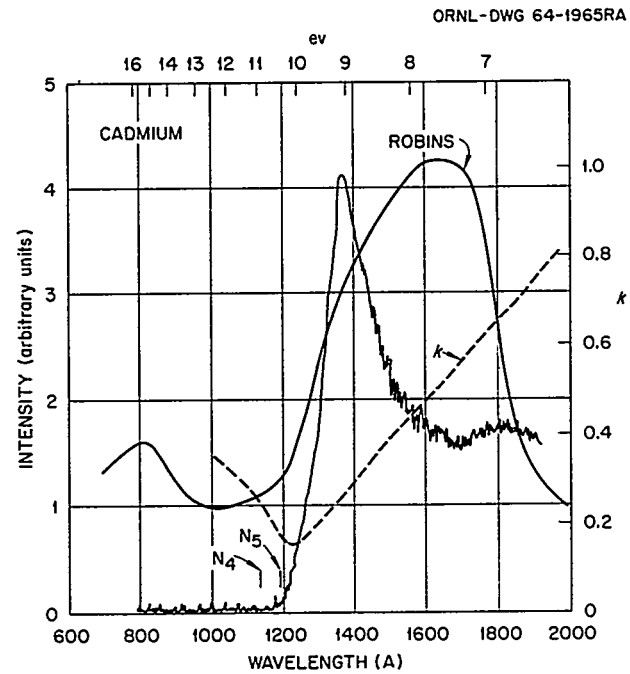

Fig. 15.5. Optical Emission Spectrum from Cd Foil Bombarded by 80-kev Electrons. Robins' electron energy-loss spectrum is shown on the same energy scale.

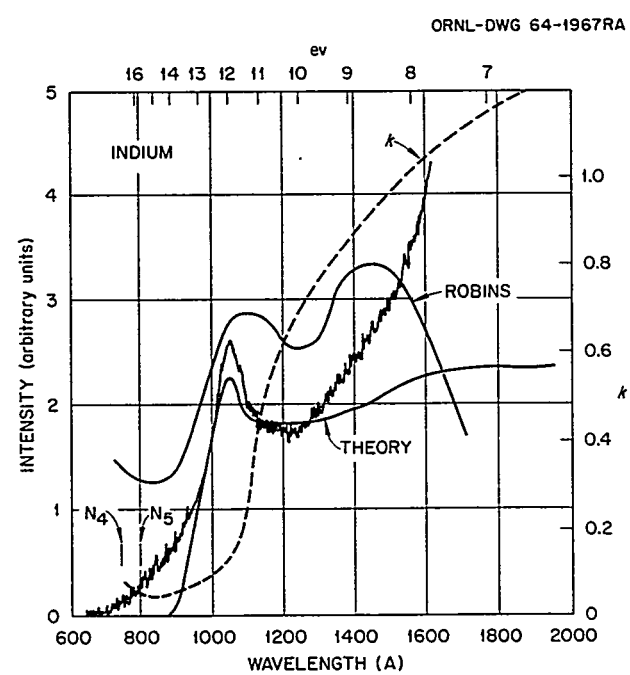

Fig. 15.6. Optical Emission Spectrum from In Foil Bombarded by 80-kev Electrons. Robins' electron energy-loss spectrum is shown on the same energy scale.

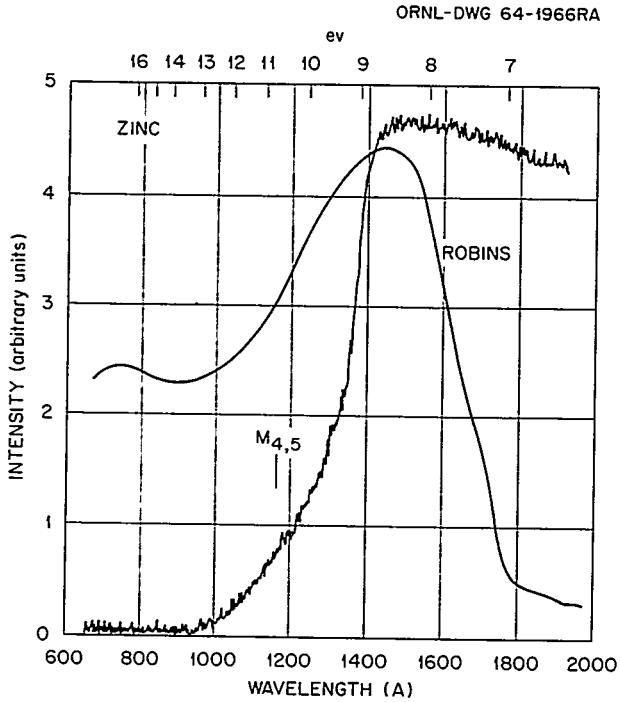

Fig. 15.7. Optical Emission Spectrum from Zn Foil Bombarded by 80-kev Electrons. Robins' electron energy-loss spectrum is shown on the same energy scale.

metals showed an edge beyond which the intensity of emission dropped sharply. These edges correspond quite well with soft-x-ray energy levels. The emissions could therefore arise from transitions of the electrons in the metals from the valence band to holes created by the incident electron in the N_4 and N_5 levels in Cd and In, and in the unresolved $M_{4,5}$ levels in Zn.

Another interpretation of the emission peak in In at 11.8 ev is that it corresponds to the decay of the plasma oscillation. The calculated value of the plasma energy $\hbar\omega_p$ is 12.5 ev, where the number of free electrons per atom is taken to be 2. Robins found a sharp loss at 11.3 ev in his electron energy-loss experiments which was identified by him to be the plasma loss. The loss observed by Robins at 8.7 ev and identified by him as the surface loss did not lead to observable emission. This is in agreement with theoretical predictions that surface plasmons should not radiate.[11]

Robins reports a weak peak at 15 ev in the electron energy-loss experiment for Cd which he identifies as the volume plasma loss. Our data show no enhanced emission at this energy. Likewise, the 17.0-ev peak in Robins' data for Zn was not observed in the present work. Robins found intense losses at 7.5 ev in Cd and at 8.6 ev in Zn which he identifies as surface plasmon losses. The emissions observed by us at 9.1 ev in Cd and at around 8.6 ev in Zn must be due either to transitions from the valence band to holes in inner shells or to volume plasma oscillations. Either interpretation would lead to the conclusion that the identification of these losses by Robins as surface plasmons is incorrect. The fact that these losses are the strongest and sharpest in these elements also leads one to doubt their identification as surface plasmons. Further experiments of this type should help to clarify the nature of these characteristic losses.

TRANSITION RADIATION AND BREMSSTRAHLUNG FROM SOLIDS IRRADIATED BY OBLIQUELY INCIDENT ELECTRONS

Recent experimental data[12] on the emission of light from thick solids bombarded by energetic nonnormally incident electrons show a very strong peaking in light emitted as θ, the angle of incidence relative to the normal to the surface, approaches 90°.

The generation of transition radiation and optical bremsstrahlung due to multiple small-angle scattering of electrons obliquely incident on planar foils has been determined theoretically, extending earlier work along these lines.[13] Our considerations apply to foils which are very thin compared with the range of the incident electrons but thick compared with the attenuation length of photons in the foil.

---

[11] R. A. Ferrell, *Phys. Rev.* 111, 1214 (1958). Ferrell has shown that the phase velocity of surface plasmons generated in a planar foil does not become large enough to permit coupling with the transverse electromagnetic field. Radiation from surface plasmons is possible through the intermediary of electron-hole excitation in the metal. Rough estimates of the probability of such a process (R. H. Ritchie, private communication) indicate that it is very small compared with the probability of volume plasmon radiation.

[12] P. von Blanckenhagen *et al.*, *Phys. Letters* 11, 296 (1964).

[13] R. H. Ritchie *et al.*, *Phys. Rev.* A135, 759 (1964).

It is found that the intensity of transition radiation should vary approximately as $\cos^2 \theta$, while the intensity of observable bremsstrahlung should vary approximately as $(\cos \theta)^{-1}$ for $\theta \sim \pi/2$. Interference between these two kinds of radiation should give rise to an observable effect which is roughly independent of θ.

This work will be submitted for publication in the near future.

OPTICAL CONSTANTS AND ENERGY-LOSS FUNCTIONS OF VACUUM-EVAPORATED FILMS OF Cd AND Tl IN THE VACUUM ULTRAVIOLET

The optical constants, n and k, and energy-loss functions of vacuum-evaporated Cd and Tl films were determined in the wavelength region 500 to 2800 A from reflectance measurements made at 20, 45, and 70° angles of photon incidence.

The real and imaginary parts of the complex dielectric constant, ϵ_1 and ϵ_2, respectively, evaluated from these n and k values are shown in Figs. 15.8 and 15.9. The conditions for collective electron oscillation (ϵ_2 is small and $\epsilon_1 = 0$)[14] are satisfied well at 1450 A or 8.55 ev for Cd and at 1210 A or 10.25 ev for Tl. Figures 15.10 and 15.11 show the energy-loss functions, Im $(1/\epsilon)$, of Cd and Tl. The energy-loss function for Cd reaches a maximum at 8.55 ev, as compared with the value of 8.0 ev found by Leder[15] in characteristic energy-loss experiments for 20-kev electrons passing through Cd vapor. Also a value of 8.1 ev was found by Leder *et al.*[16] for characteristic

[14] H. Frolich and H. Pelzer, *Proc. Phys. Soc.* (*London*) A68, 525 (1955).

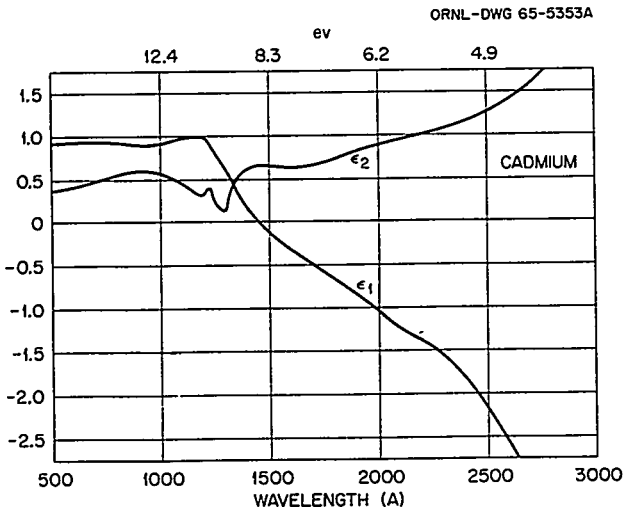

Fig. 15.8. Dielectric Constants of Cd vs Wavelength.

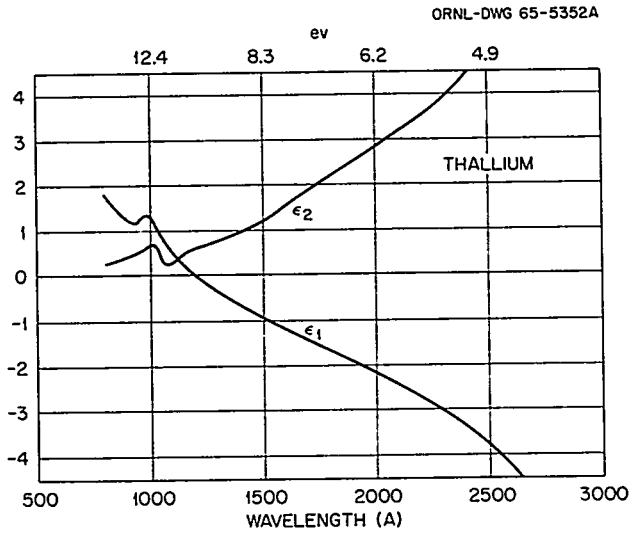

Fig. 15.9. Dielectric Constants of Tl vs Wavelength.

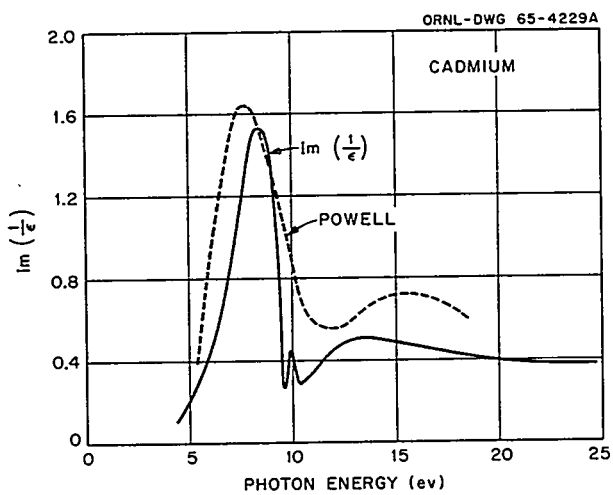

Fig. 15.10. Energy-Loss Function Im $(1/\epsilon)$ of Cd vs Photon Energy.

[15] L. B. Leder, *Phys. Rev.* 107, 1569 (1957).

[16] L. B. Leder *et al.*, *Phys. Rev.* 101, 1460 (1956).

energy losses in thin Cd films. Powell[17] has found an intense electron energy loss in Cd at 7.8 ± 0.1 ev (also shown in Fig. 15.10) for initial electron energies of 750 and 1500 ev. Leder explains the 8.0-ev loss in Cd vapor as an interband transition, while the 7.8-ev loss found by Powell is explained as a surface plasmon loss. Herickhoff *et al.*[18] have observed the optical emission spectra of electron-bombarded thin Cd films and found an intense peak in the emitted light at 9.1 ev. Herickhoff suggests that this emission might be due to a valence to N_4, N_5 interband transition. The energy loss at 8.55 ev found in this experiment is interpreted to be a volume plasmon loss. This interpretation results from two considerations: First, the value of ϵ_2, at and near the region where $\epsilon_1 = 0$, is seen to be fairly constant and has no relative maximum. This indicates that the loss is due to a plasma loss, surface or volume, and not due to an interband transition. Second, the peak in the optical emission spectrum of an electron-bombarded Cd film found by Herickhoff is the same as the one reported here. If the loss were a surface plasma loss, it would not have been seen by Herickhoff since the probability of radiation from a surface plasmon is very small. Hence, it is concluded that the energy loss at 8.55 ev is due to a volume plasma loss. The broad loss at about 950 A or 13.1 ev corresponds to the loss found by Robins at 15.1 ev.[19] The interpretation of this loss is not certain, but it is not a plasma loss since ϵ_1 is not zero and ϵ_2 exhibits a relative maximum at this point. The small bump in the energy loss at 1240 A might correspond to the N_4, N_5 x-ray emission of Cd and again is not a plasma loss, since ϵ_1 is not zero and ϵ_2 has a relative maximum at that point.

A sharp peak was found in the energy-loss function of Tl at 10.25 ev, as compared with the value of 9.6 ± 0.2 ev found by Robins[20] (also shown in Fig. 15.11) in his energy-loss spectra using reflected electrons with primary energies of 1500 and 800 ev. The loss was interpreted by

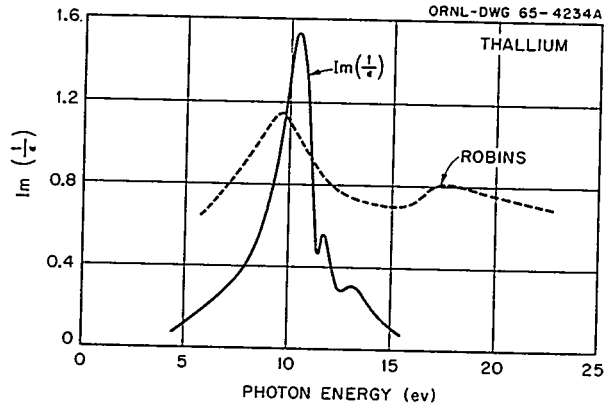

Fig. 15.11. Energy-Loss Function Im (1/ε) of Tl vs Photon Energy.

Robins to be a plasma loss. The energy loss reported here at 10.25 ev is interpreted to be a volume plasma loss for the same reasons as discussed in the case of the large loss in Cd, except that this peak has not yet been found in optical emission studies of electron-bombarded foils of Tl. The small peaks in the energy-loss function at 950 and 1060 A are as yet unidentified.

The agreement of energy losses found from the optical constants presented here and characteristic energy-loss experiments shows that the present n and k values accurately predict the optical characteristics of evaporated Cd and Tl foils.

THE DIELECTRIC CONSTANT OF AN ELECTRON GAS

Lindhard[21] and Hubbard[22] have given different expressions for $\epsilon(k,\omega)$, the dielectric constant of a degenerate free-electron gas. For certain ranges of k, ω, and electron density these expressions differ appreciably. The static dielectric constant $\epsilon(k,0)$, which we write as $\epsilon(k)$, is of importance in the theory of positron annihilation in metals, in determining the shielding of impurity atoms in metals, the influence of impurities on the Knight shift in metals, etc.

[17] C. J. Powell, *Proc. Phys. Soc. (London)* **76**, 593 (1960).

[18] R. J. Herickhoff *et al.*, *Phys. Rev.* **137**, A1433 (1965).

[19] J. L. Robins, *Proc. Phys. Soc. (London)* **78**, 1177 (1961).

[20] J. L. Robins, *Proc. Phys. Soc. (London)* **79**, 119 (1962).

[21] J. Lindhard, *Kgl. Danske Videnskab., Selskab., Mat.-Fys. Medd.* **28**, 8 (1954).

[22] J. Hubbard, *Proc. Roy. Soc. (London)* **A243**, 336 (1957).

In the approximation that the basic polarization bubble diagram[23] may contain 0, 1, 2, ... static interactions between the electron and hole which make up the bubble, the dielectric constant is given by

$$\epsilon(\mathbf{k}) = 1 + 2v_c(\mathbf{k}) \sum_{\mathbf{q}} H_{\mathbf{k}}(\mathbf{q})\, L_{\mathbf{k}}(\mathbf{q}) ,$$

where

$$H_k(\mathbf{q}) = \frac{2m}{\hbar^2} \frac{f_0(\mathbf{q}) - f_0(\mathbf{q} - \mathbf{k})}{(\mathbf{q} - \mathbf{k})^2 - \mathbf{q}^2}$$

and $L_{\mathbf{k}}(\mathbf{q})$ is the solution of the equation

$$L_k(\mathbf{q}) = 1 + \sum_{\mathbf{p}} v(\mathbf{q} - \mathbf{p})\, H_{\mathbf{k}}(\mathbf{P})\, L_{\mathbf{k}}(\mathbf{P}) .$$

The quantity $v_c(\mathbf{k})$ is the Fourier transform of the two-body Coulomb interaction potential in the electron gas, $f_0(\mathbf{q})$ is the Fermi distribution of states in the noninteracting gas, and the sums indicated run over three-dimensional momentum space.

A Monte Carlo program has been written to solve the equation for $L_{\mathbf{k}}(\mathbf{q})$ and is being checked. The function $\epsilon(\mathbf{k})$ so obtained will be employed to determine annihilation rates of positrons in a free-electron gas as described above.

EFFECT OF PHOTON REFRACTION ON ANGULAR DEPENDENCE OF PHOTOELECTRIC YIELDS IN THE WAVELENGTH REGION 300 to 1200 A

Heroux *et al.*[24] have reported results of measurements of photoelectric yields from tungsten and their dependence on the angle of photon incidence for wavelengths between 300 and 1300 A. They found that near 300 A the ratio of the yield per absorbed photon at a given angle of incidence ϕ to the yield at normal incidence was equal to sec ϕ, in agreement with an expression derived by Rumsh *et al.*[25] in connection with photoelectric measurements using x rays. According to Rumsh's derivation, the ratio of the yield per absorbed photon at an angle of incidence ϕ to the yield at normal incidence is given by

$$\frac{Y(\phi)}{Y(0^\circ)} = \left(1 + \frac{\mu}{\alpha}\right) \frac{\sec\phi}{1 + (\mu/\alpha)\sec\phi} .$$

Here μ (cm^{-1}) is the photon extinction coefficient and α (cm^{-1}) is an electron attenuation coefficient defined by setting the escape probability of photoelectrons created at a depth x below the surface equal to $e^{-\alpha x}$. If $(\mu/\alpha)\sec\phi \ll 1$, then $Y(\phi)/Y(0^\circ) \approx \sec\phi$. Optical studies,[26] theoretical calculations of electron mean free paths,[27] and experimental data tending to confirm these calculations[28,29] indicate that this approximation should hold for $\phi \ll 75^\circ$ in the wavelength region of interest here.

For radiation of wavelength greater than 300 A, Heroux and co-workers found that the above ratio increased more slowly than sec ϕ as ϕ increased, becoming practically angle independent near 1200 A. However, they did not take into account the refraction of the light beam at the vacuum-metal interface. The angle of refraction may be calculated using Snell's law for an absorbing medium,[30]

$$\sin\phi' = \frac{\sqrt{2}\sin\phi}{\{n^2 - k^2 + \sin^2\phi + [4n^2k^2 + (n^2 - k^2 - \sin^2\phi)^2]^{1/2}\}^{1/2}} ,$$

where ϕ is the angle of incidence measured with respect to the normal to the vacuum-metal interface, ϕ' is the angle of refraction, and n and k are,

[23] A. J. Glick, *Phys. Rev.* **129**, 1399 (1963).

[24] L. Heroux *et al.*, *J. Opt. Soc. Am.* **55**, 103 (1965).

[25] M. A. Rumsh *et al.*, *Dokl. Akad. Nauk SSSR* **135**, 55 (1960) [English transl.: *Soviet Phys. Dokl.* **5**, 1231 (1960)].

[26] L. R. Canfield *et al.*, *J. Phys.* **25**, 124 (1964).

[27] J. J. Quinn, *Phys. Rev.* **126**, 1453 (1962).

[28] R. N. Stuart *et al.*, *Phys. Rev. Letters* **10**, 7 (1963); *Phys. Rev. Letters* **10**, 119 (1963).

[29] C. R. Crowell *et al.*, *Phys. Rev.* **127**, 2006 (1962).

[30] T. S. Moss, *Optical Properties of Semi-Conductors*, 2d ed., chap. 1, p. 10, Academic, New York, 1961.

respectively, the real and imaginary parts of the complex index of refraction $\tilde{n} = n - ik$ determined for the photocathode used.

The results of photoelectric measurements on commercially pure, 1-mil-thick foils of Pt and Au, outgassed by resistance heating in a separate vacuum chamber, are shown in Fig. 15.12. The ratios $Y(45°)/Y(0°)$ and $Y(70°)/Y(0°)$ are plotted vs wavelength for wavelengths between 300 and 1200 A. For angles of incidence of 45 and 70°, values of sec ϕ (indicated by solid lines in Fig. 15.12) have been calculated for wavelengths between 500 and 1200 A, for which the n and k values have been determined. Neglect of refraction would have led to values of sec ϕ' of 1.41 and 2.92 for angles of incidence of 45 and 70° respectively, whereas the use of the correct internal angles gives quite good agreement with the experimental results for wavelengths in this region. For the wavelength region below 600 A, n and k values for evaporated Au (ref. 26) are such that for a given angle of incidence the angle of refraction increases with decreasing wavelength, approaching the angle of incidence as the photon energy increases. A trend of this nature is observed in the experimental data in Fig. 15.12, where it is seen that the yield ratio for an angle of incidence of 70° increases rather rapidly with decreasing wavelength at the shorter wavelengths. This is consistent with the agreement found by Heroux *et al.* at 300 A, but not at the longer wavelengths, between their data and theory using the angle of incidence in the secant law.

The results presented here indicate that the secant law dependence of volume photoelectric yields on angle of incidence is a good representation of the experimental data for wavelengths between 300 and 1200 A if the refraction of the light beam is taken into account.

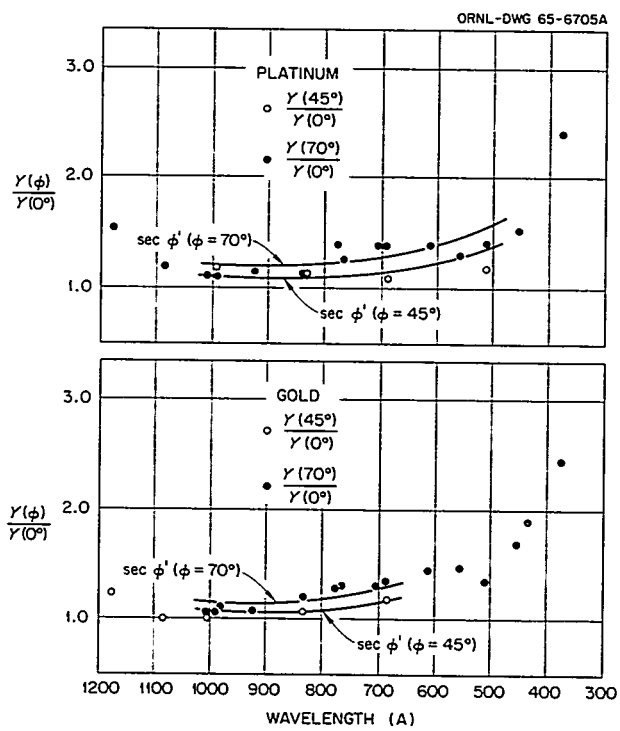

Fig. 15.12. Ratio of the Photoelectric Yield per Absorbed Photon at Angles of Incidence of 45 and 70° to the Yield at 0° Angle of Incidence for Samples of Pt and Au. Experimental values are compared with values of the secant of the corresponding angles of refraction (sec 45° = 1.41, sec 70° = 2.92).

POSITRON ANNIHILATION IN METALS

Careful experimental work by Bell and Jørgensen[31] has established total two-photon annihilation rates, as well as the dependence of annihilation rate upon electron momentum, for positrons in "free-electron" metals of various densities. These results have stimulated considerable theoretical work[32–35] on the many-body theory of the interaction of a positron with a free-electron gas. Attempts have been made to solve numerically the Bethe-Goldstone equation for a positron-electron pair in an electron gas using a static screened interaction between charges in the system,[32,34] but the results are strictly valid only for a zero-momentum electron-positron pair.

We have evolved a Monte Carlo scheme for computing the annihilation rate of positrons interacting with electrons of any momentum up to the Fermi momentum. This approach is based on a theoretical analysis of static interactions in

[31] R. E. Bell and M. H. Jørgensen, *Can. J. Phys.* 38, 652 (1960).

[32] S. Kahana, *Phys. Rev.* 129, 1622 (1963).

[33] D. Butler, *Proc. Phys. Soc.* 80, 741 (1962).

[34] H. Kanezawa, *Phys. Rev.* 138, A1155 (1965).

[35] F. Brouers and A. Lucas, *J. Phys. Soc. Japan* 19, 2351 (1964).

terms of ladder Feynman diagrams for an electron-positron pair, but the scheme is also being used to evaluate the contribution from processes not included in the Bethe-Goldstone approximation.

In order to assess the accuracy of our approach, the annihilation rate has been calculated by conventional techniques of numerical integration up to first order in the interaction potential for all electron momenta and to second order for zero momentum. We have also calculated to second order the annihilation rate of electrons with a fictitious positron having infinite mass, since several workers[32,35] have employed this simplified model for the purpose of computing annihilation rates. Our results indicate that the infinite-mass model may be in error by a factor as large as 4 for low electron densities. Our results for some processes not included in the Bethe-Goldstone series indicate that these will probably make comparatively small contributions in general, even at low electron densities.

Figure 15.13 shows some preliminary results on the annihilation rate for positrons in electron gases of various densities. The quantity r_s is the radius of a sphere which on the average contains one electron in the gas. The dashed line gives the experimental results of Bell and Jørgensen, and the open points give the results of our Monte Carlo calculations using the Lindhard[21] first-order static dielectric constant $\epsilon_L(k)$. The dielectric constant enters our calculation through the Fourier-transformed interaction potential $v(k) = 4\pi q_1 q_2 / k_2\ \epsilon(k,0)$, which we assume to exist between electrical charges q_1 and q_2 immersed in the electron gas. Hubbard[22] has derived an approximate dielectric constant $\epsilon_H(k)$ which should be more accurate than Lindhard's. The solid points in Fig. 15.13 show our results using $\epsilon_H(k)$. We believe that the upturn in the rate for large r_s using $\epsilon_L(k)$ is real and represents the effect of a bound state of the positron-electron pair at a value of $r_s > 6.0$.

The dot-dash line shows Kahana's[32] numerical results using $\epsilon_L(k)$. These values are strictly appropriate only for a zero-momentum pair. Our values using $\epsilon_L(k)$ are generally larger than his and show an appreciable momentum dependence of the annihilation rate.

It is clear that a better approximation to $\epsilon(k)$ is desirable. Work in progress along these lines is described in "The Dielectric Constant of an Electron Gas," this chapter. The improved $\epsilon(k)$ relation will be used to determine a better and more nearly consistent set of annihilation rates using our basic Monte Carlo approach.

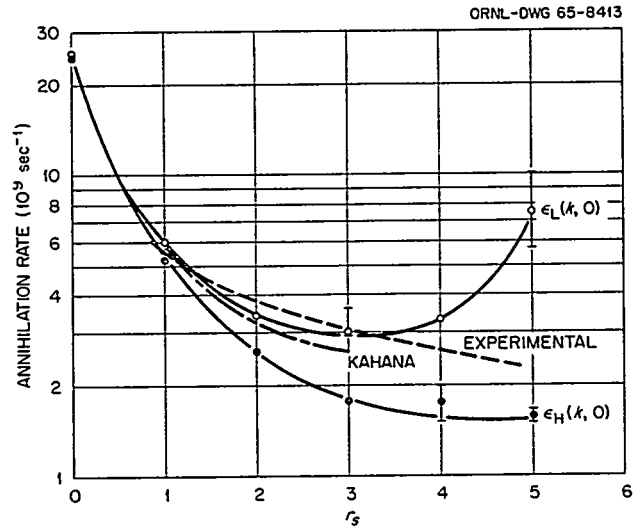

Fig. 15.13. Annihilation Rate of Positrons in Electron Gases of Various Densities. The parameter T_s is the radius of a sphere containing one electron at the density of the gas. The present calculations using the Lindhard dielectric constants are labeled ϵ_L, while those with the Hubbard dielectric constant are labeled ϵ_H.

POLARIZATION STUDIES IN THE VACUUM ULTRAVIOLET

We have studied reflection-type polarizers using silver and gold surfaces which are stable and can be used in the regions of the spectrum (500 to 1300 A) for which polarizers have not previously been available. The polarizers were initially evaluated by rotating them about the direction of the beam from a vacuum ultraviolet monochromator. The intensity $I(\theta)$ measured as a function of angle θ between the planes of incidence of the grating and the polarizer should follow the relationship

$$I(\theta) = a \cdot \cos^2 \theta + b \ .$$

These data are plotted in Fig. 15.14, where the experimental intensities have been normalized to compare with the equation above, with $a = 1$ and $b = 0$. The $\cos^2 \theta$ dependence is indeed verified. In addition, the data show that the light emerging from the exit slit of our Seya-Namioka monochromator is partially plane polarized, with the maximum along the length of the slit.

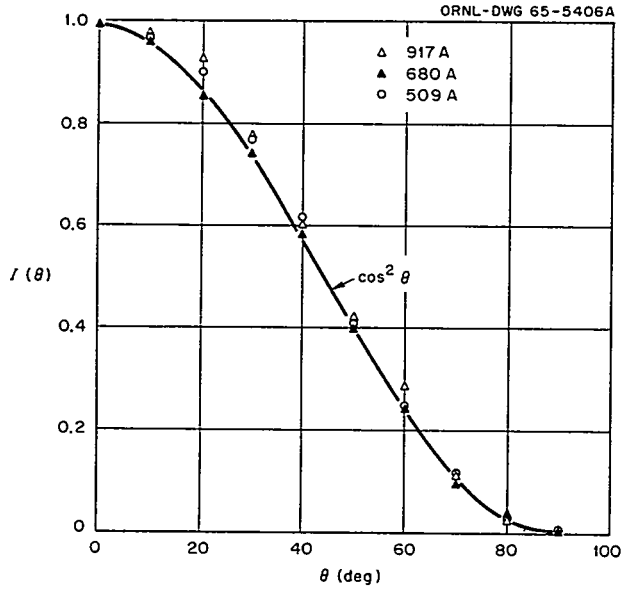

Fig. 15.14. Evaluation of $\cos^2 \theta$ Dependence of Reflection Polarizer.

The ratio $P = R_p/R_s$ for a platinized Bausch and Lomb grating blazed at 700 A used in the Seya geometry is plotted in Fig. 15.15. The polarizations produced by 45° reflections from silver and gold surfaces are also shown. The solid lines are calculated reflectance ratios ($\rho = r_p/r_s$) using the optical constants of Ehrenreich and Phillip[36] for Ag and of Canfield *et al.*[26] for Au. The fraction of the incident light available from these polarizers is simply the reflectivities of these surfaces, which range from 5 to 9% of the unpolarized incident intensity for Ag and from 10 to 15% for Au. The reflectivities are increased to 17 to 22% for Ag and 24 to 29% for Au when the angle of incidence is increased to 70% with approximately the same degree of polarization.

In certain cases, it may be desirable to improve the polarization with an additional reflecting surface of Ag or Au in the light path which decreases P to about 0.1. If the deviation of the light path is objectionable or a greater degree of polarization is required, a triple-reflection polarizer may be used as shown in Fig. 15.16. The high degree of polarization introduced with such a polarizer is also shown in Fig. 15.16. The transmission for such a system is 3.5 to 5.0% of unpolarized light. Finally, it should be noted that one or two reflecting surfaces at angles of incidence from 45 to 80° can easily be introduced

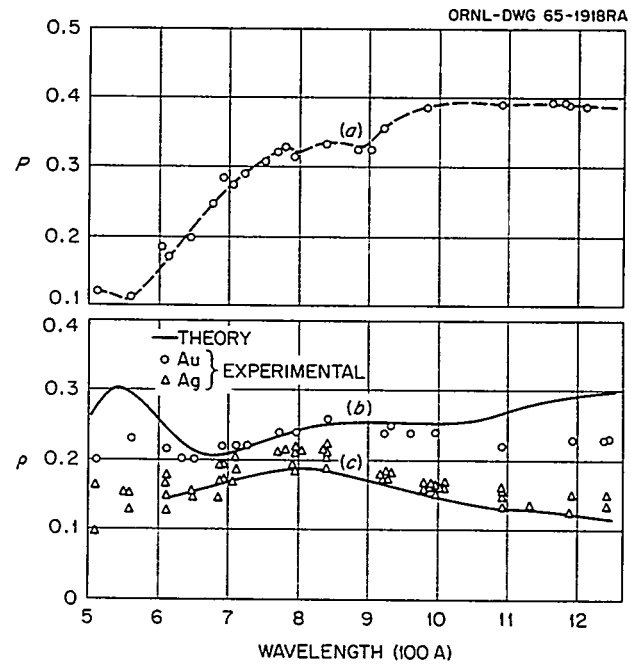

Fig. 15.15. (*a*) R_p/R_s for a Platinized Bausch and Lomb Grating Blazed at 700 A, (*b*) r_p/r_s for a 45° Reflection from Au Shown by Dots, and (*c*) from Ag Shown by Triangles.

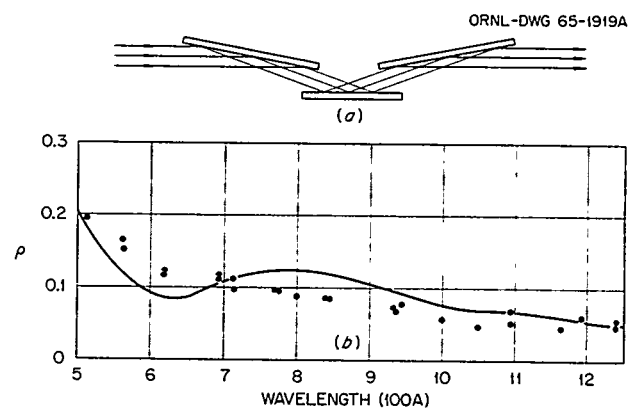

Fig. 15.16. (*a*) Schematic Diagram of and (*b*) Polarization Produced by 80°–70°–80° Triple-Reflection Polarizer of Au Surfaces. Dots represent experimental data, and solid curve shows the results obtained by using optical constants of Au determined by Canfield, Hass, and Hunter.

[36]H. Ehrenreich and H. R. Phillip, *Phys. Rev.* 128, 1622 (1962).

into the light path of vacuum ultraviolet spectrographs with minor modifications since these mirrors need not be rotated. Investigations using polarized light can then be made simply by taking two sets of measurements, one with the plane of incidence of the sample parallel to the common plane of incidence of the grating and mirrors and another with the planes of incidence perpendicular.

POLARIZATION CALCULATIONS

Calculations have been carried out in order to obtain the degree of plane polarization of a light beam from measurements made with partially polarizing elements. These calculations have been applied to the construction and evaluation of reflection-type polarizers for use in the vacuum ultraviolet.

An analysis has also been made of the requirements of a polarizer which is to be used to make accurate measurements of optical properties depending on polarization. The analysis shown here is for measurement of the reflectance of a surface for light polarized parallel (r_p) and perpendicular (r_s) to the plane of incidence using a polarizer characterized by a ratio $P = R_p/R_s$, where R_p and R_s are the reflectances of the polarizer for light of parallel and perpendicular polarization respectively. The graph (Fig. 15.17) gives the ratios of the relative error in r_p and r_s to that in the measured reflectance plotted as a function of the grating polarization P and for various r_p/r_s ratios for the surface.

It is evident that so long as the ratio r_p/r_s does not become too small, a polarizing element giving only a modest degree of polarization is sufficient for accurate measurements with polarized light to be made. Since many vacuum ultraviolet monochromator gratings have a P of about 0.4 or less, often the grating alone may be used as a polarizer.

ABSOLUTE PHOTON INTENSITY MEASUREMENTS WITH RARE-GAS ION CHAMBERS

Intensity measurements in the vacuum ultraviolet region are made using a tandem ion chamber filled with one of the rare gases. The simultaneous measurement of the two ion currents is used in the determination of the absorption cross section of the gas within the chambers. From these measurements the absolute photon intensity may be directly determined. By then removing the gas from the chamber, the photon beam, now of known intensity, passes unattenuated through the chamber to a secondary detector. With this technique absolute calibrations are routinely performed for a variety of low-energy photon detectors.

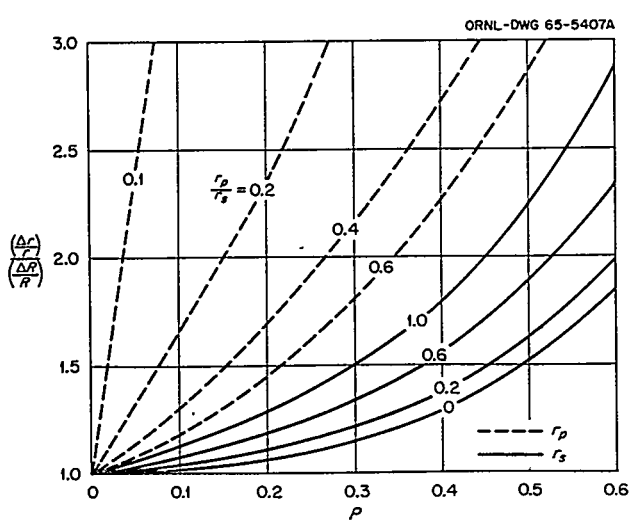

Fig. 15.17. Relative Error in the Determination of r_p and r_s as a Function of Degree of Polarization.

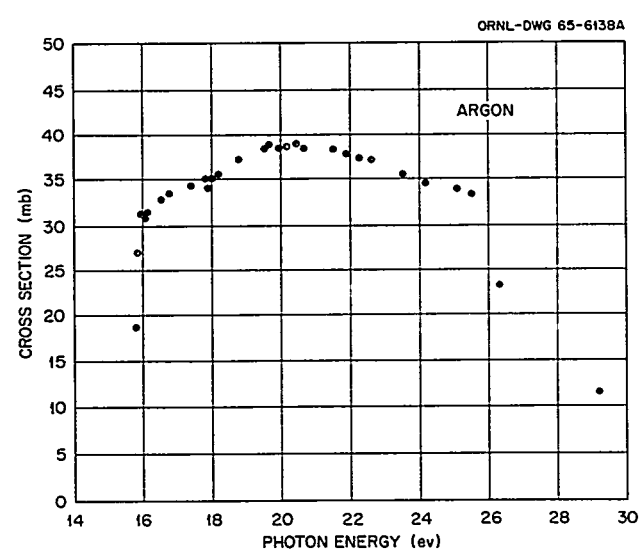

Fig. 15.18. Photoelectric Cross Section for Argon Between 16 and 30 ev.

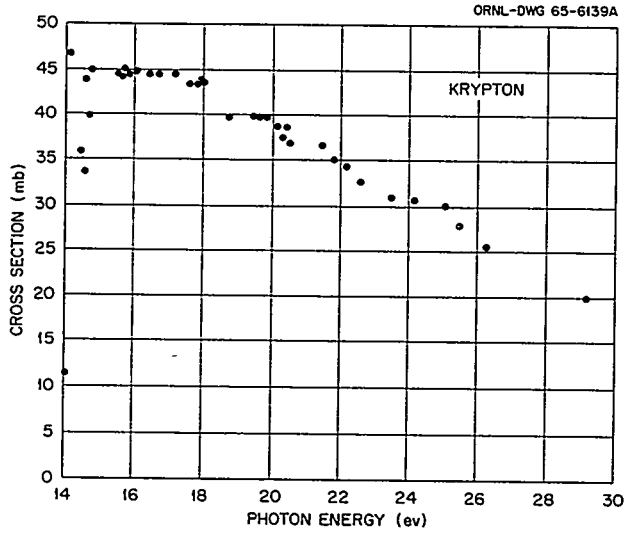

Fig. 15.19. Photoelectric Cross Section for Krypton Between 15 and 30 ev.

For the rare gases the absorption of photons occurs solely by the photoelectric effect, and the measurement of the absorption coefficient yields the photoelectric cross section directly. Experimental measurements of these cross sections have been carried out in argon and krypton at energies ranging between 15 and 30 ev. The cross section for argon, shown in Fig. 15.18, gradually rises from the autoionization region near 15.8 ev to a maximum near 20.5 ev and then decreases monotonically out to 30 ev. For krypton, the cross section shown in Fig. 15.19 is flat from the autoionization region near 14.6 out to 18 ev. From this point the cross section exhibits a gradual fall throughout the remainder of the energy region studied.

ELECTRON-SLOWING-DOWN SPECTRA IN CHROMIUM, YTTRIUM, AND GOLD

A new source approximating a "cavity" was designed for electron-slowing-down experiments. The source consists of two parallel, coaxial disks surrounded on the sides and outer faces by a magnesium shield. The exposed surface of one disk is placed tangent to the inner sphere. Ignoring boundary effects, this surface, which is irradiated on one side by the bulk of the disk it bounds and on the opposite side by the other disk, represents a plane in an infinite medium. Since the correction for boundary effects involves the geometry of the source, the double-disk source requires much simpler calculations than the frustum-type sources used previously. The double-disk source also has the advantage of being completely assembled before reactor irradiation, thus eliminating the need for final assembly behind shielding and reducing the problem of self-shielding[37] during reactor irradiation.

Improved data were obtained for copper and gold using double-disk sources. A detailed discussion of the experiment and results for ^{64}Cu beta rays slowing down in copper may be found elsewhere.[38]

The electron flux spectra resulting from ^{198}Au beta rays slowing down in gold is shown in Fig. 15.20 and compared with the Spencer-Attix and Spencer-Fano theories. The experimental flux varies from 2.9×10^{-8} electron cm^{-2} ev^{-1} per primary electron cm^{-3} at 63 kev to 1.2×10^{-4} at 11 ev above the bottom of the conduction band. There is a small step in the experimental flux at 7 kev and a broad hump from 600 to 80 ev. These are assumed to be due to *LMM* and *MNN* Auger electrons arising from photoelectric absorption of

[37] R. D. Birkhoff *et al.*, *Health Phys. Div. Ann. Progr. Rept. July 31, 1964*, ORNL-3697, p. 142.

[38] W. J. McConnell *et al.*, *Phys. Rev.* 138, A1377 (1965).

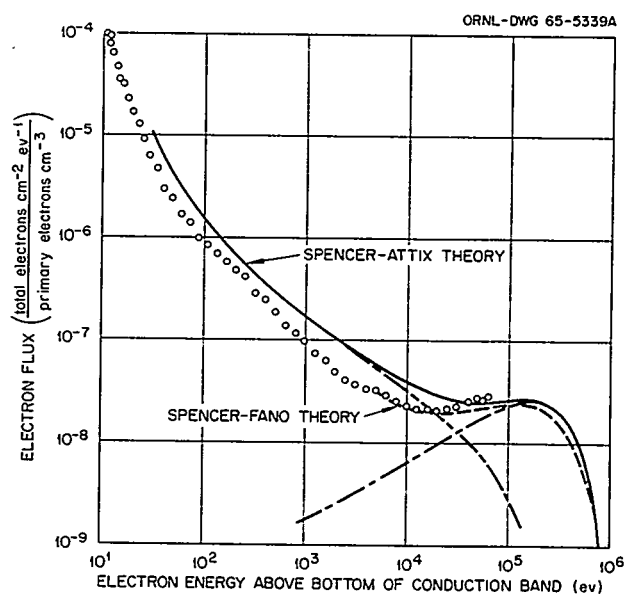

Fig. 15.20. Electron Flux Spectrum of ^{198}Au Beta Rays Absorbed in Gold.

the 411-kev gamma rays in the L and M shells respectively. A similar effect must take place in the K shell, and the data show that the flux is increasing more rapidly than either theory predicts as the KLL energy is approached. Both theories neglect Auger and bremsstrahlung effects.

The primary electrons in previously measured slowing-down spectra have been beta-ray continua. However, monoenergetic sources are also of interest. Chromium-51, which decays by electron capture (0.9 K capture and 0.1 L capture), provides a source of monoenergetic electrons. The origins of these electrons are illustrated in Fig. 15.21. The vacancies resulting in the K and L shells from the electron capture initiate an Auger cascade. The Auger electrons have the characteristic energy of vanadium because the electron capture reduces the charge of the chromium nucleus. There are 0.68 KLL, 1.68 LMM, and 3.36 MNN Auger electrons per decay. The filling of the K vacancies results in an Auger electron 76% of the time and an x ray 24% of the time. Since the source is 0.25 mm thick and the linear absorption coefficient in Cr for a 5-kev x ray is about 750 cm^{-1}, all the x rays will be absorbed in the source. Assuming that all the x rays will undergo photoelectric absorption in the L shell, the resulting vacancy will initiate another Auger cascade. In addition to the 0.22 photoelectron per decay having energy of the vanadium K_α x ray less the binding energy of the chromium K electron, there are 0.22 LMM and 0.44 MNN Auger electrons per decay having energies characteristic of chromium. Within the resolution of the spectrometer used, these electrons appear as three monoenergetic sources. Figure 15.22 compares the electron flux spectrum resulting from monoenergetic electrons from ^{51}Cr slowing down in Cr with the Spencer-Attix theory. The theory was extended to 33 ev above the bottom of the conduction band using a stopping power derived by Ritchie over the range from 33 to 230 ev and a value for manganese at 2 kev measured by Nakai, Garber, and Birkhoff. A linear extrapolation was used between Ritchie's theory and the measured value and again between the measured value and the Bethe-Bloch formula to obtain a stopping power at those intervals. Ritchie's theory includes both the volume plasmon loss and the electron-electron interaction. The stopping power is shown in Fig. 15.23. Although the theoretical and experimental curves have the same shape (Fig. 15.22), the experimental curve is a factor of 2 higher than the theoretical. Several possible causes of discrepancy are being studied. In the data shown here, the theory has

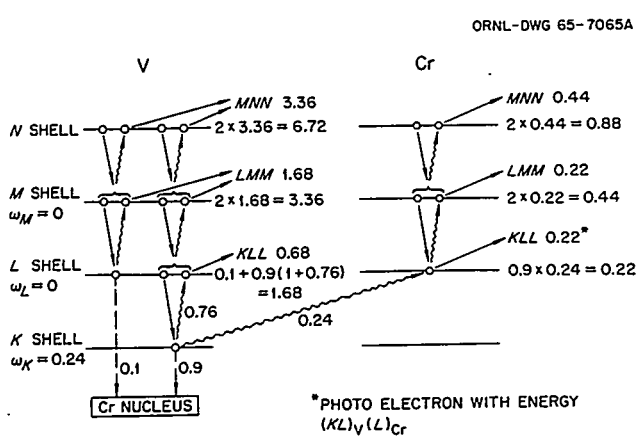

Fig. 15.21. Schematic Diagram of Electrons from Chromium Source.

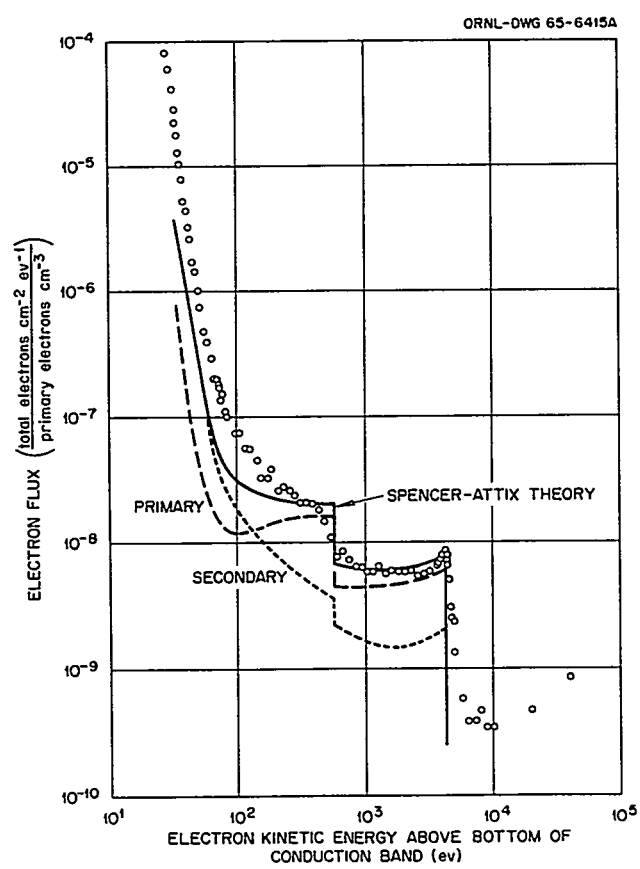

Fig. 15.22. Electron Flux Spectrum of ^{51}Cr Auger Electrons Absorbed in Chromium.

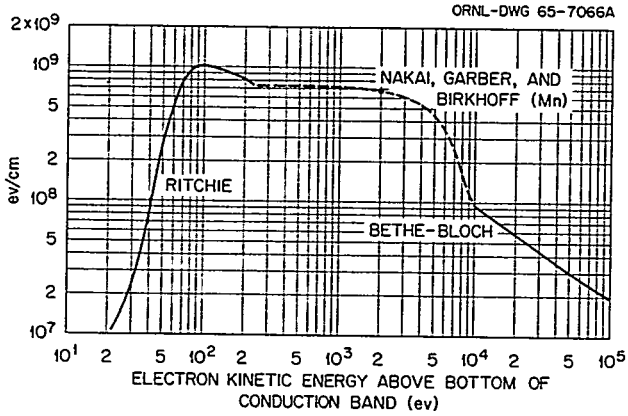

Fig. 15.23. Electron Stopping Power for Chromium.

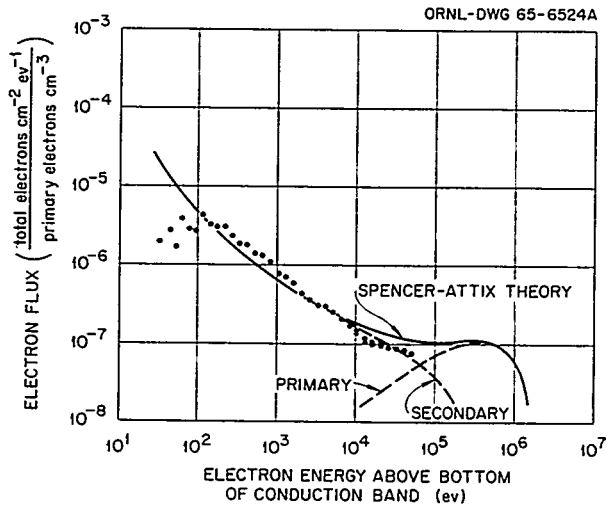

Fig. 15.24. Electron Flux Spectrum of ^{90}Y Beta Rays Absorbed in Yttrium.

been normalized to fit the experimental data at 4.3 kev. The appearance in the theory of secondary electrons at the maximum energy is due to our definition of a secondary electron (see ref. 38). The experiment shows a sharp step at 4.3 kev and is more or less constant with a value of 7×10^{-8} electron cm^{-2} ev^{-1} per primary electron cm^{-3} down to the *LMM* energy at about 460 ev. The *LMM* step is broadened due to the width of the *M* shell. Below the *LMM* step the rapid rise of the secondary electrons obscures the *MNN* step. This rise is due to the buildup of secondary electrons and the decrease in the stopping power. Our results with copper and gold indicate that the secondary electrons do not make a significant contribution to the flux until the energy falls a factor of 10 below the primary energy. When the secondary electrons begin to make a significant contribution to the flux, they rapdily cascade and dominate the flux spectrum. A source of electrons at a lower energy, such as the *LMM* electrons in this case, can cause some local structure in the spectrum, but the secondary electrons from this new source do not build up until some lower energy, with the result that they are an order of magnitude or more lower than the secondary electrons produced by the higher-energy sources. In addition, a source of electrons at some still lower energy, such as the *MNN* electrons in this case, may not cause any significant change in the shape of the electron flux spectrum. Thus, a theory which includes the radiative energy losses due to bremsstrahlung, but does not include the subsequent production of lower-energy electrons due to Compton scattering and photoelectric

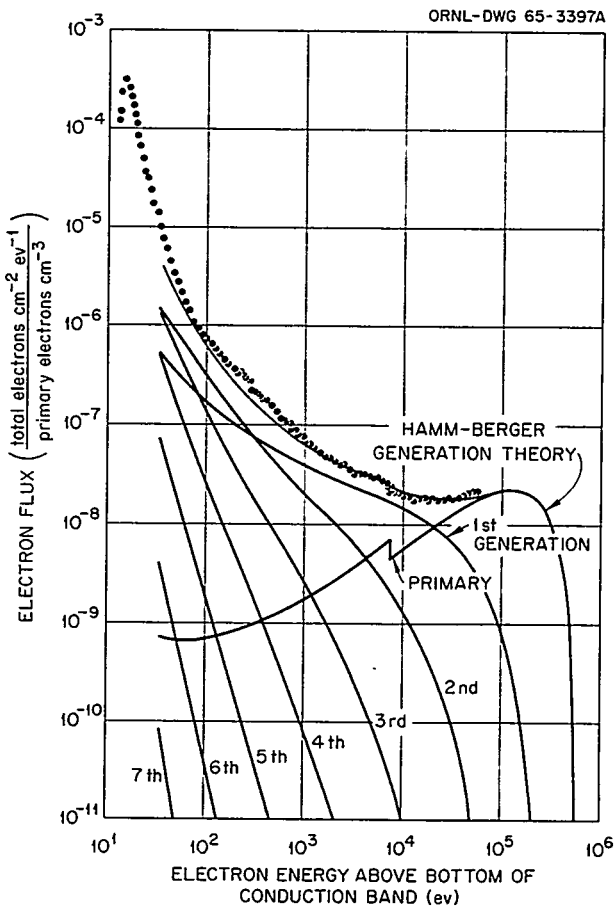

Fig. 15.25. Electron Flux Spectrum of ^{64}Cu Beta Rays Absorbed in Copper.

absorption of the bremsstrahlung, should not lead to significant errors in either the shape or the magnitude of the electron flux spectrum.

Figure 15.24 shows the electron flux spectrum from a single disk of yttrium. The flux varies from 7.7×10^{-8} electron cm^{-2} ev^{-1} per primary electron cm^{-3} at 50 kev to about 3×10^{-6} at about 100 ev. The decrease in the flux below 100 ev is attributed to surface corrosion that probably resulted from the high temperatures during reactor irradiation and surface roughness caused by a tendency of the surface to flake.

Berger[39] has modified the Spencer-Attix theory to allow calculations of each generation of flux (primary, secondary, tertiary, etc.). Figure 15.25 shows such a calculation for ^{64}Cu beta rays slowing down in copper. The total electron flux above 35 ev was obtained by summing the contribution of 13 individual generations. However, nearly all the flux above 35 ev is shown to be due to the first three generations.

INTERSTITIAL DIFFUSION IN ELEMENTS

The following criterion is proposed: The interstitial positions for a small, chemically inert diffusing atom in a crystalline element are the vertices of the Wigner-Seitz cellular polyhedra associated with the atoms of the host structure, and the diffusion path is from vertex to neighboring vertex along a connecting edge. (The Wigner-Seitz cellular polyhedron associated with an atom is the portion of space closer to that atom than to any other atom.) The diffusion coefficient D is derived according to the above model and is checked from the equivalent definition $D = \frac{1}{6}(d\overline{R^2}/dt)$, where $\overline{R^2}$ is the mean squared distance diffused by an atom in time t. The results are: (1) simple cubic elements (for which there is one interstitial site per unit cell), $D_{sc} = \lambda a^2$; (2) body-centered cubic elements (for which there are six interstitial sites per basic unit cell), $D_{bcc} = \lambda a^2/12$; (3) face-centered cubic elements (for which there is one site of type 1 and two sites of type 2 per basic unit cell), $a^2/4D_{fcc} = (2\lambda_1)^{-1} + \lambda_2^{-1}$; (4) diamond structure (for which there are two sites of type 1 and four sites of type 2 per basic unit cell), $a^2/32D_{dia} = (2\lambda_{12})^{-1} + (\lambda_{21})^{-1}$. (In these formulas, λ_1 and λ_{12} are one-channel jump probabilities per unit time from a site of type 1, λ_2 and λ_{21} are the one-channel jump probabilities per unit time from a site of type 2, and a is the length of side of the cubic unit cell.) Advantages were found for displaying graphically the logarithm of $a^2/4D_{fcc}$ vs the reciprocal of the absolute temperature.

[39] R. N. Hamm *et al.*, *Bull. Am. Phys. Soc.* 10(4), 477 (1965).

16. Physics of Tissue Damage

R. D. Birkhoff
J. G. Carter
L. G. Christophorou[1]
T. M. Jelinek[2]
M. Y. Nakai
D. R. Nelson[3]
F. W. Garber[2]
J. A. Elder[2]
A. K. Roecklein[2]

LOW-ENERGY ELECTRON TRANSMISSION IN SOLIDS

The technique used last year for studying kilovolt proton transmission[4] through conducting films has been modified and used this year for electron transmission studies. The target system consists of a thin (150 A → 500 A) top foil vacuum evaporated onto a thick (>2000 A) aluminum foil having a 75-A Al_2O_3 insulating surface. The details of preparations of the foils and insulator have been given in a recent report.[5] When a monoenergetic electron beam is normally incident on the top foil, electrons interact with the electron system of the metal in such a way as to be stopped in the top layer, and/or to generate secondary electrons, and/or to be transmitted through the layer and insulator to the back foil. Primary and secondary electron currents to the top and bottom layers are measured by Philbrick P-2 operational amplifiers and displayed on a Texas Instrument dual pen recorder. A typical graph of electron current to the top foil normalized to unit incident current is shown in Fig. 16.1 for an aluminum foil of 250 A thickness. Four fairly distinct regions are seen as the electron energy is increased from 6 to 1200 ev. At the lowest energy, many of the electrons entering the foil lose one quantum (10 ev) of energy to surface plasmon excitation, resulting in absorption (and top current) increasing with energy. From 20 to about 400 ev, absorption falls but with a convex upward characteristic which mirrors the stopping power due to volume plasmon production and electron-electron interactions as calculated by R. H. Ritchie and as plotted in Fig. 16.1. Monte Carlo calculations are in progress (see next topic) to ascertain if the secondary-electron production and transmission cross sections predict the top-current characteristic found. In the meantime, data have been analyzed in the following fashion.

The bottom current, when plotted vs energy in the region 20 to 100 ev, yields a straight line increasing with energy with a current intercept of 0.23. If this zero-energy intercept is taken as the transmission probability for the primary electron through the top layer, then all secondaries may be

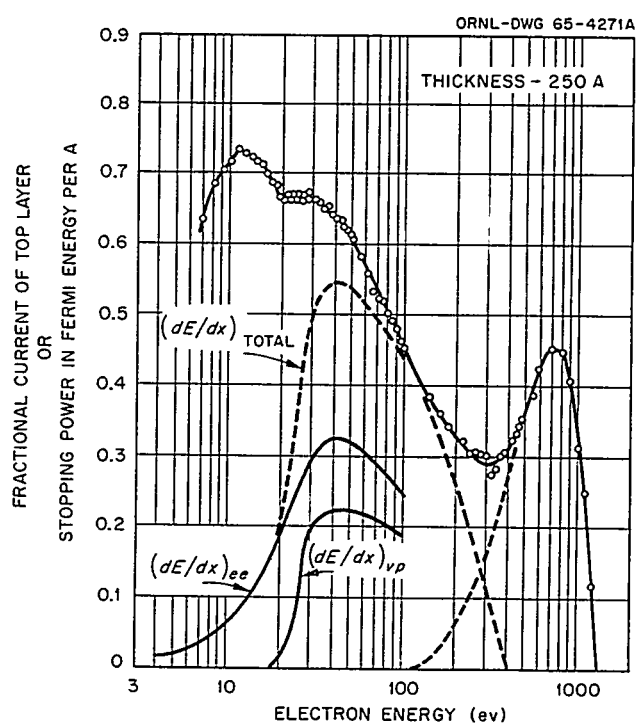

Fig. 16.1. Current to Top Layer vs Electron Energy. Also, theoretical stopping powers due to electron-electron collisions and volume plasmon production and the sum of these.

[1]Consultant.

[2]Graduate student.

[3]Temporary leave.

[4]A. K. Roecklein *et al.*, *A New Technique for Measuring Range of Low Energy Charged Particles in Conducting Solids*, ORNL-3702 (1965).

[5]F. W. Garber *et al.*, *Low Energy Electron and Proton Transmission in Aluminum and Silver*, ORNL-TM-1153 (1965).

assumed to have the same transmission probability, for they are all generated at the top surface, as the primary loses all but a few electron volts of its energy within a few angstroms of the top surface. Primaries and secondaries alike of such low energies have been found recently to have very long mean free paths (~400 A) in metals.[6] From the bottom-current plot and transmission factor, it is a simple matter to calculate the average energy per inelastic event and the attenuation length[7] as 78 ev and 272 A respectively. The former is to be compared with the value 93 ev obtained recently by Rauth and Simpson[8] for 20-kev electrons using a completely different experimental situation. The latter is of the order predicted by Quinn.[9] The foregoing analysis must be regarded as tentative pending results from the Monte Carlo calculations.

If the top current just discussed is extrapolated to zero and this extrapolated current is subtracted from the data at each energy, an absorption starting at 115 ev is found which is identified as due to *L*-shell ionization. This value of the *L*-shell energy in aluminum has been verified recently by Fahlman *et al.*[10]

At the highest energy the top current goes to zero, indicating complete transmission. The energy intercept where this occurs is found to move to the right as the top-foil thickness is increased. If this is attributed to absorption of the higher-energy beams in the surface layers of the top foil, then a stopping power may be calculated. The data are shown in Fig. 16.2 along with the theoretical stopping powers of Ritchie and of Bethe and Bloch, the latter being taken from the tabulation by Nelms.[11] The data represent the only measurements reported below 10 kev and present a heartening agreement with the two theories. Additional work is in progress on aluminum, silver, and copper.

[6]See for instance R. W. Soshea and R. C. Lucas, *Phys. Rev.* 138A, 1182 (1965).

[7]R. Stuart *et al.*, *Phys. Rev.* 135A, 495 (1964).

[8]A. N. Rauth and J. A. Simpson, *Radiation Res.* 22, 643 (1964).

[9]J. J. Quinn, *Phys. Rev.* 126, 1453 (1962).

[10]A. Fahlman *et al.*, *Phys. Rev. Letters* 14(5), 127 (1965).

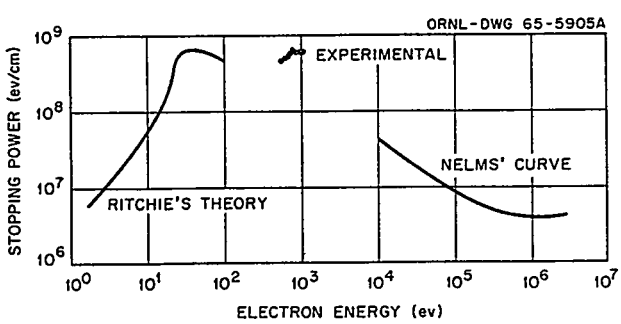

Fig. 16.2. Electron Stopping Power in Aluminum. Bethe-Bloch theory calculated by Nelms is shown above 10 kev. Theory of Ritchie (see Fig. 16.1) is shown below 100 ev. Data are taken at about 1 kev.

THE PENETRATION OF LOW-ENERGY ELECTRONS IN METALS

Experimental results[12] on the range of hot electrons, that is, electrons excited only slightly above the Fermi energy in metals, have been interpreted[7] on the basis of a simplified model of interactions between an excited electron and (1) conduction electrons and (2) lattice vibrations. An energetic electron traveling in a metal at energies comparable with or larger than the Fermi energy may create observable secondary electrons and may be capable of exciting coherent collective oscillations in the metal plasma. These possibilities were not included in the analysis of ref. 7.

We have undertaken a calculation of the penetration and cascade of energetic electrons in such systems, in connection with the experimental work of Nakai *et al.*[13] For simplicity, we assume that scattering processes involving encounters of an electron with the lattice are elastic and isotropic in the laboratory system of coordinates. Encounters with conduction electrons are described in terms of the dynamic frequency and wave-dependent dielectric constant of a free electron gas[14] having the density of the conduction-band electrons in the metal under consideration.

Figure 16.3 shows some preliminary data obtained with a simplified version of a Monte Carlo

[11]Ann J. Nelms, "Energy Loss and Range of Electrons and Positrons," NBS-577 and suppl., U.S. Department of Commerce, 1958.

[12]C. R. Crowell *et al.*, *Phys. Rev.* 127, 2006 (1962).

[13]M. Y. Nakai *et al.*, submitted to the *Journal of Physics and Chemistry of Solids.*

[14]R. H. Ritchie, *Phys. Rev.* 114, 644 (1959).

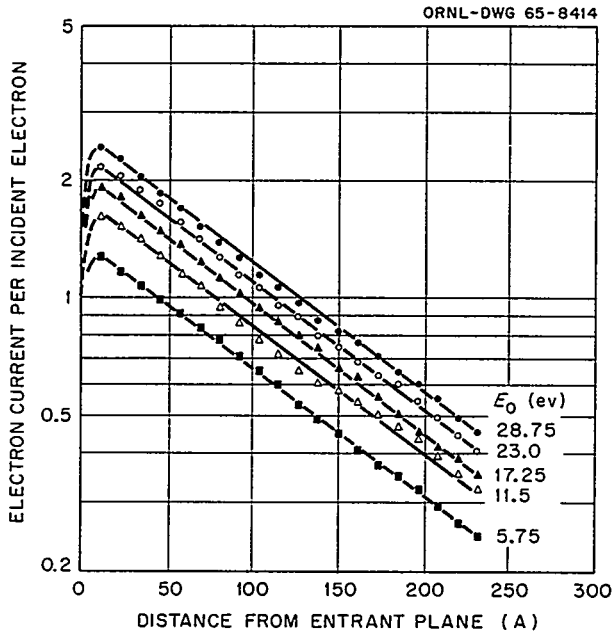

Fig. 16.3. Monte Carlo Results on the Penetration of Low-Energy Electrons in a Plane Aluminum Foil. The quantity E_0 is the energy of the incident electron measured with respect to the vacuum level.

code embodying these physical ideas. Here it is assumed that electrons of various energies E_0 are incident normally on a semi-infinite slab of Al with work function $E_\phi = 4$ ev, and that an electron which strikes the entrant surface from the interior side is specularly reflected. This condition is used to simulate the effects of the retarding electric field used in the experiments of Nakai *et al.*[13] The current of electrons having energies $\geqq$ the barrier energy $E_B = 2$ ev at planes at various distances from the entrant plane is plotted as a function of distance from the entrant plane. The current is normalized to one electron entering the system. The several curves are plotted for different values of the incident energy E_0.

The effect of electron multiplication in the system is marked in all cases considered here. The number of secondary electrons born in the system with energies above E_B ranges from ~ 7 to ~ 11 over the range of energies considered here.

These calculations are being extended to take into account the generation of surface plasmons and their conversion into secondary electrons in the system.

OPTICAL PROPERTIES OF POLYSTYRENE

The optical properties of polystyrene are being studied in the wavelength region below 3000 A. Preliminary data obtained down to 1500 A are presented. Considerable interest has been exhibited in the energy losses of polystyrene in the region from 3000 A to about 400 A. This interest is derived from the fact that polystyrene contains the benzene ring with its associated π and σ electrons, which are thought to be involved in energy losses at approximately 7 and 20 ev. It has been shown that the approximate 7-ev loss is correlated with the available ultraviolet absorption data of polystyrene and benzene. The measurement of the 7-ev loss as obtained by characteristic electron energy loss experiments differs from our value by about 0.5 ev. This is not surprising in that energy losses obtained by optical methods are more accurate than those from experiments where a small energy loss is observed from a high-energy electron. However, our value and the value obtained by optical absorption experiments agree quite well. Only the data down to 1500 A are shown here although data are now being obtained which include the 21-ev loss. The effective number of electrons taking part in any portion of the energy loss spectrum can be calculated by the sum rule

$$\int_0^{\omega_0} \omega\, \epsilon_2(\omega)\, d\omega = \left(\frac{2\pi^2 N e^2}{m}\right) n_{\text{eff}} ,$$

where n_{eff} is the effective number of electrons per molecule and N is the molecular density. Such sum-rule calculations are being carried out in order to establish the role of the π and σ electrons in these losses.

The polystyrene samples were machined from a rod 1 ft long and 3 in. in diameter of commerically obtainable polystyrene. Each sample was a block measuring $1 \times 1\frac{1}{2} \times \frac{1}{4}$ in. Data are presented on the sample that was polished, annealed, and then lapped to 0.000033 in. of optical flatness as measured by optical interference. The sample was annealed according to the Bell Telephone Laboratories method, which involves holding the sample at a temperature of 170 ± 20°F in an air oven for 16 hr followed by cooling at room temperature in still air. The polystyrene block was then attached to a holder for the reflectivity measurements. The

apparatus used to obtain the reflectance data has been described in detail in a previous report.[15]

Reflectance curves for light incident at 20 and 70° are shown in Fig. 16.4. The real (n) and imaginary (k) parts of the complex index of refraction obtained from Fig. 16.4 are presented in Fig. 16.5. The complex dielectric constant ϵ (where $\epsilon = \epsilon_1 + i\epsilon_2$) is related to the complex index of refraction $n + ik$ by the equation $\epsilon = (n + ik)^2$. The real part, $\epsilon_1 = n^2 - k^2$, and the imaginary part, $\epsilon_2 = 2nk$, shown in Fig. 16.6, were calculated from the n and k values in Fig. 16.5. The energy loss function, Im $(1/\epsilon)$, is presented in Fig. 16.7 and can be seen to have a major peak at about 1900 A or at an energy of 6.5 ev. Smaller peaks occur at 2400 A (5.2 ev) and 2700 A (4.6 ev).

[15] T. M. Jelinek *et al.*, *Optical Properties of Vacuum Evaporated Films of Cadmium, Thallium, and Zinc in the Vacuum Ultraviolet*, ORNL-TM-1164 (1965).

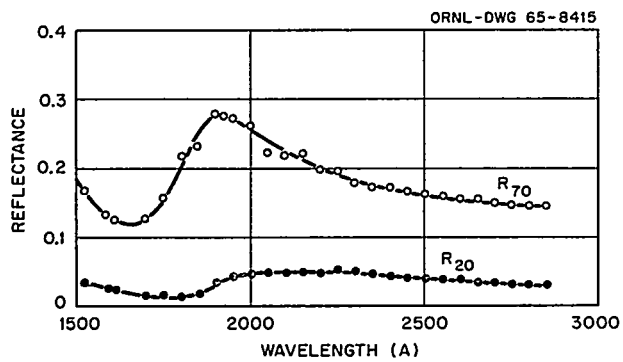

Fig. 16.4. Reflectance of Polystyrene vs Wavelength for 20 and 70° Photon Incidence.

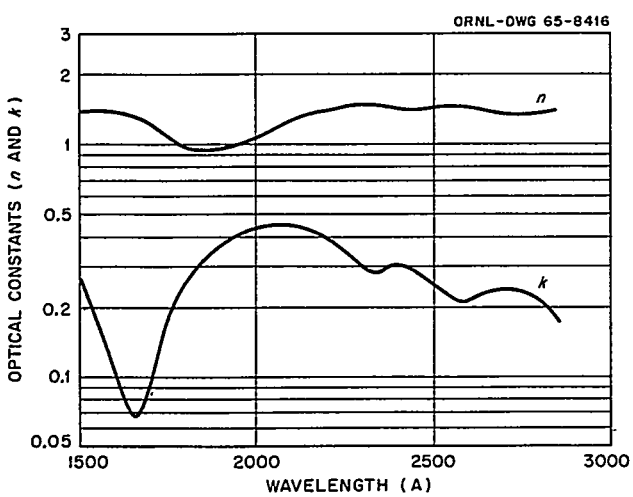

Fig. 16.5. Optical Constants (n and k) of Polystyrene vs Wavelength.

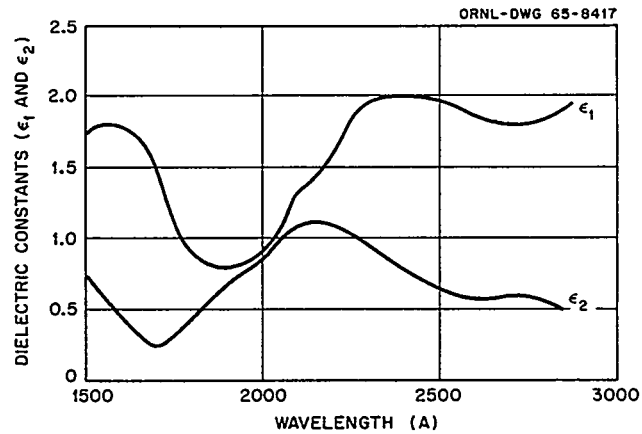

Fig. 16.6. Dielectric Constants (ϵ_1 and ϵ_2) of Polystyrene vs Wavelength.

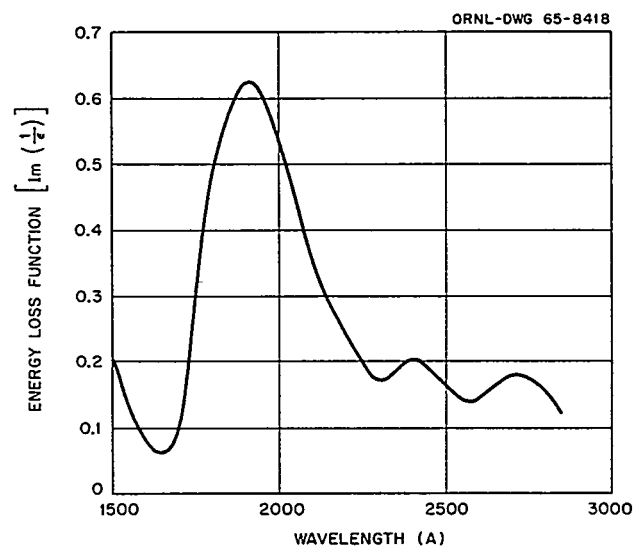

Fig. 16.7. Energy Loss Function Im $(1/\epsilon)$ of Polystyrene vs Wavelength.

EXCIMER X-RAY INVESTIGATION

An investigation has been made of the effect of the modes of excitation on excimer formation in solution and in the liquid phase. Also, the binding energy of excimers formed in organic liquids is determined for some naphthalene derivatives.

Pyrene Solutions

Pyrene oxygen-free solutions in cyclohexane were excited at room temperature by 230-kev x rays. The relative quantum intensities, I_λ, were measured by a Bausch and Lomb 500-mm grating monochromator for various solute concentrations, c, and are plotted in Fig. 16.8. The spectra are normalized at a fixed wavelength λ = 410 nm (mμ), as were the photofluorescence spectra.[16] The shape and position of the monomer-excimer bands are identical to those obtained under ultraviolet excitation. The ratio of the excimer quantum yield, I_D, to that, I_M, of the monomer, I_D/I_M, varies almost linearly with c up to $c \leqq 10^{-2}$ M.

If X and M are the solvent and solute molecules, respectively, and D* is the excimer, then we may consider the following two-step process:

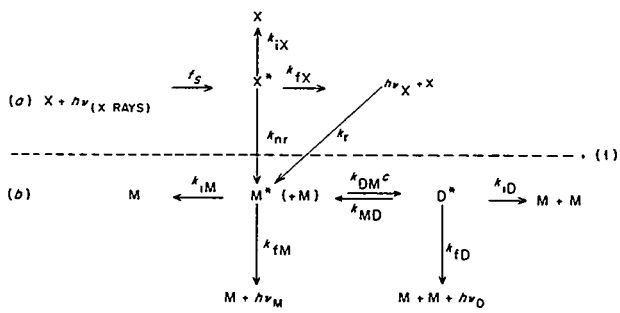

where f_s are the oscillator strengths for the various transitions in X, k_{iX} and k_{fX} are the rate parameters for internal quenching and fluorescence of X, k_{nr} and k_r are the rate parameters for nonradiative and radiative energy transfer from X to M, and k_{fM}, k_{iM}, k_{fD}, k_{iD}, $k_{DM}c$, and k_{MD} are the rate parameters for M fluorescence, M internal quenching, D* fluorescence, D* internal quenching, D* formation, and D* dissociation respectively. Thus, if it is assumed that X is initially excited and that M is subsequently excited by energy transfer from X, the formation of D and emission of M*, which follow M* formation, should be independent of the mode of excitation of X. Considering the kinetics of step (*b*), we have ($c \leqq 10^{-2}$ M)

$$\frac{I_D}{I_M} = \frac{k_{fD}k_{DM}c}{k_{fM}(k_{fD} + k_{iD} + k_{MD})} = Kc\ . \qquad (2)$$

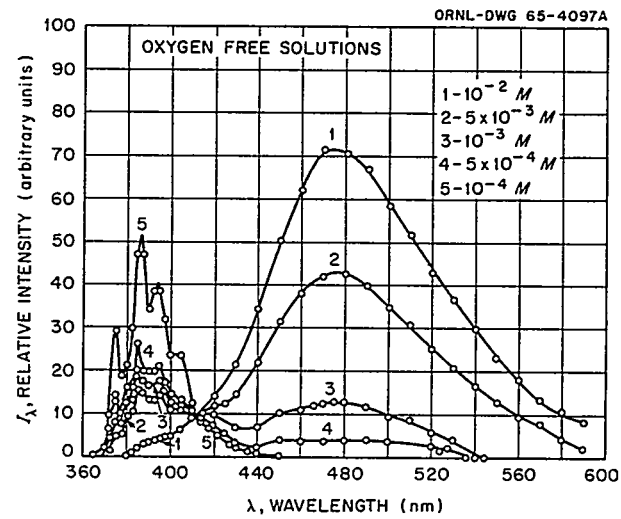

Fig. 16.8. Emission Spectra of Pyrene in Cyclohexane at Various Concentrations.

The value of K is independent of the x-ray energy E_x (120 to 204 kev) and/or x-ray intensity I_x (5 to 20 ma), and it is about 4 times smaller than its value under ultraviolet excitation of the same system. Step (*a*) in (1) is not likely to affect K, and the difference in the K value for the two modes of excitation indicates changes in the values of the rate parameters in Eq. (2). If the entropy change of the system due to excimer formation and the excimer binding energy are the same for ultraviolet and x-ray excitation, then the difference in K for the two modes of excitation is due to changes in the ratio k_{fD}/k_{fM}. Figure 16.8 and Eq. (2) ($c \leqq 10^{-2}$ M), however, indicate that excimers are formed subsequent to M* formation by collision of M and M*, as suggested by Birks *et al.*,[17] the process being collision controlled.

Liquid 2-Ethyl and 1:2-Dimethyl Naphthalene

In the liquid state, only stage (*b*) of (1) is to be considered, that is, M is excited directly by the ionizing radiation. The scintillation spectra of liquid 2-ethyl naphthalene at various temperatures (25 to 142.5°C) are presented in Fig. 16.9. Similar

[16] J. B. Birks and L. G. Christophorou, *Spectrochim. Acta* 19, 401 (1963).

[17] J. B. Birks *et al.*, *Brit. J. Appl. Phys.* 15, 399 (1964).

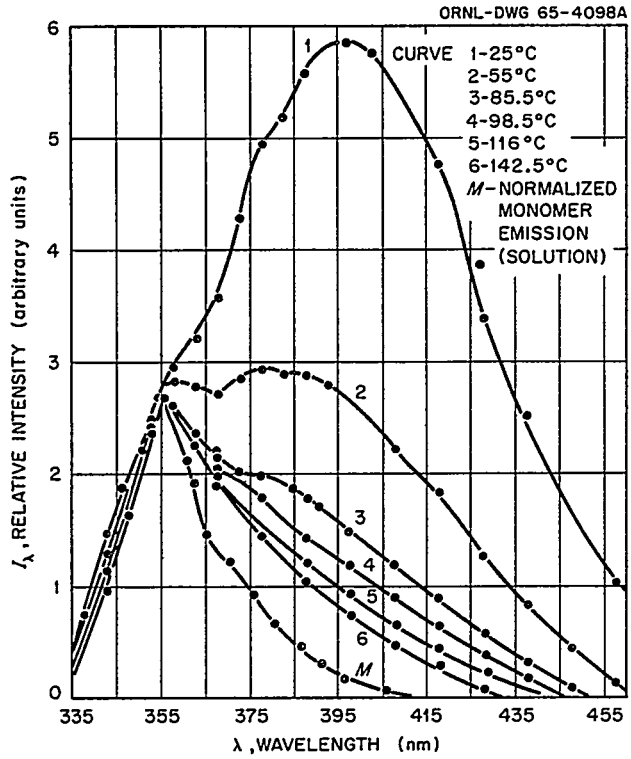

Fig. 16.9. Emission Spectra of Liquid 2-Ethyl Naphthalene at Various Temperatures.

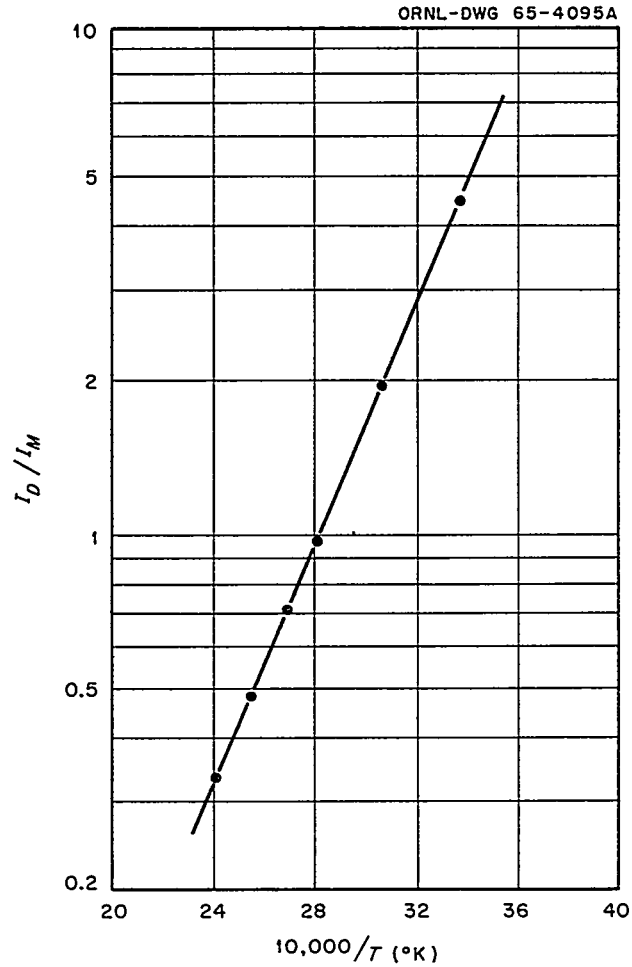

Fig. 16.10. Liquid 2-Ethyl Naphthalene, I_D/I_M vs T^{-1}.

spectra were obtained for liquid 1:2-dimethyl naphthalene for the same temperature range. As the temperature increases, the excimer emission decreases and the monomer emission becomes more pronounced due to the dissociation of D*.[18]

In case of solutions, Birks, Braga, and Lumb[19] have shown that for high temperatures, T, where k_{MD} is large compared to $k_{fD} + k_{iD}$, Eq. (2), for a given X-M system, can be written as

$$\frac{I_D}{I_M} = \text{const} \exp (B/kT) , \qquad (3)$$

where B is the excimer binding energy and k is the Boltzmann's constant. From Eq. (3), which applies also to liquids, B can be obtained from the slope of the $\log_{10} I_D/I_M$ vs T^{-1} curves. In Fig. 16.10 the observed temperature dependence of the emission spectra of liquid 2-ethyl naphthalene is plotted as $\log_{10} I_D/I_M$ vs T^{-1}. From the slope of these curves, we have calculated a binding energy equal to 0.25 ev for 2-ethyl naphthalene. A binding energy of 0.28 ev is calculated for 1:2-dimethyl naphthalene. For solutions excited by ultraviolet light, Aladekomo and Birks[20] have recently reported a binding energy of 0.29 ± 0.02 ev for 2-ethyl naphthalene and 0.31 ± 0.03 ev for 1:2-dimethyl naphthalene. They also reported identical values for the binding energy of 1:6-dimethyl naphthalene in solution and in the liquid state. It can then be concluded that excimers in liquids and solutions are formed subsequent to

[18] J. B. Birks and L. G. Christophorou, *Proc. Roy. Soc. (London)* 274A, 552 (1963).

[19] J. B. Birks *et al.*, *Proc. Roy. Soc. (London)* 283A, 83 (1965).

[20] J. B. Aladekomo and J. B. Birks, *Proc. Roy. Soc. (London)* 284A, 551 (1965).

M* formation in a diffusion-controlled process, independently of the mode of excitation. The shape and position of the monomer-excimer emission are unaffected by the mode of excitation, but the excimer-monomer quantum yield is not. The excimer binding energy seems to be the same for solutions and liquids and to be unaffected by the mode of excitation. From our results on the temperature dependence of the emission spectra of liquids, it is also suggested that since excimers are more easily formed in the liquid state than in solution, the excimer binding energy can be measured more easily by heating a compound in the liquid state than by cooling or heating it in a solution (where problems of solubility on cooling and solvent boiling on heating arise).

TIME-OF-FLIGHT ELECTRON BEAM SPECTROMETER

The pulsed electron gun, drift tube, and fast electronics discussed in the last annual report[21] were used to study the transmission of 2-ev electrons through a stream of N_2 gas crossing the electron beam at right angles to it and very close to the gun. Energy measurements by time-of-flight seem particularly attractive for the lowest electron energies, where electron drift times are relatively long ($\sim 2\mu$sec) and accurately measured (± 2 nsec) and electron deflection measurements are very difficult. A time-of-arrival distribution for 2-ev electrons is shown in Fig. 16.11 without and with the N_2 jet turned on. The electrons all started within about 2 nsec, and the distribution in arrival time after a drift distance of 143 cm is attributable to the energy distribution at the gun. When gas is added, certain energy components are reduced in size or shifted to longer drift times. The explanation is more easily visualized in Fig. 16.12, which shows the preceding distributions converted to energy distributions, that is, all ordinates

[21] R. D. Birkhoff *et al.*, *Health Phys. Div. Ann. Progr. Rept. July 31, 1964*, ORNL-3697, pp. 147–50.

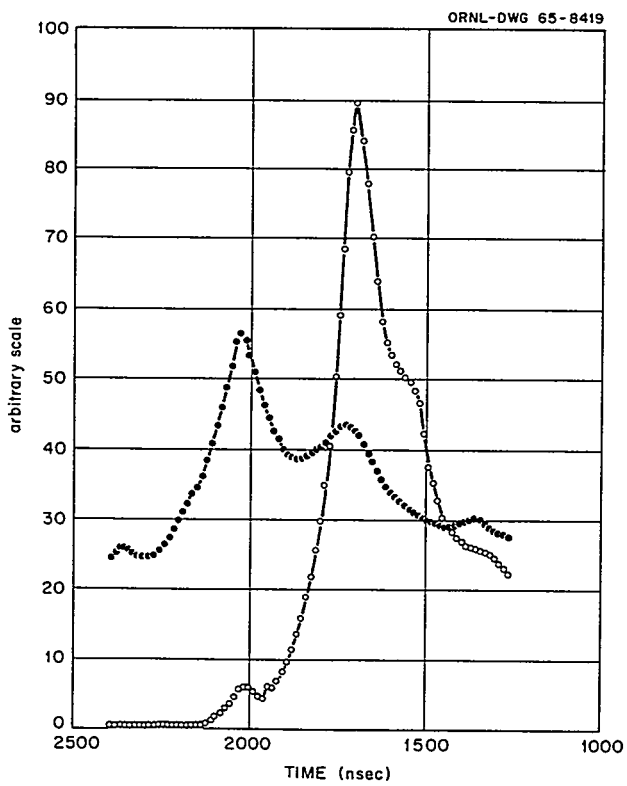

Fig. 16.11. Time-of-Arrival Distribution for 2-v Electrons Without and With Passage Through a Jet of Nitrogen Gas.

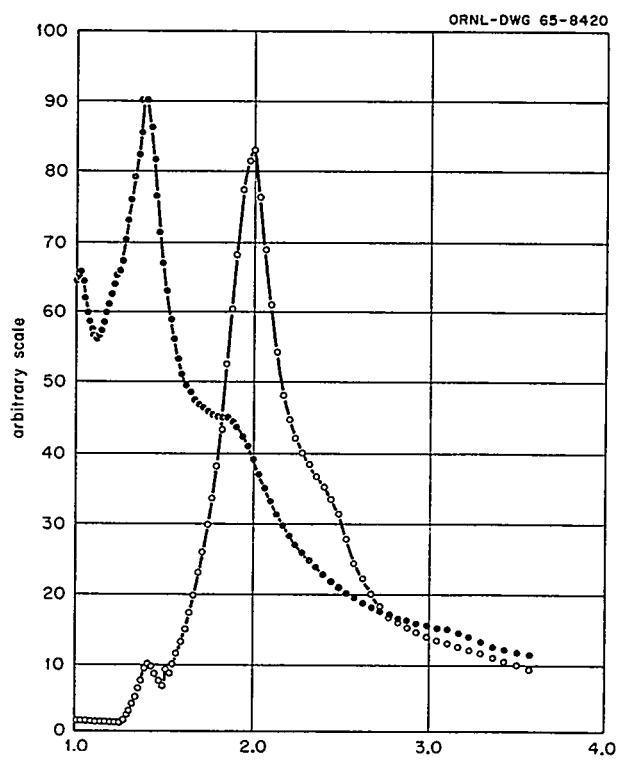

Fig. 16.12. Energy Distribution of 2-v Electrons Without and With Passage Through a Jet of Nitrogen Gas.

are multiplied by t^3. It is apparent that the electrons originally at about 2 ev have lost 0.6 or 1.0 ev as a result of passage through the N_2 jet. These losses are attributable to N_2 vibrational excitation from $v = 0$ to $v = 2$ or $v = 3$, respectively, corresponding to a quantum energy of about 0.3 ev.[22]

DIFFUSION PUMP OIL DEPOSITION MEASUREMENTS UTILIZING RADIOACTIVE TRACERS

The initial experiments conducted last year and reported in the 1964 annual report have been extended and completed.[23]

The tracer technique used simply involves the activation of $^{30}_{14}Si$, which comprises 0.54% by weight of the oil, to $^{31}_{14}Si$, which has a 2.6-hr half-life and emits a beta ray of 1.48 Mev end-point energy.

Procedure

In order to test the applicability of the use of activated silicone oil as a means of determining minute quantities of pump oil in a system, the simple bell jar system shown in Fig. 16.13 was assembled. The system was comprised of the following components: Welch 1397B fore pump, MCF 300 type CVC diffusion pump, CVC multicoolant 4-in. baffle, and a 4-in. NRC gate valve. The oil was irradiated in the Low-Intensity Test Reactor at ORNL. The system was operated under basically two operating conditions. The first phase involved 1-hr pumping times, whereas the second phase involved pumping times of 10-min duration. The 1-hr runs gave results indicating oil deposition at the rate of 6 A/hr at the top of the bell jar. The baffle was not cooled in these runs.

The second phase of the experiment, the 10-min runs, was conducted when it became necessary to determine how the oil was evolved; that is, what was the time profile of the evolved oil. Changes were also made at this time in the counting techniques that were employed during the 1-hr runs. Instead of positioning the end-window Geiger tube inside the bell jar, glass slides were placed on a metal support positioned above the opening in the base plate. The oil passed through a $2\frac{1}{2}$-cm hole in the metal support and deposited on the glass slide. The slide was then removed and positioned approximately 1 mm from the counter window. Since the diameter of the counter window was 30% greater than $2\frac{1}{2}$ cm, it was possible to assume 2π counting geometry with little error. In addition to the greater efficiency in counting that the glass slides permitted, they also eliminated the error associated with cleaning the surface of the bell jar to the same degree before each run. The glass slides were treated identically by washing with trichloroethylene before each run. With the glass slides, it was possible to measure the oil deposited on the slides as a function of time. Figure 16.14 shows data obtained with the 10-min deposition time procedure. On the abscissa, $t = 0$ is the time when the diffusion pump was turned on. The counting time for each slide was 14 min, and the points on the

ORNL-DWG 65-8535A

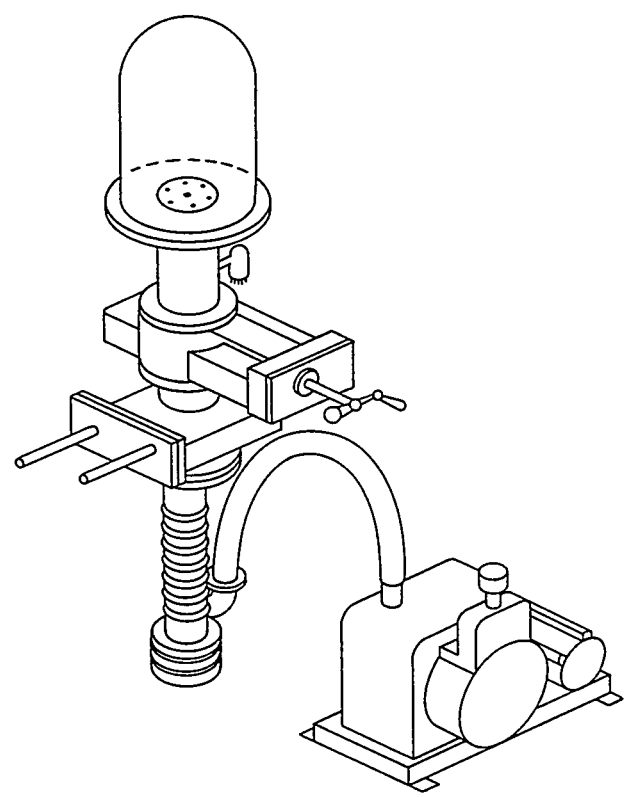

Fig. 16.13. Schematic of Apparatus Used in the Bell Jar System.

[22] G. J. Schultz, *Phys. Rev.* 125, 229 (1962).

[23] R. D. Birkhoff *et al.*, *Health Phys. Div. Ann. Progr. Rept. July 31, 1964*, ORNL-3697, p. 150.

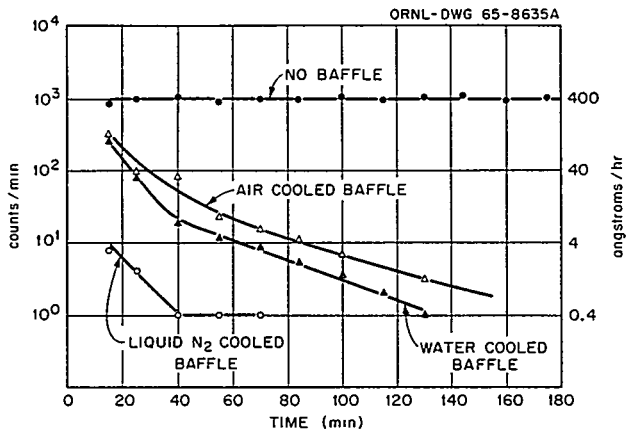

Fig. 16.14. Plots of Counts per Minute vs Time for Four Operating Conditions of the Pumping System. 10-min runs, 14-min counting times. (1) No baffle, 2×10^{-5} torr. (2) Air-cooled baffle, 2×10^{-5} torr. (3) Water-cooled baffle, 2×10^{-5} torr. (4) Liquid-nitrogen-cooled baffle, 2×10^{-6} torr.

curve are plotted at the midpoint of each counting time. The first point represents the time when the fore pump was on and the diffusion pump oil was being heated. On the right side of the graph, the deposition rates are given in angstroms per hour corresponding to count rates of 1000, 100, 10, and 1 count/min.

From the first curve one can see that without the baffle in place the oil backstreams at a constant rate, as is indicated by the constant values of the counting rate during the entire time. The second curve represents the activated oil deposited on the glass slides with the baffle air cooled. The third curve was obtained by maintaining the baffle at approximately 17°C by circulating water through it. The fourth curve was obtained by refrigerating the baffle with liquid nitrogen. The baffle takes about 5 min to reach liquid-nitrogen temperatures. The first point of the fourth curve includes this cooling-down time and is somewhat high due to this fact. The second point of this same curve, however, does represent the time when the system was operating normally with the baffle at liquid-nitrogen temperature. The pressures obtained at the end of each 10-min cycle, with the exception of the first cycle, were approximately 2×10^{-5} torr for the first three curves and approximately 2×10^{-6} torr for the last curve. The limit of our measurement is less than 0.4 A/hr for a 10-min run corresponding to a minimum detectable thickness of <0.1 A.

This tracer technique can be used not only to determine the pressure and precise location of minute quantities of oil in a system but also to evaluate the operational effectiveness of various vacuum system components. There are a number of areas of vacuum technology that could conceivably utilize this technique with suitable improvements of the methods that have been described in this report. Studies in such areas as the design and operation of cold traps and diffusion pumps might benefit from these tracer techniques. Larger quantities of oil could be irradiated, and other counting techniques such as incorporating the counting tube in the system or using solid-state detectors could be employed. Another possibility is the production of a tagged pump oil. It should be possible to tag one of the regular pump oils with an isotope which when irradiated has a longer half-life and more suitable decay characteristics than the $^{31}_{14}Si$ isotope. This tagging would not affect the pumping characteristics of the oil but would permit the oil to be more efficiently used in tracer studies.

17. Professional Health Physics Training

K. Z. Morgan[1] M. F. Fair[2]

Nineteen fellowship students reported to the Division in June for summer training. Sixteen of the fellows were supported by the USAEC and three by the USPHS. The first week was spent in the ORINS Special Training Division and the second week at ORNL in a program of orientation. The remainder of the training period included five weeks with the research groups and five weeks in applied health physics.

In the applied health physics training, the student gains practical experience in all phases of radiation protection under the supervision of a senior health physicist. The student learns of all the radiation protection services that are provided for the Physics Division, Reactor Chemistry Division, Metals and Ceramics Division, Solid State Division, Chemical Technology Division, Rolling Mill, Tracer Facilities, High-Level Radiochemical Development Laboratory, Fission Products Pilot Plant, Waste Disposal Group, Isolation Laboratory, Pilot Plant Operations, and the Ecology Research Group. In addition, they learn of personnel monitoring, instrument calibration, counting facilities, bioassay techniques, and whole-body counters.

In health physics research, the students are first given a brief summary of all the research projects which are in progress in the Division. They then choose the group in which they will remain for the five-week period. They become part of the team and are truly engaged in doing basic research under senior scientist supervision. The fields of investigation include: interaction of radiation with gases, solids, and matter; theoretical radiation physics; health physics research reactor; dosimetry; radioactive waste disposal; and radiation ecology.

It is felt that during this first summer the student is given sufficient experience in applied health physics to enable him to take a position in this field. Also, he learns of the tremendous breadth in research health physics and is made aware of the diverse problems available for thesis work should he decide to continue his education for the Ph.D. degree under the fellowship.

The course in General Health Physics (Physics 472–473) at the University of Tennessee was completed. This was a two-quarter course which met 3 hr/week. There were three AEC fellows, four U.S. Public Health Service fellows, one student from India, and one from Indonesia.

The course in Applied Radiation Physics (Physics 234) at Vanderbilt University was also completed. This was a one-semester course which met 4 hr/week. There were 13 AEC fellows, 1 engineer, and 1 student from Formosa.

Sixteen students were selected for the 1965–66 Fellowship Program. Eleven will enroll at Vanderbilt University and five at the University of Tennessee in September 1965.

One member of the Education and Training Section spent two months at ORINS heading the Health Physics Fellowship Office. During this period he visited 13 universities which were conducting USAEC-NSF summer institutes in Radiation Physics and Biology for college and high school teachers. The USAEC Health Physics Fellowships were discussed and actively promoted. These universities and others at which ORNL health physics research and education activities were discussed by various members of the Division are listed below.

Wayne State University
Purdue University
Butler University
University of Minnesota
Bemidji College
Creighton University
University of Arkansas
La Mar State College
Texas Woman's University
Southern Methodist University
Howard College
Philadelphia College of Science
Ohio State University
Lenoir-Rhyne College
Ohio University
University of Tennessee

[1]Acting Chief, Education and Training Department.
[2]Assistant Chief, Education and Training Department.

Knoxville College
Vanderbilt University
Roanoke College
Florida State University
Florida Atlantic University
East Carolina College
Medical College of Virginia
University of Texas
Southwestern State College
Duke University
North Carolina State College
Georgia Institute of Technology
Mississippi State University
Millsaps College
Texas A and M University
Berea College

One member of the Radiation Physics Section spent part of his time with the University-ORNL Co-Op Program in setting up a new graduate curriculum at the University of Tennessee. This new course of study includes, in addition to the General Health Physics course, one-quarter courses entitled Radiation Chemical Physics, Radiation Biology, Physics of Polyatomic Molecules, Interaction of Electrons with Gases, Interaction of Electrons with Solids, and Interaction of Radiation with Matter. These new courses will be taught by University of Tennessee faculty members and by members of the Radiation Physics Section on loan to the University of Tennessee. It is felt that the availability of this new curriculum leading to a Ph.D. in Radiation Physics will prove attractive to Health Physics fellows who desire education beyond the master's level.

There were seven Oak Ridge graduate fellows and five AEC fellows in the Division working on theses as partial requirements for advanced degrees.

Four research participants and ten ORINS undergraduate students arrived in June to spend the summer in the Division.

Various members of the Division participated in the Traveling Lecture Program, the ORNL Orientation Program, and various other community activities.

A seven-week course in Health Physics was given for the Oak Ridge School of Reactor Technology. The course consisted of lectures with selected visits to health physics facilities. There were 33 students with representation from 9 countries.

A seven-week course was presented for 20 members of the Ecology Section. The course covered the physical principles of dosimetry of internal and external emitters as well as the new recommendations in regard to the fundamental units of measurements.

The Division, in cooperation with ORINS, presented a ten-week course in Health Physics for State personnel sponsored by the Atomic Energy Commission. This was part of the overall AEC program to turn over to the individual States the responsibility for regulation and control of radioactive materials. Ten students completed the program.

The demands for education in Health Physics will continue to rise as they have in the past. Emphasis will be on education to the Ph.D. level to provide personnel for positions of leadership in industrial, academic, and medical institutions. Although the advanced program will be emphasized, education will continue to be offered during the summer at the master's level to provide vocational training which includes a knowledge of health physics principles and procedures.

Part IV. Radiation Dosimetry

J. A. Auxier

18. Ichiban Studies

J. A. Auxier
J. S. Cheka
H. H. Hubbell, Jr.
D. R. Johnson
T. D. Jones
P. T. Perdue
J. H. Thorngate

In the past year considerable progress has been made in clearing up details of the calculation of radiation doses to survivors of the wartime atomic bombings of Hiroshima and Nagasaki. Studies of numerous old reports, letters, photographs, and other data have revealed a number of estimates of the hypocenters and burst heights of the bombs and additional information on yield values.

Radiation leakage was measured from a critical assembly at Los Alamos Scientific Laboratory, which resembled the Hiroshima bomb in structure and materials.

From these and other data, new air dose vs distance formulas and curves were constructed for neutrons and gamma rays in both cities.

ICHIBAN LEAKAGE EXPERIMENT

As a part of the continuing program to evaluate the dose received by the survivors at Hiroshima and Nagasaki, an experiment was performed at Los Alamos Scientific Laboratory to determine the neutron fluence and dose leakage and the gamma dose leakage from a critical assembly designed to have nuclear characteristics similar to the Hiroshima weapon. The assembly is shown in Fig. 18.1. Neutron measurements were made with Hurst proportional counters[1] and threshold foil systems[2,3] for dose and a ^{6}Li "sandwich" spectrometer[4] for neutron spectrum. Additional neutron normalization and measurements were made using a $^{10}BF_3$ counter with the moderator originally designed for Operation BREN (Bare Reactor Experiment Nevada)[5] and the fission counter designed for use with the HPRR[6] and sulfur pellet activations.[7] Gamma measurements were made with the "Phil"[8,9] and photoluminescent glass.[10]

Spectrum measurements were made 2 m from the center of the assembly. Dose measurements were made at 1, 2, 3, and 4 m in air and at approximately 9.5 m in a collimator. For the neutron measurements, a borated paraffin shadow cone was used to determine the scattered radiation. Good internal consistency was obtained for the measurements.

---

[1] E. B. Wagner and G. S. Hurst, *Rev. Sci. Instr.* 29, 153 (1958).

[2] G. S. Hurst *et al.*, *Rev. Sci. Instr.* 27, 153 (1956).

[3] T. A. Love and R. B. Murray, *Use of Silicon Surface-Barrier Counter in Fast Neutron Detection and Spectroscopy*, ORNL-CF-60-5-121 (1960).

[4] J. A. Auxier *et al.*, *General Correlative Studies — Operation BREN*, CEX-62.03 (1963).

[5] J. H. Thorngate *et al.*, *Neutron and Gamma Ray Leakage from the "Ichiban" Critical Assembly*, CEX-64.7 (to be published).

[6] G. S. Hurst and R. H. Ritchie, *Radiation Accidents: Dosimetric Aspects of Neutron and Gamma-Ray Exposures*, ORNL-2748, Pt. A (November 1959).

[7] D. R. Johnson *et al.*, *An Experimental Calibration of Fission Foil Threshold Detectors*, to be published in *Health Physics*.

[8] E. B. Wagner and G. S. Hurst, *Health Phys.* 5, 20 (1961).

[9] J. H. Thorngate and D. R. Johnson, *Health Phys.* 11, 133 (1965).

[10] W. T. Thornton and J. A. Auxier, *Some X-Ray and Fast Neutron Response Characteristics of Silver Metaphosphate Glass Dosimeters*, ORNL-2912 (August 1960).

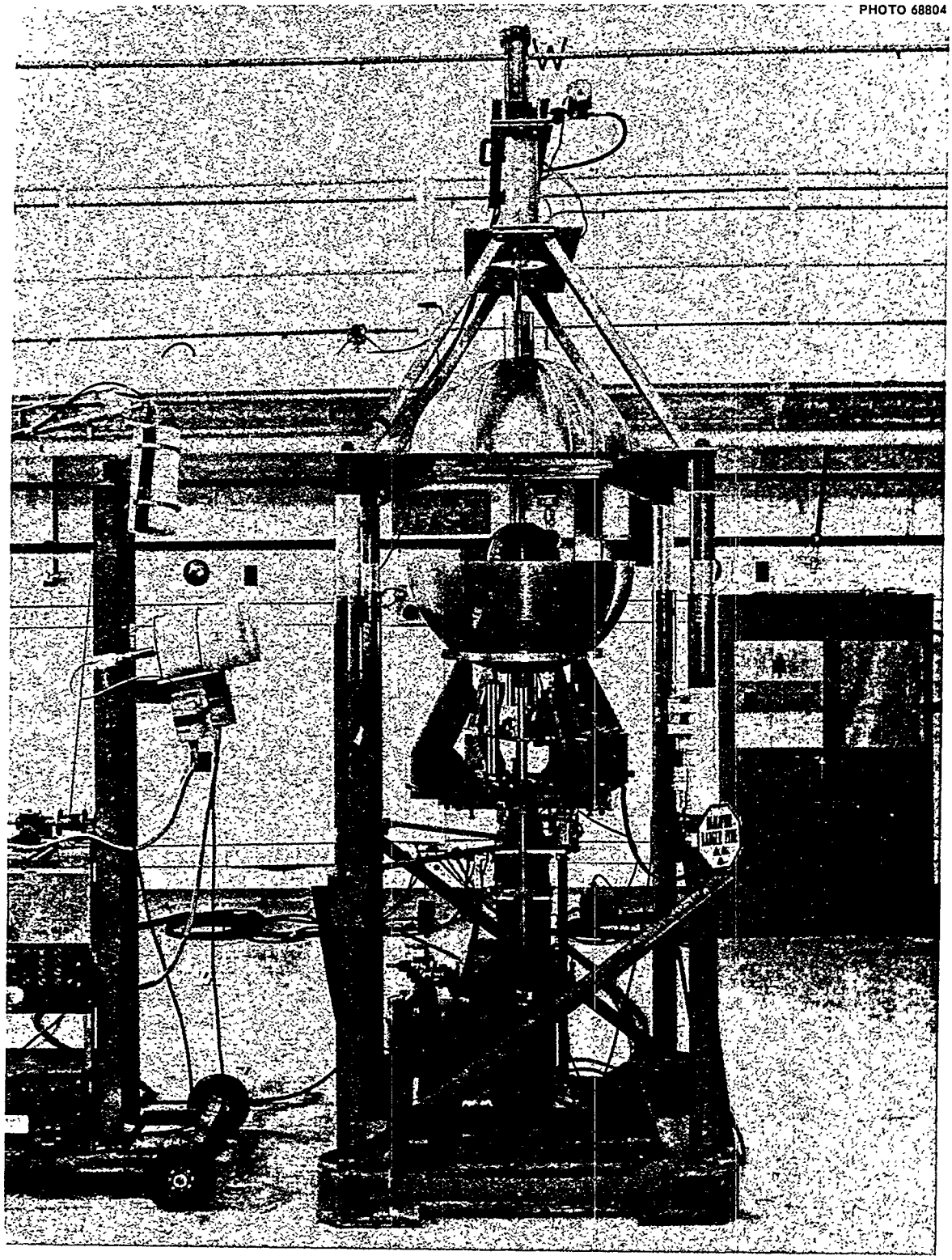

Fig. 18.1. "Ichiban" Critical Assembly.

After the necessary corrections due to the neutron spectrum were made, good agreement was achieved between the neutron dose as measured with the threshold detector unit and with the proportional counter system. Good agreement was also obtained between the several means of normalizing source output and total fissions.

The results indicate a total neutron leakage of 0.76 neutron/fission and a neutron dose leakage of 7.71×10^{-17} rad/fission at 9.46 m. The neutron spectrum is presented in Fig. 18.2. Definitive gamma-ray data could not be obtained because no adequate method was available for separating direct from room-returned gamma rays. Data were good enough to indicate that the prompt gamma contribution to the total dose field was small.

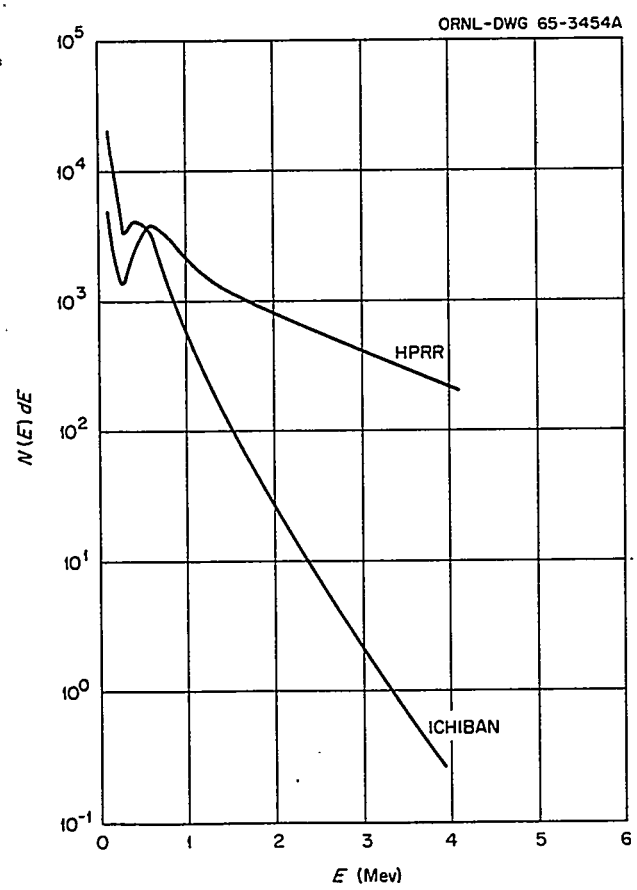

Fig. 18.2. Neutron Energy Spectra of HPRR and Ichiban.

WEAPONS RADIATION YIELD

In the light of more recent maps and other data, Sir William Penney, Chairman of the United Kingdom Atomic Energy Authority, very kindly undertook to restudy the blast pressure data he obtained in Japan in 1945. He writes that another good yield estimate for the weapon should be obtained from this work soon. Also, the Naval Ordnance Laboratory is assisting with a reevaluation of the pressure records from the telemetering canisters which were dropped over Hiroshima and Nagasaki. This too may provide a better estimate for the blast yield.

BURST POINT

Recent investigations in what might be called "nuclear archaeology" by ORNL and AEC personnel have revealed a number of old results and some original data on the epicenters. About 10 or 11 different and apparently independent estimates of these points have been located. A study of these reports indicates that, wherever possible, the data should be reanalyzed on the basis of good maps and aerial surveys now available, since the maps used by early workers were often small and inaccurate. Also, the correction for the finite size of the fireball was seldom made.

Studies on some shadows formed on stone by the bomb thermal radiation and still visible today confirmed a few of the original angle measurements in Hiroshima. Most calculations of the hypocenter and burst heights used such shadows. Similar efforts in Nagasaki yielded no useful data – most of the shadows are gone.

Members of the group at ORNL and the Civil Effects Branch of the Division of Biology and Medicine, AEC, Washington, interviewed a number of the senior scientists, aircrew members, and military personnel who participated in the bomb construction and delivery. Useful data were obtained on the location and calibration of the blast canisters.

AIR DOSE CURVES

Revision of the weapons yield figures and further data from tests and the BREN experiment have permitted the calculation of revised air dose vs distance curves for Hiroshima and Nagasaki.

Nagasaki

The weapon used here was of similar design to those used at several early weapons tests. Good yield and gamma-ray air dose vs distance data are available, but little information on neutron leakage or spectrum has been found. This was an implosion-type device, so a great deal of high explosive surrounded the plutonium at the instant of detonation. Leakage neutrons interacted with the nitrogen of the explosive, producing an intense source of very high-energy gamma rays (about 7 Mev). These are very penetrating, so the relaxation length is long. The scatter and capture of neutrons in the low-Z elements of the explosive resulted in a much lower neutron yield than for the Hiroshima device.

The fast-neutron component determines the neutron attenuation rate for both devices. As shown by Ritchie and Hurst,[11] both gamma and neutron doses fall off with distance as

$$D(R) = \frac{G_0 \exp(-R/L)}{R^2}, \qquad (1)$$

where $D(R)$ is the dose in rads at distance R meters, L is the relaxation length in meters for the appropriate air density and radiation, and G_0 is the normalization for the particular weapon type, yield, and radiation. We take the best gamma dose vs distance data from many tests and determine by least-squares solution the $G_{0\gamma}L_\gamma$. We then assume York's value for the ratio $(G_{0\gamma}/G_{0n})$ of gamma to neutron dose extrapolated to $R = 0$.[11] The value for L_n was derived from weapons tests, corrected to the air density in Japan at the time of the bomb, 1.133 g/liter. The results are given in Table 18.1.

Hiroshima

The normalization problem is much more difficult since a device of this design has never been tested. York relied entirely on calculations. The general structure is that of a large-bore gun firing one piece of uranium as a bullet against another as a target at the end of the barrel, as described in the original Smyth report. The amount of low-atomic-number material in the propellant charge was quite small compared to the quantity of high explosive in the Nagasaki bomb, so there was less moderation or capture of neutrons, hence more leakage of fast neutrons. The relaxation length for the neutrons is assumed to be the same as in Nagasaki. For the gamma rays the dose relaxation length is much less in Hiroshima than in Nagasaki because the hard component of the initial spectrum is so much weaker.

The radiation yield is calculated stepwise from a number of experiments. Several results indicate that the probable blast yield in Hiroshima was equivalent to a total energy release of between 10 and 15 kilotons of TNT equivalent.[12] The fraction, approximately 50%, of this total release which appears as blast wave energy was measured at many tests, so the total release can be inferred from the blast energy.[13] At present the best approximation is 12.5 kilotons total yield.

This yield may be expressed as 12.5 kilotons $\times$ (1.45×10^{23} fissions/kiloton) = 1.815×10^{24} fissions. The number of fissions is multiplied by the neutron leakage factor derived from the Ichiban reactor assembly described above, 6.91×10^{-15} neutron rad m^2 per fission at 1 m, giving the Hiroshima radiation yield as 1.25×10^{10} rads m^2 at 1 m.

The neutron dose builds up in the region close to the source because of air scattering. This buildup factor was calculated from data measured in the BREN experiment[14] and is equal to 6.96,[15] giving a value of $G_{0n} = 8.70 \times 10^{10}$ rads m^2.

The constants for the gamma-dose equation in Hiroshima were derived as follows. The air-dose equation (1) may be rewritten for gamma rays as

$$(\ln R^2 D) = \ln G_{0\gamma} - (R/L) . \qquad (2)$$

---

[11] R. H. Ritchie and G. S. Hurst, *Health Phys.* 1, 390 (1959).

[12] One kiloton of TNT equivalent is now defined as a total energy release of 10^{12} g-cal.

[13] S. Glasstone (ed.), *The Effects of Nuclear Weapons*, USAEC, Washington, 1962.

[14] F. F. Haywood *et al.*, *An Experimental Investigation of the Spatial Distribution of Dose in an Air-over-Ground Geometry*, CEX-62.14 (1964).

[15] The data are shown in Fig. 17, p. 81, and Fig. 18, p. 83, in ref. 17. The ratio of the observed (DR^2) at 10 ft to the calculated (DR^2) is 6.96. This calculated (DR^2) is obtained from the ordinate intercept of the ln (DR^2) vs R line passing through the observed point for 1500 ft reactor height parallel to the linear parts of the other curves on Fig. 17. Figure 18 indicates that increasing the height to 1885 ft, the Hiroshima burst height, would change this ratio only about 1%.

If ($\ln R^2D$) is plotted as a function of R, it is linear, so one point and the slope ($1/L$) will determine the line. The relaxation length, L, was measured for similar gamma-ray spectra in BREN and weapons tests and is 250 m. It was observed at BREN (and at several of the most nearly appropriate weapons tests) that the dose due to neutrons was equal to that due to gamma rays at about 825 m slant range if the "fireball" gamma rays, missing in BREN, amount to 33% of the total at this distance. Therefore, $G_{0\gamma}$ is calculated by substituting in Eq. (2) $R = 825$ m, L_γ for Nevada air density, and the value for $\ln (R^2D)_n$ for neutrons at 825 m, the last calculated from the same equation but with G_{0n} and L_n (Nevada) for neutrons substituted. The values for L in Table 18.1 have all been corrected to the air density in Japan at the time of the bombings, 1.133 g/liter.

Several independent results tend to confirm these air-dose equations.

1. The activation by bomb neutrons of soil at the hypocenters in Hiroshima and Nagasaki was measured shortly after the bombings and the activities were found to be equal. These equations predict neutron doses at the hypocenters equal within a factor of 2. In view of the variable and uncertain composition of the soil, this is reasonable agreement.
2. Recent work by Ichikawa, Higashimura, and Sidei[16] at Kyoto University, Japan, on the thermoluminescence of roof tiles exposed to the bombs gives gamma-ray doses agreeing within about 17% (probable error) with doses calculated from these equations for Nagasaki, and the same for Hiroshima up to 800 m from the hypocenter. If several points out to 980 m are included, the probable error increases to 46%.
3. Studies on the ^{60}Co activity of iron samples which were in the cities at the time of the bombings give neutron fluxes of the same order as values calculated from the equations. Preliminary work of this type was done at ORNL, and extensive work is in progress at the National Institute of Radiological Sciences, Chiba City, Japan, under Dr. Hashizume.
4. Activation of phosphorus in animal and human bones and of sulfur used in insulators on electric distribution lines agrees roughly with these calculations. Neutron fluxes calculated from such activities are subject to considerable error because of the uncertainty of the exact locations of the samples at the time of the bombs and of the shielding and thermalizing effects of surroundings on the neutron fluence and spectrum.

The present results, together with York's values and R. R. Wilson's[17] early calculations are summarized in Tables 18.1 and 18.2 and Figs. 18.3 and 18.4.

[16] Y. Ichikawa *et al.*, *Thermoluminescent Dosimetry of Gamma Rays from Atomic Bombs in Hiroshima and Nagasaki*, to be published in *Health Physics*.

[17] R. R. Wilson, *Radiation Res.* 4, 349 (1956).

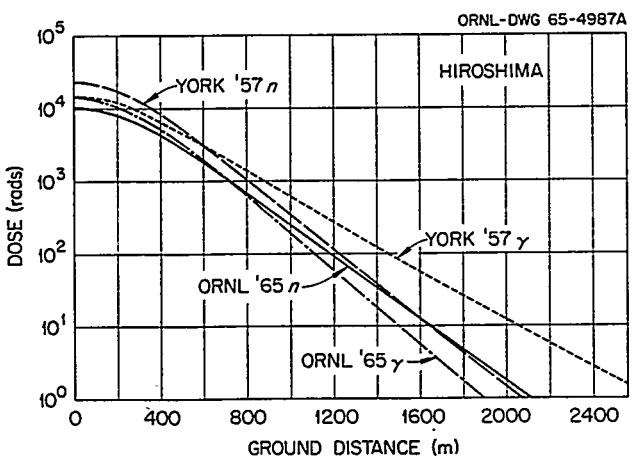

Fig. 18.3. Air Doses for Neutrons and Gamma Rays from the Atomic Bomb Dropped on Hiroshima, Japan, August 6, 1945. Current ORNL results are compared with York's 1957 calculations.

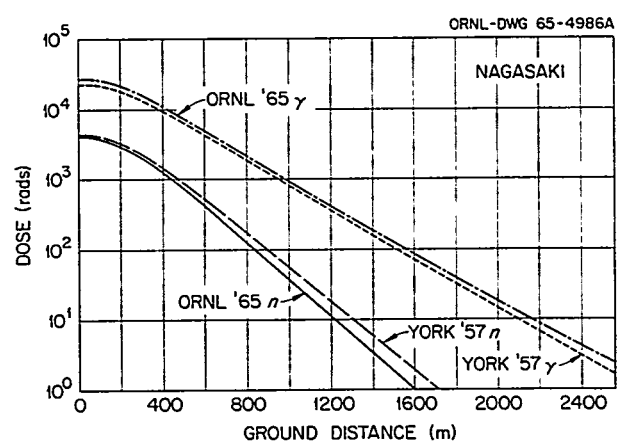

Fig. 18.4. Air Doses from Neutrons and Gamma Rays from the Atomic Bomb Dropped on Nagasaki, Japan, August 9, 1945. Current ORNL results are compared with York's 1957 calculations.

ICHIBAN LIAISON

Liaison with ABCC was continued, and this year included trips by two staff members. The first trip, from September 14 to November 18, 1964, was for the purpose of instructing the Japanese technicians in the application of the shielding formula, which has been introduced by the previous liaison representatives.[18] The second trip, from April 19 to May 20, 1965, introduced revised air-dose curves for use in conjunction with the shielding formula for estimation of exposure, superseding the "York curves" which had been used previously. Questions concerning the criteria of applicability of the shielding formula, which had arisen since the previous liaison trip, were also resolved.

[18] J. A. Auxier *et al.*, *Health Phys. Div. Ann. Progr. Rept. July 31, 1964*, ORNL-3697, p. 155.

Table 18.1. Air Dose Curve Assumptions for Atomic Bombs in Japan

	ORNL (1965)	E. N. York[11] (1957)	R. R. Wilson[17] (1951)
Hiroshima			
Energy yield, kilotons of TNT equivalent	12.5	18.5	20
Height of burst, m	570	550	600
Relaxation length, m			
Neutrons	198	218	196
Gamma rays	250	346	320
Extrapolated G_0 at burst point, $m^2 \times$ rads			
Neutrons	8.70×10^{10}	8.64×10^{10}	7.66×10^{11}
Gamma rays	3.45×10^{10}	2.16×10^{10}	2.72×10^{10}
Nagasaki			
Energy yield, kilotons	22	23	20
Height of burst, m	500	519	600
Relaxation length, m			
Neutrons	198	218	196
Gamma rays	350	346	320
Extrapolated G_0 at burst point, $m^2 \times$ rads			
Neutrons	1.30×10^{10}	1.25×10^{10}	5.65×10^{10}
Gamma rays	2.63×10^{10}	2.68×10^{10}	2.72×10^{10}

Notes: 1. York's and Wilson's values of G_0 have been converted to $m^2 \times$ rads by multiplying by $(0.9144\ m/yd)^2 \times$ (0.93 rad/r or rep).

2. Relaxation lengths are corrected to 1.133 g/liter, the surface air density in both cities at the time of the bombings.

3. Wilson gives only neutron fluxes. Values of G_0 for dose have been calculated from his fast fluxes assuming one fast fission neutron per square centimeter delivers 1.14×10^{-9} rad. Neutrons above 3 Mev and slow neutrons add only a few percent to the dose.

Table 18.2. Air Doses for Atomic Bombs in Japan[a]

Distance from Ground Zero (m)	Neutrons (rads)			Gamma Rays (rads)		
	ORNL (1965)	E. N. York (1957)	R. R. Wilson (1951)	ORNL (1965)	E. N. York (1957)	R. R. Wilson (1951)
			Hiroshima			
0	14,800	23,000	103,000	10,900	14,650	10,000
500	3,220	5,700	24,000	2,887	4,700	4,700
1000	192	380	1,140	260	680	680
1500	10.1	24	80	22.3	91	90
2000	0.54	1.6	11	1.9	15	12
			Nagasaki			
0	4,180	4,310	8,300	26,400	22,600	10,000
500	737	860	1,600	7,290	6,300	4,700
1000	37.1	56	80	903	820	680
1500	1.8	3.3	6	121	108	90
2000	0.089	0.20	0.4	17.9	15.5	12

[a]See notes on Table 18.1.

19. Spectrometry and Dosimetry Research

J. H. Thorngate
M. D. Brown[1]
D. R. Davy[2]
D. R. Johnson
P. T. Perdue
L. H. Peshori[2]

RADIATION SPECTROMETRY

The major modification of the BREN neutron spectrometer[3] for Operation HENRE (High Energy Neutron Reactions Experiment; see below) was the incorporation of circuits to provide better discrimination against gamma rays detected by the organic scintillators used. A number of systems have been reported that separate the proton-produced pulses from those caused by electrons in an organic crystal; these systems depend on the

[1]Two days/week graduate student.

[2]Alien guest.

[3]J. A. Auxier *et al.*, *Health Phys. Div. Ann. Progr. Rept. July 31, 1961*, ORNL-3189, p. 177.

greater amount of long-time-constant scintillation produced by heavier particles.[4] Methods which were tried included the systems described by De Vries and Udo,[5] Daehnick and Sherr,[6] Alexander and Goulding,[7] and Forte.[8] The system finally chosen was a revision of an approach developed by Peelle and Love[9] from the work of Alexander and Goulding. Each of the other systems had some deficiencies that prevented using them with the BREN spectrometer. The difficulties were increased due to the necessity of using anthracene as the organic scintillators; the reported separation schemes were generally designed for stilbene, which has a better ratio of long to short components. Large-diameter crystals of stilbene are not available, and plastic phosphors, which can have almost any shape desired, have a poor electron-to-proton rejection ratio and a relatively low light output. Low light output adversely affects the resolution of the detectors. For the systems tested and rejected, most had a dynamic range too limited for this application and an excessively high low-energy limit when used with anthracene. Most were designed to be used with 14-stage photomultiplier tubes which did not fit the mechanical restrictions imposed upon the spectrometer for field use.

---

[4]R. B. Owens, *IRE Trans. Nucl. Sci.* 5, 198 (1958).

[5]L. J. De Vries and F. Udo, *Nucl. Instr. Methods* 13, 153–60 (1961).

[6]W. Daehnick and R. Sherr, *Rev. Sci. Instr.* 32, 666 (1961).

[7]T. K. Alexander and F. S. Goulding, *Nucl. Instr. Methods* 13, 244 (1961).

[8]M. Forte *et al.*, "Electronic Methods for Discriminating Scintillation Shapes," *Nuclear Electronics*, vol. II, p. 277, IAEA, Vienna, Austria, 1962.

[9]R. W. Peelle and T. A. Love, "Neutron Time of Flight Zero Cross Over Pulse Shape Discriminator," *Proceedings of Conference on Instrumentation Techniques in Nuclear Pulse Analysis, Monterey, California, April 20–May 3, 1963*, National Academy of Sciences–National Research Council Publication 1184, Nuclear Science Series Report No. 40, 1964.

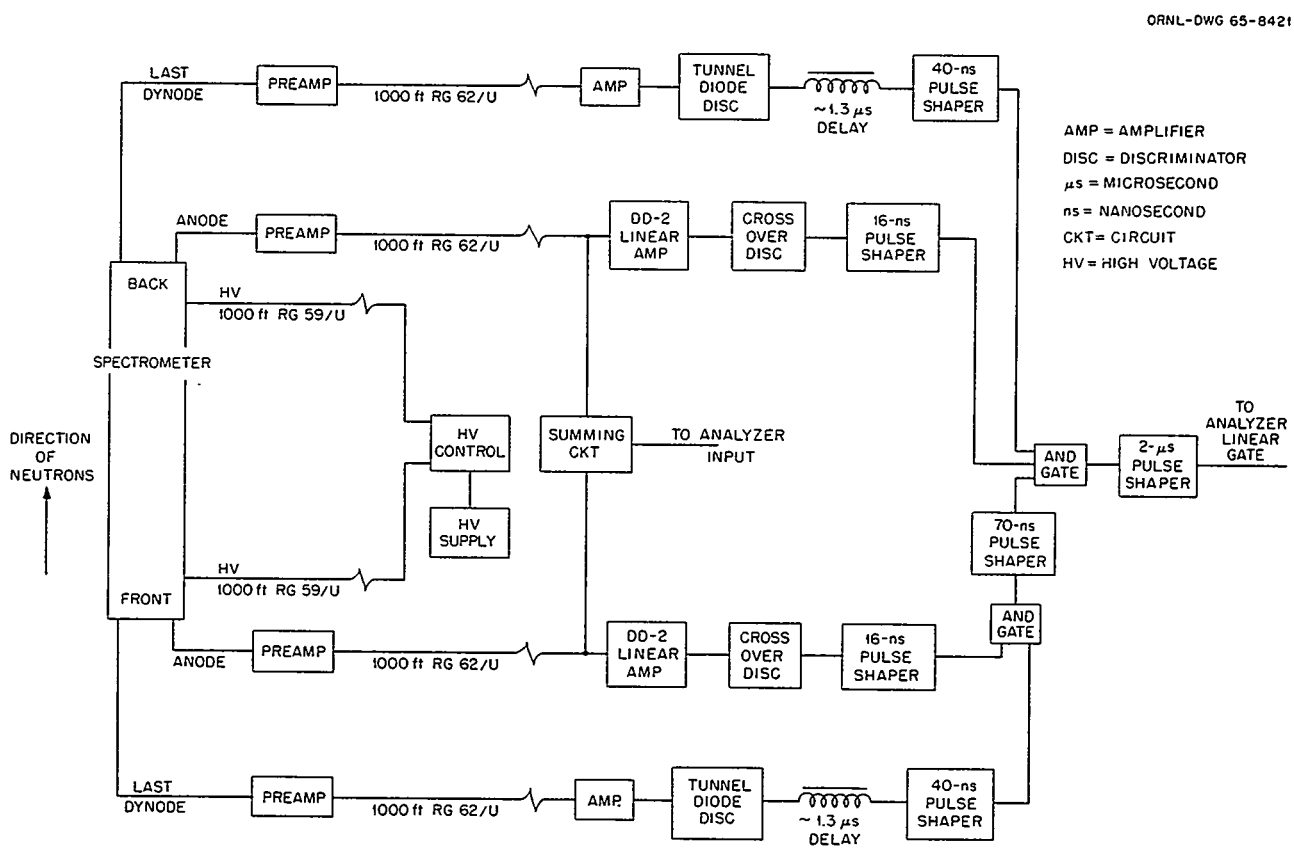

Fig. 19.1. Block Diagram of Neutron Spectrometer.

The system selected is shown in the block diagram in Fig. 19.1. The time from the start of a pulse to the time of "crossover" of the pulse after amplification with a doubly differentiated amplifier is measured. Proton-produced pulses cross back through zero after a longer time than gamma pulses. By using delay lines of the proper length, a coincidence circuit was evolved which will operate only when a proton pulse is obtained from both crystals. An additional timing requirement results from the finite time required by the recoil proton to traverse the length of the spectrometer.

A scintillation gamma spectrometer that uses a five-crystal scheme and a three-out-of-five coincidence circuit to detect pair-producing interactions of the gamma rays with the crystals was designed for use during Operation HENRE. Pair-producing reactions in a central NaI crystal 1 in. in diameter by 1.5 in. long are identified by the 0.511-Mev annihilation gamma rays which are detected in a surrounding NaI annulus 9 in. in outer diameter by 6 in. high. The outer crystal is divided into quadrants, each of which operates a discriminator that produces output pulses only when 0.511 Mev is deposited in the crystal. Two of these signals plus a signal from any energy in the central crystal must occur within 16 nsec of one another in order to open the linear gate of a multichannel analyzer which measures the output of the central crystal. The electronic circuits chosen for use with this device are similar to those used with the neutron spectrometer. Figure 19.2 gives a block diagram of this system.

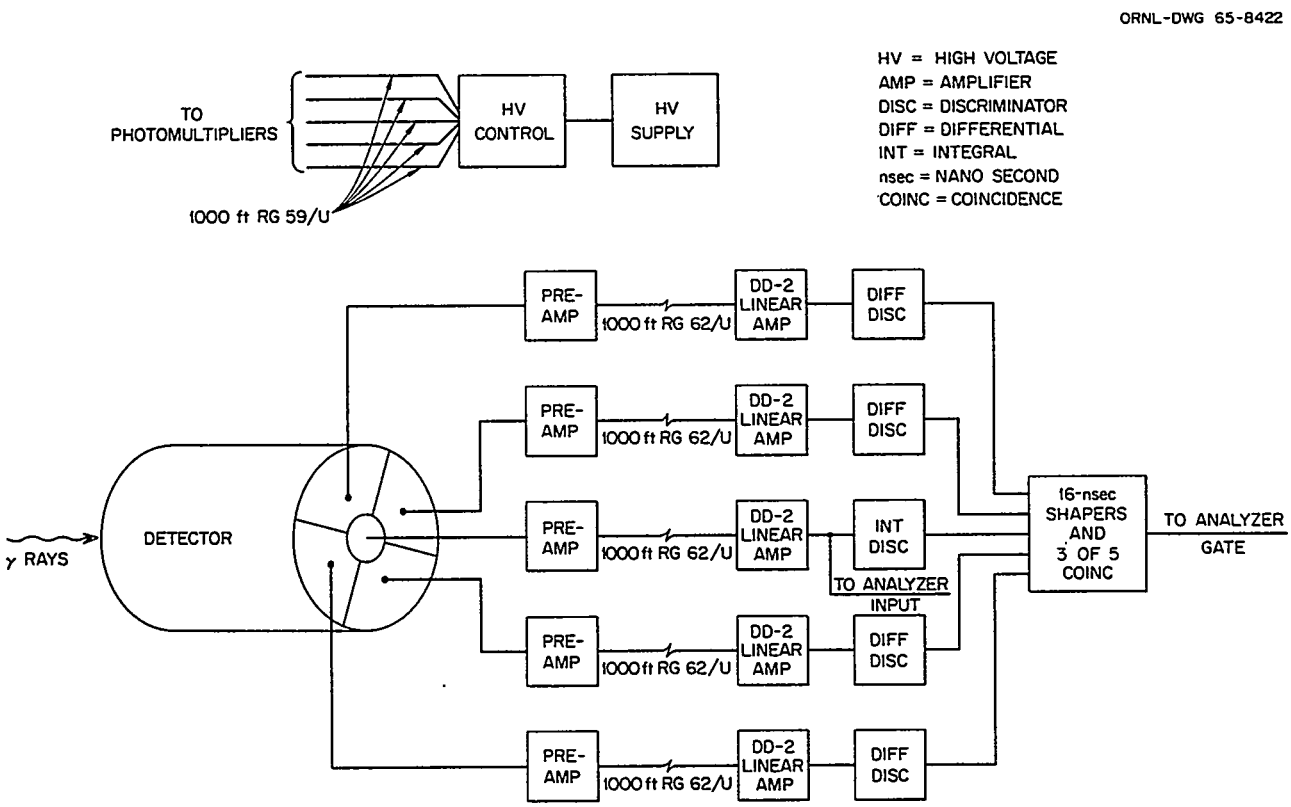

Fig. 19.2. Gamma Spectrometer.

NEUTRON-DOSE-CONVERSION FACTORS FOR AmBe AND AmB SOURCES

The results of measurements and calculations of the average dose per neutron from PoBe and PuBe neutron sources were reported earlier.[10] Due to the increasing use of AmBe and AmB sources, dose-conversion factors for these sources were measured. Source outputs were determined by comparison with a 1-curie PuBe standard source using a Hansen-McKibben long counter.[11] The PuBe source had been calibrated by the National Bureau of Standards and had been constructed so as to be nearly isotropic in emission. Neutron dose rate comparisons were made with a Radsan fast-neutron dosimeter[12] with fixed source-detector geometry. Values for average dose per neutron for AmBe and AmB were then calculated relative to the previously determined value of $(3.9 \pm 0.2) \times 10^{-9}$ rad neutron^{-1} cm^2 for PuBe. This experimental technique had the advantage of canceling systematic errors such as small uncertainties in the proportional counter volume and gas pressure.

The measured output of the 5-curie AmBe source was $(1.22 \pm 0.04) \times 10^7$ neutrons/sec and the average dose per neutron was $(4.05 \pm 0.30) \times 10^{-9}$ rad neutron^{-1} cm^2. The corresponding values for the 10-curie AmB source were $(5.55 \pm 0.17) \times 10^6$ neutrons/sec and $(3.51 \pm 0.26) \times 10^{-9}$ rad neutron^{-1} cm^2. The value for AmBe is still within the error limit quoted for PuBe. Therefore, (4.0×10^{-9}) rad neutron^{-1} cm^2 should be an accurate dose-conversion factor for all three beryllium sources studied.

BURRO DEPTH DOSE STUDY

A study was conducted in collaboration with University of Tennessee–Atomic Energy Commission Agricultural Research Laboratory (UT-AEC ARL) personnel to determine depth-dose distributions in a burro irradiated side-on with the HPRR. In the radiobiological studies at the UT-AEC ARL and in the dosimetry studies at the DOSAR Facility, burros are used frequently. An embalmed burro cadaver was fitted with several thin-walled aluminum tubes extending vertically into its body cavity so that small neutron and gamma-ray dosimeters could be positioned at points of interest. One tube was positioned at the center line, while two others were positioned approximately halfway between the center line and the sides of the burro. A fourth tube was inserted into the center of the brain. The reactor was positioned at the same height as the center line of the burro (1.15 m) and at a distance to the center line of 3 m. First-collision tissue dose rates were normalized to reactor output and compared with "in air" measurements at the burro center-line distance. The dose distribution data are shown in Table 19.1.

[10] T. D. Jones *et al.*, *Health Phys.* 11, 519 (1956).

[11] A. O. Hansen and J. L. McKibben, *Phys. Rev.* 72, 673 (1947).

[12] E. B. Wagner and G. S. Hurst, *Rev. Sci. Instr.* 29, 153 (1958).

Table 19.1. Burro Depth Dose Studies of January 28, 1965

Position	Neutron Dose Rate (millirads/hr)	Relative Neutron Dose Rate	Gamma Dose Rate (mr/hr)	Relative Gamma Dose Rate
Center line of burro, "in air"	1680	1.00	304	1.00
Front side	1870	1.11	625	2.06
Front hole	576	0.34	760	2.50
Center hole	396	0.24	638	2.10
Back hole	170	0.10	406	1.34
Back side	134	0.08	223	0.73
Brain	1792	1.07	380	1.25

20. Dosimetry Applications

J. A. Auxier
J. S. Cheka
K. W. Crase[1]
Mary P. Haydon[2]
W. R. Hendee[3]
T. D. Jones
J. W. Poston
T. D. Strickler
J. H. Thorngate
D. R. Davy[4]
D. R. Johnson
L. H. Peshori[4]

GAMMA-ALBEDO EXPERIMENT

Experimental measurements have been made of the exposure due to ^{60}Co and ^{137}Cs gamma rays scattered from thick, semi-infinite slabs of concrete, lead, and water for various source-detector separation distances and for various heights of source and detector above the scattering slabs.

The experiment was designed to provide data for checking the existing albedo theories and for practical application in instrument calibration. A small isotropic ^{60}Co or ^{137}Cs source, a slender lead attenuator, and a small gamma dosimeter were centered axially on an aluminum crossbeam. The beam was suspended above a thick concrete pad which measured 9.2 × 9.2 m. The crossbeam was suspended near the center so that the source-attenuator-dosimeter array could be rotated about a horizontal axis, that is, alignment could be maintained even though the source was positioned higher than the detector or vice versa. The lead attenuator could be removed in order to make direct measurements of the radiation from the source. The entire array could be positioned at any height above the pad up to about 3 m, and the source-detector separation was varied from 80 to 200 cm. Lead slabs 5 cm thick were placed on the concrete slab for lead-scatter measurements, and a 5.5-m-diam pool filled to 60 cm of H_2O was used for the water-scatter measurements.

The ratio of scattered to unscattered exposure (D_s/D_0) as a function of the ratio of height to separation of source and detector for a fixed separation is shown in Figs. 20.1 to 20.3 for the ^{60}Co source. Figure 20.1 shows the distribution above concrete; Fig. 20.2 shows the same distribution for lead; and Fig. 20.3 shows the distribution above water, each for source-detector separations of 80, 120, 160, and 200 cm. The symbols ($h_d/h_s > 1$) and ($h_d/h_s < 1$) indicate values obtained with the support beam oriented 60° with the normal to the slab such that the detector was higher or lower, respectively, than the source. From these and similar data, the dose albedos were determined for both ^{60}Co and ^{137}Cs for each slab material. The albedos are 0.050, 0.0113, and 0.049 for ^{60}Co gamma radiation on concrete, lead, and water, respectively, and 0.100, 0.013, and 0.083 for ^{137}Cs gamma radiation on concrete, lead, and water, respectively.

BODY SODIUM ACTIVATION AS A DOSIMETRIC TOOL IN NUCLEAR ACCIDENTS

The activation of ^{23}Na in the blood of an individual in the vicinity of accidental or unscheduled criticality excursions has proved to be one of the best criteria for evaluation of his neutron exposure. When the shielding and the neutron and the gamma-ray leakage per fission from a critical assembly are known, the overall exposure and dose equivalent may be calculated from data on the activation of ^{23}Na in blood.

A Monte Carlo computer code was used to predict the number of ^{24}Na atoms produced per incident neutron in an infinite slab of tissue 30 cm thick and for an assortment of cylindrical geometries. To simplify the "debugging" of the code, monoenergetic neutrons were assumed to present a parallel beam unilateral to the phantom. The

[1]ORINS student trainee.

[2]Consultant.

[3]Summer research participant, 1964.

[4]Alien guest.

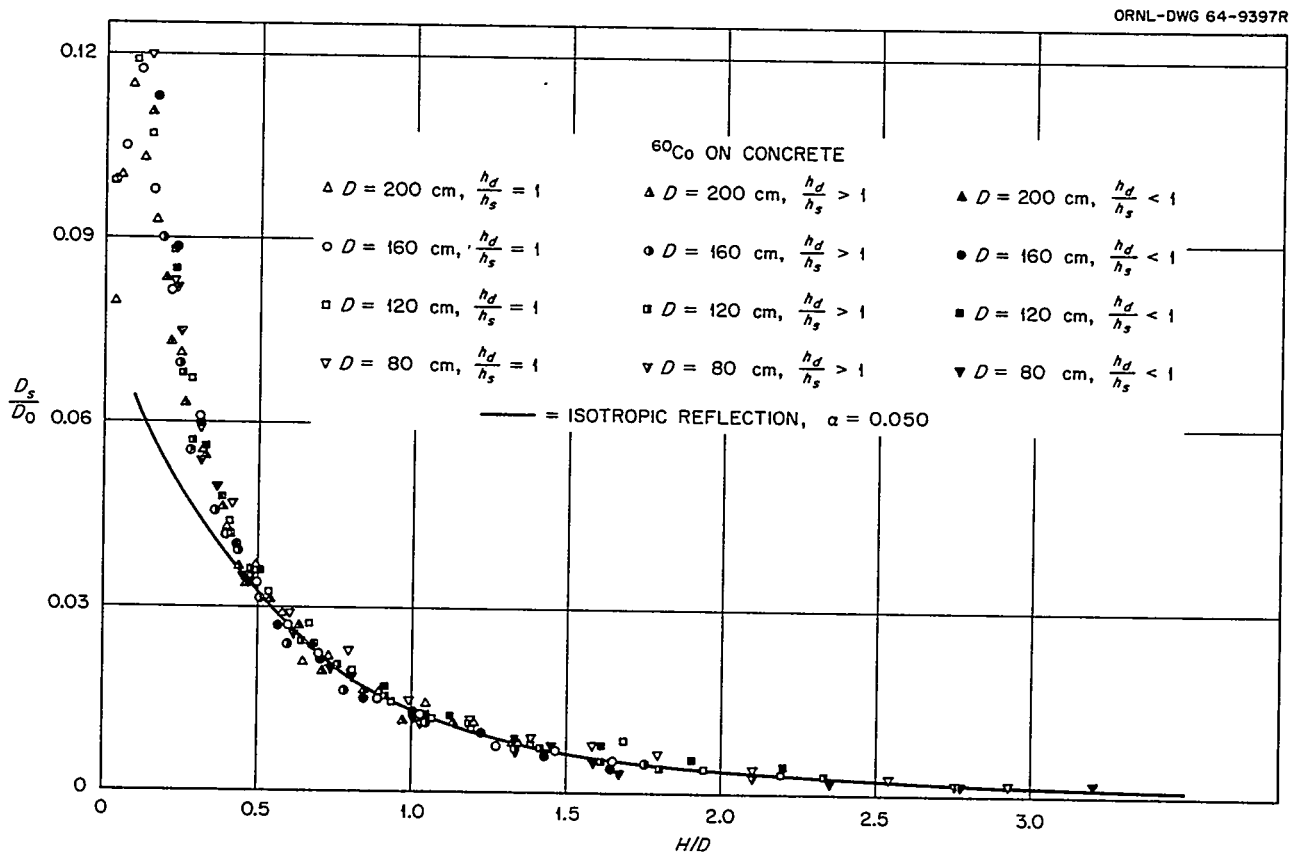

Fig. 20.1. Ratio of Scattered to Unscattered Gamma-Ray Dose as a Function of the Ratio of Source-Detector Height to Separation of Detector and ^{60}Co Source Above the Scattering Slab of Concrete for Several Separation Distances.

results compare with Smith's experimental data[5] as shown in columns 2 and 3 of Table 20.1. Smith listed 11 sources of error which add to ±33% in the unlikely event that all were in the same direction. The code was run for cylinders of varying radii using the fission spectrum of the Health Physics Research Reactor (HPRR), as is shown in Fig. 20.4. The results of these calculations are shown in Fig. 20.5. From Fig. 20.5 and Smith's data, it was apparent that a consistent error existed in one of the assumptions upon which the Monte Carlo code was based.

Various parameters from the computer output are shown in Fig. 20.6 as a function of cylinder radius. The relative difference of the Monte Carlo results compared to HPRR experimental results is also shown and is parallel to the curve indicating the number of fast neutrons escaping from the phantom. This implies that something is wrong with the activation cross sections used in the code.

The cross sections for ^{23}Na which are shown in Figure 20.7 are essentially $1/V$ from 0.025 to 600 ev, but have a narrow resonance peak at 2.9 kev, reaching a maximum value of 325 mb.[6] Hurst,[7] Smith,[5] and others assume that "the neglect of epithermal activation of ^{23}Na is not serious"[7] and for practical purposes may be ignored. In order to expedite the programming and the running time, the capture cross section at 0.025 ev was

[5] J. W. Smith, *Sodium Activation by Fast Neutrons in Man Phantoms*, AERE-R-3697 (1962).

[6] M. D. Brown, ORNL, personal communication, January 1965.

[7] G. S. Hurst *et al.*, *Health Phys.* 2, 121 (1959).

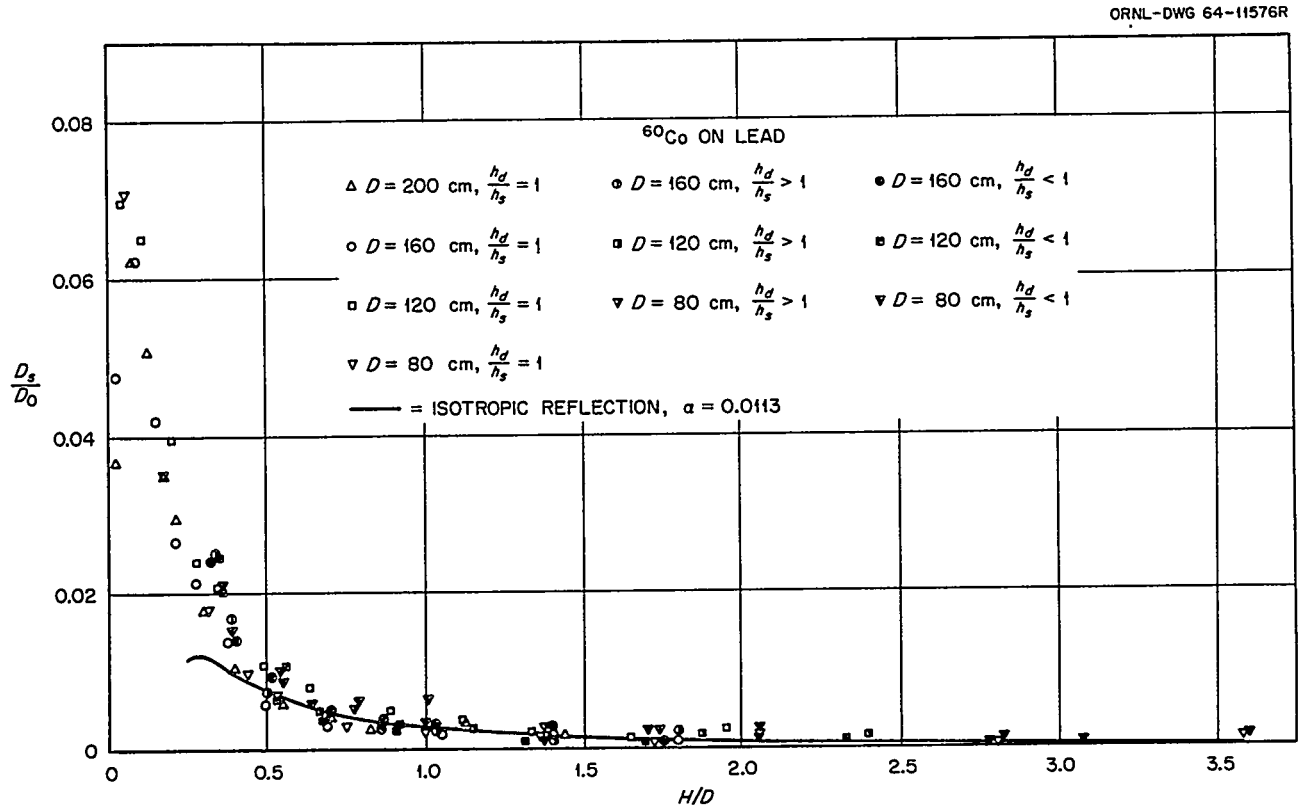

Fig. 20.2. Ratio of Scattered to Unscattered Gamma-Ray Dose as a Function of the Ratio of Source-Detector Height to Separation of Detector and ^{60}Co Source Above the Scattering Slab of Lead for Several Separation Distances.

taken[8] and assumed to follow a $1/V$ law for higher energies as shown by the dotted line in Fig. 20.7.

It appears that for a fast neutron moderated to thermal energy, the probability of producing an ^{24}Na atom in the resonance region is insignificant when compared to the probability that it will do so in the thermal region. However, if a large number of the incident neutrons escape from the phantom before thermalizing, the contribution from this region can become quite significant in the total ^{24}Na production probability. With the data in Table 20.2 and selected data from the computer output, it was possible to estimate a correction factor for large phantoms. For cylinders of 15, 18, and 23 cm radii, 60 cm high, a correction factor of +17% was estimated. The magnitude of the correction must increase as phantom size decreases, since fewer and fewer neutrons will be thermalized. This correction, when applied to the results of the code, yields the data shown in column 4 of Table 20.1. A comparison of this to Smith's data[5] is in column 5.

Smith observed a 14 to 16% overestimation due to polyethylene containers and applied a −8% correction to reduce the maximum error to ±8%. For the HPRR experimental data, a +20% difference was observed, and the polyethylene containers were replaced by aluminum ones. If an additional minus 8 to 12% correction is applied to Smith's data, the two agree quite well. Applying the same correction for the neutron fission spectrum results produces three new points, as seen in Fig. 20.5.

[8]D. J. Hughes and R. B. Schwartz, *Neutron Cross Sections*, BNL-325, 2d ed. (1958).

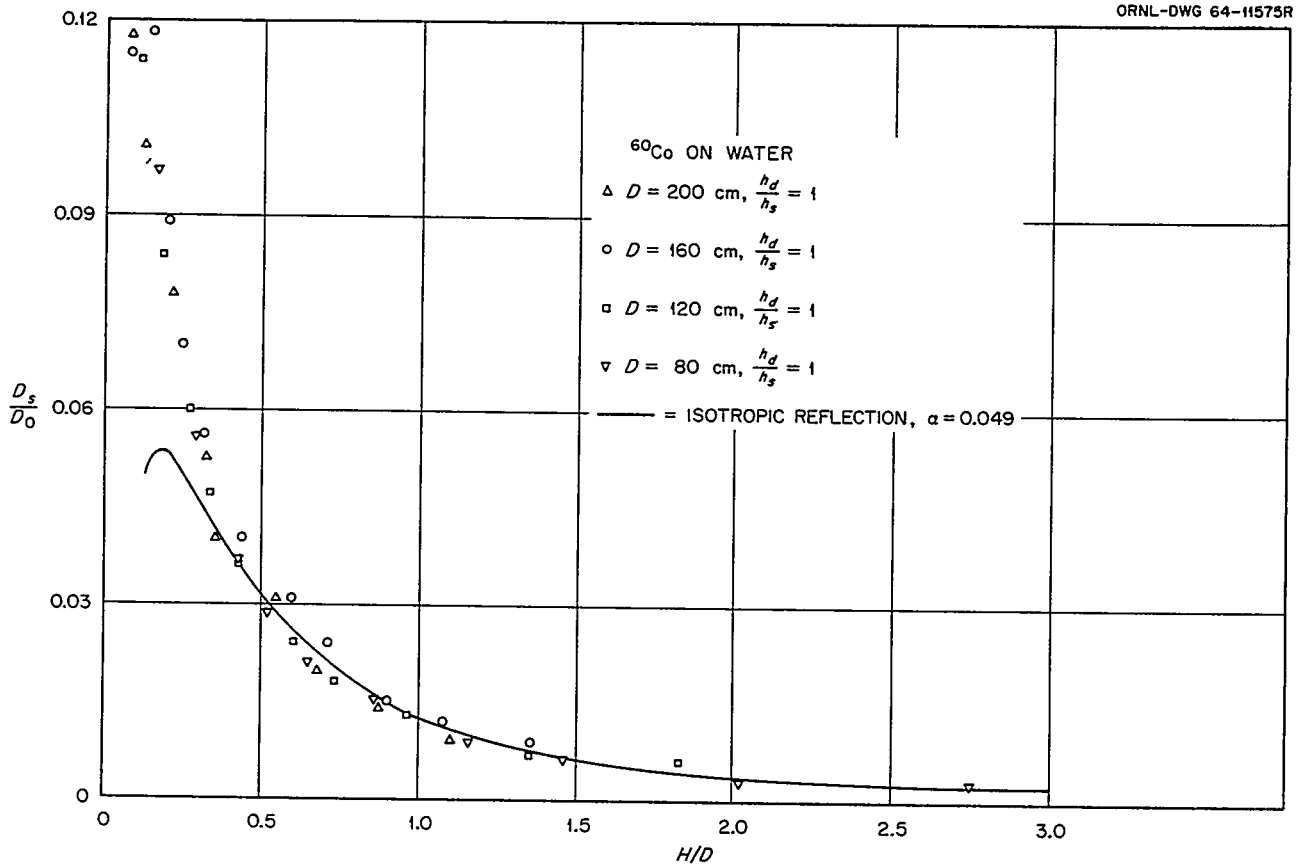

Fig. 20.3. Ratio of Scattered to Unscattered Gamma-Ray Dose as a Function of the Ratio of Source-Detector Height to Separation of Detector and ^{60}Co Source Above the Scattering Slab of Water for Several Separation Distances.

DISTRIBUTION OF DOSE AND DOSE EQUIVALENT IN A CYLINDRICAL TISSUE PHANTOM FROM FISSION SOURCES OF NEUTRONS

The International Commission on Radiological Protection (ICRP) and the National Commission on Radiation Protection (NCRP) have recommended that the relative biological effectiveness (RBE) of ionizing radiation be based on linear energy transfer (LET) between the incident particle and the particles or medium which it irradiates. The RBE of radiation depends, among other things, on: (1) rate of LET along the tracks of the ionizing particles, (2) dose level, (3) dose rate, (4) biological end point, (5) size and composition of phantom, and (6) the general situation during and after exposure.[9]

Thus, in order to calculate the rem dose equivalent of radiation in tissue by charged particles, it is necessary to know the values of LET.[10] When neutrons irradiate tissue phantoms, the dose will be delivered by recoil protons and recoil ions of the elements carbon, oxygen, and nitrogen by inelastic collisions, and by thermal-neutron capture resulting for the most part in the production of gamma rays.

The computer codes used consisted of a neutron code, O5R,[11,12] and a gamma-ray analysis code.

[9] W. S. Snyder, *Some Data on the Relationship of RBE and LET*, TID-7652, Book 1, p. 402.

[10] J. Neufeld and W. S. Snyder, *Selected Topics on Radiation Dosimetry*, p. 35, IAEA, Vienna, 1961.

[11] R. R. Coveyou *et al.*, *Codes for Reactor Computations*, p. 267, IAEA, Vienna, 1961.

[12] W. S. Snyder, *Biological Effects of Neutrons and Proton Irradiations*, vol. 1, p. 3, IAEA, Vienna, 1964.

Table 20.1. Comparison of Calculated Data with Experimental Results with Monoenergetic Neutrons Using a Cylinder Phantom (15 cm radius, 60 cm height)

E (Mev)	Microcuries of ^{24}Na per Milligram of ^{23}Na at 1 neutron/cm^2			Error (%)
	Exptl. Data[a]	Calculated Data	Improved Calculations	
	$\times 10^{-15}$	$\times 10^{-15}$	$\times 10^{-15}$	
0.2	3.12	3.04	3.53	+11
0.5	4.58	3.25	3.69	−20
2.5	4.65	3.44	3.90	−16
6.25	3.70	2.45	3.07	−17

[a]J. W. Smith, *Sodium Activation by Fast Neutrons in Man Phantoms*, AERE-3-3697 (1962). Smith estimated an error of +14–16% due to polyethylene containers and only applied −8% correction. We observed an error of +20% with the HPRR spectrum using polyethylene containers.

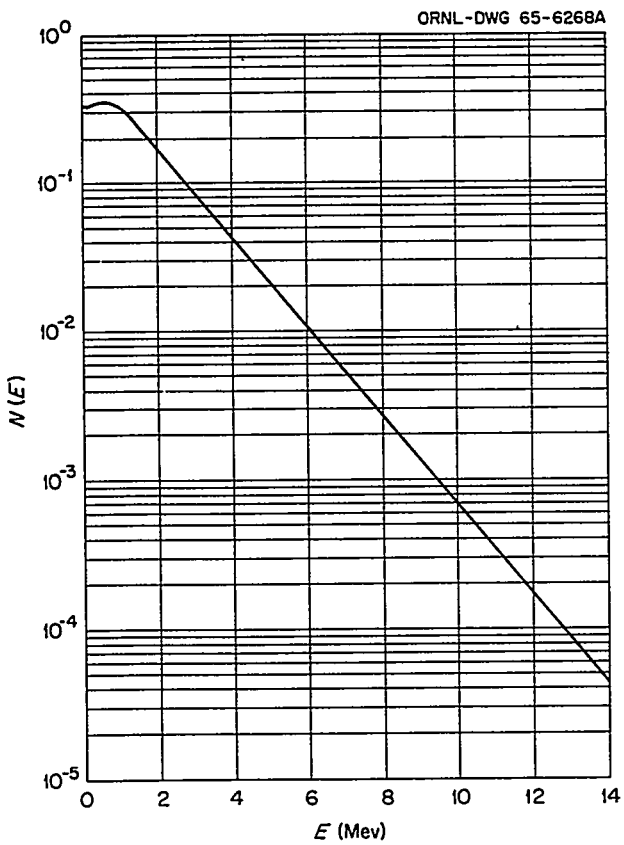

Fig. 20.4. Fast-Neutron Spectrum for the HPRR.

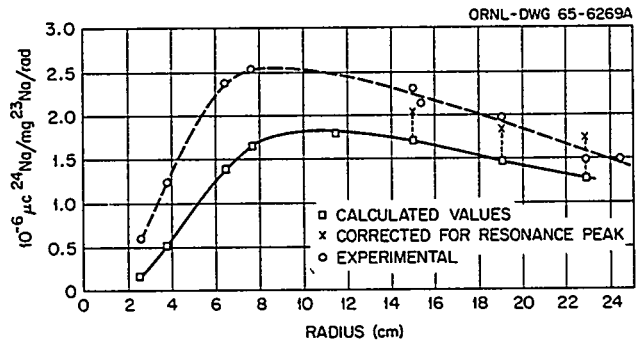

Fig. 20.5. ^{23}Na$(n,\gamma)^{24}$Na as a Function of Cylinder Size for the HPRR Spectrum.

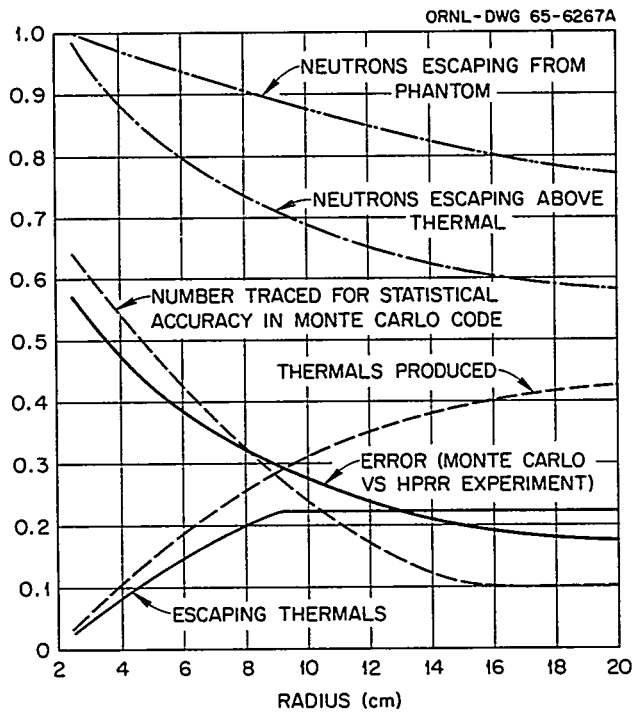

Fig. 20.6. Distribution of Error Compared to Thermal-Neutron Distributions as a Function of Cylinder Size.

The O5R code produces independent histories of neutrons. The histories are computed using appropriate cross sections.[8] Neutrons absorbed in the hydrogen (n,γ) reaction give birth to a photon of 2.2 Mev energy, and the pertinent information concerning this gamma is written on the magnetic tape which serves as input to the gamma-ray

Table 20.2. Neutron Collision Parameters in the Resonance Region of the ^{23}Na Capture Cross-Section Curve[a]

Element	Fractional Energy Loss per Collision (L.S.)	σt (barns) (in ^{23}Na Resonance Region)	Atoms per cm^3 (tissue)	Probability[b]	Maximum Number of Collisions in Resonance Region
Hydrogen	0.63	20	5.74×10^{22}	0.885	1
Carbon	0.14	5	8.69×10^{21}	0.0335	5
Nitrogen	0.13	8	1.24×10^{21}	0.00765	5
Oxygen	0.11	4	2.35×10^{22}	0.0725	5

[a]Average number of collisions per neutron (for those degraded through 2 kev) is 1.46 collisions in the resonance region.

[b]Assuming a collision in resonance region, this is probability of colliding with given element.

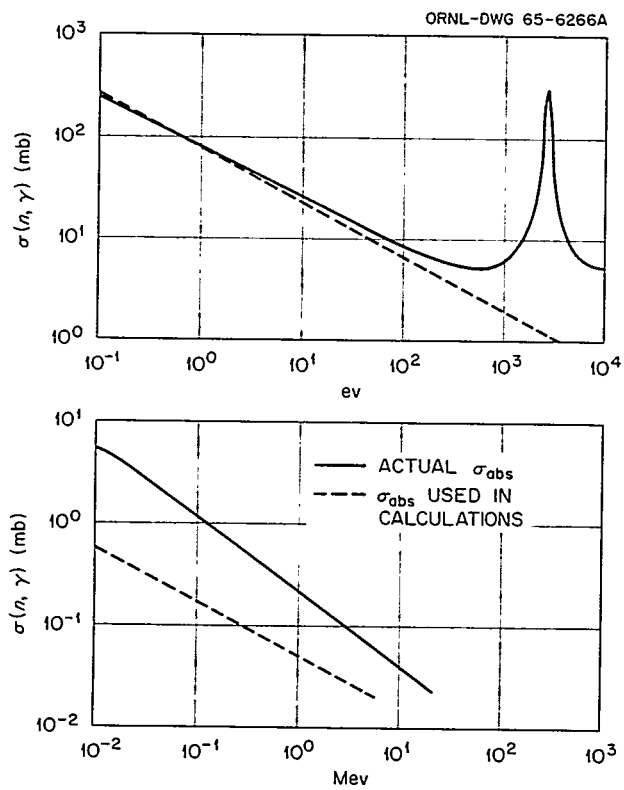

Fig. 20.7. Cross Sections for the ^{23}Na Capture Reaction as a Function of Energy.

analysis code. This code traces the photon much the same as O5R traces the neutron, and it has provisions for the generation of secondary gamma rays.

The machine time on a CDC 1604 digital computer was 26⅔ hr. A total of 90,000 neutrons was traced, producing 62,432 photons, and these in turn produced 35,908 more for a total of 189,340 individual histories analyzed by the two codes.

The average rate of LET along the tracks of recoil nuclei of hydrogen, carbon, nitrogen, and oxygen is shown in Fig. 20.8.

The phantom (Fig. 20.9) is considered to be composed of standard tissue[13] consisting of only the four main elements, which constitute 99% of standard soft tissue by weight. This yielded a medium of density of 0.96 g/cm^3. The phantom was taken to be a right circular cylinder of height 60 cm and radius 15 cm. It was divided into 150 volume elements. The cases considered in this paper all correspond to the phantom being irradiated either unilaterally or bilaterally by broad, parallel beams of fission neutrons.

[13]"Measurement of Absorbed Dose of Neutrons, and of Mixtures of Neutrons and Gamma Rays," *Natl. Bur. Std. (U.S.), Handbook* 75, U.S. Govt. Printing Office, Washington 25, D.C., 1961.

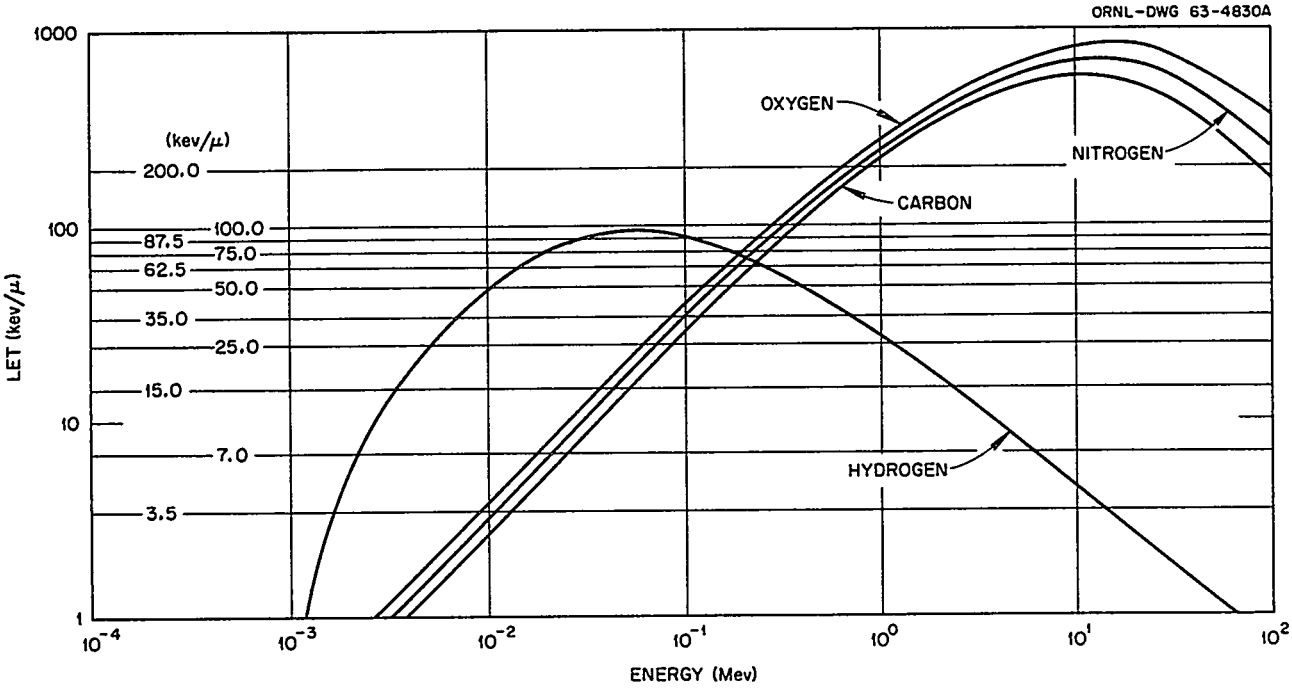

Fig. 20.8. Average Rate of LET Along the Tracks of Recoil Nuclei of H, C, N, and O.

The following spectra were chosen as representative of typical reactors:

The *Y-12* accidental neutron spectrum was produced by a critical assembly of aqueous UO_2F_2 solution 15 cm in height and 25.4 cm radius. The ^{235}U density was 0.0259 g/cm^3.

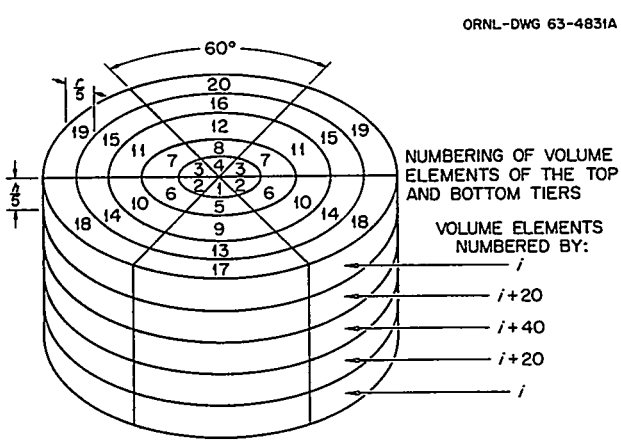

Fig. 20.9. Man-Equivalent Phantom Used in the Monte Carlo Code.

The *Godiva II* and Health Physics Research Reactor (*HPRR*) neutron spectra (Fig. 20.10) are essentially identical and are typical of the fast reactor systems; they show few neutrons of energy lower than 10 kev escaping the assembly. The HPRR ^{235}U core is a right circular cylinder 8 in. in diameter and 9 in. high.

The *Yugoslav* (Boris Kidric) reactor assembly consists of a matrix of natural uranium rods 2.5 cm in diameter immersed in D_2O. The reactor vessel has a radius of 100 cm and a height of 178 cm. This is a large thermal reactor exhibiting a near $1/E$ spectrum below 100 kev.

ORNL UO_2F_2 is typical of an "intermediate" reactor and consists of an aqueous UO_2F_2 solution of ^{235}U density equal to 0.643 g/cm^3. The radius is 15.2 cm and the height is 29.4 cm.

Argonne CP-5 biological port consists of a 4-in. bismuth shield over a 1-in. uranium converter plate.[14]

[14] "Physical Aspects of Irradiation," ICRU Report 10B, *Natl. Bur. Std. (U.S.), Handbook* 85, U.S. Govt. Printing Office, Washington 25, D.C., 1964.

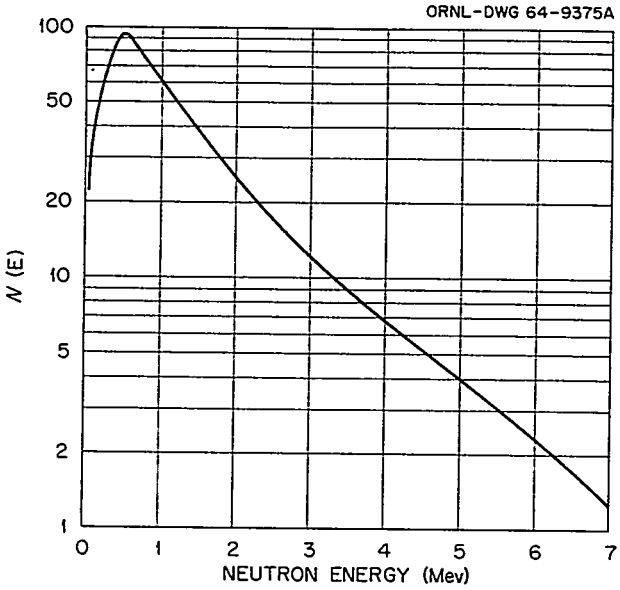

Fig. 20.10. Fission Spectrum of Godiva II and the HPRR.

Table 20.3. Total Dose per Incident Neutron vs Penetration for Unilateral Exposure

Values normalized to Y-12

Spectrum	Dose for Average Penetration Depth (cm) of –						
	1.5	5	10	15	20	25	28.5
Y-12	1.00	1.00	1.00	1.00	1.00	1.00	1.00
ORNL UO_2F_2	0.98	0.95	0.92	0.97	0.97	0.96	1.00
Godiva II	0.70	0.62	0.50	0.41	0.33	0.25	0.22
Argonne CP-5	0.53	0.38	0.31	0.21	0.17	0.13	0.13
Yugoslav	0.30	0.21	0.14	0.10	0.09	0.07	0.07

Table 20.3 gives the values of dose vs penetration for unilateral exposure. All values of dose per incident neutron have been normalized to Y-12, because this spectrum showed the least amount of attenuation and most nearly approached the theoretical spectrum given analytically by $N(E) = Ae^{-E} \sinh \sqrt{2E}$ (ref. 15).

The dose distribution due to recoil ions, for Godiva II spectrum, was only about one-sixth of that for the critical solution assemblies of Y-12 and ORNL UO_2F_2, and it was too small to be considered a contributing factor in either the CP-5 or Yugoslav calculations. In general, the total dose in the elements of the second tiers (volume elements 20 to 40 and 60 to 80) increased about 9.5% over that of the elements in the first tiers (volume elements 1 to 20 and 80 to 100), and the middle tier (volume elements 40 to 60) increased 10.5% in total dose over the values in the first tiers. Sample calculations are given for the HPRR spectrum in Figs. 20.11 through 20.15.

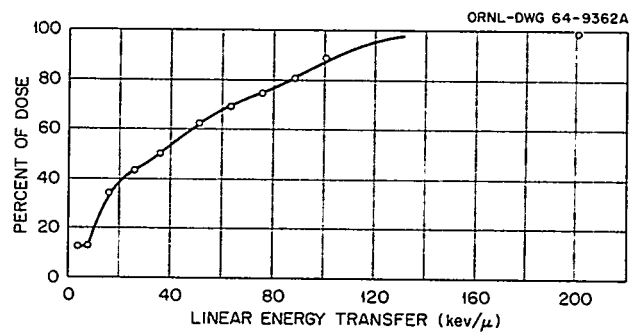

Fig. 20.11. Distribution of Dose with LET – Godiva II and HPRR Assemblies. Volume element 1.

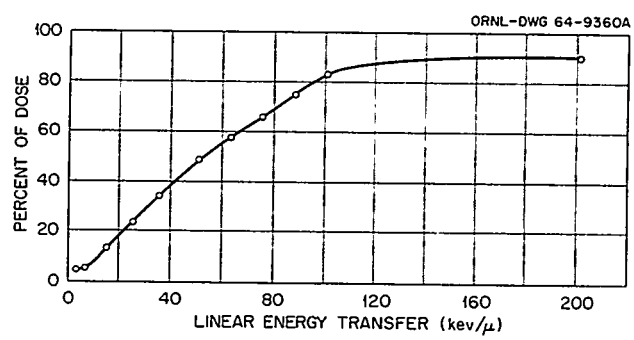

Fig. 20.12. Distribution of Dose with LET – Godiva II and HPRR Assemblies. Volume element 17.

[15]R. L. Murray, *Nuclear Reactor Physics*, chap. 2, Prentice Hall, Englewood Cliffs, N.J., 1957.

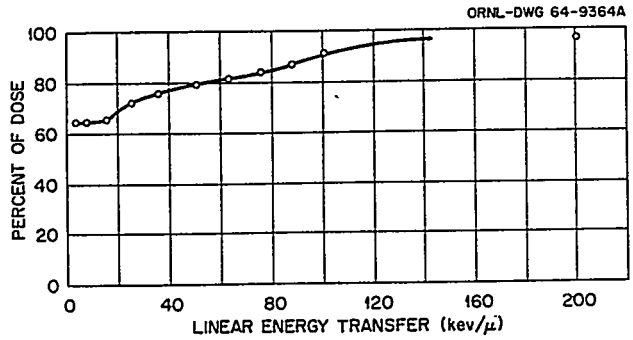

Fig. 20.13. Distribution of Dose with LET – Godiva II and HPRR Assemblies. Volume element 20.

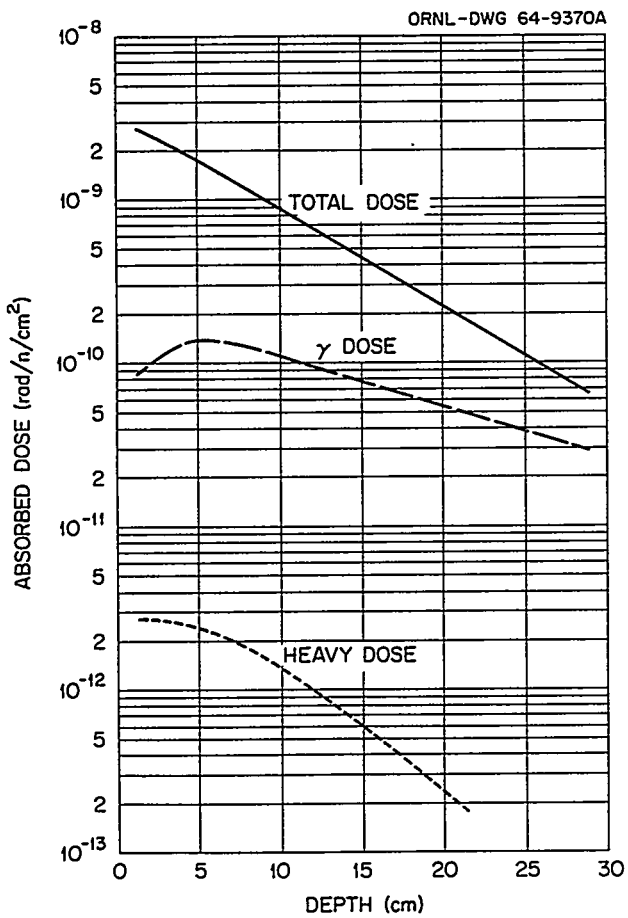

Fig. 20.14. Distribution of Dose with Depth for Unilateral Exposure – Godiva II and HPRR Assemblies. Volume elements 1 to 20 and 80 to 100.

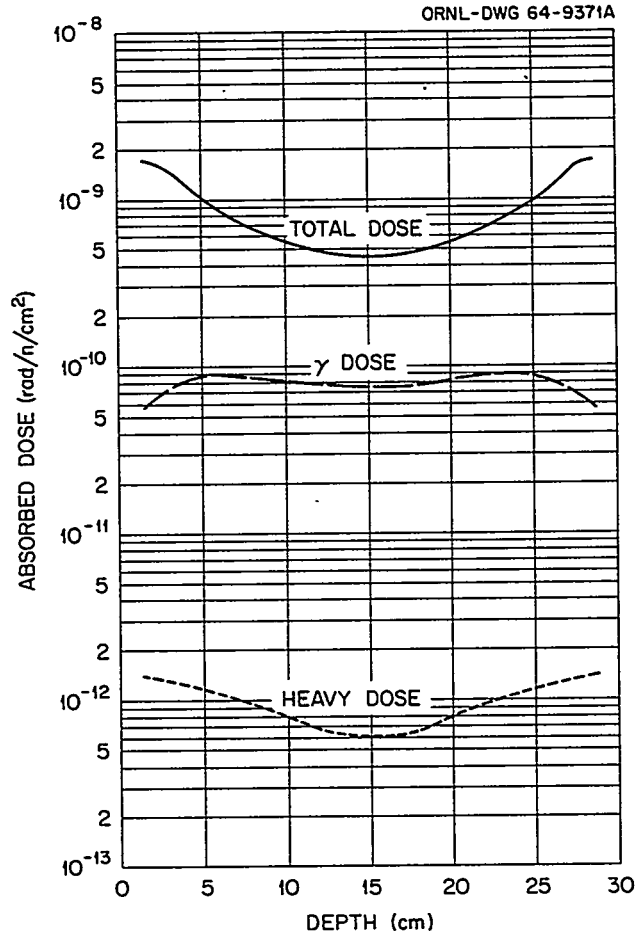

Fig. 20.15. Distribution of Dose with Depth for Bilateral Exposure – Godiva II and HPRR Assemblies. Volume Elements 1 to 20 and 80 to 100.

GLASS DOSIMETRY

The experiment, begun in 1962, to investigate the change of fluorescence of three types of metaphosphate glass microdosimeters with time in dark storage after single exposures to gamma radiation[16,17] was continued. At first, Mn-activated glass rods were used as standards, but these became scarred and chipped in the course of time and were discarded. In the later stages

[16] J. S. Cheka, *Health Phys.* 10, 303 (1964).

[17] J. A. Auxier *et al.*, *Health Phys. Div. Ann. Progr. Rept. July 31, 1964*, ORNL-3697, p. 158.

of the experiment an "internal standard" was used whereby a new series of fluorods was exposed. All the readings from previously exposed rods were compared directly with the readings of the new specimens at 24 hr postexposure at the corresponding exposures.

For all three types of glass exposed to 1000 r or less, the readings at two and three years after exposure show little change from those at one year, as shown in Table 20.4. These results indicate that metaphosphate glass, especially the Toshiba type, indeed lends itself to long-term integrating dosimetry.

Table 20.4. Ratios to Readings 24 Hr After Exposure on Bausch and Lomb Reader

Exposure (r)	1 Year	2 Years	3 Years
	Bausch and Lomb High Z		
100	0.78	0.75	0.72
1000	0.79	0.83	0.89
	Bausch and Lomb Low Z		
100	1.04	1.10	1.12
1000	1.05	1.12	1.17
	Toshiba		
100	1.03	1.05	1.05
1000	1.05	1.04	1.05

STANDARDIZATION OF NUCLEAR ACCIDENT DOSIMETER SYSTEMS FOR APPLIED HEALTH PHYSICS AND THE PUERTO RICO NUCLEAR CENTER

On April 6, 1965, the Applied Health Physics (AHP) Section requested a review of its equipment and experimental procedures for evaluating Hurst threshold detector units in the event of a criticality. In addition, the method of data reduction as originally outlined in ORNL-2748-A was to be updated to include all improvements currently in use at the DOSAR Facility.[18] A prompt investigation showed that the AHP Section was well equipped and fully prepared to evaluate their nuclear accident dosimeter (NAD) detectors if the need should arise. Several minor changes were made in data-reduction techniques to improve the accuracy of the fission foil threshold detectors.

On April 26, 1965, a DOSAR staff member traveled to Mayaguez, Puerto Rico, to evaluate the NAD system at the Puerto Rico Nuclear Center (PRNC). The evaluation was requested by PRNC because of difficulties encountered in use of the NAD counting system. After installation of revised electronics, the NAD counting system operated according to specifications and was used satisfactorily by PRNC personnel to evaluate an NAD detector which was exposed in the reactor to approximately 18,500 rads of fast neutrons. No further problems are anticipated in the operation of the NAD counting system at PRNC.

NUCLEAR ACCIDENT DOSIMETER INTERCOMPARISON STUDY

For a number of years, ORNL and other AEC installations have used a nuclear accident dosimeter (NAD) system based on the Hurst threshold detector system; however, Savannah River Plant (SRP), Pacific Northwest Laboratory (PNL), and Phylatron Corporation recently have developed several NAD systems, and an intercomparison study seemed advisable. On March 23, 1965, seven groups representing SRP, PNL, Phylatron, and four dosimetry groups from Oak Ridge (Y-12, K-25, X-10, and DOSAR) participated in an inter-

[18] D. R. Johnson *et al.*, "An Experimental Calibration of Fission Foil Threshold Detectors," to be published in *Health Physics*.

comparison study of NAD systems at the DOSAR Facility. The HPRR was pulsed at 7.74×10^{16} fissions with the dosimeters and a burro positioned 3 m from the core and approximately 1.5 m from the floor (Fig. 20.16). On March 24, the experiment was repeated, without the burro, using a moderated neutron energy spectrum which was produced by placing an 8-in.-thick graphite shield between the reactor and the dosimeters. The second pulse yielded 6.76×10^{16} fissions. Tables 20.5 and 20.6 show the results of both experiments as of March 26, 1965, and after modifications as of April 22, 1965. The large discrepancies, especially in the response of the same detector system, indicate the need for further intercomparison and calibration. A follow-up experiment is tentatively being planned for late fall.

ORNL-DWG 65-9458

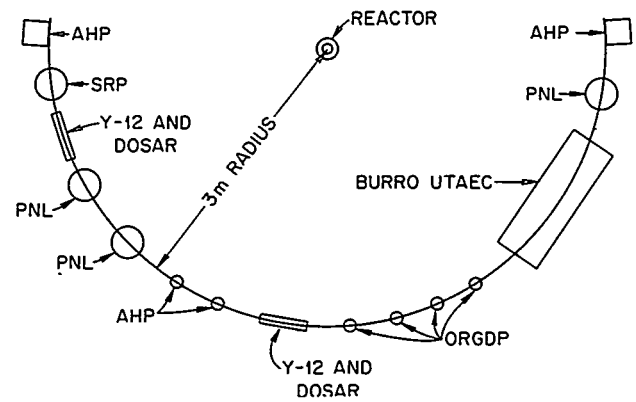

Fig. 20.16. Experimental Arrangement for NAD Intercomparison Study.

Table 20.5. Intercomparison Data for Burst B7ID, March 23, 1965

Study Group	Date	D_f (rads)	D_{th} (rads)	D_γ (r)	n/γ	Neutron Fluence (neutrons/cm^2)									^{24}Na (μc/cm^3)	Burro Dose Based on ^{24}Na (rads)
						ϕ_{th}[a]	ϕ_{Pu}	ϕ_{Np}	ϕ_U	ϕ_S	ϕ_{In+Cd}	$\phi_{In^{115m}}$	ϕ_{Cu}	ϕ_{tot}		
						$\times 10^{10}$	$\times 10^{10}$	$\times 10^{10}$	$\times 10^{10}$	$\times 10^{10}$	$\times 10^{10}$	$\times 10^{10}$	$\times 10^{10}$	$\times 10^{10}$	$\times 10^{-3}$	
SRP	3-26	462	0.6	73	6.3					1.4	0.02	13.0	4.7	18.5	2.14[b]	
	Revised	337		65										16.0		401
PNL	3-26	468	0.16	79	5.9	0.7				3.7	0.47	4.2	4.7	12.6		
		337														
DOSAR	3-26	320		58	5.3	1.04	12.6	8.9	4.2	2.5				12.6	1.0[c]	
		300														
	Revised	320	0.29				13.1	9.2	4.3					13.1		284
Y-12	3-26	332		56	5.9	0.6	15.0	9.0	4.3	2.2				15.0	1.47[c]	331
		356														
	Revised		0.19	57 (glass)	5.8	0.69		9.2								
				53 (film)												
K-25	3-26	466 TDU		52	8.6	0.69	19.0	10.4	5.23	2.4		5.0		19.0	1.3[b]	
		431 BB					17.0	10.8	4.96							
	Revised	339 TDU			6.5		12.8	8.44	4.31						2.14[b]	
		333 BB			6.4		11.6 (calc)	9.49 (calc)								
Phylatron	3-26	330					12.0									
AHP, X-10	3-26	346	0.20	52 (glass)	5.3	0.73	15.0	10.5	4.7	2.4				15.0	2.9[b]	
	Revised	316					12.8	9.3	4.4	2.4				12.8		

[a]Determined by gold and cadmium-covered gold foil.

[b]Serum.

[c]Whole blood.

Note: D_f = absorbed dose (first collision) due to fast neutrons; D_{th} = absorbed dose due to thermal neutrons; D_γ = absorbed dose (first collision) due to gamma rays; n/γ = ratio of neutron to gamma dose; ϕ_{th} = thermal neutron fluence; ϕ_{Pu}, ϕ_{Np}, ϕ_U, and ϕ_S = neutron fluence above the fission threshold of ^{239}Pu (^{10}B), ^{237}Np, and ^{238}U, and the ^{32}S $(n,p)^{32}$P threshold of sulfur respectively; ϕ_{In+Cd} = fluence as determined by the cadmium difference activation of indium; ^{115m}In, fluence above the ^{115m}In threshold; ϕ_{Cu} = fluence as determined with a copper foil; ϕ_{tot} = total neutron fluence; and ^{24}Na = activation of sodium in the burro blood.

Table 20.6. Intercomparison Data for Burst B72D, March 24, 1965[a,b]

Study Group	Date	D_f (rads)	D_{th} (rads)	D_γ (r)	n/γ	Neutron Fluence (neutrons/cm^2) ϕ_{th}[c]	ϕ_{Pu}	ϕ_{Np}	ϕ_U	ϕ_S	ϕ_{In+Cd}	$\phi_{In^{115m}}$	ϕ_{Cu}	ϕ_{tot}	^{24}Na ($\mu c/cm^3$)	Dose in Air
						$\times 10^{10}$	$\times 10^{10}$	$\times 10^{10}$	$\times 10^{10}$	$\times 10^{10}$	$\times 10^{10}$	$\times 10^{10}$	$\times 10^{10}$	$\times 10^{10}$		
SRP	3-26	193	0.5	32	5.8					0.24	0.02	2.3	4.0	9.0	8.3×10^{-4}	
		188		33												
	Revised	129		30	4.3									7.8		
PNL	3-26	132	0.15	44	3.0	0.63				0.47	0.48	1.4	4.4	6.3		
		120														
DOSAR	3-26	81	0.30	22	3.7	1.08	3.8	2.0	0.8	0.38				3.8	1.0×10^{-3}	295
Y-12	3-26	79		24	3.3	0.84	4.2	2.1	0.8	0.31				4.2		273
	Revised		0.15	22 (glass)	3.6	0.53									1.3×10^{-3}	
				21 (film)												
K-25	3-26	120 TDU		23		0.524	5.4	2.43	0.97	0.33		0.9		5.4	4.7×10^{-3}	
		91 ORGDP														
	Revised	86			3.7		3.63	1.94	0.79			0.89			1.56×10^{-3}	
		73			3.2											
Phylatron	3-26	75					2.7									313
	Revised	80					3.2									

[a]AHP X-10 did not participate.
[b]Symbols are as defined in Table 20.5.
[c]Determined by gold and cadmium-covered gold foil.

21. Special Projects and HPRR Operations

F. F. Haywood
E. G. Hill[2]
D. G. Inman[2]
J. E. Jackson
W. G. Markland[2]
W. C. Plake[3]
E. M. Robinson
W. H. Shinpaugh
T. G. Provenzano[4]
L. W. Gilley[1]
E. D. Carroll[5]
J. W. Poston
D. R. Ward[1]

OPERATION HENRE

During the last few years, there has been an extensive experimental and theoretical research effort directed toward the description of the total radiation field from an isotropic radiation source positioned at various heights above the ground. An accurate knowledge of such radiation fields is of fundamental importance in radiation physics as well as in practical application to civil and military defense. A facility was provided during Operation BREN[6,7] that had the capability to position a small fission source (HPRR) at heights up to 1500 ft. Shortly after the completion of the experiments in Operation BREN, the suggestion was made to assess the feasibility of building a monoenergetic neutron source which could be used in the same source facility and which would have a neutron yield of at least 10^{13} neutrons/sec for exposures of 4 hr each. This value was based on an evaluation of the sensitivity of the various dosimetry and spectrometry instruments and on the calculated transmission of neutrons and gamma rays in air. During 1964 the feasibility of constructing such a source was determined.[8]

The basic design criteria may be stated as follows: the neutron source to be constructed must have a yield of 10^{13} neutrons/sec for a 4-hr period for each target, the total weight of all system components including the hoisting device containing the neutron source must be less than 16,000 lb, and quick release mechanisms must be incorporated for removing radioactive components, for example, used targets.

Design, Construction, and Testing

During this report period, the neutron source has been designed, fabricated, and tested. Some of the system components which required special design or developmental work will be mentioned here.

The vacuum system was designed for an operating pressure of 2×10^{-6} torr. The amount of deuterium passing through the system (throughput) is 50 μl/sec, exclusive of outgassing of components. To obtain operating pressure, the pumping speed must be about 25,000 liters/sec. A 10-in. oil diffusion pump and a titanium evaporation (getter) pumping surface were used. Tests to date with the system have yielded operating pressures of 1×10^{-6} torr and less.

The neutron-producing target for the neutron source is a layer of erbium 3 to 4 mg/cm^2 sublimed onto a copper disk 14 in. in diameter (Fig. 21.1) and saturated with ^{3}H. The maximum power put into the target by D^+ beam bombardment is 75 w/cm^2. Therefore, channels for liquid coolant were constructed in the back of the target plate to increase the area for heat transfer (see Fig. 21.2).

[1]On loan from Neutron Physics Division, ORNL.

[2]Visiting investigator from Edgerton, Germeshausen and Grier, Inc., Las Vegas, Nev.

[3]Visiting investigator from Edgerton, Germeshausen and Grier, Inc., Santa Barbara, Calif.

[4]Visiting investigator from Armed Forces Radiobiology Research Institute, Bethesda, Md.

[5]On loan from Instrumentation and Controls Division, ORNL.

[6]F. W. Sanders *et al.*, *Operation Plan and Hazards Report — Operation BREN*, CEX-62.02 (1962).

[7]J. A. Auxier *et al.*, *General Correlative Studies — Operation BREN*, CEX-62.03 (1963).

[8]T. G. Provenzano *et al.*, *Feasibility Study: Intense 14 Mev Neutron Source for Operation HENRE*, CEX-65.01 (in preparation).

A developmental program was required to have firm fabrication procedures for this copper target backing. In order to have individually sealed channels for coolant flow, it was necessary to electroplate one surface with silver prior to cutting the channels, then braze a thin cover to this surface. To have even distribution of coolant (demineralized water) over the target back, a 20- to 30-psi drop across the target was a design criterion. Experiments with individual coolant channels indicated that 0.034- by 0.080-in. channels on $\frac{1}{8}$-in. centers across the target would provide the desired coolant distribution for a flow rate of 18 gpm. To date, an unloaded target backing has been bombarded with a 500-ma H^+ beam at 150 kv with no apparent structural damage to the target.

Because the neutron source is to operate on a tower, it was necessary to design a closed-circuit cooling system. Heat dissipated in the target by the deuterium beam will be about 75 kw maximum.

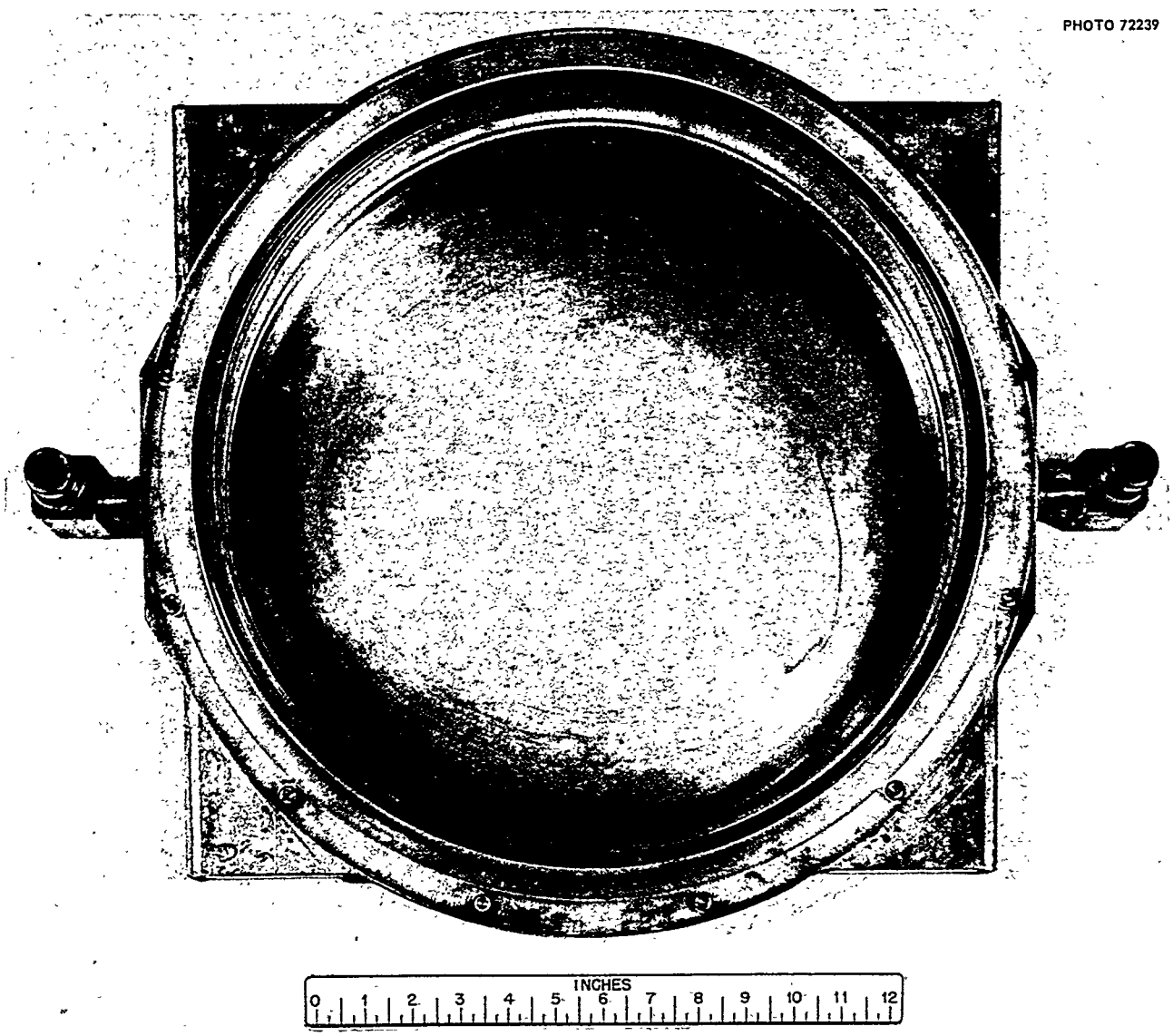

Fig. 21.1. HENRE Neutron Source Target Backing.

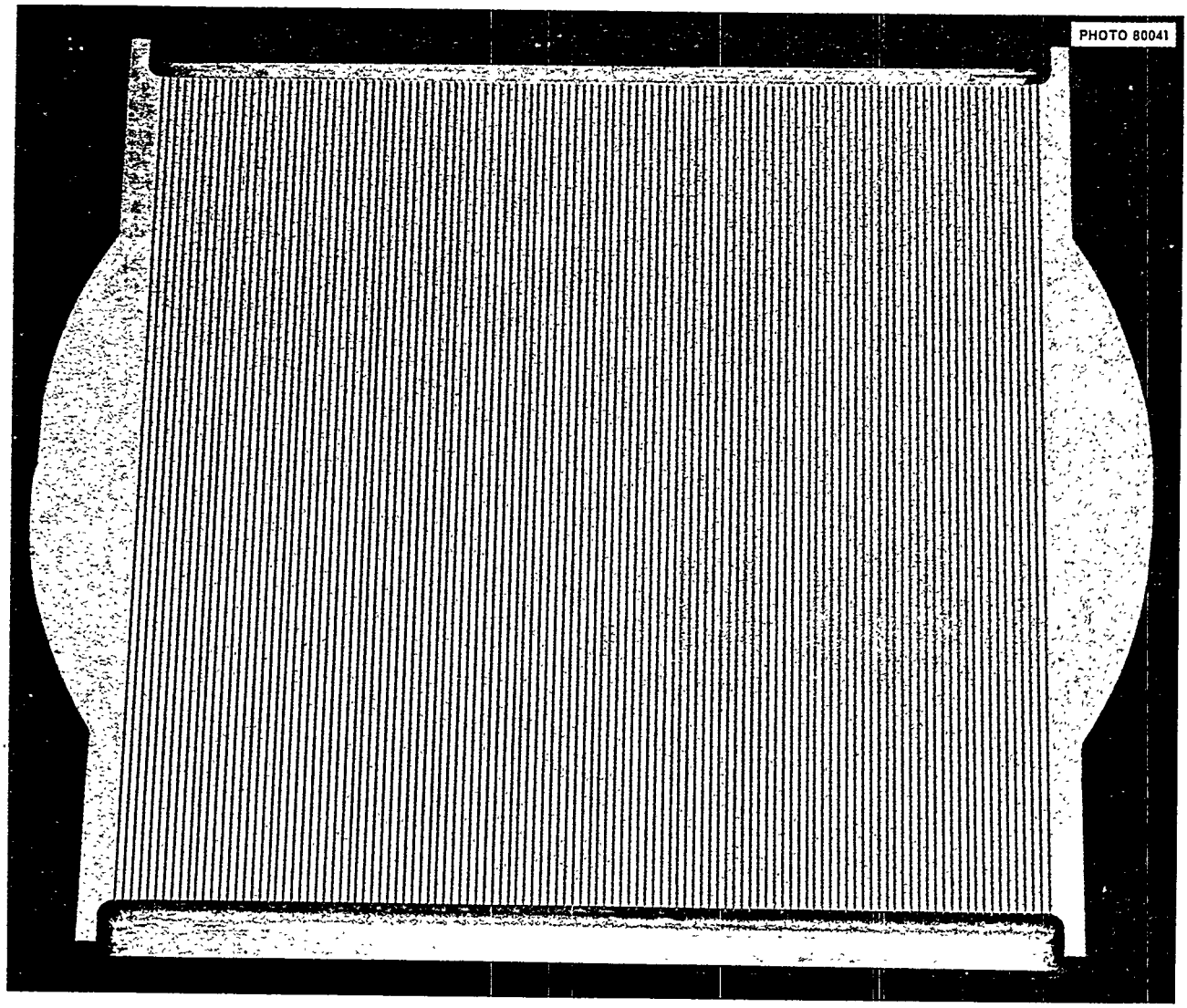

Fig. 21.2. Coolant Channels on $\frac{1}{8}$-in. Centers.

Heat from other components (duoplasmatron ion source, diffusion pump, and vacuum manifold liner) will be 15 kw. Therefore, the cooling system was designed to dissipate 90 kw at an ambient temperature of 38°C. The system utilizes a large (16 ft^2) automotive-type heat exchanger and an axial blower (see Fig. 21.3). Tritium diffuses from targets at a rate which is dependent on the target temperature. An experiment was performed to determine if the rate of release of ^3H from a target is strongly dependent on small changes in the temperature of the coolant. It was learned in this experiment that the relative release rate of ^3H between coolant at 10°C and coolant at 75°C was 36% (see Fig. 21.4). The cooling system was designed to dissipate 90 kw at 38°C ambient with the return coolant at a temperature of about 43°C. Based on results of the experiment, this system was considered adequate.

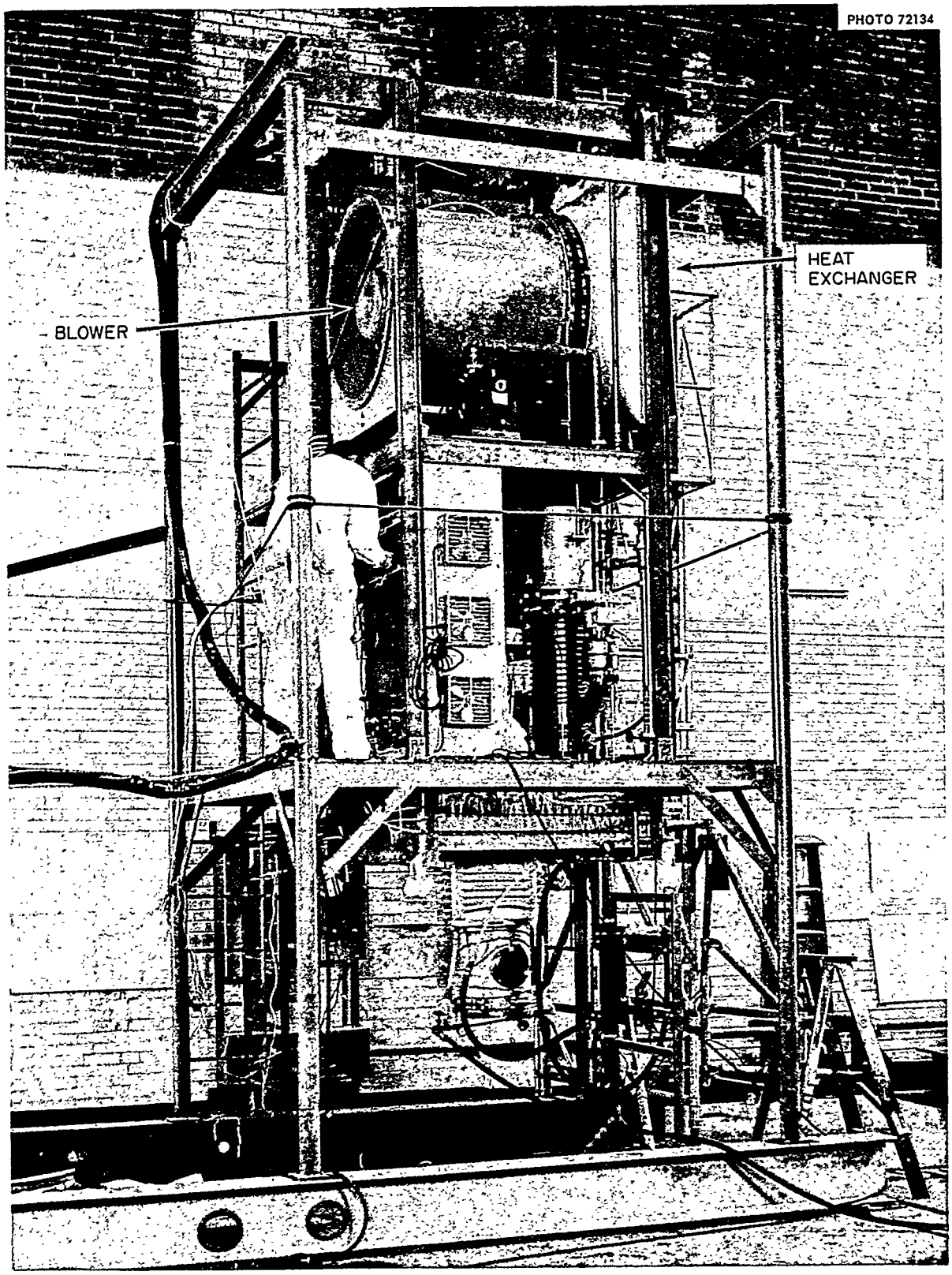

Fig. 21.3. Operation HENRE Testing Stand Showing Cooling System.

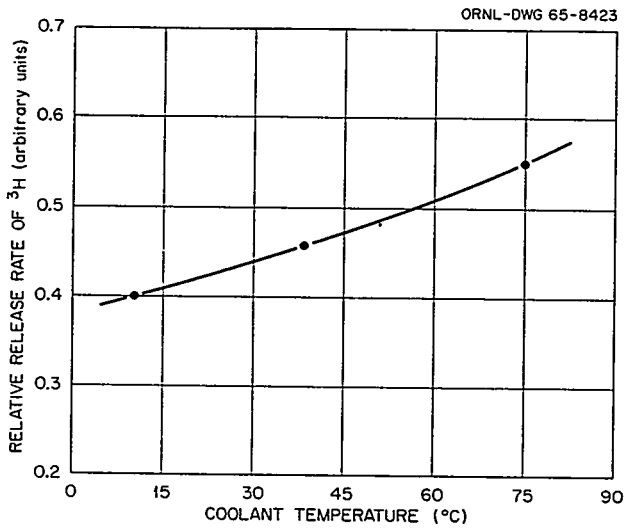

Fig. 21.4. Rate of ^{3}H Release from an ErT_2 Target as a Function of Coolant Temperature.

Neutron Source Status

The neutron source has been assembled on a test stand in the Thermonuclear Division facilities. All systems are complete and final testing is under way. To date, a 500-ma H^+ beam at 150 kw has been run to determine certain final design characteristics associated with suppression of electrons at the target (one or more electrons are released for every H^+ ion impinging on the target). It is necessary to suppress these electrons in order to prevent damage to the ion source filament and extractor electrode due to the sudden "slowing down" of the electrons. Tritium targets will not be used until the source is installed on the tower at the Nevada Test Site (NTS) because of the effect of ^{3}H contamination on packing and shipping and because of a lack of personnel shielding at the test stand location.

Field Experiment Projection

The neutron source will be the primary tool for a large-scale field experiment, designated Operation HENRE (High Energy Neutron Reactions Experiment), which will be conducted at the NTS. The experiment has been planned and organized during this report period. Details of Operation HENRE are given in other reports.[9,10]

The participants of this operation represent a total of 15 different U.S. organizations and representatives from two foreign organizations (see Fig. 21.5). The individual field experiments[9,10] are scheduled to start in early March 1966 and continue through June 1966.

HEALTH PHYSICS RESEARCH REACTOR

Reactor Operations

Health Physics Research Reactor (HPRR) operations during the past year consisted of 50 operations in the burst mode and 200 operations as a steady-state source of neutrons. Power levels for the steady-state exposures ranged from 0.1 w to 8.0 kw with durations from 40 sec to 6.25 hr. Animal irradiations and dosimetry research account for the major portion of the experiments. In addition to the Health Physics Division, users of reactor time included several ORNL divisions, university groups, AEC contractors, other national laboratories, military laboratories and their contractors, and representatives of two foreign nations.

The experiments performed with the HPRR have included a broad spectrum of dosimetry, biological, and reactor physics experiments. Dosimetry research and applications included such experiments as an intercomparison of nuclear accident dosimeter systems with the major USAEC facilities, blood sodium studies in phantoms, and depth dose measurements using a burro cadaver. Some of the more significant radiobiological work included such experiments as a study of the ability of trained primates to perform tasks after being subjected to large doses of neutron and gamma radiation. Genetic studies with mice and central nervous system studies in the burro, the rabbit, and the rat also represented other biomedical experiments of interest. A feasibility study in an attempt to pump a laser to power and measurements of the diffusion time of a burst of fast neutrons through graphite were typical of the physics experiments for which the HPRR was used.

---

[9]F. F. Haywood and J. A. Auxier, *Technical Concept — Operation HENRE*, CEX-65.02 (1965).

[10]Technical Director's Staff, *Operations Plan — Operation HENRE*, CEX-65.03 (ed. by F. F. Haywood *et al.*) (to be published).

ORNL Dwg. 65-7606

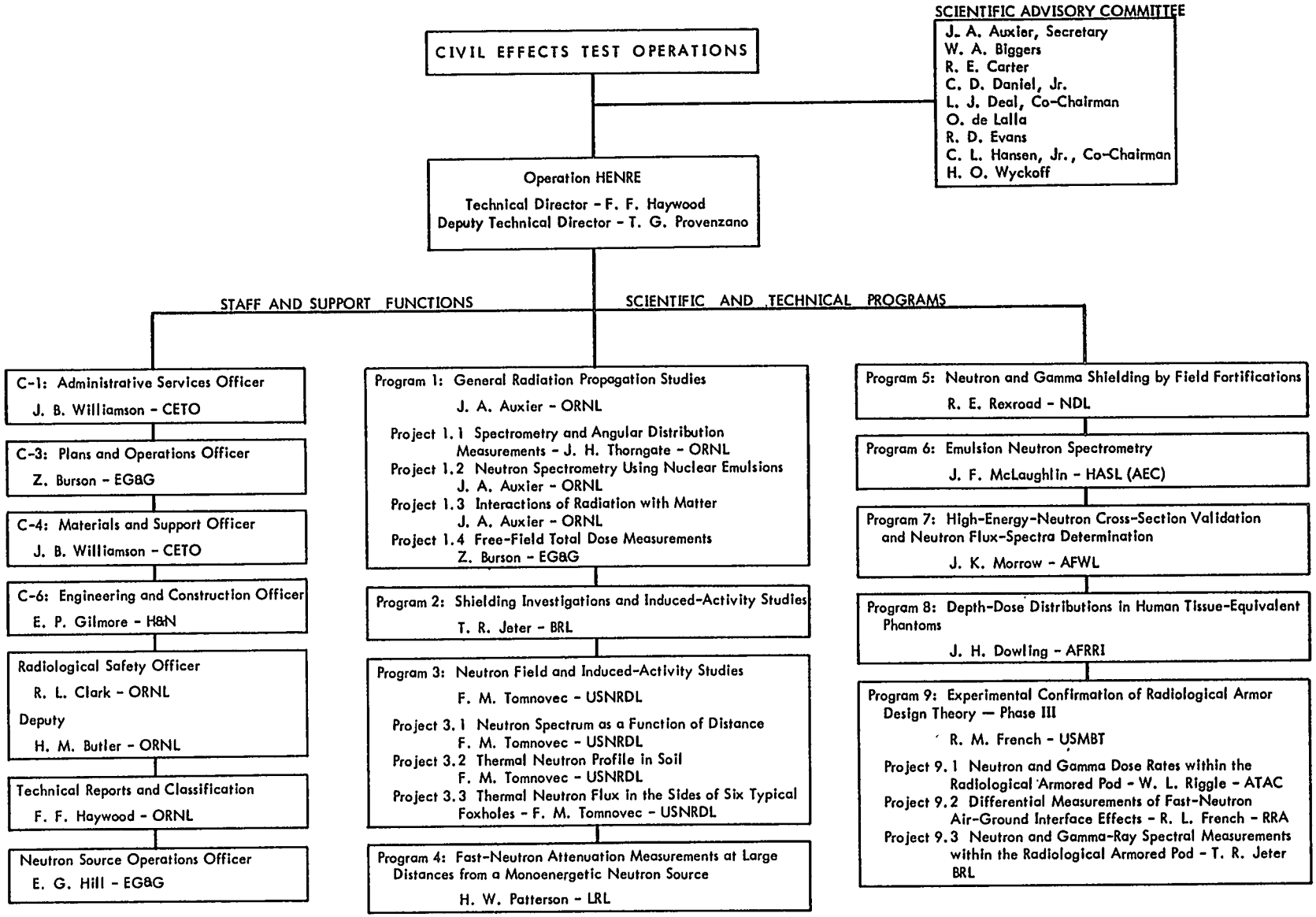

Fig. 21.5. Operation HENRE Organization.

Reactor Investigations

Examination of data obtained in burst experiments has shown a greater variation in yield for a given introduction of reactivity than was expected. A program is being conducted to investigate sources of small errors in the introduction of reactivity and variations in response of the core to a given introduction of reactivity. High-speed camera pictures show that the burst rod bounces at the end of its insertion stroke for about 140 msec, the highest bounce being $^{15}/_{16}$ in. Some bursts occur during this time interval, and when a burst occurs with the burst rod above its inserted position, a burst of reduced yield is obtained. A new burst rod, long enough to protrude $1\frac{1}{8}$ in. outside the core, has been installed so as to minimize the effects of bouncing on the yield. An improved pneumatic system is being developed to reduce the bounce and shock. High-speed camera pictures have also shown that the safety block bounces off its seat for about 160 msec in response to the shock of inserting the burst rod. Again a burst occurring while the safety block is displaced will be of reduced yield. Repeated measurements of changes in reactivity due to withdrawing and reinserting the safety block (a step in the burst procedure) show that errors in repositioning are not significant.

Any additional effects which seem to have the potential of varying the yield will be similarly investigated.

Part V. Internal Dosimetry

W. S. Snyder

22. Internal Dose Estimation

W. S. Snyder
S. R. Bernard
Mary Jane Cook
H. L. Fisher, Jr.[1]
Mary R. Ford

A DOSE ESTIMATE BASED ON STABLE-ISOTOPE DATA

W. S. Snyder

Data on intake and on concentration of stable elements in human tissue have been used in many cases as a check on the adequacy of metabolic models for radioactive isotopes. It is clear that if individuals in the population are supposed to have a nearly constant intake and to be nearly in a state of equilibrium with respect to a given element, then the amounts in grams of the element in the various tissues are a direct measure of average gram-days of residence of the isotope in those tissues for the given level of intake. If a radioactive isotope of this element is taken into the body in similar chemical form, the number of microcurie-days of residence in the tissue will be less than that indicated by the data on the stable isotope because of radioactive decay. However, it is clear that neglect of decay will produce an overestimate of dose rate and that it may be possible to make some correction for the decay. Although all this is quite obvious, the question does not seem to have been treated quantitatively in the literature until quite recently.

Brues and Tyler[2] have discussed the variation of dose and dose rate in a multicompartment system which is in a state of equilibrium. They find that "there is a predictable maximum radiation given by any compartment of any steady-state multicompartment open system in which the 'external' compartment is specified as to its specific activity in time." Marshall has generalized the argument of Brues and Tyler in his discussion of the metabolism of the alkaline earths.[3] However, his discussion applies almost without change for other elements. In the present note a related result is obtained without the assumption of a multicompartment or mammillary system, and the final estimate of dose does not directly involve the rate constants of the various compartments. Thus the present result appears somewhat more general than those mentioned above. On the other hand, the argument presented here demands a knowledge of the daily intakes and of the mean concentrations in the organs involved of a stable isotope of the radionuclide in question. In this sense, the argument may be more special than that of Brues and Tyler or that of Marshall.

Assume an individual is taking in a stable element E and is in a state of equilibrium with respect to this element, and consider that this individual takes in an amount A (in microcuries) of a radioactive isotope of E, the latter being designated by E*. It is assumed that E* enters the body by the same route as does the stable element E and that the chemical forms of E and E* are similar or, preferably, identical. If this is the case, one can expect that E and E* will metabolize in similar or identical fashion. It is desired to estimate the total dose delivered to an arbitrary tissue T of mass M in the body of this individual. The tissue in question need not be a complete organ or physiological entity. For example, one may choose it to be the lower third of the heart,

[1] U.S. Public Health Service.

[2] A. M. Brues and S. A. Tyler, *Atompraxis* 5, 253 (1959).

[3] J. H. Marshall, *J. Theoret. Biol.* 6, 386 (1964).

or the tissue in a sphere with its center at the center of gravity of the body and radius 5 cm, etc.

Let $R(t)$ be the retention function for element E in tissue T, that is, if 1 g of stable element E is taken in at time 0, then t days later, $R(t)$ g of element E is present in tissue T. Since the route of entry and chemical form in which E is encountered are assumed to be similar or identical to those for E*, the same function $R(t)$ describes the fraction of an intake of E* which is present in tissue T, t days following intake, corrected for radioactive decay.

The total microcurie-days accumulated in T during the first L days following exposure due to the intake of A μc of E* is given by

$$A \int_0^L R(t) e^{-\lambda t}\, dt \text{ microcurie-days} , \quad (1)$$

where λ is the radioactive decay constant for E*. The dose delivered to tissue T during these L days is then

$$D_L = \frac{A \int_0^L R(t) e^{-\lambda t}\, dt \times 3.2 \times 10^9 \times \mathcal{E} \times 1.6 \times 10^{-8}}{M} \text{ rads} , \quad (2)$$

where

3.2×10^9 = dis day^{-1} μc^{-1},

$\mathcal{E}$ = energy (Mev) absorbed in T per disintegration of E*,

1.6×10^{-8} = gram-rad/Mev, and

M = mass of tissue T in grams.

In many cases, $R(t)$ is not known or is not known very precisely.

If the hypothetical individual is taking in I g of stable element E per day, then, at equilibrium, tissue T should contain $\int_0^\infty R(t)\, dt$ g of element E. The integration over an infinite range is purely symbolic, and one may substitute any finite number of days, say L days, for infinity, provided L is so large that equilibrium is attained effectively within L days. Mathematically, this means that $\int_0^L R(t)\, dt$ and $\int_0^\infty R(t)\, dt$ are effectively equal. That is, L must be specified as a number of days so great that the individual will be effectively in equilibrium when maintained on a constant daily intake of E for a period of L days.

With L so specified, the equilibrium concentration of stable element E in tissue T is given approximately by

$$C = I \int_0^L R(t) \frac{dt}{M} \frac{\text{grams of E}}{\text{grams of } T} . \quad (3)$$

One may solve (3) for M and substitute in (2), obtaining

$$D_L \cong \frac{51\, A\mathcal{E}C}{I} \times \frac{\int_0^L R(t) e^{-\lambda t}\, dt}{\int_0^L R(t)\, dt} \text{ rads} . \quad (4)$$

From (4) one has the immediate overestimate of dose

$$D_L \leqq \frac{51\, A\mathcal{E}C}{I} \text{ rads} . \quad (5)$$

The estimate will be of most interest when E* has a radioactive half-life which is long compared with the time for an individual to reach effective equilibrium, that is, long compared to L days. Under these conditions $e^{-\lambda t} \sim 1$ for $0 < t < L$, and the estimate in (5) should be a good approximation to the actual dose.

As a first application of this result, consider the exposure of an infant to ^{90}Sr. Comar[4] has suggested that in early infancy the bone is remodeling rapidly and that effective equilibrium on a steady diet should be reached in a matter of a few weeks or perhaps a month. The infant is growing during this period, and doubtless a true and precise state of equilibrium is not attained. However, growth during a month usually would not be so great as to be a considerable factor in dose estimation, and we may suppose that there is a state of transient equilibrium. Applying formula (5), one finds that an intake of 1 μc of ^{90}Sr in a very young infant would produce an estimated dose to bone of 1.7 rads. This estimate is obtained by using

$\mathcal{E}$ = 1.1 Mev,[5]

$C = 1.5 \times 10^{-5}$ = concentration of stable Sr in infant bone,

$I = 5 \times 10^{-4}$ g = daily intake of stable Sr by the infant.

---

[4] C. L. Comar *et al.*, *Health Phys.* 11, 609 (1965).

[5] *ICRP Publication 2*, Pergamon, Oxford, 1964.

The value of C is found by assuming that the skeleton of the one-year-old child contains 100 g of Ca and weighs 1.30 kg and by using the value 200 μg of Sr per gram of Ca in the skeleton obtained from ref. 6. The value of I is taken from ref. 7. This estimate is somewhat lower than a similar estimate given by Rivera.[8]

If formula (5) is applied for an adult, one obtains

$$D_L = 2.8 \text{ rads per microcurie of intake .}$$

This value is obtained by using

$$C = 5 \times 10^{-5} \text{ g of Sr per gram of bone,}^{9}$$

$$I = 10^{-3} \text{ g of Sr per day .}^{7}$$

The use of (5) for the adult is questionable since the very long retention time of Sr in adult bone, while not known with precision, may not be long compared to the 28-year radioactive half-life of ^{90}Sr. Thus the exponential factor $e^{-\lambda t}$ in (5) may be significantly less than 1 during a part of the residence time. Putting this another way, (5) neglects the effect of radioactive decay and thus may produce an overestimate of D_L. According to the ICRP rule,[10] a yearly intake of ^{90}Sr will produce a dose of 30 rems or, equivalently, of 6 rads over the ensuing 50 years. Using the latest MPC value recommended by ICRP of 4×10^{-6} μc/cc for continuous occupational exposure by ingestion, a yearly intake is found to be 3.2 μc. Thus, 1 μc of intake should, by this rule, deliver 2 rads to bone. It is gratifying that the estimate from (5) is so close and that it is high as would be expected.

Finally, the case of an intake of $^1H^3HO$ will be discussed. In the 1964 annual report[11] a human exposure was reported for which $R(t)$ seemed to involve two exponentials. This suggests that some tissues other than the body water are involved and may accumulate a greater dose than that received by body water. According to (5), any tissue T would receive a total dose of 1.8 rads per microcurie of intake. This is obtained by assuming

$$C = 0.1 \text{ g of H per gram of soft tissue,}$$

and

$$I = 2500 \text{ g of } H_2O \text{ per day,}$$

which is equivalent to 278 g of H per day. The value of I is probably an underestimate since some hydrogen will be taken in with the solids of the diet. This is essentially the same as the dose to body water. In fact, all soft tissues for which data have been found show a concentration of hydrogen close to 10% and thus have essentially the same dose according to (5). The concentration of hydrogen in bone is approximately 5%, and thus bone should receive a smaller dose. Tritium is, perhaps, the isotope least favorable for this type of estimation. The ratio of the masses of ^{3}H and ^{1}H is far greater than in the case of other isotopes, and so it is questionable as to how nearly the retention function for ^{1}H corresponds to the retention function for ^{3}H. The argument assumes ^{1}H and ^{3}H have the *same* retention function in the body when they are taken in as H_2O or $^1H^3HO$ respectively. No doubt there are differences in the metabolism of ^{1}H and ^{3}H, but it does not seem easy to obtain an indication of the degree of disparity that might exist. Except for this factor, (5) yields essentially the same estimate for all tissues. In the case of other elements where this difference in mass ratio is much smaller, one may use (5) with more confidence. However, even for tritium it seems unlikely that the retention would differ by orders of magnitude, and thus (5) may serve to allay any fears that some tissue might receive a dose which is orders of magnitude greater than the dose to body water.

---

[6] Medical Research Council, *Assay of Sr^{90} in Human Bone in the United Kingdom Results for 1963, Part II*, H. M. Stationery Office, London, 1964.

[7] F. J. Bryant and J. F. Loutit, *Human Bone Metabolism Deduced from Strontium Assay*, AERE-R3718 (1961).

[8] Joseph Rivera, *Second AEC Conference on Radioactive Fallout from Nuclear Weapons Tests, Germantown, Maryland, Nov. 3–6, 1964*, CONF-765 (1965), paper No. 7.

[9] Derived from ref. 5.

[10] *ICRP Publication 6*, Pergamon, London, 1959.

[11] *Health Phys. Div. Ann. Progr. Rept. July 31, 1964*, ORNL-3697, p. 173.

A COMPUTER CODE FOR ESTIMATION OF BODY BURDEN OF ^{90}Sr BASED ON OBSERVED RATIO AND BONE REMODELING WHICH ARE AGE DEPENDENT

H. L. Fisher, Jr. W. S. Snyder

The principal concern in occupational exposure to internal ionizing radiation is with adult man. However, in extending the concept of radiation protection to a population consisting of people of all ages, one is faced with additional problems. For an adult, many of the physiological parameters such as body weight, water intake, and absorption or uptake of an element into an organ may be considered practically constant with time. It is not always possible to use such simplifying assumptions for the general population. Obviously, the weight of a person and his water intake change considerably from birth to adulthood. The model presented below is an initial attempt at using some of the primary age-dependent parameters in an effort to estimate the dose rate to the skeleton from the oral ingestion of ^{90}Sr.

If the skeletal burden of ^{90}Sr, $S(t)$, and the weight of the skeleton, $W(t)$ (see Fig. 22.1), as a function of age are known, then the average dose rate over the skeleton is

$$D(t) = \frac{k\ S(t)}{W(t)},$$

where k is a constant. Langham and Anderson[12] first described a materials-balance method for finding $S(t)$. A first-order, linear, differential materials-balance equation for estimating the skeletal burden of ^{90}Sr as given by Kulp[13] is

$$\frac{d}{dt}S(t) = -\left[\lambda_r + f(t)\right]S(t) + K(t)\,Z(t)\left[f(t)\,\mathrm{Ca}(t) + \frac{d}{dt}\mathrm{Ca}(t)\right],$$

where

$S(t)$ = the skeletal ^{90}Sr burden,

λ_r = the ^{90}Sr radiological decay constant,

$f(t)$ = the calcium bone turnover rate,

$K(t)$ = the $(^{90}\mathrm{Sr/Ca})_{\mathrm{bone}}/(^{90}\mathrm{Sr/Ca})_{\mathrm{diet}}$,

$Z(t)$ = the $(^{90}\mathrm{Sr/Ca})$ in the diet, and

$\mathrm{Ca}(t)$ = the calcium content of the skeleton.

Mitchell[14] has given values for $\mathrm{Ca}(t)$ (see Fig. 22.1), and Rivera[15] has used measured values of $Z(t)$ and $S(t)$ to estimate the functions $f(t)$ and $K(t)$. These functions are graphed in Fig. 22.2.

The equation was coded for computer solution for $S(t)$, assuming inputs for $Z(t)$ are given. Before computer solution, however, the equation was converted to a difference equation. The stop interval was one month during 0 to 2 years, three months during 2 to 24 years, and one year from 24 to 70 years. Results for the cases of a constant ^{90}Sr concentration in water, of a one-month exposure to an arbitrary ^{90}Sr concentration in milk, and of a constant daily intake of ^{90}Sr for a period of one month are presented in Figs. 22.3–22.5. Results for an exposure to the calculated ^{90}Sr concentrations in Clinch River water were also obtained.

---

[12] W. H. Langham and E. C. Anderson, *Science* 126, 205 (1957).

[13] J. L. Kulp, *Radioactive Fallout from Nuclear Weapons Tests, Proceedings of a Conference Held in Germantown, Maryland, Nov. 15–17, 1961*, TID-7632 (1962), book 2, p. 457.

[14] H. H. Mitchell *et al.*, *J. Biol. Chem.* 158, 625 (1945).

[15] Joseph Rivera, *Second AEC Conference on Radioactive Fallout from Nuclear Weapons Tests, Germantown, Maryland, Nov. 3–6, 1964*, CONF-765 (1965), paper No. 7.

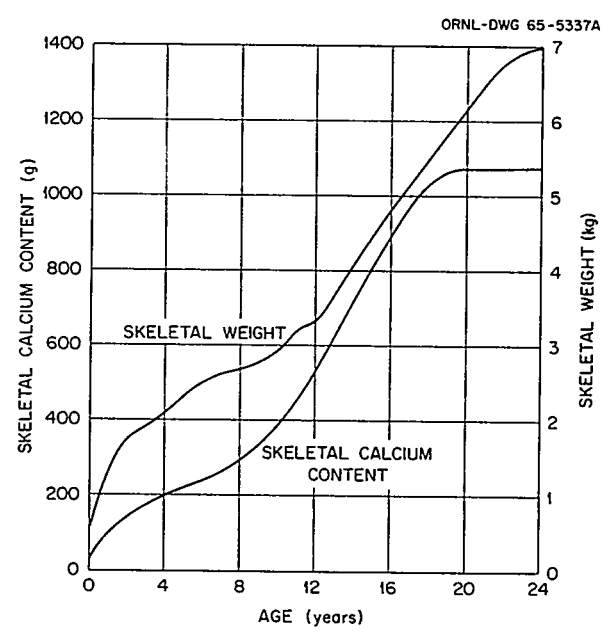

Fig. 22.1. Parameters for Strontium Bone Burden Model (Weight).

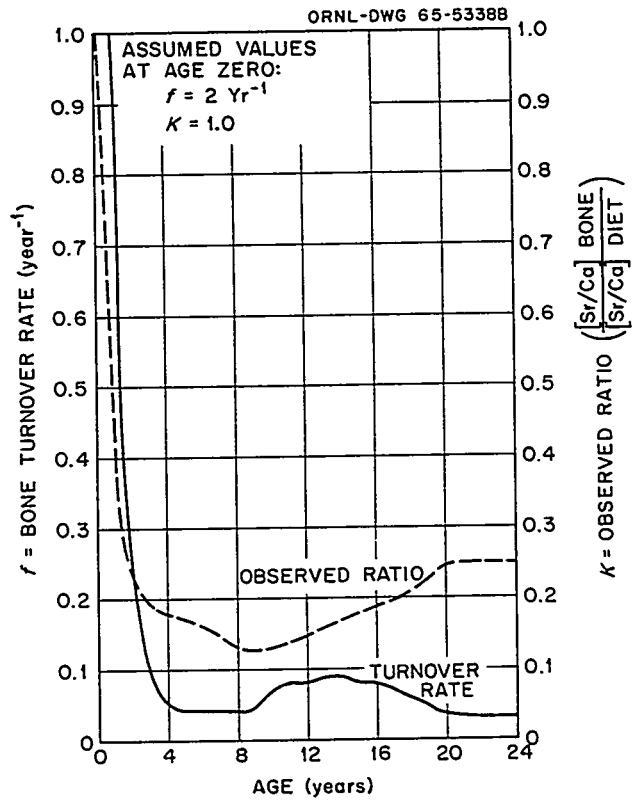

Fig. 22.2. Parameters for Strontium Bone Burden Model (Observed Ratio).

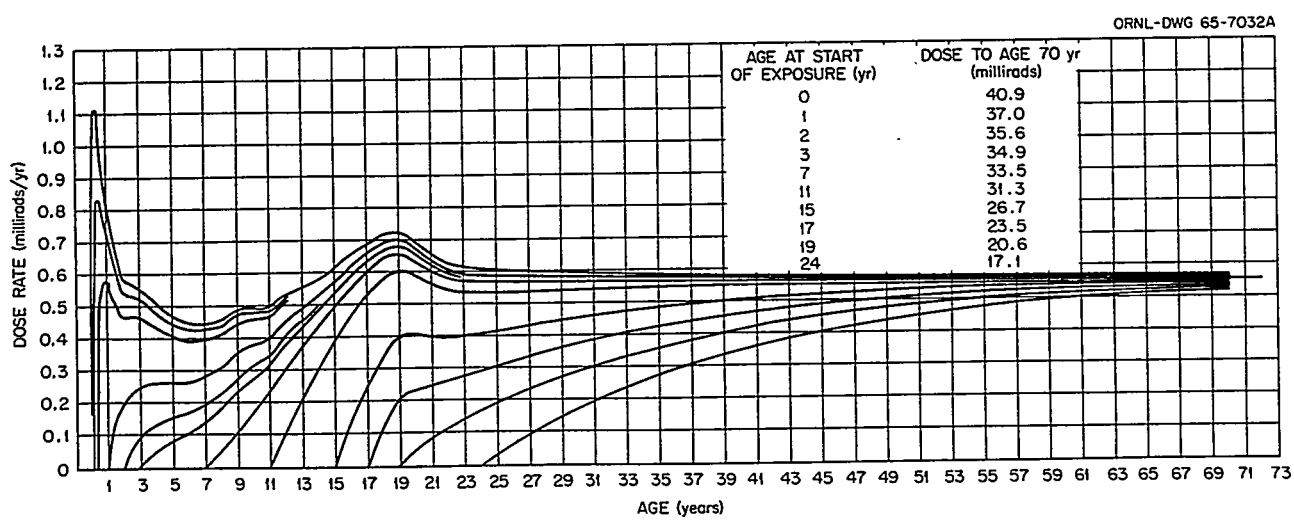

Fig. 22.3. Dose Rate to the Skeleton from a Constant Exposure of 1 pc of ^{90}Sr per Liter of Water.

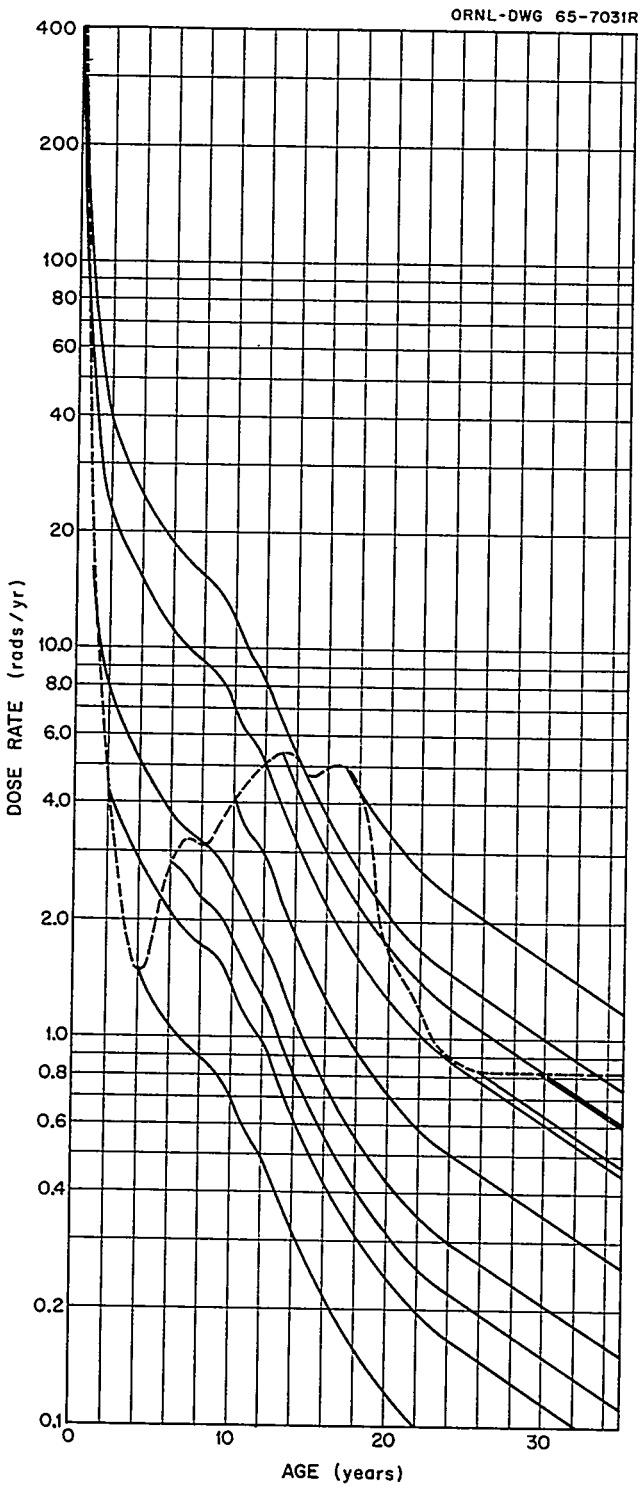

Fig. 22.4. Dose Rate to the Skeleton from a 1-month Exposure to 1 μc of ^{90}Sr per Liter of Milk at Various Ages.

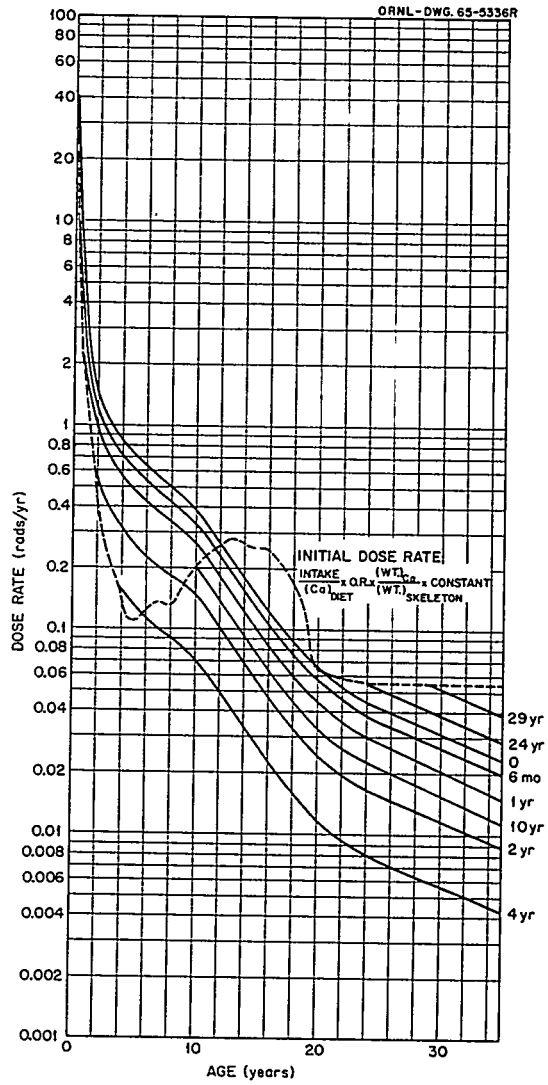

Fig. 22.5. Dose Rate After Oral Intake of 1 μc of ^{90}Sr for 1 Month at Indicated Age.

AGE DEPENDENCE OF THE BIOLOGICAL HALF-LIFE OF IODINE AND CESIUM IN MAN

Mary Jane Cook W. S. Snyder

Until the 1959 Report of the Subcommittee on Permissible Internal Dose of the NCRP[16] and the 1958 Recommendations of the ICRP,[17] the radiation

[16] "Maximum Permissible Body Burdens and Maximum Permissible Concentrations of Radionuclides in Air and Water for Occupational Exposure," *Natl. Bur. Std. (U.S.), Handbook 69*, GPO, Washington, 1959.

[17] Recommendations of the International Commission on Radiological Protection, *ICRP Publication 2, Report of Committee II on Permissible Dose for Internal Radiation (1959)*, p. 151, Pergamon, London, 1959.

worker had been, in general, the primary concern for radiation protection, and relatively little attention had been focused on the exposure of the population at large. In these reports some general guidance was given pertaining to the exposure of the population, but this was not very detailed. Since that time, data from many sources have been assembled to estimate such age-dependent factors as the intake of milk, water, fat, carbohydrates, proteins, etc.; the total body and organ weights; and chemical composition of the total body or of various organs. These biological factors are utilized in constructing metabolic models which may be used in calculating MPC and body-burden values.

Iodine is one example in which a metabolic rate is found to be age dependent. In Fig. 22.6 are presented the change in concentration of iodine in the thyroid with age, the change in the weight of the thyroid with age, the daily intake of stable iodine as estimated from standard diets, and an indication of the fraction of iodine going to the thyroid. For adults the metabolic model for retention of iodine in the thyroid is represented adequately

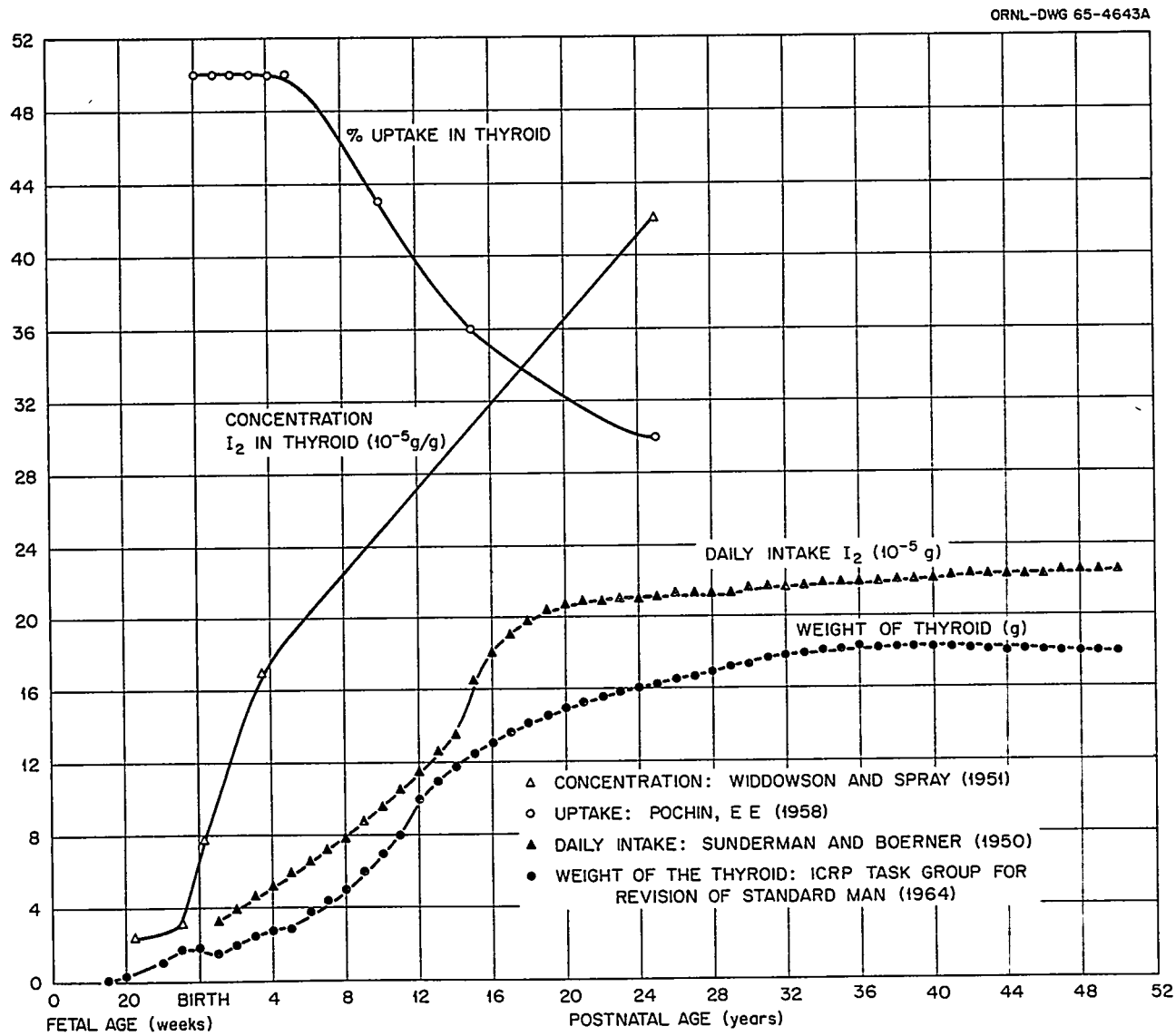

Fig. 22.6. Change in Metabolic Rate of Iodine.

by a single exponential. The exponential model predicts an equilibrium concentration

$$\frac{If_w T_b}{W \ln 2} = c ,$$

where I is the daily intake in grams, f_w is the fraction going to the thyroid, T_b is the biological half-time in days for elimination from the thyroid, and W is the weight of the thyroid in grams. Using the above data, the biological half-life of iodine in the thyroid is seen to be age dependent. This age-dependent biological half-life is presented in Fig. 22.7. For comparison, values measured by Van Dilla, Bernard, Ogborn, and Morrison are shown. Although the data used to obtain this estimate are not highly accurate, the indicated age dependence is so large that the existence of an age effect can scarcely be doubted. The actual values shown are not likely to be very accurate.

It has been estimated that approximately 85% of the ^{137}Cs enters the body through the intake of milk, and retention in the body is largely of the single-exponential type. By using the same exponential model as for iodine, the biological half-life for cesium is seen to be age dependent. In this case, the intake of milk is used rather than water and the total body weight rather than the thyroid weight for W. These biological half-lives are presented in Fig. 22.8. For comparison, measurements are included on Japanese, Laplanders, Swedes, and other nationalities. Using excretion data, rather than intake data, C. W. Mays, Jr.,[18] also has found that the biological half-life for cesium varies with age, and his data agree reasonably well with these presented.

[18] R. C. Pendleton, C. W. Mays, *et al.*, "A Trophic Level Effect on ^{137}Cs Concentration," submitted to *Health Physics* for publication.

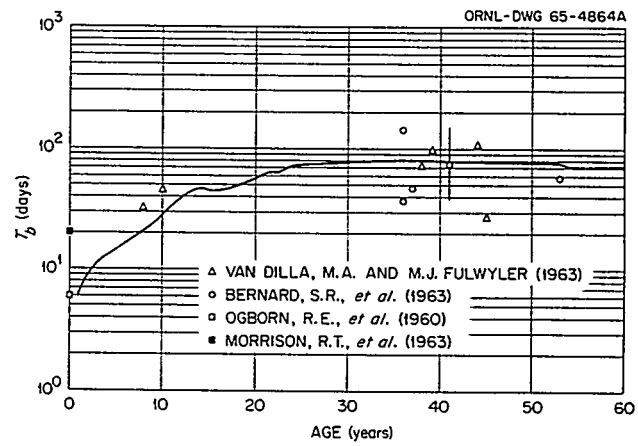

Fig. 22.7. Variation of Biological Half-Life for Iodine with Age.

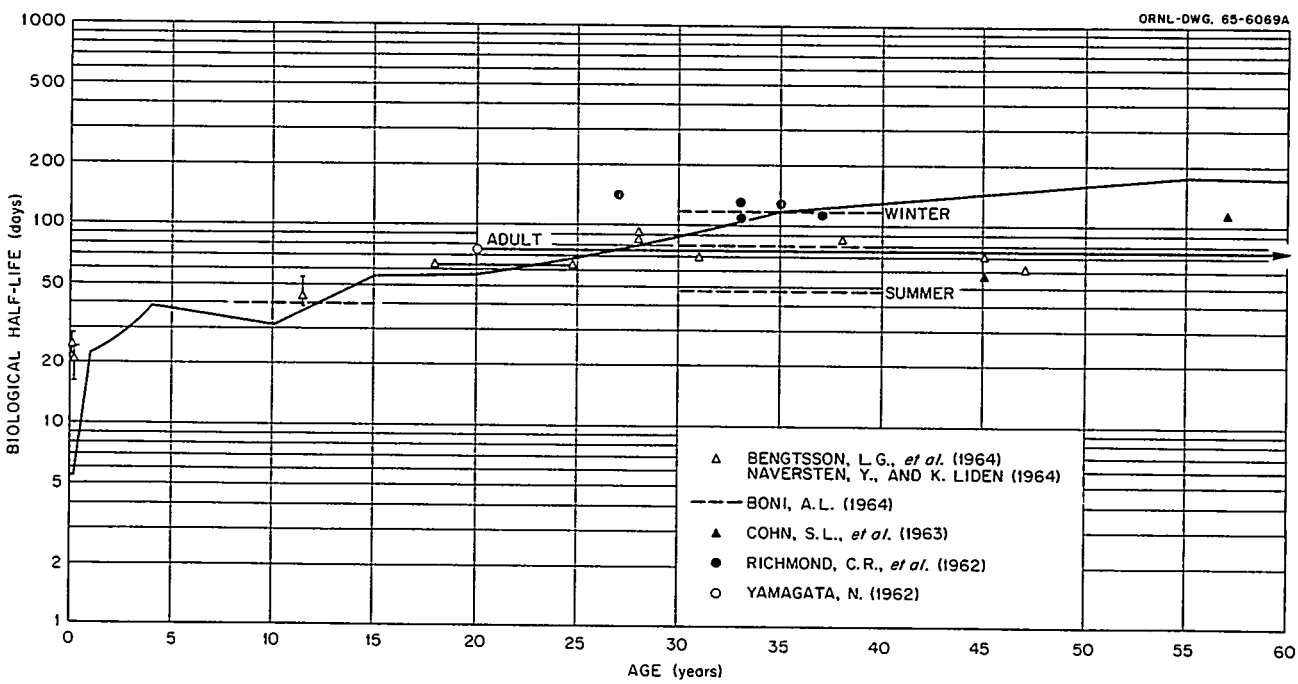

Fig. 22.8. Variation of Biological Half-Life for Cesium with Age.

From these and similar calculations, one will be able to calculate exposures for each age group of a population rather than use such interim rules as set forth in 1958 and 1959 by the ICRP and NCRP.

A MONTE-CARLO CODE FOR ESTIMATION OF DOSE FROM GAMMA-RAY SOURCES

W. S. Snyder Mary R. Ford

A Monte-Carlo-type program for estimating dose from gamma-ray sources has been designed so that the gamma dose can be estimated for a wide variety of exposure situations. The source subroutine can be rewritten to suit the specific problem but must deliver photons on demand, specifying energy, the coordinates of the point in the phantom where they enter or originate, and a direction of propagation. Thus the source may be exterior to the phantom or within the phantom. In particular, the source may be photons produced by neutrons undergoing the (n,γ) process within the phantom. To improve on the statistics, the photons are never absorbed, although they may escape from the phantom. Each photon is assigned a weight of 1 in starting, and the weight is reduced following each interaction by multiplying by the ratio of the cross section for Compton scattering to the total cross section. This improves the statistics, since photons have a better chance to reach distant portions of the phantom.

Cross sections are taken from *NBS Circular 583* and its supplement and are programmed on a separate subroutine. The energy scale is divided into major regions, each major region corresponding to a decrease of the energy by one-half. Values of the cross sections are listed on magnetic tape at 64 energy values intercalated in each such major region. The machine uses the cross sections corresponding to the nearest listed energy on the magnetic tape. Only the cross sections for the photoelectric effect, for pair production, and the total cross section are listed, the cross section for Compton scattering being obtained by subtraction.

Preliminary results concerning a particular case of some interest for clinical practice are shown in Fig. 22.9. Neohydrin, a compound of mercury, is known to concentrate in the cortex of the kidney, and thus neohydrin labeled with radioactive mercury is often used in scanning procedures. C. C. Harris of ORNL asked us to consider this case and attempt to estimate the dose from ^{203}Hg to the cortex, to the medulla, and to various other regions of the body, particularly the ovaries. We acknowledge his advice in designing the model shown schematically here. The body is taken as a homogeneous right circular cylinder with the composition of standard man and with dimensions in centimeters as shown. Each kidney is simulated by an ellipsoid with a wedgelike indentation, and each has a mass of 87 g. The cortex consists of the outer shell of this ellipsoid with a thickness of 1 cm. The ovaries are represented by the two spheres below the kidneys, the thyroid by the thin cylinder at the top of the phantom, and the sphere between the kidneys might be a portion of the gastrointestinal tract.

Mercury-203 is assumed to be present only in the cortex of the kidney and to be uniformly distributed there with an assigned activity. The starting subroutine selects a point at random in the cortex and also produces a random direction for the photon.

Five planes have been inserted between the ovaries and the kidneys and five below the ovaries. These planes define "splitting regions." To each splitting region a weight standard is assigned. If a photon has a collision in a splitting region, its weight is compared to the weight standard for that region. If the photon's weight is greater than the weight standard, it is replaced by two photons, each having a statistical weight one-half that of the parent. The weight standards are chosen so that the probability of splitting is greatest for photons close to the ovaries. By such a technique, enough low-energy photons arrive at the ovaries to give good statistical accuracy on the estimate of dose to these organs.

The dose rate in rads hr^{-1} mc^{-1} corresponding to the 0.280-Mev gammas of ^{203}Hg is given in the margin of the figure for the simulated organs of interest. Mercury-203 decays to stable ^{203}Tl by emitting 0.208-Mev beta particles followed by the emission either of 0.280-Mev gammas or of conversion electrons and resultant x rays and Auger electrons from the electron shells.[19] The gamma rays occur in 82% of the disintegrations. Thus

[19] *Nuclear Data Sheets*, prepared by the Nuclear Data Group, ORNL.

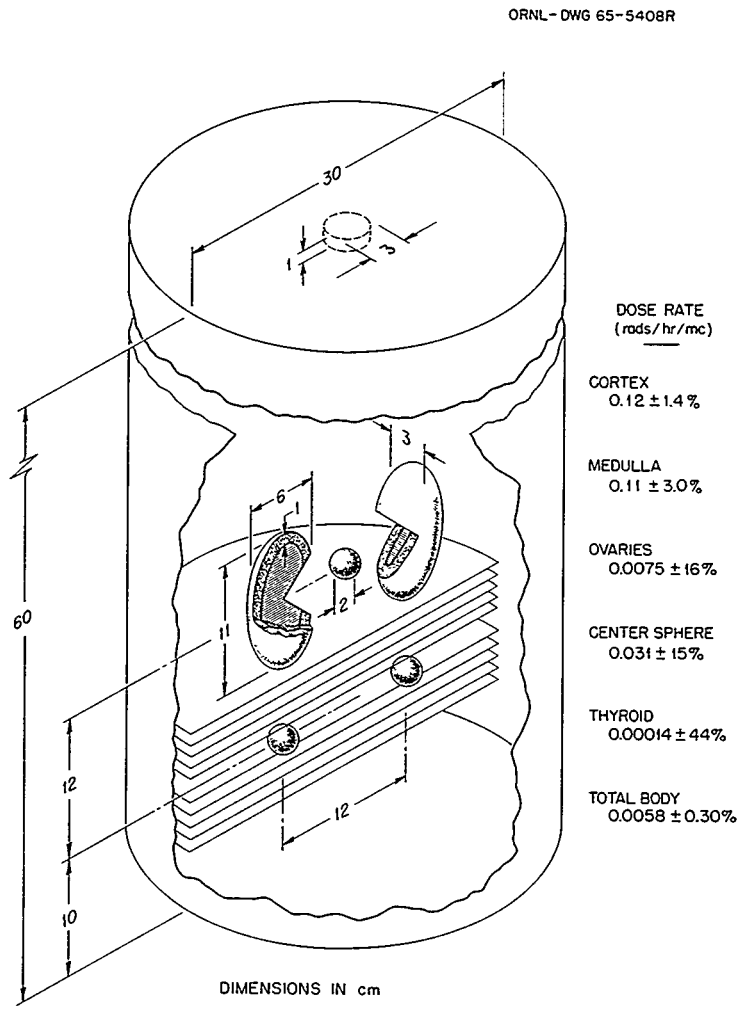

Fig. 22.9. Model for Estimation of Dose to Ovaries from ^{203}Hg Therapy.

the doses given in the figure are the contributions from the 82%, 0.280-Mev gammas of ^{203}Hg located in the cortex of the kidneys. The total dose would include the gamma contributions given in the figure, plus contributions from the 0.208-Mev betas, conversion electrons, x rays, and Auger electrons. The contribution of the x rays, electrons, and betas to the dose is very small except in the case of the kidney itself, where this contribution to the dose is readily evaluated by conventional methods.

The standard deviation for each value in the figure as a percentage of the mean dose is also shown, that is, the coefficient of variation is given. Although the ovaries receive a much smaller dose than the center sphere, they are estimated with essentially the same accuracy. The fact that the coefficient of variation is nearly the same in the two cases is attributed to the use of the splitting technique in estimating the dose to the ovaries.

After this code was completed, it was found that Ellett and Brownell[20] had designed a basically

[20] W. H. Ellett, A. B. Callahan, and G. L. Brownell, *Brit. J. Radiol.* 37, 45 (1964); "Gamma-Ray Dosimetry of Internal Emitters, Part II. Monte Carlo Calculations of Absorbed Dose from Uniform Sources," to be published in *The British Journal of Radiology*.

similar code and reported on a number of cases of interest to internal dose. Comparison of results obtained with these codes is under way. The present code offers somewhat more flexibility in programming the source and target regions and also allows for splitting, which enables one to estimate the dose at rather large distances from the source. We intend to use this code to estimate the dose to a variety of organs for many of the exposure situations of interest.

While the authors are responsible for the basic design of the program, the coding and running of the code on the CDC 1604-A computer have been the responsibility of Al Craig of the Mathematics Division. His efficient work is gratefully acknowledged.

AN AGE-DEPENDENT MODEL FOR ^{90}Sr METABOLISM

S. R. Bernard

The purpose in this section is to develop an age-dependent model for estimation of internal exposure to ^{90}Sr. The model developed here is almost identical to and can be considered an extension of that employed by Kulp[21] and by Rivera[22] and originally proposed by Langham and Anderson.[23] These investigators arrived at their model from physiological considerations of the accumulation of Ca in the growth of the skeleton. The approach employed here is to modify the single-exponential metabolic model used by ICRP and NCRP in the case of continuous exposure of adults. The parameters in that model are assumed to be age dependent and are based on data on physiological growth. Insight on how to modify the model is gained from consideration of experimental data on dogs which were administered single injections or fed ^{90}Sr chronically from birth to 500 days of age. The models of Kulp and Rivera are not continuous, that is, they compute levels in the body at discrete periods of time and for discrete intakes. Their model can be made continuous, as will be shown later, and a comparison with the present model is made later in this report. We also mention that there is some advantage in having a continuous-type model since one can estimate maxima and minima simply (provided they exist). Also, analytical methods permit an estimate of what intake as a function of time and age is required to result in the same body burden of ^{90}Sr (which delivers a constant dose rate throughout life) for any aged member of the population. This has important application in a civil defense situation when one has a limited supply of uncontaminated (canned) foods available, together with contaminated foods. Thus some estimate of that age group which should eat a larger proportion of an uncontaminated diet can be made with the model.

We begin by employing the standard metabolic model approach mentioned above and compare the estimates made from this model with Kulp's 1960 measurements on bones. In this model let $R_c(t)$ denote the microcuries of ^{90}Sr in bone for a continuous intake of $I(t)$ μc of ^{90}Sr per day, $R_s(t)$ the fractional retention in the body for a single intake, and f_w the fraction going from the gut into the body. It can be shown that

$$R_c(t) = f_w \int_0^t I(\tau)\, R_s(t-\tau)\, d\tau. \qquad (1)$$

Here t is the time over which the intake occurs. Denote the weight of Ca in the body by $W(t)$. We use the data of Mitchell *et al.* for $W(t)$,[24] and for $I(\tau)$ we employ the data cited by Kulp, which are shown plotted in Fig. 22.10. On the ordinate is plotted the picocuries of ^{90}Sr per gram of Ca in the milk, and on the abscissa is the year in which this measurement was made, the zeroth year being 1953 (see top of graph). A straight line has been drawn through the points to approximate the measured values. Its equation is

$$\frac{\text{picocuries of } ^{90}\text{Sr}}{\text{grams of Ca}} = 2x \ (x \text{ in years}) . \qquad (2)$$

Now, assuming an intake of 365 g of Ca per year (which might be too high by a factor of 2 for infants), then

$$I(x) = 730 \times \frac{\text{picocuries of } ^{90}\text{Sr}}{\text{year}} . \qquad (3)$$

---

[21] As cited in *Radioactive Fallout from Nuclear Weapons Test, Proceedings of a Conference Held in Germantown, Maryland, Nov. 15–17, 1961*, TID-7632 (1962), p. 470.

[22] Joseph Rivera, *Second AEC Conference on Radioactive Fallout from Nuclear Weapons Tests, Germantown, Maryland, Nov. 3–6, 1964*, CONF-765 (1965), paper no. 7.

[23] W. H. Langham and E. C. Anderson, *Science* 126, 205 (1957).

[24] H. H. Mitchell *et al.*, *J. Biol. Chem.* 158, 625 (1945).

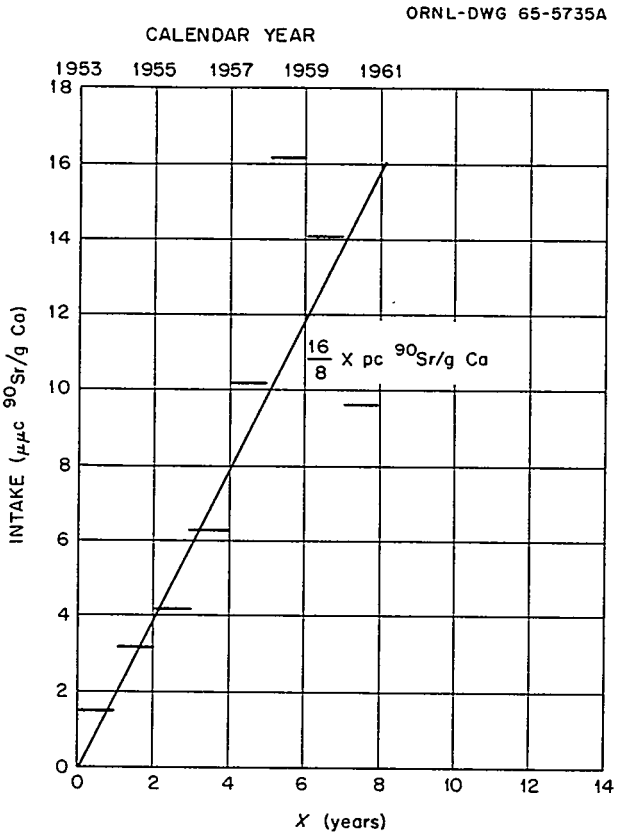

Fig. 22.10. Average Yearly Levels of ^{90}Sr in American Milk for Years 1953–61 (Data from Kulp).

For $R_s(t)$ we use the function suggested by Snyder *et al.*,[25] that is,

$$R_s(t) = 0.73e^{-0.693t/0.008} + 0.10e^{-0.693t/0.12} + 0.17e^{-0.693t/11}, \quad (4)$$

where t is in years. For f_w we take the value of 0.3 cited in the ICRP report. Before we insert the above data into the equation and calculate the burden, we have to modify Eq. (1) to apply to children whose age is less than seven years in the 1960 calendar year. These children were born in the interval calendar years of 1953 to 1960. They had an initial body burden at birth acquired during intrauterine life. We denote this by R_{bx}, where x is the number of years measured from the calendar year of 1953, which is taken to be the zeroth year for fallout exposure to begin. Also, the input function has to be modified to take into consideration the fact that the individual who is t years of age in 1960, where $0 \leq t \leq 7$, received an intake in the interval from $7 - t$ to t years. To modify Eq. (1) such that these factors are accounted for, we write

$$R(t) = R_{bx}\, R_s(t) + f_w \int_0^t I(\tau + 7 - t)\, R_s(t - \tau)\, d\tau, \quad (5)$$

where $0 \leq t \leq 7$ and where we have assumed that the retention function for ^{90}Sr is age independent, for example, any ^{90}Sr acquired during intrauterine life would follow the same retention function $R_s(t)$ as for adults. Admittedly, these assumptions are crude, but these calculations are made to see how great the difference is between the estimated and measured levels.

To estimate the burden acquired during fetal stages and present at birth, R_{bx}, for births in the xth year after exposure began (1953 in the case of Kulp's 1960 data), we assume as a first approximation that the accumulation in the fetal bone is identical to that acquired by the mother's bone over a period of $\frac{3}{4}$ year. Thus

$$R_{bx} = f_w \int_0^{0.75} I(\tau + x)\, R_s(0.75 - \tau)\, d\tau. \quad (6)$$

When we insert the preceding equation for $R_s(t)$, $I(\tau + x)$, and the value for f_w, we find

$$R_{bx} \sim 26 \times \text{pc}, \quad 0 \leq x \leq 7,$$

and taking the weight of Ca in the newborn as 28 g,

$$\frac{R_{bx}}{28} \sim x \text{ pc/g}. \quad (7)$$

Thus we would predict in the seventh year (calendar year 1960) newborns would have a level of 7 pc/g. This is too high and conservatively overestimates the level as can be seen from Fig. 22.11, in which the measurements obtained in fetuses born in the various calendar years have been plotted. As is noted, in 1960 the level was ~1.1 pc/g, or a factor of 7 lower than that predicted from the crude model above. In the calculations that follow, we employ a lower estimate of the

[25] W. S. Snyder, M. J. Cook, and M. R. Ford, *Health Phys.* 10, 171 (1964).

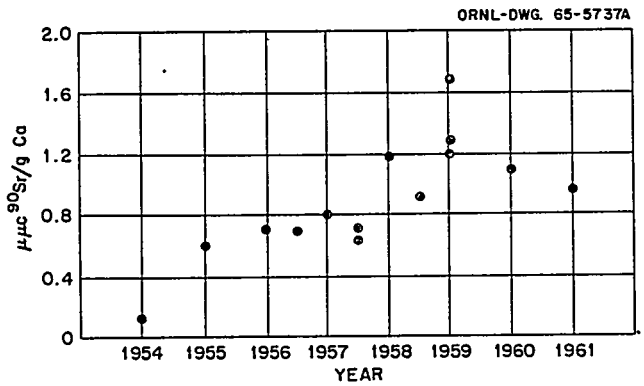

Fig. 22.11. Strontium-90 Levels in Fetuses for Various Calendar Years (Kulp's Data).

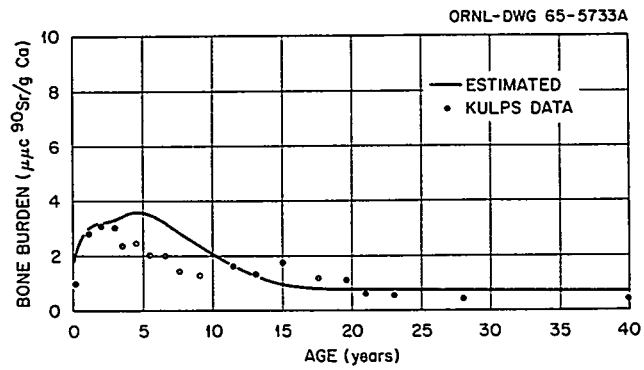

Fig. 22.12. Comparison of Estimated Levels of ^{90}Sr in the Body of Humans with Kulp's Measured Levels in 1960.

^{90}Sr level in the newborn by arbitrarily lowering the right side of Eq. (7) by dividing by 7. In later estimates we employ Comar's observed ratio (O.R.) method for estimation in fetal tissues.

Now from Eqs. (7), (5), and (4), we can calculate the retention for the ages zero to seven years in 1960, and from Eqs. (3) and (1) we estimate the retention for seven years and beyond seven years of age. Making these calculations and dividing by the appropriate weight of calcium in the skeleton, $W(t)$ (from Mitchell data), we then plot the ^{90}Sr levels in the body vs the age of the members of the population. Figure 22.12 shows this plot. Also shown are Kulp's measured levels for the year 1960. As can be seen, the estimated level and measured level do not agree over the entire age span, but the ratios do not exceed a factor of 2. Also, the estimated peak level occurs at four or five years of age, whereas the measured level peaks at approximately two years of age. In spite of the admittedly crude assumptions, namely, that the retention curve derived by Snyder *et al.* for adults was applicable for children and newborns as well and that the intakes were additive, the estimate is comfortably conservative.

Next, we make some modifications in this simple model to bring in age dependence of the parameters and physiological data. To see where we have to modify the model, we appeal to the experimental data obtained by Glad *et al.*,[26] who injected, intravenously, dogs of different ages with ^{85}Sr in a citrate buffer solution and measured the retention in the whole body. Figure 22.13 shows a plot of the retention curves for these dogs of different ages. Equations containing two exponential terms were fitted to these data, and these equations appear on the graphs. Glad *et al.* plotted the data on log × log plots, and the retention over this 200-day interval can also be represented by the power function. We employ the exponential function for convenience in manipulation, as will be seen later. From inspection of Fig. 22.13 it can be noted that the general function representing the data is of the form

$$R(t,T) = \left[1 - a_2(T)\right]e^{-\alpha_1 t} + a_2(T)e^{-\alpha_2 t}, \quad (8)$$

that is, the coefficients of the exponential terms are functions of age, T, while the decay constants are not highly age dependent. In the studies of Speckman *et al.*[27] and Decker *et al.*[28] on mice and dogs, a similar type of phenomenon was observed. The older animals had a lower retention than the younger animals at long times after injection. When these authors plotted their measurements on log by log graphs, they observed that the curves could be fitted by power functions with an age-dependent parameter, and they were parallel curves, that is, the intercept of the power function was age dependent while the exponent was relatively constant. They set up the equation for retention

[26] B. W. Glad, C. W. Mays, and W. Fisher, *Radiation Res.* 12(6), 672 (1960).

[27] T. W. Speckman and W. P. Norris, *Radiation Res.* 23, 461 (1964).

[28] C. F. Decker, L. V. Caspar, and W. P. Norris, *Radiation Res.* 23, 475 (1964).

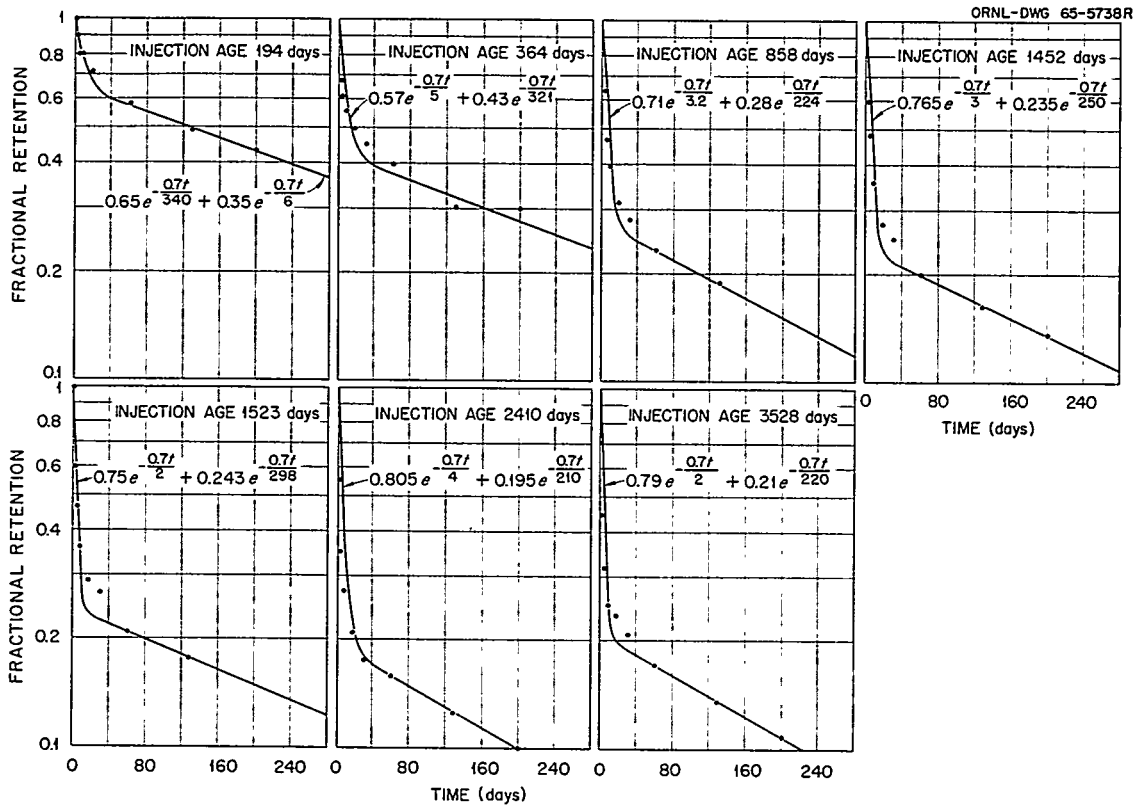

Fig. 22.13. Strontium-85 Retention in Dogs (Glad *et al.*)

during a continuous intake. The equation could not be expressed in closed form but could be evaluated numerically. By using exponential functions we can obtain some expressions in closed form and get a little more insight into the phenomenon of age effects on retention. To make Eq. (8) represent the retention for a continuous input into the blood of a dog, we assume linear superposition and let the coefficients be functions of time. Again, we ignore the exponential term having the shortest half-life, the first term, and write

$$R_c(t) = I \int_0^t a_2(\tau + A_0) e^{-a_2(t-\tau)} d\tau. \quad (9)$$

Here A_0 is the age of the animal at the time of injection, and I is the constant daily input into the blood. Now, we appeal to the single-compartment model used in the ICRP report to understand the meaning of this age-dependent parameter. In that model the retention for a continuous intake is given by

$$\dot{R} = f_2' I - \lambda R , \quad (10)$$

the solution of which is

$$R = \int_0^t f_2' I e^{-\lambda(t-\tau)} d\tau , \quad (11)$$

where f_2' is the fraction of the injected dose going from blood to an organ of long-term retention – the bone in the case of Sr injection – and $\lambda(=\lambda_b + \lambda_r)$ is the effective decay constant (= the sum of the biological and radiological decay constants). In comparing Eqs. (9) and (11) we see that the $a_2(T)$ corresponds to the f_2', and thus the only difference seems to be that the fraction going from the blood to the bone is a function of time (or age).

Admittedly this is a crude interpretation, but within the framework of the simple one-compartment (or exponential) model, it is the only one which seems to be admissible. Values of α_2 and $a_2(\tau + A_0)$ were inserted into Eq. (9), and $R_c(t)$ was calculated. Estimates of intake were not available from the published accounts of these experiments. The intake to blood, $f_1 I$, was considered as a parameter, and corresponding estimates of $R_c(t)$ were compared with the measurements of retention in dogs continuously fed ^{90}Sr by the group at Davis, California.[29] By proper choice of $f_2 I$, the agreement was fairly good. Figure 22.14 shows a plot of the retention of ^{90}Sr in dogs who were continuously fed ^{90}Sr at levels indicated on the right-hand side of the graph, together with a plot of the estimated retention equation. This was obtained from Eq. (9) by letting

$$a_2(\tau + A_0 = 0) = \left(0.21 + 0.78e^{-0.693\tau/365}\right),$$

$$\alpha_2 = \frac{0.693}{365}\ \text{day}^{-1},$$

$$I = 7.8\ \mu\text{c/day}.$$

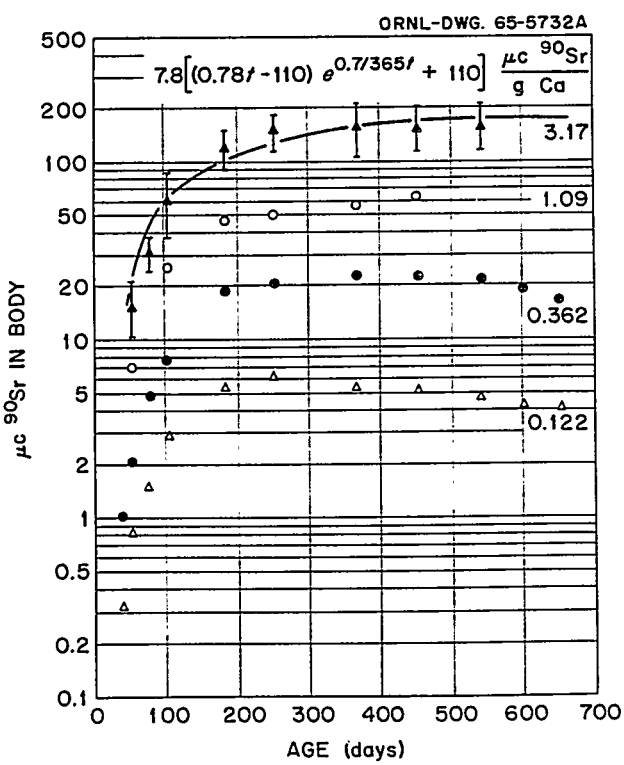

Fig. 22.14. California Dog Data. ^{90}Sr in whole body during feeding of various levels in diet.

The function $a_2(\tau)$ was obtained from a plot of the coefficient fitted to the data of Glad *et al.* (Fig. 22.13) vs age. Note, in Fig. 22.14, that the equation predicts that the retention will go through a maximum (its value is ~1800 μc) and then decrease to a steady value of ~860 μc. It is not known whether or not this will be observed. We also mention that in making the above calculations we assumed that the fraction absorbed into the blood from the gut, f_1, was age dependent. The value chosen for $f_1 I = 7.8$ μc/day contains this fraction f_1. If we had data on the actual daily intake by the dog, we could obtain an estimate of f_1.

In application to the case of human ingestion, we assume the retention occurring during continuous intake is, again, given by the equation

$$R_c(t) = \int_0^t f_w(\tau)\, I(\tau)\, R_s(t - \tau)\, d\tau. \qquad (12)$$

For $R_s(t)$, we employ the retention function of Snyder *et al.*, Eq. (4), and assume, as we did in the case of the dogs, that only the coefficients of the exponentials are age dependent; the decay constants are taken to be age independent. We do not have controlled human experimental data to determine $f_w(\tau)$. However, we can employ the observed ratio concept of Comar and obtain a crude estimate of $f_w(\tau)$. Remembering that

$$\text{O.R.} = \frac{(\text{microcuries of } ^{90}\text{Sr per gram of Ca})_{body}}{(\text{microcuries of } ^{90}\text{Sr per gram of Ca})_{diet}} \qquad (13)$$

and if we let $R_c(t)$ denote the microcuries of ^{90}Sr in the body, $W(t)$ the grams of Ca in the body, $I(t)$ the daily microcuries of ^{90}Sr taken into the body, and $I'(t)$ the daily intake of Ca into the gut, then we can write (13) as

$$R_c(t) = \text{O.R. } W(t)\, \frac{I(t)}{I'(t)}. \qquad (14)$$

We equate (14) to (12) and assume $I(t)$ and $I'(t)$ (≈1 g/day) are constants, and then

$$\text{O.R. } W(t) = \int_0^t f_w(\tau)\, R_s(t - \tau)\, d\tau. \qquad (15)$$

[29] *Fifth Annual Progress Report*, AEC Project No. 6, UCD-106 (1962).

The left-hand side is known, and for $R_s(t)$ we take the single long-term exponential in Snyder's equation. Then it can be shown, assuming O. R. is constant, that

$$f_w(t) = \text{O. R.}\left[\frac{d}{dt} W(t) + \lambda\, W(t)\right] \qquad (16)$$

is the solution of this simple integral equation. Thus, in order to estimate the age dependence of f_w, we can use Mitchell's data on the weight of Ca in the body. Figure 22.15 shows a plot of his data. We assumed O. R. = $\frac{1}{4}$ and numerically differentiated the data in Fig. 22.15. We set $\lambda = 0.089$ year^{-1} (from Snyder's equation and the radiological decay constant). Figure 22.16 shows a plot of f_w as a function of age. As can be seen, it starts at 0.069 at birth, decreases to a minimum of ~0.025 at 5 years of age, increases to a maximum of 0.115 at 15 years of age, and then returns to 0.065 at 20 years. For ages greater than or equal to 20, it remains constant at 0.069.

The age-dependent f_w can be inserted into (12), and $R_c(t)$ for any arbitrary intake of ^{90}Sr can be estimated. However, as in the case of the simpler model, we must add a term to account for the burden acquired by the fetus during its intrauterine life. We use Comar's O. R. model for this, that is, we assume the O. R. for the newborn to be one-half that of the adult. Denoting by R_{bx} the burden of an infant born x years after the exposure began, then

$$R_{bx} = \frac{1}{8}\,\frac{I(x)}{365} \times 28\,, \qquad (17)$$

where $I(x)$ is the yearly intake of ^{90}Sr, 365 g is the yearly intake of Ca by the mother, and 28 is the amount (in grams) of Ca in the newborn infant. Our equation for estimating $R_c(t)$ is thus

$$R_c(t) = R_{bx}\; R_s(t)\Big]_{A_0>0} + \int_0^t f_w(\tau + A_0)\, I(\tau + x)\, R_s(t-\tau)\, d\tau. \qquad (18)$$

Here, A_0 is the age of the individual, and the bracket on the first term signifies that this term is not to be added if A_0 is not 0 at the time of exposure. The xth year is to account for birth in the years after exposure began. The various values for the functions were inserted into (18), and calculations of $R_c(t)$ were made. These were divided by $W(t)$, and the resulting quotient is plotted in Fig. 22.17.

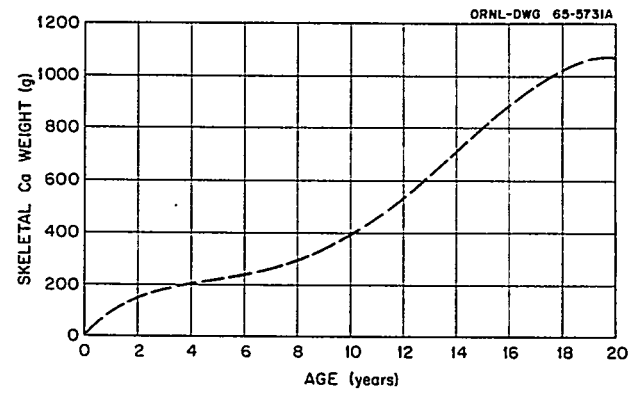

Fig. 22.15. Plot of Mitchell's Data on Calcium in the Body.

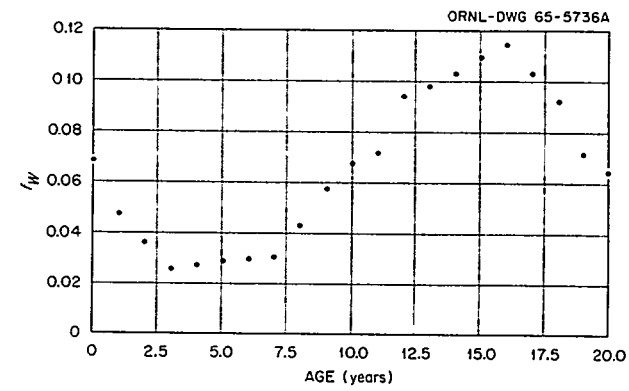

Fig. 22.16. Estimated f_w for ^{90}Sr Uptake by Man.

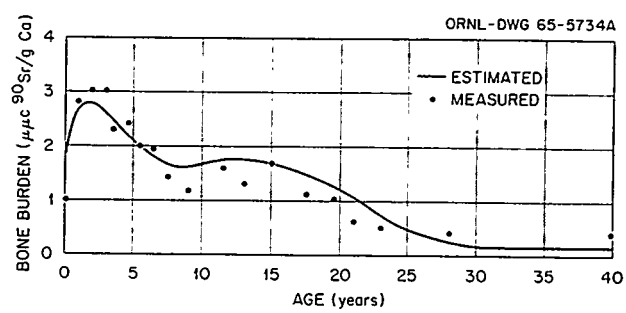

Fig. 22.17. Comparison of Estimated Levels of ^{90}Sr in the Body of Humans with Kulp's Measured Levels in 1960.

The agreement between the estimated and measured levels is somewhat better than was observed in Fig. 22.12. Still better agreement would probably obtain had we included an age-dependent O.R. value. Also, the calculations should be made with all exponential terms in Eq. (4) of Snyder *et al.*

The equation for estimation of body burden given by Kulp[20] can be written, as was shown by Rivera,[21] as

$$\mathrm{Ca}_n X_n = \mathrm{Ca}_{n-1} X_{n-1} - f_n \mathrm{Ca}_{n-1} X_{n-1} + f_n \mathrm{Ca}_{n-1} K_n Z_n + (\mathrm{Ca}_n - \mathrm{Ca}_{n-1}) K_n Z_n ,$$

where Ca_n is the skeletal Ca of an individual at the end of year n, X_n is the $^{90}\mathrm{Sr/Ca}$ ratio of the skeleton at the end of year n, f_n is the fraction of the skeletal Ca exchanged during the year, K_n is the bone-diet observed ratio, and Z_n is the $^{90}\mathrm{Sr/Ca}$ ratio of the diet. Now in this model, let

$$\mathrm{Ca}_n X_n = \mathrm{Ca}_{n-1} X_{n-1} + \Delta\mathrm{Ca}\, X$$

and

$$\mathrm{Ca}_n = \mathrm{Ca}_{n-1} + \Delta\mathrm{Ca} .$$

Then the above equation can be written as

$$\Delta\mathrm{Ca}\, X = -f(t)\mathrm{Ca}X\ \Delta t + K(t)\ A(t)\left[f(t)\mathrm{Ca}\ \Delta t + \Delta\mathrm{Ca}\right]$$

after dropping the subscript n and replacing the variables with continuous functions of time. Dividing through by Δt and taking the limit as $\Delta t \to 0$, we have

$$\frac{d\ \mathrm{Ca}X}{dt} = K(t)\ Z(t)\left[f(t)\mathrm{Ca} + \frac{d\mathrm{Ca}}{dt}\right] - f(t)\mathrm{Ca}X .$$

The solution of this differential equation is identical to our Eq. (18) when $K(t)$ and $f(t)$ are taken to be constants. The quantity in brackets times $K(t)$ is what we have called $f_w(t)$, the age-dependent absorption factor. We mention here that Kulp employed constant values for $K(t)$ and $f(t)$, while Rivera chose to let these parameters be age dependent.

DERIVATION OF A POWER FUNCTION FROM A LINEAR COMBINATION OF EXPONENTIALS

S. R. Bernard

Recently, a number of papers dealing with the problem of derivation of the power function for retention of bone-seeking radionuclides from fundamental considerations of the physiology and chemistry involved in incorporation of calcium in bone crystals have appeared in the literature.[30–32] The purpose here is to present another derivation of the power function from purely mathematical considerations. No chemical or physiological bases for the retention to be either a power function or a sum of exponential functions are assumed.

In the studies on stochastic models mentioned elsewhere in this report, some attempts to pass from a sum of exponential terms to a power function representation were made. In the case of one of the models, the sum of the amounts in all compartments for a very large number of compartments was found to be described by the equation

$$\sum_i p_i e^{-p_i K t} , \qquad (1)$$

where p_i and K are constants and t is the time. When these p_i are distributed uniformly, the summation is replaced by the integral, and then

$$\int_0^\infty p e^{-pKt}\, dp = (Kt)^{-2} . \qquad (2)$$

Thus, a power function of slope −2 is generated by this particular set of exponentials. It turns out that the expression

$$\sum_i p_i^{-n} e^{-p_i K t} , \qquad (3)$$

where n is a small positive number, gives rise to a power function of slope $n - 1$. To see this, we pass to the integral

$$\int_0^\infty p^{-n} e^{-Ktp}\, dp , \qquad (4)$$

[30] J. H. Marshall, J. *Theoret. Biol.* 6, 386 (1964).

[31] D. N. Edgington, *Radiation Res.* 25, 257 (1965).

[32] R. B. Holtzman, *Radiation Res.* 25, 277 (1965).

and letting $Ktp = x$, then on substitution we obtain

$$(Kt)^{n-1} \int_0^\infty x^{-n} e^{-x}\, dx\,. \qquad (5)$$

As can be seen, when $0 < n < 1$, we have a power function

$$\Gamma(1-n)(Kt)^{n-1}\,, \qquad (6)$$

where

$$\Gamma(1-n) = \int_0^\infty x^{-n} e^{-x}\, dx$$

is the well-known gamma function.

Although Eq. (3) gives rise to the power function, note from (4) that, when $t = 0$,

$$\int_0^\infty p^{-n}\, dp \qquad (7)$$

is not finite for positive values of $n \leqq 1$. This is inherent in any power function with a negative exponent. However, this difficulty seems to be removed by assuming the smallest p is not zero and the largest p is not infinity. Thus, denoting the smallest p by P_e and the largest by P_u, then instead of (4) we have

$$\int_{P_e}^{P_u} p^{-n} e^{-tKp}\, dp\,, \quad P_u > P_e\,, \qquad (8)$$

and when $t = 0$, the integral is finite. Equation (8) also can be rewritten as

$$(tK)^{n-1} \int_{tKP_e}^{tKP_u} x^{-n} e^{-x}\, dx\,, \qquad (9)$$

$$(tK)^{n-1} \left[\Gamma(1-n) - \int_0^{tKP_e} x^{-n} e^{-x}\, dx - \int_{tKP_u}^\infty x^{-n} e^{-x}\, dx \right], \qquad (10)$$

or

$$(tK)^{n-1} \left[\int_0^{tKP_e} x^{-n} e^{-x}\, dx - \int_0^{tKP_e} x^{-n} e^{-x}\, dx \right]. \qquad (11)$$

Here, as can be noted, we obtain two incomplete gamma functions whose limits are dependent on time. When t is finite and fixed and $P_u \to \infty$ while $P_e \to 0$, the limit is a power function of slope $n - 1$. Also, the function in Eq. (10) is finite at the origin as can be seen in (8). As t becomes large, then the first incomplete gamma function in (10) approaches $\Gamma(1-n)$, the second one approaches zero, and the value of the function approaches zero. It intuitively seems from examination of (8) that the function will be an exponential function for large t and small Kp, for then, in a linear combination of exponential functions such as (3), those which have large tKp values will have become negligible, and only the terms with Kp small will be significant. Thus there is some interval in time during which this function is approximately a power function of time, but for sufficiently long times the function follows the path of an exponential function. Further studies to determine the interval over which the function (10) can adequately represent Eq. (3) are being made.

STOCHASTIC MODELS FOR REPRESENTATION OF THE DISTRIBUTION OF RADIONUCLIDES IN ORGANS AND TISSUES

S. R. Bernard V. R. R. Uppuluri[33]
L. R. Shenton[34]

In the previous progress report[35] a simple two-compartment model having random variable connections was presented and discussed. The behavior of the expected amounts present in each of the compartments following a single injection was determined. Mention was made of determining the behavior of the distribution in a more complex model – a j-compartment model – and the possibilities that this model had in representing the distribution of "hot spots" of activity in bone were also pointed out. In the past year this work has been carried on, and the purpose here is to present briefly some of the findings. More details on these studies are presented in a separate report.[36] A mammillary system with $j-1$ peripheral compartments, each of which is in random communication with a central compartment, is treated,

[33]Mathematics Division.

[34]University of Georgia, Athens.

[35]S. R. Bernard and V. R. R. Uppuluri, *Health Phys. Div. Ann. Progr. Rept. July 31, 1964*, ORNL-3697, p. 193.

[36]S. R. Bernard, V. R. R. Uppuluri, and L. R. Shenton, *Stochastic Models for the Distribution of Radioactive Material in a Connected System of Compartments*, ORNL-3809 (1965).

and its application to the interpretation of a specific model for the ^{85}Sr retention data on dogs of different ages is discussed briefly in the following.

The mammillary system is presented in Fig. 22.18. In this model the peripheral compartments are labeled 1 through $j-1$. Denoting the probability for the jth peripheral compartment to be open by P_{jc} and the mean or expected concentration of the radionuclide in the whole system in the mth time interval after initially injecting into S an amount U and into each of the $j-1$ peripheral compartments an amount $(1-U)/(j-1)$ by $\mu_{t,m}$, then the following equation was derived for the case where all P_j's are equal:

$$\mu_{t,m} = d\lambda_1^m + (1-d)\,\lambda_2^m\,, \qquad (1)$$

where

$$d = \frac{a}{j}\,\frac{[1-(j-1)\,U\,] + \theta(1-U) - \lambda_2}{\lambda_1 - \lambda_2}$$

and

$$\theta = \frac{a}{(j-1)} + \frac{j-2}{j-1}\,.$$

Here, $\lambda_1 > \lambda_2$ are the roots of

$$\lambda^2 - \lambda\left[\frac{a\,(j^2-2j+2)}{j\,(j-1)} + \frac{j-2}{j-1}\right] + a\left(\frac{j-2}{j}\right) = 0\,, \qquad (2)$$

$a = e^{-K\Delta t}$ is the reduction factor for the S compartment, and K is a constant corresponding to the fractional release from the S compartment. The interval of time during which the jth peripheral compartment remains open is denoted by Δt. The more general case where the P_j's are not equal gives rise to a $j \times j$ matrix, the eigenvalues of which are evaluated in ORNL-3809. Also, the equations for the raw moments corresponding to the probability distributions of the amounts in each compartment are derived in that report. We will not list these equations here. Instead, we apply this special mammillary model to the ^{85}Sr data of Glad *et al.*[37]

[37] B. W. Glad, C. W. Mays, and W. Fisher, *Radiation Res.* 12, 672 (1960).

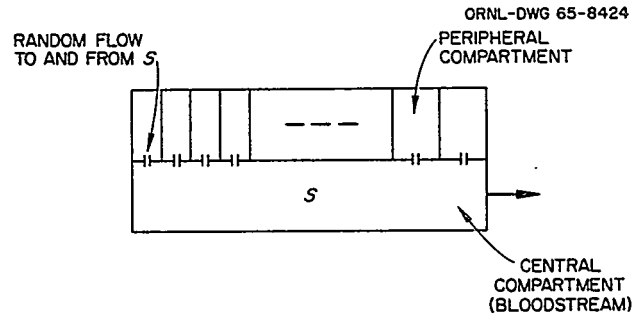

Fig. 22.18. Mammillary System with Random Flows Between S and Each of the Peripheral Compartments.

Table 22.1. Values of Parameters to Represent the Data of Glad *et al.*[a]

Parameter	$\Delta t = 1$	$\Delta t = 2$	$\Delta t = 4$
	194-day-old Dogs		
λ_1, λ_2	0.997, 0.890	0.994, 0.792	0.988, 0.627
j	3.35	826	233
a	0.888	0.788	0.623
U	0.360	0.361	0.363
	1452-day-old Dogs		
λ_1, λ_2	0.997, 0.793	0.994, 0.629	0.989, 0.395
j	1727	483	149
a	0.791	0.626	0.393
U	0.278	0.759	0.761

[a] The parameters are chosen so that Eq. (1) will superimpose on the data described by the equations

$$R(t) = 0.65e^{-0.693t/240} + 0.35e^{-0.693t/6}$$

and by

$$R(T) = 0.24e^{-0.693t/250} + 0.76e^{-0.693t/3}\,,$$

which represent the whole-body retention of ^{85}Sr in 194- and 1452-day-old dogs, respectively, administered a single intravenous injection.

Equation (2) was used to interpret the whole-body retention of ^{85}Sr in dogs, as determined by Glad *et al.*, which, as discussed in the previous progress report, could be represented over a 200-day period by the equation

$$R(t) = de^{-K_1 t} + (1 - d)e^{-K_2 t} . \qquad (3)$$

(In Glad *et al.*'s experiment, it was observed that the parameter d was age dependent.) In this model there are four parameters – a, j, Δt, and U – to align with the three parameters d, K_1, and K_2 in (3). When we set $U = 1$, the values of a, j, and Δt compatible with the other assumption do not provide a reasonable approximation to the data of Glad *et al.* By choosing to let Δt take on values of 1 day, 2 days, and 4 days, then the values of j, a, and U corresponding to these choices are possible and do give a reasonable approximation to the data of Glad *et al.* These values appear in Table 22.1. As can be seen in this table, whether the peripheral compartments interact daily ($\Delta t = 1$) or once every 2 or 4 days, there has to be a larger number of them to represent retention in a 194-day-old dog and a smaller number to represent retention in a 1452-day-old dog. This suggests that during aging some of the compartments (or regions of bone) become inaccessible to the blood supply (decreased vascularization in bone), and to include the effect of age on the uptake of ^{85}Sr, further modification of the model, probably by varying the number of compartments with age, is required.

At present the equation for the probability distribution of the total amount in the system has not been derived. Some preliminary studies on a simpler three-compartment model have been carried out. All that can be said at the present is that the distributions appear to be multimodel in structure.

---

23. Stable Element Metabolism

W. S. Snyder
Isabel H. Tipton [1]
Mary Jane Cook
Judy J. Eatherly [2]
Cyrus Feldman [3]
James Rhyne [1]
F. S. Jones [3]
Jane J. Shafer [1]
Peggy L. Stewart [1]

With increasing use of atomic energy in industry, medicine, and research, problems of exposure of the population are increasingly important. Therefore, it is necessary that dose estimates be made for members of the population, including fetuses, infants, children, teen-agers, and adults. Of necessity, most methods of estimation are indirect.

Long-term residents of a region who are grossly normal may be presumed, on the average, to be in a state of approximate equilibrium so far as intake and excretion of trace elements are concerned. Allowing for radioactive decay, the concentration of the stable elements indicates the extent to which the corresponding radionuclide would accumulate under conditions of chronic exposure. Thus by knowing the concentration, the dose may be estimated under chronic conditions. With this and related objectives in view, human tissues from many age groups have been analyzed for their stable-element content.

With the expanded uses of radioactivity, exposure of the population and, in particular, estimates of genetic dose are of increasing interest. Recent

[1]Physics Department, University of Tennessee.
[2]Mathematics Division.
[3]Analytical Chemistry Division.

experiments[4] have indicated that the LD_{50} for the earliest oocyte stages of a 10-day-old mouse is 8.4 r, which is believed to be the lowest known LD_{50}. Because these germinal cells of female mice are extremely radiosensitive, it may be postulated that these similar germinal cells in man also may be radiosensitive. Therefore, special emphasis has been given to studying the inorganic element content of the gonads. Gonads of grossly normal adults are being collected under specified procedures, and each tissue is evaluated histologically by a pathologist. A total of 71 gonads have been received of which 45 are testes and 26 are ovaries. The ashing and analysis of these samples have been started.

In calculating maximum permissible concentrations (MPC) and body-burden values for radionuclides, the fraction of the body burden in an organ is needed. Plans and procedures for obtaining one or more whole bodies are under discussion, because data on trace-element content of the whole body are extremely scarce. Since this will involve much larger quantities of tissues than ordinarily handled in the analytical laboratory, special techniques are being developed to process large amounts of tissue.

Three samples of the results obtained under this program during the past year are presented in this report. These include (1) "Tissue Analysis Laboratory Progress Report," (2) "Improvements in the Methods for Analysis of Trace Elements in Biological Materials," and (3) "Further Statistical Studies on Trace Elements in Subjects from the United States." These presentations are concerned largely with the immediate results of the technical staff and do not attempt to integrate these data with other data on Standard Man in order to arrive at estimates of population exposure.

TISSUE ANALYSIS LABORATORY PROGRESS REPORT

Cyrus Feldman F. S. Jones

The program for the spectrographic analysis of human tissue was continued using the previously described procedures.[5] Analytical results for approximately 544 soft-tissue samples analyzed for 23 elements were forwarded to the University of Tennessee for compilation in their computer program. These samples included autopsies collected previously from Richmond and Baltimore as well as numerous smaller organs, such as the lymph nodes, thyroid, and adrenal glands, which had not been analyzed previously because of their small size.

Most of the above samples were analyzed using the data acquisition computer system which processes the data from the Quantometer and presents them in the form of a typewritten, computer-output sheet. To provide increased sensitivity as well as data on additional elements, the samples also are analyzed on a film spectrograph. The computer program was further developed to provide the analytical data directly on IBM cards in a format compatible with the University of Tennessee computer's requirements. After a trial run of 229 samples, this procedure was abandoned because of the potential error and difficulty of posting the spectrographic data with the Quantometer data at a location distant from the source of the data. The spectrographic and Quantometer results are now combined and edited at ORNL and manually keypunched to the University of Tennessee's requirements, and each IBM card is checked against the original data before shipment to the university.

There is a need for a method of pulverizing large samples of wet tissue so that a small analytical sample representative of the whole may be obtained. This would improve the sampling of large organs and permit the preparation of aggregate samples large enough for distribution to different laboratories for comparison purposes. A hammer mill made by the Pulverizing Machinery Company of Summit, New Jersey, was installed and tested on beef fat, bone, and muscle, which had been frozen and mixed with dry ice. Fat gave a white powder and muscle a fine shredded fiber. As long as the product was kept frozen, it could be mixed and blended using simple equipment.

A blender was constructed, consisting of an inclined rotating platform on which a plastic tub containing the pulverized tissue and chunks of dry ice is rotated at 20 rpm. Initial tests using pulverized fat containing a dye indicated adequate mixing. Contamination in the pulverizer and

[4] E. F. Oakberg, *Proc. Soc. Exptl. Biol.* 109, 763 (1962).

[5] S. R. Koirtyohann and C. Feldman, TID-7606, pp. 51–63 (Jan. 24, 1961).

blender is negligible, because only carbon steel or plastic contacts the sample. Analysis of the residue from evaporated dry ice revealed no significant contamination from that source. Although testing of the equipment is not complete, the feasibility of the method for pulverizing tissue and mixing has been demonstrated. Freeze-drying and gamma-ray sterilization are being investigated as methods of preventing spoilage and facilitating the handling of the blended samples.

IMPROVEMENTS IN THE METHODS FOR ANALYSIS OF TRACE ELEMENTS IN BIOLOGICAL MATERIALS

Peggy L. Stewart Isabel H. Tipton
James Rhyne

To make a survey of a large number of elements in low concentrations in a large number of samples in the shortest time, the methods of emission spectroscopy are the best available. These methods are better for some elements than others, and, as in any method, when speed and broad coverage are of primary consideration, precision is sacrificed. In the survey of trace elements in human tissues carried out in the spectroscopy laboratory at the University of Tennessee, variations from individual to individual proved to be very large, and the precision of the method was adequate for the study.[6–8]

In the study of diets and excreta, however, finer distinctions have required that the analytical methods be made more sensitive and precise. This has been done by making a careful study of comparative methods for every step of the procedure from ashing of the sample to determination of concentration and by choosing the method which combined the greatest accuracy and precision with good sensitivity.

Ashing

The old method of ordinary dry ashing at 450°C was compared with wet ashing with HNO_3, wet ashing with H_2SO_4, dry ashing after ignition with heptane, and dry ashing at 550°C after the addition of spectroscopically pure sulfur and reduction of water content. The last method proved most satisfactory from several standpoints – the reproducibility of the ash percent in replicates of the same sample, the consistency of the anionic composition of the ash (chiefly sulfates and oxides) which is desirable in emission spectroscopy, and the reduction of loss of volatile metals such as zinc, tin, cadmium, etc., during ashing. To be sure of its purity, the sulfur is analyzed before it is used.

Determination of Dry Weights of Foods and Feces

The old method of oven drying was compared with a method involving distillation of the wet sample with organic components added in sufficient quantity to make an azeotropic mixture. Toluene proved to be the best. This method is simpler, quicker, more accurate, and more reproducible than the old method. The only disadvantage, that the aliquot of the sample is not recoverable, does not apply when large samples are available as is the case with most dietary and excretory studies.

"Major" Trace Elements

When a sample of human tissue or of food or excreta is ashed, the chief constituents of the ash are sodium, potassium, calcium, and magnesium. These elements are in such high concentrations that emission spectrography is not really appropriate. Therefore, a method by flame photometry is being developed for sodium and potassium, and a method involving EDTA titrations has been developed for calcium and magnesium. The precision of the latter method is improved fourfold over the old method by emission spectrography.

Film Calibration

The old method, involving a single calibration of an entire batch of film, has been replaced by the periodic calibration of seven different regions of wavelength. This has made possible the use of

[6] I. H. Tipton *et al.*, *Health Phys.* 9, 89 (1963).
[7] I. H. Tipton and M. J. Cook, *Health Phys.* 9, 103 (1963).
[8] I. H. Tipton *et al.*, *Health Phys.* 11, 403 (1965).

SA-1 film, which responds to much finer gradations in concentration than SA-2 and SA-3 film previously used but which varies more in response to different wavelengths and thus must be calibrated in several regions.

Volatilization, Atmosphere, and Internal Standard

A detailed study was carried out on the effects of different atmospheres (air, 80% argon—20% oxygen, 80% helium—20% oxygen) on the volatilization rates of elements and internal standards in the arc in which the sample is excited to emit the characteristic lines of elements. The argon-oxygen atmosphere provided the most stable conditions. Every analytical line and its corresponding internal standard line have been chosen on the basis of similarity in behavior in this atmosphere. The spectrum of palladium provides appropriate internal standard lines for all elements. The calibration of every region of the film makes it possible to use line pairs which are widely separated in wavelength.

Standards – Exposure Time

A great many more standards have been prepared, covering a wider range and with finer gradations of concentration. The problem of mixing of both standards and samples has been solved by the use of a tungsten wire spiral containing a trapped tungsten carbide ball as the pestle in the plastic vial of a mixer mill.

The standards and the samples to be analyzed are arced for 90 sec. From this time, exposures of 10, 30, and 90 sec are selected and recorded on different portions of the film by means of a Hartman diaphragm. Low concentrations are determined from the 90-sec exposure and higher concentrations at the shorter times. Thus, the range and sensitivity of the method are increased without having to use lines that are too light or too dark.

Working Curves – Concentration

Working curves from the standards of known concentration are plotted using a third-degree approximation method. Concentrations of the unknowns are read from these curves.

Use of Computer

In the comparative studies which have led to establishing the refined methods briefly described here, the computer was used to determine the number of trials to make, to calculate variance and significance of differences between methods, and to carry out statistical operations generally.

In the actual analytical method itself, the computer plays a vital role. Sample preparation, arcing, film development, and densitometry are carried out in the laboratory. Data from the densitometer are sent directly to the computing center, where they are punched on cards and fed into the computer, which performs the film calibrations, converts densitometer data on standards and unknowns to intensities, calculates ratios of intensities of analytical line to internal standard line, generates working curves, and determines concentrations. Values for concentration are put on punched cards, from which they may be reported on typed sheets or used in further operations, such as the calculation of average daily intake of an element.

FURTHER STATISTICAL STUDIES ON TRACE ELEMENTS IN SUBJECTS FROM THE UNITED STATES

Isabel H. Tipton Jane J. Shafer
Mary Jane Cook Judy J. Eatherly

Preliminary studies on correlations between concentration and age indicate that the concentration of certain trace elements in some tissues does tend to vary with age (Table 23.1). Therefore, in attempting to determine MPC values for various segments of the population, it is desirable to determine whether there is a quantitative relation between concentration and age, and thereby obtain information relating to possible age differences in the metabolic model. It is useful to calculate intercept and slope of a regression line relating these two quantities and to make a plot of the line for quick visual reference.

Table 23.1. Correlation of Concentration of Trace Elements in Human Tissue Ash with Age

Correlation coefficient ≥ 0.32, $p \leq 0.001$

Element	Tissue	Number of Individuals	Correlation Coefficient[a]
Aluminum	Lung	153	0.41
Barium	Trachea	57	0.41
	Uterus	33	0.54
Cadmium	Kidney	157	0.35
	Prostate	52	0.48
Calcium	Aorta	94	0.43
	Kidney	129	0.44
	Prostate	40	0.52
	Testis	71	0.55
	Trachea	54	0.50
Chromium	Lung	151	0.39
Copper	Aorta	105	−0.51
Iron	Bone-Rib	92	0.41
	Brain	114	0.37
	Kidney	131	0.32
	Lung	128	0.39
	Larynx	49	−0.46
	Pancreas	124	0.36
	Spleen	131	0.43
	Testis	71	0.37
Lead	Bone-Rib	92	0.40
	Cartilage	70	0.58
	Larynx	50	0.43
	Prostate	52	0.43
	Trachea	57	0.56
Phosphorus	Lung	118	−0.35
	Testis	68	−0.42
Potassium	Adrenal	8	0.94
	Aorta	91	−0.70
	Larynx	48	−0.52
	Trachea	52	−0.54
	Uterus	28	−0.69
Strontium	Kidney	155	0.32
	Trachea	57	0.41
Tin	Heart	151	0.33
	Lung	152	0.52
	Prostate	52	0.49
	Trachea	57	0.46
	Uterus	33	0.55
Titanium	Lung	153	0.39
	Urinary Bladder	114	0.33

Table 23.1 (continued)

Element	Tissue	Number of Individuals	Correlation Coefficient[a]
Vanadium	Lung	153	0.32
Zinc	Bone-Rib	92	0.44
	Cartilage	70	0.40
	Prostate	52	0.42
	Uterus	33	−0.64

[a]For method used in calculating and testing the level of significance of the correlation coefficient, see I. H. Tipton and J. J. Shafer, *Arch. Environ. Health* 8, 58 (1964).

Before a meaningful regression line can be plotted, it is necessary to establish the fact that the quantities can be expected to have a linear relation. If, for every fixed value of the independent variable (in this case age), the values for the dependent variable (in this case concentration) show a normal statistical distribution about a mean value, then the linear regression line may be determined by the method of least squares. However, most of the values for concentration of a trace element in human tissue prove not to be distributed normally. In this case a regression line for the concentration with age may be obtained, but it is not easily used to obtain confidence intervals on the means or percentiles as functions of age. Therefore, in this study, before plotting regression lines for an element, the data have been tested for normality and for log normality.[9] For those elements whose values for concentration show a normal distribution, a regression line of concentration on age is plotted; for those which show a log-normal distribution, the log of the concentration is used instead of concentration in plotting the regression line.

For some elements, a single line does not give the true picture. Since, for the most part, the differences occur between children and adults, slopes of lines are calculated for subjects under 20 (0–19) and for subjects over 20. If the slopes of these two segments do not differ significantly from the slope of the line calculated for the entire group of subjects of all ages, the latter line is the only one drawn.

[9]Memo, D. A. Gardiner to W. S. Snyder (June 20, 1963).

The figures are included as examples of the kinds of variation that occur. Age is plotted as abscissa, and log of concentration of an element in a wet tissue *(not ash)* is plotted as ordinate. The equation of the line or the segment of a line is included in the figure under the legend for the ordinate. Individual values are indicated as points. The 95% confidence interval is indicated by the dotted (x-ed) curves on each side of the regression line. This interval is not bounded by straight lines, because there were different variabilities and different numbers of observations for different age groups.

Figure 23.1 shows the variation of the concentration of cadmium in wet kidney with age. All data came from subjects from the United States. This element shows a highly significant positive correlation with age in tissue ash (Table 23.1). As the regression lines indicate, the concentration of cadmium in kidney increases markedly up to age 20 and more gradually after that.

The concentration of calcium in wet kidney (Fig. 23.2) shows a slight decline from infancy through 19 years of age and a gradual increase after 20.

The rate of increase of concentration of strontium in wet kidney proved to be the same for children and adults, and so Fig. 23.3 contains only one line.

The concentration of zinc in kidney increases slightly with age (Fig. 23.4).

The concentration of lead in lung (Fig. 23.5) increases significantly from birth up to age 20 and then remains almost constant.

Correlations Between Tissues

To determine whether an element was highly specific for one tissue or more generally distributed, correlations between the various wet tissues of individuals were investigated. The element which showed the most striking general distribution was lead. The concentration of lead in bone was significantly correlated ($p < 0.05$) with the concentration in almost every other tissue and highly correlated ($r \geqq 0.50$; $p < 0.001$) with the concentration in cartilage, larynx, lung, and omentum. The concentration of strontium in bone and cartilage also showed significant correlations with the concentration in soft tissues. Calcium showed the highest specificity. This element showed significant correlations in only three pairs of tissues. The concentration of calcium in bone was negatively correlated with the concentration of this element in aorta ($r = 10.29$; $p = 0.05$), in jejunum ($r = -0.55$; $p = 0.02$), and in testis ($r = -0.74$; $p = 0.05$).

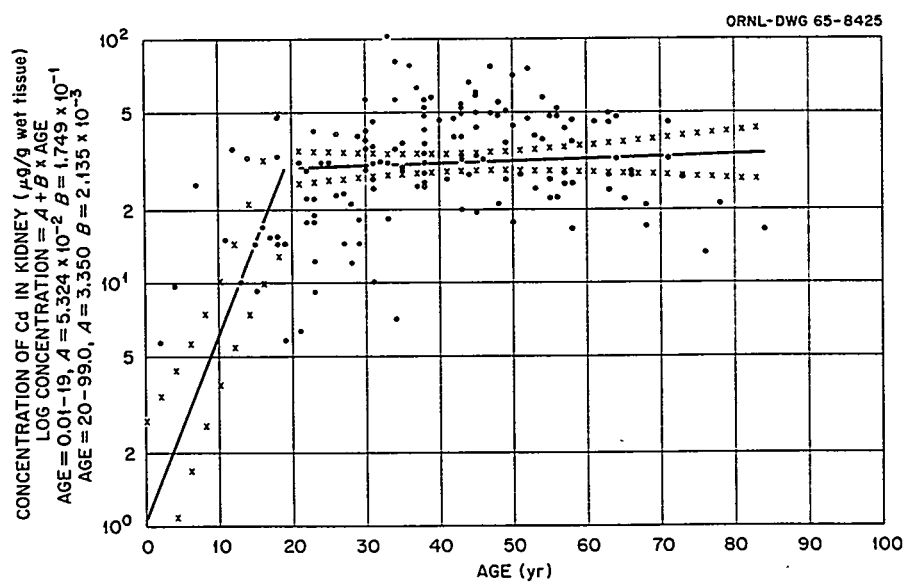

Fig. 23.1. Concentration of Cadmium in Kidney as a Function of Age.

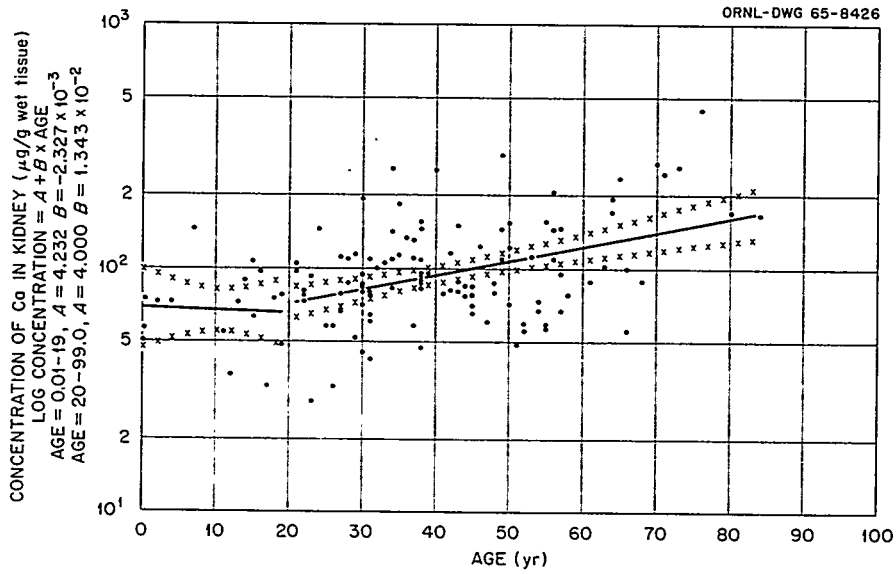

Fig. 23.2. Concentration of Calcium in Kidney as a Function of Age.

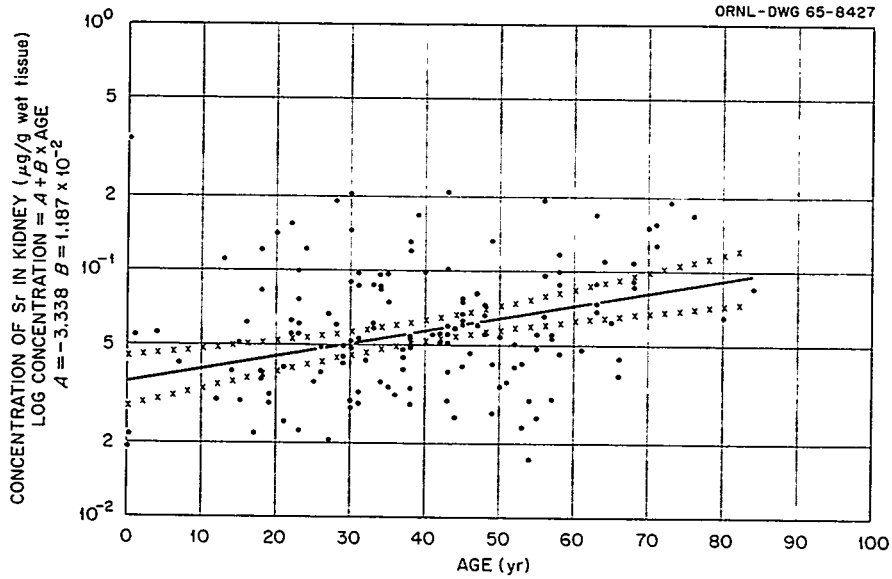

Fig. 23.3. Concentration of Strontium in Kidney as a Function of Age.

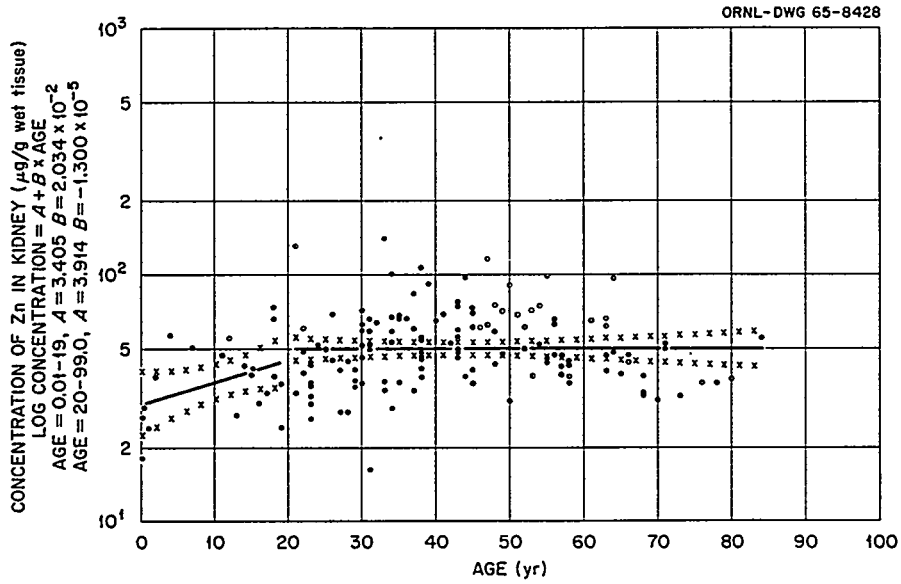

Fig. 23.4. Concentration of Zinc in Kidney as a Function of Age.

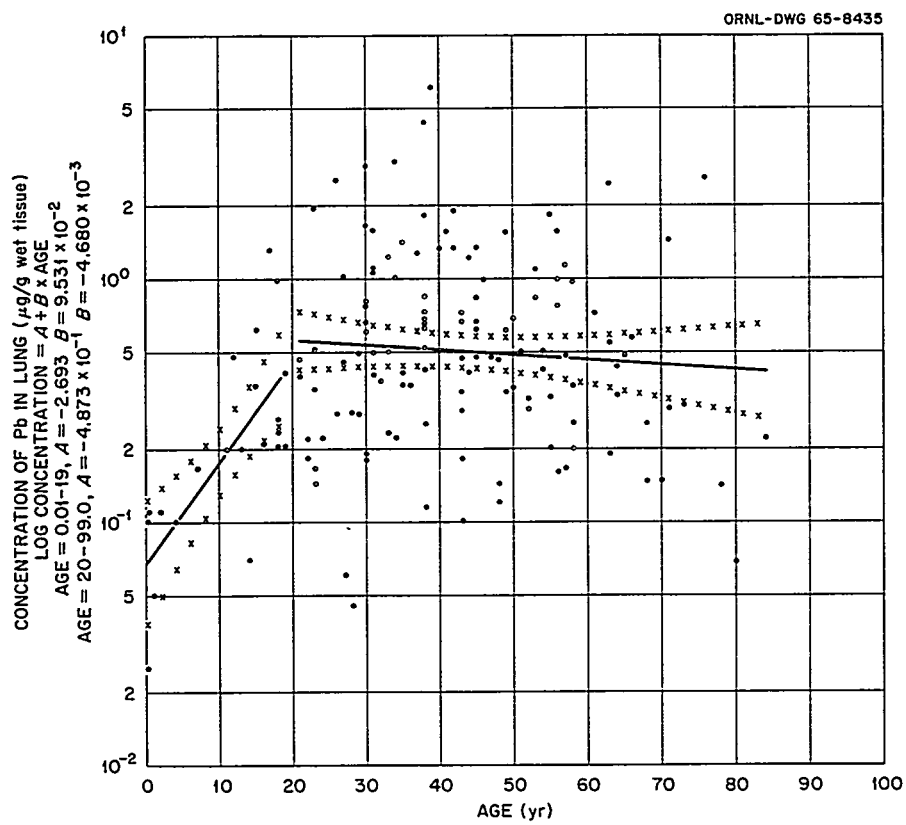

Fig. 23.5. Concentration of Lead in Lung as a Function of Age.

24. Information Center for Internal Exposure

W. S. Snyder S. R. Bernard
C. F. Holoway

ESTIMATES OF f_1 FOR PLUTONIUM COMPOUNDS

S. R. Bernard C. F. Holoway

The experimental data of Weeks *et al.*[1] and Ballou[2] permit some estimates of f_1 to be made for some compounds of plutonium. In the study by Weeks *et al.*, f_1 values were measured on rats for ingestion of Pu nitrates and Pu citrates existing in various valence states and at different pH's (Table 24.1). Ballou measured f_1 of $Pu(NO_3)_4$ at pH = 2 on rats of various ages (Table 24.2).

In Table 24.1, the first column gives the anion, the second lists the pH, the next three columns give the valence states present in percent, and the last column lists the estimated f_1.

For the citrate solutions, a linear relationship was assumed to exist between f_1 and the fraction of Pu^{4+} in the citrate solution at pH = 2. The best-fitting equation by least squares representing the citrate data of Weeks *et al.* is

$$f_1 = 0.023 - 0.022\left(\frac{Pu^{4+}}{Pu^{4+} + Pu^{6+}}\right).$$

Thus in a solution of pH = 2 where 100% of the Pu is Pu^{6+} citrate

$$f_1 = 0.02,$$

and when it is 100% Pu^{4+} citrate

$$f_1 = 1 \times 10^{-3}.$$

[1]M. H. Weeks *et al.*, *Radiation Res.* 4, 339 (1956).

[2]J. E. Ballou, *Proc. Soc. Exptl. Biol. Med.* 98, 726 (1958).

Table 24.2. f_1 Values for $Pu(NO_3)_4$ at pH = 2 Measured on Rats of Different Ages[a]

Age (days)	f_1
1	2.5×10^{-3}
7	1×10^{-3}
21	2×10^{-4}
33	3×10^{-5}

[a]J. E. Ballou, *Proc. Soc. Exptl. Biol. Med.* 98, 726–27 (1958).

Table 24.1. f_1 for Different Compounds of Plutonium in Different pH's and Valence States[a]

Anion Present	pH	Valence State Administered (%)			Percent of Dose Deposited in Rats at Four Days (= f_1)
		III	IV	VI	
Nitrate	1		68		2.8×10^{-3}
	1			100	1.9×10^{-2}
	2	90	10		6.3×10^{-5}
	2	7	93		5×10^{-5}
	2		96		1.3×10^{-5}
	4		97		1.7×10^{-5}
Citrate	2		99		2.9×10^{-4}
	2		96	4	2.5×10^{-3}
	2		85	15	4.1×10^{-3}

[a]M. H. Weeks *et al.*, *Radiation Res.* 4, 339–47 (1956).

For the nitrate solutions from Weeks' measurements on absorption of the nitrate compound, it is evident that f_1 is a sensitive function of the pH and of the valence state. The f_1 values for the nitrate solutions in different valence states appear in Table 24.3. It is known from the chemistry of plutonium that nitrate solutions of Pu consist of different cationic forms in dilute solutions.[3–6] These forms are a function of the pH, the cation-to-anion mole ratio, the actual molarity of the stoichiometric compound itself, the length of time following its preparation from the metal, the temperature, and the mode and extent of dilution. Also, if the solution is ultrafiltered, the size distribution of the colloid ($PuO_2 \cdot xH_2O$) will be changed. Weeks *et al.* do not state all the conditions under which their solutions were prepared. Appearing in the fourth column of Table 24.3 are possible cationic forms which were deduced from the chemical literature. The age of the colloid present in the solutions used by Weeks was not specified. We assume that a polymeric form of plutonium ($PuO_2 \cdot xH_2O$) is present. Also, it is assumed that this is an aged colloid (molecular weight $>10^6$). In this table it is seen that when 90% or more of the Pu exists as aged colloid, then the f_1 value should be $\sim 3 \times 10^{-5}$. On the other hand, in solutions which contain no colloid, we then assume the Pu is in a monomeric form (molecular weight <500) and that f_1 should be $\sim 2 \times 10^{-2}$. For the present it is suggested that $f_1 = 2 \times 10^{-2}$ for ingestion of monomeric Pu and 2×10^{-5} for ingestion of Pu as an aged colloid. It is not known what value should be used for nonaged colloidal solutions of Pu^{4+}. It is known that the molecular weight of $PuO_2 \cdot xH_2O$ increases with time.[7] The absorption of a larger aggregate may be less than that of a smaller aggregate. More data on f_1 as a function of the size of the colloidal aggregate are needed to estimate adequately the appropriate f_1 value. In cases where a mixture of monomeric and polymeric forms exists, one could use the rule for mixtures.

[3]G. Goldstein, *Equilibrium Distribution of Metal-Ion Complexes*, ORNL-3620 (November 1964).

[4]R. E. Biggers and D. Costanzo, *Studies of the Polymers of Plutonium IV, the Precipitation of Polymeric Plutonium for, and the Kinetics of, the Depolymerization of Polymeric Pu IV in Acidic Nitrate Media*, ORNL-3799 (to be published).

[5]Gel'man, Moskvin, Zaitsev, and Mefod'eva, *Complex Compounds of Transuranium Elements*, translated and published by Consultants Bureau, New York, 1962.

[6]J. J. Katz and G. T. Seaborg, *The Chemistry of the Actinide Elements*, Methuen and Co., Ltd., London, 1957.

[7]D. W. Ockenden and G. A. Welch, *J. Chem. Soc.* 1956, p. 3361.

Table 24.3. f_1 Values for Different pH's and Valence States of Pu Nitrate

Valence State	pH	f_1	Possible Cationic Form
III	1	5×10^{-5}	Pu^{3+} $Pu(OH)^{2+}$ $Pu(NO_3)^{2+}$
IV	1	2×10^{-2}	Pu^{4+} (99%) $PuOH^{3+}$ (0.1%) $PuO_2 \cdot xH_2O$ (0.9%)
	2	6×10^{-5}	Pu^{4+} $PuOH^{3+}$ $PuO_2 \cdot xH_2O$ (90%)[a]
	4	2×10^{-5}	$PuO_2 \cdot xH_2O$ (90%)[a]
	7	3×10^{-5}	$PuO_2 \cdot xH_2O$ (100%)[a]
VI	1	2×10^{-2}	PuO_2^{2+} $PuO_2(NO_3)^{+}$

[a]Here the molecular weight is probably a maximum of 10^7 (D. W. Ockenden and G. A. Welch, *J. Chem. Soc.* 1956, pp. 3358–63).

Part VI. Health Physics Technology

B. R. Fish

25. Aerosol Physics

B. R. Fish

R. H. Boyett
T. G. Clark, Jr.
G. W. Royster, Jr.
F. G. Karioris[1]
J. L. Thompson
R. L. Walker
W. H. Wilkie, Jr.
C. F. Parrish[2]

STUDIES OF SURFACE CONTAMINATION

G. W. Royster, Jr. B. R. Fish

Redispersion of deposited particulates from surfaces in a semi-isolated environment is being studied with regard to the probability of a given particle population being resuspended by the movement of persons in the area. Major emphasis is on the comparison of sampling techniques for measuring particulate contamination on surfaces and application of redispersion test results to the establishment of contamination control criteria.

Comparisons of methods for measuring surface contamination have been reported[3] as they relate to measurement techniques and surface characteristics. The "smair" measuring technique employs air impingement to redisperse loose contamination from a surface and is seen to be more consistently related to the probability of inhalation exposure than other available methods of assessing "removable" contamination. Originally, the design of this sampler employed a vacuum pump to pull air through the sampler in the same manner as standard air samplers. However, the mobility of that apparatus is limited, depending on the availability of electrical outlets and because of the bulkiness of the necessary vacuum pump, rotameter, etc. The sampler head has been redesigned to include a small chamber surrounding the air jets so that air pressure may be used instead of a pump (Fig. 25.1). This pressure is obtained from a small, easily transported source of compressed gas.

In order to relate the various measuring procedures to the probability of a given particle population being resuspended by the movement of persons in the area, a large room-size test chamber is used.[4] Since the use of a radioactive dust presents the possibility of unnecessary exposure

[1]Temporary summer employee, Marquette University, Milwaukee.

[2]Research participant, Indiana State College, Terre Haute.

[3]G. W. Royster, Jr., and B. R. Fish, *Techniques for Assessing "Removable" Surface Contamination*, ORNL-TM-1045 (Feb. 4, 1965).

[4]B. R. Fish *et al.*, *Health Phys. Div. Ann. Progr. Rept. June 30, 1964*, ORNL-3697, p. 213.

ORNL-DWG. 65-6033

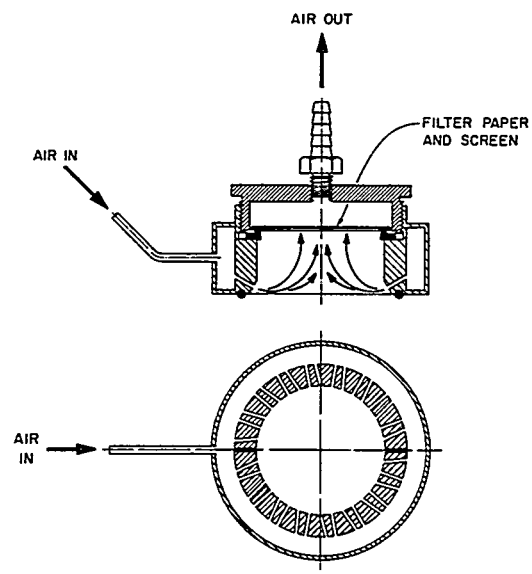

Fig. 25.1. Sampler Head Using Air Pressure.

to the experimenter, stable cupric oxide is used and the collected samples are irradiated with neutrons to form ^{64}Cu. Gamma counting yields estimates of the relative amounts of copper in the different samples. Each of the two resuspension rooms is 8 × 12 × 8 ft high and is constructed of painted wallboard. One room has an asphalt-tile floor and the other is of concrete. Tracer dust is dispersed from a Wright dust feed into a small mixing chamber outside the room and is introduced into the room through a short length of flexible hose.

To understand the resuspension of settled particulates in a room, it is helpful to refer to some model such as that outlined in Fig. 25.2. Clearly, whatever relationship may exist between the concentration of airborne particles and that of surface deposits must be affected by several major factors. First, the original source of the particles may be an intermittent or a continuous source; in addition, the source may be located in one or a few single spots or it may be more or less uniformly distributed throughout the room. Second, the movement of air in the room controls the transport and deposition of particles released by the primary source, as well as contributing to reentrainment from surfaces and determining the residence time of particles in the air. Redispersion of particles depends upon other important factors, including the physical and chemical characteristics of the surfaces and of the particles, the kind and degree of work going on in the room, and the cleaning schedule and techniques.

Some of these parameters are being evaluated by means of the resuspension studies. Cupric oxide dust is introduced into the test room and allowed to settle undisturbed for two days. For the redispersion tests a man wearing coveralls, gloves, shoe covers, a cap, and a respirator enters the room and obtains various types of samples. The amount of tracer collected on the respirator filter is taken to be related to the amount he would have inhaled without a respirator. During the time the man is in the room taking samples (assumed to represent moderate human activity), air samples are collected by conventional samplers. In addition, the relative particle size distribution is monitored with a recording light-scattering particle size analyzer. After the samples have been obtained, the filters are changed and another series of samples are collected while sweeping in order to simulate redispersion under conditions of vigorous human activity in the room.

The fractional removal of dust from floors under a variety of floor conditions is recorded in Table 25.1. It is seen that the mask (respirator filter)

Table 25.1. Fractional Removal of Dust from Floors

Trial[a]	Activity on Floor (counts/min per 100 cm^2)	Fraction Removed per 100 cm^2		Fraction Redispersed per Hour			
				Moderate Activity		Sweeping	
		Smair	Smear	Mask	Air Sample	Mask	Air Sample
1	9866	0.23	0.25	0.28	0.23	1.82	0.94
2	8999	0.30	0.36	0.49	0.21	2.60	1.28
3	3648	0	0.12	0	0	0	0
4	599	0.03	0.86	0.08	0.05		
5	1429	0.13	0.55	0.15	0.10	1.30	0.84
6	9383	0.67	0.08	0.21	0.19	10.4	3.40
7	7956	0.29	0.05	0.13	0.10	6.2	1.86

[a]Surface: 1 Asphalt tile, waxed and buffed.
2 Asphalt tile, waxed and buffed.
3 Asphalt tile, oiled.
4 Asphalt tile, waxed not buffed.
5 Asphalt tile, waxed and buffed.
6 Asphalt tile, dusty.
7 Concrete.

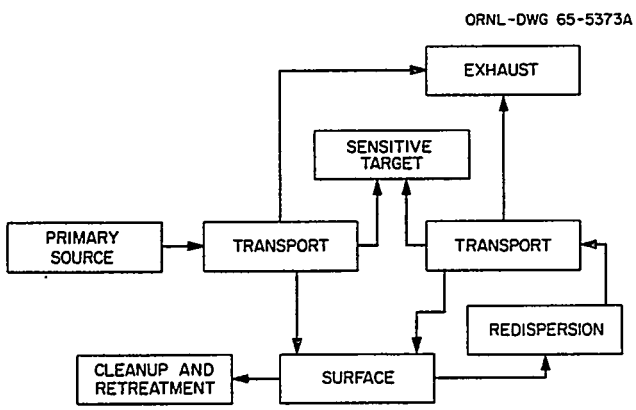

Fig. 25.2. Schematic Model of Transport, Deposition, and Redispersion of Dust in a Room.

and air sample data compare rather well for moderate activity in the room. For example, 28% of the concentration of deposited dust on 100 cm^2 of floor space was found on the mask filter after 1 hr of breathing, and 23% was on the air sampler in 1 hr. Air samplers were operated at 15 liters/min in order to approximate the breathing rate for light work activity. After sweeping, however, the respirator filter data indicate a greater increase in concentration than that shown by the air samplers; this may be explained by a factor of 2 increase in breathing rate during vigorous activity. The air sample data show about an order of magnitude higher air concentration during sweeping than during moderate activity. The smair sample results are better correlated (smear to air correlation coefficient, $r = -0.222$; smair to air, $r = +0.68$) with the mask and air sample data than the results of smear sampling.

STUDY OF THE EFFECTS OF RADIOACTIVE IODINE ON AEROSOLS

R. L. Walker B. R. Fish
J. L. Thompson

The decrease with time of the airborne concentration of radioactive and nonradioactive particles is studied in an aerosol chamber described in a previous report.[5] For the work reported here, a silver aerosol, made by the exploding-wire technique,[6] is introduced into the test chamber through a diffusion ionizer of a design suggested by Whitby.[7] In the test chamber, the aerosol can be mixed with radioactive iodine, and the particle concentration is monitored by several different sampling techniques.

Theoretically, the number concentration of airborne particles in the chamber can decrease by any one of four major mechanisms: (1) Particles may agglomerate, thus reducing the number concentration but not affecting the mass concentration in suspension. (2) Some of the agglomerates may grow to sufficient size to settle under the action of gravity. (3) Individual particles can diffuse to interior surfaces under the action of convective currents and thermal diffusion. (4) If the aerosol is made to bear a unipolar charge, the rate of diffusion to the interior surfaces will be enhanced by space-charge repulsion.

In the present study, the number concentration, which ranged from 3×10^3 to 1.8×10^5 particles/cm^3, was measured with a Nolan-type condensation nuclei counter. The number concentration data expressed in percent of the initial concentration is presented in Fig. 25.3. Two runs were made in which the ionizer was operated so as to produce a local high concentration of positive and negative air ions, thus promoting the approach to charge equilibrium. The addition of 1 mc of ^{130}I made no obvious change in the loss of particle concentration from that observed for the particles without radioactivity. In contrast, when the particles were deliberately given a net excess of positive charge, the addition of radioactive iodine made a definite change in the rate of loss of particles compared with the nonradioactive runs.

These observations indicate that for conductive particles and for radioactivity levels of 0.1 to 1 mc/m^3 the major difference in behavior is that radioactive particles cannot retain a significant asymmetry of charge for an appreciable length of time, whereas nonradioactive particles can. Thus, the results of this ad hoc experiment, while not providing direct insight into the detailed aerosol physics of radioactive particles, nevertheless do emphasize the importance of the electrical charge

[5] R. L. Walker, *Health Phys. Div. Ann. Progr. Rept. June 30, 1963*, ORNL-3492, p. 187.

[6] F. G. Karioris *et al.*, *Exploding Wires* 2, 299 (1962).

[7] K. T. Whitby, *Rev. Sci. Instr.* 32, 1351 (1961).

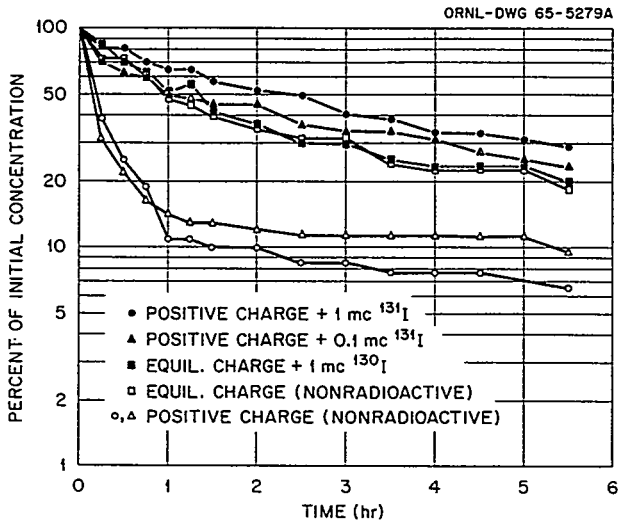

Fig. 25.3. Effect of Radioactivity and Electrostatic Charge on Number Concentration of Airborne Particles.

distribution on test aerosols which may be used to simulate airborne radioactive particles. Further work in this program is directed toward investigation of the effects of radiation and radioactivity on the individual mechanisms affecting deposition, agglomeration, and resuspension of particulates.

ADHESION OF SOLID PARTICLES TO SOLID SURFACES

B. R. Fish R. L. Walker
F. G. Karioris C. F. Parrish

A review of the literature indicates four basic mechanisms for adhesion of particles to surfaces. These are related to capillary, electrostatic, and molecular forces and to a time-dependent force due to a viscous-flow phenomenon which has been referred to as Stefan flow.[8]

When a liquid capillary layer exists between a particle and a surface, the surface tension of the liquid acting on the particle produces a component of force normal to the surface, provided that both the particle and the surface are wetted by the liquid. If the particle and the surface both have an electrostatic charge, there will be a second type of force which is attractive or repulsive depending on the relative sign of the charge.

Another force of adhesion between particles and surfaces is that due to molecular interactions. The best known of these is the London–van der Waals force, where an attractive force results from the interaction between fluctuating electric dipoles and the dipoles that these induce in adjacent molecules. Other examples of molecular forces include the interaction of dipoles with other dipoles or with polarizable molecules, hydrogen bonds, metallic bonds, and image bonds.[9]

A time-dependent force due to viscous flow seems to have been studied first by Stefan.[10] In a liquid system, including a capillary layer, as a particle is pulled away from a surface there is resistance to the flow of the liquid into the gap. This tends to retard the movement of the particle away from the surface. Thus, a given force must be applied for a finite time in order to separate the particle a given distance from the surface. There are three basic types of forces available for removing particles from surfaces. These are fluid dynamical (e.g., liquid or air streams), inertial (centrifugal, vibrational, gravitational), and direct mechanical contact (e.g., brushing or grinding).

Preliminary results from work with a high-speed centrifuge are presented in Fig. 25.4. The re-

[8] J. J. Bikerman, *Surface Chemistry*, p. 384, Academic, New York, 1958.

[9] F. M. Fowkes, *Am. Soc. Testing Mater., Tech. Publ.* 360, p. 20 (1964).

[10] J. Stefan, *Akad. Wiss. Sitzber.* 69, 713 (1874).

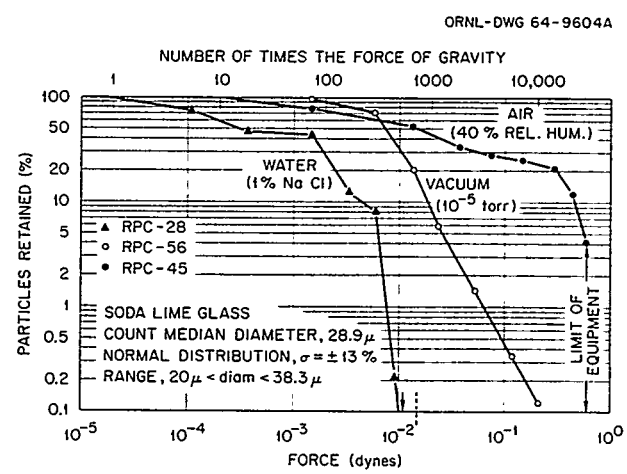

Fig. 25.4. Centrifuge Study – Retention of Glass Particles on Glass Surface.

tention of glass particles with a count median diameter of 28.9 μ on glass surfaces is studied under three different conditions. The significant part of the graph is the limits that each of the curves seems to be approaching. Each is separated by about one order of magnitude. For the case of the surface in air at 40% relative humidity, it is postulated that three major forces hold the particles to the surface. These result from the effects of a liquid capillary layer, electrostatic charge, and molecular interactions. In a vacuum the electrostatic and molecular forces could still be present, but the capillary layer would be eliminated, thus reducing the force of adhesion. In the conductive liquid system, surface charges are eliminated and the capillary layer is not present since the particles are completely submersed in the liquid. This condition leaves only the molecular forces, again reducing the force of adhesion.

The forces of adhesion of solid particles to solid surfaces are in no way simple or well understood. These preliminary studies suggest that the most meaningful results can be obtained by emphasizing the maximum force required to remove 100% of the particles rather than the 50%, or other intermediate, removal force. Additional work is being done to examine each of the forces of adhesion separately.

ADHESION OF PARTICLES TO SKIN

R. H. Boyett T. G. Clark, Jr.
B. R. Fish J. L. Thompson

In addition to the dependence on the usual source parameters, surface and tissue depth dose from a radioactive particle on the skin is also a function of particle sticking probability and retention time. An investigation of the retention of small particles on skin is now under way, and a study of fluorescent wax particles on skin has been completed. Some of the data are summarized in this progress report.

No formal study of the initial retention of particles falling onto the skin has been found in the literature; however, an experiment is planned to yield this information. A preliminary inquiry suggests an initial retention of 10 to 20% for 1-mm particles and approximately 100% for particles smaller than about 200 μ in diameter.

A pilot study of particle retention on human skin was made using particles composed of a thermosetting plastic (Turtox) mixed with ZnS-CdS(Ag) powder. Except for the composition and the fact that the particles were more angular than rounded, the techniques used were the same as in the work with fluorescent wax particles discussed below. The results with the angular plastic particles were essentially the same as observed when the wax spheres were used. The differences in the average retention times for the two materials were less than differences seen between individuals with the same type of particles. These and other observations suggest that the major parameters are the level of moisture on the skin (and of other liquids, e.g., oiliness), weight of the particle, degree and kind of physical activity of the subject, and, probably somewhat less important, the geometry and composition of the particle. These questions will be explored in more detail using graphite (sp gr 2.0) and other particles.

Carnauba wax was chosen for the study of the retention of particles on skin because it melts at a temperature between 86 and 90°C; thus it can be spheroidized in water, yet remains hard at normal human body temperature (37°C). The fluorescent powder ZnS-CdS(Ag) was selected because of its superior light output and also because its color (brilliant yellow-orange) contrasts well with the background of fluorescent material found on the forearms of local volunteers. Normal fluorescent background, in our experience, has been widespread and fluoresces a medium-bright light blue, due mainly to the presence of detergents in lint collected on the skin. It is to be expected that background may depend upon various factors of local geology as well as of local customs; accordingly, the choice of a fluorescent tracer should be verified before using the technique in a new geographical area.

Wax spheres, produced by the procedure outlined in ORNL-TM-1053 (classified), were separated into limited size ranges by wet sieving. Six sizes were used in this study: 50 to 74 μ, 74 to 88 μ, 125 to 149 μ, 250 to 297 μ, 500 to 595 μ, and 1 mm diameter. The particles were dropped from a height of about 5 cm onto the flexor and the extensor surfaces of the forearms of human volunteers. From three to six subjects participated in each run, which consisted of a set of determinations of retention time for one particle size. Figure 25.5

is a photograph of a 1-mm particle on the forearm of one of the subjects. A minimum of 60 particles (1 mm) were used on each subject, and usually there were more than 100 per subject. Detailed results of the study will be published as a separate report. In the interim, the following summary of the major findings may suffice for estimating retention time as a basis for radiation dose calculations.

Particle retention as a function of time varies widely for individual subjects. Nevertheless, the general trends with particle size (mass) are about the same; that is, for two subjects having grossly different fractions retained after the initial half hour, the adhering particles are lost at approximately the same rate. It appears that there are two components of retention. One component consists of particles relatively loosely held on comparatively dry regions of the skin; these are the easiest to remove, and the rate of removal is related to particle mass and to degree of movement (acceleration). The second component may consist of particles more tightly bound in moist or oily areas of the skin; removal of these particles may require greater force than normal accelerations afford; thus the probability of a direct hit of the particle and removal by some brushing or abrasive action may control the rate of loss from skin. Since this is a study of natural attrition of adherent particles, deliberate decontamination by washing was not included in the schedule; however, it was observed that normal bathing is essentially 100% effective for removing particles in the size range $>50\ \mu$ from skin.

In this experiment, the retention of particles on skin is seen to decrease with time and follows a two-component exponential function. Retention of smaller particles is described adequately by a single exponential function of time,

$$R = Ae^{-t/T}\ , \qquad (1)$$

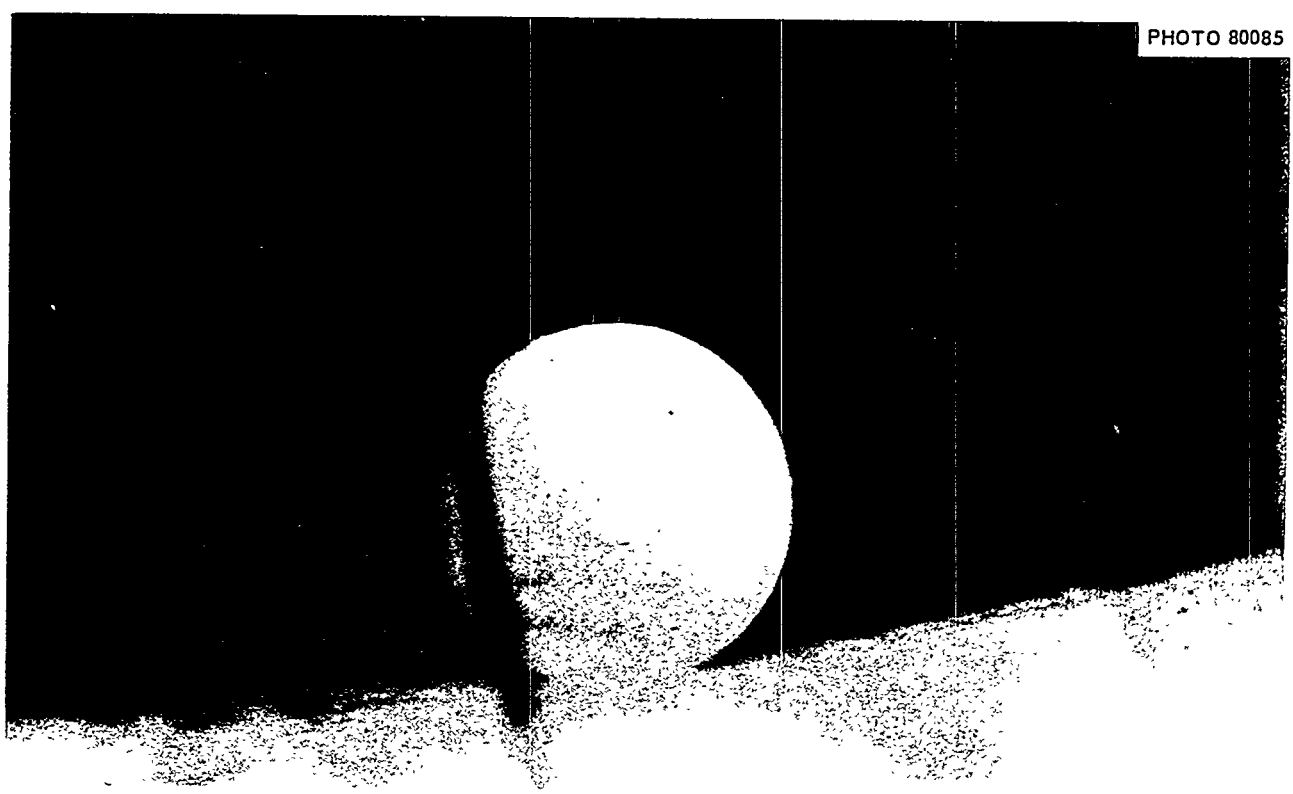

Fig. 25.5. One-Millimeter Wax Particle on Human Subject.

where

A = the fraction sticking initially,

T = average lifetime of a particle on the skin (equals $T_{1/2} \div 0.693$, where $T_{1/2}$ is the half-life for retention),

R = the fraction remaining at time t.

Our data indicate that the retention of larger particles may be described by

$$R = Be^{-t/T_B} + Ce^{-t/T_C} , \qquad (2)$$

where

B = the fraction retained with the average lifetime T_B,

C = the fraction with average lifetime T_C,

$B + C = 1.0$.

The average lifetime is determined by integrating $R\,dt$ from zero to infinity; thus from (2),

$$T = \int_0^\infty R\,dt = BT_B + CT_C , \qquad (3)$$

which is just the weighted average retention time for the given size particle. Figure 25.6 presents the average retention time of wax particles on human skin for the six particle size groups noted above.

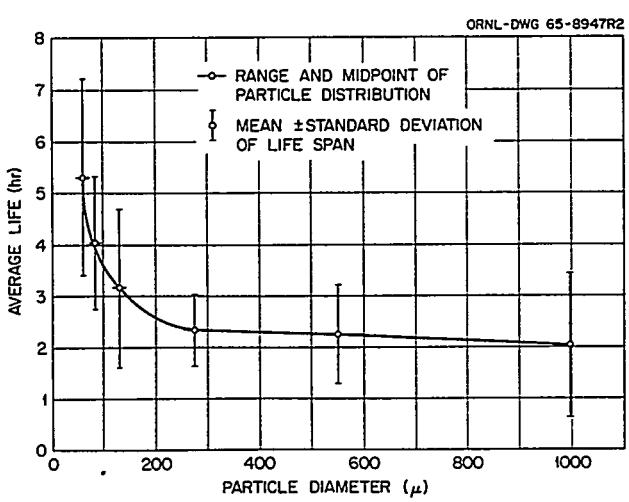

Fig. 25.6. Particle Retention on Skin.

RETENTION OF SMALL PARTICLES IN THE GASTROINTESTINAL TRACT AND THEIR PROXIMITY TO THE WALL DURING TRANSIT

T. G. Clark, Jr. J. L. Thompson
B. R. Fish

Literature reports dealing with the hazards of ingested, nonabsorbable radionuclides most often are based on the assumption that the radioactivity is mixed uniformly with the contents of the gastrointestinal tract. Radiation dose rate to tissue is calculated from assumed or measured residence times of the source in each segment of the tract. The assumption of uniform distribution of radioactivity in the GI tract contents is equivalent to assuming uniformity of radiation exposure to the walls. Thus, a dosing technique in which the radionuclide is given as a solution or as a suspension of very small particulates greatly simplifies the comparison of radiobiological effect with radiation dose delivered; hence, it is not surprising that most radiobiological studies employ some variation of this technique of dose administration. However, in order to apply the results of such studies to the estimation of relative biological significance, it is necessary that one be able to assume that the radioactivity is finely divided and thoroughly mixed with other ingesta, that the average transit times through segments of the GI tract are well known, and that the resulting irradiation of the gut does not alter these "normal" transit times. Unfortunately, in many cases of interest, the validity of these assumptions ranges from questionable to erroneous.

If the radioactivity should be contained in a single insoluble particle, additional questions must be answered. One of the more important ones deals with the residence time of the particle in each division of the GI tract. A literature search was begun on the passage of inert material through the GI tract of man, and preliminary indications are that transit times of such material are more variable than those of ordinary foodstuffs. Hoelzel[11] has reported transit times ranging from 1½ hr to 22 days; the average time varies directly with the specific gravity of the test material. Bizzell *et al.*[12] dosed one rat with a Bakelite powder labeled

[11] F. Hoelzel, *Am. J. Physiol.* 92, 466 (1930).

[12] O. M. Bizzell *et al.*, *Nucleonics* 8(4), 17 (1951).

Table 25.2. Fluorescent Wax Particles[a] in the Gastrointestinal Tract of a Rat

Organ	Particles Within 500 μ of Wall		Total Particles in Organ	
	Number	Percent of Total in Organ	Number	Percent of Total in Organ
Stomach	48	63	76	19
Duodenum	1	33	3	<1
Jejunum-ileum	5	56	9	2
Cecum	64	47	137	35
Ascending and transverse colon	29	51	57	14
Descending colon	55	48	114	29
Total	202	51	396	

[a]Specific gravity = 1.22 g/cm^3.

with 54 μc of ^{32}P and reported that only 50% had been eliminated by 36 hr. A pilot study by Fish *et al.*[13] revealed significant amounts of radioactivity remaining in the stomach of a pig one week following an oral dose of ^{90}Sr-^{90}Y titanate in powdered form. This was due in part to the entrapment of particles by areas of ulcerated mucosa.

In order to estimate dose delivered by small insoluble particles to the wall of the GI tract, it is necessary to obtain information on their pattern of movement as they traverse the alimentary canal. A technique based on a suggestion by Decker and Goldman[14] for determining the proximity of particles to the gut wall is being evaluated. Spherical particles of variable composition and density and containing a fluorescent tracer are given to experimental animals via food, drinking water, or gavage. Phosphors of various colors may be used to tag particles given at different times or of different physical characteristics. At a specified time the animal is sacrificed, and the viscera are removed and immersed immediately in isopentane at liquid-nitrogen temperature. Thin transverse sections of the gut are examined microscopically under ultraviolet light, and the position of the particles with respect to the wall is noted.

[13]B. R. Fish *et al.*, ORNL-TM-927 (1964) (classified).

[14]R. S. Decker, Jr., and M. I. Goldman, *Nuclear Utility Services Report*, NUS-167 (1964).

One rat was fed spherical particles of carnauba wax containing ZnS-CdS(Ag) (diameters ranged from 149 to 177 μ) which were maintained in the drinking water for 30 hr before necropsy. Two-millimeter-thick sections were made of the entire length of the GI tract, and counts were made of the particles within an arbitrary distance of the wall (Table 25.2). Figure 25.7 shows a section of the duodenum with one particle about 500 μ away from the nearest mucosal surface.

AN ANTHRACENE EXTRAPOLATION DOSIMETER

W. H. Wilkie, Jr. B. R. Fish

The importance of assessing the biological effects of ionizing radiation to humans and of relating tissue damage to the radiation dose delivered has prompted considerable research effort in the field of dosimetry. Primarily, the experimental approach has been focused on attempts to measure directly or indirectly the rate of energy absorption in tissue. Many of these attempts have utilized ionization extrapolation chambers[15,16] to measure

[15]R. Loevinger, *Rev. Sci. Instr.* 24(10), 407 (1953).

[16]B. R. Fish *et al.*, *Environmental Studies: Radiological Significance of Nuclear Rocket Debris. Semiann. Progr. Rept. July 1–Dec. 31, 1964*, ORNL-1053 (classified).

the ionization per unit volume as a function of the depth of a plane air gap. This function may be extrapolated to give the ionization per unit mass in an infinitely small volume. The Bragg-Gray equation relating the total ionization to the absorbed energy may then be invoked to arrive at an estimate of the absorbed dose in tissue at the depth of interest. While this technique continues to be of great significance in the field of experimental dosimetry, it has several limitations. The method yields no information regarding linear energy transfer (LET) or the absorbed energy spectrum. In addition, it necessitates the use of moderately high source activities (~10 mc).

Preliminary measurements using a series of progressively thinner scintillators indicate that an extrapolation dosimeter utilizing anthracene can be made to have a sensitivity two or three orders of magnitude greater than that of the standard ionization extrapolation chambers. If tissue-equivalent dosimetry is desired, the detection components should be made up of low-Z materials with a density near unity. An anthracene crystal (density of 1.25 g/cm^3) mounted on Lucite (density 1.18 g/cm^3) satisfies these requirements. Anthracene is the obvious choice for a scintillator, because it has the highest luminous efficiency and the best resolution of the organic scintillators. Its response to charged particles has been studied in detail. With suitable corrections for stopping power, nonlinearity, and finite resolution, a pulse-height distribution can be converted to an energy distribution, the integral of which in energy per unit time is equivalent to the dose rate that would be delivered to tissue having the same dimensions as the anthracene. It is not necessary that hollow-crystal or split-crystal techniques be used in order to obtain spectrometer-quality results with anthracene, as has been thought by some. A Fermi plot linear to energies less than 15 kev has been demonstrated for beta particles incident on the surface of a right circular cylinder of anthracene in a spectrometer system designed and constructed at ORNL.[17]

The beta particles from a discrete source deposit a fraction of their energies in the anthracene depending on the path length of the primary and secondary electrons in the crystal; the resulting photon emission is converted into a distribution of pulse height as a function of channel number using a multichannel analyzer.[18] Data obtained in this manner provide information on surface and depth doses as a function of absorbing layers between the source and the crystal face. LET data can also be generated using crystals with thickness in the micron range and with the beta radiation traversing the crystal normal to the surface. In addition, extrapolation curves may be drawn through data points taken with crystals of the same diameter and a series of thicknesses approaching zero.

Particles of spherical shape have been formed from purified and tetradistilled sulfur with diameters between 200 and 4000 μ. These are activated using neutrons to produce ^{32}P by an (n,p) reaction with ^{32}S. Dosimetry measurements will be made with these sources to simplify the comparison with calculational models developed at ORNL.[19,20]

Calibration of the anthracene crystals will be made with the aid of a monoenergetic beam of negatrons produced in a linear accelerator with energy variable from zero to 60 kev. The primary purpose of the apparatus will be to provide working calibration curves for each of some 20 to 30 anthracene crystals to be used for extrapolation dosimetry. An alpha-emitting source, ^{242}Cm, will provide a single point reference to standardize the spectrometer for dose measurements after the initial response curves are determined. The paucity of theory and experimental data concerning the response of anthracene to negatrons of energies <20 kev would cast some doubt on dose measurements in this range if no absolute response curve were available. In addition to providing energy calibration curves, the accelerator will provide the resolution curves required for making necessary iterative corrections to the pulse-height distribution.

---

[17] W. H. Wilkie and R. D. Birkhoff, *Measurement of Spectral Distribution of Positron Flux in an Infinite Copper Medium Containing ^{64}Cu*, ORNL-3469 (Dec. 10, 1963).

[18] Nuclear Data, Inc., model ND-130AT.

[19] P. A. Thompson *et al.*, *ZAP-1: A Program to Calculate Radiation Dose Rates near a Spherical Source*, ORNL-TM-803 (October 1964).

[20] P. A. Thompson *et al.*, *FORTRAN and CODAP Listings for ZAP-1 (a CDC-1604 Computer Program to Calculate Radiation Dose near a Spherical Source)*, ORNL-TM-817 (November 1964).

Suitable techniques have been developed for the preparation of extremely thin anthracene crystals. Preliminary measurements have been made using crystals as small as 1 mm in diameter and <20 μ thick. A specially selected low-noise phototube (Amperex XP-1010) is necessary for measuring spectra from crystals having small volumes. The lower energy limit of this technique is probably between 1 and 2 kev, the limit being determined by statistical variations due to the low number of photoelectrons produced and the electronic noise level.

Fig. 25.7. Fluorescent Wax Particle (Arrow) in a Transverse Section of a Rat Duodenum. ½-mm scale in upper left corner.

26. Applied Internal Dosimetry

B. R. Fish

ORNL IN VIVO GAMMA-RAY SPECTROMETRY FACILITY

P. E. Brown L. B. Farabee
G. R. Patterson, Jr. Rose J. McBath
W. H. Wilkie, Jr.

The program for obtaining a base-line count on essentially every person with a potential for future exposure was completed in May 1965. This program was implemented by having the Radiation Control Office in each division select the persons to be counted and schedule the counting time. The primary emphasis was placed on counting first those with the greatest potential for exposure.

Beginning with the third week in May 1965, the method of selecting and scheduling persons to be counted was changed to provide for the selection of persons by radiation survey personnel of the Applied Health Physics Section on the basis of a five-part priority system. Radiation survey headquarters serves as liaison to regulate the counting load and forward the requests for schedule time from the several area survey representatives to the In Vivo Gamma-Ray Spectrometry (IVGS) Facility. As before, persons suspected of having sustained an exposure have the first priority for in vivo counts; persons being recounted as a follow-up to the findings of previous in vivo counts have the second priority; persons who work directly with radioactive materials have third priority and are scheduled for approximately one count every three months; the fourth priority, which entails a count every six months, is for persons who work in the areas where radioactive materials are handled but do not work directly with the materials themselves; the last priority group includes any newly hired or other persons requiring base-line counts before beginning work with radioactive materials and a limited number of persons prior to termination of employment.

The in vivo counting program for the period between July 1, 1964, and June 30, 1965, included 1623 counts on 1462 persons; approximately 88% showed a normal human spectrum. Table 26.1 summarizes the data for those cases in which measurable amounts of internal radioactive contamination other than normal ^{40}K and ^{137}Cs were observed.

IN VIVO DETECTION AND MEASUREMENT OF ^{90}Sr-^{90}Y INTERNAL CONTAMINATION

The estimated ^{90}Sr-^{90}Y lung burdens of three persons exposed to airborne particulate $^{90}SrTiO_3$ in January 1964 (ref. 1) has been followed by chest counts at approximately one-month intervals using a lead-collimated 8 × 4 in. NaI(Tl) crystal. Figure 26.1 shows the estimated chest burdens for the two persons calculated to have an average of 100% of the maximum permissible level for the first year postexposure. At the present time, the third person involved in the exposure incident has an estimated chest burden less than 10% of the permissible level. The half-time for lung clearance appears to be >500 days.

DISTRIBUTION OF ^{40}K AND ^{137}Cs IN CALIBRATION MANNIKIN

Calibration standards for the ORNL In Vivo Gamma-Ray Spectrometry (IVGS) Facility are obtained either by counting a distilled-water-filled Alderson Research Laboratory mannikin which has discrete sources of the isotope of interest inserted in the location of the critical organs or by counting a tank-type mannikin filled with distilled water and a known quantity of the isotope. Heretofore, in the latter type of calibrations, it had been assumed that the ^{40}K and ^{137}Cs isotopes were uniformly distributed, both in the mannikin and in human subjects. However, nonuniform distributions of both ^{40}K and ^{137}Cs have been noted by

[1]B. R. Fish *et al.*, *Health Phys. Div. Ann. Progr. Rept. July 31, 1964*, ORNL-3697, p. 223.

Table 26.1. Measurable Radioactivity Found in Routine Whole-Body Monitoring Program July 1, 1964, to June 31, 1965

Isotope	Individuals Counted	Maximum Detected (μc)	Percent of Maximum Permissible Body Burden (MPBB)
^{51}Cr	3	Trace	
^{56}Co	1	0.015	*a*
^{58}Co	2	Trace	
^{60}Co	8	0.005	0.05
^{65}Zn	2	Trace	
^{90}Sr-^{90}Y	4	0.8	100[b]
^{95}Zr-^{95}Nb	2	0.018	0.09
^{106}Ru-^{106}Rh	2	0.020	0.20
^{131}I	6	0.054	40
^{137}Cs	93	0.104	0.3
^{144}Ce-^{144}Pr	3	0.075	0.75
^{203}Hg	1	0.169	*c*
^{242}Cm	5	Trace	
d	2		

[a]No MPBB data (approximately the same as ^{58}Co).
[b]Calculated maximum permissible lung burden (~0.76 μc).
[c]Medical procedure (nonoccupational).
[d]Short-half-life (9.8 min to 1.7 days) isotopes of Ir, Os, and Re (cyclotron target).

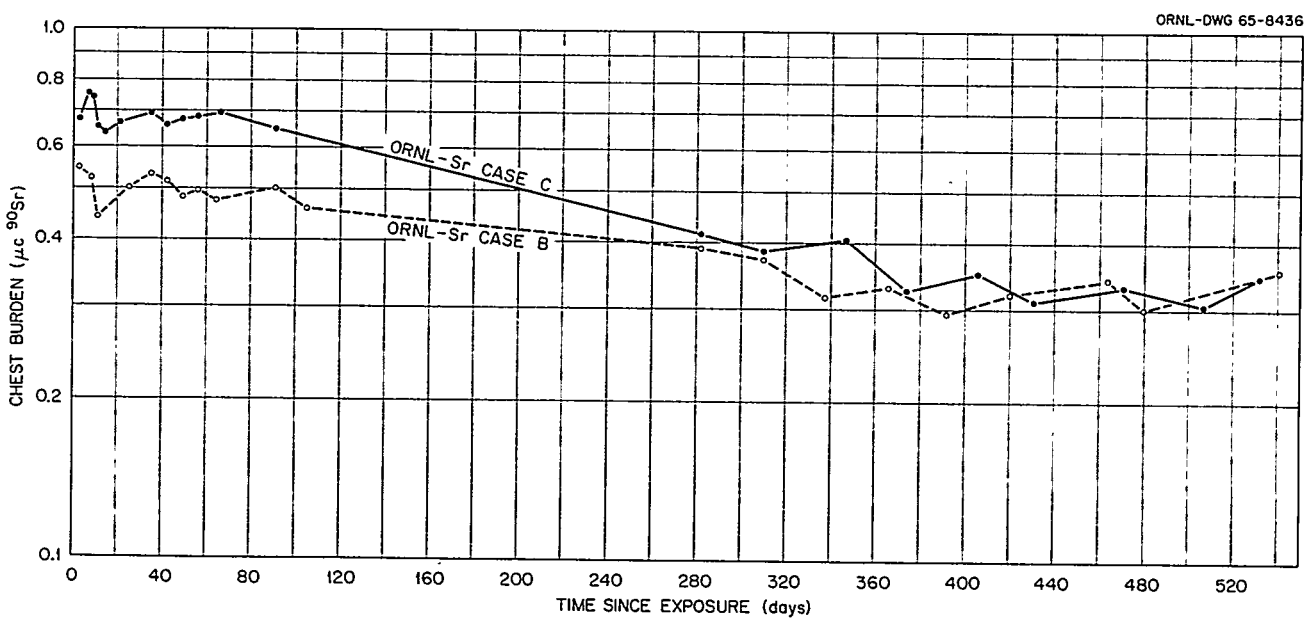

Fig. 26.1. Estimated Lung Burdens of Subjects Inhaling $^{90}SrTiO_3$. Counts were made by use of a lead-collimated 8 × 4 in. NaI(Tl) Crystal.

workers at AERE, Harwell,[2] and at the Savannah River Plant, Aiken, S.C.[3] During this report period, personnel of the ORNL-IVGS facility have investigated the distribution of ^{40}K and ^{137}Cs in normal human subjects.

Six employees of about the same body size as "standard man" were counted in the horizontal position with a lead-collimated 8 × 4 in. NaI(Tl) crystal. The crystal was positioned over the body successively at five different locations, as shown in Fig. 26.2. The distance shown for the crystal to bed surface is the same as that used in routine whole-body scan counts. Subsequently, the mannikin was filled with the usual uniform distributions of the isotopes and counted in the same manner as the human subjects. A comparison of the averages found in each sectional count of the humans to the counts found in the mannikins is given in Table 26.2. The data listed are the fractions in each section of the total counts in all sections. Because of differences in the distance between the subject and the crystal from one section of the body to the next, and because of unavoidable overlapping of the fields of view for the various crystal positions, the fractions given in the table do not represent the actual ratio of radioactivity in these parts of the human body or the mannikin; nevertheless, the data can be used successfully to adjust the proportions used in filling the mannikin to yield more realistic calibrations. The calibrations with which the human counts are presently being compared for evaluation of ^{137}Cs and of total potassium content have been made with an adjusted, nonuniform filling of the mannikin based on the findings of these studies. Based on the new calibrations the old estimates of potassium and ^{137}Cs were high by approximately 4%.

[2] J. Rundo, personal communication.

[3] J. R. Watts *et al.*, "Savannah River Plant Whole Body Counter Calibration and Operation," paper presented at the Ninth Annual Meeting of the Health Physics Society, Cincinnati, Ohio, June 1964.

Table 26.2. Comparison of Sectional Counts for Human Subjects (Average) and Mannikin Filled with Uniformly Distributed Activity

Section	^{40}K, Fraction of Total Count		^{137}Cs, Fraction of Total Count	
	Mannikin	Human	Mannikin	Human
Head	0.139	0.167	0.109	0.136
Chest	0.290	0.270	0.262	0.267
Abdomen	0.269	0.250	0.280	0.249
Thighs	0.191	0.221	0.206	0.236
Legs	0.111	0.092	0.143	0.112

ORNL-DWG 65-8437

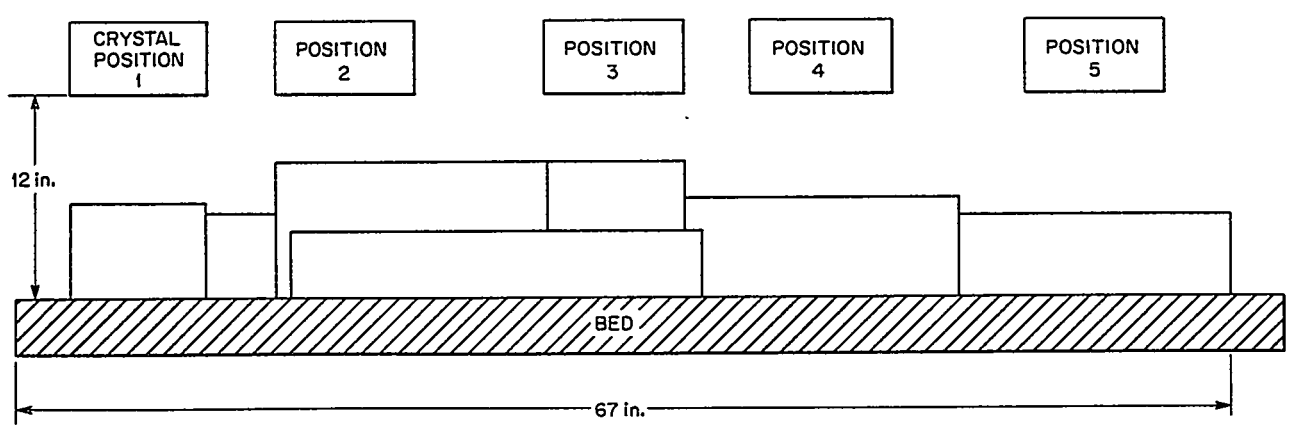

Fig. 26.2. Crystal to Subject Configuration for Sectional Counts.

Papers, Publications, and Lectures

Papers

G. A. Andrews, J. A. Auxier, and C. C. Lushbaugh
The Importance of Dosimetry to the Medical Management of Persons Accidentally Exposed to High Levels of Radiation, IAEA Symposium on Personnel Dosimetry for Accidental High-Level Exposure to External and Internal Radiation, March 8–12, 1965, Vienna, Austria. (Andrews and Lushbaugh are ORINS employees; paper presented by Andrews.)

S. I. Auerbach
Mineral Cycling Studies in Forest Ecosystems Using Radioactive Cesium, Xth International Botanical Congress, August 3–12, 1964, Edinburgh, Scotland.

Cycling of Radioactive Materials in Natural Communities, Xth International Botanical Congress, August 3–12, 1964, Edinburgh, Scotland.

Radionuclide Cycling: Current Status and Future Needs, Symposium on Radiation and Terrestrial Ecosystems, May 3–5, 1965, Richland, Washington.

J. A. Auxier
Civil Defense, Ten-Week Course in Health Physics, sponsored by the Oak Ridge Institute of Nuclear Studies, given at ORNL, November 19, 1964, Oak Ridge, Tennessee.

Ichiban: The Dosimetry Program for Nuclear Bomb Survivors of Hiroshima and Nagasaki, Protective Structures Symposium, April 19–23, 1965, Washington, D.C.

S. R. Bernard
Maximum Permissible Body Burdens and Maximum Permissible Concentrations Estimated by an Equivalence Relation Between External Dose and Internal Dose, Health Physics Society, June 14–17, 1965, Los Angeles, California.

S. R. Bernard and S. V. Kaye
Evaluation of Internal Exposure Resulting from Hypothetical Use of Former White Oak Lake Bed for Grazing, Health Physics Society, June 14–17, 1965, Los Angeles, California.

B. G. Blaylock
Chromosomal Polymorphism in Irradiated Natural Populations of Chironomus tentans, December 29, 1964, American Society of Zoologists, Knoxville, Tennessee.

W. J. Boegly, Jr., R. L. Bradshaw, F. M. Empson, W. C. McClain, F. L. Parker, and W. F. Schaffer, Jr.
Disposal of High-Level Power Reactor Wastes in a Salt Mine, 94th Annual Meeting of the American Institute of Mining Engineers, February 14–18, 1965, Chicago, Illinois.

W. J. Boegly, Jr., R. L. Bradshaw, F. M. Empson, W. C. McClain, F. L. Parker, and W. F. Schaffer, Jr.
Project Salt Vault: Radioactive Waste Disposal in a Salt Mine, 20th Annual Industrial Waste Conference, Purdue University, May 4–6, 1965, Lafayette, Indiana.

R. H. Boyett and B. R. Fish
Empirical Approach to the Beta Dosimetry of Discrete Sources in Inhomogeneous Media, Tenth Annual Health Physics Society Meeting, June 14–17, 1965, Los Angeles, California.

R. L. Bradshaw, J. O. Blomeke, W. J. Boegly, Jr., F. L. Parker, J. J. Perona, and W. F. Schaffer, Jr.
A Concept and Field-Scale Test of Disposal of High-Activity Power Reactor Wastes in Salt Mines, 1964 Winter Meeting of the American Nuclear Society, November 30–December 3, 1964, San Francisco, California.

R. L. Bradshaw, W. J. Boegly, Jr., and F. M. Empson
Correlation of Convergence Measurements in Salt Mines with Laboratory Creep-Test Data, Sixth Symposium on Rock Mechanics, University of Missouri, October 28–30, 1964, Rolla.

G. N. Brown
Ribonucleic Acid Characteristics and Varying Growth Rates for Mimosa Seedlings, AIBS Meetings (Plant Physiology Section), August 23–28, 1964, Boulder, Colorado.

J. G. Carter, R. H. Huebner, R. N. Hamm, R. D. Birkhoff, and E. T. Arakawa
Optical Properties of Graphite in the Region of 1100 Å to 3000 Å, American Physical Society, Southeastern Section, November 5–7, 1964, Chattanooga, Tennessee.

J. G. Carter, A. K. Roecklein, and R. D. Birkhoff
Diffusion Pump Oil Deposition Measurements Utilizing Radioactive Tracers, American Vacuum Society, September 30–October 2, 1964, Chicago, Illinois.

J. S. Cheka
Glass Dosimetry, Ten-Week Course in Health Physics, Oak Ridge Institute of Nuclear Studies, October 5, 1964, Oak Ridge, Tennessee

L. G. Christophorou and J. G. Carter
X-Ray Investigation of the Pyrene and Naphthalene Excimers, Symposium on Molecular Structure and Spectroscopy, June 14–18, 1965, Columbus, Ohio.

L. G. Christophorou and G. S. Hurst
Interaction of Low-Energy Electrons with Organic Molecules, Health Physics Society, June 15–18, 1964, Cincinnati, Ohio.

L. G. Christophorou and G. S. Hurst
Molecular Interactions with Low-Energy Electrons, American Physical Society, Southeastern Section, November 5–7, 1964, Chattanooga, Tennessee.

L. G. Christophorou, G. S. Hurst, R. N. Compton, and P. W. Reinhardt
Interactions of Low-Energy Electrons with Polyatomic Molecules, Radiation Research Society, May 23–26, 1965, Philadelphia, Pennsylvania.

M. J. Cook and W. S. Snyder
Estimation of Population Exposure, Health Physics Society, June 14–17, 1965, Los Angeles, California.

K. E. Cowser and W. S. Snyder
Evaluation of Radiation Dose to Man from Radionuclides Released in the Clinch River, Tenth Meeting of Health Physics Society, June 14–17, 1965, Los Angeles, California.

P. B. Dunaway
Problems in Evaluating Consequences of Irradiation on Populations of Native Rodents, Radiation Research Society, May 23–26, 1965, Philadelphia, Pennsylvania.

P. B. Dunaway, Lovell Lawrence, J. A. Payne, and J. D. Story
Intrafamily Relation of Erythrocyte Count, Mean Corpuscular Volume, and Weight in Mammals, Society of Systematic Zoology, December 27–29, 1964, Knoxville, Tennessee.

L. C. Emerson
Gamma Radiation Fields from Large Exponentially Distributed Volume Sources, Health Physics Society, June 14–17, 1965, Los Angeles, California.

L. C. Emerson and E. T. Arakawa
The Photoelectric Effect in Atomic and Molecular Gases Between 15 and 25 Electron Volts, Health Physics Society, June 14–17, 1965, Los Angeles, California.

L. C. Emerson and J. O. Blomeke
The Hazards Associated with the Tank Storage of High-Level Liquid Wastes, Health Physics Society, June 14–17, 1965, Los Angeles, California.

F. M. Empson, W. J. Boegly, Jr., R. L. Bradshaw, W. C. McClain, F. L. Parker, and W. F. Schaffer, Jr.
Demonstration of Disposal of High-Level Radioactive Solids in Salt, Second Symposium on Salt, May 3–5, 1965, Cleveland, Ohio.

B. R. Fish and R. L. Walker
Aerosol Physics of Radioactive Particles, International Symposium on Fission Product Release and Transport Under Accident Conditions, April 5–7, 1965, Oak Ridge, Tennessee.

Kenneth Fox
Theory of Vibration-Rotation Interactions in Spherical Top Molecules, American Physical Society, Southeastern Section, November 5–7, 1964, Chattanooga, Tennessee.

Kenneth Fox
Theory of Vibration-Rotation Interactions in Spherical Top Molecules – I. A New Overtone Band, International Symposium on Atomic and Molecular Quantum Theory, January 13–23, 1965, Sanibel Island, Florida.

R. N. Hamm, R. A. MacRae, and E. T. Arakawa
Polarization Studies in the Vacuum Ultraviolet, Optical Society of America, March 31–April 2, 1965, Dallas, Texas.

R. N. Hamm, W. J. McConnell, R. D. Birkhoff, and M. Berger
Contributions of Successive Generations of Secondary Electrons to the Electron Slowing Down Flux, American Physical Society, April 26–29, 1965, Washington, D.C.

W. F. Hanson, R. J. Herickhoff, E. T. Arakawa, and R. D. Birkhoff
The Angular Distribution and Thickness Dependence of Transition Radiation from Thin Aluminum Foils, American Physical Society, April 26–29, 1965, Washington, D.C.

R. J. Herickhoff, E. T. Arakawa, and R. D. Birkhoff
Characteristic Energy Loss Studies of Cd, In, and Zn Using the Optical Method, American Physical Society, Southeastern Section, November 5–7, 1964, Chattanooga, Tennessee.

H. Hollister and J. E. Turner
On the Relationship of Linear Momentum Transfer to RBE: Remarks on the 1962 ICRP/ICRU Report, Health Physics Society, June 14–17, 1965, Los Angeles, California.

H. J. Howe and R. H. Ritchie
Light from Electron Irradiated Metals, American Physical Society, April 26–29, 1965, Washington, D.C.

D. G. Jacobs
Use of Negative Sorption in Studies of Ion Fixation by Hydrobiotite, Clay Mineral Society Meeting, October 5–9, 1964, Madison, Wisconsin.

T. M. Jelinek, R. H. Huebner, R. N. Hamm, and E. T. Arakawa
The Optical Constants of Vacuum Evaporated Tl, Cd, and Zn from 500 Å to 2800 Å, American Physical Society, April 26–29, 1965, Washington, D.C.

D. R. Johnson, J. H. Thomgate, and P. T. Perdue
Neutron and Gamma-Ray Leakage from the "Ichiban" Critical Assembly, Health Physics Society, June 14–17, 1965, Los Angeles, California (presented by J. A. Auxier).

T. D. Jones
Distribution of Dose and Dose Equivalent in a Cylindrical Tissue Phantom from Fission Sources of Neutrons, International Symposium on the Dosimetry of Irradiations from External Sources, French Section of Health Physics Society, November 23–27, 1964, Paris, France.

Body Sodium Activation as a Dosimetric Tool in Nuclear Accidents, Health Physics Society, June 14–17, 1965, Los Angeles, California.

C. E. Klots
Energy Partition in Gaseous Mixtures, Radiation Research Society, May 23–26, 1965, Philadelphia, Pennsylvania.

T. F. Lomenick, D. G. Jacobs, and F. L. Parker
The Distribution of ^{90}Sr and ^{137}Cs in Abandoned Seepage Pits, Health Physics Society, June 14–17, 1965, Los Angeles, California.

A. L. Marusak and J. E. Turner
Preliminary Analytic Fits to Shell Corrections in Stopping Power, American Physical Society, Southeastern Section, November 5–7, 1964, Chattanooga, Tennessee.

W. J. McConnell and R. D. Birkhoff
Electron Slowing-Down Spectrum in Cr of Monoenergetic Electrons from Cr^{51}, Radiation Research Society, May 23–26, 1965, Philadelphia, Pennsylvania.

W. J. McConnell, H. H. Hubbell, Jr., and R. D. Birkhoff
Slowing Down Spectrum of Au^{198} Beta Rays in Gold, American Physical Society, Southeastern Section, November 5–7, 1964, Chattanooga, Tennessee.

K. Z. Morgan
The Need for Research Programs to Provide Data Applicable to the Estimate of Maximum Permissible Exposure Values for Internally Deposited Radionuclides, Fourth Inter-American Conference on Toxicology and Occupational Medicine, August 24–27, 1964, Miami Beach, Florida.

K. Z. Morgan
What Is the Importance of Dosimetry of Internally Administered Emitters? Fifth Annual Meeting of the Society of Nuclear Medicine, October 23, 1964, Emory University, Atlanta, Georgia.

K. Z. Morgan
Compatibility of Science and Religion, Vesper Service, Gloria Dei Lutheran Church, November 1, 1964, Knoxville, Tennessee.

Y. Nakai, W. Garber, R. H. Ritchie, and R. D. Birkhoff
Detection of Plasmon Excitation by Low-Energy Electrons in Aluminum, American Physical Society, April 26–29, 1965, Washington, D.C.

J. Neufeld and Harvel Wright
Excitation of Whistler and Hydromagnetic Waves in a Stream of Gyrating Electrons, International Scientific Radio Union, April 20–23, 1965, Washington, D.C.

J. Neufeld and Harvel Wright
Generation of Whistler Waves by a Helical Electron Beam, International Scientific Radio Union, October 11–14, 1964, Urbana, Illinois.

J. S. Olson
Equations for Cesium Transfer in Liriodendron *Forest,* Symposium on Radiation and Terrestrial Ecosystems, May 3–5, 1965, Richland, Washington.

J. S. Olson
Use of Tracer Techniques for the Study of Biogeochemical Cycles, 1st International Symposium on Ecosystems, July 29, 1965, Copenhagen, Denmark.

F. L. Parker
Comparison of United States and Soviet Union Waste Disposal Standards, Health Physics Society, June 14–17, 1965, Los Angeles, California.

F. L. Parker
Disposal of Radioactive Waste Solids, National Academy of Sciences–National Research Council Seminar on Pollution, April 29–30, 1965, Washington, D.C.

J. A. Payne, P. B. Dunaway, G. D. Martin, and J. D. Story
Plasma Protein Alterations in Peromyscus leucopus *Infested with* Cuterebra angustifrons, American Society of Zoologists, December 27–29, 1964, Knoxville, Tennessee.

D. E. Reichle and D. A. Crossley, Jr.
Radiocesium Dispersion in a Cryptozoan Food Web, Symposium on Radiation and Terrestrial Ecosystems, May 3–5, 1965, Richland, Washington.

R. H. Ritchie
Plasmons and Electrons in Metals, American Physical Society, Southeastern Section, November 5–7, 1964, Chattanooga, Tennessee.

A. S. Rogowski and Tsuneo Tamura
Movement of Cesium-137 by Runoff, Erosion, and Infiltration on the Alluvial Captina Silt Loam, Symposium on Radiation and Terrestrial Ecosystems, May 3–5, 1965, Richland, Washington.

G. W. Royster, Jr., and B. R. Fish
Redispersion of Surface Dust in a Room, Fourth National Technical Meeting, American Association for Contamination Control, May 25–28, 1965, Miami, Florida.

G. W. Royster, Jr., and B. R. Fish
Studies of Surface Contamination. IV. Resuspension of Particulate Contamination in a Room, Tenth Annual Health Physics Society Meeting, June 14–17, 1965, Los Angeles, California.

H. C. Schweinler
Interstitial Diffusion in Crystalline Cubic Elements, American Physical Society, March 24–27, 1965, Kansas City, Missouri.

A. F. Shinn
Radioecology of Mud-Dauber Wasps, Annual Meetings, Entomological Society of America, December 1, 1964, Philadelphia, Pennsylvania.

Radioecology of Sceliphron *and* Trypoxylon *Mud-Dauber Wasps,* American Society of Zoologists, December 27, 1964, Knoxville, Tennessee.

W. S. Snyder
Recent Developments in Internal Dose Concepts, Joint Technical Meeting of New England Sections of Air Pollution Control Association, Health Physics Society, and American Industrial Hygiene Association, May 20, 1965, Yankee Drummer Inn, Auburn, Massachusetts.

W. S. Snyder and Mary R. Ford
A Monte-Carlo Code for Estimation of Dose from Gamma-Ray Sources, Health Physics Society, June 14–17, 1965, Los Angeles, California.

J. L. Stanford, R. D. Birkhoff, and E. T. Arakawa
Photoelectric Yields of Pt, Au, and Pd from 300 Å to 1300 Å, American Physical Society, April 26–29, 1965, Washington, D.C.

I. H. Tipton, Jane J. Shafer, and Fred W. Roberts
The Use of Computers in Spectrochemical Analysis, 8th Conference on Analytical Chemistry in Nuclear Technology, October 7, 1964, Gatlinburg, Tennessee.

I. H. Tipton and Peggy L. Stewart
Spectrographic Analysis of Biological Material, 16th Annual Mid-America Symposium on Spectroscopy, June 1965, Chicago, Illinois.

J. E. Turner
The Application of Shell Corrections in Stopping Power to Theoretical Dose Studies, International Symposium on the Dosimetry of Irradiations from External Sources, November 23–27, 1964, Paris, France.

G. M. Van Dyne
Application of Some Operations Research Techniques to Food Chain Analysis Problems, Symposium on Radiation and Terrestrial Ecology, May 3–5, 1965, Richland, Washington.

G. M. Van Dyne
Distance Traveled by Sheep on Winter Range, Annual Meeting, Western Section, American Society of Animal Science, July 12–14, 1965, Fort Collins, Colorado.

G. M. Van Dyne
Probabilistic Estimates of Range Forage Intake, Annual Meeting, Western Section, American Society of Animal Science, July 12–14, 1965, Fort Collins, Colorado.

R. L. Walker and B. R. Fish
Adhesion of Particles to Surfaces in Liquid and Gaseous Environments, Fourth National Technical Meeting, American Association for Contamination Control, May 25–28, 1965, Miami, Florida.

J. P. Witherspoon
Radiation Damage to Forest Surrounding an Unshielded Fast Reactor, Symposium on Radiation and Terrestrial Ecosystems, May 3–5, 1965, Richland, Washington.

Martin Witkamp
Environmental Influences on Microbial Populations and Activity of the Forest Floor, VIIIth International Congress of Soil Science, Section of Soil Biology, August 31–September 9, 1964, Bucharest, Rumania.

Martin Witkamp and D. A. Crossley, Jr.
Effects of a Pesticide on Biota and Breakdown of Forest Litter, VIIIth International Congress of Soil Science, Section of Soil Biology, August 31–September 9, 1964, Bucharest, Rumania.

Harvel Wright, G. S. Hurst, and E. B. Wagner
An Application of the Generalized Concept of Dosimetry to Space Radiations, Second Symposium on the Protection Against Radiations in Space, October 12–14, 1964, Gatlinburg, Tennessee.

Publications

G. A. Andrews, J. A. Auxier, and C. C. Lushbaugh
"The Importance of Dosimetry to the Medical Management of Persons Accidentally Exposed to High Levels of Radiation," *IAEA Symposium on Personnel Dosimetry for Accidental High-Level Exposure to External and Internal Radiation, Vienna, Austria* (to be published in proceedings) (Andrews and Lushbaugh are ORINS employees.)

J. C. Ashley and R. H. Ritchie
"Photon Emission from Irradiated Dielectric Slabs," *J. Appl. Phys.* **35**, 2313–21 (1964).

S. I. Auerbach *et al.*
"Postattack Recovery in Civil Defense," *Project Harbor Summary Report,* Natl. Acad. Sci.–Natl. Res. Council, Publ. 1237 (1964).

L. Augenstein, James Carter, Jaynati Nag-Chaudhuri, DeVaughn Nelson, and Edward Yeargers
"Comparison of Emission from Excited States Produced in Proteins and Amino Acids by Ultraviolet Light and Ionizing Radiation," pp. 73–92 in *Physical Processes in Radiation Biology,* Academic, New York, 1964.

J. A. Auxier
Ichiban: The Dosimetry Program for Nuclear Bomb Survivors of Hiroshima and Nagasaki–A Status Report as of April 1, 1964, CEX-64.3 (July 31, 1964).

"The Health Physics Research Reactor," *Health Phys.* 11, 89–93 (1965).

"Nuclear Accident at Wood River Junction," *Nucl. Safety* 6(3), 298–301 (1965).

Report of Trip Abroad by J. A. Auxier During Period May 10, 1965–May 12, 1965, ORNL-CF-65-6-7 (June 7, 1965).

R. D. Birkhoff
"Energy Loss Spectra for Charged Particles Traversing Metal and Plastic Films," pp. 145–59 in *Physical Processes in Radiation Biology,* Academic, New York, 1964.

R. E. Blanco and F. L. Parker
Waste Treatment and Disposal Quarterly Progress Report, November 1963–January 1964, ORNL-TM-830 (August 1964).

B. G. Blaylock
"A Method for Preparing Salivary-Gland Chromosomes," *Drosophila Information Service* 40, 97 (1965).

"Chromosomal Aberrations in a Natural Population of *Chironomus tentans* Exposed to Chronic Low-Level Radiation," *Evolution* (in press).

"Chromosomal Polymorphism in Irradiated Natural Populations of Chironomidae," submitted for publication in *Genetics.*

"Chromosomal Polymorphism in Irradiated Natural Populations of *Chironomus tentans,*" *Am. Zoologist* 4, 405 (1965) (abstract).

B. G. Blaylock and J. P. Witherspoon, Jr.
"Environmental Factors Affecting Dosimetry," *Health Phys.* 11, 549 (1965).

R. L. Bradshaw
Analysis of Data from Plastic Flow Gages in Experimental Area of Lyons, Kansas, Salt Mine with Special Consideration of Roof Stability, ORNL-CF-65-4-56 (Apr. 20, 1965).

Book review of "Treatment and Storage of High-Level Radioactive Wastes," *Nucl. Sci. Eng.* 18(4), 534 (1964).

Discussion of: "Heat Generation by Radioactive Wastes," *J. Sanit. Engr. Div., Am. Soc. Civil Engrs.* 90(SA5), Pt. 1, 55–57 (1964).

R. L. Bradshaw, J. O. Blomeke, W. J. Boegly, Jr., F. L. Parker, J. J. Perona, and W. F. Schaffer, Jr.
"A Concept and Field-Scale Test of Disposal of High-Activity Power Reactor Wastes in Salt Mines," *Trans. Am. Nucl. Soc.* 7(2), 399–400 (1964).

R. L. Bradshaw, W. J. Boegly, Jr., and F. M. Empson
"Correlation of Convergence Measurements in Salt Mines with Laboratory Creep-Test Data," pp. 501–14 in *Proceedings of the 6th Symposium on Rock Mechanics, October 1964,* University of Missouri at Rolla (1964).

R. L. Bradshaw, J. J. Perona, and J. O. Blomeke
Demonstration Disposal of High-Level Radioactive Solids in Lyons, Kansas, Salt Mine: Background and Preliminary Design of Experimental Aspects, ORNL-TM-734 (Jan. 10, 1964).

G. N. Brown
"Temperature Controlled Growth Rates and Ribonucleic Acid Characteristics in Mimosa Epicotyl Tissue," *Plant Physiology* (in press).

G. N. Brown and A. W. Naylor
"Quantitative Studies of Nucleic Acids in Contrasting Zones of Tissue Differentiation in Germinating Mimosa Seedlings," *Botan. Gaz.* (in press).

J. G. Carter, J. A. Elder, R. D. Birkhoff, and A. K. Roecklein
"Diffusion Pump Oil Deposition Measurements Utilizing Radioactive Tracers," *J. Vacuum Sci. Technol.* **2**, 59–62 (1965).

J. G. Carter, R. H. Huebner, R. N. Hamm, and R. D. Birkhoff
"Optical Properties of Graphite in the Region 1100 to 3000 Å," *Phys. Rev.* **137**, A639–41 (1965).

J. G. Carter, D. R. Nelson, and L. G. Augenstein
"The Effect of Temperature on X-Ray Induced Light Emission from Powders of Amino Acids and Trypsin," *Arch. Biochem. Biophys.* (in press).

J. S. Cheka
Report of Trip Abroad by J. S. Cheka During Period April 13, 1965–May 22, 1965, ORNL-CF-65-6-18 (June 10, 1965).

J. S. Cheka, F. W. Sanders, T. D. Jones, and W. H. Shinpaugh
Distribution of Weapons Radiation in Japanese Residential Structures, CEX-62.11 (in press).

L. G. Christophorou, R. N. Compton, G. S. Hurst, and P. W. Reinhardt
"The Determination of Electron Capture Cross Sections with Swarm-Beam Techniques," to be published in the *Journal of Chemical Physics.*

G. E. Cosgrove and T. P. O'Farrell
"Papillomas and Other Pathologic Findings in the Stomachs of Pine Mice," *J. Mammal.* (in press).

G. E. Cosgrove, T. P. O'Farrell, S. V. Kaye, and P. B. Dunaway
"Infection of Laboratory-Reared and Wild Cotton Rats with Cat Tapeworm Larvae," *J. Tenn. Acad. Sci.* **39**, 140–41 (1964).

K. E. Cowser
"Current Practices in the Release and Monitoring of ^{131}I at NRTS, Hanford, Savannah River, and ORNL," *Nucl. Safety* **6**(2), 212–18 (1964–65).

Current Practices in the Release and Monitoring of ^{131}I at NRTS, Hanford, Savannah River, and ORNL, ORNL-NSIC-3 (Aug. 11, 1964).

D. A. Crossley, Jr.
"Radioisotope Measurement of Food Consumption by a Leaf Beetle Species, *Chrysomela knabi* Brown," *Ecology* (in press).

D. A. Crossley, Jr. (with E. W. Baker)
"A New Species of Mite, *Fusoherecia lawrencei,* from an Artificial Tree-Hole (Acarina: Glycyphagidae)," *Ann. Natal Museum* **16**, 3–8 (1964).

D. A. Crossley, Jr. (with G. L. Plummer and D. A. Gardiner)
"A Growth Response of Two Sedges Inhabiting a Radioactive Waste Disposal Area," *Ecology* **46**(3), 346–48 (1965).

D. A. Crossley, Jr., and Martin Witkamp
"Effects of a Pesticide on Biota and Breakdown of Forest Litter," *Proc. Intern. Congr. Soil Sci., 8th, Bucharest, Rumania* (in press).

"Forest Soil Mites and Mineral Cycling," *Proc. Intern. Congr. Acarology, 1st (Acarologia Publ.),* 137–46 (1964).

Wallace de Laguna
"Importance of Deep Permeable Disposal Formations in Siting a Nuclear Fuel Reprocessing Plant," Foreword to *Radioactive Waste-Disposal Potentials in Selected Geologic Basins*, SAN-413-2, A Reconnaissance Study by Subcommittee on Atomic Waste Disposal of AAPG, Midland, Texas, for U.S. Atomic Energy Commission, John E. Galley, Chairman, June 24, 1964.

P. B. Dunaway and L. L. Lewis
"Taxonomic Relation of Erythrocyte Count, Mean Corpuscular Volume, and Body Weight in Mammals," *Nature* **205**, 481–84 (1965).

F. M. Empson
"Demonstration of Disposal of High-Level Radioactive Solids," *Newsletter*, Kansas State Department of Health, Topeka, October 26, 1964.

F. M. Empson and Hisashi Kubota
"Problems in Disposal of Radioactive Liquid Wastes in Salt," *Chem. Eng. Progr.*, Symp. Ser., **60**(53), 68–73 (1964).

U. Fano and J. E. Turner
"Contributions to the Theory of Shell Corrections," pp. 49–67 in *Studies in Penetration of Charged Particles in Matter*, Natl. Acad. Sci.–Natl. Res. Council, Publ. 1133 (1964).

B. R. Fish, R. H. Boyett, T. G. Clark, J. L. Thompson, and W. H. Wilkie, Jr.
Environmental Studies: Radiological Significance of Nuclear Rocket Debris. Semi-Annual Progress Report for Period Ending December 31, 1964, ORNL-TM-1053 (April 1965) (classified).

B. R. Fish, T. G. Clark, R. H. Boyett, W. C. McWhorter, and G. W. Royster, Jr.
Environmental Studies: Radiological Significance of Nuclear Rocket Debris. Annual Progress Report for Period Ending June 30, 1964, ORNL-TM-927 (Sept. 1964) (classified).

B. R. Fish, R. L. Walker, G. W. Royster, Jr., and J. L. Thompson
Redispersion of Settled Particulates, ORNL-TM-1049 (Feb. 5, 1965).

Kenneth Fox
"A Theorem on the Reduced Matrix Element of an Irreducible Spherical Tensor Operator," submitted for publication in the *Journal of Chemical Physics*.

"Theory of Vibration-Rotation Interactions in Spherical Top Molecules. I. A New Overtone Band," *J. Mol. Spectry.* (in press).

"Theory of Vibration-Rotation Interactions in Spherical Top Molecules. I. A New Overtone Band" (Proceedings of International Symposium on Atomic and Molecular Quantum Theory, January 18–23, 1965, Sanibel Island, Florida), submitted for publication in the *Journal of Chemical Physics*.

W. F. Hanson, R. J. Herickhoff, E. T. Arakawa, and R. D. Birkhoff
Investigation of Plasma Radiation from Electron Bombarded Aluminum Foils as a Function of the Angle of Observation and the Foil Thickness, ORNL-TM-1126 (June 1965).

F. F. Haywood
"Spatial Dose Distribution in Air-over-Ground Geometry," *Health Phys.* **11**, 185–92 (1965).

F. F. Haywood and J. A. Auxier
Technical Concept – Operation HENRE, CEX-65.02 (March 1965).

F. F. Haywood, J. A. Auxier, and E. T. Loy
An Experimental Investigation of the Spatial Distribution of Dose in an Air-over-Ground Geometry, CEX-62.14 (October 1964).

F. F. Haywood, J. A. Auxier, and T. G. Provenzano (eds.)
Operations Plan – Operation HENRE (prepared by Operation HENRE Technical Director's Staff), CEX-65.03 (in press).

R. J. Herickhoff, E. T. Arakawa, and R. D. Birkhoff
Characteristic Energy Loss Studies of Electron-Bombarded Al, Cd, In, Mg, and Zn Foils with Vacuum Ultraviolet Spectroscopy, ORNL-TM-1107 (Apr. 14, 1965).

"Optical Emission Studies of the Characteristic Energy Losses in Cd, In, Tl, and Zn," *Phys. Rev.* 137, A1433–35 (1965).

R. J. Herickhoff, W. F. Hanson, E. T. Arakawa, and R. D. Birkhoff
"The Angular Distribution and Thickness Dependence of Transition Radiation from Thin Al Foils," submitted for publication in the *Physical Review.*

H. Hollister and J. E. Turner
"On the Relationship of Linear Momentum Transfer to RBE: Remarks on the 1962 ICRP/ICRU Report," submitted for publication in *Health Physics.*

H. H. Hubbell, W. J. McConnell, and R. D. Birkhoff
"The Spherical Condenser as a High Transmission Particle Spectrometer – III. Construction and Calibration," *Nucl. Instr. Methods* 31, 18–24 (1964).

R. H. Huebner, E. T. Arakawa, R. N. Hamm, and R. A. MacRae
Optical Constants of Evaporated Metal Films of Silver and Indium, ORNL-TM-1104 (Apr. 8, 1965).

R. H. Huebner, E. T. Arakawa, R. A. MacRae, and R. N. Hamm
"Optical Constants of Vacuum-Evaporated Silver Films," *J. Opt. Soc. Am.* 54, 1434–37 (1964).

G. S. Hurst, T. E. Bortner, and R. E. Glick
"Ionization and Excitation of Atomic Argon with Alpha Particles," *J. Chem. Phys.* 42, 713–19 (1964).

D. R. Johnson, J. H. Thorngate, P. W. Reinhardt, and F. J. Davis
"An Experimental Calibration of Fission Foil Threshold Detectors," submitted for publication in *Health Physics.*

R. M. Johnson
The Herpetofauna of the Oak Ridge Area, ORNL-3653 (December 1964).

T. D. Jones
Report of Trip Abroad by T. D. Jones During Period September 14, 1964–November 28, 1964, ORNL-CF-64-12-36 (Dec. 29, 1964).

"Distribution of Dose and Dose Equivalent in a Cylindrical Tissue Phantom from Fission Sources of Neutrons," to be published in *Proceedings of International Symposium on the Dosimetry of Irradiations from External Sources,* Health Physics Society French Section Series, Paris, France.

T. D. Jones, D. R. Johnson, and J. H. Thorngate
"Neutron Dose Conversion Factors for PuBe and PoBe Sources," *Health Phys.* 11, 519–22 (1965).

S. V. Kaye
"Use of Miniature Glass Rod Dosimeters in Radiation Ecology," *Ecology* 46, 201–6 (1965).

N. R. Kevern
"Relative Strontium and Calcium Uptake by Green Algae," *Science* 146, 1488 (1964).

"Strontium and Calcium Uptake by the Green Algae, *Oocystis eremosphaeria,*" *Science* 145, 1445–46 (1964).

N. R. Kevern and R. C. Ball
"Primary Productivity and Energy Relationships in Artificial Streams," *Limnol. Oceanog.* 10(1), 74–87 (1965).

L. L. Lewis and P. B. Dunaway
Techniques for Hematological Studies of Wild Mammals, ORNL-3806 (June 1965).

T. F. Lomenick
Lithology of Ceiling in the Experimental Area of the Lyons Mine, ORNL-CF-65-4-57 (Apr. 26, 1965).

T. F. Lomenick and R. L. Bradshaw
"Accelerated Deformation of Rock Salt at Elevated Temperatures," *Nature* **207**, 158–59 (1965).

T. F. Lomenick and D. A. Gardiner
"The Occurrence and Retention of Radionuclides in the Sediments of White Oak Lake," *Health Phys.* 11(6), 567–77 (1965).

Liliana Masironi and B. R. Fish
Direct Observation of Particle Reentrainment from Surfaces, ORNL-TM-1054 (Feb. 10, 1965).

W. J. McConnell, H. H. Hubbell, Jr., R. N. Hamm, R. H. Ritchie, and R. D. Birkhoff
"Electron Slowing-Down Spectrum in Cu of Beta Rays from Cu^{64}," *Phys. Rev.* **138**, A1377–83 (1965).

W. M. McMaster and H. D. Waller
Geology and Soils of Whiteoak Creek Basin, Tennessee, ORNL-TM-1108 (May 1965).

E. F. Menhinick
Design of ^{90}Sr Sources for Ecological Studies Involving Beta Irradiation, ORNL-TM-997 (Nov. 11, 1964).

"^{90}Sr Plaques for Beta Radiation Studies," submitted for publication in *Health Physics.*

K. Z. Morgan
"The Need for Research Programs to Provide Data Applicable to the Estimate of Maximum Permissible Exposure Values for Internally Deposited Radionuclides," *Ind. Med. Surg.* 33(7), 496 (July 1964); also, *J. Nucl. Med.* **6**, 79 (1965).

"Recommendations of Publication 6 of the ICRP," *Nucl. Safety* 6(1), 20 (1964).

"Radiation Hazards Associated with Tritium," Introduction for report of the Symposium on Tritium Hazards, Vesinet, France, Apr. 16–18, 1964.

Yohta Nakai, F. W. Garber, R. H. Ritchie, and R. D. Birkhoff
"Electronic Energy Levels in Aluminum – A Solid State Franck and Hertz Experiment," *J. Phys. Chem. Solids* (in press).

D. J. Nelson
"Biological Vectors and Reservoirs of Strontium-90," *Nature* **203**(4943), 420 (1964).

"Strontium in Calcite: New Analysis," *Institute of Marine Science* (University of Texas) (in press).

D. J. Nelson (with G. M. Rosenthal and D. A. Gardiner)
"Deposition of Strontium and Calcium in Snail Shell," *Nature* (in press).

D. J. Nelson (with C. W. Wiser)
"Uptake and Elimination of Cobalt-60 by Crayfish," *Amer. Midland Naturalist* **71**(1), 181–202 (1964).

D. R. Nelson, J. G. Carter, R. D. Birkhoff, and L. G. Augenstein
"Yield of Luminescence from X-Irradiated Biochemicals," submitted for publication in *Radiation Research.*

J. Neufeld
Report of Trip Abroad by J. Neufeld During the Period April 18–May 6, 1965, ORNL-CF-65-6-21 (June 4, 1965).

J. Neufeld and Harvel Wright
"Excitation of Magnetodynamic Waves by a Helical Proton Beam," submitted for publication in the *Physics of Fluids.*

"Generation of Whistler Waves by Helical Electron Beams," *Nature* **206**, 288–89 (1964).

"Hydromagnetic Instabilities Caused by a Gyrating Proton Stream," *Nature* **206**, 498 (1965).

"Instabilities Produced in a Plasma by a Helical Proton Beam," submitted for publication in the *Physical Review.*

"Instabilities Produced in a Stationary Plasma by an 'Almost Circular' Electron Beam," *Phys. Rev.* **137**, A1076–83 (1965).

"Interaction of a Plasma with a 'Helical' Electron Beam," *Phys. Rev.* **135**, A1175–89 (1964).

"Multiple Instability in a Plasma-Beam System," *Phys. Fluids* **7**, 1527–34 (1964).

T. P. O'Farrell
"Home Range and Ecology of Snowshoe Hares in Interior Alaska," *J. Mammal.* (in press).

"The Rabbits of Middleton Island, Alaska," *J. Mammal.* (in press).

J. S. Olson
"Advances in Radiation Ecology," *Nucl. Safety* 6(1), 78–81 (1964).

"Eolian Transport," submitted for publication in *Encyclopedia of Earth Sciences.*

"Equations for Cesium Transfer in *Liriodendron* Forest," *Health Phys.* (Proceedings of Symposium on Radiation and Terrestrial Ecosystems, Richland, Washington, May 3–5, 1965) (in press).

F. L. Parker
"Disposal of Radioactive Wastes in Fresh Water," *Nucl. Safety* 6(1), 89–97 (1964).

"United States and Soviet Union Waste Disposal Standards," *Nucl. Safety* 6(4) (1965).

F. L. Parker and R. E. Blanco
Waste Treatment and Disposal Semiannual Progress Report, July–December 1964, ORNL-TM-1081 (May 1965).

B. C. Patten
Community Organization and Energy Relationships in Plankton, ORNL-3653 (February 1965).

"The Biocoenetic Process in an Estuarine Phytoplankton Community," submitted for publication in *Estuaries* (Proceedings of AAAS Symposium).

"Equilibrium Behavior of Specific Activity in Two-Compartment Tracer Experiments," submitted for publication in *Health Physics.*

"Odd-Even Relationships in Food Webs," submitted for publication in *Ecology.*

The Systems Approach in Radiation Ecology, ORNL-TM-1008 (November 1964).

B. C. Patten and B. F. Chabot
"Factorial Productivity Experiments in a Shallow Estuary," submitted for publication in *Limnology and Oceanography.*

B. C. Patten and A. L. Kretchmar
"Analog Computer Solutions of the Lotka-Volterra Equations," submitted for publication in the *American Scientist.*

B. C. Patten, D. K. Young, and M. H. Roberts
"Vertical Distribution and Sinking Characteristics of Seston in the Lower York River, Virginia," submitted for publication in *Limnology and Oceanography.*

J. A. Payne
"A Summer Carrion Study of the Baby Pig, *Sus scrofa* Linnaeus," *Ecology* (in press).

J. A. Payne and G. E. Cosgrove
"Tissue Changes Following *Cuterebra* Infestations in Rodents," *Am. Midland Naturalist* (in press).

J. A. Payne, P. B. Dunaway, G. D. Martin, and J. D. Story
"Effects of *Cuterebra angustifrons* on Plasma Proteins of *Peromyscus leucopus,*" *J. Parasitol.* (in press).

D. E. Reichle and D. A. Crossley, Jr.
"Radiocesium Dispersion in a Cryptozoan Food Web," *Health Phys.* (in press).

D. E. Reichle, J. D. Palmer, and O. Park
"Persistent Rhythmic Locomotor Behavior in the Cave Cricket, *Hadenoecus subterraneus*, and Its Ecological Significance," *Am. Midland Naturalist* (in press).

R. H. Ritchie
"The Damping of Electromagnetic Waves in an Electron Gas," to be published in the *Physical Review*.

R. H. Ritchie and J. C. Ashley
"The Interaction of Hot Electrons and Holes with a Free Electron Gas," submitted for publication in the *Journal of Physics and Chemistry of Solids*.

R. H. Ritchie, J. C. Ashley, and L. C. Emerson
"Optical Bremsstrahlung and Transition Radiation from Irradiated Media," *Phys. Rev.* **135**, A759–63 (1964).

A. K. Roecklein
A New Technique for Measuring Range of Low-Energy Charged Particles in Conducting Solids, ORNL-3702 (March 1965).

G. W. Royster, Jr., and B. R. Fish
Techniques for Assessing "Removable" Surface Contamination, ORNL-TM-1045 (Feb. 4, 1965).

H. A. Schroeder, J. J. Balassa, and I. H. Tipton
"Abnormal Trace Metals in Man – Tin," *J. Chronic Diseases* **17**, 483 (1964).

A. F. Shinn
"Three New Species of the Bee Genus *Calliopsis* (Hymenoptera, Andrenidae)," *Am. Museum Novitates* **2211**, 1–19 (1965).

W. S. Snyder
"On the Estimation of a Systemic Body Burden of Plutonium," *Assessment of Radioactivity in Man*, vol. II, pp. 583–88, IAEA, Vienna, 1964.

"The Distribution of ^{239}Pu in the Body Following Exposure by Inhalation," *Health Phys.* **10**(12), 1035 (1964).

J. L. Stanford, R. N. Hamm, and E. T. Arakawa
"Angular Dependence of Photoelectric Yields in the Wavelength Region 300 Å to 1200 Å," to be published in the *Journal of the Optical Society of America*.

J. A. Stockdale, G. S. Hurst, and L. G. Christophorou
"Capture of Low-Energy Electrons in Chlorobenzene and Bromobenzene," *Nature* **202**, 459–61 (1964).

"Capture of Low-Energy Electrons in Chlorobenzene and Bromobenzene," *Nature* **203**, 1270 (1964).

T. D. Strickler and E. T. Arakawa
"Optical Emission from Argon Excited by Alpha Particles: Quenching Studies," *J. Chem. Phys.* **41**, 1783–89 (1964).

F. G. Taylor, Jr.
"Nuclear Volume Changes in Southeastern Tree Species Before Spring Growth," *Radiation Botany* **5**, 61–64 (1965).

P. A. Thompson, S. A. Lewis, and T. G. Clark
FORTRAN and CODAP Listings for ZAP-1 (a CDC-1604 Computer Program to Calculate Radiation Dose near a Spherical Source), ORNL-TM-817 (November 1964).

P. A. Thompson, S. A. Lewis, T. G. Clark, B. R. Fish, and R. H. Boyett
ZAP-1: A Program to Calculate Radiation Dose Rates near a Spherical Source, ORNL-TM-803 (October 1964).

J. H. Thomgate
"A Medium Speed Coincidence Circuit Using Tunnel Diodes," *Health Phys.* 10(4), 283–84 (1964).

"A Versatile Frequency Divider," *Health Phys.* 10, 687–89 (1964).

J. H. Thorngate and D. R. Johnson
"The Response of a Neutron-Insensitive Gamma-Ray Dosimeter as a Function of Photon Energy," *Health Phys.* 11, 133–36 (1965).

J. H. Thorngate and J. E. Parks
"A Portable Scaler," submitted for publication in *Health Physics.*

I. H. Tipton and Ann Calhoun
"A Modified Electrode Loader for Spectrochemical Analysis," *Appl. Spectry.* 18(2), 64 (1964).

I. H. Tipton, H. A. Schroeder, H. M. Perry, Jr., and M. J. Cook
"Trace Elements in Human Tissue. Part III. Subjects from Africa, the Near and Far East and Europe," *Health Phys.* 11(5), 403 (1965).

J. E. Turner
"Effects of Shell Corrections to Stopping Power in Theoretical Dose Studies," submitted for publication in *Proceedings of International Symposium on the Dosimetry of Irradiations from External Sources, November 23–27, 1964, Paris, France.*

"Electron Capture by Rotational Excitation of Polar Molecules," to be published in the *Physical Review.*

"On the Experimental Verification and Determination of Parameters in Stopping Power Theory," pp. 39–47 in *Studies in Penetration of Charged Particles in Matter,* Natl. Acad. Sci.–Natl. Res. Council, Publ. 1133 (1964).

Report of Trip Abroad by J. E. Turner During the Period November 23–December 8, 1964, ORNL-CF-65-1-5 (Jan. 4, 1965).

"The Possible Role of Momentum in Radiation Dosimetry. II. Extension to Charged Particles and Further General Considerations," *Health Phys.* (in press).

"Values of I and I_{adj} Suggested by Subcommittee," pp. 99–101 in *Studies in Penetration of Charged Particles in Matter,* Natl. Acad. Sci.–Natl. Res. Council, Publ. 1133 (1964).

J. E. Turner and Hal Hollister
"On the Relationship of the Velocity of a Charged Particle to Its Relative Biological Effectiveness (RBE)," submitted for publication in *Nature.*

J. E. Turner, C. D. Zerby, R. L. Woodyard, H. A. Wright, W. E. Kinney, W. S. Snyder, and J. Neufeld
"Calculation of Radiation Dose from Protons to 400 MeV," *Health Phys.* 10, 783–808 (1964).

G. M. Van Dyne
"A Further Note on Random Locations for Sample Units," *J. Range Management* 18(3), 150–51 (1965).

"Application of Some Operations Research Techniques to Food Chain Analysis Problems," *Health Phys.* (in press).

"Chemical Composition and Digestibility of Range Plants from Annual Range and from Pure-Stand Plots," *J. Range Management* (in press).

"Probabilistic Estimates of Range Forage Intake," *Proc. West. Sect. Am. Soc. Animal Sci.* 16(LXXVII), 1–6 (1965).

G. M. Van Dyne (with H. G. Fisser)
"Effect of Variation in Number and Spacing of Points on Accuracy and Precision of Estimates of Basal Cover of Foothill Grassland," submitted for publication in the *Journal of Range Management.*

G. M. Van Dyne and H. F. Heady
"Dietary Botanical Composition of Cattle and Sheep Sharing a Mature California Annual Range," *Hilgardia* (in press).

"Dietary Chemical Composition of Cattle and Sheep Grazing in Common on a Dry Annual Range," *J. Range Management* 18(2), 78–86 (1965).

"Interrelations of Botanical and Chemical Dietary Components of Livestock on Dry Annual Range," *J. Animal Sci.* 24(2), 305–12 (1965).

G. M. Van Dyne (with H. F. Heady)
"Prediction of Weight Composition from Point Samples on Clipped Herbage," *J. Range Management* 18(3), 144–48 (1965).

G. M. Van Dyne and G. F. Payne
"Grazing Responses of Western Range Plants," Department of Animal and Range Science, Montana State College, Bozeman (multilith).

G. M. Van Dyne, O. O. Thomas, and J. L. Van Horn
"Diet of Cattle and Sheep Grazing on Winter Range," *Proc. West. Sect. Am. Soc. Animal Sci.* 14(LXI), 1–6 (1964).

G. M. Van Dyne and J. L. Van Horn
"Distance Grazed by Sheep on Winter Range," *Proc. West. Sect. Am. Soc. Animal Sci.* 16(LXXIV), 1–6 (1965).

G. M. Van Dyne (with W. G. Vogel)
"Vegetation Responses to Grazing on a Central Montana Foothill Sheep Range," submitted for publication in the *Journal of Range Management.*

G. M. Van Dyne and W. C. Weir
"Comparison of Microdigestion Techniques Under Range and Dry-Lot Conditions," submitted for publication in the *Journal of Agricultural Science.*

W. H. Wilkie and R. D. Birkhoff
"Measurement of Spectral Distribution of Positron Flux in an Infinite Copper Medium Containing Cu^{64}," *Phys. Rev.* 135, A1133–38 (1964).

J. P. Witherspoon
"Cycling of Cesium-134 in White Oak Trees," *Ecol. Monographs* 34, 403–20 (1964).

"Radiation Damage to Forest Surrounding an Unshielded Fast Reactor," *Health Phys.* (Proceedings of Symposium on Radiation and Terrestrial Ecosystems, Richland, Washington, May 3–5, 1965) (in press).

J. P. Witherspoon and G. N. Brown
"Translocation of Cesium-137 from Parent Trees to Seedlings of *Liriodendron tulipifera,*" *Botan. Gaz.* (in press).

Martin Witkamp
"Biological Concentrations of ^{137}Cs and ^{90}Sr in Arctic Food Chains," submitted for publication in *Nuclear Safety.*

"Decomposition of Leaf Litter in Relation to Environmental Conditions, Microflora, and Microbial Respiration," *Ecology* (in press).

"Environmental Effects of Microbial Turnover of Some Mineral Elements," submitted for publication in *Ecology.*

"Environmental Influences on Microbial Populations and Activity of the Forest Floor," *Proc. Intern. Congr. Soil Sci., 8th, Bucharest, Rumania,* vol. III, *Soil Biology* (in press).

"Macroflora, Mycoflora, and Soil Relationships in a Pine Continuum," submitted for publication in *Ecology.*

"Rates of Carbon Dioxide Evolution from the Forest Floor: Measurement, Environmental Effects, and Relation to CO_2 from Litter," submitted for publication in *Ecology.*

Martin Witkamp and Marilyn L. Frank
"First Year of Movement, Distribution, and Availability of Cs-137 in the Forest Floor Under Tagged Tulip Poplars," *Radiation Botany* 4, 485–95 (1964).

Harvel Wright, C. L. Wiginton, and J. Neufeld
"Almost Longitudinal Instabilities in a Plasma-Beam System," submitted for publication in the *Physics of Fluids.*

Lectures

E. T. Arakawa
Studies of Solid State Plasmas by Optical and Electron Beam Methods, Millsaps College, December 7, 1964, Jackson, Mississippi; Texas A and M College, December 9, 1964, College Station; University of Texas, December 10, 1964, Austin; Mississippi State University, April 13, 1965, Starkville; Georgia Institute of Technology, April 14, 1965, Atlanta; Howard College, April 15, 1965, Birmingham, Alabama.

S. I. Auerbach
Ecology and Ecological Research at ORNL, ORINS Navy Seminar, December 4, 1964, Oak Ridge, Tennessee.

Radioactivity in Ecological Systems, ORINS Health Physics Course, November 1964, Oak Ridge, Tennessee.

Current Trends in Radiation Ecology Research at ORNL, Department of Zoology, University of North Carolina, December 10, 1964, Chapel Hill.

Radiation Ecology at a National Laboratory, Department of Zoology, Rutgers University, September 24, 1964, New Brunswick, New Jersey.

Systems Analysis in Ecology, Department of Zoology, University of Georgia, April 14, 1965, Athens.

J. A. Auxier
Ichiban: The Dosimetry Program for Nuclear Bomb Survivors of Hiroshima and Nagasaki, Medical College of Virginia, April 21, 1965, Richmond.

R. D. Birkhoff
Theory and Experiments on Electron Slowing-Down Spectra in Infinite Isotropic Media, Physics Department, Vanderbilt University, March 23, 1965, Nashville, Tennessee; Physics Department, University of Tennessee, March 30, 1965, Knoxville; Institute of Molecular Biophysics, Florida State University, April 12, 1965, Tallahassee.

Theory and Experiments on Plasmon Production and Decay in Solids, Department of Chemistry and Physical Sciences, Florida Atlantic University, April 14, 1965, Boca Raton.

B. G. Blaylock
Ecological Dosimetry, Radioecology Institute, ORINS, June 28, 1965, Oak Ridge, Tennessee.

W. J. Boegly, Jr.
Project Salt Vault, Meeting of the National Academy of Sciences–National Research Council Committee on Geologic Aspects of Radioactive Waste Disposal, ORNL, April 14, 1965, Oak Ridge, Tennessee.

Geologic Methods of Disposal – Salt, Course on Reactor Safety and Hazards Evaluation for Personnel of U.S. Public Health Service, Robert A. Taft Sanitary Engineering Center, ORNL, April 12, 1965, Oak Ridge, Tennessee.

Salt Demonstration, University of North Carolina School of Public Health Students, ORNL, August 19, 1964, Oak Ridge, Tennessee.

R. L. Bradshaw

Stress, Strain, and Temperature Relationships in Project Salt Vault, Meeting of the National Academy of Sciences–National Research Council Committee on the Geologic Aspects of Radioactive Waste Disposal, The Carey Salt Company, May 7, 1965, Lyons, Kansas.

J. S. Cheka

Dosimetry for Human Exposure, Rensselaer Polytechnic Institute, November 20, 1964, Troy, New York.

Civil Defense, Tokyo Boeki Kaikan, April 16, 1965, Tokyo, Japan.

K. E. Cowser

Process Waste Treatment Plant, USSR Waste Disposal Delegation, ORNL, June 8–9, 1965, Oak Ridge, Tennessee.

Waste Water Treatment Plant and Low Level Waste System, State Health Department Personnel, ORNL, November 9, 1964, Oak Ridge, Tennessee.

Progress Report No. 4, Subcommittee on Safety Evaluation, Clinch River Study Steering Committee, December 14–16, 1964, Oak Ridge, Tennessee.

D. A. Crossley, Jr.

Radiation Ecology, Summer Institute in Radiation Chemistry, Texas Woman's University, August 6, 1964, Denton; U.S. Army Nuclear Science Seminar, ORINS, August 20, 1964, Oak Ridge, Tennessee.

Food Chains and Radionuclide Transfer, Radioecology Institute, ORINS, June 9, 1965, Oak Ridge, Tennessee.

Radionuclide Transfer in ^{137}Cs Tagged Forest Food Chains, Radioecology Institute, ORINS, July 6, 1965, Oak Ridge, Tennessee.

Wallace de Laguna

Hydrofracturing, Southern Interstate Nuclear Board Briefing on Waste Disposal, ORNL, May 6, 1965, Oak Ridge, Tennessee.

Pits and Trenches, Meeting of the National Academy of Sciences–National Research Council Committee on Geologic Aspects of Radioactive Waste Disposal, ORNL, April 15, 1965, Oak Ridge, Tennessee.

Seepage Pits and Trenches and Intermediate Level Waste System, State Health Department Personnel, ORNL, November 9, 1964, Oak Ridge, Tennessee.

Liquid Disposal Trenches, USSR Waste Disposal Delegation, ORNL, June 8–9, 1965, Oak Ridge, Tennessee.

Hydrofracture Test, USSR Waste Disposal Delegation, ORNL, June 8–9, 1965, Oak Ridge, Tennessee.

Hydrofracturing Experiment, University of North Carolina School of Public Health Students, ORNL, August 19, 1964, Oak Ridge, Tennessee.

Post Injection Coring, Water Levels, Pressures, and Their Implications, Meeting of the National Academy of Sciences–National Research Council Committee on Geologic Aspects of Radioactive Waste Disposal, ORNL, April 14–15, 1965, Oak Ridge, Tennessee.

Concept, Geology, and Water Tests, Meeting of the National Academy of Sciences–National Research Council Committee on Geologic Aspects of Radioactive Waste Disposal, ORNL, April 14–15, 1965, Oak Ridge, Tennessee.

P. B. Dunaway

Radiation Effects in Mammals, Radioecology Institute, ORINS, June 24, 1965, Oak Ridge, Tennessee.

F. M. Empson

Mine Preparation, Meeting of the National Academy of Sciences–National Research Council Committee on the Geologic Aspects of Radioactive Waste Disposal, The Carey Salt Company, May 10, 1965, Lyons, Kansas.

H. H. Hubbell, Jr.

Hiroshima's Contribution to Health: The Radiation Doses to Survivors of the Atomic Bombings in Japan, Texas College of Arts and Industries, December 3, 1964, Kingsville (traveling lecture).

G. S. Hurst

Photon Trapping in Atomic Systems – Effects on Ion Yield Interpretation, Physics Department, University of Tennessee, April 6, 1965, Knoxville.

Excitation and Ionization of Argon Atoms by Alpha Particles, Physics Department, Vanderbilt University, May 4, 1965, Nashville, Tennessee.

D. G. Jacobs

Hazards Analyses, University of North Carolina School of Public Health Students, ORNL, August 19, 1964, Oak Ridge, Tennessee.

Tritiated Water Tracer Tests, Meeting of the National Academy of Sciences–National Research Council Committee on Geologic Aspects of Radioactive Waste Disposal, ORNL, April 14, 1965, Oak Ridge, Tennessee.

Tank Farm Hazard Analysis, Meeting of the National Academy of Sciences–National Research Council Committee on Geologic Aspects of Radioactive Waste Disposal, ORNL, April 14, 1965, Oak Ridge, Tennessee.

Disposal of Gases, Ground Disposal of Radioactive Gaseous Wastes Meeting, January 28–29, 1965, University of California, Berkeley.

N. R. Kevern

Aquatic Food Chain Studies, Radioecology Institute, ORINS, July 21, 1965, Oak Ridge, Tennessee.

T. F. Lomenick

Geologic Considerations in Radioactive Waste Disposal, Course in Nuclear Geology, ORINS, January 1965, Oak Ridge, Tennessee.

Distribution and Movement of Fission Products in the Sediments of White Oak Lake and *Waste Disposal Operations,* USGS Briefing, ORNL, February 11, 1965, Oak Ridge, Tennessee.

Geohydrological Considerations in Solid Waste Burials, Meeting of the National Academy of Sciences–National Research Council Committee on Geologic Aspects of Radioactive Waste Disposal, ORNL, April 14, 1965, Oak Ridge, Tennessee.

Burial Grounds for Solid Waste, Meeting of the National Academy of Sciences–National Research Council Committee on Geologic Aspects of Radioactive Waste Disposal, ORNL, April 15, 1965, Oak Ridge, Tennessee.

Burial Ground Facilities, USSR Waste Disposal Delegation, ORNL, June 8, 1965, Oak Ridge, Tennessee.

Solid Waste Disposal, Southern Interstate Nuclear Board Briefing on Waste Disposal, ORNL, May 6, 1965, Oak Ridge, Tennessee.

Safety and Hazard Analyses of Burial Grounds, State Health Department Personnel and Tour of Waste Disposal Facilities, November 9, 1964, Los Angeles, California.

Waste Disposal, 15th Annual Navy Nuclear Sciences Seminar, December 2, 1964, Oak Ridge, Tennessee.

K. Z. Morgan

Health Physics, ASEE-AEC Summer Institute, ORNL, August 17, 1964, Oak Ridge, Tennessee; Navy Nuclear Science Seminar, December 9, 1964, Oak Ridge, Tennessee; ORSORT, December 15, 16, and 18, 1964, Oak Ridge, Tennessee; Southwestern State College, February 15, 1965, Weatherford, Oklahoma; AEC Fellowship Students, Vanderbilt University, March 1–2, 8–9, and 22–23, 1965, Nashville, Tennessee.

Maximum Permissible Exposure to Ionizing Radiation, University of Texas, February 16, 1965, Austin; Medical College of Virginia, April 12, 1965, Richmond; East Carolina College, April 13, 1965, Greenville, North Carolina.

Radiation Health Physics, Nuclear Engineering Department, North Carolina State College, January 21, 1965, Raleigh.

Radiation Safety Training Program, ORNL, June 28, 1965, Oak Ridge, Tennessee.

Internal Exposure Dose, ORINS-ORNL 10-Week Health Physics Course, ORNL, November 3, 1964, Oak Ridge, Tennessee.

Health Physics Division Program, Research Committee Meeting, ORNL, November 10, 1964, Oak Ridge, Tennessee.

University of Tennessee Lectures, March 26 and 31 and April 2, 7, and 9, 1965, Knoxville.

D. J. Nelson

Strontium-90 and Stable Strontium in the Environment, Radioecology Institute, ORINS, July 13, 1964, Oak Ridge, Tennessee.

Interpretation of Radioisotope Tracer Studies Using Specific Activities and Biological Half-Lives, Radioecology Institute, ORINS, July 14, 1964, Oak Ridge, Tennessee; Department of Civil Engineering, University of Texas, October 15, 1964, Austin.

The Inorganic Chemistry of Life, Department of Geology, Rice University, October 14, 1964, Houston, Texas; Department of Biology, Knoxville College, January 6, 1965, Knoxville, Tennessee; Science Department, Jersey City State College, March 17, 1965, Jersey City, New Jersey; Sigma Xi Club, University of Southwestern Louisiana, April 22, 1965, Lafayette (traveling lectures).

J. S. Olson

Ecosystem Processes, Radioecology Institute, ORINS, June 10, 1965, Oak Ridge, Tennessee.

Fundamental Problems of Productivity and Mineral Cycling in Forests, University of Washington College of Forestry, May 7, 1965, Seattle.

F. L. Parker

Clinch River Studies, USSR Waste Disposal Delegation, ORNL, June 8–9, 1965, Oak Ridge, Tennessee.

Waste Disposal and Problems of Environmental Contamination, Oak Ridge Institute on Nuclear Science and World Politics, ORINS, April 20, 1965, Oak Ridge, Tennessee.

Clinch River Study, Civil Engineering Department, Harvard University, November 2, 1964, Cambridge, Massachusetts.

General Introduction to Waste Disposal, University of North Carolina School of Public Health Students, ORNL, August 19, 1964, Oak Ridge, Tennessee.

Flume Research, Atomic Energy Commission River Research Seminar, University of Texas, April 26–27, 1965, Austin.

Introduction to Waste Disposal Practices and Research, State Health Personnel, ORNL, November 9, 1964, Oak Ridge, Tennessee.

Background Briefing – Objectives of Project Salt Vault, Meeting of the National Academy of Sciences–National Research Council Committee on the Geologic Aspects of Radioactive Waste Disposal, The Carey Salt Company, May 10, 1965, Lyons, Kansas.

Radioactive Waste Disposal, Nuclear Engineering Seminar, University of Tennessee, May 25, 1965, Knoxville; U.S. Army Nuclear Sciences Seminar, ORINS, August 20, 1964, Oak Ridge, Tennessee.

B. C. Patten

Diversity and Productivity in Estuarine Phytoplankton, University of Tennessee, February 18, 1965, Knoxville.

A. Biocoenetics: Adaptive Control in Natural Communities. I. The Biocoenetic Problem; B. Biocoenetics. II. Basic Concepts About Systems; C. Biocoenetics. III. The Optimum Diversity Problem; D. Biocoenetics. IV. Structure and Behavior of Coupled Systems; E. Information Processing Structure of a Natural Plankton Community, Oklahoma State University, December 15–16, 1964, Stillwater.

Ecological Models: A Coupled Exponential Food Chain, Radioecology Institute, ORINS, June 10, 1965, Oak Ridge, Tennessee.

D. E. Reichle

Use of Radioisotopes in Studies of the Structure and Function of an Old-Field Ecosystem, Radioecology Institute, ORINS, August 1964, Oak Ridge, Tennessee.

Arthropod Studies in Tagged Forests, Radioecology Institute, ORINS, July 1965, Oak Ridge, Tennes-

R. H. Ritchie

Electron Interactions in Solid State Electron Plasmas, Physics Department, Vanderbilt University, March 9, 1965, Nashville, Tennessee; Physics Department, University of Tennessee, April 6, 1965, Knoxville.

Isabel H. Tipton

Lectures to Science Department, Sweet Briar College, February 1965, Sweet Briar, Virginia.

A. F. Shinn

Ecological Dosimetry, Radioecology Institute, ORINS, July 1964, Oak Ridge, Tennessee.

Mud-Dauber Wasps and Radioactive Mud: How a Scientist Attacks His Problems, Powell High School Science Club, October 5, 1964, Knoxville, Tennessee.

Radioecology of Sceliphron *and* Trypoxylon *Mud-Dauber Wasps,* Tennessee Academy of Science, Collegiate Division, Tennessee Polytechnic Institute, May 8, 1965, Cookeville.

Introduction to Radioecology I, Radioecology Institute, ORINS, June 8, 1965, and *Introduction to Radioecology II,* Radioecology Institute, ORINS, June 9, 1965, Oak Ridge, Tennessee.

Tsuneo Tamura

Mix Development, Meeting of the National Academy of Sciences–National Research Council Committee on Geologic Aspects of Radioactive Waste Disposal, ORNL, April 14, 1965, Oak Ridge, Tennessee.

Mineral Exchange, Meeting of the National Academy of Sciences–National Research Council Committee on Geologic Aspects of Radioactive Waste Disposal, ORNL, April 14, 1965, Oak Ridge, Tennessee.

Mineral Exchange Studies, USSR Waste Disposal Delegation, ORNL, June 8–9, 1965, Oak Ridge, Tennessee.

G. M. Van Dyne

The Program of the Radiation Ecology Section, Southeastern Forest Experimental Station, November 13, 1964, Asheville, North Carolina; Biological Sciences Division, Oregon State University, May 7, 1965, Corvallis; Department of Agronomy and Range Management, University of Nebraska, July 9, 1965, Lincoln; College of Forestry, Range and Wildlife Sciences, Utah State University, July 21, 1965, Logan; Division of Biological Sciences, Fort Hays Kansas State College, July 26, 1965, Hays.

The Future of Renewable Resource Management, Range Management Department, Oregon State University, May 7, 1965, Corvallis.

Nutritional Implications of Nonlinear Programming Analyses, Animal Sciences Department, Oregon State University, May 6, 1965, Corvallis.

Feces, Fistulas, and Forages, Zoology Department, University of Tennessee, February 1965, Knoxville.

Ecosystems, Systems Ecology, and Systems Ecologists, Radioecology Institute, ORINS, June 8, 1965, Oak Ridge, Tennessee.

J. P. Witherspoon

Ecological Dosimetry, June 28, 1965; *Cesium Cycling in Forests,* June 29, 1965, and *Radiation Effects on Plants,* July 7, 1965, Radioecology Institute, ORINS, Oak Ridge, Tennessee.

Effects of Postirradiation Environment on Expression of Radiation Damage in Pine Seedlings, AIBS Meetings, August 1964, Boulder, Colorado.

ORNL-3849
UC-41 – Health and Safety
TID-4500 (44th ed.)

INTERNAL DISTRIBUTION

1. Biology Library
2. Reactor Division Library
3–5. Central Research Library
6. Laboratory Shift Supervisor
7–8. ORNL – Y-12 Technical Library, Document Reference Section
9–62. Laboratory Records Department
63. Laboratory Records, ORNL R.C.
64. S. I. Auerbach
65. J. A. Auxier
66. S. E. Beall
67. S. R. Bernard
68. R. D. Birkhoff
69. W. J. Boegly
70. T. H. J. Burnett
71. R. L. Clark
72. W. E. Cohn
73. M. J. Cook
74. F. L. Culler
75. D. M. Davis
76. L. C. Emerson
77. B. R. Fish
78. J. L. Gabbard
79. J. H. Gillette
80. C. S. Harrill
81. J. A. Harter
82. A. Hollaender
83. L. B. Holland
84. A. S. Householder
85. G. S. Hurst
86. L. C. Johnson
87. W. H. Jordan
88. M. T. Kelley
89. C. E. Larson
90. T. A. Lincoln
91. R. S. Livingston
92. H. G. MacPherson
93. F. C. Maienschein
94. A. J. Miller
95. K. Z. Morgan
96. J. S. Olson
97. F. L. Parker
98–99. R. B. Parker
100. R. W. Peelle
101. H. P. Raaen
102. M. L. Randolph
103. R. M. Richardson
104. H. E. Seagren
105. M. J. Skinner
106. W. S. Snyder
107. E. G. Struxness
108. C. D. Susano
109. N. Tarr
110. E. H. Taylor
111. O. D. Teague
112. A. C. Upton
113. A. D. Warden
114. A. M. Weinberg
115. G. C. Williams
116. G. Young
117. R. J. Morton (consultant)
118. T. E. Bortner (consultant)
119. P. H. Doyle (consultant)
120. U. Fano (consultant)
121. T. D. Strickler (consultant)
122. J. C. Frye (consultant)
123. J. B. Hursh (consultant)
124. J. L. Magee (consultant)
125. E. P. Odum (consultant)
126. H. O. Wyckoff (consultant)

EXTERNAL DISTRIBUTION

127. R. W. McNamee, Union Carbide Corporation, New York
128. Physics and Engineering Group, Balcones Research Center, RFD 4, Box 189, Austin, Texas
129. G. E. Thoma, St. Louis University Hospital, 135 South Grand Boulevard, St. Louis, Missouri
130. Vanderbilt University (Physics Library)
131. Paul Jones, U.S. Geological Survey, Washington, D.C.
132. Lola Lyons, Librarian, Olin Industries, Inc., East Alton, Illinois
133. Jack Story, Health Physicist, North Carolina State College, Raleigh, North Carolina
134. J. H. Ebersole, USS Nautilus, c/o Fleet Post Office, New York, New York
135. W. L. Templeton, Health and Safety Division, U.K. Atomic Energy Authority, Seascale, Cumberland, England
136. David S. Smith, Health and Safety Division, U.S. Atomic Energy Commission, Chicago Operations Office, P.O. Box 59, Lemont, Illinois
137. Research and Development Division, AEC, ORO
138. S. C. Sigoloff, Office of the Executive Vice President, Electro-Optical Systems, Inc., 300 North Halstead Street, Pasadena, California 91107
139. Robert Wood, Department of Physics, Memorial Center, 444 E. 68th St., New York 21, New York
140. John Wolfe, Division of Biology and Medicine, U.S. Atomic Energy Commission, Washington, D.C.
141. Orlando Park, Department of Biology, Northwestern University, Evanston, Illinois
142. W. T. Ham, Medical College of Virginia, Richmond, Virginia
143. F. H. W. Noll, Department of Physics, Berea College, Berea, Kentucky
144. Herbert E. Stokinger, Bureau of State Service, Department of Health, Education and Welfare, Penn 14 Broadway, Cincinnati 2, Ohio
145. J. B. Lackey, University of Florida, Gainesville, Florida
146. J. J. Davis, Biology Operation, Hanford Atomic Power Operations, Seattle, Washington
147. Robert B. Platt, Department of Biology, Emory University, Atlanta, Georgia
148. C. H. Bernard, Dept. of Physics, Midwestern University, Witchita Falls, Texas
149. C. E. Dady, Watertown Arsenal, Ordnance Material Research Office, Watertown, Massachusetts
150. John I. Hopkins, Davidson College, Department of Physics, P.O. Box 327, Davidson, North Carolina
151. W. J. Lacy, Office of Civil Defense, Pentagon, Washington, D.C.
152. G. A. Andrews, Oak Ridge Institute of Nuclear Studies, Oak Ridge, Tennessee
153. E. P. Resner, States Marine Lines, c/o New York Shipbuilding Corp., Camden, New Jersey

154–158. Walter Belter, Division of Reactor Development, AEC, Washington, D.C.

159. H. J. Carey, Jr., The Carey Salt Company, Hutchinson, Kansas
160. C. Orr, Georgia Institute of Technology, Atlanta, Georgia
161. E. F. Gloyna, Department of Civil Engineering, University of Texas, Austin 12, Texas
162. J. S. Cragwall, Jr., U.S. Geological Survey, Surface Water Branch, 823 Edney Building, Chattanooga, Tennessee
163. H. H. Waesche, AEC Liaison Officer, Geochemical and Petrology Branch, U.S. Geological Survey, Naval Gun Factory, Building 213, Washington 25, D.C.
164. S. Leary Jones, Tennessee Department of Public Health, Cordell Hull Building, Nashville, Tennessee
165. H. C. Thomas, Chemistry Department, University of North Carolina, Chapel Hill, North Carolina
166. Glenn Gentry, Fish Management Division, Game and Fish Commission, Cordell Hull Building Nashville, Tennessee
167. Vincent Schultz, Environmental Sciences Branch, Division of Biology and Medicine, U.S. Atomic Energy Commission, Washington 25, D.C.
168. O. W. Kochtitzky, Tennessee Valley Authority, 717 Edney Building, Chattanooga, Tennessee
169. Leslie Silverman, Industrial Engineering, Department of Industrial Hygiene, School of Public Health, Harvard University, 55 Shattuck Street, Boston 15, Massachusetts

170. J. Wade Watkins, U.S. Bureau of Mines, Washington, D.C.
171. Kansas State Board of Health, Topeka, Kansas (Lee Mayes)
172. Kansas State Geological Survey, Lawrence, Kansas (Frank Foley)
173. Linn Hoover, Executive Secretary, Division of Earth Sciences, National Academy of Sciences–National Research Council, Washington, D.C.
174. C. S. Shoup, Biology Division, U.S. Atomic Energy Commission, Oak Ridge, Tennessee
175. L. Garcia, Naval Research Laboratory, Washington, D.C.
176. J. A. Lieberman, Division of Reactor Development, AEC, Washington, D.C.
177. Conrad Straub, Robert A. Taft Sanitary Engineering Center, Cincinnati, Ohio
178. M. Vidmar, Boris Kidric Institute, Vinča, Yugoslavia
179. Warren J. Kaufman, University of California, Berkeley, California
180. Sakai Shimizu, Institute for Chemical Research, Kyoto University, Kyoto, Japan
181. Toshio Aoki, J. A. E. R. I., Tokai-Mura, Naka-Gun, Ibaraki-Ken, Japan
182. K. A. Mahmoud, Radiation Protection and Civil Defense Department, Atomic Energy Establishment, Abou-Zaabal Post Office, Cairo, U.A.R. (Egypt)
183. New York Operations Office, Radiation Physics Division, Health and Safety Laboratory
184. D. C. Conway, Purdue University, Department of Chemistry, West Lafayette, Indiana
185. John Myhill, The Royal North Shore Hospital of Sydney, Crows Nest, Sydney, N.S.W., Australia
186. R. L. Shearin, Environmental Radiological Health Training, R. A. Taft Sanitary Engineering Center, 4676 Columbia Parkway, Cincinnati, Ohio 45226
187. H. N. Gardner, Division of Medical Sciences, National Academy of Sciences, National Research Council, 2101 Constitution Avenue, N.W., Washington, D.C.
188. W. P. Bennett, University of California, Radiation Laboratory, P.O. Box 808, Livermore, California
189. R. J. Anderson, Assistant Surgeon General, Chief, Bureau of State Services, USPHS, Department of Health, Education, and Welfare, Washington, D.C.
190. A. K. Ganguly, Head, Health Physics Division, Atomic Energy Establishment, Trombay, Bombay 73, India
191. Miriam Sachs, Department of Health, Metropolitan State Health District, 1100 Raymond Boulevard, Newark 2, New Jersey
192. Kazuo Simokawa, Library of Faculty of Science, Osaka City University, Sugimoto-Cho, Sumiyoshi-Ku, Osaka, Japan
193. G. R. Holeman, Department of University Health, Health Physics Division, Yale University, New Haven, Connecticut

194–603. Given distribution as shown in TID-4500 (44th ed.) under Health and Safety category (100 copies – CFSTI)